Université de Montréal

Relevé et analyse spectroscopiques d'étoiles naines blanches brillantes et riches en hydrogène

par

Alexandros Gianninas

Département de physique

Faculté des arts et des sciences

Thèse présentée à la Faculté des études supérieures

en vue de l'obtention du grade de

Philosophiæ Doctor (Ph.D.)

en physique

Août, 2011

Université de Montréal

Faculté des études supérieures

Cette thèse intitulée:

Relevé et analyse spectroscopiques d'étoiles naines blanches brillantes et riches en hydrogène

présentée par:

Alexandros Gianninas

a été évaluée par un jury composé des personnes suivantes:

François Wesemael,	Président-rapporteur
Pierre Bergeron,	Directeur de recherche
Nicole St-Louis,	Membre du jury
Martin Barstow,	Examinateur externe
Karen Waldron,	Représentante du Doyen de la FES

Thèse acceptée le: _____

Sommaire

Nous présentons un relevé et une analyse spectroscopiques de plus de 1300 naines blanches brillantes ($V \leq 17.5$) et riches en hydrogène. Des spectres dans le domaine du visible avec un rapport signal-sur-bruit élevé ont été obtenus et les données ont ensuite été analysées avec notre méthode spectroscopique habituelle qui compare les profils observés des raies de Balmer à des spectres synthétiques calculés à partir de la dernière génération de modèles d'atmosphère. D'abord, nous présentons une analyse détaillée de 29 naines blanches de type DAO utilisant une nouvelle grille de modèles qui inclut du carbone, de l'azote et de l'oxygène aux abondances solaires. Nous démontrons que l'ajout de ces métaux dans les modèles d'atmosphère est essentiel pour surmonter le problème des raies de Balmer qui empêche un ajustement simultané de toutes les raies de Balmer avec des paramètres atmosphériques cohérents. Nous identifions également 18 naines blanches chaudes de type DA qui souffrent aussi du problème des raies de Balmer. Des spectres dans l'ultraviolet lointain obtenus des archives du satellite *FUSE* sont ensuite examinés pour démontrer qu'il existe une corrélation entre les abondances métalliques élevées et les cas du problème des raies de Balmer. Les conséquences de ces résultats pour toutes les naines blanches chaudes et riches en hydrogène sont discutées. En particulier, le scénario évolutif pour les naines blanches DAO est révisé et nous n'avons plus besoin d'évoquer l'évolution post-EHB pour expliquer la majorité des étoiles DAO. Finalement, nous élaborons un scénario dans lequel les métaux engendrent un faible vent stellaire qui expliquerait la présence d'hélium dans les étoiles DAO.

Ensuite, nous présentons les résultats globaux de notre relevé, ce qui inclut une analyse spectroscopique de plus de 1200 naines blanches de type DA. En premier lieu, nous présentons le contenu spectroscopique de notre échantillon qui contient de nombreuses classifications er-

ronées ainsi que plusieurs naines blanches de type DAB, DAZ et magnétiques. Nous discutons ensuite des nouveaux modèles d'atmosphère utilisés dans notre analyse. De plus, nous utilisons des modèles de naines M pour obtenir de meilleures valeurs des paramètres atmosphériques pour les naines blanches qui sont membres de systèmes binaires DA+dM. Certaines naines blanches uniques et quelques systèmes binaires double-dégénérées sont également analysés de manière plus détaillée. Nous examinons ensuite les propriétés globales de notre échantillon incluant la distribution de masse et la distribution de masse en fonction de la température. Nous étudions également la façon dont les nouveaux profils de raies de Balmer affectent la détermination des paramètres atmosphériques. Nous testons la précision et la robustesse de nos méthodes en comparant nos résultats avec ceux du projet SPY, dans le cadre duquel plus de 300 des mêmes naines blanches ont été analysées d'une manière complètement indépendante. Finalement, nous faisons un retour sur la bande d'instabilité des naines blanches pulsantes de type ZZ Ceti pour voir quels effets ont les nouveaux profils de raies sur la détermination de ses frontières empiriques.

Mots clefs:

étoiles : abondances – étoiles : atmosphères – étoiles: évolution – étoiles: paramètres fondamentaux – naines blanches

Abstract

We present a spectroscopic survey and analysis of over 1300 bright ($V \leq 17.5$), hydrogen-rich white dwarfs. High signal-to-noise ratio optical spectra were obtained and are then analyzed using our standard spectroscopic technique which compares the observed Balmer line profiles to synthetic spectra computed from the latest generation of model atmospheres. First, we present a detailed analysis 29 DAO white dwarfs using our new up-to-date model atmosphere grids in which we have included carbon, nitrogen, and oxygen at solar abundances. We demonstrate that the inclusion of these metals in the model atmospheres is essential in overcoming the Balmer-line problem, which manifests itself as an inability to fit all the Balmer lines simultaneously with consistent atmospheric parameters. We also identify 18 hot DA white dwarfs that also suffer from the Balmer-line problem. Far ultraviolet spectra from the *FUSE* archive are then examined to demonstrate that there exists a correlation between higher metallic abundances and instances of the Balmer-line problem. The implications of these findings for all hot, hydrogen-rich white dwarfs are discussed. Specifically, the possible evolutionary scenario for DAO white dwarfs is revised and post-EHB evolution need no longer be invoked to explain the evolution for the majority of the DAO stars. Finally, we discuss how the presence of metals might drive a weak stellar wind which in turn could explain the presence of helium in DAO white dwarfs.

We then present the complete results from our survey, including the spectroscopic analysis of over 1200 DA white dwarfs. First we present the spectroscopic content of our sample which includes many misclassifications as well as several DAB, DAZ and magnetic white dwarfs. We then discuss the new model atmospheres we employ in our analysis. In addition, we use M dwarf templates to obtain better estimates of the atmospheric parameters for those white

dwarfs which are in DA+dM binary systems. A handful of unique white dwarfs and double-degenerate binary systems are also analyzed in greater detail. We then examine the global properties of our sample including the mass distribution and mass distribution as a function of temperature. Next, we look at how the new Balmer-line profiles affect the determination of the atmospheric parameters. We then proceed to test the accuracy and robustness of our method by comparing our results to those of the SPY survey which has analyzed over 300 of the same white dwarfs in a completely independent manner. Finally, we also re-visit the ZZ Ceti instability strip and how the determination of its empirical boundaries is affected by the latest line profile calculations.

Subject headings:

stars: abundances – stars: atmospheres – stars: evolution – stars fundamental parameters – white dwarfs

Table des matières

Liste des figures

Liste des tableaux

Remerciements

"Ideal teachers are those who use themselves as bridges over which they invite their students to cross, then having facilitated their crossing, joyfully collapse, encouraging them to create bridges of their own." – Nikos Kazantzakis

Je crois que cette citation représente bien la philosophie de mon directeur de recherche, Pierre Bergeron, vis-à-vis de ses étudiants au doctorat et sans lui, je n'aurais jamais réussi à me rendre jusqu'ici. Je suis endetté à Pierre pour tout son appui, son enthousiasme, son encouragement et l'encadrement qu'il m'a fourni, mais également pour tous les coups de pied aux fesses qu'il m'a donnés au fil des années.

J'aimerais également remercier mes collaborateurs Jean Dupuis et Maria Teresa Ruiz. Je veux aussi remercier Gilles Fontaine de son aide indispensable durant la découverte de ma première étoile ZZ Ceti, pour toutes les histoires qu'il raconte, et également pour son enthousiasme envers son travail. J'espère que ma passion pour l'astronomie demeurera aussi forte que la sienne.

Je dois aussi remercier tous mes collègues de bureau, ceux qui sont encore ici ainsi que certains qui sont déjà partis : Robert, Patrick, Pier-Emmanuel, Guy, Pierre, Marie-Michèle et Noemi avec qui j'ai passé de bons moments, tant au bureau qu'en mission d'observation, en assistant à des conférences et bien sûr au pub!

Finalement, j'aimerais remercier ma mère et mon frère de leur appui et encouragement durant des moments difficiles; mes amis, Tony, Sevy, Christos, Alexandra et Ritsa qui sont toujours là pour moi; tous mes coéquipiers au soccer avec qui je me défoule au moins une fois par semaine; et la dernière, mais certainement non la moindre, ma dulcinée Dina, qui a cru en moi dès le début.

À Dina, qui est arrivée juste au bon moment.

Chapitre 1

Introduction

Depuis les débuts de l'astrophysique, l'évolution stellaire est demeurée un des champs de recherche les plus importants sur lequel se penchent les astrophysiciens. On cherche ici à comprendre comment les étoiles se forment, évoluent et finalement meurent. Contrairement aux étoiles massives qui finiront leur vie de manière spectaculaire dans une explosion de supernova, les étoiles qui ont une masse inférieure à huit fois la masse du Soleil finiront leur vie de façon plus paisible. Ces étoiles subiront une phase de perte de masse importante où les couches externes de l'étoile seront éjectées et le noyau résiduel se contractera pour former ce qu'on appelle une étoile naine blanche. Les naines blanches représentent le stade final dans la vie d'environ 97% de toutes les étoiles dans la Galaxie. Donc, si on veut en arriver à une compréhension globale de l'évolution stellaire, il est impératif d'étudier et de comprendre comment les étoiles naines blanches se forment et évoluent.

Dans cette thèse, nous présenterons les résultats de notre relevé spectroscopique d'étoiles naines blanches tirées de la plus importante référence dans le domaine des naines blanches : le catalogue de McCook & Sion (1999). Dans le but de placer notre étude dans un contexte approprié, il est important de comprendre les origines du catalogue. Dans les prochaines sections, nous présenterons l'histoire de la découverte des toutes premières naines blanches, des importants relevés qui ont suivi, jusqu'aux résultats récents du *Sloan Digital Sky Survey*. L'ensemble de ces efforts a permis la découverte de la grande majorité des naines blanches qui sont le sujet de notre analyse. Nous exposerons ainsi les raisons qui ont motivé la création

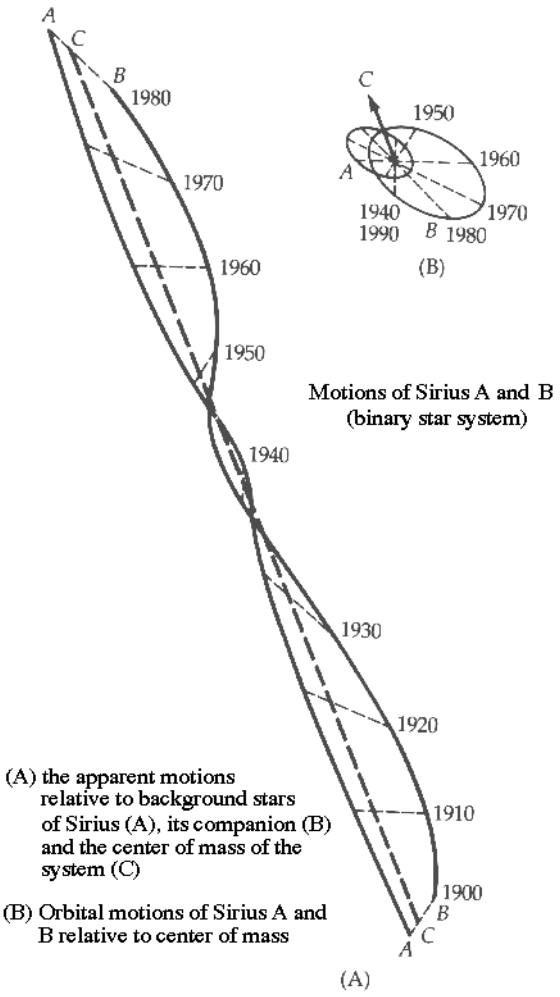

FIGURE 1.1 – (A) Mouvement propre de Sirius A et B dans le ciel et (B) mouvement orbital de Sirius A et B relatif au centre de masse.

du catalogue de McCook & Sion mais également la motivation derrière ce projet.

1.1 Les premières naines blanches

La première naine blanche observée est une des étoiles du système triple 40 Eridani, spécifiquement 40 Eri B. La paire d'étoiles 40 Eri B/C a été observée pour la première fois par l'astronome anglais, d'origine allemande, Friedrich Willhelm Herschel en 1783. Plus tard, en 1910, Henry Norris Russell, Edward Charles Pickering et Williamina Fleming ont découvert que 40 Eri B, en dépit du fait qu'elle soit très peu brillante, était de type spectral "A". Le type spectral de 40 Eri B est officiellement décrit par Adams (1914) (et de nouveau dans Adams

& Pease 1914) qui la classifie comme une étoile de type A0.

La deuxième naine blanche observée est Sirius B. Dans un premier temps, en 1844, l'astronome allemand Friedrich Bessell déduit que Sirius A devait avoir un compagnon parce que le mouvement propre de l'étoile ne suivait pas une trajectoire rectiligne (voir Figure 1). En 1862, l'opticien américain Alvan Graham Clark observe le compagnon de Sirius A pour la première fois durant une mise au point du nouveau réfracteur de 18.5 pouces destiné au Dearborn Observatory à Evanston en Illinois. Ensuite, Adams (1915) observe Sirius B et détermine que c'est une étoile de faible magnitude dont le spectre est quasiment identique à celui de Sirius A, une étoile de type spectrale A. Cela vient confirmer que Sirius B est la deuxième naine blanche à être identifiée, après 40 Eri B.

Finalement, en 1917, Adriaan van Maanen découvre "l'étoile de van Maanen" (van Maanen 2), une naine blanche isolée (van Maanen 1917). Mais la valeur de la parallaxe mesurée par van Maanen implique que ce soit l'étoile de type F la moins brillante, en magnitude absolue, connue à l'époque. Plus tard, Luyten (1923) publie une étude d'étoiles ayant des mouvements propres supérieurs à $0''.50$ par année. Parmi ces étoiles, Luyten identifie l'étoile de van Maanen comme une des trois naines blanches connues. Ce sont toutes des étoiles peu brillantes compte tenu de leur type spectral. Dans la Figure 1.2, on peut voir les trois naines blanches bien en dessous et à la gauche des étoiles de la séquence principale. Dans un contexte plus général, Luyten (1922a) identifie les trois étoiles mentionnées ci-haut comme des étoiles blanches peu brillantes (*faint white stars*) pour ensuite utiliser le terme "naine blanche" (*white dwarf*) pour la première fois dans Luyten (1922b). Les naines blanches sont ainsi baptisées.

1.2 Les relevés de mouvements propres: Luyten et Giclas

Que Willem Jacob Luyten fût en quelque sorte le "parrain" des naines blanches n'est peut-être pas une coïncidence puisqu'il allait, durant une longue carrière, découvrir des centaines de nouvelles naines blanches. Premier étudiant à obtenir son doctorat sous la direction d'Ejnar Hertzsprung en 1921, Luyten s'établit éventuellement à l'Université du Minnesota en 1931, où il travaillera le reste de sa vie. Comme en témoigne la section précédente, Luyten s'intéresse aux naines blanches très tôt dans sa carrière. Après les premières découvertes,

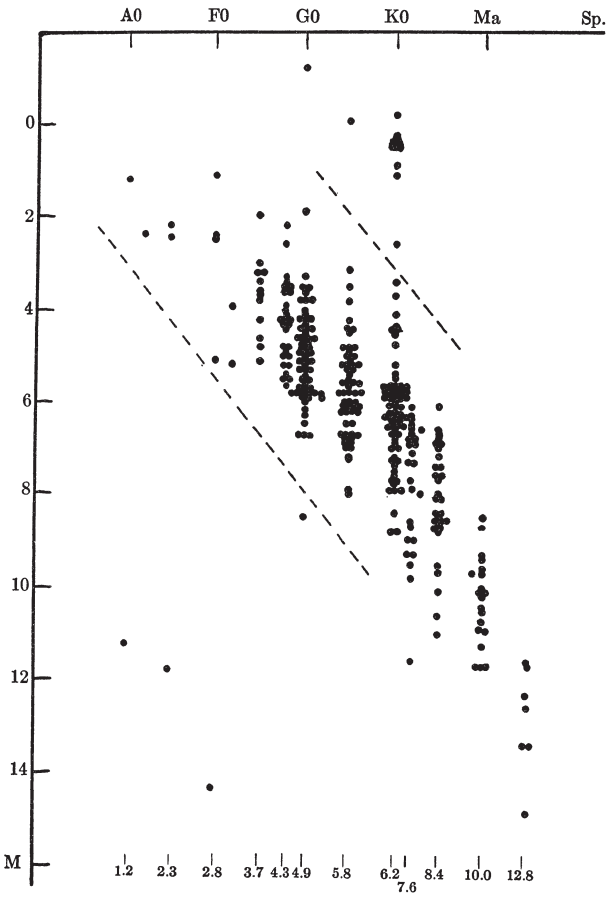

FIG. 1
RELATION BETWEEN ABSOLUTE MAGNITUDE AND SPECTRAL CLASS

FIGURE 1.2 – Diagramme de type spectral versus la magnitude absolue pour les étoiles étudiées dans Luyten (1923). On voit bien les trois naines blanches (40 Eri B, Sirius B et Van Maanen 2) en bas à gauche.

l'identification de nouvelles naines blanches fut lente: en 1939, seulement 18 naines blanches étaient connues (Schatzman 1958). Luyten (1950) explique qu'après les découvertes initiales, il entame un relevé spectroscopique d'étoiles faibles avec un grand mouvement propre. Il se rend compte que cette technique n'est pas très efficace pour trouver de nouvelles naines blanches et il concentre donc ses efforts pour augmenter le nombre potentiel de naines blanches par l'entremise de relevés de mouvements propres complétés par des observations photométriques. La photométrie ainsi obtenue permet de calculer des indices de couleurs à partir desquels les naines blanches peuvent être identifiées. Ainsi, Luyten publie durant une période de 40 ans les résultats de ses travaux dans une série de catalogues dans lesquels il rapporte la découverte

de plusieurs centaines de naines blanches. Parmi les plus connus de ces relevés on retrouve les relevés Luyten Two Tenths (LTT, Luyten 1957), Bruce Proper Motion (BPM, Luyten 1963) et Luyten Half Second (LHS Luyten 1979).

Henry Lee Giclas, un contemporain de Luyten, travaillait au Lowell Observatory, à Flagstaff en Arizona, où il entreprend également un relevé de mouvements propres. Avant l'époque de Giclas, Percival Lowell, le fondateur de l'observatoire, avait établi comme projet la recherche de la planète Pluton. Pour ce faire, il initie un relevé de tout le ciel nocturne observable depuis Flagstaff. Malheureusement, il ne réussit pas à trouver Pluton avant son décès en 1916, et le projet est éventuellement accordé à Clyde Tombaugh qui réussit l'exploit le 18 février 1930. Giclas, lui, cherche une façon d'exploiter toutes les plaques photographiques qui avaient été obtenues durant la quête de Pluton. Giclas (1958) présente le projet qui définira le reste de sa carrière. Une nouvelle série de plaques photographiques sera obtenue pour ainsi mener un relevé de mouvements propres en conjonction avec les vieilles plaques photographiques de Lowell. Le produit final consiste en deux grands catalogues. Premièrement, un catalogue d'objets qui ont un mouvement propre, $\mu > 0\farcs26\ yr^{-1}$ (les objets G, Giclas et al. 1971) et un deuxième catalogue d'objets avec $\mu < 0\farcs26\ yr^{-1}$ et choisis selon leurs couleurs $U-B$ et $B-V$ dans le but d'identifier de nouvelles naines blanches (les objets GD, Giclas et al. 1965). Il contribue ainsi à l'essor de la recherche sur les naines blanches avec la découverte de plusieurs centaines de nouvelles étoiles de ce type.

1.3 Les relevés par excès dans l'ultraviolet: Palomar-Green et Kiso Ultraviolet Excess

Les années 80 ont vu l'arrivée de relevés qui avaient pour but d'identifier des objets avec des excès dans l'ultraviolet. Dans un premier temps, le relevé Palomar-Green (PG, Green et al. 1986) avait été entamé pour tenter de trouver des quasars. Le relevé PG s'étend sur presqu'un quart du ciel avec des latitudes galactiques $b \geq 30°$ et des déclinaisons plus grandes que $-10°$. Des plaques photographiques sont obtenues sur le télescope de 18 pouces du Mont Palomar et tous les objets avec $U-B < -0.46$ sont ensuite observés en spectroscopie. Malheureusement,

le relevé PG fut un échec à cet égard avec seulement 93 nouveaux quasars détectés sur un total de 1715 objets. Par contre, le relevé PG a permis la découverte de centaines d'objets bleus, notamment des étoiles de type sous-naine, mais également plusieurs centaines de naines blanches (Fleming et al. 1986; Liebert et al. 2005). En parallèle, mais de l'autre côté de l'océan Pacifique, s'effectuait le relevé Kiso Ultraviolet Excess (KUV, Noguchi et al. 1980; Kondo et al. 1984). En utilisant le télescope de 105 cm de l'observatoire Kiso, 1186 objets sont identifiés dans une ceinture du pôle nord au pôle sud galactique à une longitude galactique de 180°. Encore une fois, plusieurs centaines de naines blanches sont cataloguées (Darling 1994; Limoges & Bergeron 2010). Un des avantages de ce genre de relevé est la possibilité de définir une magnitude limite en deça de laquelle on peut considérer que le relevé est complet. Ceci permet de calculer une fonction de luminosité pour la population de naines blanches, ce qui mène à une mesure de la densité spatiale et du taux de formation de ces étoiles dans le voisinage solaire.

1.4 Les relevés Montréal-Cambridge-Tololo et Edinburgh-Cape

Contrairement aux relevés PG et KUV, les relevés Montréal-Cambridge-Tololo (MCT, Demers et al. 1986) et Edinburgh-Cape (EC, Stobie et al. 1987) avaient comme but principal la découverte d'objets stellaires bleus, surtout des étoiles naines blanches. Ces deux relevés se distinguent également par le fait qu'ils ont été réalisés dans l'hémisphère sud. Demers et al. (1986) avaient noté le besoin d'exploiter le ciel de l'hémisphère sud puisque seulement environ 18% des naines blanches connues à l'époque s'y trouvait. Cependant, les difficultés reliées à la gestion, à partir de Montréal, d'un relevé dans l'hémisphère sud, plus précisément au Chili, ont fait en sorte que seulement le tiers du suivi spectroscopique du relevé MCT fut complété. Lamontagne et al. (2000) présentent ces résultats et les statistiques indiquent qu'environ 30% des candidats observés en spectroscopie sont des naines blanches. De façon très similaire, des résultats partiels du relevés EC sont présentés dans Kilkenny et al. (1997), mais le rendement en naines blanches est plus faible; seulement 15% de leurs cibles se sont avérées être des naines blanches. Ceci étant dit, contrairement au relevé MCT, le suivi spectroscopique du relevé EC continue à ce jour (Kilkenny et al. 2010).

1.5 Les relevés Hamburg-Schmidt et Hamburg-ESO

Les relevés Hamburg-Schmidt (HS, Hagen et al. 1995) et Hamburg-ESO (HE, Wisotzki 1994) constituent des relevés complémentaires de l'hémisphère nord et sud, respectivement, qui utilisent un prisme objectif pour obtenir, tout d'abord, des spectres à basse résolution spectrale pour l'identification de candidats. Les cibles ainsi identifiées sont ensuite réobservées à plus haute résolution. Encore une fois, le but principal de ces deux relevés était la détection de quasars. L'avantage d'utiliser un prisme objectif plutôt que des méthodes colorimétriques (voir les relevés PG et KUV) est qu'on obtient, du premier coup, un spectre de chaque objet. Cela augmente considérablement l'efficacité du relevé pour trouver des quasars. Néanmoins, la plus grande contamination dans un relevé d'objets bleus provient d'objets stellaires chauds, incluant les étoiles naines blanches. Homeier et al. (1998) présentent une analyse spectroscopique de 80 naines blanches provenant du relevé HS, tandis que Christlieb et al. (2001) élaborent un algorithme pour détecter des naines blanches dans les données du relevé HE. Ainsi, Christlieb et al. (2001) identifient 440 naines blanches potentielles qui ne sont pas listées dans McCook & Sion (1999).

1.6 Le Sloan Digital Sky Survey

Le *Sloan Digital Sky Survey* (SDSS) est un grand relevé visant la création d'une carte tri-dimensionnelle de la distribution de galaxies dans l'Univers. La première étape du relevé a été de recueillir de la photométrie en cinq bandes (*ugriz*) pour 35% du ciel avec le télescope de 2.5 m du Apache Point Observatory, au Nouveau-Mexique. À partir des données photométriques, une sélection de cibles est faite selon une liste de priorités bien établies. Ensuite, 660 fibres optiques sont attribuées à des cibles dans chaque champ. Ces fibres optiques sont ensuite acheminées vers un spectrographe spécialement conçu pour ce relevé qui permet de prendre un spectre pour chaque fibre optique simultanément. Cependant, les champs ne contiennent pas tous 660 galaxies et donc les fibres restantes sont attribuées à d'autres types d'objets, incluant des étoiles naines blanches. Des milliers de nouvelles naines blanches ont été ainsi découvertes comme produit secondaire du SDSS. Malheureusement, la majorité des

No.	Star	R.A. 1900	Decl. 1900	P.M.	m_{vis}	p(tr)	M_{vis}	Sp	C	Reference
1	Wolf 1	0^h08^m5	− 0°14′	0″.53	15.0	.....	....	wA	b	1
2	vMaanen 2	0 43.9	+ 4 55	3.00	12.4	0″.243±6	14.3	wG	a6	2
3	Wolf 1516	1 12.7	+15 40	0.69	13.6	.....	....	Con	o	1
4	Ross 548	1 31.2	−11 51	0.42	13.5	.....	....	wA	b	1
5	L 870–2	1 33.0	− 5 31	0.67	12.2	.....	....	wAs	a	3
6	AC 25°6725	2 03.1	+24 46	0.43	12.7	.....	....	wA	b	1
7	1166 h Per	2 10.5	+56 39	0.16	13.5	0.011±6	....	wA	b5	4
8	L 587–77A	3 24.7	−27 44	0.81	13.0	.....	....	wA	b	3
9	Wolf 219	3 38.8	+18 09	1.25	15.2	0.067±8	14.3	Con	b	5
10	40 Eri B	4 10.7	− 7 49	4.08	9.6	0.202±3	11.1	wA	b7	6
11	Hyad 7	4 18.2	+16 07	0.10	14.1	(0.027)	11.3	wA	b	7
12	Hyad 16	4 22.9	+16 45	0.10	14.0	(0.027)	11.2	wA	b	7
13	Sel. A. W82	6 36.0	+44 45	0.05	16.3	.....	....	wA	b	8
14	α CMa B	6 40.7	−16 35	1.32	8.5	0.376±3	11.4	wA5	a	9
15	Hertzsp. 3	6 40.9	+37 39	0.96	11.7	0.072±7	11.0	wA	b5	10
16	L 384–24	7 30.4	−42 41	0.66	14.0	.....	....	wA	b	3
17	α CMi B	7 34.1	+ 5 29	1.24	10.8	0.291±4	13.1	?	?	11
18	L 745–46	7 35.8	−17 10	1.29	13.1	0.177±14	14.3	wF	b	3
19	−32°5613	8 37.7	−32 37	1.68	11.5	.....	....	wA	b	3
20	Fu I, 182	9 40.3	+44 22	0.29	13.1	.....	....	wA	b	12
21	L 898–25	10 52.6	− 6 59	0.80	14.3	.....	....	Con	a	3
22	L 971–14	11 13.2	− 2 42	0.54	14.7	.....	....	Con	a	3
23	Ross 627	11 19.1	+21 55	1.23	14.1	0.080±8	13.6	wAs	b	13
24	Wolf 457	12 55.1	+ 4 02	1.05	15.6	0.078±8	15.1	Con	a	1
25	−7°3632A	13 25.1	− 8 03	1.18	12.0	0.064±8	11.0	wA	b5	5

FIGURE 1.3 – Extrait de la Table 1 de Kuiper (1941) qui montre le premier système de classification spectrale pour les étoiles naines blanches.

données du SDSS ont un rapport signal-sur-bruit (S/N) faible en raison du temps de pose fixe pour chaque champ. En d'autres mots, moins une étoile est brillante, plus le S/N du spectre obtenu est faible. Néanmoins, avec la publication du catalogue de naines blanches découvertes dans le *Data Release 4*, Eisenstein et al. (2006) ont quadruplé le nombre de naines blanches connues. Depuis ce temps, les publications subséquentes des ensembles de données du SDSS ont fait en sorte que le nombre de naines blanches connues et identifiées spectroscopiquement frôle maintenant les 13,000. Ce nombre va bientôt augmenter de nouveau avec la publication des résultats du *Data Release 7* (Kleinman 2010).

1.7 Classification spectrale

Même avant la découverte de ces centaines, voire milliers, de nouvelles naines blanches dans tous ces divers relevés, il devenait nécessaire de pouvoir classifier les spectres de ces étoiles. Une première tentative a été faite par Kuiper (1941) qui présenta une liste de 38 étoiles naines

Star	1950 R.A.	1950 Dec.	m_{pg}	Sp.	p	M_{pg}	I.C.
v Ma 1	0h46m5	+ 5°11′	12.9	DF	0″.245	14.8	+0.69
L 870-2	1 35.5	− 5 16	13.0	DA	.065	12.1	+0.13
h Per 1166	2 14.0	+56 53	13.2	DA	.011	8.4	−0.59
W 219	3 41.6	+18 18	15.1	DF	.066	14.2	+0.73
o_2 Eri B	4 13.0	− 7 44	9.5	DA	.200	11.0	−0.1:
L 82-61	6 15.5	−59 11	13.7	a–f	.041	11.8	+0.2:
α CMa B	6 43.0	−16 39	8.8	DA	.376	11.7	+0.3:
He 3	6 44.3	+37 36	11.2	DA	.066	10.3	−0.80
α CMi B	7 36.7	+ 5 21	11.3	f:	.294	13.6	+0.4:
L 745-46 A	7 38.0	−17 17	12.8	DA	.158	13.8	−0.17
L 97-12	7 52.8	−67 38	15.0	g	.170	16.2	+0.5:
L 532-81	8 39.7	−32 47	11.7	DA	.102	11.8	+0.05
SA 29-130	9 43.5	+44 08	12.9	DA	.035	10.6	−0.57
R 627	11 21.7	+21 39	13.8	DA	.079	13.3	−0.54
L 145-141	11 42.9	−64 34	11.9	DA	.204	13.2	−0.1:
W 457	12 57.7	+ 3 46	16.0	DC	.076	15.4	+0.15
BD−7°3632	13 27.7	− 8 18	12.1	DA	.062	11.1	−0.40
W 489	13 34.3	+ 3 58	15.5	DC	.129	16.1	+0.77
Grw+70°5824	13 37.8	+70 33	12.3	DA	.028	9.5	−0.62
CPD−37°6571 B	15 44.2	−37 45	13.5	DA	.074	12.8	0.0:
Grw+70°8247	19 00.6	+70 34	12.7	DC:	.074	12.0	−0.31
L 997-21	19 54.0	− 1 09	13.7	DA	.074	13.0	0.00
W 1346	20 32.3	+24 55	11.2	DA	.074	10.5	−0.30
LDS 749 B	21 29.6	0 00	14.2	DA	.025	11.2	−0.39
Grw+82°3818	21 36.7	+82 49	12.5	DA	.050	11.0	−0.55
L 362-81	23 59.6	−43 25	12.8	DA	.127	13.3	0.0:
VR 7	4 21.0	+16 14	14.1	DA	.026	11.2	+0.09
VR 16	4 25.7	+16 52	13.5	DA	.026	10.6	−0.47
Z 9	4 29.4	+17 38	14.0	DA	.026	11.1	+0.24
Z 7	4 31.0	+12 35	13.6	DA	.026	10.7	−0.54
L 68-28	12 25.6	−71 13	15.7	k–m	.15:	16.6	+1.1:
L 68-27	12 25.6	−71 13	17.7	k–m	.15:	18.6	+1.0:
BD+4°4048 B	19 14.6	+ 5 05	19.5	m	.170	20.7	+1.4
L 587-77 A	3 26.8	−27 34	13.9	DA	.045	11.2	+0.3:
LDS 235 B	8 45.3	−18 48	14.6	DA	.013	10.2	−0.45
L 1405-40	11 47.7	+23 35	15.4	DA	.015	11.3	−0.27
LDS 455 A	13 34.3	−16 04	14.9	DA	.008	9.4	−0.35
L 619-50	13 48.1	−27 18	15.0	DA	.023	11.8	−0.35
W 672 A	17 16.2	+ 2 00	14.2	DA	.025	11.2	−0.03
LDS 678 A	19 17.7	− 7 46	11.9	DC	.030	9.3	−0.14
LDS 683 B	19 32.9	−13 36	15.3	DA	.011	10.5	−0.11
L 1512-34	23 41.4	+32 15	12.9	DA	.048	11.3	+0.06
LDS 826 A	23 51.5	−33 33	14.6	DA	0.025	11.6	+0.25:

FIGURE 1.4 – Table 3 de Luyten (1952) qui montre un nouveau système de classification spectrale pour les étoiles naines blanches.

blanches. Le système élaboré par Kuiper était basé sur le système de classification spectrale de Harvard établi par Cannon & Pickering (1912) avec un w devant la classification Harvard pour indiquer que c'est une naine blanche. Ainsi, une naine blanche dont le spectre ressemble à une étoile de type A est classifiée wA (ex. 40 Eri B) et ainsi de suite pour les autres types spectraux (wF, wG, etc). Les naines blanches dont les spectres n'affichent aucune raie spectrale sont classifiées *Con.* Dans la Figure 1.3, nous présentons un extrait de la Table 1 tiré de Kuiper (1941) où l'on voit la classification dans la colonne *Sp.* Cependant, un nouveau système est introduit dans Luyten (1952), un système qui formera la base du système de classification

Symbol	Characteristics
DC	Continuous spectrum; no lines deeper than 10%
DO	He II strong; He I and/or H present
DB	He I strong; no H
DA	H present; no He I
DA, F	H sharper and weaker; Ca II weak
DF	Ca II, Fe I, no H
DK	Weak Ca II
DM	Ca II; Ca I weak; TiO?
λ4135	Broad "Minkowski" bands, unidentified
λ4670	Broad bands at λλ4670, 5165; probably C_2
C_2	Same as definition of λ4670 stars
Subscripts:	
p or P	polarization; also sometimes used for peculiar
wk	weak
e	emission
s	sharp
ss	very sharp
n	diffuseness
PEC	peculiar

FIGURE 1.5 – Table 1 de Sion et al. (1983) qui présente le système de classification spectrale pour les étoiles naines blanches de Greenstein (1960).

spectrale actuel. Dans le système de Luyten, les *w* sont remplacés par un "D". Ainsi une étoile classifiée *wA* par Kuiper est maintenant classifiée DA dans le nouveau système. Luyten définit les naines blanches DA comme des étoiles dont le spectre est dominé par les raies de Balmer de l'hydrogène tandis que les étoiles qui montrent uniquement des raies d'hélium dans leur spectre sont classifiées DB. D'autre part, van Maanen 2, dont le spectre est caractérisé par la présence de raies de calcium, est désignée DF et les naines blanches anciennement classifiées *Con* sont rebaptisées DC. Outre l'appellation DF, les définitions des autres types spectraux demeureront inchangées. On peut voir le nouveau système de Luyten (1952) dans la Figure 1.4.

Avec la découverte de divers nouveaux types d'étoiles naines blanches, Greenstein (1960) étend le système de Luyten et y introduit de nouvelles catégories (ex. DO, pour les étoiles avec des raies d'hélium ionisé), mais aussi une classification hybride (DA,F) pour les naines blanches qui montrent à la fois des raies d'hydrogène et de calcium dans leur spectre. Le nouveau système de classification de Greenstein est présenté dans la Figure 1.5. Cependant, Sion et al. (1983) discutent du fait qu'au fil des années plusieurs types spectraux sont devenus obsolètes et/ou peu pratiques. De plus, des spectres à plus haute résolution permettent la détection de raies plus faibles, ce qui a pour conséquence le développement de classifications hybrides du genre DAZ, DBA, etc. Ainsi, Sion et al. (1983) proposent un nouveau système de

DEFINITION OF PRIMARY SPECTRAL SYMBOLS

Spectral Type	Characteristics
DA	Only Balmer lines; no He I or metals present
DB.....	He I lines; no H or metals present
DC	Continuous spectrum, no lines deeper than 5% in any part of the electromagnetic spectrum
DO	He II strong; He I or H present
DZ	Metal lines only; no H or He lines
DQ	Carbon features, either atomic or molecular in any part of the electromagnetic spectrum
P.....	Magnetic white dwarfs with detectable polarization
H	Magnetic white dwarfs without detectable polarization
X.....	Peculiar or unclassifiable spectrum
E.....	Emission lines are present
?	Uncertain assigned classification; a colon (:) may also be used
V.....	Optional symbol to denote variability

FIGURE 1.6 – Table 1 de McCook & Sion (1999) qui démontre le système de classification spectrale pour les étoiles naines blanches présentement en vigueur.

classification spectrale mais l'application systématique de celui-ci devra attendre la publication de McCook & Sion (1999).

Les symboles primaires du nouveau système sont présentés dans la Figure 1.6. Ces symboles indiquent quelles raies dominent le spectre observé de l'étoile. Si des raies secondaires sont présentes, on peut joindre un (ou deux) symbole(s) supplémentaire(s) selon le cas. On peut alors se retrouver avec des étoiles de types DQA, DAOZ, etc. D'autres symboles peuvent également être rajoutés pour indiquer la présence de raies d'émission (E) ou d'un champ magnétique (P et H). Toutefois, ce système ne permet pas de distinguer entre une étoile DA avec une température effective $T_{\rm eff} = 30{,}000$ K ou $T_{\rm eff} = 8000$ K, malgré des différences notables entre les deux spectres respectifs. Luyten (1952) avait déjà introduit un chiffre à la fin du type spectral entre 0 et 7, pour distinguer les étoiles DA avec des raies larges, peu profondes et un maximum d'intensité dans le bleu (0-3) contrairement aux DAs avec des raies plus étroites et un maximum d'intensité dans le rouge (5-7). Ce concept revient dans Sion et al. (1983) et il est ensuite raffiné dans McCook & Sion (1999) qui proposent le système actuel où l'indice de température est défini de manière quantitative et est donné par $10 \times \theta_{\rm eff} (= 50,400/T_{\rm eff})$. Donc, une naine blanche DA avec $T_{\rm eff} = 30{,}000$ K serait classifiée DA1.7 tandis qu'une étoile avec $T_{\rm eff} = 8000$ K serait classifiée DA6.3.

1.8 Le catalogue de McCook & Sion

Un premier catalogue regroupant toutes les naines blanches connues ainsi que toutes les données astrométriques disponibles pour chaque objet fut publié par Eggen & Greenstein (1965). Dans les années suivantes, le nombre de naines blanches augmente considérablement et continuera d'augmenter avec l'aide de nombreux groupes qui obtiennent de nouvelles observations photométriques et spectroscopiques. Le volume de données est immense et l'information pertinente est dispersée à travers la littérature. George McCook et Ed Sion, de l'Université Villanova, prennent alors l'initiative de répertorier toutes les naines blanches connues dans un seul catalogue. Ils décident que ce serait utile, autant pour les observateurs que pour les théoriciens, d'avoir accès à une référence qui contient une liste exhaustive de tous les naines blanches identifiées spectroscopiquement. La première version du catalogue, McCook & Sion (1977), inclut moins de 600 naines blanches. Plusieurs mises à jour ont suivi (McCook & Sion 1983, 1987) et la dernière version publiée est celle de McCook & Sion (1999) avec 2239 naines blanches. Le catalogue, qui continue d'être mis à jour régulièrement, est maintenant disponible en ligne[1] et contient presque 13,000 naines blanches, en grande partie en raison des contributions récentes du SDSS.

En dépit de toute l'information contenue dans McCook & Sion (1999)[2], il reste que beaucoup de ces étoiles n'ont jamais été observées avec des instruments modernes, ni étudiées de manière détaillée avec la dernière génération de modèles d'atmosphère. Nous avons donc défini un échantillon de naines blanches basé sur McCook & Sion (1999) qui inclut toutes les naines blanches DA (et tous les types secondaires ex. DAO, DAB, DAZ, etc.) avec une magnitude $V < 17.5$. Tout d'abord, nous voulons obtenir un spectre visible de haut S/N pour chaque étoile. Cela nous permet de confirmer la classification de l'objet et ensuite d'effectuer une analyse spectroscopique détaillée. On peut alors mesurer de façon précise les paramètres atmosphériques de chaque naine blanche. Cela nous permet d'étudier les objets individuellement, mais également d'étudier les propriétés globales de notre échantillon.

[1] http://www.astronomy.villanova.edu/WDCatalog/index.html
[2] On veut se concentrer ici sur la version du catalogue avant l'inclusion des étoiles du SDSS.

1.9 Format de cette thèse

Cette thèse comprend un article publié et un article en préparation pour l'*Astrophysical Journal*. De plus, nous incluons dans les annexes un compte rendu de conférence dans lequel nous avons publié des résultats préliminaires de ce projet de thèse. Dans l'ensemble, nous présentons les résultats de notre relevé d'étoiles naines blanches brillantes et riches en hydrogène tirées de McCook & Sion (1999).

Au Chapitre 2, nous présentons notre analyse des naines blanches chaudes de type DA et DAO. Nous présentons également les nouveaux modèles que nous avons calculés pour analyser ces étoiles. Ces nouveaux modèles sont nécessaires pour surmonter le problème des raies de Balmer qui affecte une majorité des étoiles DAO, mais aussi plusieurs étoiles DA chaudes. Nous présentons ensuite notre analyse spectroscopique de ces étoiles et nous discutons des conséquences que ces nouvelles déterminations des paramètres atmosphériques entraînent sur notre compréhension de l'évolution de ces naines blanches chaudes. De plus, nous exploitons des données ultraviolettes du satellite *FUSE* pour comprendre le mécanisme à l'origine du problème des raies de Balmer. Dans le Chapitre 3, nous présentons les résultats globaux de notre relevé de McCook & Sion (1999). Nous examinons le contenu spectroscopique de notre échantillon de plus de 1300 étoiles et nous procédons ensuite à une analyse détaillée de toutes les étoiles naines blanches avec la dernière génération de modèles d'atmosphère. Ceci inclut des analyses particulières pour des systèmes binaires de type DA+DB et des naines blanches de type DAZ. Une attention particulière est portée à l'analyse des systèmes binaires de type DA+dM où la contribution du compagnon dM est soustraite du spectre composite. Nous étudions ensuite les propriétés globales de notre échantillon. Tout d'abord, nous comparons nos résultats à ceux d'autres analyses avec lesquelles nous avons plusieurs étoiles en commun. Ensuite, nous discutons de la distribution de masse et de la distribution de masse en fonction de la température effective de notre échantillon. Finalement, nous faisons un retour sur la détermination empirique de la bande d'instabilité des naines blanches de type ZZ Ceti. Au Chapitre 4, nous concluons avec un résumé des résultats importants obtenus par l'entremise de ce projet de thèse et un aperçu de relevés futurs qui auront un impact important dans l'étude des étoiles naines blanches.

Chapitre 2

SPECTROSCOPIC ANALYSIS OF HOT, HYDROGEN-RICH WHITE DWARFS: THE PRESENCE OF METALS AND THE BALMER-LINE PROBLEM [1]

A. Gianninas[1,4], P. Bergeron[1], J. Dupuis[2] and M. T. Ruiz[3,4]

[1] *Département de Physique, Université de Montréal, C.P. 6128, Succ. Centre-Ville, Montréal, Québec H3C 3J7, Canada*

[2] *Canadian Space Agency, 6767 Route de l'Aéroport, Longueuil, Québec J3Y 8Y9, Canada*

[3] *Departamento de Astronomía, Universidad de Chile, Casilla 36-D, Santiago, Chile*

[4] *Visiting astronomers at Las Campanas Observatory operated by Carnegie Institution of Washington.*

Received 2010 May 3; Accepted 2010 July 4

Published in the *Astrophysical Journal*,

September 2010, *Vol.* 720, *page* 581

[1] Based on observations made with ESO Telescopes at the La Silla or Paranal Observatories under program ID 078.D-0824(A).

2.1 ABSTRACT

We present an analysis of optical spectra for 29 DAO white dwarfs. First, we present our new up-to-date model atmosphere grids computed without the assumption of local thermodynamic equilibrium in which we have included carbon, nitrogen, and oxygen at solar abundances. We demonstrate that the addition of these metals in the model atmospheres is essential in overcoming the Balmer-line problem, which manifests itself as an inability to fit all the Balmer lines simultaneously with consistent atmospheric parameters. We then present the spectroscopic analysis of our sample of DAO white dwarfs for which we determine the effective temperature, surface gravity, and helium abundance. We also present 18 hot DA white dwarfs that also suffer from the Balmer-line problem. We analyze these stars with models analogous to those for the DAO white dwarfs save for the presence of helium. Systematic differences between our newly determined atmospheric parameters with respect to previous determinations are explored. Far ultraviolet spectra from the *FUSE* archive are then examined to demonstrate that there exists a correlation between higher metallic abundances and instances of the Balmer-line problem. The implications of these findings for all hot, hydrogen-rich white dwarfs are discussed. Specifically, the possible evolutionary scenario for DAO white dwarfs is revised and post-extreme horizontal branch evolution is no longer needed to explain the evolution for the majority of the DAO stars. Finally, we discuss how the presence of metals might drive a weak stellar wind which in turn could explain the presence of helium in DAO white dwarfs.

2.2 INTRODUCTION

One of the great achievements in white dwarf research over the last 20 years has been the ability to accurately measure the atmospheric parameters of these stars by comparing the theoretical predictions of model atmosphere calculations to observations throughout the electromagnetic spectrum. In particular, the spectroscopic technique developed by Bergeron, Saffer, & Liebert (1992) for analyzing the hydrogen-line (DA) white dwarfs has become the standard method for measuring the effective temperature and surface gravity of these stars which represent 80% of the white dwarf population.

Over the last several years, we have been conducting a spectroscopic survey based largely on the catalog of McCook & Sion (1999) and focusing on all the DA white dwarfs brighter than $V = 17.5$. High signal-to-noise ratio (S/N > 50) optical spectra for over 1300 white dwarfs have been secured and a preliminary analysis is presented in Gianninas, Bergeron, & Ruiz (2009). Of particular interest in this paper is that our sample includes a number of DAO white dwarfs. These are hot white dwarfs ($T_{\rm eff} > 40{,}000$ K) that are characterized by optical spectra that exhibit absorption lines due to helium present in the atmosphere. Specifically, most DAO white dwarfs are distinguished by the He II λ4686 absorption feature in addition to the hydrogen Balmer lines. Since these stars clearly contain more than just hydrogen in their atmospheres, they need to be analyzed separately from the rest of our sample and require models which differ from our pure hydrogen models in order to properly measure their atmospheric parameters. We believe that this presents an opportunity to revisit in detail the DAO phenomenon and the connection with their hot DA counterparts.

Bergeron et al. (1994) presented an overview of the history and status of research on hot DA and DAO stars prior to their work. For the benefit of the reader, we provide a brief summary of that overview here. Initially, hot white dwarfs were expected to be sources of soft X-rays and extreme ultraviolet (EUV) radiation (Shipman 1976), but *Einstein* and *EXOSAT* data revealed instead that most hot DA stars had an X-ray flux deficiency (Vennes et al. 1988). It was thought that the presence of helium could explain the flux deficiency but Vennes et al. (1988) showed that radiation pressure could not support sufficient amounts of helium in the atmosphere to provide the necessary opacity. As an alternative, Vennes et al. (1988) proposed a model where a thin hydrogen layer floated in diffusive equilibrium above a more massive helium layer. These stratified models reproduced the X-ray and EUV data rather well (Koester 1989; Vennes & Fontaine 1992). Unfortunately, the survey conducted with *ROSAT* (Pounds et al. 1993) detected only 119 sources out of an expected $1000 - 2000$ white dwarfs (Barstow 1989). Barstow et al. (1993) showed that neither homogeneous nor stratified models could explain these observations and they suggested that an additional opacity source, most likely metals, would provide a better match to the data.

The launch of the *Extreme Ultraviolet Explorer* (*EUVE*) and the spectroscopic data that

it gathered permitted a more detailed study of the EUV flux of hot DA white dwarfs than the previous photometric surveys could. Analyses of the *EUVE* spectra showed that stratified atmospheres could not reproduce the data nearly as well as models that included metals (Barstow et al. 1997; Wolff et al. 1998). More sophisticated models that included the diffusion of the various metals through the atmosphere, in a self-consistent way, were subsequently computed and these matched the *EUVE* data even better (Dreizler & Wolff 1999; Schuh, Dreizler & Wolff 2002). As such, the notion that the flux deficiency in hot DA stars could be explained by stratified atmospheres, composed only of hydrogen and helium, was abandoned.

DAO white dwarfs, on the other hand, presented a different challenge since they clearly contained a much higher abundance of helium as evidenced by the appearance of the He II λ4686 absorption line in their optical spectra. It was possible that at least for this subgroup of white dwarfs the stratified atmospheres proposed by Vennes et al. (1988) might yet be valid. Indeed, DAO white dwarfs were unique in that their hybrid spectra provided a diagnostic tool by which the abundance and distribution of helium in the atmosphere could be studied directly.

The prototype of the DAO class, HZ 34, was identified as such by Wesemael, Green & Liebert (1985) who presented the first spectroscopic analysis of DAO white dwarfs using homogeneous model atmospheres. Holberg (1987) significantly increased the number of known DAO stars and Holberg et al. (1989) combined optical and *International Ultraviolet Explorer* (*IUE*) observations to determine the atmospheric parameters of these stars. At the same time, Fontaine & Wesemael (1987) discussed the idea that most white dwarfs possibly descended from helium-rich PG 1159 stars. However, several studies had begun to show that several old planetary nebulae nuclei have hydrogen-rich atmospheres (Napiwotzki & Schönberner 1993). DAO white dwarfs might then represent a transition between the PG 1159 stars where hydrogen is diffusing upward to eventually form a hydrogen-rich layer at the surface. If that scenario were to be true, the stratified atmospheres of Vennes et al. (1988) would be the only viable models. However, a comprehensive analysis comparing the predictions of homogeneous and stratified model atmospheres to observations had never been conducted. It is for this reason that the study of Bergeron et al. (1994) is of particular importance as they were the

first to perform a detailed analysis comparing optical and UV spectra to the predictions of both homogeneous and stratified atmospheres. Although their analysis of the UV spectra ultimately proved inconclusive, the He II λ4686 line profiles clearly pointed to homogeneous models as the stratified atmospheres produced line cores that were too shallow. Indeed all of the DAO white dwarfs in their sample were best reproduced with the homogeneous models, with the exception of PG 1305−017. As a consequence of this result, all subsequent analyses of DAO stars have employed homogeneous model atmospheres.

In addition to DAO white dwarfs, Bergeron et al. (1994) also looked at a number of hot DA stars. In particular, they explored the effects that trace amounts of helium (number ratios in the range He/H = 10^{-5} to 10^{-4}) would have on the atmospheric parameter determinations. They found significant differences between the pure hydrogen models and those including helium. However, it was later shown by Napiwotzki (1997) that this was due to the fact that Bergeron et al. (1994) computed models assuming local thermodynamic equilibrium (LTE) since the effects due to the presence of helium vanish when models are computed assuming non-LTE (NLTE) conditions. It should also be noted that the stratified models were also computed in LTE, and NLTE versions of those models, and the subsequent helium line profiles associated with them, have never been explored.

Another important result from that study was the realization that most of the DAO stars in their sample were afflicted with the so-called Balmer-line problem. This problem manifests itself as an inability to simultaneously fit all the Balmer lines with consistent values of $T_{\rm eff}$ and $\log g$, and it was first observed by Napiwotzki (1992, 1993) in his analysis of central stars of planetary nebulae (hereafter, CSPNe). More specifically, the line profiles of Hβ, and to a lesser extent Hγ, are predicted too shallow and thus require a lower temperature to correctly fit the observations. It should be noted that the Balmer-line problem was not observed in any of the hot DA stars analyzed by Bergeron et al. (1994). This would suggest that the mechanism responsible for the Balmer-line problem was operating only in DAO stars. Consequently, several solutions to this problem were explored. Bergeron et al. (1993) included blanketing due to iron in their model atmospheres in an effort to fit the line profiles of Feige 55. Although they were successful, they used an iron abundance of log Fe/H = −3.0 which is unrealistically

high (15 times solar) and their models were computed assuming LTE conditions. Furthermore, Napiwotzki & Rauch (1994) reviewed several failed explanations to the Balmer-line problem such as magnetic fields, wind effects, and pressure ionization. They also explored another possibility by looking at ion-dynamical effects on the Stark broadening of hydrogen lines, but this also proved unsuccessful.

A solution to the Balmer-line problem was eventually achieved and presented by Werner (1996). His solution was to include carbon, nitrogen, and oxygen (hereafter, CNO) at solar abundances in the calculation of the model atmosphere. Although such calculations had already been performed in the past (Werner & Heber 1991; Werner & Dreizler 1993), Werner (1996) showed that the decisive ingredient was the necessity to include the proper Stark broadening of the metallic lines. The net effect was a cooling of the upper layers of the atmosphere where the core of the Balmer lines is formed. In this temperature regime, cooler temperatures translate to deeper line cores. As such, these new models were in very good agreement with the observed line profiles.

Other important studies of hot DAO white dwarfs since then have come from Napiwotzki (1999) who analyzed a large sample of CSPN, 15 of which turned out to be DAO white dwarfs. Interestingly, Napiwotzki (1999) did not implement the solution to the Balmer-line problem outlined by Werner (1996). Instead, he relied on the fits of the higher Balmer lines, namely Hδ and Hϵ, which are formed deeper in the atmosphere where the thermodynamic structure is not affected by the presence of CNO. The reasons for omitting the solution are twofold. First, Napiwotzki (1999) argued that CNO abundances would need to be known for each star and that the computational time required to include CNO in NLTE models was too great.

More recently, far-ultraviolet (FUV) spectra of DAO white dwarfs obtained with the *Far-Ultraviolet Spectroscopic Explorer* (*FUSE*) were analyzed in a series of papers by Good et al. First, Good et al. (2004) wanted to verify if consistent temperatures can be obtained by independently fitting the Balmer lines in the optical spectrum and the Lyman lines in the FUV spectrum. Instead, they observed a similar trend to the one highlighted by Barstow et al. (2003) with the Lyman lines systematically yielding higher temperatures as compared to those derived from the Balmer lines. It should be noted that the NLTE model atmospheres

used by Good et al. (2004) in their analysis did include CNO as prescribed by Werner (1996). Second, Good et al. (2005a) exploited the time-resolved nature of *FUSE* data to check for binarity among DAO white dwarfs. They did not detect evidence for any new binaries but their technique did detect radial velocity variability for all the known binaries in their sample. Finally, Good et al. (2005b) obtained abundance measurements for the various metals whose absorption lines abound in the FUV of these DAO white dwarfs. However, due to the difficulties of computing a full grid of models to measure, in an absolute manner, the abundances of all the observed species (C, N, O, Si, Fe, and Ni), the abundance determinations are measured relative to the measured abundances in G191-B2B (Barstow et al. 2001b).

Finally, one of the biggest developments in recent times in the white dwarf community has been the wealth of observational data produced by the Sloan Digital Sky Survey (SDSS). Having now surpassed the 10,000 mark in terms of newly discovered white dwarf stars, it should come as no surprise that new DAO white dwarfs are among them. Hügelmeyer et al. (2007) present an analysis for 16 new DAO white dwarfs discovered in the SDSS up to and including Data Release 4 (Eisenstein et al. 2006). Unfortunately, as is often the case, many of the spectra lack the S/N necessary in order to accurately measure their atmospheric parameters (Gianninas et al. 2005, see also Section 2.3). Furthermore, Hügelmeyer et al. (2007) use H/He model atmospheres that do not include CNO to deal with the Balmer-line problem. In addition, they do not restrict their analysis to the higher Balmer lines like Napiwotzki (1999) did, instead they include both Hβ and Hγ in their fits thus increasing the uncertainty of their measured atmospheric parameters.

We believe that the time is right to take a fresh look at the DAO phenomenon using high S/N spectra coupled with model atmospheres that take into account all that we have learned about these stars over the past 15 years. In addition, and similarly to Bergeron et al. (1994), we also include an analysis of hot DA white dwarfs found in the same range of effective temperature as the DAO stars. Indeed, we will see that several distinct groups of objects emerge from this analysis and that DAO and hot DA stars have more in common than we might have been led to believe in the past. We present in Section 2.3 our spectroscopic observations and in Section 2.4 we describe the various grids of model atmospheres and synthetic spectra that

we computed for our analysis. The results from our analysis of optical spectra are presented in Section 2.5. In Section 2.6, we examine the *FUSE* data for our ensemble of white dwarfs. In Section 2.7 we discuss the implications of our findings and finally, we make some concluding remarks in Section 2.8.

2.3 SPECTROSCOPIC OBSERVATIONS

Our optical data are taken from the ongoing spectroscopic survey of DA white dwarfs outlined in Gianninas et al. (2009). Since we are interested in the temperature range where DAO stars are found, we restrict ourselves to stars with $T_{\rm eff} > 40{,}000$ K. This translates to a total of 152 white dwarfs of which 29 are DAO white dwarfs. However, the spectrum we obtained for 0625−253 was completely dominated by the emission lines of the associated planetary nebula (A15) and so we were forced to drop this object from our sample. The spectra of the 29 DAO white dwarfs come from several sources. First of all, there are 12 stars for which the spectra are identical to those used by Bergeron et al. (1994) in their analysis. Of the remaining 17 spectra, 13 have been obtained as part of our ongoing spectroscopic survey (Gianninas et al. 2009). This includes new spectra of Feige 55 (1202+608) and PG 1210+533, both of which are white dwarfs analyzed in Bergeron et al. (1994). With the exception of five spectra (Feige 55, 0458−303, 0950+139, 1136+667, and 1958−501), all of our data were obtained at Steward Observatory's 2.3 m telescope equipped with the Boller & Chivens spectrograph. The $4\farcs5$ slit together with the 600 line mm^{-1} grating blazed at 3568 Å in first order provides a spectral coverage from about 3000–5250 Å at a resolution of ~ 6 Å (FWHM). The spectrum of Feige 55 was obtained at the 1.6 m telescope of the Observatoire du Mont-Mégantic where the 600 line mm^{-1} grating provided a spectral coverage from about 3100-7500 Å at a similar resolution. 0458−303 was observed at ESO's 3.6 m telescope at La Silla, Chile with the ESO Faint Object Spectrograph and Camera (v.2) (EFOSC2). The no. 7 grism and a $1\farcs0$ slit provided a spectral coverage from about 3300–5200 Å with a resolution of ~ 6 Å (FWHM). The spectrum of 0950+139 was obtained using the Mt. Hopkins 6.5 m MMT telescope using the Blue Channel of the MMT Spectrograph. The 500 lines mm^{-1} grating and a $1\farcs0$ slit provided a spectral coverage from about 3400–6300 Å with a resolution of ~ 4 Å (FWHM). 1136+667 is in a

binary system with a K dwarf and the spectrum we obtained was heavily contaminated with emission lines to the point where our spectroscopic analysis technique was rendered useless. Luckily, this object had been previously studied by Sing et al. (2004). In their work, they obtained a spectrum at inferior conjunction (see their Figure 9) which is almost devoid of contamination and which they kindly provided to us. Finally, the spectrum of 1958−501 was obtained at Carnegie Observatories' 2.5 m Irénée du Pont Telescope at Las Campanas, Chile with the Boller & Chivens spectrograph. The 1.″5 slit with the 600 line mm^{-1} grating blazed at 5000 Å provided a spectral coverage from about 3500–6600 Å at a slightly better resolution of ~ 3 Å (FWHM).

Of these 29 white dwarfs, 26 have already been identified as being of the DAO spectral type. The remaining three (0458−303, 1201−049, and 1958−501) are identified as members of the DAO class for the first time in this paper. Finally, we wish to address the case of 2218+706. This star was classified as a DAO white dwarf by Barstow et al. (2003) based on their detection of a "trace" of He II λ1640 in the ultraviolet (Barstow et al. 2001a). This detection is not an especially strong indicator as He II λ1640 has only rarely been detected in DAO white dwarfs (Holberg et al. 1989; Bergeron et al. 1994). More importantly, white dwarfs are classified based on features observed in their *optical* spectra. In that respect, we concur with Barstow et al. (2003) as we detect no sign of He II λ4686 in our optical spectrum. However, if we consider the abundance of He/H $= 3 \times 10^{-5}$ determined by Barstow et al. (2001a), it would be impossible to detect any trace of He II λ4686 with our medium resolution spectrum. Therefore, for the purposes of our analysis, we will consider 2218+706 as a simple DA white dwarf.

The 29 spectra of our DAO white dwarfs are displayed in Figure 2.1. First of all, we note that all the spectra have a relatively high signal-to-noise ratio with a minimum of S/N ~ 50. Second, we see that all the spectra show, besides the hydrogen Balmer lines from Hβ to Hϵ, the He II λ4686 line signaling the presence of helium in the atmosphere (the weakness of the helium line observed in 1201−049 is further discussed in Section 2.7.1; see also Figure 2.21). However, this is not the only feature of note in the spectra of these DAO white dwarfs. Several spectra (0950+139 and 2011+398) also contain emission lines. In the case of 0950+139, these

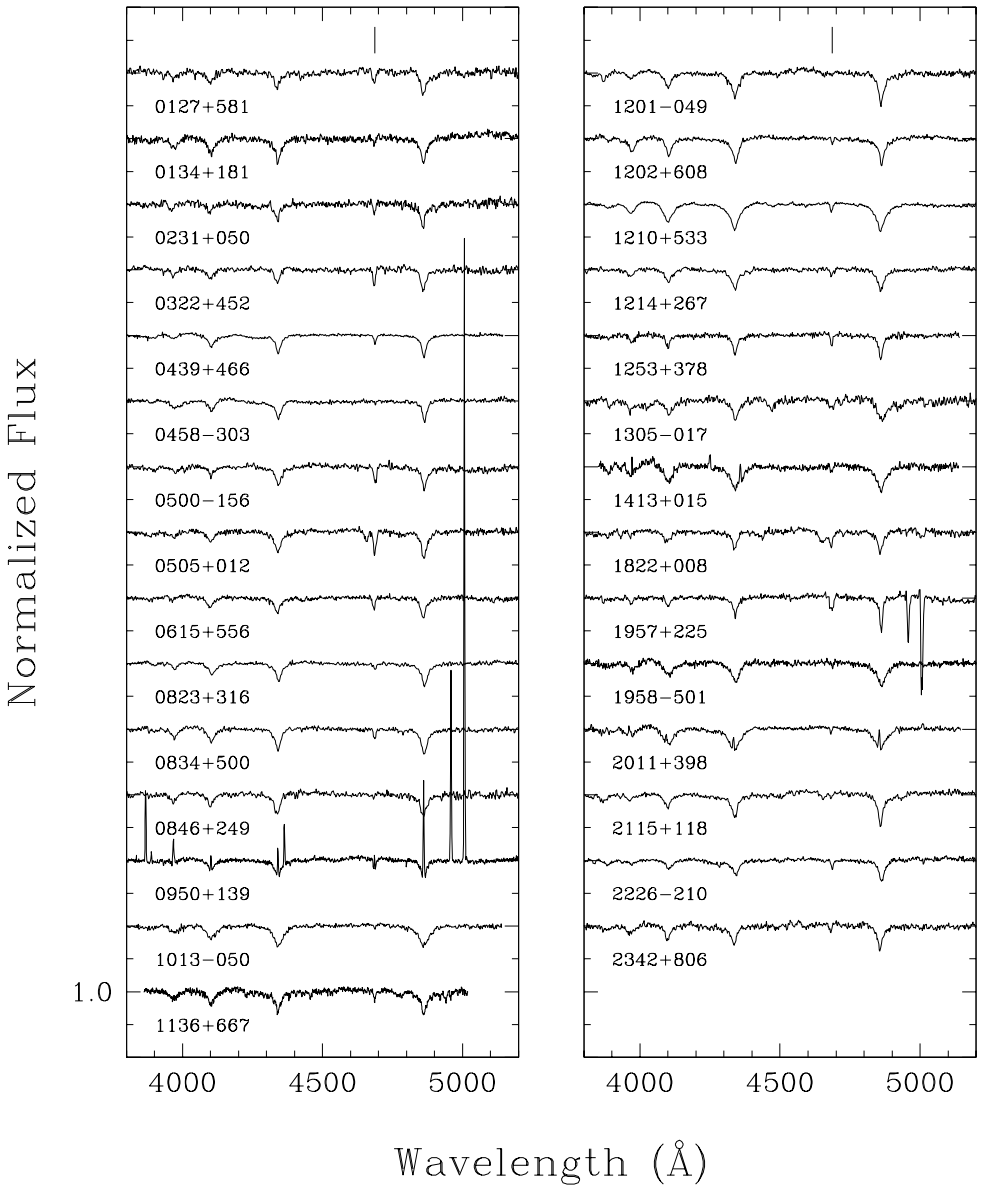

FIGURE 2.1 – Optical spectra for the 29 DAO stars in our sample in order of increasing right ascension from top left to bottom right. The spectra have been normalized to a continuum set to unity and vertically shifted for clarity. The tick mark at the top of each panel indicates the location of the He II λ4686 absorption line.

are due to the contribution of a planetary nebula still present around the star. On the other hand, the emission lines in 2011+398 are the result of this star being in a binary system with an M dwarf (Barstow et al. 1995). The contamination due to the emission lines varies from one spectrum to another and will complicate our analysis, especially in cases where there is emission in the core of the Balmer lines. In the case of 1957+225, emission lines

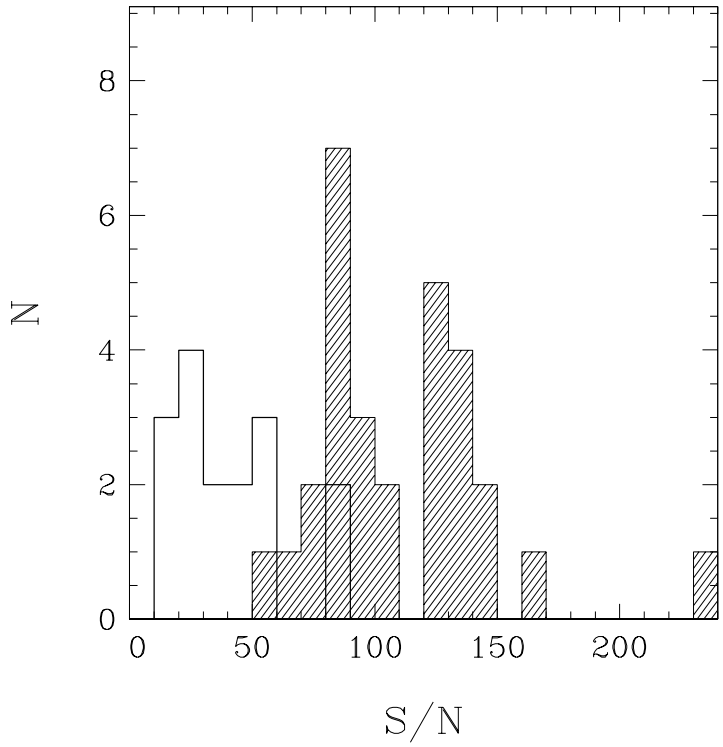

FIGURE 2.2 – Distribution of S/N for our sample of 29 DAO white dwarfs (dashed histogram) and the 16 SDSS DAO white dwarfs from Hügelmeyer et al. (2007) (solid line histogram).

from the accompanying planetary nebula were slightly over-subtracted during the removal of the background during data reduction and now appear as two deep and narrow absorption lines redward of Hβ. Furthermore, four of these stars (0505+012, 1201−049, 1822+008, and 2115+118) are actually of spectral type DAOZ due to the presence of metallic absorption lines in their spectra. Specifically, it is the C IV λ4658 line which is observed just blueward of He II λ4686 in all of these stars. 0505+012 was originally identified by Heber, Dreizler, & Hagen (1996) whereas we classify 1201−049 as DAOZ for the first time in this work. 1822+008 was classified as both a DAOZ white dwarf and a PG 1159 star by Napiwotzki & Schönberner (1995). In the subsequent analyses of Dreizler et al. (1995b) and Napiwotzki (1999), the DAOZ classification was dropped altogether and 1822+008 was considered as a hybrid PG 1159 star due to the presence of strong Balmer lines. However, as we will see below, the atmospheric parameters we obtain for this star place it squarely in the realm of the DAO stars. Specifically, we obtain a lower $T_{\rm eff}$ and a higher $\log g$ value than Napiwotzki (1999, see his Table 1). As such, we believe that the initial classification of DAOZ is the correct one. Finally, Dreizler

et al. (1995a) were the first to identify 2115+118 as being of the DAOZ spectral type. Indeed, in their spectrum of 2115+118 (see their Figure 1), they identify absorption lines due to highly ionized C, N, O, and even Ne.

Finally, we show in Figure 2.2 a comparison of the S/N of our sample of DAO stars with the SDSS DAO stars analyzed by Hügelmeyer et al. (2007). We see that *all* of the DAO white dwarfs from our sample have S/N greater than 50 whereas the peak of the SDSS distribution is near 20. We see once again the great weakness of the SDSS whose spectra have S/N too low to precisely measure the atmospheric parameters of these stars (Gianninas et al. 2005).

2.4 MODEL ATMOSPHERES AND SYNTHETIC SPECTRA

For the analysis of our sample of DAO white dwarfs, we have computed several new grids of model atmospheres and synthetic spectra that take into account advances (since Bergeron et al. 1994) in our knowledge and understanding of DAO white dwarfs as well as the physics and composition of their stellar atmospheres. In particular, we have computed separate grids assuming both LTE and NLTE as well as models containing CNO in order to study their effects on the thermodynamic structure of the atmosphere and how those changes translate to the theoretical Balmer-line profiles. Our models and synthetic spectra were all computed using the TLUSTY atmosphere code and the accompanying spectrum synthesis code SYNSPEC, both developed by Hubeny & Lanz (1995). All the model atmospheres are homogeneous in terms of their chemical composition (cf. Section 2.2).

As for the emergent spectra, we use the improved Stark profiles developed by Tremblay & Bergeron (2009) for our hydrogen line profiles, instead of the tables of Lemke (1997) and the calculations of Schöning & Butler (1989) for the profiles of He II λ1640 and λ4686. The implications of the improved hydrogen line profiles from Tremblay & Bergeron (2009) on our derived atmospheric parameters will be qualitatively discussed in Section 2.5.4. The atmospheric parameters cover a range of $T_{\rm eff}$ = 40,000 (5000) 90,000 K and $T_{\rm eff}$ = 90,000 (10,000) 150,000 K (where the quantity in parentheses indicates the step size), $\log g$ = 6.5 (0.5) 8.5 and log He/H = $-$5.0 (1.0) 0.0.

The first major change relative to the models used in the Bergeron et al. (1994) analysis

is the computation of models in NLTE. The combination of modern computing power and the TLUSTY code makes it possible to compute NLTE models rather easily and within a reasonable time frame, a much more difficult task in the past. In particular, it is clear that NLTE effects are important in white dwarfs in this temperature range (Napiwotzki, Green, & Saffer 1999). DAO white dwarfs are particularly susceptible since they are all hot and generally have lower surface gravities than normal DA stars, which favors departures from LTE conditions. Bergeron et al. (1994) had demonstrated that traces of helium in hot DA stars had an effect on the Balmer-line profiles, and consequently on the atmospheric parameters measured for those stars. However, the models in Bergeron et al. (1994) were all computed assuming LTE conditions. Napiwotzki (1997) showed that when these same models are computed assuming NLTE, the presence of helium has no effect on the Balmer-line profiles. They concluded that for an LTE analysis of the Balmer lines, pure hydrogen models should be used even if traces of helium are present in the atmosphere. Consequently, for an analysis of the Balmer lines in DAO white dwarfs which, by definition, contain helium in the atmosphere, it is imperative to compute models in NLTE.

As a first test of our new models, we show in Figure 2.3 a comparison between line profiles computed in LTE and NLTE, and with varying traces of helium for a model atmosphere at $T_{\rm eff} = 65{,}000$ K, $\log g = 7.5$. We see that in the LTE case the presence of helium affects the line cores producing shallower lines as the helium abundance increases. In contrast, the line profiles computed in NLTE are identical regardless of the helium abundance and thus we are in perfect agreement with the results of Napiwotzki (1997). This result further reinforces the need to calculate NLTE atmospheres in order to properly model white dwarfs in this temperature regime, the more so that our technique for determining the atmospheric parameters for these stars rests on our ability to reproduce the Balmer-line profiles in detail.

The second, and possibly more important difference with the previous generation of models, is the addition of CNO at solar abundances (as listed in Asplund et al. 2005) as the solution to the Balmer-line problem. Werner (1996) showed that the inclusion of these metals with the proper Stark broadening effectively solves the Balmer-line problem by cooling the upper layers of the atmosphere where the core of the lower Balmer lines are formed, most

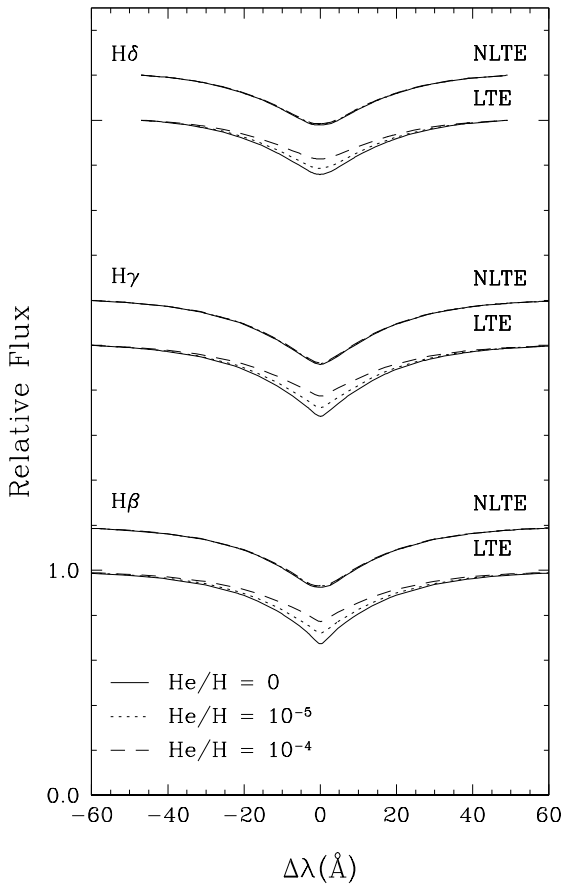

FIGURE 2.3 – Normalized Balmer-line profiles for Hβ, Hγ, and Hδ computed for different He abundances both in LTE and NLTE for a model atmosphere at $T_{\rm eff}$ = 65,000 K and $\log g$ = 7.5.

notably Hβ and to a lesser extent Hγ. The addition of these metals is further supported by the fact that they have since been detected in the UV spectra of many DAO white dwarfs and hot white dwarfs in general (Barstow et al. 2003; Good et al. 2005a). For completeness, we list in Table 2.1 all the ions of CNO included in our models along the with the number of super levels (as defined in Hubeny & Lanz 1995) and total transitions included for each ion. All the model atoms are taken from the TLUSTY Web site.[2]

To better illustrate the effects of the addition of CNO and the assumption of NLTE on the thermodynamic structure of the atmosphere, we show in Figure 2.4 the temperature structure for four reference model atmospheres computed at $T_{\rm eff} \simeq$ 65,000 K, $\log g \simeq$ 7.5 and log He/H = −3.0. The first model is a model with H and He computed assuming LTE, the

[2]http://nova.astro.umd.edu/Tlusty2002/tlusty-frames-data.html

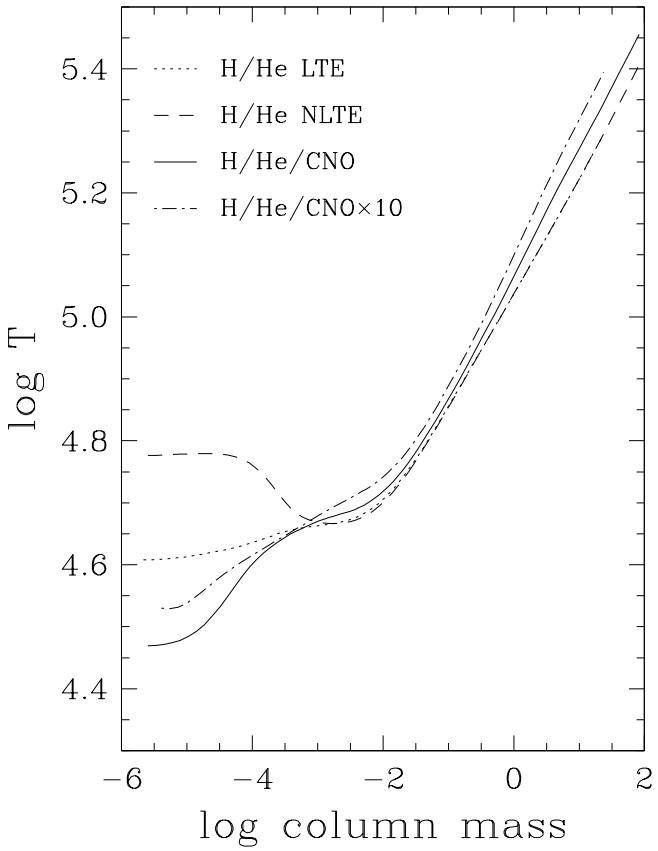

FIGURE 2.4 – Temperature structure as a function of column mass for a reference model atmosphere at $T_{\rm eff}$ = 65,000 K, $\log g = 7.5$ and log He/H = −3.0. The dotted line represents a model with H and He computed with the assumption of LTE whereas the dashed line was computed in NLTE. The solid line depicts a model with H, He and CNO computed in NLTE. Finally, the dash-dotted line represents a model with H, He, and a CNO abundance enhanced by a factor of 10 and computed assuming NLTE.

second is identical but computed in NLTE, and in the third we have the addition of CNO. The fourth model was computed with the CNO abundances enhanced by a factor of 10; this model will be discussed in greater detail later. We see that the NLTE effects actually cause the classical heating of the surface regions with respect to the LTE model. In contrast, the inclusion of CNO causes a cooling of the surface regions, even cooler than the LTE model. Let us now examine what effect these changes have on the Balmer-line profiles. In Figure 2.5, we compare Balmer-line profiles for two models, both computed in NLTE, one with CNO and one without. We see that the cooling effect of the CNO in the upper atmosphere produces line profiles with much deeper cores. The core of the Balmer lines is formed higher up in the

TABLE 2.1 – Ions Included in the Model Atmospheres

Ion	Levels	Super Levels	Transitions
C III	16	7	92
C IV	21	4	150
N III	25	7	184
N IV	15	8	97
N V	10	6	86
O III	20	9	141
O IV	31	8	270
O V	34	6	222
O VI	15	5	116

atmosphere due to the higher opacity in the line center, and since the Balmer lines become deeper as temperature decreases in this temperature regime, we obtain line profiles with deeper cores, as required. Our results are thus in agreement with the results of Werner (1996) and we have essentially overcome the Balmer-line problem. As a test of this statement, we have attempted to reproduce in Figure 2.6 the analysis shown in Figure 3 of Werner (1996) for the same two stars, namely BD+28 4211 and LS V+46 21 (0439+466). In both cases, we are not showing formal fits to the data but simply a superposition of the synthetic spectrum and the observed spectrum. In the case of LS V+46 21, we note the significant difference seen in the line cores, in particular for Hβ and Hγ. The models that include CNO allow for much deeper line cores, as previously stated, and thus reproduce the observed line profiles of LS V+46 21 quite well, as was the case for Werner (1996). We should note however that the effect of the CNO is exaggerated when comparing two models for a given set of atmospheric parameters. As we will see, the effect is less pronounced when comparing two fits of the same star since all three parameters ($T_{\rm eff}$, $\log g$, and log He/H) are allowed to vary to achieve the best possible match between the models and the data.

The case of BD+28 4211 is somewhat different. First of all, the parameters used by Werner (1996), $T_{\rm eff}$ = 82,000 K, $\log g$ = 6.2, and log He/H = -1.0, are based on an analysis of the Fe V/Fe VI ionization balance by Napiwotzki (1993). Neither Werner (1996) or Napiwotzki (1993) performed a formal fit to the observed line profiles of BD+28 4211 with an appropriate

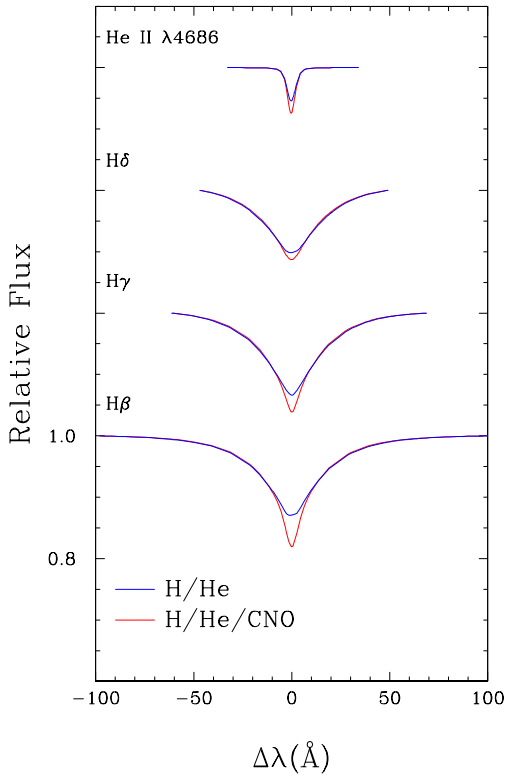

FIGURE 2.5 – Normalized Balmer-line profiles for Hβ, Hγ, Hδ and He II λ4686 computed in NLTE with (red) and without (blue) CNO for a model atmosphere at $T_{\rm eff}$ = 65,000 K and $\log g$ = 7.5 and log He/H =−3.0.

set of models. As such, our parameters ($T_{\rm eff}$ = 63,210 K, $\log g$ = 6.57, and log He/H = −1.14) differ significantly from those used by Werner (1996). Furthermore, we see that the effect of the CNO in the case of BD+28 4211 is much more subtle than what is seen in Werner (1996). This is because we are comparing H/He models in NLTE with similar models to which we have added CNO. In contrast, Werner (1996) compared H/He models computed with *Doppler* profiles to his final Stark broadened CNO models. In any case, the relevance of BD+28 4211 in this discussion is mitigated by the fact that it is not even a white dwarf, but rather a subdwarf O star.

As a final consistency check of our models, we have taken our reference model which includes CNO and have artificially added noise to the corresponding synthetic spectrum to simulate an S/N of 200. We then fitted this synthetic spectrum with our grid that does not contain any metals. Similarly, we created a synthetic spectrum based on our model with

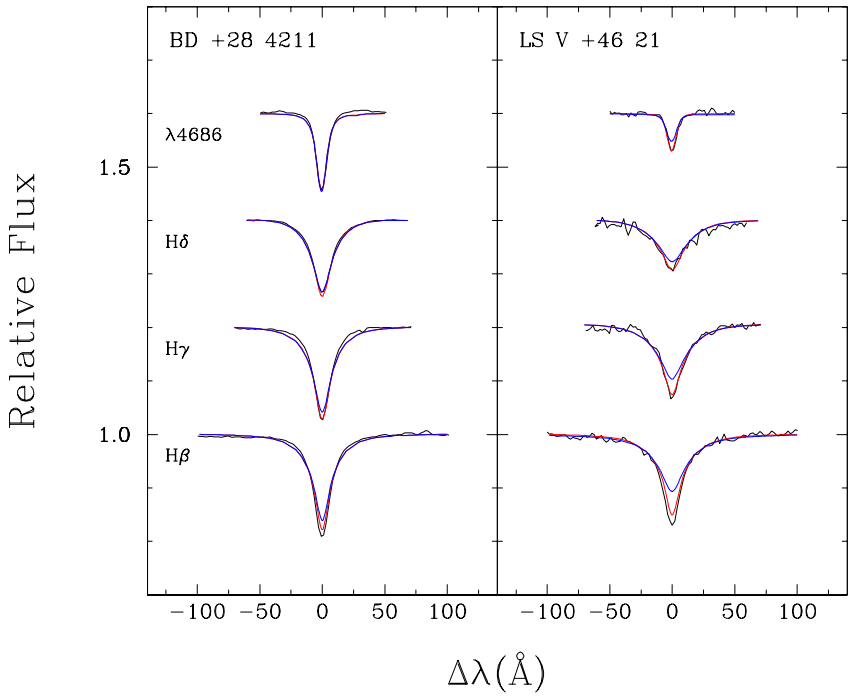

FIGURE 2.6 – Comparison of the observed line profiles for BD+28 4211 and LS V+46 21 with synthetic spectra obtained from model atmospheres with (red) and without (blue) CNO.

enhanced CNO abundance (CNO×10) and fitted it with our CNO grid. These fits are displayed in Figure 2.7. We can see that in both cases we are able to reproduce the Balmer-line problem since in both cases the model grids we used are "inappropriate" for fitting the spectrum at hand. It should also be noted that the amount by which the atmospheric parameters are underestimated is larger in the first case ($\Delta T_{\rm eff} \approx 4000$ K, $\Delta \log g = 0.15$ dex, $\Delta \log$ He/H $=$ 0.10 dex) than in the second. This suggests that the increase in CNO abundance has a smaller effect on the atmospheric parameter determinations than the inclusion of CNO altogether.

Having shown the necessity of computing models in NLTE and that the addition of CNO is compulsory in order to deal with the Balmer-line problem, it is these models that we will use in order to analyze our sample of DAO white dwarfs. We should note that although the solution to the Balmer-line problem has been known since Werner (1996), several analyses of DAO white dwarfs have been performed without implementing it (Napiwotzki 1999; Hügelmeyer et al. 2007).

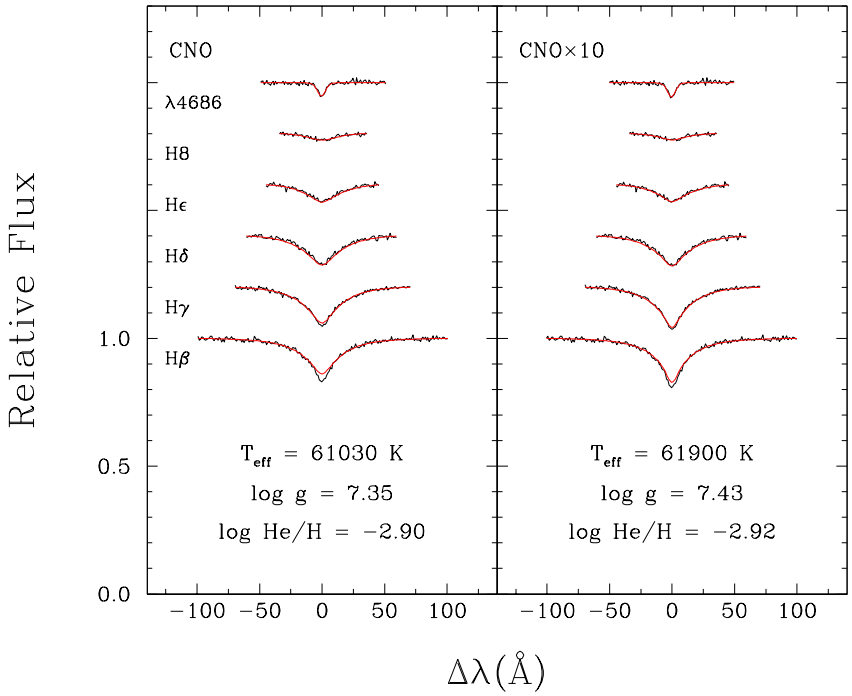

FIGURE 2.7 – Fits of the Balmer lines from Hβ to Hϵ and He II λ4686 for models at $T_{\rm eff}$ = 65,000 K, $\log g = 7.5$ and log He/H = -3.0. On the left, a synthetic spectrum computed from a model containing CNO is fit with a pure H/He grid. On the right, a synthetic spectrum computed from a model with a CNO abundance enhanced by a factor of 10 is fit with an H/He/CNO grid.

2.5 SPECTROSCOPIC ANALYSIS

2.5.1 Fitting Technique

Our fitting technique is identical to the one employed by Liebert, Bergeron, & Holberg (2005) with the exception that we include the He II λ4686 line in addition to the Balmer lines from Hβ to H8. The first step is to normalize the flux from an individual line, in both observed and model spectra, to a continuum set to unity at a fixed distance from the line center. The comparison with model spectra, which are convolved with the appropriate Gaussian instrumental profile (3, 4, and 6 Å), is then carried out in terms of these line shapes only. The most sensitive aspect of this fitting technique is to define the continuum of the observed spectra. In this temperature range, we rely on theoretical spectra to reproduce the observed spectrum, including a wavelength shift, a zero point, as well as several order terms in λ (up to λ^6) using the nonlinear least-squares method of Levenberg–Marquardt (Press et al. 1986).

The normal points are then fixed at the points defined by this smooth model fit. Note that the values of $T_{\rm eff}$, $\log g$, and log He/H at this stage are meaningless since too many fitting parameters are used, and the model just serves as a smooth fitting function to define the continuum of the observed spectrum. Once the lines are normalized to a continuum set to unity, we use our grid of model spectra to determine $T_{\rm eff}$, $\log g$, and log He/H in terms of these normalized profiles only. Our minimization technique again relies on the nonlinear least-squares method of Levenberg–Marquardt, which is based on a steepest descent method.

As we have shown in Section 2.3, several of the spectra contain emission lines that are due to the presence of a companion or a planetary nebula. These emission lines can affect both our determination of the continuum and the actual fit of the spectral lines. In order to avoid this problem, we have excluded the contaminated regions from our fits, both in terms of the normalization procedure and the fitting of the line profiles themselves. Furthermore, we have the four DAOZ white dwarfs whose spectra notably contain the C IV λ4658 line immediately blueward of He II λ4686. We have also omitted the spectral range where this line is found from our fits and extended the normalization region blueward of the C IV λ4658 line in order to properly determine the continuum for He II λ4686 in particular.

2.5.2 DAO white dwarfs

Let us now examine the results obtained from combining the spectroscopic method described above with our new grid of NLTE model atmospheres that include CNO. We show in Figure 2.8 typical fits for several of our DAO white dwarfs. To better appreciate the difference between the models with and without CNO, we display in the top panels of Figure 2.8 fits with our NLTE H/He grid whereas the fits in the bottom panels are performed with our CNO grid. First and foremost, we note that the Balmer-line problem is no longer present when fitting with our CNO grid. Although this is a clear indication of the cooling effect of the CNO in the upper atmosphere, we would like to stress that this is by no means an indication of the abundance of CNO in the atmosphere.

Besides resolving the Balmer-line problem, we also obtain atmospheric parameters ($T_{\rm eff}$, $\log g$, and log He/H) that are significantly different in both cases, especially with respect to

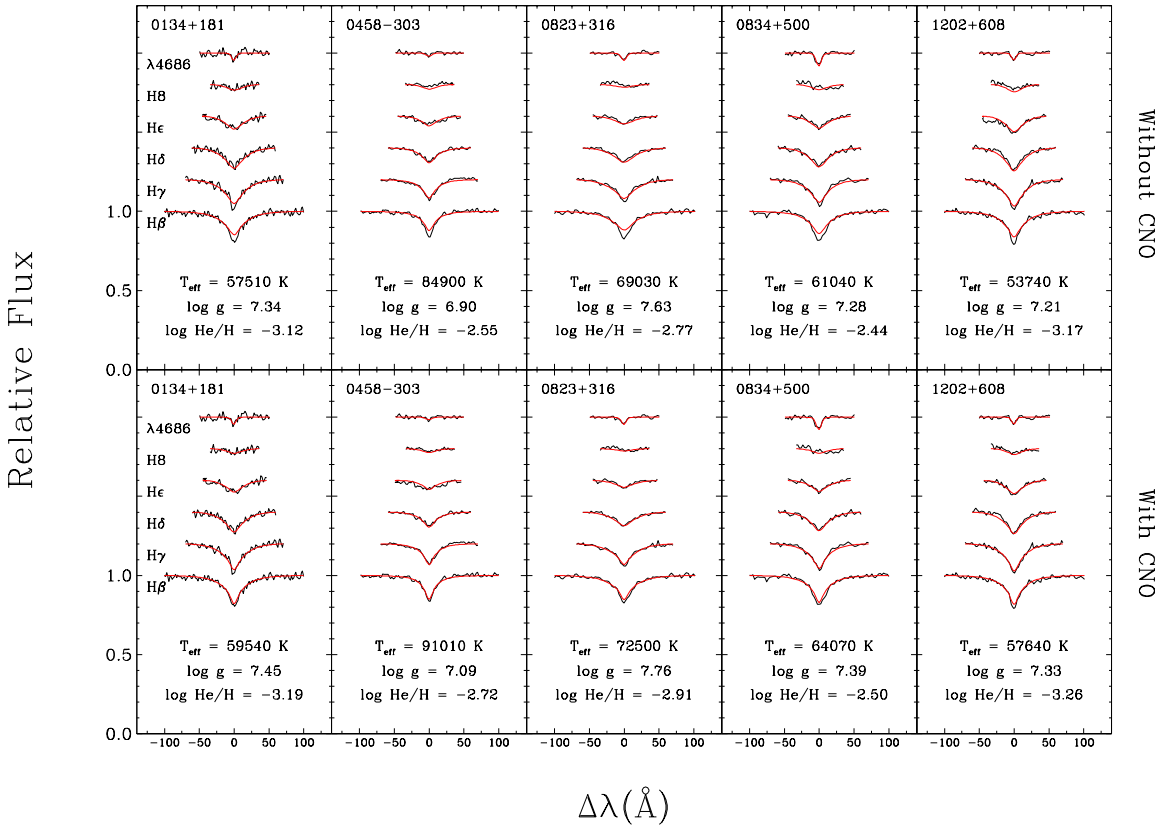

FIGURE 2.8 – Typical fits of observed Balmer-line profiles and He II λ4686 for DAO white dwarfs. The fits in the top panels are performed with a grid of models assuming an H/He atmosphere. The fits in the bottom panels are performed using a grid of models containing H, He and CNO. We clearly see how the inclusion of CNO improves the fits of Hβ and Hγ.

$T_{\rm eff}$ and $\log g$. In general, the fits with our CNO grid imply higher values for the surface temperature and gravity and slightly lower helium abundances. The fits without CNO tend to underestimate $T_{\rm eff}$ by $\sim 2000 - 5000$ K and $\log g$ by $\sim 0.1 - 0.2$ dex, which is in line with the differences we saw in Figure 2.7 when fitting a synthetic spectrum containing CNO with a H/He grid. As far as $T_{\rm eff}$ is concerned, the underestimate, when using the models without CNO, can be understood as the consequence of the fitting procedure attempting to reproduce the depth of the observed line profile and in this temperature regime that is accomplished by going to lower $T_{\rm eff}$. We will see below that the combined effect of higher $T_{\rm eff}$ and $\log g$ values shifts the position of DAO stars in the $T_{\rm eff}$–$\log g$ plane down toward the normal DA cooling sequence. This has important consequences for their possible evolutionary history.

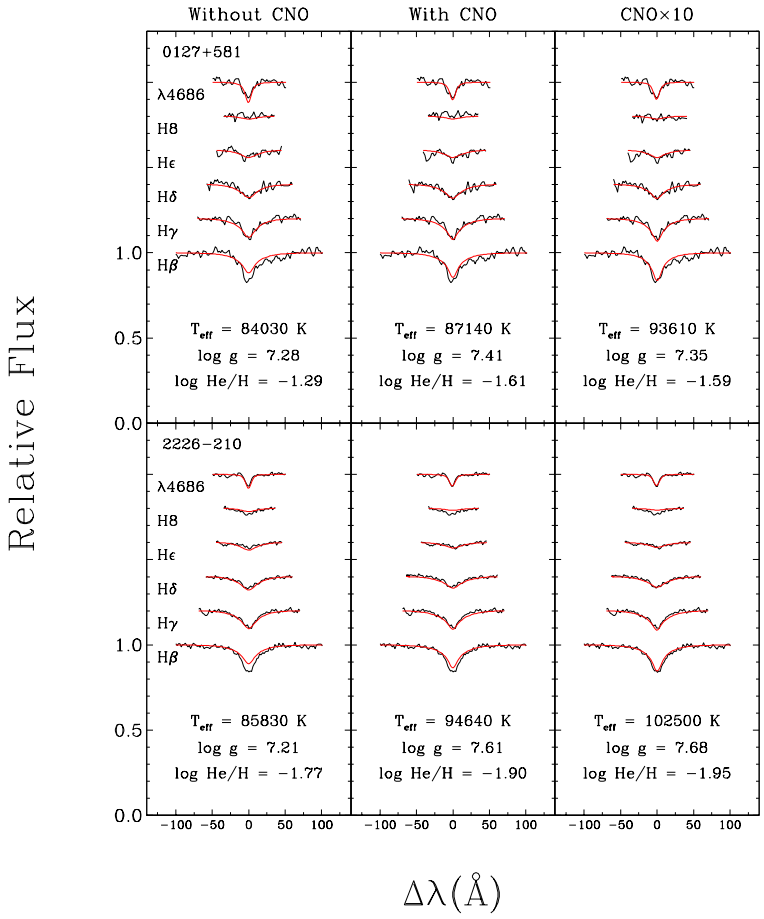

FIGURE 2.9 – Fits to the observed Balmer-line profiles and He II λ4686 for 2 DAO white dwarfs, 0127+581 (top) and 2226−210 (bottom). Fits from left to right are performed with increasing abundances of CNO from none (left), to solar (middle) and finally 10 times solar (right).

Although the results displayed in Figure 2.8 are very encouraging, not all of the DAO stars in our sample produce the same results. Indeed, several DAO stars still show the Balmer-line problem even when fitting them with our CNO grid. In Figure 2.9, we present two such examples with 0127+581 and 2226−210. As we can see, even with the presence of CNO, the fits are not satisfactory although there is a definite improvement with respect to the grid without CNO, especially for 2226−210. In an attempt to fit these particular objects, we have computed a grid with the CNO abundances increased by a factor of 10 (CNO×10, see Figure 2.4). We can see that we obtain an excellent fit in both cases with this new grid of models. However, as we have stated before, the CNO we have included in our model atmospheres

essentially acts as a proxy for all metals. It is perfectly reasonable to believe that simply increasing the abundance of CNO cannot mimic the effect other metals, like iron for example, might have on the thermodynamic structure of the atmosphere, and consequently on the Balmer-line profiles. Furthermore, the abundances we are using for CNO (Asplund et al. 2005) are, by all accounts, much too high as it is. Increasing them by an order of magnitude would then be even more unrealistic. For these reasons, the parameters we will adopt for our DAO white dwarfs are those obtained using our CNO grid only, even if this means that the Balmer-line problem will still be present, to varying degrees, in several of our fits.

On the other hand, a few DAO's either do not show the Balmer-line problem or we simply cannot tell whether the problem is present or not. 1013−050 and 1413+015 are fit perfectly with our H/He NLTE grid. Both of these stars are relatively cool and have higher $\log g$ values than all of the other DAO stars in our sample. The combination of age (i.e., lower $T_{\rm eff}$) and higher surface gravity has likely allowed any surplus of metals to diffuse out of the atmosphere. 2011+398 is similarly cool and massive, however emission in the line cores from its M dwarf companion prevents us from determining whether the Balmer-line problem is actually present. However, parameters obtained with our H/He NLTE and CNO grids are virtually identical for this star. This is not at all surprising since in both cases we are only fitting the line wings where the presence, or lack thereof, of CNO in the atmosphere is essentially irrelevant since the line wings form deeper in the atmosphere where the effect of CNO is negligible. For these reasons, we adopt the parameters obtained from our H/He grid for 2011+398 as well. The case of 0950+139 is similar in that there is also emission in the line core but due to the surrounding planetary nebula this time. We will see below that the parameters for this star place it squarely in the realm of DAO white dwarfs that exhibit the Balmer-line problem. Consequently, we adopt the parameters from our CNO grid for this object.

We now wish to address the particular case of PG 1210+533. Bergeron et al. (1994) had encountered difficulties in fitting the He II λ4686 line profile for this star. Indeed, neither homogeneous nor stratified models allowed for satisfactory fits to the observed He II λ4686 line profile. In both cases, the theoretical line profiles were predicted to be too shallow (see Bergeron et al. 1994, Figure 6). As per their own suggestion that PG 1210+533 required

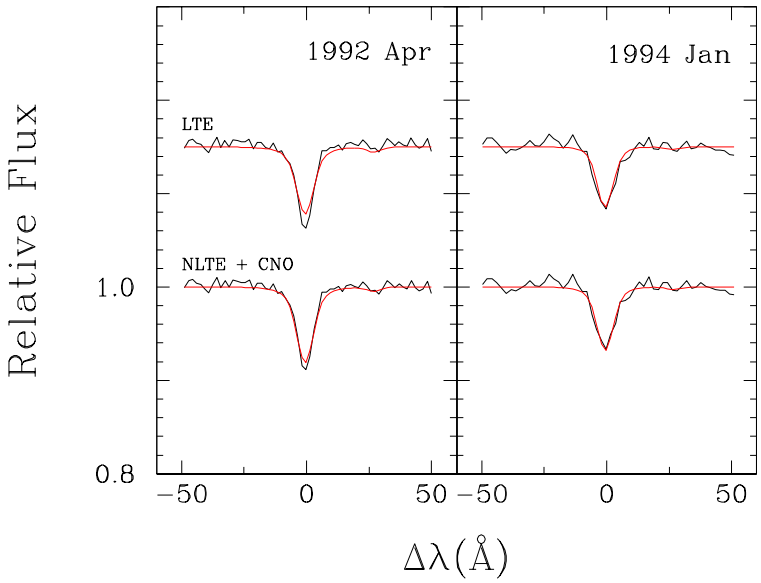

FIGURE 2.10 – Fits to the He II λ4686 line profile of PG 1210+533 for spectra taken in 1992 April (left) and 1994 January (right) using models computed in LTE (top) and models computed in NLTE that also include CNO (bottom).

further monitoring, a new spectrum of this star was obtained in 1994 January. We display in Figure 2.10 fits to the He II λ4686 line from the two separate observations using the LTE models employed by Bergeron et al. (1994) and our new NLTE models containing CNO. We see that for the 1992 April observation, neither set of models can properly reproduce the observed line profile although the newer models do a slightly better job. In contrast, both model grids have no difficulty in fitting the He II λ4686 line profile of the 1994 January observation. As such, we conclude that the issue encountered by Bergeron et al. (1994) can be attributed to the spectroscopic variability of PG 1210+533, which shall be discussed in Section 2.7.2, more so than any inadequacy of the models they were using.

Finally, the only DAO white dwarf that was successfully modeled with a stratified atmosphere by Bergeron et al. (1994) was PG 1305−017. Our new model grid is thus inappropriate for analyzing this particular object and as such, we adopt the atmospheric parameters they obtained for this star.

2.5.3 Hot DA white dwarfs

In addition to the DAO white dwarfs, Bergeron et al. (1994) also analyzed 29 hot DA stars. In particular, they studied the effects that spectroscopically invisible traces of helium would have on the Balmer-line profiles and consequently on the determination of the atmospheric parameters for those stars. Of course, as we have seen, when models are computed in NLTE, the addition of helium has no discernible effect on the Balmer lines of hot DA white dwarfs. As such, there is no evidence to suggest that these stars contain helium in their atmospheres and one could thus conclude that DAO stars form a class of objects that is quite distinct from the DA white dwarfs found in the same temperature regime. Indeed, of the 29 hot DA stars analyzed by Bergeron et al. (1994), the Balmer-line problem did not manifest itself in any of them. As such, Bergeron et al. (1994) concluded that the Balmer line problem must be unique to DAO stars. On the other hand, our ongoing survey (Gianninas et al. 2009) has provided us with a sample of 152 white dwarfs with $T_{\rm eff} > 40{,}000$ K. With a sample over five times larger than that of Bergeron et al. (1994), we have discovered that 18 of these hot DA white dwarfs are also afflicted with the Balmer-line problem (hereafter DA+BP), just like their DAO counterparts.

This is not the first time that this problem has been reported in stars other than DAO stars. There was a note added at the end of Bergeron et al. (1994) regarding the detection of the Balmer-line problem in 0948+534. Vennes et al. (1999) also reported observing the Balmer-line problem in 0621−376 (EUVE J0623−376) and 2211−495 (EUVE J2214−493), both of which are in our sample. However, there was never any follow-up to these detections in subsequent works. A search of the literature also turned up a case where the Balmer-line problem can be seen but is not reported or discussed by the authors: 0556−375 (EUVE J0558−375; Vennes et al. 1997, see their Figure 2). We should also mention that 2218+706 was shown to exhibit the Balmer-line problem by Barstow et al. (2001a). However, 2218+706 was later deemed to be a DAO star (see Section 2.3) and so the Balmer-line problem in regular DA white dwarfs remained a non-issue.

In similar fashion to the previous section, we show in Figure 2.11 typical fits to five of the hot DA stars that we have found to exhibit the Balmer-line problem. The top panels show

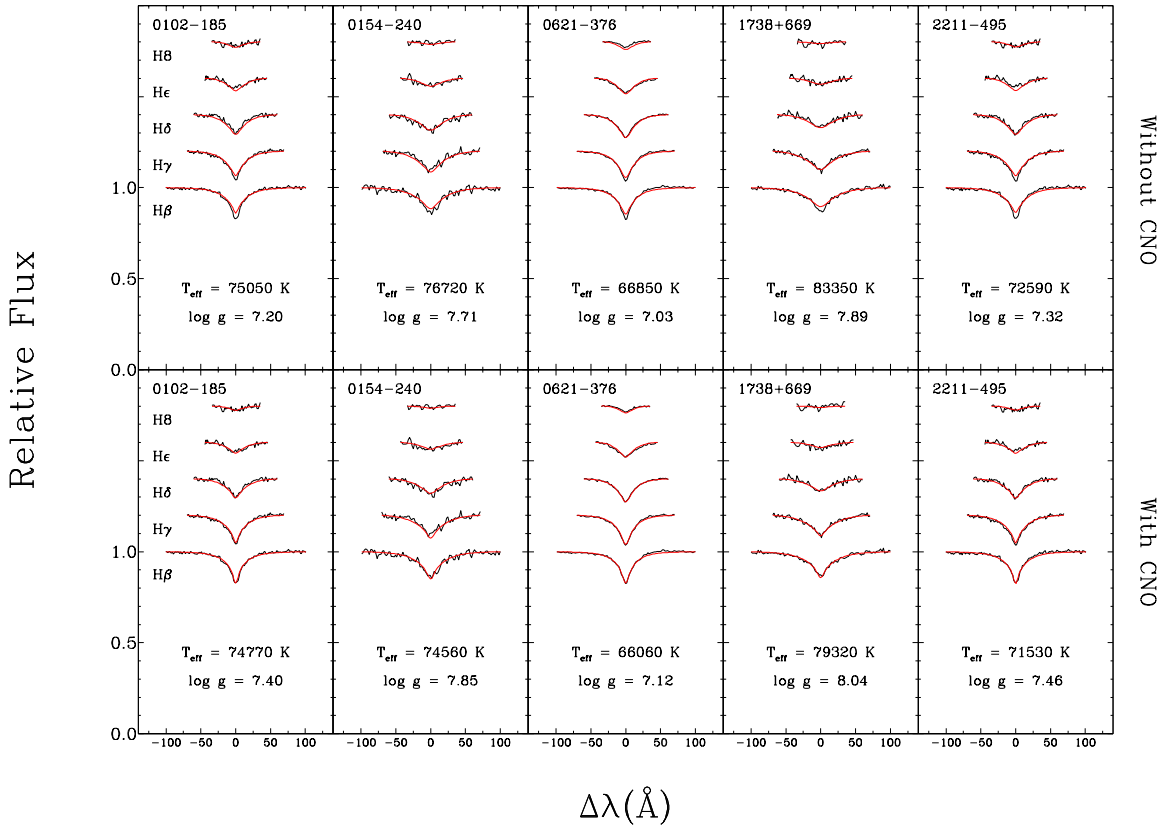

FIGURE 2.11 – Same as Figure 2.8 but for DA white dwarfs showing the Balmer-line problem.

fits performed using a grid of pure H atmospheres computed in NLTE and we can clearly see the inability of these models to fit the core of Hβ. In the bottom panels, we show an identical analysis but here we use a grid analogous to our CNO grid for the DAO stars but without the presence of helium. We see once again, that the inclusion of CNO in the models allows us to overcome the Balmer-line problem and adequately fit the line profiles of these stars with the exception of two that are discussed below. As far as the new atmospheric parameters obtained, we note that $\log g$ is systematically higher for all the stars in Figure 2.11 and indeed for all 18 hot DA stars exhibiting the Balmer-line problem, as was the case for the DAO stars. However, unlike the DAO stars, which yielded systematically higher temperatures when fit with the CNO grid, most of the hot DAs curiously yield lower temperatures. This dichotomy in the shifts of $T_{\rm eff}$ values when fitting with and without CNO in the models for DA and DAO white dwarfs can be ascribed to the presence of helium. We took synthetic spectra computed

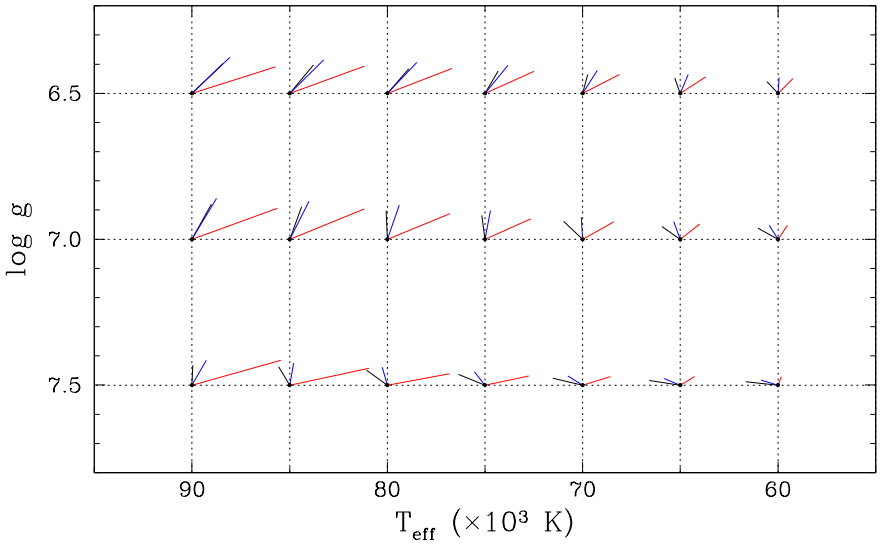

FIGURE 2.12 – Results from the fits of our CNO grid (dots) using a grid that does not contain any metals. The vectors point to the values obtained from the fits with He/H = 0 (black), 10^{-4} (blue), and 10^{-2} (*red*). The shifts in temperature have been reduced by a factor of 2 for clarity.

with CNO and fit them with our grid that does not contain any metals in order to examine the systematic differences in the derived atmospheric parameters while assuming different helium abundances. The results of this exercise are presented in Figure 2.12. The dots represent the correct values for the CNO models while the vectors point to the values obtained from the fits for He/H = 0, 10^{-4}, and 10^{-2}. As observed in the actual fits of our observed spectra, all the solutions underestimate the true surface gravity when fitting without CNO in the models. What is more interesting is the behavior as we change the helium abundance. The difference vectors "rotate" in the $T_{\rm eff}$–$\log g$ plane from left to right as the helium abundance is increased. In other words, stars analyzed with CNO models will yield lower temperatures in cases where there is no helium (DA stars) but higher temperatures when sufficient helium is present (DAO stars), which is exactly what we observe in the fits of our spectroscopic sample.

As we did in Figure 2.9, we show in Figure 2.13 fits using three different model grids (H/He only, CNO, and CNO×10) for the only two hot DA stars that still exhibit a case of the Balmer-line problem despite the addition of CNO: 0237+241 and 0311+480. As in the case of the DAO stars, the increasing metal abundance produces successively better fits to the

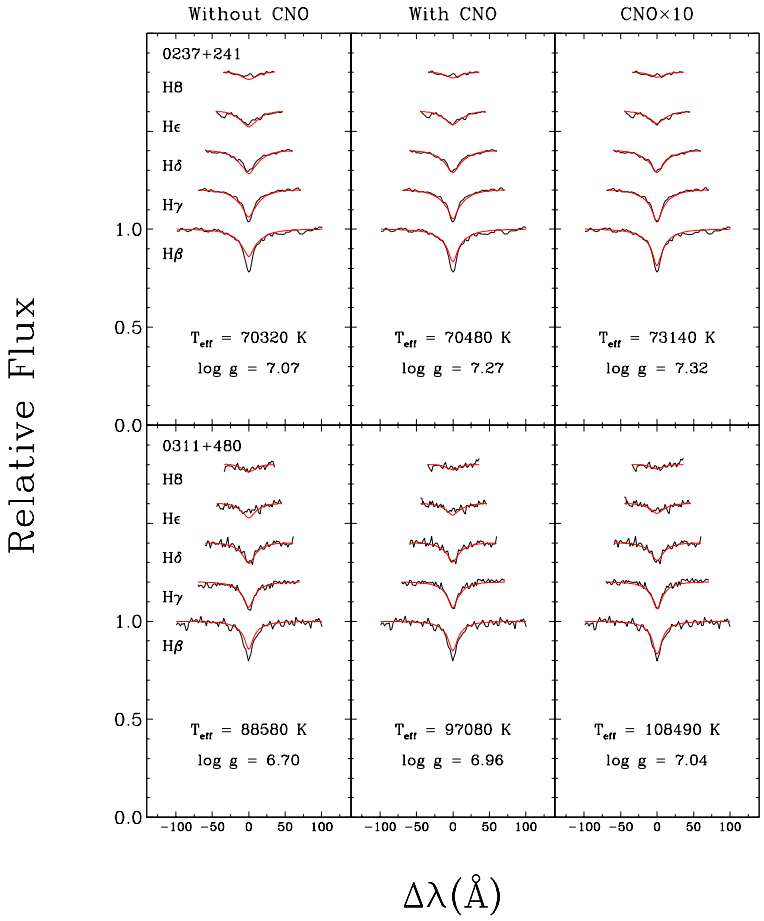

FIGURE 2.13 – Fits to the observed Balmer-line profiles for two DA white dwarfs, 0237+241 (top) and 0311+480 (bottom). Fits from left to right are performed with increasing abundances of CNO from none (left), to solar (middle), and finally 10 times solar (right).

observed line profiles. Curiously, these are the only two DA+BPs where $T_{\rm eff}$ actually increases with the addition of CNO. As with the DAO stars, although the fits with the CNO×10 grid are qualitatively better, we adopt the atmospheric parameters from the CNO fits for these two stars for the same reasons outlined earlier. The reason why these two stars in particular would show a more acute case of the Balmer-line problem is not immediately obvious but there is a clue in each case as to the cause of this discrepancy. A closer inspection of the optical spectrum of 0247+241 reveals what seem to be metallic absorption lines near Hϵ. With an abundance of metals large enough to produce absorption lines in the optical, it is then not surprising that 0247+241 should display a more severe form of the Balmer-line problem. On

the other hand, 0311+480, is the DA+BP star with the lowest $\log g$ measurement in which the Balmer-line problem manifests itself. It is therefore not unlikely that the lower gravity allows for a larger quantity of metals to be supported in the star's atmosphere by radiation pressure, thus causing a more severe case of the Balmer-line problem as well.

2.5.4 Atmospheric Parameters

The atmospheric parameters we have adopted for the DAO stars in our analysis are summarized in Table 2.2 where we list the values of $T_{\rm eff}$, $\log g$, and log He/H determined from our spectroscopic fits using our CNO grid as well as the masses derived from the evolutionary models of Wood (1995) with thick hydrogen layers, and absolute visual magnitudes determined using the photometric calibrations from Holberg & Bergeron (2006). We list, as a reference, the sources where each of these white dwarfs was first identified as belonging to the DAO spectral type. Additionally, we also indicate which objects are known CSPN, which parameters were determined using only our H/He NLTE grid, which stars contain emission lines in their optical spectrum, which stars are in binary systems, and finally we identify those stars that are of the DAOZ spectral type. Furthermore, since we have opted to use the atmospheric parameters from Bergeron et al. (1994) for PG 1305−017, this means we do not have a measurement of the helium abundance for this star. This is because the fit by Bergeron et al. (1994) using their stratified models used, instead, a quantity related to the thickness of the hydrogen layer as a free parameter. In Table 2.3, we list the atmospheric parameters, masses, and absolute visual magnitudes obtained for the DA+BP stars. All of these results are summarized in Figure 2.14 where we plot the location in the log $T_{\rm eff}$-log g plane of the 29 DAO white dwarfs, 18 DA+BP stars, and the remaining 104 hot DA white dwarfs from our sample. The filled and open symbols represent the DAO and DA white dwarfs, respectively, whereas the triangles denote stars where the Balmer-line problem has been detected. The dashed lines represent cooling sequences from Wood (1995) for C/O core white dwarfs with thick hydrogen layers and they are labeled by their values of stellar mass. We note that these cooling sequences use post-AGB evolutionary sequences as a starting point (M. A. Wood,

TABLE 2.2 – Atmospheric Parameters of DAO White Dwarfs

WD	Name	$T_{\rm eff}$ (K)	$\log g$	log He/H	$M/M_\odot$	M_V	Ref.	Notes
0127+581	Sh 2–188	87,140	7.41	−1.61	0.58	7.20	1	CSPN
0134+181	PG 0134+181	59,540	7.45	−3.18	0.51	7.83	2	
0231+050	PG 0231+051	89,470	7.52	−1.95	0.62	7.42	3	
0322+452	HDW 3	91,200	7.32	−1.29	0.57	6.95	1	CSPN
0439+466	LS V +46 21	86,980	7.23	−2.10	0.54	6.83	1	CSPN
0458−303	MCT 0458−3020	91,010	7.09	−2.72	0.53	6.46	4	
0500−156	A66 7	82,710	7.47	−1.36	0.59	7.43	5	CSPN
0505+012	HS 0505+0112	60,340	7.67	−1.09	0.58	8.25	3	DAOZ
0615+556	PuWe 1	93,150	7.57	−1.65	0.64	7.42	1	CSPN
0823+316	Ton 320	72,500	7.76	−2.91	0.64	8.16	6	CSPN
0834+500	PG 0834+501	64,070	7.39	−2.50	0.51	7.61	7	
0846+249	Ton 353	70,180	7.48	−3.37	0.55	7.67	6	
0950+139	PG 0950+139	93,230	7.36	−1.60	0.59	7.00	8	CSPN, emission
1013−050	RE J1016−053	57,250	8.03	−3.54	0.72	8.93	9	DA + dM, no CNO
1136+667	HS 1136+6646	83,090	7.31	−2.36	0.55	7.06	3	DA + dK
1201−049	PG 1201−049	57,260	7.61	−3.46	0.55	8.19	4	DAOZ
1202+608	Feige 55	57,640	7.33	−3.26	0.47	7.65	10	Double degenerate
1210+533	PG 1210+533	46,320	7.88	−2.20	0.63	8.98	7	Spectroscopic variable
1214+267	LB 2	67,850	7.72	−2.79	0.62	8.18	2	
1253+378	HZ 34	87,670	7.02	−1.81	0.50	6.38	7	
1305−017	PG 1305−017	44,400	7.76	...	0.57	8.80	7	Stratified
1413+015	PG 1413+015	47,770	7.72	−2.56	0.56	8.64	11	DA + dM, no CNO
1822+008	Sh 2–68	84,460	7.24	−0.86	0.53	6.93	1	CSPN, DAOZ
1957+225	NGC 6853	86,670	7.36	−1.29	0.57	7.13	1	CSPN
1958−501	BPS CS 30302-17	56,870	7.97	−3.55	0.69	8.85	4	
2011+398	RE J2013+400	49,650	7.94	−2.79	0.66	8.97	12	DA + dM, emission, no CNO
2115+118	HS 2115+1148	62,230	7.76	−2.97	0.62	8.36	13	DAOZ
2226−210	NGC 7293	94,640	7.61	−1.90	0.65	7.49	1	CSPN
2342+806	GD 561	74,160	7.16	−2.65	0.48	6.94	14	CSPN, binary

References. – (1) Napiwotzki 1995; (2) Bergeron et al. 1994; (3) Heber et al. 1996; (4) This work; (5) Greenstein 1984; (6) Kidder, Holberg & Mason 1991; (7) Green, Schmidt, & Liebert 1986; (8) Liebert et al. 1989; (9) Barstow et al. 1993; (10) Lamontagne et al. 1993; (11) Fulbright et al. 1993; (12) Barstow et al. 1995; (13) Dreizler et al. 1995a; (14) Bergeron et al. 1992.

TABLE 2.3 – Atmospheric Parameters of DA White Dwarfs with the Balmer Line Problem

WD	Name	$T_{\rm eff}$ (K)	$\log g$	$M/M_{\odot}$	M_V
0102−185	PHL 975	74,770	7.40	0.54	7.56
0113−245	KUV 01138−2431	58,880	7.56	0.54	8.19
0154−240	PHL 1248	74,560	7.85	0.68	8.46
0237+241	PG 0237+242	70,480	7.27	0.50	7.38
0311+480	KPD 0311+4801	97,080	6.96	0.53	6.23
0455−282	RE J0457−280	63,540	7.58	0.56	8.14
0615+655	HS 0615+6535	77,780	7.93	0.72	8.58
0621−376	RE J0623−374	66,060	7.12	0.45	7.19
0915+201	LB 3016	72,710	7.49	0.56	7.79
0948+534	PG 0948+534	139,500	7.56	0.75	7.04
1328−152	EC 13288−1515	57,980	7.89	0.66	8.83
1401+005	PG 1401+006	63,530	7.88	0.68	8.70
1526+013	PG 1526+013	50,000	7.89	0.64	8.99
1532+033	PG 1532+034	66,610	7.67	0.60	8.25
1738+669	RE J1738+665	79,320	8.04	0.77	8.76
2146−433	MCT 2146−4320	78,090	7.30	0.53	7.31
2211−495	RE J2214−491	71,530	7.46	0.55	7.74
2218+706	DeHt 5	76,750	7.38	0.54	7.48

private communication). We also plot, as dotted lines, two post-extreme horizontal branch (post-EHB) evolutionary sequences at 0.471 and 0.475 $M_{\odot}$ as well as a post-early asymptotic giant branch (post-EAGB) sequence at 0.495 $M_{\odot}$. These represent stars that left the AGB before the thermally pulsing stage (Dorman et al. 1993). The above three sequences are taken from Dorman et al. (1993) and all of them assume [Fe/H] = 0.

One of the first things we note is that most, but not all, of the hottest white dwarfs are DAO stars. More importantly, the sequence of DAO white dwarfs seems to seamlessly join the normal DA cooling sequence. This would suggest that the majority of these stars share a common evolutionary history. This is a very different result from that obtained by Bergeron et al. (1994) who had suggested that DAO white dwarfs might, instead, be the product of stars having evolved directly from the EHB (post-EHB evolution) to the white dwarf phase unlike most white dwarfs, which are descendants of stars having evolved off the AGB (post-AGB evolution). This new result is a direct consequence of the new parameters we have obtained, which make DAO white dwarfs hotter, and more importantly, more massive than previously measured. As mentioned above, our grid of model spectra makes use of the improved Stark

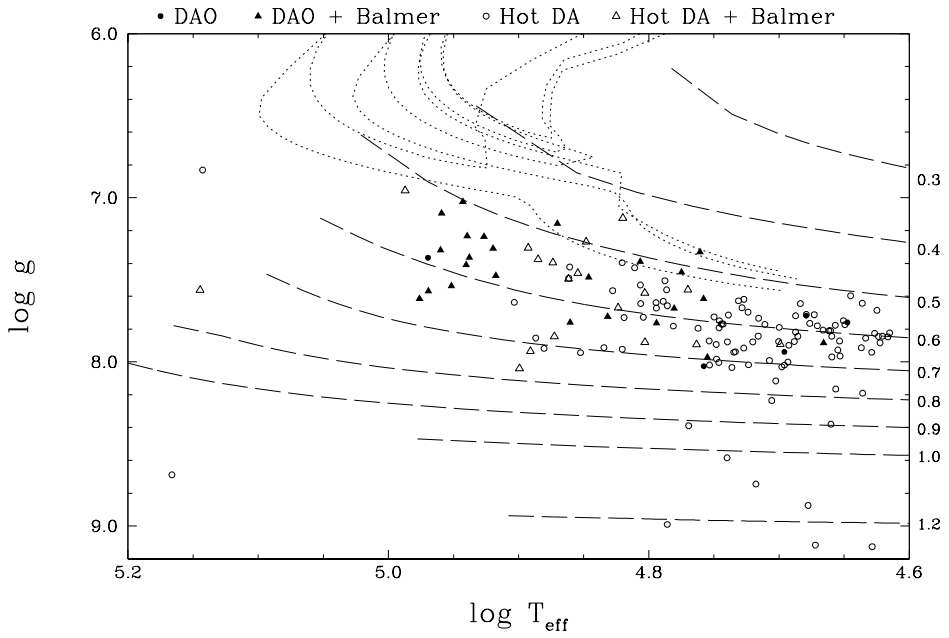

FIGURE 2.14 – Section of the $\log g$ vs. $\log T_{\rm eff}$ diagram showing the hot end of the DA white dwarf cooling sequence. Open symbols correspond to DA white dwarfs whereas filled symbols represent DAO white dwarfs. Triangles correspond to stars exhibiting the Balmer line problem. The dashed lines represent white dwarf cooling tracks with thick hydrogen layers from Wood (1995) and are labeled with their mass (in solar mass units) to the right of the figure. The dotted lines are three evolutionary tracks from Dorman et al. (1993). From top to bottom, a 0.471 $M_{\odot}$ and 0.475 $M_{\odot}$ post-EHB tracks and a 0.495 $M_{\odot}$ post-EAGB evolutionary track.

profiles developed by Tremblay & Bergeron (2009). A comparison of our grids with analogous grids computed with the older tables of Lemke (1997) reveals that temperatures increase, on average by about 3%, and the $\log g$ values by ~ 0.05 dex (see also Figure 8 of Tremblay & Bergeron 2009). However, these shifts in the atmospheric parameters are smaller than those brought on by the inclusion of CNO in the models. More importantly, the use of the new tables from Tremblay & Bergeron (2009) alone would not have allowed us to overcome the Balmer-line problem. Clearly, the addition of metals is the dominant factor to consider in comparing our results and conclusions with those of Bergeron et al. (1994).

With that being said, we must also note that there are a few stars in Figure 2.14 with somewhat lower masses. First of all, the DAO white dwarf with the lowest mass (0.47 $M_{\odot}$), Feige 55, is a known double-degenerate system (Holberg et al. 1995). As such, it is highly likely that it has lost mass through interactions with its companion, which Holberg et al.

(1995) conclude is likely a less luminous white dwarf. Another noteworthy star is GD 561 (2342+806) at log $T_{\rm eff} \sim 4.87$ and just above the 0.5 $M_{\odot}$ cooling track. Interestingly, GD 561 has a known planetary nebula (Sh 2-174; Napiwotzki & Schönberner 1993). Based on their results, Bergeron et al. (1994) had suggested that GD 561 could represent a case where post-EHB evolution produced a planetary nebula by way of H-flashes late in the star's evolution. However, Napiwotzki (1995) later discovered that GD 561 actually has a cool companion separated by $\approx 4\farcs0$. In addition, Napiwotzki (1995) reported the detection of a slight excess in the K band that also supports a binary scenario for this object. The exact nature of the companion has never been determined, to our knowledge. Later, Saffer et al. (1998) observed GD 561 in an effort to determine if it was a radial velocity variable but no variations were detected. Good et al. (2005a) did not detect any significant radial velocity variations either. Regardless, the binary nature of GD 561 likely explains why this star has a lower mass and the presence of the planetary nebula seems to point towards the canonical post-AGB evolution for white dwarfs. As such, the post-EHB scenario suggested by Bergeron et al. (1994) need no longer be invoked. The other lower mass object is 0621−376 (0.45 $M_{\odot}$), a DA+BP white dwarf. This star seems to be consistent with post-EHB evolution as it falls almost on top of the two post-EHB sequences plotted. However, this solitary object does not change our original conclusion that most of the stars in our sample, DA and DAO, are descendants from post-AGB evolution. Finally, it should also be pointed out that several stars near the 0.50 $M_{\odot}$ cooling sequence could also be compatible with the post-EAGB evolutionary scenario.

With respect to the Balmer-line problem, we see in Figure 2.14 that it is found mostly in the hotter stars although not in all of them, and there are also a few cooler stars that are also afflicted. More importantly, *all* the hot DAO stars exhibit the Balmer-line problem with the exception of the previously discussed case of PG 0950+139. Of the other four DAO white dwarfs that do not show the Balmer-line problem, the coolest one is PG 1305−017, which represents the only case of a stratified atmosphere. The other three cool white dwarfs that do not display the Balmer-line problem are 1013−050, 1413+015, and 2011+398. These three stars are members of DA+dM binary systems (probably pre-cataclysmic variables (CVs)). It is likely that in the case of these stars, the helium observed in the spectrum of the white

dwarf primary results from interactions with their M dwarf companion. The helium could have been accreted from the companion star or the system may have undergone a common envelope phase during which much of the white dwarf's hydrogen was stripped away. In the latter case, even a moderate mass-loss rate could bring sufficient helium to the surface of the star. As we will discuss later, there is likely a link between the fact that these three stars do not show the Balmer-line problem and that the source of their helium is the result of their membership in DA+dM binary systems. The coolest DAO star showing the Balmer-line problem is PG 1210+533, unique among DAO white dwarfs in that it displays spectroscopic variability. It is interesting to note that PG 1210+533 and PG 1305−017, possibly the two most unique DAO white dwarfs, are the only ones where the He II λ1640 line has been detected in their UV spectra.

We now turn our attention to the DA white dwarfs in Figure 2.14. We first remark that the DA+BP stars are all hotter than $\sim$ 55,000 K ($\log T_{\rm eff} \sim 4.75$). The lone exception to this rule is 1526+013 ($\log T_{\rm eff} \sim 4.7$). However, our spectrum for 1526+013 has a somewhat lower S/N and this makes the detection of the Balmer-line problem more difficult. It is thus quite possible that 1526+013 does not suffer from the Balmer-line problem at all. More importantly, the DA+BP white dwarfs do not seem to dominate over their normal DA counterparts. Specifically, in the range $4.8 < \log T_{\rm eff} < 4.9$, there seem to be just as many normal DA stars as DA+BP stars. This would seem to imply a transition region where the phenomenon responsible for the Balmer-line problem slowly ceases to operate. As we have already noted, most of the hottest stars are DAO white dwarfs but there also four very hot DA white dwarfs among them. Of these four stars, two are normal DAs while the other two are DA+BP stars. The two DA white dwarfs are 0556+106 and 2246+066. 0556+106 is actually a CSPN (Liebert et al. 1994) while 2246+066 was discovered during the course of the Hamburg Quasar Survey (Homeier et al. 1998). As for the two very hot DA+BPs, 0311+480 represents one of the two extreme cases of the Balmer-line problem in DA stars as shown in Figure 2.11. On the other hand, despite being the hottest DA+BP star ($\log T_{\rm eff} \sim 5.15$), and consequently having rather shallow Balmer lines to begin with, we do detect the Balmer-line problem in 0948+534 as well.

In Figure 2.15, we display the mass distribution of our entire sample of hot white dwarfs

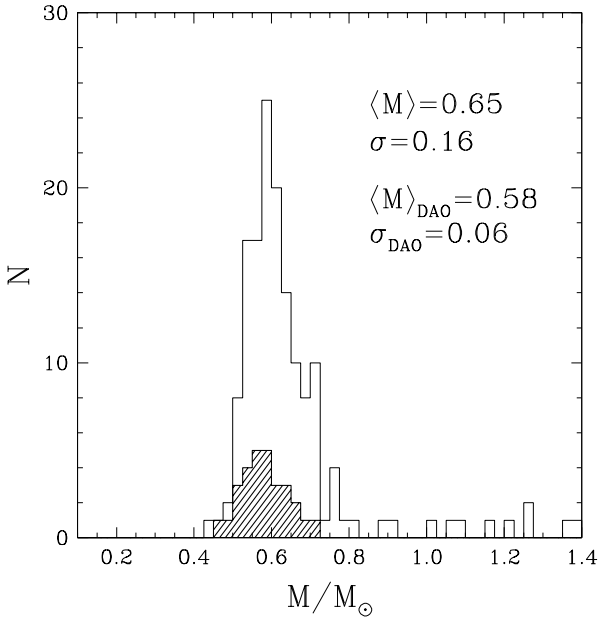

FIGURE 2.15 – Mass distribution for our entire sample of hot white dwarfs (solid line histogram) and of the DAO white dwarfs (hatched histogram).

as compared to that of the 29 DAO stars. We see that the mass distribution of the whole sample is strongly peaked around $\sim 0.6\ M_{\odot}$ with a mean mass of $0.65\ M_{\odot}$ and a dispersion of $0.16\ M_{\odot}$. The dispersion would probably be lower were it not for the presence of a number of higher mass white dwarfs in the sample. The hatched histogram shows the mass distribution for the DAO stars only. The latter is strongly peaked around $\sim 0.55{-}0.60\ M_{\odot}$ with a mean of $0.58\ M_{\odot}$ and a dispersion of $0.06\ M_{\odot}$. Although the mean mass is lower than that of the whole sample it is not uncomfortably lower. Indeed, if we take into account the dispersions of each distribution, both mass distributions are consistent with a single population of white dwarfs. This is yet another strong indication that most DAO white dwarfs stem from the same evolutionary channel as their DA brethren.

2.6 FUSE Observations

In this section, we turn our attention to the FUV spectra of these hot white dwarfs. We have seen that the inclusion of CNO in our models greatly improves the fits for both DA and DAO stars that suffer from the Balmer-line problem, and we now wish to understand its

TABLE 2.4 – List of *FUSE* Observations

WD	Name	Exposures	Exposure time (s)	Aperture
0001+433	RE J0003+433	18	26827	LWRS
0004+330	GD 2	79	83276	LWRS/MDRS
0027−636	RE J0029-632	5	14619	LWRS
0131−163	PHL 1043	4	8619	LWRS
0229−481	LB 1628	4	10704	LWRS
0343−007	KUV 03439−0048	2	3869	LWRS
0346−011	GD 50	21	43407	LWRS
0421+740	RE J0427+741	16	61145	LWRS
0455−282	RE J0457−280	31	47464	MDRS
0501+527	G191-B2B	149	68575	LWRS/MDRS
0505+012	HS 0505+0112	4	7111	LWRS
0615+655	HS 0615+6535	17	30146	LWRS
0621−376	RE J0623−374	40	18147	LWRS
0718−316	RE J0720-318	6	17659	LWRS
0802+413	KUV 08026+4118	4	9163	LWRS
0823+316	Ton 320	9	8427	LWRS
0834+500	PG 0834+501	4	9730	LWRS
0948+534	PG 0948+534	5	10855	LWRS
0950+139	PG 0950+139	11	21418	LWRS
1029+537	RE J1032+532	5	7408	LWRS
1040+492	RE J1043+490	63	57466	LWRS
1057+719	PG 1057+719	13	34203	LWRS
1136+667	HS 1136+6646	4	14098	LWRS
1202+608	Feige 55	36	49096	LWRS/MDRS
1210+533	PG 1210+533	3	4597	LWRS
1214+267	LB 2	6	9209	LWRS
1234+481	PG 1234+482	20	31542	LWRS
1253+378	HZ 34	7	7474	LWRS
1302+597	GD 323	7	17448	LWRS
1314+293	HZ 43	120	66227	LWRS/MDRS
1342+443	PG 1342+444	4	10679	LWRS
1444+636	RE J1446+632	8	10720	LWRS
1528+487	RE J1529+483	50	46737	LWRS/MDRS
1611−084	RE J1614−083	6	9643	LWRS
1631+781	RE J1629+780	32	57347	LWRS/MDRS
1711+668	RE J1711+664	16	35002	LWRS
1725+586	LB 335	7	18154	LWRS
1738+669	RE J1738+665	14	33648	LWRS

TABLE 2.4 – Continued

WD	Name	Exposures	Exposure time (s)	Aperture
1740−706	RE J1746−703	27	56187	LWRS
1800+685	KUV 18004+6836	23	63824	LWRS
1819+580	RE J1820+580	8	5411	LWRS
1950−432	MCT 1950−4314	7	14779	LWRS
2004−605	RE J2009−605	11	9718	LWRS
2011+398	RE J2013+400	95	73695	LWRS/MDRS
2046+396	KPD 2046+3940	4	8812	LWRS
2116+736	KUV 21168+7338	13	55373	LWRS
2124−224	BPS CS 29506-51	25	18938	MDRS
2146−433	MCT 2146−4320	10	13690	LWRS
2211−495	RE J2214−491	198	91639	LWRS/MDRS
2218+706	DeHt 5	3	6056	LWRS
2247+583	Lanning 23	18	62033	LWRS
2309+105	BPM 97895	91	45617	LWRS/MDRS
2321−549	RE J2324-544	6	14471	LWRS
2353+026	PB 5617	4	5604	LWRS

underlying causes. To this end, we will make use of FUV spectra from the FUSE archive[3]. The spacecraft and instrumentation are described in Moos et al. (2000, 2002). We retrieved spectra from the archive for as many of the DAO and hot DA stars in our sample that we could find. In total, we were able to obtain spectra for 10 of our DAO white dwarfs, 8 of the DA+BP stars, and 53 for the rest of our hot DA stars. The list of FUSE observations is presented in Table 2.4 where we indicate the number of exposures, total exposure time, and the aperture(s) used. The data provide a wavelength coverage from $\sim$ 905 to 1185 Å, and the majority of the observations were obtained using the low-resolution LWRS aperture that provides a resolution of $R \sim 20,000$. The spectra were processed using the latest version of the calibration pipeline, CalFUSE 3.2.3 (Dixon et al. 2007). The processed spectra were then co-aligned from individual exposures by cross-correlating the spectra in pixel space over small regions that include narrow absorption lines. Finally, the spectra were combined by taking an exposure-weighted average of all observations.

FUSE spectra have already been exploited in an effort to study DAO white dwarfs in a series of papers by Good et al. (2004, 2005a,b). In particular, Good et al. (2005a) fit several

[3]http://archive.stsci.edu/fuse/

TABLE 2.5 – Selected Wavelength Intervals and Central Wavelengths in *FUSE* Data

Ions	Wavelength Interval (Å)	Central Wavelengths (Å)
C IV	1106.5–1109.5	1107.59
...	...	1107.93
...	...	1107.98
N IV	921.5–924.5	921.99
...	...	922.52
...	...	923.05
...	...	923.22
...	...	923.68
...	...	924.28
O VI	1030.5–1033.5	1031.91
P V	1126.5–1129.5	1128.01
Si IV	...	1128.34
P V	1116.5–1119.5	1117.98
S VI	931.5–934.5	933.38
Fe VI/Fe VII	1164.5–1167.5	1165.10
...	...	1165.70
...	...	1166.18

of the observed metallic lines in the *FUSE* spectra with a grid of models whose metallicities were scaled to the measured abundances in G191-B2B. DA stars have also been the target of numerous studies aimed at determining the abundances of metals present in their atmospheres. Our analysis of the available FUV data will be a qualitative one as we are not interested in determining metal abundances for each individual star. Rather, our goal is to demonstrate that the presence of metals is the main culprit where the Balmer-line problem is concerned. We shall proceed from the most metal-poor stars, the normal DA white dwarfs, and work our way up to the most metal-rich objects, the DAO stars. For each group of stars, we will examine a set of seven wavelength intervals that probe well-known metallic absorption lines present in the FUV spectra of many hot white dwarfs. We list in Table 2.5 the extent of these intervals as well as the central wavelengths[4] for the spectral lines of interest. We wish to also point out a few particularities in the *FUSE* data. First, there is a very deep absorption feature seen near $\sim$ 923 Å, which is ubiquitous in the spectra. This absorption feature is of

[4]Taken from the NIST Web site, http://physics.nist.gov/PhysRefData/ASD/lines_form.html

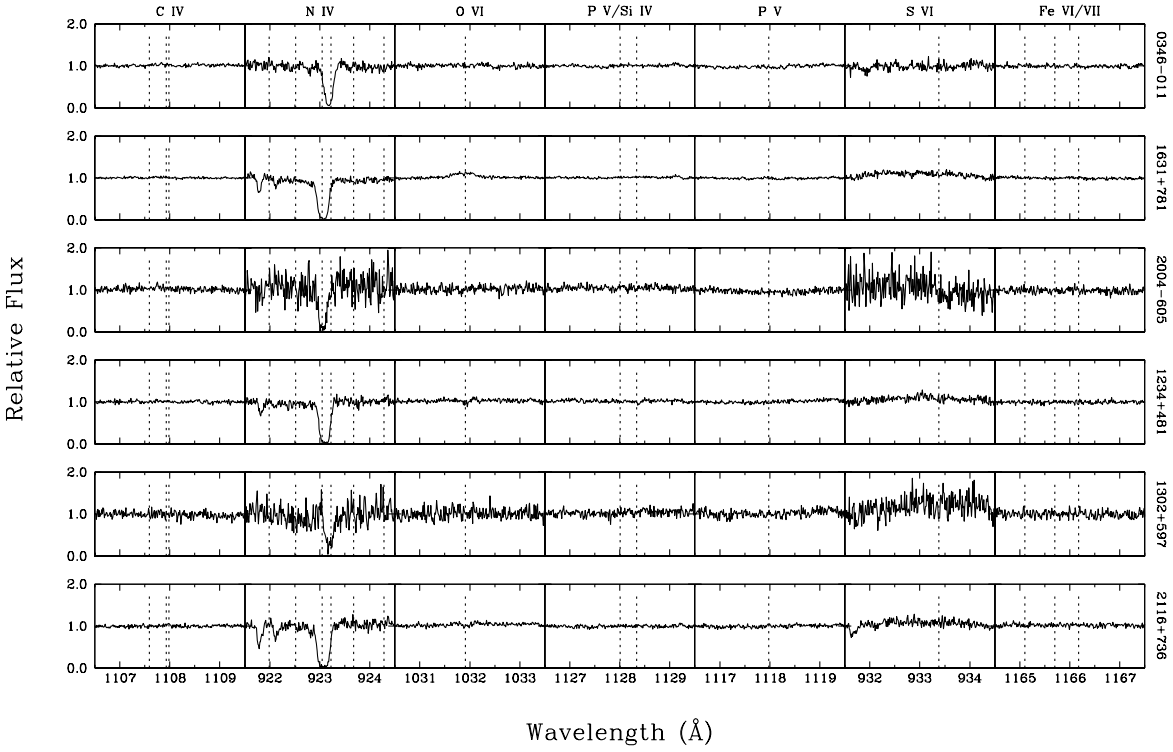

FIGURE 2.16 – Selected regions of the *FUSE* spectra for six normal DA white dwarfs. Each segment has been normalized to a continuum set to unity. The vertical dotted lines correspond to the central wavelengths of selected lines as listed in Table 2.5.

interstellar origin and is due to neutral hydrogen. Second, many of the lines appear shifted with respect to the central wavelengths indicated by the dotted lines in the figures. These shifts are due to the stellar radial velocity and actually help to distinguish the photospheric lines from interstellar lines.

The first group of stars is shown in Figure 2.16. These are six normal DA white dwarfs that do not exhibit the Balmer-line problem. The top three stars in the figure are somewhat cooler with $T_{\rm eff} \sim 45{,}000$ K, whereas the bottom three have $T_{\rm eff}$ in the range 50,000 K $< T_{\rm eff} <$ 60,000 K. With the exception of a few weak N IV lines in some cases, no other metal lines are observed in any of these stars. In particular, 0346−011, one of the coolest objects in Figure 2.16, is also quite massive with $\log g = 9.13$ and $M = 1.27\ M_{\odot}$; in fact it is the most massive white dwarf seen in Figure 2.14. This combination of age and high mass has clearly contributed here to produce an FUV spectrum completely devoid of any metal lines. Indeed,

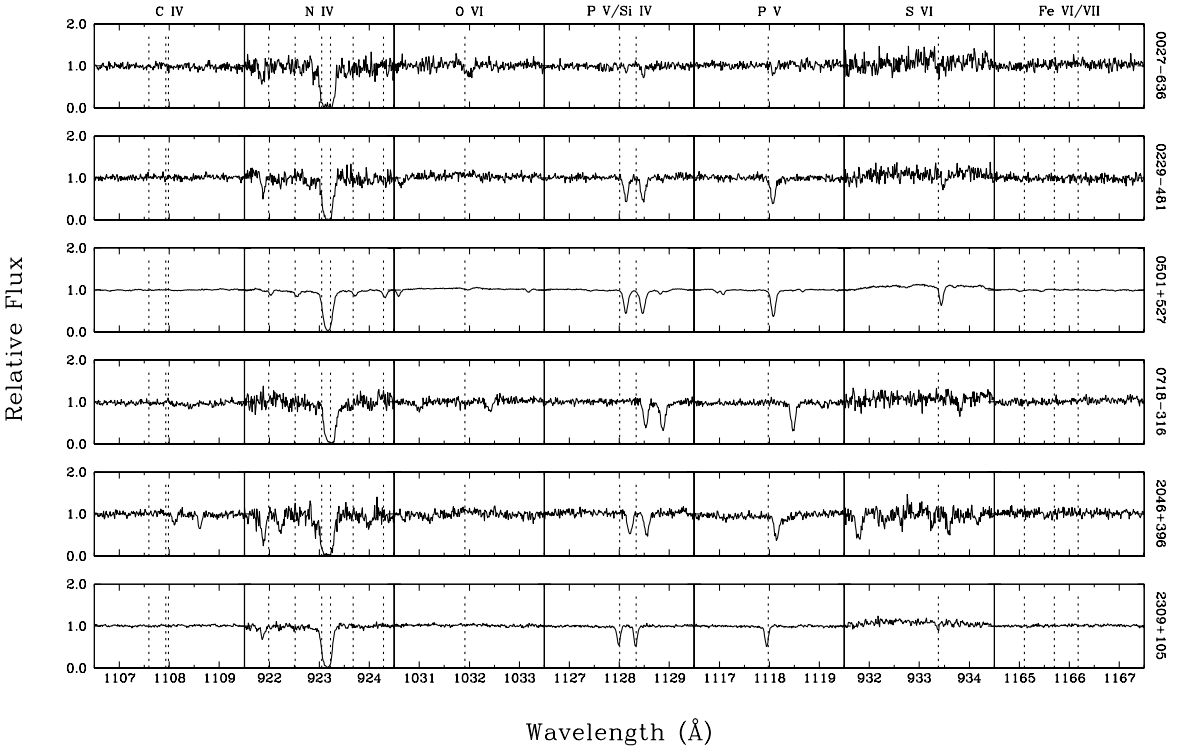

FIGURE 2.17 – Same as Figure 2.16 but for six normal DA white dwarfs with some metals.

any metals in this star likely diffused out of the atmosphere of this star a long time ago and rather quickly at that. These six stars clearly represent the template for metal-poor DA white dwarfs, and consequently they do not suffer from the Balmer-line problem.

Next, we see in Figure 2.17 examples of hot DA white dwarfs where at least some metal lines are present, particularly the P V/Si IV doublet as well as the P V line near 1118 Å. However, like the stars displayed in Figure 2.16, they are not afflicted by the Balmer-line problem. In addition, all these stars have $T_{\rm eff}$ in the range 55,000 K $\lesssim T_{\rm eff} \lesssim$ 65,000 K and thus overlap with the bottom three stars of Figure 2.16 in the $T_{\rm eff}$–$\log g$ plane. Since we find stars with and without metals occupying the same range of atmospheric parameters, we must conclude that the presence of metals itself is not only a function of $T_{\rm eff}$ or $\log g$ but must also be related to the evolutionary history of each individual object. Of note here is G191-B2B (0501+527), as one of the brightest known white dwarfs ($V = 11.78$) it is consequently one of the most studied white dwarfs as well (Barstow et al. 2001b; Vennes & Lanz 2001; Holberg et al. 2002), and a well-known photometric standard for both ground- and space-

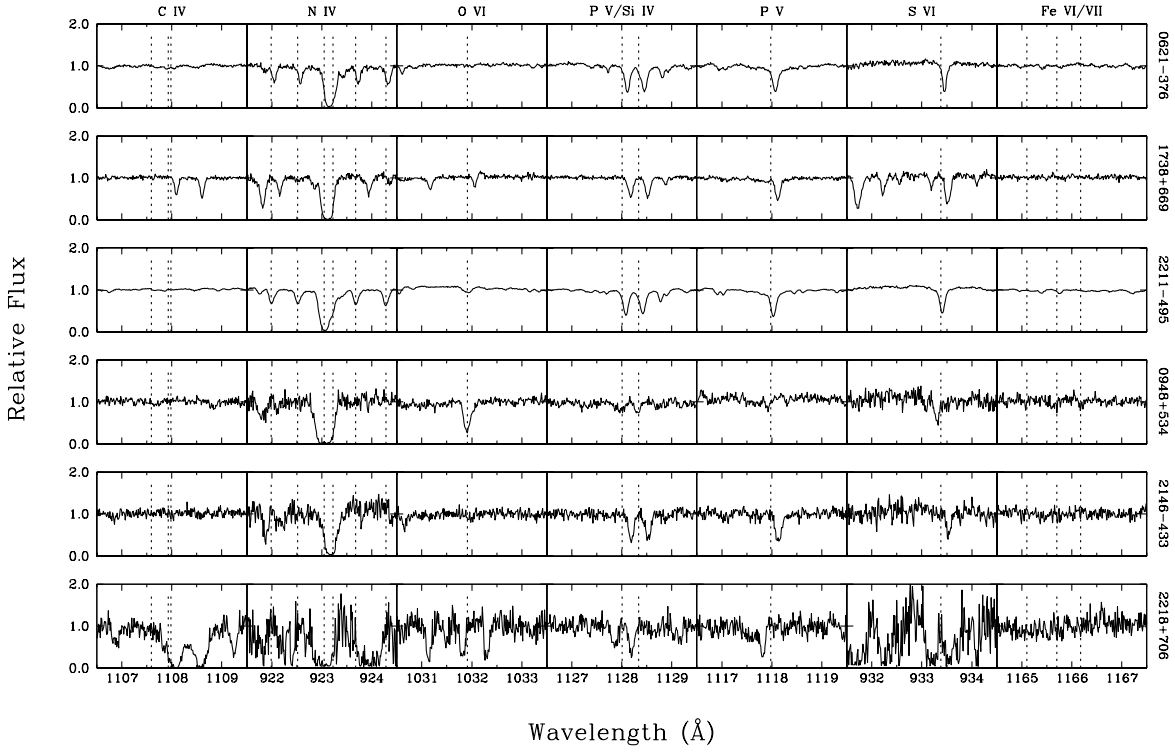

FIGURE 2.18 – Same as Figure 2.16 but for six DA white dwarfs exhibiting the Balmer-line problem.

based observations (Massey et al. 1988; Turnshek et al. 1990). We see in Figure 2.17, however, that in the present context G191-B2B does not really stand out and seems to be rather typical of these hot DA white dwarfs that contain some metals, yet do no exhibit the Balmer-line problem.

We now move to Figure 2.18 where we look at six DA+BP stars. We first note that, in addition to the metal lines observed in the previous group, we see here the appearance, in particular, of O VI and S VI lines, but no iron lines are observed, as in the two previous cases. Some might suggest that these lines are interstellar in origin. However, the strength of the lines and the fact that they are shifted in the same way as the rest of the observed lines in the spectrum strongly suggest they are truly photospheric in nature. The stars in the top three panels have 60,000 K $< T_{\rm eff} <$ 80,000 K but more importantly, they span a large range in surface gravity, from $\log g = 7.13$ for 0621−376 to $\log g = 8.04$ for 1738+669, yet the spectra of all three stars are quite similar. Furthermore, as we can see in Figure 2.11, the Balmer

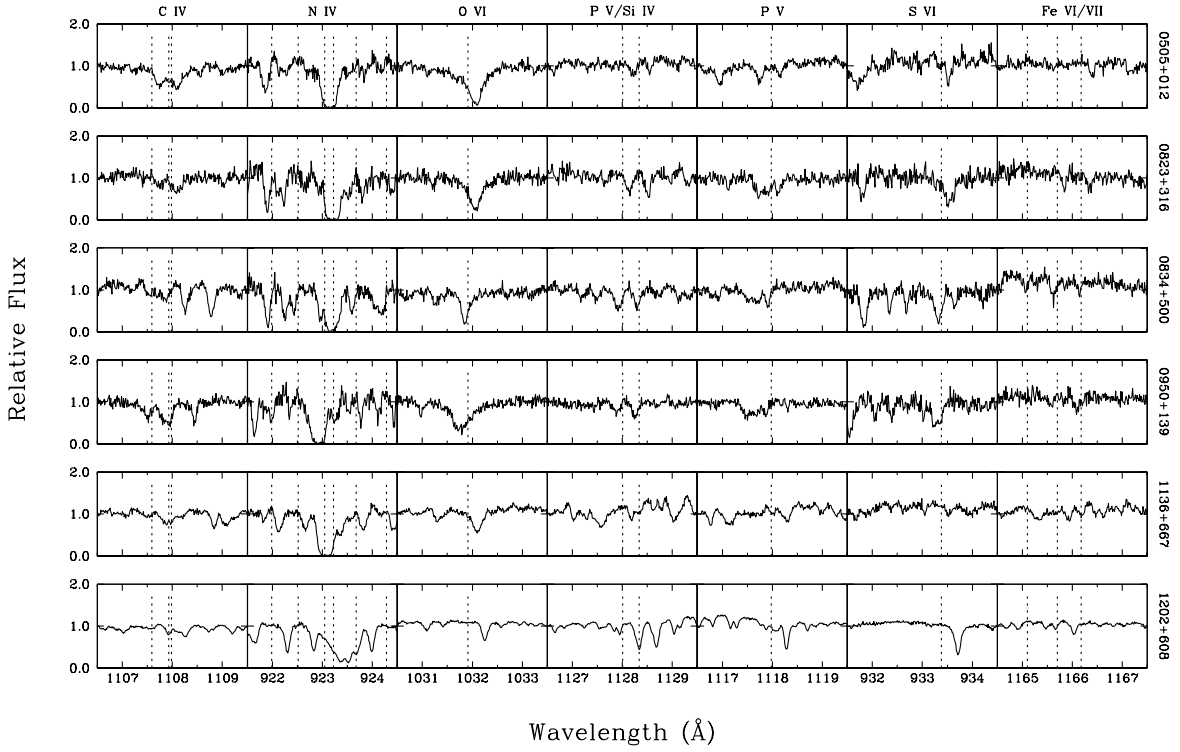

FIGURE 2.19 – Same as Figure 2.16 but for six DAO white dwarfs exhibiting the Balmer-line problem.

line problem is fairly obvious in these three white dwarfs. This once again seems to support our earlier assertion that the presence, or lack thereof, of metals is not only a function of the atmospheric parameters of a star. 0948+534 is the hottest DA+BP in our sample and we see that some of its metallic lines are weaker (P V/Si IV and P V), yet it also shows the strongest O VI lines of these three stars. The higher effective temperature ($T_{\rm eff} \sim 140{,}000$ K) likely induces a different ionization balance that favors O VI but depletes the abundance of the other ions. 0948+534 is also somewhat more massive with $M = 0.67\ M_{\odot}$, and the Balmer-line problem is not quite as severe in this case. Finally, the spectrum of 2218+706 shows some very deep and wide absorption features which are due to a rather high column density of molecular hydrogen.

We have now arrived at the DAO white dwarfs, which are plotted in Figure 2.19. We see here a large number of metallic lines in each of the individual wavelength intervals we have chosen, and we finally see the appearance of iron lines. This is in stark contrast to the normal

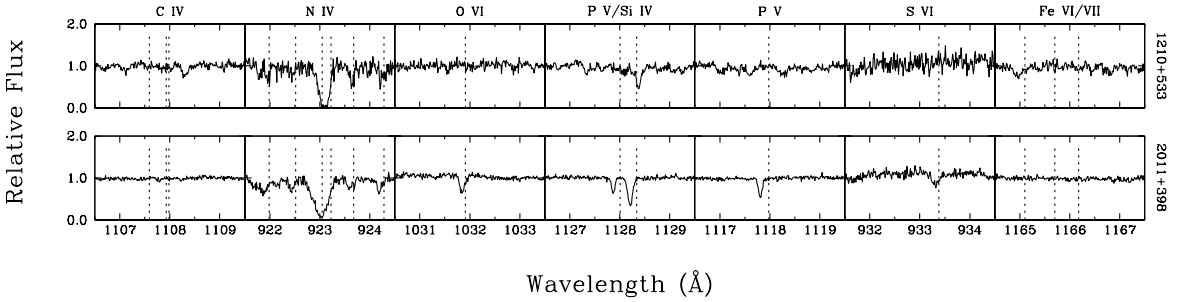

FIGURE 2.20 – Same as Figure 2.16 but for two peculiar DAO white dwarfs.

DA white dwarfs we saw in Figures 2.16–2.18. DAO white dwarfs are thus clearly the most metal-rich group of stars in our sample and it is not surprising that all the hot DAO stars suffer from the Balmer-line problem. There was, however, one slight exception: 0950+139. As we discussed earlier, the optical spectrum of this star prevents us from determining whether it suffers from the Balmer-line problem. However, its atmospheric parameters are consistent with the bulk of the hotter DAO stars and on that basis we chose to use our CNO grid to fit 0950+139. We see in Figure 2.19 that it does indeed resemble all the other DAO stars in terms of the presence of metals, thus supporting our earlier decision. Finally, in Figure 2.20 we show *FUSE* data for two particular DAO white dwarfs. 1210+533 is the DAO white dwarf that Bergeron et al. (1994) had discussed as being spectroscopically variable whereas 2011+398 is one of the three DAO white dwarfs in a DA+dM binary system and does not show the Balmer-line problem. These two stars do not show nearly as many metallic lines as the other DAO stars in Figure 2.19. Indeed, these two objects are more akin to the DA stars in Figure 2.17. As such, the fact that 2011+398 contains less metals and does not show the Balmer-line problem is perfectly consistent with the trend we have observed thus far. As for 1210+533, it also seems to be rather metal poor. In this case, the presence of the Balmer-line problem is likely related to its spectroscopic variability than to the presence of metals in the atmosphere.

In summary, we see that, with a few exceptions, the stars in our sample can essentially be divided into four categories in terms of the presence of metals and the Balmer-line problem. First, there are DA white dwarfs almost completely devoid of metals that do not suffer from

the Balmer-line problem, and DA white dwarfs that contain some metals, but do not suffer the Balmer-line problem either. On the other hand, there are DA stars that seem to be quite rich in metals and are afflicted by the Balmer-line problem. Finally, we have the hot DAO white dwarfs that all seem to contain important quantities of metals and consequently all exhibit the Balmer-line problem. It should be clear by now that there is a direct correlation between the presence of metals in the atmospheres of hot white dwarfs and instances of the Balmer-line problem.

2.7 DISCUSSION

Our analysis of DAO and hot DA white dwarfs has led to some interesting results that have a direct bearing on how we interpret the origin and evolution of these stars. The stars studied in this work represent the largest sample of DAO white dwarfs analyzed in a homogeneous fashion with appropriate model atmospheres. However, one important caveat to keep in mind is that our results would most certainly change if we had precise determinations for the metal abundances in each star. Nonetheless, the new atmospheric parameters, obtained with our improved CNO grid, imply that DAO white dwarfs are hotter, and more massive than previous studies have shown. As a result, we can conclude that most DAO stars are indeed products of post-AGB evolution just like the vast majority of white dwarfs. This is further supported by the knowledge that several of the DAO stars in our sample are CSPN. Indeed, the suggestion by Bergeron et al. (1994) that DAO stars required post-EHB evolution, due to their previously determined lower masses, is no longer valid. We have clearly shown that DAO stars follow the same evolutionary path as the rest of the hydrogen-rich white dwarfs.

This connection is further supported by our discovery that several hot DA stars also suffer from the Balmer-line problem just like DAO stars. In both cases, we used FUV spectra from *FUSE* to demonstrate rather convincingly that the presence of metals is clearly the source of the Balmer-line problem. The only thing that seems to distinguish the DAO stars from their DA counterparts is the presence of helium. As previously discussed, stratified atmospheres and radiative levitation are not able to explain the presence of helium in the atmosphere of these white dwarfs. The most probable cause, as suggested by Bergeron et al. (1994), must therefore

be the presence of a weak stellar wind. In that context, the work presented in Unglaub & Bues (2000) is of particular interest here. Although many of their results do not, in a quantitative sense, agree with our own, qualitatively at least, much of what is presented and discussed in Unglaub & Bues (2000) seems to match our results.

The calculations of Unglaub & Bues show that a stellar wind, driven by the presence of metals, can support sufficient amounts of helium in the atmospheres of a white dwarf to explain the observed abundances in DAO stars. However, this is only true up to a limiting temperature known as the "wind limit". Beyond the wind limit, mass loss ceases and heavier elements begin to sink under the influence of gravitational settling. More importantly, Unglaub & Bues showed that when the wind limit is reached, helium sinks more rapidly than CNO. This would allow for a transition region where stars would still have some metals in their atmospheres but no helium. The one major discrepancy between the results of Unglaub & Bues and ours is that their wind limit for DAO stars is $\sim$ 80,000 K whereas we find several DAOs in the range 60,000 K $< T_{\rm eff} <$ 80,000 K. Otherwise, one can imagine a scenario whereby DAO's are stars with a wind, driven by metals, that maintains helium in the atmosphere. At the same time, these same metals are also the driving force behind the Balmer-line problem. If the star does not have sufficient helium left, we see it as a DA+BP star instead. On a star-by-star basis, the distinction between a DAO and a DA+BP star would stem from the evolutionary history of each individual object and the initial abundances of helium and metals upon the formation of the white dwarf.

Furthermore, in the presence of mass loss, stratified atmospheres cannot exist because diffusive equilibrium cannot be reached. This would explain why PG 1305$-$017 is the only DAO white dwarf with a stratified atmosphere as it is cooler than the predicted wind limit. Other stars that are below the wind limit are the three DA+dM systems, this scenario would not apply to them as the DAO nature of these stars most probably stems from interactions with their companion and not from a wind driven by the presence of metals which maintains helium in the atmosphere.

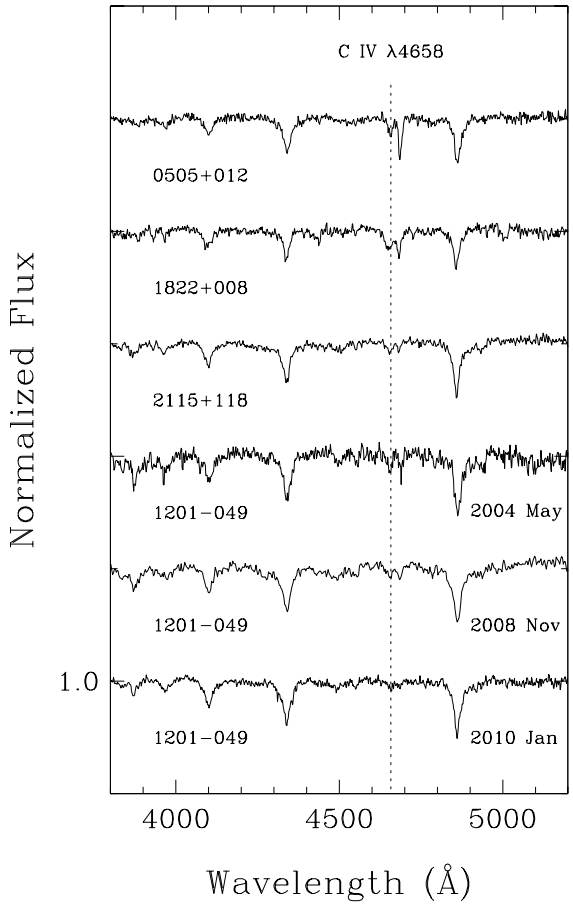

FIGURE 2.21 – Optical spectra of the four DAOZ white dwarfs in our sample. The bottom three spectra correspond to observations of 1201−049 taken in 2004 May, 2008 November, and 2010 January.

2.7.1 DAOZ

We show in Figure 2.21 the four DAOZ white dwarfs in our sample. However, as we alluded to in Section 2.3, these objects have also been classified as hybrid PG 1159 stars. The first of these objects was uncovered by Napiwotzki & Schönberner (1991). The designation derives from the similarity of their spectra with those of the normal PG 1159 stars, particularly the combination of the He II λ4686 and C IV λ4658 lines. The "hybrid" nature refers to the presence of hydrogen, as evidenced by the strong Balmer lines observed in their spectra. Of particular interest to us is the statement by Dreizler et al. (1995b) that with sufficient hydrogen left in the atmosphere, a PG 1159 star could become a DA (or DAO) white dwarf once all the metals have diffused out of the atmosphere. The three spectra at the bottom of

Figure 2.21 are all of 1201−049 and span a timescale of almost six years. Specifically, there seems to be an important decrease in the strength of He II λ4686 and C IV λ4658 from the oldest to the most recent observation. It is possible we are witnessing the effects of the metals diffusing out of the atmosphere and this star will eventually present itself as a simple DA or DAO star. Thus, these DAOZ white dwarfs probably represent the transition phase between PG 1159 stars and hot hydrogen-rich white dwarfs corroborating, to a certain extent, the ideas of Fontaine & Wesemael (1987).

2.7.2 PG 1210+533

One of the unique DAO stars discussed in Bergeron et al. (1994) is PG 1210+553. However, one of the mysteries associated with this object has been solved. We showed in Section 2.5.2 that the inability of Bergeron et al. (1994) to properly fit the He II λ4686 line profile was a consequence of the one remaining enigma presented by PG 1210+533: its spectroscopic variability. Bergeron et al. (1994) had suggested that further monitoring of this star was necessary in order to decipher its true nature. Since then, two new optical spectra have been obtained in 1994 January (see Section 2.3 and Figure 2.1) and more recently in 2007 January at the Observatoire du Mont-Mégantic with the instrument and setup described in Section 2.3. We compare in Figure 2.22 these two spectra with the four spectra shown in Bergeron et al. (1994, see their Figure 16) which were obtained by Wesemael et al. (1985, 1977 February), Holberg (1987, 1987 April), Kidder (1991, 1989 February), and Bergeron et al. (1994, 1992 April). The same type of variability as reported by Bergeron et al. (1994) is observed even in the most recent observations; specifically, the variable strength of He II λ4686 and the appearance and disappearance of He I λ4471, which has re-appeared in the most recent spectrum. We are at odds to explain this strange behavior. Perhaps PG 1210+533 is a hotter counterpart of GD 323, a spectroscopically variable DAB white dwarf (Pereira et al. 2005). In the case of GD 323, Pereira et al. (2005) surmised that the likely causes of the observed variability are inhomogeneities in the surface abundance of helium either as spots, or equatorial belts and polar caps. Similarly, Bergeron et al. (1994) drew comparisons to Feige 7 (Achilleos et al. 1992), a magnetic white dwarf where the spectroscopic variability was

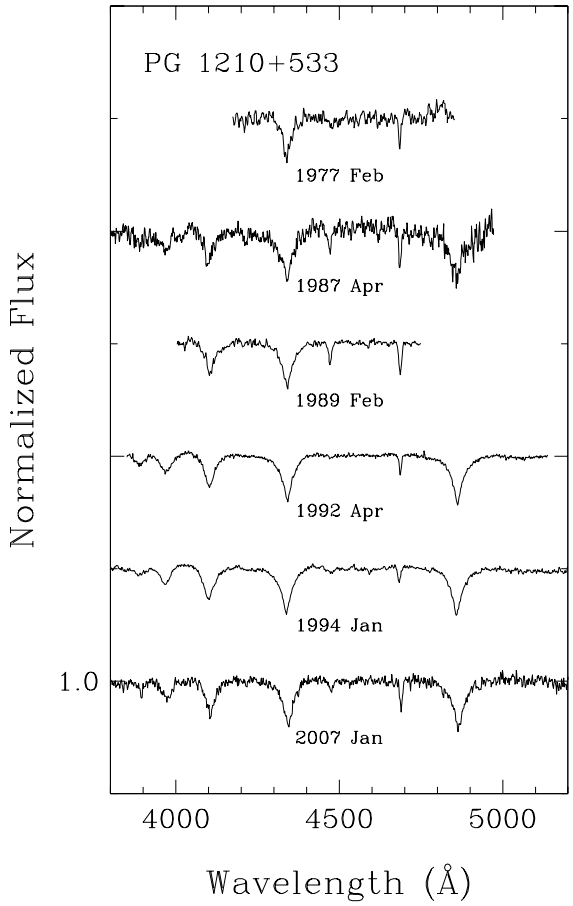

FIGURE 2.22 – Comparison of our spectrum of PG 1210+533 (1994 January) with spectra obtained over the course of 30 years by Wesemael et al. (1985, 1977 February), Holberg (1987, 1987 April), Kidder (1991, 1989 February), Bergeron et al. (1994, 1992 April), and A. Gianninas (unpublished, 2007 January).

interpreted as the surface abundance inhomogeneities of a rotating white dwarf. However, another scenario might also be plausible. Within the paradigm of mass loss as the driving force behind the DAO phenomenon, we established that the stratified nature of PG 1305−017 follows from the extinguishing of the stellar wind which then allows diffusive equilibrium to set in. PG 1210+533 is only ≈ 2000 K hotter than PG 1305−017. Perhaps we are witnessing a star in the process of establishing that diffusive equilibrium but has not quite gotten there yet. Whatever the case may be, the one certainty is that yet further study is required before the true nature of PG 1210+533 is fully understood.

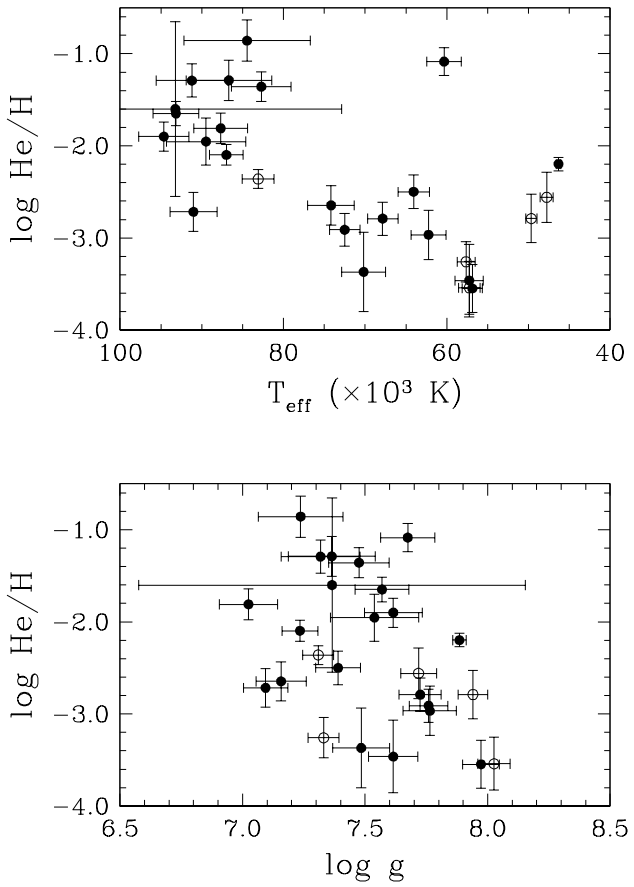

FIGURE 2.23 – Correlations between the atmospheric parameters of DAO stars (excluding PG 1305−017). DAO stars that are in binary systems are denoted by open circles.

2.7.3 Correlations

We plot in Figure 2.23 the relations between the measured helium abundances of our DAO white dwarfs with respect to $T_{\rm eff}$ and $\log g$. All the values are taken from Table 2.2. It should be noted that PG 1305−017 is not included in this figure since we have no measurement for the helium abundance in that star. Unlike Bergeron et al. (1994) we do not observe any correlation, in the bottom panel, between $\log g$ and the helium abundance. We do note, however, that the three most massive stars near $\log g \sim 8.0$ all have rather low helium abundances, two of these being DA+dM binaries (1013−050 and 2011+398). More striking is the rather clear correlation between the helium abundance and $T_{\rm eff}$ seen in the top panel of Figure 2.23. If the mass loss scenario we have described above holds, then this is yet another indication

of how the weakening stellar wind can no longer maintain helium in the atmosphere of the white dwarf. The three coolest stars in this panel consist once again of two DA+dM binaries (1413+015 and 2011+398) along with PG 1210+533. That the helium abundances in the DA+dM binaries do not match the observed trend is not surprising since the helium in their atmospheres likely results from their binary evolution. Similarly, the fact that PG 1210+533 does not conform to the observed trend is not surprising considering the variable nature of this star and, specifically, of its helium abundance. The DAO star near $T_{\rm eff} \sim 60{,}000$ and log He/H ~ -1.0 is 0505+012, one of the four DAOZ white dwarfs in our sample.

Finally, the object with the very large error bars is 0950+139. The optical spectrum of this star was contaminated with many emission lines from its planetary nebula. All the affected regions, including the core of virtually all the Balmer lines, were necessarily excluded from the fitting procedure thus greatly increasing the uncertainty in the measured atmospheric parameters.

2.8 CONCLUSION

We have presented a spectroscopic analysis of hot DA and DAO white dwarfs. First, we presented our new grids of NLTE model atmospheres that include CNO to overcome the Balmer-line problem, as prescribed by Werner (1996). By coupling these new models with our standard spectroscopic technique, we were then able to revise the atmospheric parameters of these stars. Our results show that DAO white dwarfs are hotter and more massive as compared to previous determinations. This leads us to the conclusion that DAO white dwarfs are products of post-AGB evolution, not post-EHB evolution as Bergeron et al. (1994) had suggested. Our analysis also uncovered an important number of DA+BP white dwarfs which we analyzed with analogous models. We then employed spectra taken from the *FUSE* archive to show that the presence of metals in both DAO and DA+BP stars are at the origin of the Balmer-line problem.

Clearly, DAO stars form a rather mixed bag of objects. Most of them are products of post-AGB evolution, including many CSPN, and owe their helium to a metal-driven stellar wind. On the other hand, there are also three DA+dM binary systems where the DAO nature is a

consequence of interactions with their companion, either through mass exchange or a common envelope phase. Also, we have the two special cases of PG 1305−017 and PG 1210+533. PG 1305−017 is the sole DAO white dwarf that requires a stratified atmosphere. However, even this case can be explained by the mass-loss paradigm because the star is cool enough that mass loss would have ceased, allowing for diffusive equilibrium to be established. On the other hand, PG 1210+533 and its spectroscopic variability still defy explanation.

In the future it would be interesting to see the models of Unglaub & Bues (2000) revisited with new and improved calculations of the mass-loss rates for these stars. In particular, obtaining a better match for the location of the "wind limit" would further cement the case for mass loss as the driving force behind the DAO phenomenon. Additionally, further analyses of the FUSE spectra would be in order to precisely determine, in an absolute manner, the abundances of all metals that are present. This would allow for the calculation of models tailor-made for each object and thus permit the most precise determination of the atmospheric parameters for each star. Finally, as PG 1210+533 still remains a mystery, further monitoring of this object would be warranted if we are ever to truly understand the particular nature of this object.

We thank the director and staff of Steward Observatory and of the Carnegie Observatories for the use of their facilities. We also thank I. Hubeny for his help with the TLUSTY and SYNSPEC packages, P. Dufour for obtaining the spectrum of 0950+139, J. B. Holberg for providing us with his spectrum of HS 1136+6646, and G. Fontaine for useful discussions. Some of the data presented in this paper were obtained from the Multimission Archive at the Space Telescope Science Institute (MAST). STScI is operated by the Association of Universities for Research in Astronomy, Inc., under NASA contract NAS5-26555. Support for MAST for non-HST data is provided by the NASA Office of Space Science via grant NAG5-7584 and by other grants and contracts. This work was supported in part by the NSERC Canada and by the Fund FQRNT (Québec). M. T. R. acknowledges support from FONDAP (15010003) and Proyecto BASAL PB06 (CATA). P. B. is a Cottrell Scholar of Research Corporation for Science Advancement.

2.9 REFERENCES

Achilleos, N., Wickramasinghe, D. T., Liebert, J., Saffer, R. A., & Grauer, A. D. 1992, ApJ, 396, 273

Asplund, M., Grevesse, N., & Sauval, A. J. 2005, in ASP Conf. Ser. 336, Cosmic Abundances as Records of Stellar Evolution and Nucleosynthesis, ed. T. G. Barnes III & F. N. Bash, (San Francisco, CA: ASP), 25

Barstow, M. A. 1989, in IAU Colloq. 114, White Dwarfs, ed. G. Wegner (New York: Springer), 156

Barstow, M. A., Bannister, N. P., Holberg, J. B., Hubeny, I., Bruhweiler, F. C., & Napiwotzki, R. 2001a, MNRAS, 325, 1149

Barstow, M. A., Burleigh, M. R., Bannister, N. P., Holberg, J. B., Hubeny, I., Bruhweiler, F. C., & Napiwotzki, R. 2001b, in 12th European Workshop on White Dwarfs, Vol. 226, 128

Barstow, M. A., Dobbie, P. D., Holberg, J. B., Hubeny, I., & Lanz, T. 1997, MNRAS, 286, 58

Barstow, M. A., Good, S. A., Holberg, J. B., Hubeny, I., Bannister, N. P., Bruhweiler, F. C., Burleigh, M. R., & Napiwotzki, R. 2003, MNRAS, 341, 870

Barstow, M. A., et al. 1993, MNRAS, 264, 16

Barstow, M. A., et al. 1995, MNRAS, 272, 531

Bergeron, P., Saffer, R. A., & Liebert, J. 1992, ApJ, 394, 228

Bergeron, P., Wesemael, F., Beauchamp, A., Wood, M. A., Lamontagne, R., Fontaine, G., & Liebert, J. 1994, ApJ, 432, 305

Bergeron, P., Wesemael, F., Lamontagne, R., & Chayer, P. 1993, ApJ, 407, L85

Dixon, W. V. et al. 2007, PASP, 119, 527

Dorman, B., Rood, R. T., & O'Connell, R. W. 1993, ApJ, 419, 596

Dreizler, S., Heber, U., Napiwotzki, R., & Hagen, H.-J. 1995a, A&A, 303, L53

Dreizler, S., Werner, K., & Heber, U. 1995b, White Dwarfs, ed. D. Koester & K. Werner (Lecture Notes in Physics, Vol. 443; Berlin: Springer), 160

Dreizler, S., & Wolff, B. 1999, A&A, 348, 189

Eisenstein, D. J., et al. 2006, ApJS, 167, 40

Fontaine, G., & Wesemael, F. 1987, in IAU Colloq. 95, The Second Conference on Faint Blue Stars, ed. A. G. D. Philip, D. S. Hayes, & J. Liebert (Schenectady, NY: Davis), 319

Fulbright, M. S., Liebert, J., Bergeron, P., & Green, R. 1993, ApJ, 406, 240

Gianninas, A., Bergeron, P., & Fontaine, G. 2005, ApJ, 631, 1100

Gianninas, A., Bergeron, P., & Ruiz, M. T. 2009, J. Phys.: Conf. Ser., 172, 012021

Good, S. A., Barstow, M. A., Burleigh, M. R., Dobbie, P. R., Holberg, J. B., & Hubeny, I. 2005a, MNRAS, 363, 183

Good, S. A., Barstow, M. A., Burleigh, M. R., Dobbie, P. R., Holberg, J. B., & Hubeny, I. 2005b, MNRAS, 364, 1082

Good, S. A., Barstow, M. A., Holberg, J. B., Sing, D. K., Burleigh, M. R., & Dobbie, P. D. 2004, MNRAS, 355, 1031

Green, R. F., Schmidt, M., & Liebert, J. 1986, ApJS, 61, 305

Greenstein, J. L. 1984, ApJ, 276, 602

Heber, U., Dreizler, S., & Hagen, H.-J. 1996, A&A, 311, L17

Holberg, J. B. 1987, in IAU Colloq. 95, The Second Conference on Faint Blue Stars, ed. A. G. D. Philip, D. S. Hayes, & J. Liebert (Schenectady, NY: Davis), 285

Holberg, J. B., Barstow, M. A., Hubeny, I., Sahu, M. S., Bruhweiler, F.C., & Landsman, W. B. 2002, BAAS, 34, 765

Holberg, J. B., & Bergeron, P. 2006, AJ, 132, 1221

Holberg, J. B., Kidder, K., Liebert, J., & Wesemael, F. 1989, in IAU Colloq. 114, White Dwarfs, ed. G. Wegner (New York: Springer), 188

Holberg, J. B., Saffer, R. A., Tweedy, R. W., & Barstow, M. A. 1995, ApJ, 452, L133

Homeier,D., Koester, D., Hagen, H.-J., Jordan, S., Heber, U., Engels, D., Reimers, D., & Dreizler, S. 1998, A&A, 338, 563

Hubeny, I., & Lanz, T. 1995, ApJ, 439, 875

Hügelmeyer, S., Dreizler, S., Rauch, T., & Krzesiński. J. 2007, in ASP Conf. ser. 372, 15th European Workshop on White Dwarfs, ed. R. Napiwotzki & M. R. Burleigh, (San Francisco, CA: ASP), 187

Kidder, K. M. 1991, PhD thesis, Univ. Arizona, Tucson

Kidder, K. M., Holberg, J. B., & Mason, P. A. 1991, AJ, 101, 579

Koester, D. 1989, ApJ, 342, 999

Lamontagne, R., Wesemael, F., Bergeron, P., Liebert, J., Fulbright, M. S., & Green, R. F 1993, in White Dwarfs: Advances in Observation and Theory, ed. M. A. Barstow (Dordrecht: Kluwer), 347

Lemke, M. 1997, A&AS, 122, 285

Liebert, J., Bergeron, P., & Holberg, J. B. 2005, ApJS, 156, 47

Liebert, J., Bergeron, P., & Tweedy, R. W. 1994, ApJ, 424, 817

Liebert, J., Green, R., Bond, H. E., Holberg, J. B., Wesemael, F., Fleming, T. A., & Kidder, K. 1989, ApJ, 346, 251

Massey, P., Strobel, K., Barnes, J. V., & Anderson, E. 1988, ApJ, 328, 315

McCook, G. P., & Sion, E. M. 1999, ApJS, 121, 1

Moos, H. W., et al. 2000, ApJ, 538, L1

Moos, H. W., et al. 2002, ApJS, 140, 3

Napiwotzki, R. 1992, in The Atmospheres of Early-Type Stars, ed. U. Heber & C. S. Jeffery (Berlin: Springer), 310

Napiwotzki, R. 1993, Acta Astron., 43, 343

Napiwotzki, R. 1995, in White Dwarfs, ed. D. Koester & K. Werner (Lecture Notes in Physics, Vol 443; Berlin: Springer), 176

Napiwotzki, R. 1997, A&A, 322, 256

Napiwotzki, R. 1999, A&A, 350, 101

Napiwotzki, R., Green, P. J., & Saffer, R. A. 1999, ApJ, 517, 399

Napiwotzki, R., & Rauch., T. 1994, A&A, 285, 603

Napiwotzki, R., & Schönberner, D. 1991, A&A, 249, L16

Napiwotzki, R., & Schönberner, D. 1993, in IAU Symp. 155, Planetary Nebulae, ed. R. Weinberger, & A. Acker (Dordrecht: Kluwer), 495

Napiwotzki, R., & Schönberner, D. 1995, A&A, 301, 545

Pereira, C., Bergeron, P., & Wesemael, F. 2005, ApJ, 623, 1076

Pounds, K. A. et al. 1993, MNRAS, 260, 77

Press, W. H., Flannery, B. P., Teukolsky, S. A., & Vetterling, W. T. 1986, Numerical Recipes (Cambridge: Cambridge Univ. Press)

Saffer, R. A., Livio, M., & Yungelson, L. R. 1998, ApJ, 502, 394

Schöning, T., & Butler, K. 1989, A&AS, 78, 51

Schuh, S. L., Dreizler, S., & Wolff, B. 2002, A&A, 382, 164

Shipman, H. L. 1976, ApJ, 206, L67

Sing, D. K., et al. 2004, AJ, 127, 2936

Stroeer, A., Heber, U., Lisker, T., Napiwotzki, R., Dreizler, S., Christlieb, N., & Reimers, D. 2007, A&A, 462, 269

Tremblay, P.-E., & Bergeron, P. 2009, ApJ, 696, 1755

Turnshek, D. A., Bohlin, R. C., Williamson, R. L., II, Lupie, O. L., Koornneef, J., & Morgan, D. H. 1990, AJ, 99, 1243

Unglaub, K., & Bues, I. 2000, A&A, 359, 1042

Vennes, S. 1999, ApJ, 525, 995

Vennes, S., & Fontaine, G. 1992, ApJ, 401, 288

Vennes, S., & Lanz, T. 2001, ApJ, 553, 399

Vennes, S., Pelletier, C., Fontaine, G., & Wesemael, F. 1988, ApJ, 331, 876

Vennes, S., Thejll, P. A., Galvan, R. G., & Dupuis, J. 1997, ApJ, 480, 714

Werner, K. 1996, ApJ, 457, L39

Werner, K., & Dreizler, S. 1993, Acta Astron., 43, 321

Werner, K., & Heber, U. 1991, in Stellar Atmospheres: Beyond Classical Models, ed. L. Crivellari, I. Hubeny, & D. G. Hummer (Dordrecht: Kluwer), 341

Wesemael, F., Green, R. F., & Liebert, J. 1985, ApJS, 58, 379

Wolff, B., Koester, D., Dreizler, S., & Haas, S. 1998, A&A, 329, 1045

Wood, M. A. 1995, in Proc. 9th European Workshop on White Dwarfs, ed. D. Koester & K. Werner (Berlin: Springer), 41

Chapitre 3

A SPECTROSCOPIC SURVEY AND ANALYSIS OF BRIGHT, HYDROGEN-RICH WHITE DWARFS[1]

A. Gianninas[1,3], P. Bergeron[1], and M. T. Ruiz[2,3]

[1] *Département de Physique, Université de Montréal, C.P. 6128, Succ. Centre-Ville, Montréal, Québec H3C 3J7, Canada*

[2] *Departamento de Astronomía, Universidad de Chile, Casilla 36-D, Santiago, Chile*

[3] *Visiting astronomers at Las Campanas Observatory operated by Carnegie Institution of Washington.*

[1]Based on observations made with ESO Telescopes at the La Silla or Paranal Observatories under program ID 078.D-0824(A).

3.1 ABSTRACT

We have conducted a spectroscopic survey of over 1300 bright ($V \leq 17.5$), hydrogen-rich white dwarfs based largely on the last published version of the McCook & Sion catalog. The complete results from our survey, including the spectroscopic analysis of over 1100 DA white dwarfs, are presented. High signal-to-noise ratio optical spectra were obtained for each star and were subsequently analyzed using our standard spectroscopic technique where the observed Balmer line profiles are compared to synthetic spectra computed from the latest generation of model atmospheres appropriate for these stars. First, we present the spectroscopic content of our sample, which includes many misclassifications as well as several DAB, DAZ, and magnetic white dwarfs. When necessary, specific models and analysis techniques are used to derive the most accurate atmospheric parameters possible. In particular, we employ M dwarf templates to obtain better estimates of the atmospheric parameters for those white dwarfs that are in DA+dM binary systems. Certain unique white dwarfs and double-degenerate binary systems are also analyzed in greater detail. We then examine the global properties of our sample including the mass distribution and their distribution as a function of temperature. Next, we look at how the new Stark broadening profiles affect the determination of the atmospheric parameters. We then proceed to test the accuracy and robustness of our method by comparing our results to those of other surveys such as SPY and SDSS. Finally, we re-visit the ZZ Ceti instability strip and examine how the determination of its empirical boundaries are affected by the latest line profile calculations.

3.2 INTRODUCTION

For many years, the catalog of McCook & Sion (1999, hereafter MS99) was the most important reference in the white dwarf community including a total of 2249 spectroscopically identified white dwarf stars. Similarly, the now regularly updated online incarnation[2] is used by white dwarf researchers on a daily basis and has grown to include nearly 13,000 entries as this publication goes to press. This is due in large part to the increasingly large number of

[2]http://www.astronomy.villanova.edu/WDCatalog/index.html

white dwarfs discovered in the Sloan Digital Sky Survey (SDSS). The SDSS's huge database of newly discovered white dwarfs has permitted the discovery of previously unknown types of white dwarfs like the carbon atmosphere "Hot DQ" stars (Dufour et al. 2008), white dwarfs with gaseous disks (Gänsicke et al. 2008), and even white dwarfs with oxygen dominated atmospheres (Gänsicke et al. 2010). However, the fact remains that most of the SDSS data lack the necessary signal-to-noise ratio (S/N) to measure accurately the atmospheric parameters for each star (Gianninas et al. 2005). This is largely due to the rather faint white dwarfs observed by the SDSS and the practice of having a set exposure time for every field. Consequently, the fainter the star, the lower the S/N of the data. On the other hand, white dwarfs from MS99 are comparatively bright, especially if we restrict ourselves to stars with $V \leq 17.5$. Historically, many of the white dwarfs from MS99 have not been particularly well studied despite their relative brightness, which makes it easier to obtain high S/N spectroscopic observations. Indeed, many of these white dwarfs have only a spectral classification, based on photographic spectra, without any further analysis ever having been performed, let alone with modern CCD spectroscopy. Therefore, we believe it is both important and worthwhile to study these stars, the more so that it is much more feasible to conduct follow-up observations (i.e. high resolution spectroscopy, high-speed photometry, etc.) for objects of interest, if they are bright.

Indeed, some of the early results from our survey have already allowed us to make a few discoveries of our own. The most notable of these is likely the discovery of the unique nature of GD 362, originally reported as a highly metallic and massive DAZ white dwarf (Gianninas et al. 2004), it was later discovered that the main atmospheric constituent is helium (Zuckerman et al. 2007). Even more important was the discovery of an infrared excess due to the presence of a circumstellar debris disk (Becklin et al. 2005; Kilic et al. 2005) around this star. This lone discovery essentially opened the door to a whole new area of white dwarf research with many groups launching observational campaigns with the specific goal of discovering debris disks around other cool, metal-enriched white dwarfs. We have also successfully used our survey to refine the empirical determination of the boundaries of the ZZ Ceti instability strip and confirm its purity (Gianninas et al. 2005). We were thus able to predict the variability of several new ZZ Ceti pulsators, while also confirming the

non-variability of other DA white dwarfs near the ZZ Ceti instability strip (Gianninas et al. 2006).

Ours is not the only survey to have recently looked at a substantial number of bright white dwarfs. The ESO SN Ia Progenitor Survey (SPY, Koester et al. 2001) also observed about 800 bright white dwarfs, of which many were selected from MS99. It is not surprising then that there is a rather large overlap between the SPY sample and our own. However, in the case of SPY, the aim of the survey was to obtain multi-epoch, high resolution spectra in order to detect the radial velocity variations of double-degenerate binary systems. These could then lead to the identification of possible SN Ia progenitors, which were ultimately what they were looking to find. Results of the analysis of the DA white dwarfs from SPY are summarized in Koester et al. (2009). Finley et al. (1997) also presented an analysis of 174 hot ($T_{\rm eff} > 25{,}000$ K) DA white dwarfs selected from MS99 as well as the *ROSAT* (Pounds et al. 1993) and *EUVE* (Bowyer et al. 1994) surveys. Similarly, Marsh et al. (1997a,b) and Vennes et al. (1996, 1997, 1998) also presented analyses of DA white dwarfs selected from *ROSAT* and *EUVE* while Vennes et al. (2002) analyzed over 200 DA white dwarfs discovered in the 2dF QSO Redshift Survey (Smith et al. 2005). Other important studies of large samples of DA white dwarfs include the works of Liebert et al. (2005, hereafter LBH05) and Limoges & Bergeron (2010) who looked at the complete samples from the Palomar-Green (Green et al. 1986, PG) and Kiso (Noguchi et al. 1980; Kondo et al. 1984, KUV) surveys, respectively. These studies defined statistically significant samples of white dwarfs in an effort to derive the luminosity function of the disk white dwarf population. Finally, an analysis of over 7000 DA white dwarfs from the SDSS Data Release 4 (DR4) was presented in Kepler et al. (2007) with particular attention to the mass distribution of the sample. Tremblay et al. (2011) performed a new analysis of the aforementioned sample of DA white dwarfs from the SDSS and showed that for the analysis of ensemble properties, such as the mass distribution, the SDSS data are reliable down to S/N $\sim$ 15. However, the precise determination of the atmospheric parameters for individual stars remains problematic with such low S/N observations, as in the case of the ZZ Ceti instability strip (Gianninas et al. 2005).

In an effort to derive the most accurate atmospheric parameters possible, we also want

to incorporate all available improvements to the model atmospheres that we use to study these white dwarfs. With that in mind, we will be using models that include the improved theoretical calculations of the Balmer-line profiles, including non-ideal effects, by Tremblay & Bergeron (2009, hereafter TB09). Seeing as our spectroscopic technique relies on a detailed comparison between observed and theoretical Balmer lines, it is crucial that we employ the most accurate and up to date models at our disposal. In the same vein, two sub-categories of white dwarfs contained within our sample required particular attention in order to obtain accurate atmospheric parameters. First, there are the hot DA and DAO stars exhibiting the so-called Balmer-line problem. A comprehensive and detailed analysis of these stars has already been presented by Gianninas et al. (2010) and those results will be included in our analysis. Second, we have DA+dM binary systems whose Balmer-line profiles are contaminated, to varying degrees, by the spectrum of the dM secondary.

As a whole, we wish to present a detailed analysis of all the hydrogen-line white dwarfs from MS99 for which we have obtained optical spectra. In Section 2 we will present the spectroscopic content of our survey. Section 3 will deal with the model atmospheres used for the analysis of our data, and we will present in Section 4 the spectroscopic analysis of our entire sample, including particular analyses for certain subsets of white dwarfs. Subsequently, in Section 5 we will examine the global properties of our sample including the mass distribution and the mass distribution as a function of effective temperature, and how these compare to other large surveys. We will then revisit the PG luminosity function, and the empirical determination of the ZZ Ceti instability strip. Finally, we end with some concluding remarks in Section 6.

3.3 SPECTROSCOPIC CONTENT

The goal of our survey was to observe all the white dwarfs listed as DA in MS99, including all subtypes (DAB, DAH/P, DAO, DAZ, DA+dM), with a visual magnitude $V \leq 17.5$. Along the way, several DA stars were added to the sample through various other projects and collaborations the Montreal group was involved in. In the final reckoning, we had defined a sample of 1495 white dwarfs for which we wanted to obtain high S/N optical spectra. After nearly 7 years of observing, and a total of 18 observing runs in both the northern and

southern hemispheres, we succeeded in securing spectra for 1339 of the 1495 white dwarfs we had selected. This translates to an 90% completion rate. Indeed, the majority of the missing spectra are those of the least bright stars in our sample and objects observable only from the southern hemisphere where we were unable to secure additional telescope time.

In all, 704 spectra were obtained specifically for the purposes of this survey since it began in 2003. Of those 704 spectra, 546 were obtained between 2003 September and 2010 January at Steward Observatory's 2.3 m telescope equipped with the Boller & Chivens spectrograph. The $4\farcs5$ slit together with the 600 line mm^{-1} grating blazed at 3568 Å in first order provide a spectral coverage from about 3000 to 5250 Å at a resolution of $\sim$ 6 Å (FWHM). An additional 18 spectra were obtained in 2006 April and 2007 January at the 1.6 m telescope of the Observatoire du Mont-Mégantic where the 600 line mm^{-1} grating provided a spectral coverage from about 3100 to 7500 Å at a similar resolution. Furthermore, a total of 140 spectra from the southern hemisphere were secured during the course of two observing runs in 2007 March and 2007 October, respectively. First, 84 spectra were obtained at ESO's 3.6 m telescope at La Silla, Chile with the ESO Faint Object Spectrograph and Camera (v.2) (EFOSC2). The #7 grism and a $1\farcs0$ slit provided a spectral coverage from about 3300 to 5200 Å with a resolution of $\sim$ 6 Å (FWHM). The remaining 56 southern spectra were obtained at Carnegie Observatories' 2.5 m Irénée du Pont Telescope at Las Campanas, Chile with the Boller & Chivens spectrograph. The $1\farcs5$ slit with the 600 line mm^{-1} grating blazed at 5000 Å provided a spectral coverage from about 3500 to 6600 Å at a slightly better resolution of $\sim$ 3 Å (FWHM). There are also 169 spectra that were kindly provided by C. Moran (1999, private communication). Finally, the sources of the spectra for 0950+139, and 1136+667 (two DAO white dwarfs) are described in Gianninas et al. (2010). For the remaining 464 stars, we have used archival spectra that have been obtained throughout the years by the Montréal group during the course of various other projects (e.g. Bergeron et al. 1992, LBH05). These were acquired at Steward Observatory's 2.3 m telescope with the same instrument and setup described above.

We show in Figure 3.1 the final distribution of visual magnitudes V for our sample of white

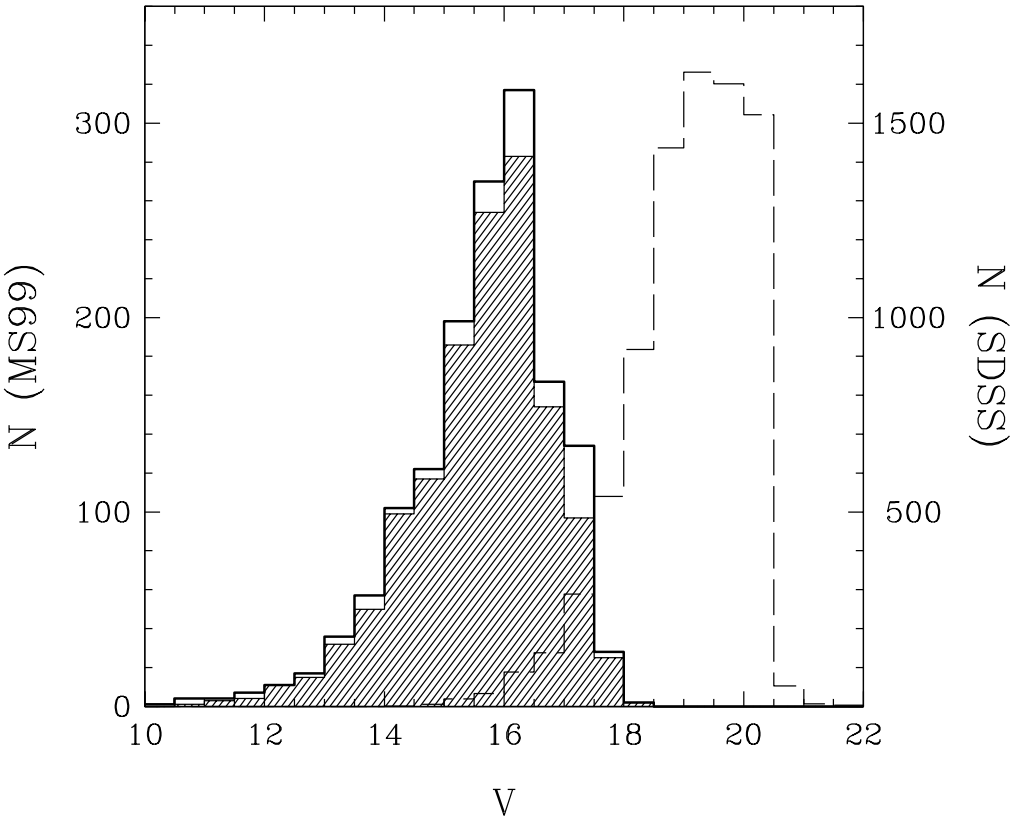

FIGURE 3.1 – Distribution of visual magnitudes V for our sample selected from MS99 (bold histogram) and for the white dwarfs for which we have obtained optical spectra (hatched histogram). In comparison, the distribution for the SDSS sample as of DR4 (Eisenstein et al. 2006) is also shown (dashed histogram). Note that the scale is different for the McCook & Sion sample (left) and the SDSS sample (right) and that we use the SDSS g magnitudes as equivalent to V.

dwarfs (see Figure 1 of Gianninas et al. 2009, as a comparison)[3]. We note that 10 white dwarfs have no magnitude listed in the literature. The bold histogram shows the distribution for the entire sample while the hatched histogram represents the stars for which we have successfully obtained spectra. We see that the distribution peaks near $V = 16.5$ and that the majority of our stars have $V \leq 16.5$. We contrast this result with the sample of DA white dwarfs from the SDSS DR4 (Eisenstein et al. 2006). Although the SDSS sample contains over six times more white dwarfs, the vast majority of these have $20.5 \geq g \geq 18.5$, which makes for a much fainter sample overall. The distribution of S/N for our entire sample of 1339 optical spectra is displayed in Figure 3.2. The S/N is determined by an estimate of the rms noise per pixel in

[3]Please refer to Annexe D.

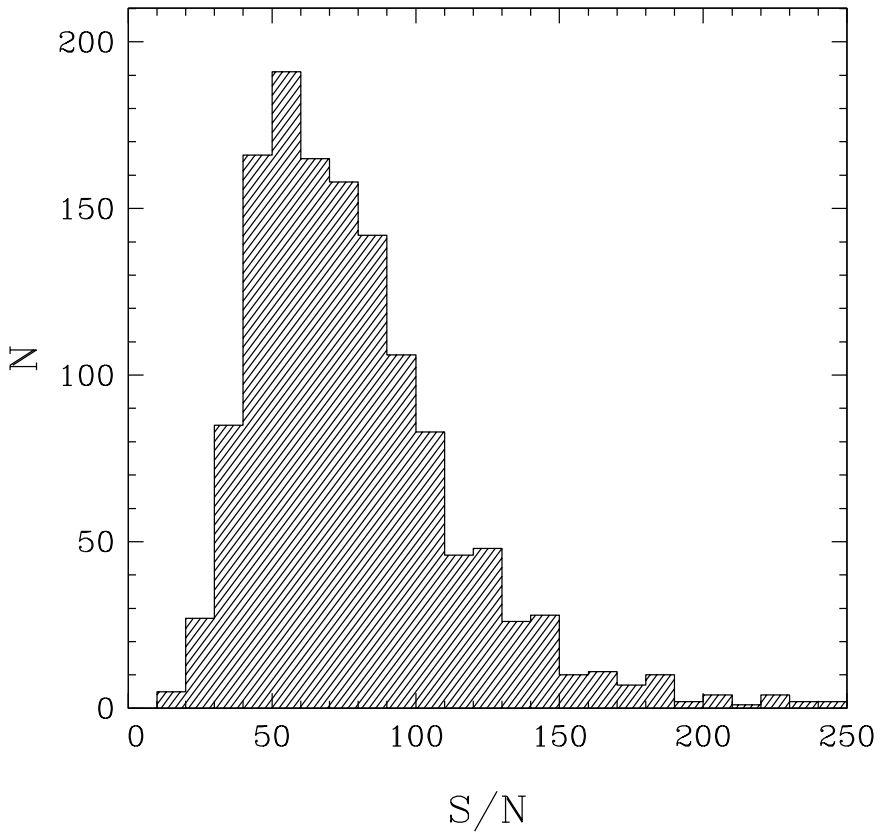

FIGURE 3.2 – Distribution of S/N for all the stars in our spectroscopic survey. The distribution peaks at the $50-60$ bin and more than 50% of the spectra have S/N ≥ 70.

the continuum between ~ 4500 and ~ 4700 Å. Over 52% of our sample have S/N > 70 and almost 80% above 50. Only the faintest objects in our sample have S/N that is significantly lower. As such, we have achieved our goal of obtaining high quality data for the majority of the white dwarfs in our survey.

As previously stated, many of these stars have never been studied using modern CCD spectroscopy. Consequently, it is not surprising to discover that many of the spectral classifications are erroneous; many of the objects listed in MS99 are not even white dwarfs. We list in Table 3.1 67 objects that are incorrectly classified as white dwarfs in MS99. We provide the spectral classification from MS99 as well as our revised spectroscopic classification for each object along with the appropriate references. Some of these have been known to be misclassified for some time but are still listed as white dwarfs in the online version of MS99. Of the 67 stars listed in Table 3.1, 20 were recently reported as being misclassified objects in Limoges

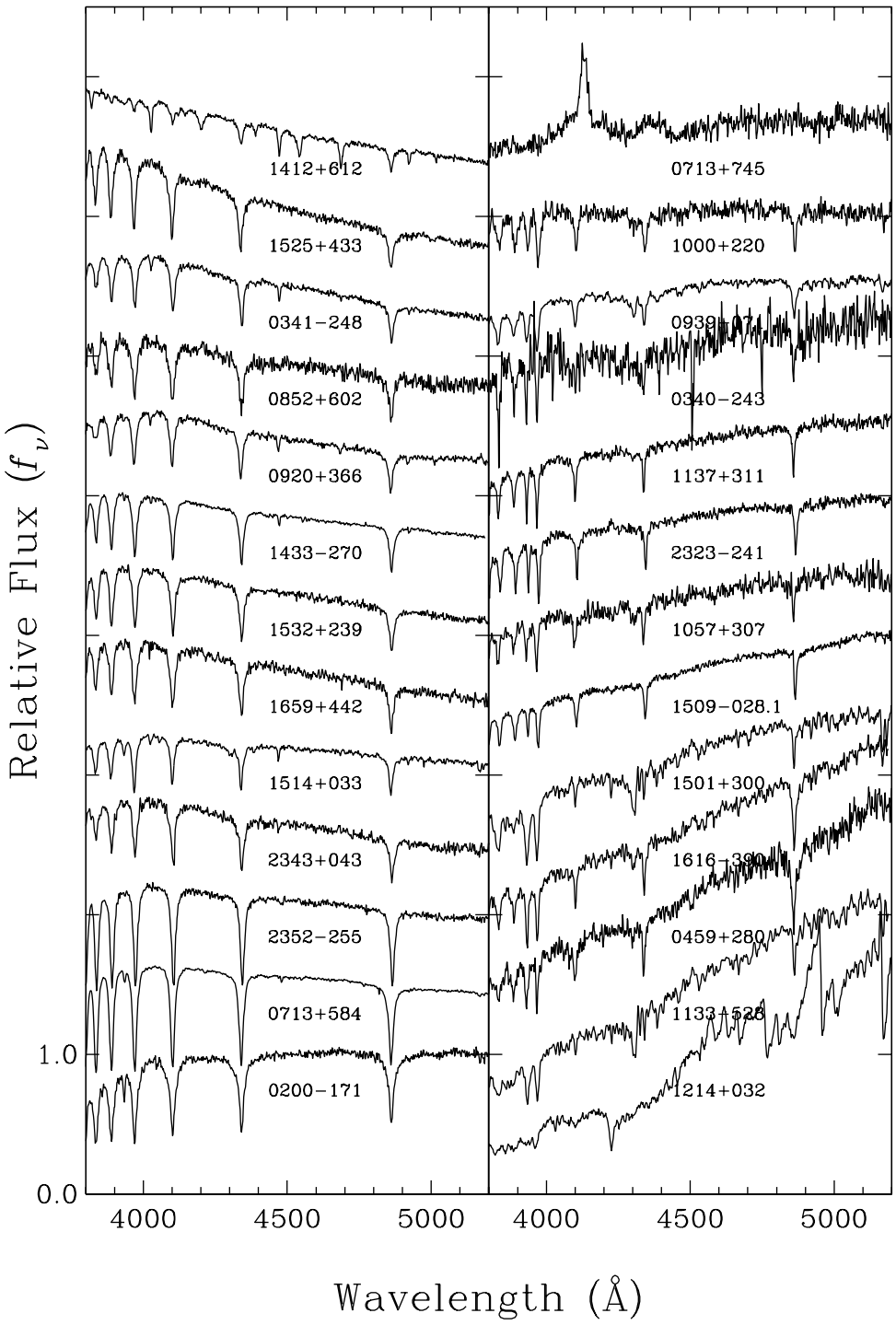

FIGURE 3.3 – Optical spectra of stars misclassified as DA white dwarfs in MS99 and reported for the first time in this work. The objects are approximately ordered as a function of their slope from upper left to bottom right. The spectra have been normalized to a continuum set to unity and vertically shifted for clarity. 0713+745 (right panel, first object at the top) is a quasar.

TABLE 3.1 – Misclassified Objects

WD	Name	ST (MS99)	ST (This Work)	Notes
0021−234	Ton S 155	DAWK	sdB	1
0031−274	Ton S 163	DA1	sdB	1
0107−342	GD 687	DA3	sdB	1
0109−264	Ton S 201	DA1	sdB	1
0113−243	GD 693	DA6	sdB	2
0154−071	PB 8949	DA1	sdB	1
0200−171	G272-B5B	DA	sdB	3
0222+314	KUV 02222+3124	DA	sdB	2
0240+341	KUV 02409+3407	DA	MS(dF)	2
0258+184	PG 0258+184	DA	sdB	1
0340−243	Ton S 372	DAWK	MS(dF)	3
0341−248	Ton S 374	DA	sdB	3
0459+280	CTI 045934.1+280335	DA	MS(dF)	3
0509+168	KUV 05097+1649	DA	MS(dF)	4
0510+163	KUV 05101+1619	DA	MS(dF)	2
0526+271	KUV 05260+2711	DA	sdB	2
0529+261	KUV 05296+2610	DA	sdB	2
0627+299	KUV 06274+2958	DA	sdB	2
0628+314	KUV 06289+3126	DA	sdB	2
0713+584	GD 294	DA4	sdB	3
0713+745	Mrk 380	DA	QSO	3
0720+304	SA 51-822A	DA2	sdB	5
0752+412	KUV 07528+4113	DA?	sdB	2
0852+602	PG 0852+602	DA2	sdB	3
0920+366	CBS 98	DA1	sdB	3
0927+388	KUV 09272+3854	DA	sdB	2
0930+376	KUV 09306+3740	DA	sdB	2
0932+396	KUV 09327+3937	DA	sdB	2
0937+395	KUV 09372+3933	DA	sdB	2
0939+071	PG 0939+072	DA7	MS(dF)	3
0943+371	KUV 09436+3709	DA	sdB	2
0944−090	GD 104	DA1	sdO	6
0946+381	KUV 09467+3809	DA	sdB	2
1000+220	Ton 1145	DA6	MS(dF)	3
1008−179	EC 10081−1757	DA1	sdO	7
1036+433	Feige 34	DA	sdO	8
1057+307	CSO 64	DA5	MS(dF)	3
1121+145	PG 1121+145	DA1	sdB	9
1133−528	BPM 21065	DA5	MS(dK)	3
1137+311	CSO 105	DA5	MS(dF)	3
1207−032	PG 1207−033	DA4	sdB	1
1214+032	LP 554-63	DA	dM	3
1256+286	KUV 12562+2839	DA?	sdB	2
1304+313	PB 3322	DA	sdB	2
1412+612	HS 1412+6115	DAH	sdO	3
1412−049	PG 1412−049	DA	DA+dM	10
1433−270	BPS CS 22874-57	DA	sdB	3
1501+300	...	DA	MS(dF)	3
1509−028.1	LP 622-13	DA:	MS(dF)	3

TABLE 1.1 – Continued

WD	Name	ST (MS99)	ST (This Work)	Notes
1514+033	PG 1514+034	DAWK	sdB	3
1524+438	CBS 246	DABZ4	sdO	11
1525+433	GD 344	DA	sdB	3
1532+239	Ton 241	DA	sdB	3
1544+009	LB 898	DA1	sdO	12
1603+175	KUV 16032+1735	DAH?	sdO+dK	2
1611+390	KUV 16118+3906	DA	sdB	2
1616−390	Ton 264	DA4	MS(dF)	3
1659+442	PG 1659+442	DA	sdB	3
2122+157	PG 2122+157	DA	sdB	1
2148+286	BD+28 4211	DA	sdO	13
2204+071	PG 2204+071	DA	sdOB	10
2309+258	KUV 23099+2548	DA	sdB	2
2323−241	G275-B16A	DA	MS(dF)	3
2329−291	Ton S 102	DAWK	sdB	1
2333−002	PB 5462	DA2	sdO	14
2343+043	PB 5529	DA	sdB	3
2352−255	G275-B17B	DA	sdB	3

References. – (1) Lisker et al. 2005; (2) Limoges & Bergeron 2010; (3) this work; (4) Kawka et al. 2004; (5) Finley et al. 1997; (6) Stroeer et al. 2007; (7) Christlieb et al. 2001; (8) Farihi et al. 2005; (9) Green et al. 1986; (10) LBH05; (11) Eisenstein et al. 2006; (12) Catalán et al. 2008; (13) Kilkenny et al. 1988; (14) Hügelemeyer et al. 2006.

& Bergeron (2010) and we refer the reader to Figure 1 of Limoges et al. for the spectra of those stars. In this paper, we report the erroneous classification of an additional 26 objects for the first time. The spectra of these 26 white dwarfs are displayed in Figure 3.3. Many of these are sdB stars that show strong Balmer lines that are not as broad as those of their white dwarf cousins due to their lower surface gravity. However, it is not too hard to see how these objects could easily have been mistaken as white dwarfs, especially using photographic spectra. On the other hand, it is harder to explain how several main sequence stars were just as easily misclassified. Indeed, even a quasar (0713+745) has found its way into MS99. Furthermore, MS99 still lists stars like BD+28 4211 (2148+286) and Feige 34 (1036+433), popular spectrophotometric standards that are known hot subdwarfs. In addition to the misclassified objects, several stars had two separate entries in MS99 under two different names. Although virtually all of these have since been corrected, we report here that at least two still remain. The entries for 0525+271 and 0526+271 refer to the same star, which also happens to be one of the misclassified objects in Table 3.1, and 1100+604 and 1104+602 are also one

in the same. We also note that 1959+059 is GD 226, not GD 266 as listed in MS99 (Giclas et al. 1965).

In Figure 3.4 we show a series of representative DA spectra in order of decreasing effective temperature, all of which have $75 \geq \mathrm{S/N} \geq 65$. We have chosen this range of S/N values to emphasize the mean quality of our data, which is quite high overall. We refer the reader to Gianninas et al. (2010, see Figure 1) for a detailed presentation of the DAO white dwarfs contained within our sample. Spectra for the 25 magnetic white dwarfs in our sample are displayed in Figure 3.5 as a function of their slope. In many of these we see the classical Zeeman splitting of the hydrogen lines for somewhat lower magnetic field strengths on the order of $\sim$1 to $\sim$10 MG. On the other hand, stars with much stronger fields, on the order of 10's to 100's of MG, are rendered almost unrecognizable as DA stars. Of note in Figure 3.5 are possibly four new magnetic white dwarfs. With regards to 1018−103 and 1610+330, there is little doubt as to their magnetic nature. On the other hand, the cases of 0321−026 and 0350+098 are more problematic. In the case of 0321−026, the Balmer lines predicted by our best fit model are too deep and we obtain a somewhat high $\log g$ value (see Section 3.5.6). This is often the case with magnetic white dwarfs as the Zeeman splitting broadens the observed line profiles leading to a higher $\log g$ value. We suggest that 0321−026 might harbor a weak magnetic field and a spectrum with higher S/N could reveal weak Zeeman splitting such as that seen in 0637+477. Second, 0350+098 was detected by *ROSAT* (Fleming et al. 1996) and we therefore conclude that it must be a relatively hot star, and the slope would seem to corroborate that conclusion. Unfortunately, nothing else is known about this object. The absence of any spectral features could be an indication of a strong magnetic field that has completed diluted any absorption lines that would otherwise be present. Spectropolarimetric observations would be needed to confirm the magnetic nature of this star. We also note that three of the magnetic white dwarfs are members of double-degenerate binary systems. Namely, 0945+245 (LB 11146, Liebert et al. 1993), 1440+753 (RE J1440+750, Vennes et al. 1999), and 1506+229 (CBS 229, Gianninas et al. 2009).

Finally, in Figure 3.6 we display spectra for white dwarfs of other miscellaneous spectral types included in our sample. This includes five DAB stars, five DAZ white dwarfs, and eight

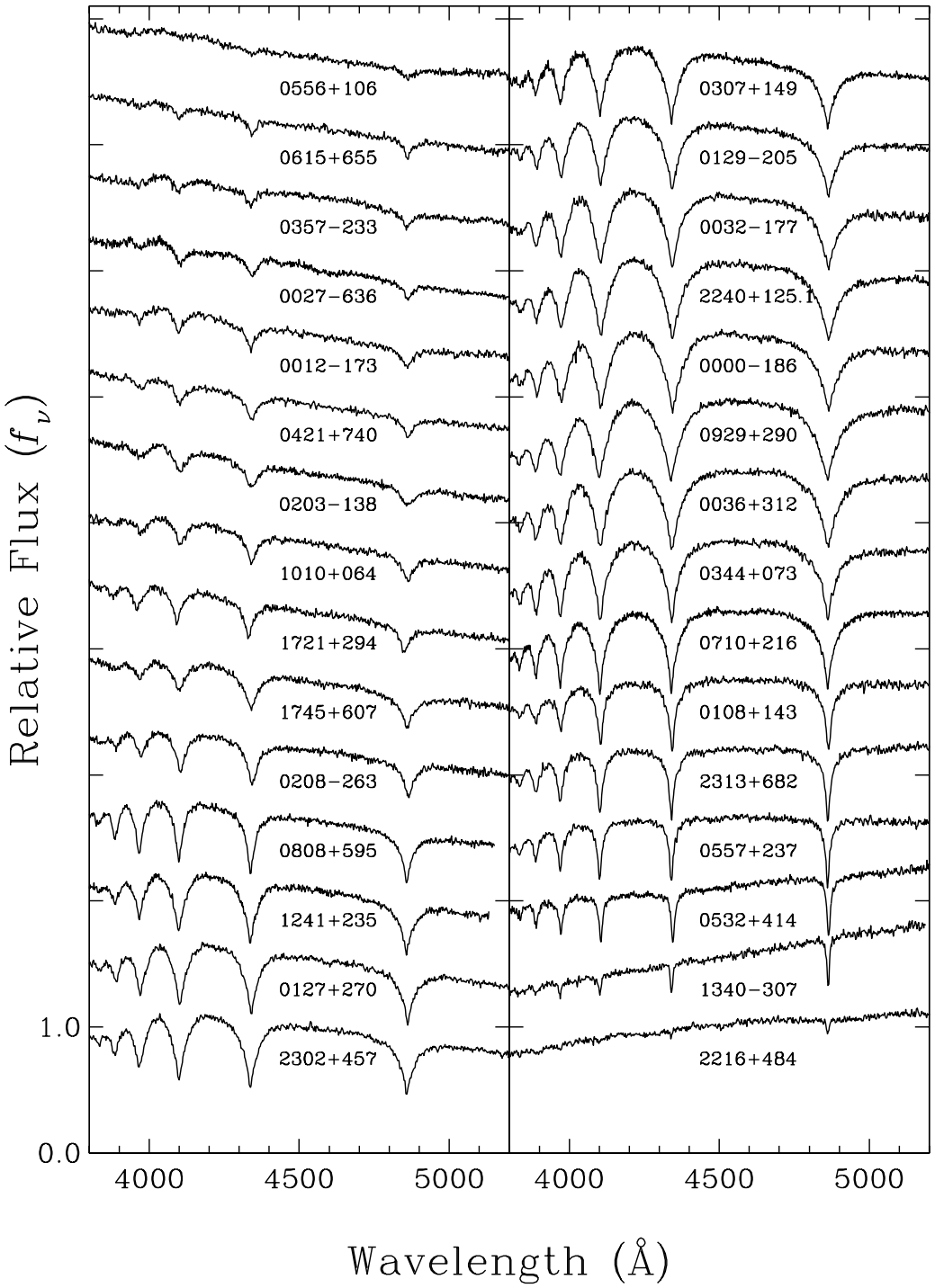

FIGURE 3.4 – Optical spectra for a subsample of the DA white dwarfs from ou survey of MS99. The spectra are normalized at 4500 Å and shifted vertically for clarity. The effective temperature decreases from upper left to bottom right. All the spectra have $75 \leq \mathrm{S/N} \leq 65$.

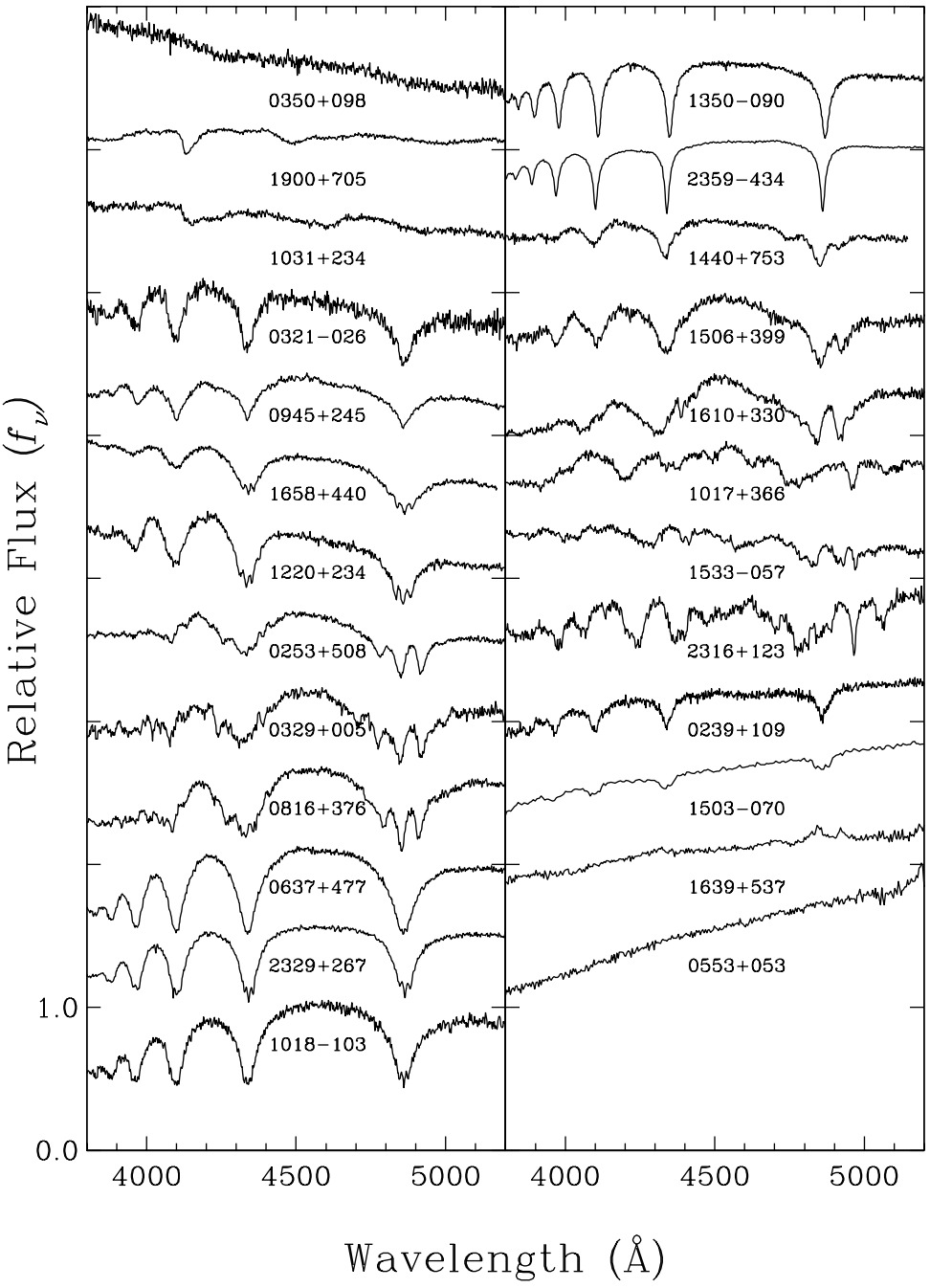

FIGURE 3.5 – Optical spectra for 25 magnetic (or suspected magnetic) DA white dwarfs from our survey of MS99. The objects are approximately ordered as a function of their slope from upper left to bottom right. The spectra are normalized at 4500 Å and shifted vertically for clarity.

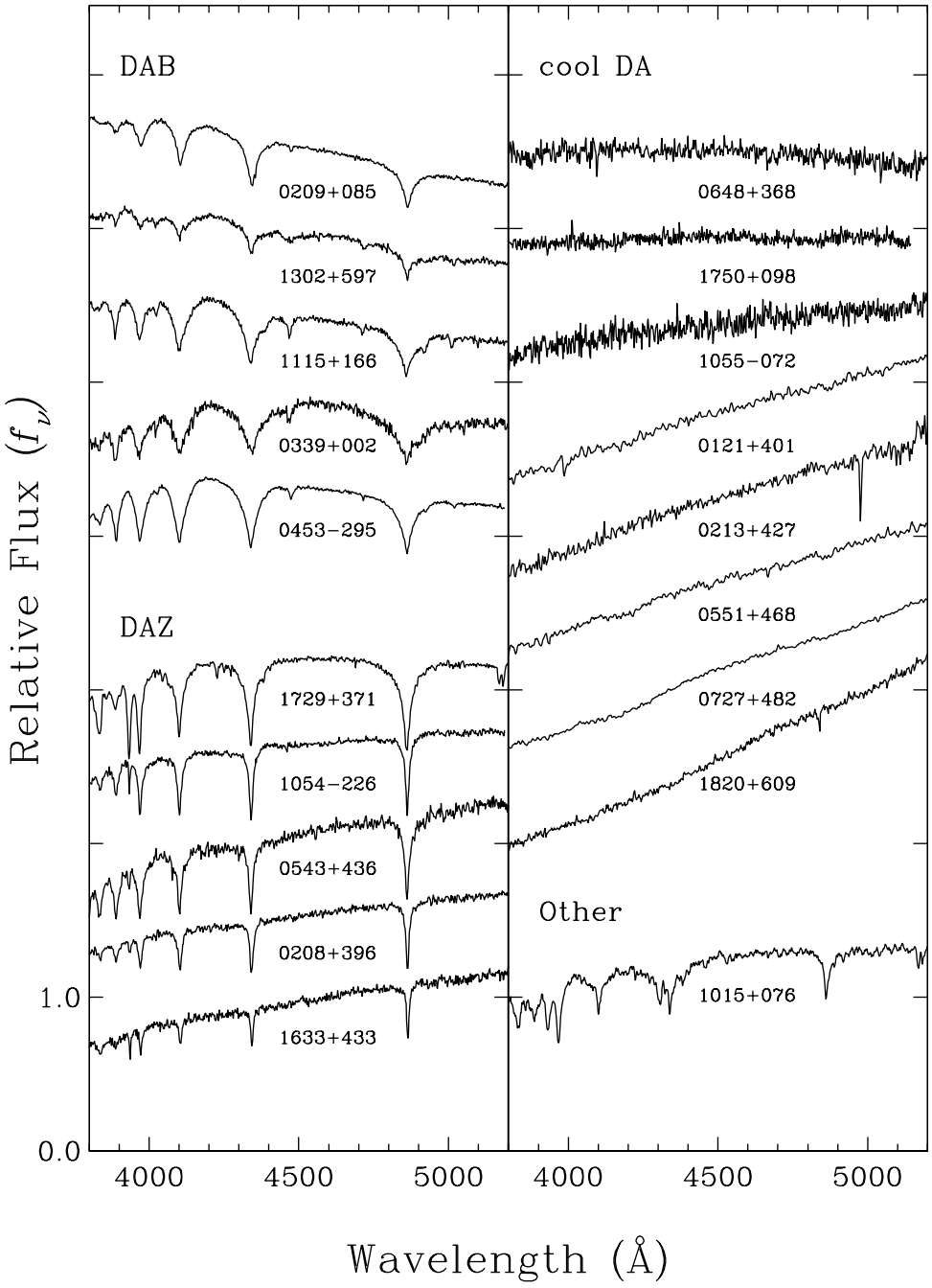

FIGURE 3.6 – Optical spectra for 19 white dwarfs from our survey of miscellaneous spectral types. The objects are approximately ordered as a function of their slope from upper left to bottom right. The spectra are normalized at 4600 Å and shifted vertically for clarity.

cool DA. Among the DAB white dwarfs we find HS 0209+0832 (0209+085) and GD 323 (1302+597), which have been shown to be spectroscopically variable (Heber et al. 1997; Pereira et al. 2005, respectively), while the other three DAB stars (0339+002, 0453−295, and 1115+166) are actually DA+DB binary systems (Limoges & Bergeron 2010; Wesemael et al. 1994; Bergeron & Liebert 2002, respectively). Regarding the DAZ white dwarfs, our sample includes the first DAZ ever discovered, G74-7 (0208+396, Lacombe et al. 1983) as well as GD 362 (1729+371, Gianninas et al. 2004). Although, as previously mentioned, GD 362 has since been shown to have a helium-dominated atmosphere (Zuckerman et al. 2007), a discovery made possible by the detection of a very faint helium line at 5877 Å. However, the dominant absorption lines in the spectrum, which define the spectral class of an object, remain the hydrogen and metal lines, as such the spectral type should at most be updated to DAZB. In addition, we report for the first time that 0543+436, and 1054−226 are also members of the DAZ class. In particular, 1054−226 was initially discovered by Subasavage et al. (2007) but their discovery spectrum lacked the necessary S/N to detect the H and K lines of calcium. In addition, there are eight white dwarfs whose spectra are completely devoid of absorption lines in the observed wavelength range. However, with the exception of 0648+368 and 1055−072, the other six cool DA stars have detections of Hα (Bergeron et al. 2001; Silvestri et al. 2001), hence their DA spectral type. We also note that 0727+482 is actually a double-degenerate system (Strand et al. 1976). Finally, we also include the peculiar spectrum obtained for 1015+076. It seems that 1015+076 is a DA white dwarf whose spectrum is completely dominated by an unresolved, background G dwarf (Farihi et al. 2005). Indeed, the SPY spectrum analyzed in Voss (2006) shows a perfectly normal DA white dwarf with $T_{\rm eff} \sim 25{,}600$ K and $\log g \sim 7.70$.

Our spectroscopic sample also contains a total of 47 DA+dM binary systems, all of which have been previously identified. In order to obtain accurate atmospheric parameters for the DA white dwarfs in these binary systems, we need to remove the contamination from the dM secondary. With that in mind, we have obtained follow-up spectra for all the DA+dM systems in our sample, with the exception of six (0208−153, 0309−275, 0419−487, 1106+316, 1541−381, 1717−345), covering a larger spectral range from 3500 to 7000 Å. These spectra were obtained at Steward Observatory's 2.3 m telescope using the same instrument and setup

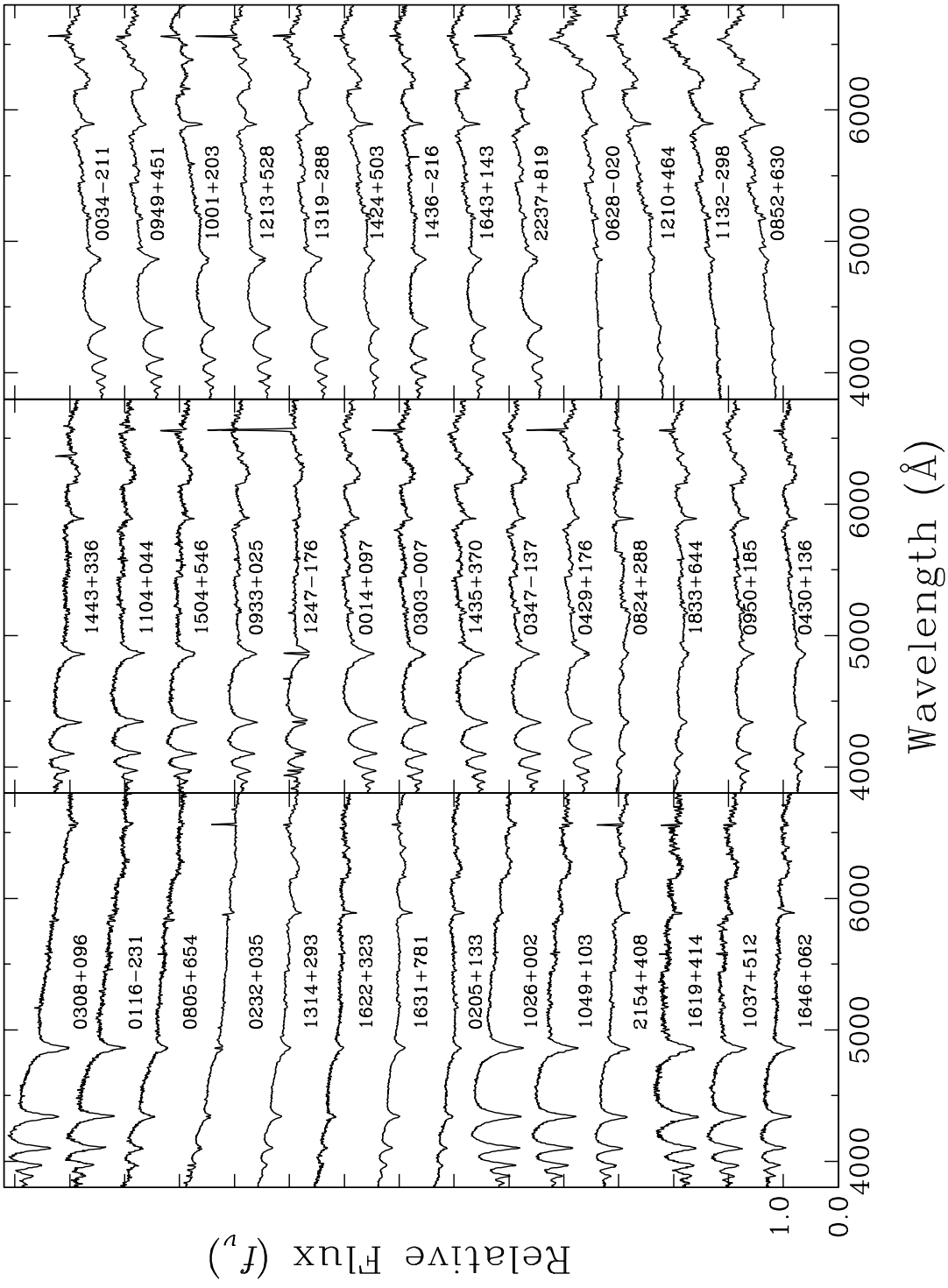

FIGURE 3.7 – Optical spectra for 41 DA+dM binary systems covering the range 3500–7000 Å. The spectra are normalized to unity at 6500 Å and shifted vertically for clarity.

TABLE 3.2 – Breakdown of Spectral Types

DA	DAO	DAZ	DAB	DAmag	DA+dM	cool DA	Total
1152	30	5	5	25	47	8	1272

as described above except that here we used the 400 line mm^{-1} grating blazed at 4800 Å to achieve the desired wavelength coverage. The one drawback was that the use of this particular grating degrades our spectral resolution to $\sim$ 9 Å (FWHM) from our usual $\sim$ 6 Å. However, this slightly reduced spectral resolution is still sufficient for our purposes. We present in Figure 3.7 what we will refer to as our *red* spectra for 41 of the 47 DA+dM binaries in our sample. These will be coupled with our usual optical spectra (3000 – 5250 Å), which we will call our *blue* spectra, for the analysis of the DA+dM systems. Several of the tell-tale features found in the spectra of DA+dM binaries can be seen in Figure 3.7. We see in these spectra how the contribution from the M dwarf becomes more significant at longer wavelengths. More specifically, we see the TiO absorption band near $\sim$ 4950 Å that produces the "kink" in the red wing of Hβ. We also note the presence of the strong Na D line near 5895 Å as well as emission, from the M dwarf, in the core of several Balmer lines, especially at Hα.

As a summary, we present in Table 3.2 a breakdown of the white dwarfs in our sample listing the number of stars in each spectral class.

3.4 MODEL ATMOSPHERES

3.4.1 Pure hydrogen atmosphere models

For the analysis of the vast majority of white dwarfs in our sample, we have employed model atmospheres and synthetic spectra appropriate for DA white dwarfs. These are described at length in LBH05 and references therein. Briefly, these are pure hydrogen, plane-parallel model atmospheres where non-local thermodynamic equilibrium (NLTE) effects are explicitly taken into account above $T_{\rm eff}$ = 20,000 K, and energy transport by convection is included in cooler models following the ML2/α = 0.8 prescription of the mixing-length theory (see Tremblay et

al. 2010). The one major upgrade from the models described in LBH05 is that we now use the new and improved Stark broadening profiles of TB09 that account for nonideal effects directly in the line profile calculation. However, since we will wish to compare our results with those of other large surveys, such as SPY, we have also fit our sample using models computed with the older broadening profiles of Lemke (1997), and consequently with the ML2/$\alpha = 0.6$ version of the mixing-length theory (Bergeron et al. 1995), since they were still in use at the time that the SPY analysis was performed. We can thus compare the independent results on a level playing field. Beyond that, performing our analysis with both sets of hydrogen line profiles will also allow us to explore the implications of these improved models on the analysis of DA white dwarfs.

3.4.2 Hydrogen atmosphere models with CNO

Although the pure hydrogen models described above are sufficient in most cases, some white dwarfs present unique challenges that require somewhat more elaborate models. This is the case with the hot DAO white dwarfs as well as the hot DA stars that exhibit the so-called Balmer-line problem (DA+BP), which manifests itself as an inability to fit all the Balmer lines simultaneously with consistent atmospheric parameters. Though the models used to properly fit the spectra of these stars are presented and described at length in Gianninas et al. (2010), for the benefit of the reader, we briefly explain them here. The above mentioned models have all been computed using the TLUSTY atmosphere code and the accompanying spectrum synthesis code SYNSPEC, both developed by Hubeny & Lanz (1995). The models are computed in NLTE and include carbon, nitrogen, and oxygen (CNO) at solar abundances (Asplund et al. 2005). As Werner (1996) demonstrated, the inclusion of CNO reduces the temperature in the upper layers of the atmosphere, which in turn produces deeper cores for the hydrogen Balmer lines, thus overcoming the Balmer-line problem. As clearly stated by Gianninas et al. (2010), CNO acts as a proxy for all metals that may be present in the atmosphere. As such, the inclusion of CNO at solar abundances should in no way be considered as a determination of the abundance of CNO in these stars. The model atmospheres used for the DAO and DA+BP stars are identical, save for the inclusion of helium in the DAO models

in order to reproduce the He II λ4686 line.

3.4.3 Helium atmosphere models

In Figure 3.6, we presented three DA+DB binary systems that are included in our sample. In order to properly fit the spectra of these stars, we will need to combine our pure hydrogen models with pure helium models. The helium models we have employed are based on the updated grid of white dwarf models described in TB09 in which the improved Stark profiles of neutral helium of Beauchamp et al. (1997) have been incorporated. These models are comparable to those described by Beauchamp (1995) and Beauchamp et al. (1996) (see also Bergeron et al. 2010), with the exception that at low temperatures ($T_{\rm eff} < 10{,}800$ K), the free-free absorption coefficient of the negative helium ion of John (1994) is now used. The models are in local thermodynamic equilibrium (LTE) and include convective energy transport within the mixing length theory. As in the analysis of Beauchamp et al. (1999), the parametrization described as ML2/$\alpha = 1.25$ is implemented.

3.5 SPECTROSCOPIC ANALYSIS

3.5.1 Fitting technique

The method used for fitting the observations relies on the so-called spectroscopic technique developed by Bergeron et al. (1992), which has been refined by Bergeron et al. (1995) and more recently by LBH05, and includes the Balmer lines from Hβ to H8. The first step is to normalize the flux from an individual line, in both observed and model spectra, to a continuum set to unity at a fixed distance from the line center. The comparison with model spectra, which are convolved with the appropriate Gaussian instrumental profile (3, 6, 9, and 12 Å), is then carried out in terms of these line shapes only. The most sensitive aspect of this fitting technique is to define the continuum of the observed spectra. The approach is slightly different depending on the temperature range in question. For stars in the interval $16{,}000 \gtrsim T_{\rm eff} \gtrsim 9000$ K, where the Balmer lines are at their strongest, the normalization procedure involves the use of several pseudo-Gaussian profiles (Bergeron et al. 1995, and references therein). This procedure is quite

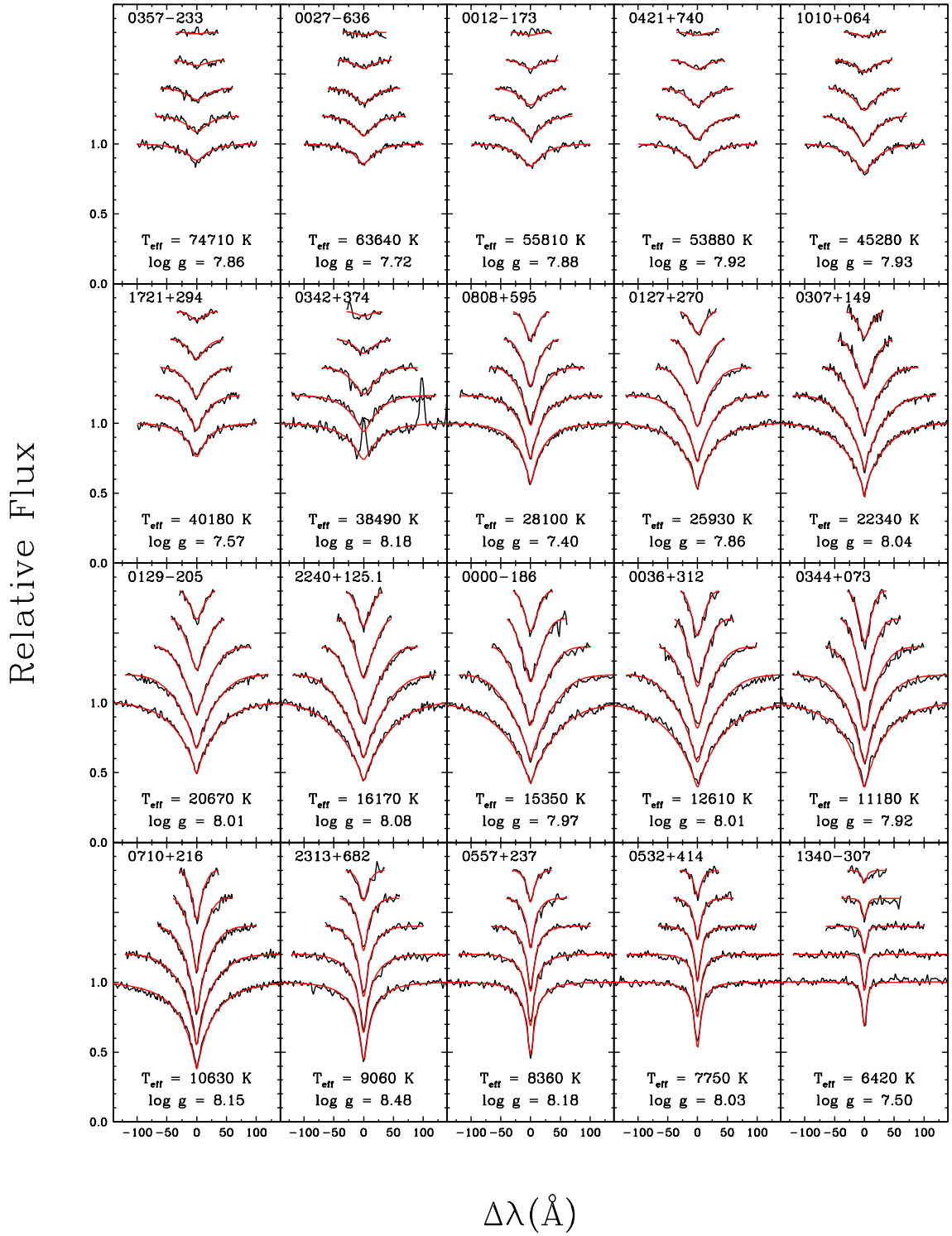

FIGURE 3.8 – Model fits (red) to the individual Balmer line profiles (black) of a sample of DA white dwarfs taken from Figure 3.4 (with the exception of 0342+374)in order of decreasing effective temperature. The lines range from Hβ (bottom) to H8 (top), each offset by a factor of 0.2. The best-fit values of $T_{\rm eff}$ and $\log g$ are indicated at the bottom of each panel.

reliable as the sum of the pseudo-Gaussian profiles represents a good approximation to the observed Balmer lines. Outside of this temperature range, the method becomes more unstable as the continuum between the Balmer lines becomes essentially linear. Consequently, for stars with $T_{\rm eff} > 16{,}000$ K and $T_{\rm eff} < 9000$ K, we rely on our synthetic spectra to reproduce the observed spectrum, including a wavelength shift, a zero point, as well as several order terms in λ (up to λ^6) using the nonlinear least-squares method of Levenberg-Marquardt (Press et al. 1986). The normal points are then fixed at the points defined by this smooth model fit. Note that the values of $T_{\rm eff}$ and $\log g$ at this stage are meaningless since too many fitting parameters are used, and the model just serves as a smooth fitting function to define the continuum of the observed spectrum. Once the lines are normalized to a continuum set to unity, we use our grid of model spectra to determine $T_{\rm eff}$ and $\log g$ in terms of these normalized profiles only. Our minimization technique again relies on the nonlinear least-squares method of Levenberg-Marquardt, which is based on a steepest descent method. Sample fits of 20 DA white dwarfs, covering almost the entire temperature range of our sample are displayed in Figure 3.8[4]. We see that the combination of high S/N spectra with the procedures described above allow us to achieve a proper normalization in each case. Hence, we are able to obtain an excellent agreement between the observed and predicted line profiles for nearly every star. The spectrum of one star (0342+374, see Figure 3.8) features emission lines from its associated planetary nebula. These emission lines can interfere with our normalization procedure but also with our fitting technique and so we simply exclude the affected spectral ranges from both the normalization and fitting procedure.

3.5.2 Effects of new Stark profile calculations

As we have mentioned, in this study we will be passing from the use of the old Lemke (1997) profiles to the new TB09 Stark broadening profiles that include nonideal effects directly in the line profile calculation. In doing so, it is important to understand what effects these new profiles will have on our atmospheric parameter determinations. TB09 explored some of these differences (see their Figure 12) using the PG sample of LBH05, but this limited them

[4]Please refer to Annexe B for the fits to all the remaining DA white dwarfs.

to a particular range of $T_{\rm eff}$ whereas we can examine the effects along virtually the entire white dwarf cooling sequence.

In Figure 3.9, we present the comparison between the atmospheric parameters measured using the older Lemke (1997) and the new TB09 Stark profiles for the 1132 DA stars in our sample. In the lower panel, we see that the correlation between the old and new values of $T_{\rm eff}$ is very tight although the overall trend is to slightly higher temperatures. This effect is somewhat more evident at higher $T_{\rm eff}$. In the upper panel of Figure 3.9, we compare the old and new values of surface gravity. Unlike with the values of $T_{\rm eff}$ we note here a much more obvious shift toward higher measurements of $\log g$ when using the new TB09 Stark broadening profiles. These results are consistent with those presented in TB09.

In Figure 3.10 we examine how these differences in the measured atmospheric parameters translate to the determination of the mass distribution as a function of $T_{\rm eff}$. Using the old profiles, we see in the top panel of Figure 3.10 that besides the high-$\log g$ problem at lower temperatures (Tremblay et al. 2010, and Section 3.6.5 below) the mass distribution dips near 13,000 K. On the other hand, the new profiles seem to even out the mass distribution with the bulk of the stars showing masses between 0.55 $M_{\odot}$ and 0.7 $M_{\odot}$ before the high-$\log g$ problem takes hold at lower $T_{\rm eff}$. As such, the new profiles permit an improved determination of the mass distribution as a function of $T_{\rm eff}$ over the older models that employ Lemke's Stark broadening profiles. Specifically, the TB09 profiles produce a relatively constant mass distribution down to about 13,000 K where the high-$\log g$ problem begins to manifest itself.

In the following sections we will focus on the spectroscopic analysis of all the objects and systems that require particular attention. These include white dwarfs of spectral types DAB, DAZ, DA+dM binary systems, magnetic white dwarfs, and a selection of other unique objects that demanded a more detailed analysis. The motivation here is to ensure that we determine the most accurate atmospheric parameters possible for each star. With that in mind, we also note that from this point forward, we will be using the new Stark profiles of TB09 exclusively.

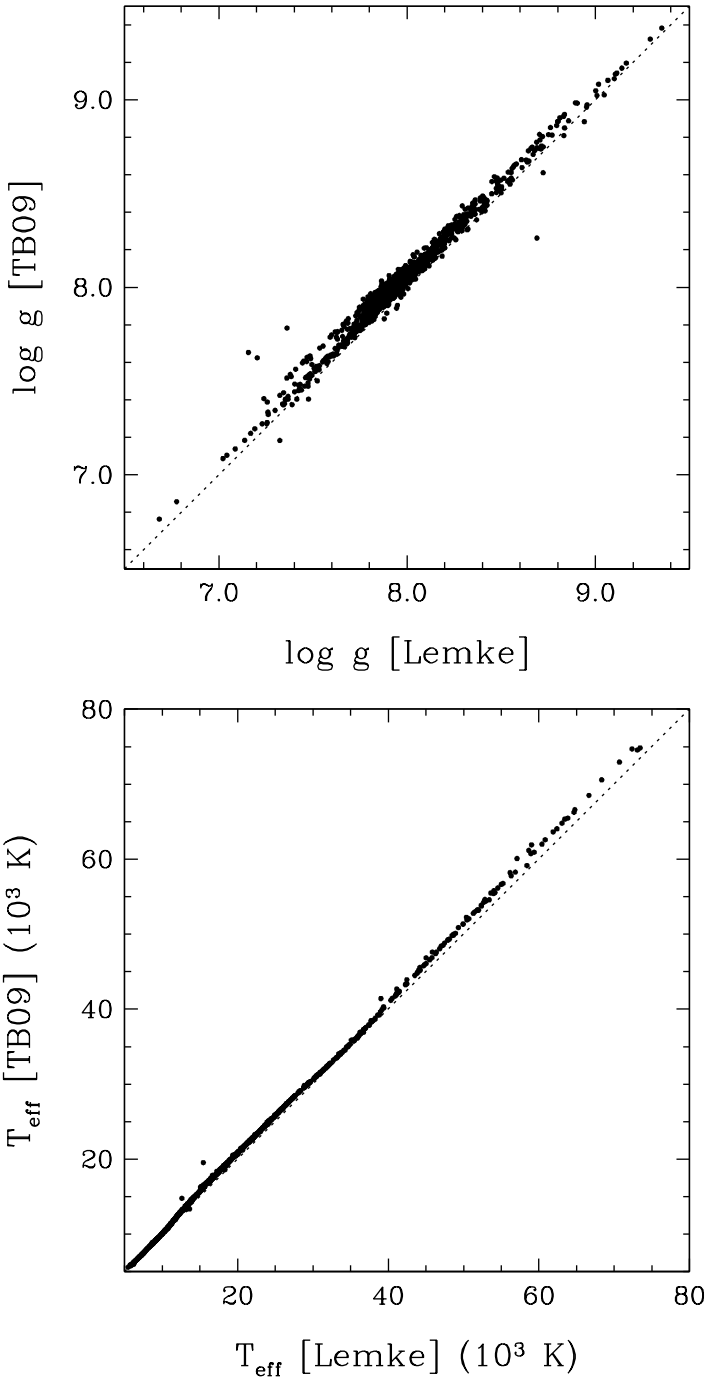

FIGURE 3.9 – Comparison of $\log g$ (top) and $T_{\rm eff}$ (bottom) values derived from fits using the improved models of TB09 and the VCS profiles of Lemke (1997) for 1132 DA white dwarfs. The dotted lines represent the 1:1 correlation.

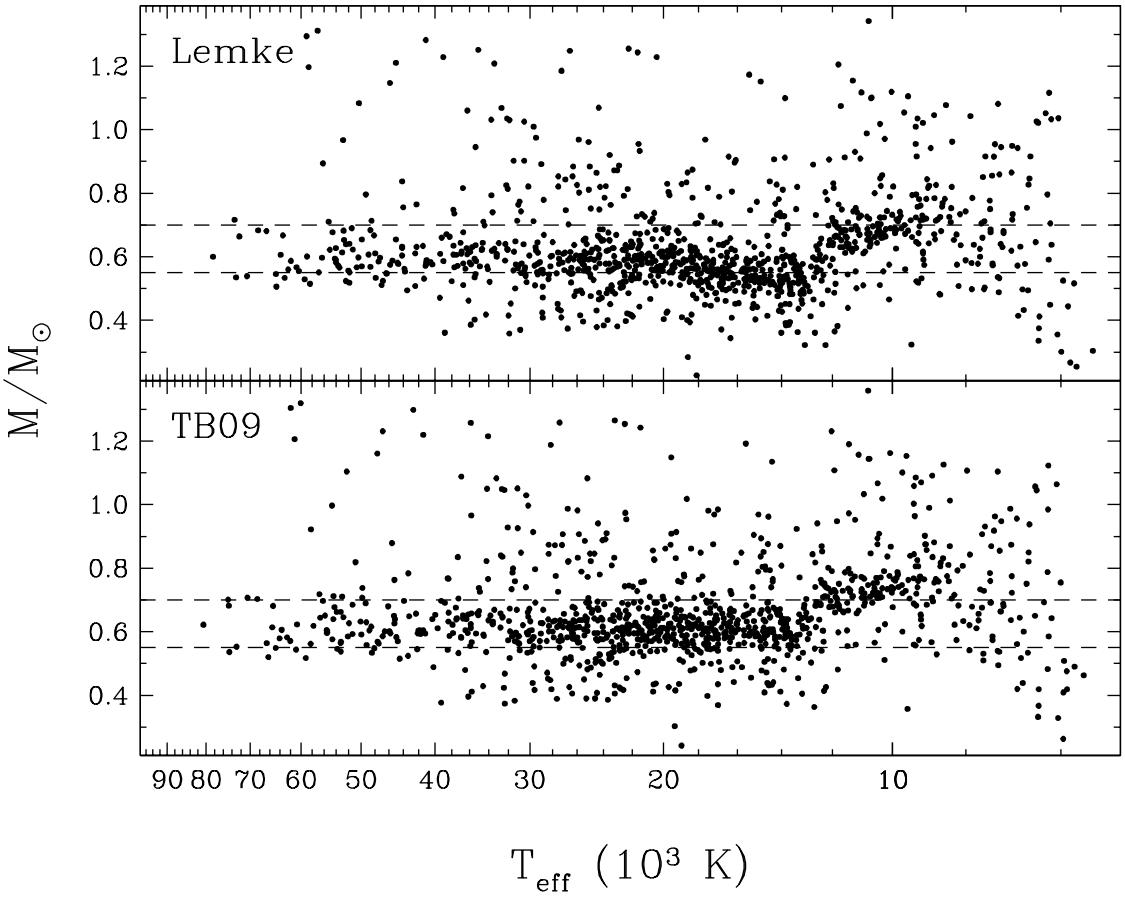

FIGURE 3.10 – Mass vs. $T_{\rm eff}$ distribution for all the DA white dwarfs in our sample using the Stark broadening profiles of Lemke (1997) (top) and the improved calculations of TB09 (bottom). Lines of constant mass at 0.55 $M_{\odot}$ and 0.7 $M_{\odot}$ are shown as a reference.

3.5.3 DAB white dwarfs

In Figure 3.6 we displayed five white dwarfs classified as DAB stars. In other words, besides the hydrogen Balmer lines, the spectra of these stars also feature lines due to neutral helium. For three of these objects (0339+002, 0453−295, 1115+166), previous analyses have shown that fits assuming a single star do not produce satisfactory results. In contrast, fits performed under the assumption that the spectrum is that of a DA+DB double-degenerate binary system have proven successful (Limoges & Bergeron 2010; Wesemael et al. 1994; Bergeron & Liebert 2002, respectively). With that in mind, we proceed to fit the spectra of these systems by combining our usual pure hydrogen models with the pure helium models

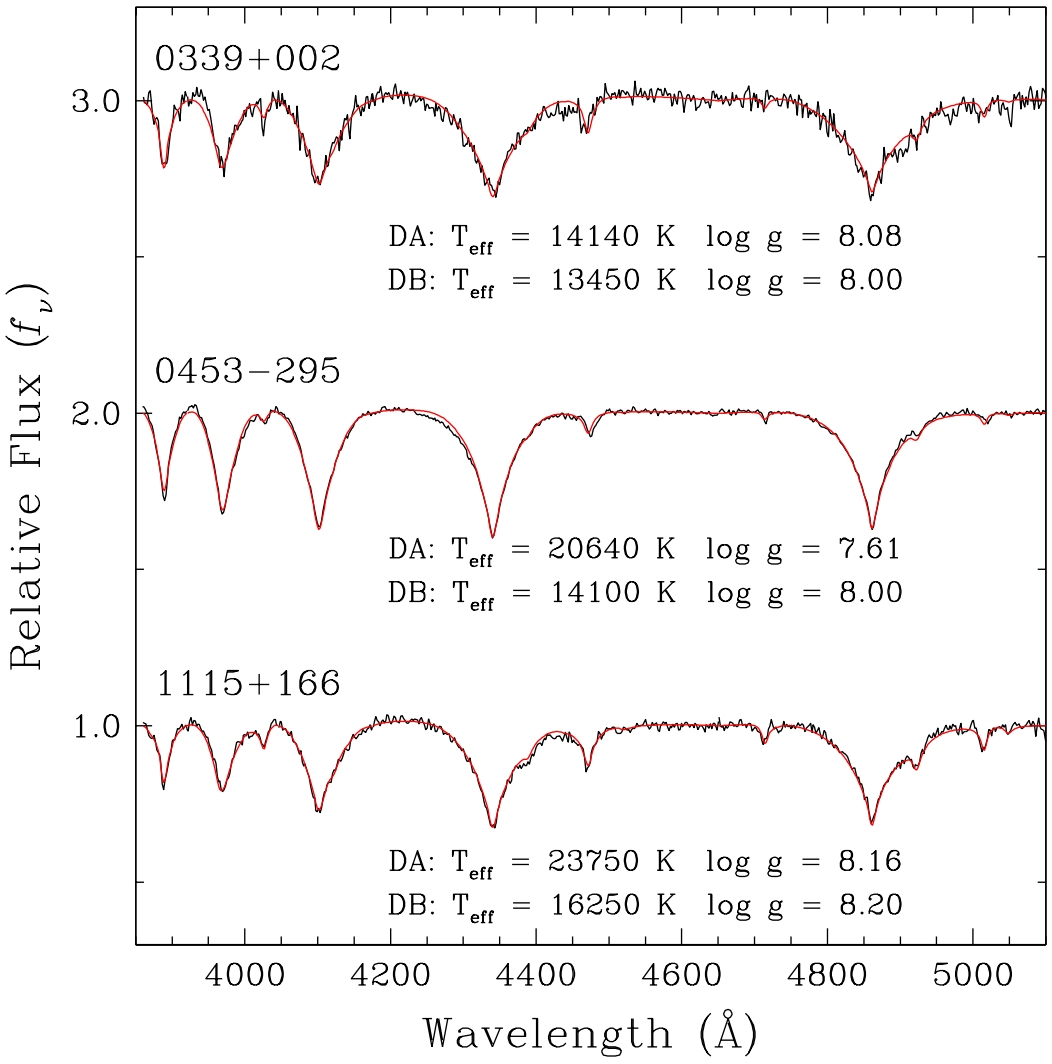

FIGURE 3.11 – Model fits (red) to the optical spectra (black) for the three DA+DB binary systems in our sample. The atmospheric parameters for each solution are given in the figure. Both the observed and theoretical spectra are normalized to a continuum set to unity and the spectra are vertically shifted for clarity.

described in Section 3.4.3. When fitting DA+DB model spectra, the total flux of the system is obtained from the sum of the monochromatic Eddington fluxes of the individual components, weighted by their respective radius. The stellar radii are obtained from evolutionary models similar to those described in Fontaine et al. (2001) but with C/O cores, $q(\mathrm{He}) \equiv \log M_{\mathrm{He}}/M_{\star} = 10^{-2}$ and $q(\mathrm{H}) = 10^{-4}$, which are representative of hydrogen atmosphere white dwarfs, and $q(\mathrm{He}) = 10^{-2}$ and $q(\mathrm{H}) = 10^{-10}$, which are representative of helium atmosphere white dwarfs.

The fitting technique for these DA+DB systems first requires that we normalize both the observed and synthetic spectra to a continuum set to unity. The calculation of χ^2 is then carried out in terms of these normalized line profiles only. The atmospheric parameters, $T_{\rm eff}$ and $\log g$, for the DA white dwarf and $T_{\rm eff}$ for the DB white dwarf are considered free parameters. We set $\log g = 8.0$ for the DB components in 0339+002 and 0453−295 since the helium lines are rather weak and are not especially sensitive to the surface gravity. The helium lines are comparatively stronger in 1115+166 so for the fit of this star, we allow $\log g$ to vary.

Our best fits to the spectra of 0339+002, 0453−295, and 1115+166 are shown in Figure 3.11. We obtain excellent fits for all three systems with the fit for 1115+166 being exceptionally good. For 0339+002, we obtain slightly higher values of $T_{\rm eff}$ and $\log g$ for the DA component as compared to the results of Limoges & Bergeron (2010) with a comparable value of $T_{\rm eff}$ for the DB component. This is not an altogether surprising result for the DA star since we are using the new profiles of TB09 in our analysis. With regards to 0453−295, we obtain a substantially higher $T_{\rm eff}$ and $\log g$ for the DA component as compared to Wesemael et al. (1994) and also a higher $T_{\rm eff}$ for the DB white dwarf. However, the models used in their analysis are considerably outdated and they also performed a four parameter fit allowing the surface gravity of DB star to vary. Finally, we get somewhat higher values of $T_{\rm eff}$ and $\log g$ than Bergeron & Liebert (2002) for the DA component but identical parameters for the DB.

The case of HS 0209+0832 is different from the above three systems as it is a true DAB white dwarf, as first reported by Jordan et al. (1993). In other words, it is a single star with both hydrogen and neutral helium lines present in its optical spectrum. Furthermore, like GD 323, this star presents neutral helium lines that are variable, in particular the He I λ4471 line (Heber et al. 1997). However, contrary to GD 323, Wolff et al. (2000) were able to explain the variability as resulting from the accretion of pockets of interstellar matter of varying densities leading to different accretion rates over the course of time. We show in Figure 3.12 the best fit to our optical spectrum of HS 0209+0832. Besides the usual Balmer lines, we also fit the He I λ4471 line in order to measure the helium abundance. To perform the fit, we have used the grid of homogeneously mixed H/He models described by Gianninas et al. (2010) for DAO white dwarfs, with some modifications. Namely, we have extended the grid down to $T_{\rm eff}$

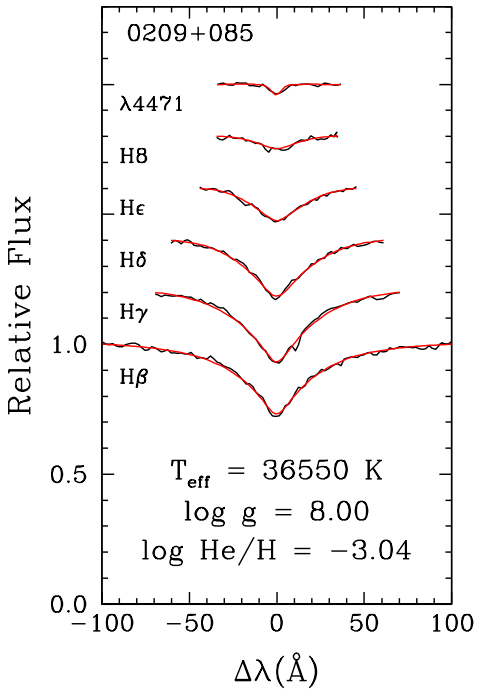

FIGURE 3.12 – Model fits (red) to the hydrogen Balmer lines and the He I λ4471 line in the observed optical spectrum (black) of the DAB white dwarf HS 0209+0832. The lines range from Hβ (bottom) to H8 in addition to He I λ4471 (top), each offset by a factor of 0.2. The best-fit values of $T_{\rm eff}$, $\log g$, and log He/H are indicated at the bottom of the figure.

= 30,000 K. However, we do not include CNO in the models as there is no evidence of the Balmer-line problem in HS 0209+0832.

Our new determinations ($T_{\rm eff}$ = 36,550, $\log g$ = 8.00) are quite comparable to the previous measurements of Heber et al. (1997, $T_{\rm eff}$= 36,100, $\log g$ = 7.91) and Wolff et al. (2000, $T_{\rm eff}$= 35,500, $\log g$ = 7.90) with our slightly higher values likely due to the use of the new TB09 Stark broadening profiles. Conversely, we determine a much lower helium abundance of log He/H = −3.04 as compared to the values compiled in Table 2 of Wolff et al. (2000) that hover around log He/H $\sim$ −2.0 with the lowest value at log He/H = −2.32 (Heber et al. 1997). It is important to note that our spectrum was obtained in 2002 December, more than three years after the last observation listed in Table 2 of Wolff et al. (2000). Furthermore, Wolff et al. state that "A lower rate would reduce the abundance within a few months due to the short diffusion timescale". Hence, the most logical explanation for our considerably lower helium abundance determination is that in the intervening time, HS 0209+0832 traversed a region of

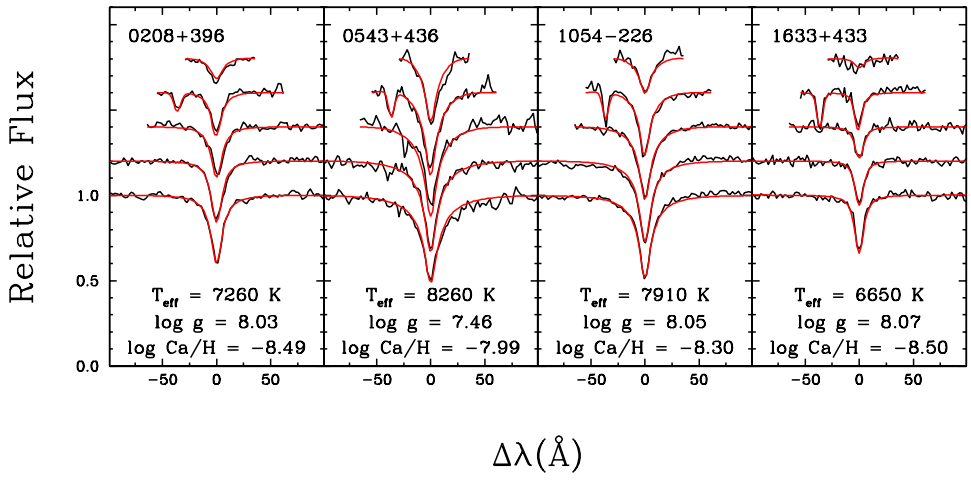

FIGURE 3.13 – Model fits (red) to the hydrogen Balmer lines and the Ca H & K lines in the observed optical spectra (black) of four DAZ white dwarfs. The lines range from Hβ (bottom) to H8 (top), each offset by a factor of 0.2. We note that the Ca K line is blended with Hϵ. The best-fit values of $T_{\rm eff}$, $\log g$, and log Ca/H are indicated at the bottom of each panel.

space where the helium density was lower, leading to a reduced accretion rate.

Finally, we do not attempt to analyze GD 323. Indeed, to date there has not been a model that has been able to achieve a satisfactory fit to the optical spectrum of GD 323 despite many attempts throughout the years. We refer the reader to Pereira et al. (2005) for a comprehensive summary of the various models that have been elaborated over the years in order to explain both the optical spectrum of GD 323, and the observed spectral variability.

3.5.4 DAZ white dwarfs

Our sample contains the five DAZ white dwarfs shown in Figure 3.6. With the exception of GD 362, we fit the remaining four DAZ white dwarfs to obtain $T_{\rm eff}$, $\log g$, as well as the calcium abundance. In order to do so, we computed a small grid of synthetic spectra based on our grid of pure hydrogen atmospheres and added calcium in the calculation of the synthetic spectrum only, as described in Billères et al. (1997). The inclusion of calcium in the calculation of the synthetic spectrum alone, and not in the model atmosphere itself, is justified since the trace amounts of calcium will have no effect whatsoever on the thermodynamic structure of the atmosphere. Our grid covers $T_{\rm eff}$ from 6000 to 9000 K in steps of 500 K, $\log g$ from 7.0 to 9.5 in steps of 0.5 dex and log Ca/H from -7.0 to -9.5 in steps of 0.5 dex. Although

our standard spectroscopic technique works well even without the inclusion of calcium in the synthetic spectra, the fact is that the calcium H-line (at 3968 Å) is blended with Hϵ (at 3970 Å). Since the upper Balmer lines are especially sensitive to the surface gravity, any failure to properly model the line profile would lead to a less precise measurement of $\log g$. Therefore, we are compelled to include the calcium lines in our spectra to avoid this potential source of uncertainty.

Our best fits of the four DAZ stars using the above grid are displayed in Figure 3.13. We have employed essentially the same fitting procedure used for our regular DA white dwarfs but here we have three free parameters, $T_{\rm eff}$, $\log g$, and the calcium abundance. Consequently, we have extended the fitting region around Hϵ blueward in order to properly include the Ca H line in the fit. We can see that we are able to reproduce the calcium lines rather well in all cases. Furthermore, we can compare the atmospheric parameters of the two known DAZ stars, G74-7 (0208+396) and G180-43 (1633+433), to previous determinations. Specifically, Billères et al. (1997) obtained $T_{\rm eff} = 7260$ K, $\log g = 8.03$, and log Ca/H $= -8.80$ for G74-7, and Zuckerman et al. (2003) obtained $T_{\rm eff} = 6569$ K, $\log g = 8.08$, and log Ca/H $= -8.63$ for G180-43. These values are quite comparable to the values we measure here. Indeed, some variation is expected considering our models contain several improvements over the ones used in the previous analyses. With respect to the two newly identified DAZ stars, G96-53 (0543+436) and LP 849-31 (1054−226), their atmospheric parameters seem to suggest that they are rather typical of DAZ white dwarfs within the same temperature range (see Figure 5 of Zuckerman et al. 2003). As new detections, these last two DAZ stars would be prime candidates for harboring circumstellar dust disks as the source of the metals present in the atmosphere. Infrared observations would be required in order to ascertain, through the detection of an infrared excess, whether a circumstellar debris disk is indeed present around these white dwarfs (Kilic et al. 2006).

3.5.5 DA+dM binary systems

As stated in Section 2, we have a total of 47 DA+dM binary systems in our sample. For ten of those systems, we employ our standard fitting technique, as described above. The fits

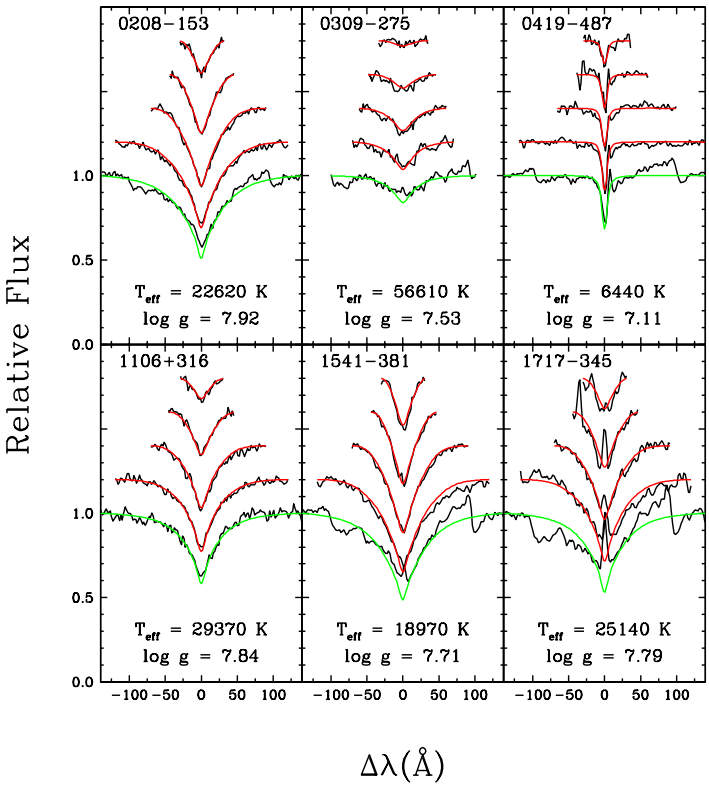

FIGURE 3.14 – Same as Figure 3.8 for six DA+dM binary systems for which we do not have red spectra. In these cases, Hβ (green) is omitted from the fitting procedure as the only contaminated spectral line.

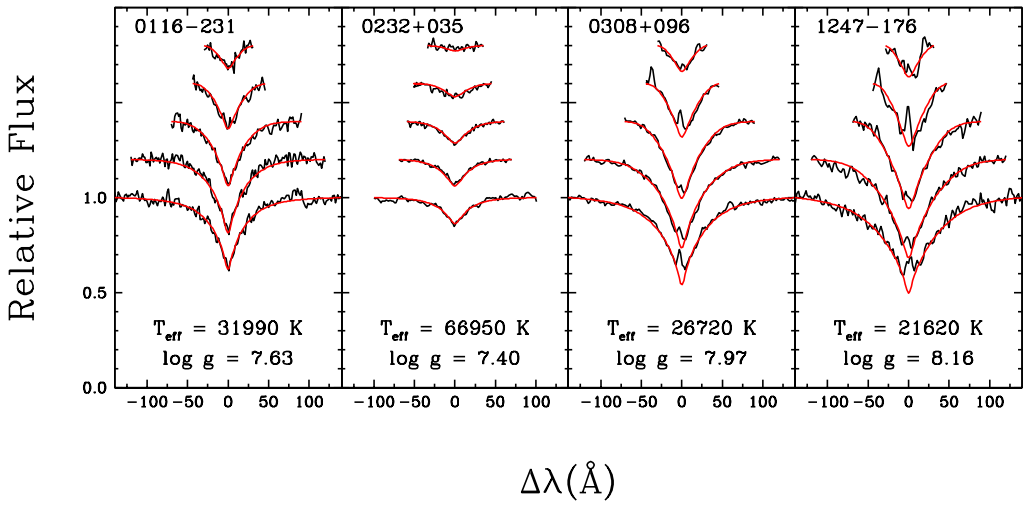

FIGURE 3.15 – Same as Figure 3.8 for four additional DA+dM binary systems where little to no contamination is detected in their blue spectra.

for these ten systems are displayed in Figures 3.14 and 3.15. Of these ten, six are the DA+dM systems, listed earlier, for which we were unable to secure red spectra (see Section 3.3). In these cases, we simply omit Hβ, the only contaminated Balmer line, from our fitting procedure and fit only the Balmer lines from Hγ to H8. We see in Figure 3.14 that we are able to achieve a more than satisfactory fit to the remaining four Balmer lines. On the other hand, the remaining four DA+dM systems, shown in Figure 3.15, display little to no contamination from their companion in their blue spectra and we obtain excellent fits to their observed line profiles without the need to omit any lines. First, the red spectrum of 0116−231 shows virtually no contamination from a companion, as we can see in the left panel of Figure 3.7. Similarly, the red spectrum of 0308+096 is also devoid of contamination except for emission at Hα. In contrast, the blue spectrum 0232+035 seems devoid of any contamination while its red spectrum has emission lines in the cores of all the Balmer lines. Finally, the blue spectrum of 1247−176 shows weak emission for some of the Balmer lines while we see strong emission in the core of all the Balmer lines in its red spectrum (see the middle panel of Figure 3.7). In the first two cases, there is insufficient contamination in the blue spectra to warrant using the procedure described below to subtract the contamination due to the secondary. In the latter two cases, the red spectrum is considerably more contaminated than the blue spectrum. As such, our procedure would likely only make matters worse. Furthermore, these seemingly contradictory detections and non-detections of emission lines from the M dwarf secondary in the latter two cases are likely due to the fact the red and blue spectra were obtained at different phases of the binary orbit. Finally, as described above for 0342+374, we exclude the centre of each Balmer line from the fitting procedure for 0308+096, 1247−176, and 1717−345, as they are contaminated by emission lines from their M dwarf companions.

For the remaining 37 systems, we will take advantage of the red spectra we obtained (see Figure 3.7) in order to remove the contamination due to the presence of the M dwarf. There have been several studies in the last few years that have analyzed DA+dM systems from the SDSS (Silvestri et al. 2006; Heller et al. 2009; Rebassa-Mansergas et al. 2010). One important distinction between these studies and our own is that in the above cases the authors were interested in recovering both the spectrum of the white dwarf and the spectrum of the M

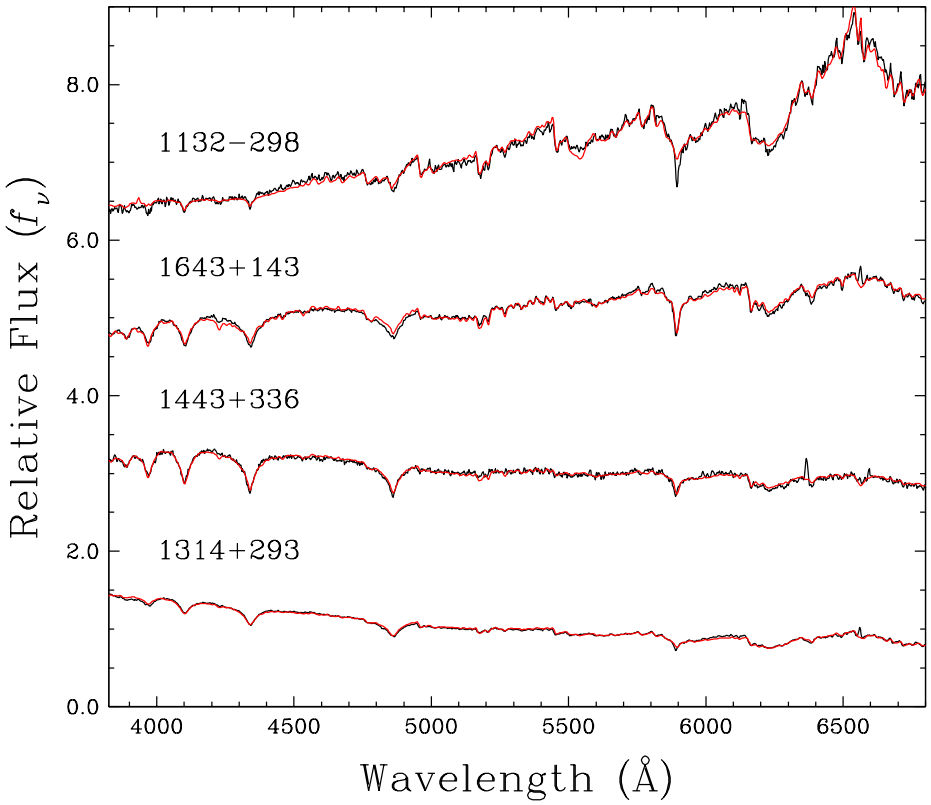

FIGURE 3.16 – Best fits of the observed red spectra (black) for four of our DA+dM binary systems using our combination of synthetic DA spectra and dM spectral templates (red). The spectra are normalized to unity at 5100 Å and shifted vertically for clarity.

dwarf in an effort to study the system as a whole and obtain atmospheric parameters for both stars. In contrast, we are only interested in obtaining a more accurate measurement of the parameters for the DA star.

Our fitting procedure for these systems combines the synthetic spectra computed from our pure hydrogen model atmospheres with the M dwarf spectral templates compiled and presented by Bochanski et al. (2007). We attempt to fit a function of the form

$$F_{\rm obs} = [F_{\rm DA}(T_{\rm eff}, \log g) + a_1 \cdot F_{\rm dM}(\text{Sp. type})] \times (a_2 + a_3\lambda + a_4\lambda^2 + a_5\lambda^3)$$

to the observed spectrum. $F_{\rm DA}$ is the flux due to the DA white dwarf and depends on $T_{\rm eff}$ and $\log g$ while $F_{\rm dM}$, the flux from the dM component, is a function solely of the M dwarf spectral type, from M0 to M9. The remaining free parameters are a_1, which is the relative contribution

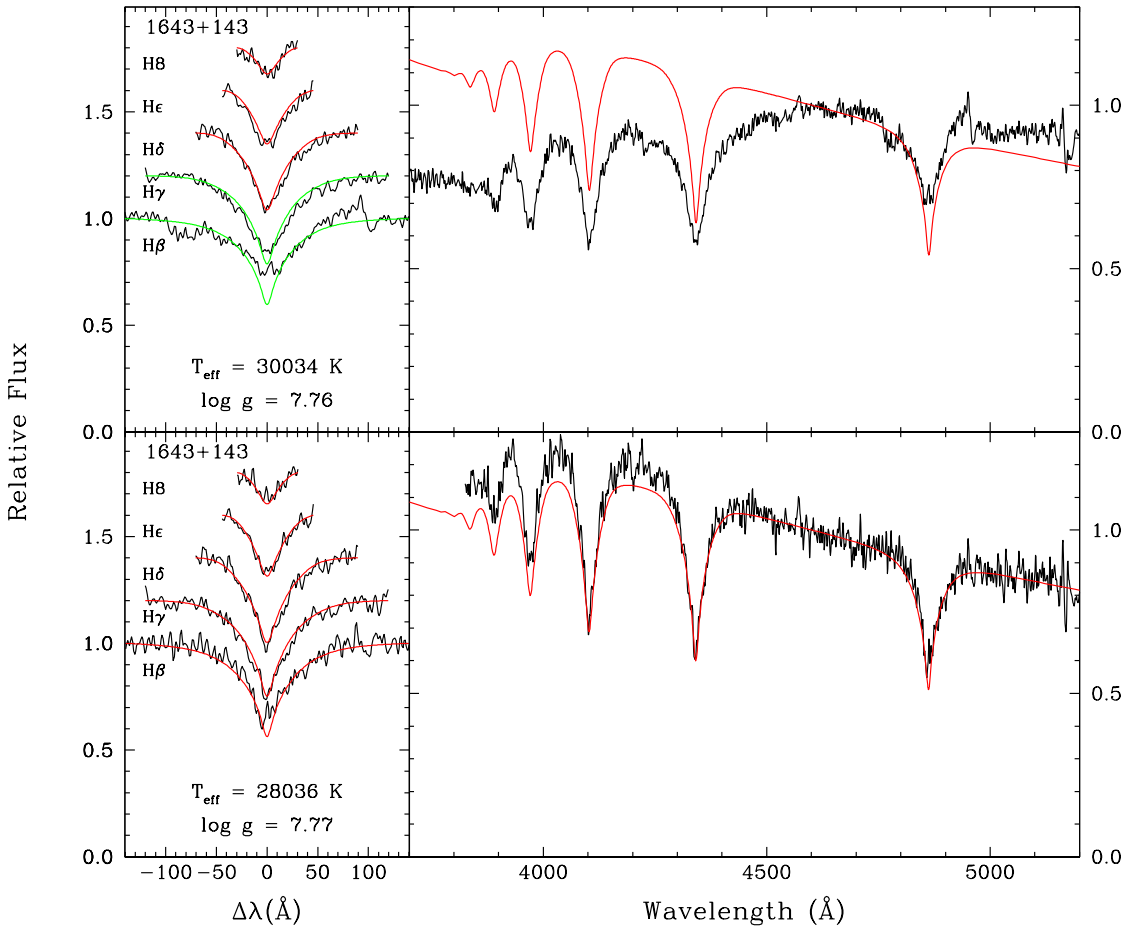

FIGURE 3.17 – Comparison of the spectroscopic solutions for 1643+143 before (top) and after (bottom) subtraction of the dM component. The left panels show the fits (red) to the observed Balmer lines (black) from Hβ to H8 where fits in green indicate spectral lines that are not taken into account in the fitting procedure. The right panels compare the observed spectrum (black) with a synthetic spectrum (red) interpolated at the values of $T_{\rm eff}$ and $\log g$ obtained from the spectroscopic fit, both are normalized to unity at 4600 Å. Note the scales for the relative flux are different in the left and right panels.

of the synthetic DA spectrum and the M dwarf spectral template, a_2, a scaling factor between the composite synthetic spectrum and the observed spectrum, and the coefficients a_{3-5} of a third order polynomial that is meant to account for errors in the flux calibration. In total, there are eight free parameters when we fit the composite spectra. This means that the values of $T_{\rm eff}$, $\log g$, and spectral type that we obtain are meaningless since there are too many parameters used in the fitting process. However, as we mentioned above, our only interest is to obtain

the necessary function to subtract from the composite spectrum in order to remove the dM contamination. We show in Figure 3.16 four examples of the fits we obtain to our composite DA+dM spectra[5]. We see that we are able to achieve some very good fits to the observed spectra. It is interesting to note the varying degrees of contamination from one system to the next. For example, 1443+336 shows only light contamination in contrast to 1132−298 where the white dwarf is nearly drowned out by the flux from its M dwarf companion. Indeed, in the case of 1132−298, and several other systems, when letting all the free parameters listed above vary, the fitting procedure produced rather poor results. In cases such as those, we forced $T_{\rm eff}$ and $\log g$ to the values obtained from fitting our blue spectra of the same objects, similar to the fits presented in Figure 3.14, and this allowed us to achieve satisfactory results as evidenced by 1132−298.

Once the spectroscopic fit to the composite spectrum is obtained, we subtract from the spectroscopic solution the contribution of the DA component [$F_{\rm DA}(T_{\rm eff}, \log g)$]. In other words, we subtract a synthetic DA spectrum interpolated to the values of $T_{\rm eff}$, and $\log g$, as determined by the fit to the composite spectrum, from the composite spectroscopic solution. The residual spectrum generated by this procedure represents the contribution of the M dwarf only. This residual spectrum is then interpolated onto the wavelength grid of the blue spectrum of the same object. Finally, we subtract the residual spectrum from the blue spectrum removing the contamination from the companion.

The next step is to fit the corrected blue spectrum with our standard fitting technique. We show in Figure 3.17 an example of the fits for 1643+143 before and after the correction has been applied. We see quite a dramatic change here. Indeed, where we had to omit the fits to Hβ and Hγ, we are now able to fit them quite well with the contamination removed. The $\log g$ value is virtually identical whereas we determine a $T_{\rm eff}$ that is over 2000 K lower. Finally, we note the greatly improved agreement between the slope of the observed spectrum and the spectroscopic solution.

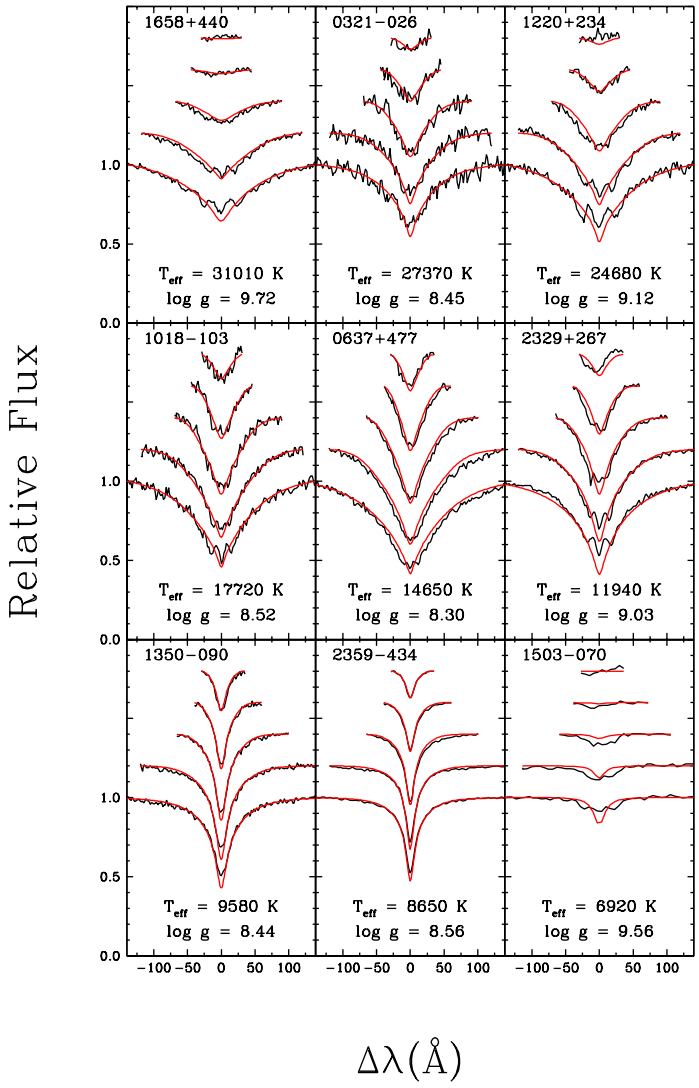

FIGURE 3.18 – Same as Figure 3.8 for nine weakly magnetic DA white dwarfs.

3.5.6 Magnetic, and cool white dwarfs

In Figure 3.5 we presented the spectra of 25 magnetic, or suspected to be magnetic, white dwarfs that are found in our sample. For most of these white dwarfs, our standard spectroscopic technique is inadequate since the Balmer line profiles are severely distorted and/or completely destroyed by a strong magnetic field. However, some of the more weakly magnetic stars can be fit with our spectroscopic method with the caveat that the values of $T_{\rm eff}$ and $\log g$ derived from such fits can only be considered, at best, as rough estimates of the atmospheric

[5]Please refer to Annexe C for the fits to all the DA+dM composite spectra

TABLE 3.3 – Parameters for Magnetic White Dwarfs

WD	Name	B_p (MG)	$T_{\rm eff}$(K)	$\log g$	Notes
0253+508	KPD 0253+5052	17	15,000	8.00	1
0329+005	KUV 03292+0035	12.1	26,500	...	2
0553+053	LTT 17891	20	5500	8.00	3
0816+376	GD 90	9	14,000	8.00	4,5
0945+245	LB 11146a	670	14,500	8.50	6,7,8
1017+366	Ton 1206	65	16,000	...	9
1031+234	Ton 527	1000	15,000	8.50	10
1440+753	RE J1440+750	15	42,000	8.80	6,11
1506+399	CBS 229	20	17,000	...	6,12,13
1533−057	PG 1533−057	31	20,000	8.50	1,14
1639+537	GD 356	13	7510	8.14	15,16
1900+705	LFT 1446	320	16,000	8.58	15
2316+123	KUV 23162+1220	45	11,000	8.00	3

References. – (1) Achilleos & Wickramasinghe 1989; (2) Gänsicke et al. 2002; (3) Putney & Jordan 1995; (4) Putney 1997; (5) Martin & Wickramasinghe 1984; (6) Double-degenerate; (7) Liebert et al. 1993; (8) Glenn et al. 1994; (9) Saffer et al. 1989; (10) Schmidt et al. 1986; (11) Vennes et al. 1999; (12) Gianninas et al. 2009; (13) Vanlandingham et al. 2005; (14) LBH05; (15) Bergeron et al. 2001; (16) Ferrario et al. 1997.

parameters. In Figure 3.18 we present the fits for nine weakly magnetic white dwarfs. For 1658+440, 1220+234, 1018−103, 0637+477, 2329+267, and 1503−070, the Zeeman splitting of the Balmer lines is fairly obvious. In the cases of 1350−090 and 2359−434, the spectroscopic solution predicts the Balmer lines to be deeper than observed, this is also evidence of a weak magnetic field, which is independently confirmed through spectropolarimetric measurements (Schmidt & Smith 1994; Aznar Cuadrado et al. 2004, respectively). Finally, the reason why we classified 0321−026 as magnetic becomes evident here as the Balmer lines are again predicted to be too strong. We note that all nine stars have $\log g$ values which are substantially higher than the canonical value of $\log g = 8.0$, this is not in the least surprising since it is known that magnetic white dwarfs have masses which are higher than the average for normal DA stars (Wickramasinghe & Ferrario 2000). When trying to fit these magnetic stars with non-magnetic models, this phenomenon is exacerbated by the Zeeman splitting which broadens the lines even further causing our spectroscopic solutions to require even higher $\log g$ values. There are no better examples of this effect than 1658+440 and 1503−070 whose $\log g$ values have actually been extrapolated outside of our model grid.

TABLE 3.4 – Parameters for Cool White Dwarfs

WD	Name	$T_{\rm eff}$(K)	$\log g$	$M/M_{\odot}$	M_V	Notes
0121+401	G133-8	5340	7.90	0.52	14.65	1
0213+427	G134-22	5600	8.12	0.66	14.72	1
0551+468	LP 159-32	5380	8.01	0.59	14.78	1
0648+368	GD 78	5700	...	...	...	2
0727+482A	G107-70A	5020	7.92	0.53	15.03	1,3
0727+482B	G107-70B	5000	8.12	0.66	15.33	1,3
1055−072	LFT 753	7420	8.42	0.85	13.91	1
1750+098	G140-B2B	9527	...	1.17	...	4
1820+609	G227-28	4780	7.83	0.48	15.16	1
			DAZ			
1729+371	GD 362	10,540	8.24	...	...	5

References. − (1) Bergeron et al. 2001; (2) Angel et al. 1981; (3) Double-degenerate; (4) Silvestri et al. 2001; (5) Zuckerman et al. 2007.

The 16 remaining magnetic white dwarfs are simply beyond the scope of this work. The same can be said of the cool white dwarfs shown in the right panel of Figure 3.6. For this reason, these white dwarfs will not be further analyzed here. However, in the interest of completeness, we have searched throughout the literature in order to compile atmospheric parameter determinations, and other derived quantities, for these white dwarfs. First, Table 3.3 lists the properties for 13 of the 16 remaining magnetic white dwarfs, including the magnetic field strength (assuming a magnetic dipole), $T_{\rm eff}$, and $\log g$, where available, along with the references to the original analyses. No information could be found for 0350+098, and 1610+330 is identified as a magnetic white dwarf for the first time in this work. Finally, 0239+109 is analyzed at length in the next section. Similarly, Table 3.4 lists the atmospheric parameters for all the cool white dwarfs in our sample. Specifically, we indicate $T_{\rm eff}$, $\log g$, mass, and the absolute visual magnitude along with the necessary references. We also include in Table 3.4 the parameters for GD 362 from Zuckerman et al. (2007) as we have not computed appropriate helium models, which include the necessary metals, for a proper re-analysis of this particular object.

We note that from here on, we shall not take into consideration the values compiled in the two tables described above in our analysis of the global properties of our spectroscopic sample. We wish to include only white dwarfs whose atmospheric parameters were determined

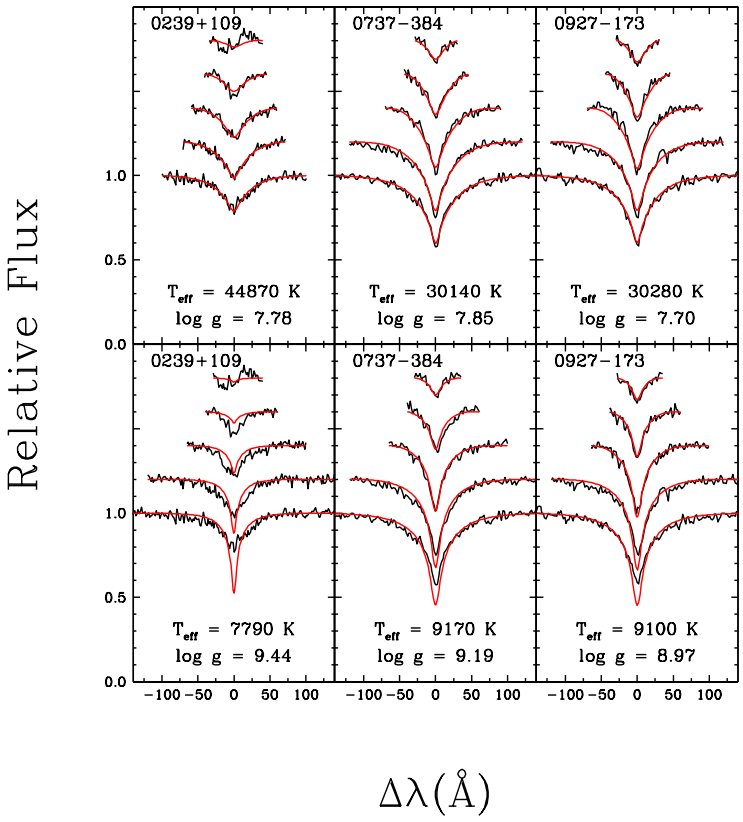

FIGURE 3.19 – Model fits (red) to the observed Balmer lines (black) for the three peculiar white dwarfs in our sample using the hot seed (top) and the cold seed (bottom) for the determination of the spectroscopic solution. The atmospheric parameters for each solution are given in the figure. Both the observed and theoretical spectra are normalized to a continuum set to unity and the lines range from Hβ (bottom) to H8 (top), each offset by a factor of 0.2.

directly by us, as we endeavor to maintain the homogeneity of our analysis.

3.5.7 Peculiar Objects

In the following section, we will take a closer look at three white dwarfs (0239+109, 0737−384, and 0927−173) whose analysis demanded particular attention in order to be certain we are obtaining the correct values for their atmospheric parameters. In all three cases, although the hot solution seemed to be the correct choice, based on our Balmer-line fits, the slopes of the corresponding spectroscopic solutions proved incompatible with those of the observed spectra. The fits for the three stars in question are presented in Figure 3.19. We see that for all three stars, the hot solutions (top panels) seem to match the observed spectra

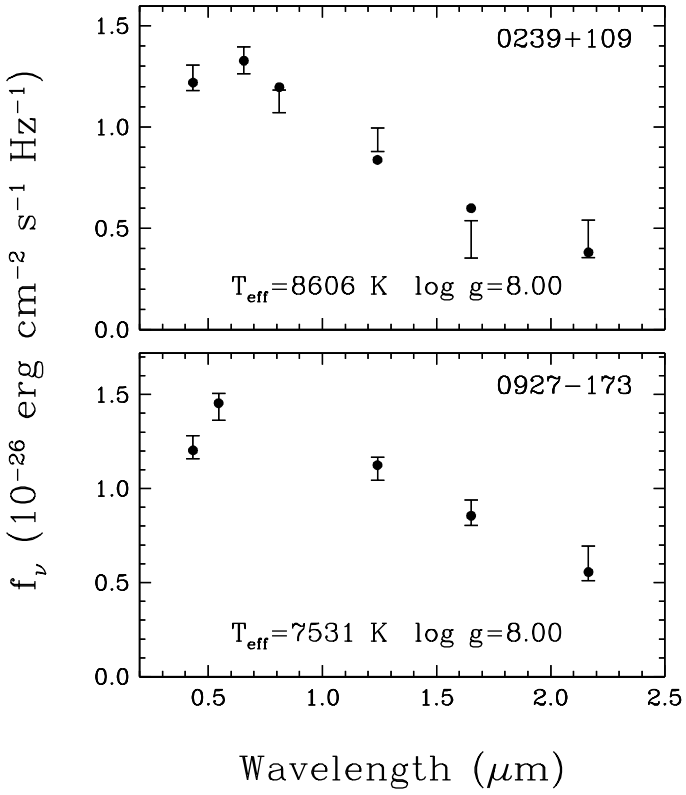

FIGURE 3.20 – Fits to the energy distribution of 0239+109 and 0927−173 with pure hydrogen models. The BVI (BV only for 0927−173) and JHK_S photometric observations are represented by error bars, while the model fluxes are shown as filled circles. The atmospheric parameters corresponding to the photometric solution are given in the figure.

rather well, whereas the cold solutions are completely incompatible with the data. We now take a closer look at each object in turn.

0239+109 (G4-34)

The star 0239+109 is actually one of the 25 magnetic white dwarfs we presented in Figure 3.5, however we will see that this case is not quite so simple. This star was analyzed in Bergeron et al. (1990a) and they had similar difficulties in properly fitting the Balmer-line profiles (see their Figure 1). To be more exact, the slope of their observed spectrum clearly suggested a cooler spectroscopic solution despite the fact that the hot solution produced the better fit to the Balmer-line profiles. As a result, their conclusion was that 0239+109 must in fact be an unresolved DA+DC binary system. More recently, this star was observed as part

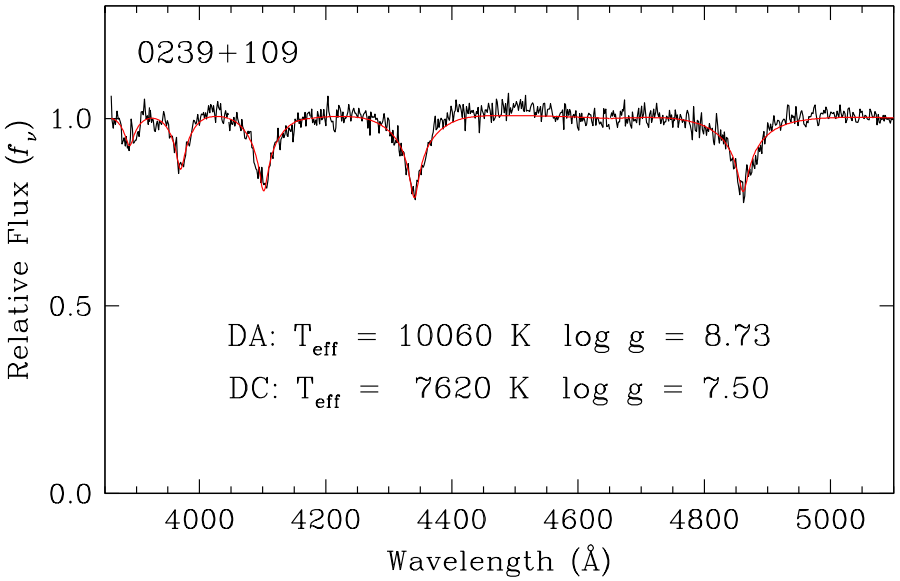

FIGURE 3.21 – Model fit (red) to the optical spectrum (black) for the DA+DC binary 0239+109. The atmospheric parameters corresponding to the spectroscopic solution are given in the figure. Both the observed and theoretical spectra are normalized to a continuum set to unity.

of the SPY survey and Koester et al. (2009) classified it instead as a magnetic white dwarf. Indeed, the SPY spectrum shown in Figure 7.3 of Voss (2006) shows what seems to be Zeeman splitting of both Hα and Hβ. Our spectrum of 0239+109 is one of the many provided to us by C. Moran, and as a result, we have no information regarding the observations (airmass, etc.). However, as we mentioned earlier, when trying to fit the Balmer-line profiles of this star, we encounter the same incoherence noted by Bergeron et al. (1990a), i.e. the hot solution produces the better fit to the observed Balmer lines, but the slope of the spectroscopic solution is incompatible with that of our observed spectrum, which suggests a much cooler temperature. Furthermore, we have in our archives the older spectrum used in the Bergeron et al. (1990a) analysis and obtained by Greenstein (1986). The slopes of the two independent observations are in perfect agreement so we are confident that there is nothing wrong with the data.

In order to get an independent estimate of $T_{\rm eff}$, we exploit the available photometry and fit the overall optical-near infrared spectral energy distribution combining the BRI photometry from the USNO-B Catalog (Monet et al. 2003) with the available Two Micron All Sky Survey (2MASS, Cutri et al. 2003) JHK_s magnitudes. Synthetic colors are obtained using the pro-

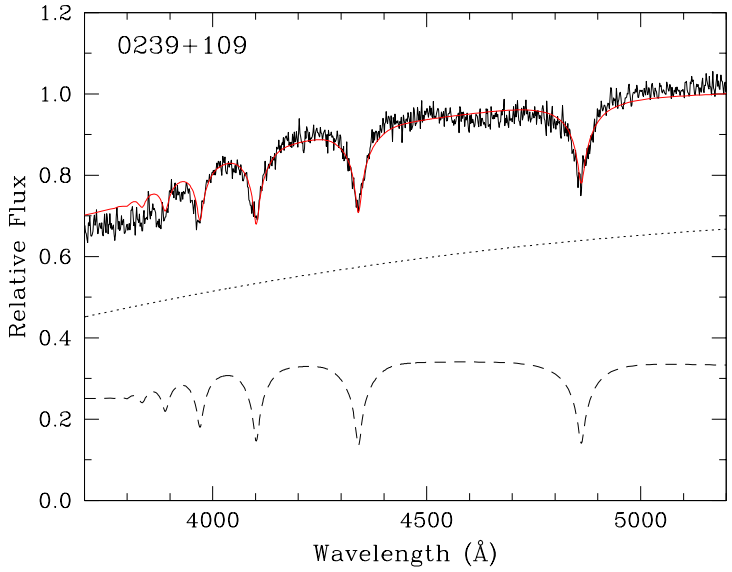

FIGURE 3.22 – Relative energy distributions for our best composite DA+DC fit displayed in Figure 3.21. The dashed line represents the contribution of the DA component while the dotted line represents the contribution of the DC component, both properly weighted by their respective radius. The red line corresponds to the total monochromatic flux of the composite system superimposed on our spectrum of 0239+109 (black line), which has been scaled to the flux of the composite model at 4600 Å.

cedure outlined in Holberg & Bergeron (2006) based on the Vega fluxes taken from Bohlin & Gilliland (2004). The method used to fit the photometric data is described in Bergeron et al. (2001). Since we have no parallax measurement, we assume $\log g = 8.0$. The best fit to the photometry is presented in the top panel of Figure 3.20. Although the photometric fit is not perfect, overall we see that this must be a cool object with $T_{\rm eff} \sim 8600$ K. To reconcile the discrepancy between the slopes of the hot solution and that of our optical spectrum, taking into account the $T_{\rm eff}$ value from the photometric fit, the only possibility is that there are two stars instead of one. Hence, we believe that in the end, both Bergeron et al. (1990a) and Koester et al. (2009) were right. In other words, the system is an unresolved double-degenerate binary composed of a magnetic DA star and a cooler DC white dwarf, a system analogous to G62-46 (Bergeron et al. 1993). In order to get a more accurate measure of the atmospheric parameters for 0239+109, we use a procedure identical to the one employed for the DA+DB binary systems but here we assume a DA and a DC component. Figure 3.21 shows our best fit to the composite spectrum and our results are very similar to those obtained by Berge-

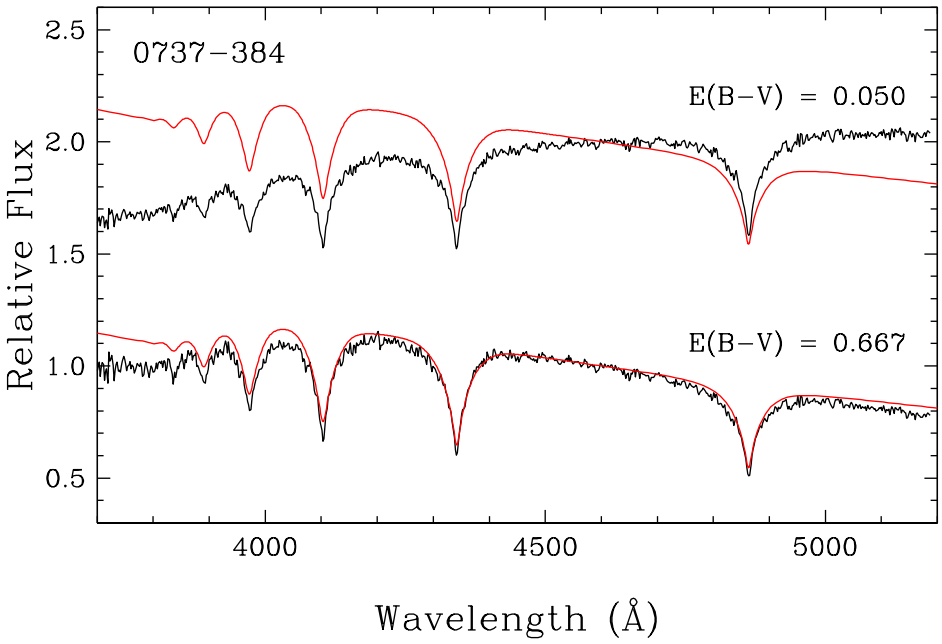

FIGURE 3.23 – Comparison of the observed spectrum (black) with the synthetic spectrum (red) corresponding to the hot solution presented in Figure 3.19 for 0737−384. The observed spectra have been corrected for interstellar reddening with values of $E(B-V)$ as indicated in the figure. Both the observed and synthetic spectra are normalized at 4600 Å and offset vertically for clarity.

ron et al. (1990a). As a final check, we plot in Figure 3.22 the model flux for the combined DA+DC spectroscopic solution and compare the slope with that of our optical spectrum of 0239+109 and see that the agreement is nearly perfect. We note, however, that despite the excellent agreement between our solution and the data, the magnetic nature of the DA component means that our measured values of $T_{\rm eff}$ and $\log g$ for this star should be considered approximate.

0737−384 (NGC 2451-6)

This white dwarf is a member of the open cluster NGC 2451 and was analyzed by Koester & Reimers (1985). Their analysis yielded $T_{\rm eff} = 31{,}000 \pm 3000$ K, which would seem to concur with our determination assuming the hot solution is indeed the correct one. Unfortunately, the slope of the hot solution does not match the slope of our observed spectrum, which suggests a much cooler temperature for this star. How can this clear discrepancy between the slopes of our observed spectrum and that of the hot solution be explained? First, we verified our

observing logs to see if our observations were obtained at high airmass. This could lead to a significant loss of flux in the blue portion of the spectrum, due to atmospheric extinction, if the instrument is not properly rotated to match the parallactic angle. As it turns out, 0737−384 was observed at an airmass of $z = 1.08$ so any such effects would be minimal and we discount that possibility. In the analysis of Koester & Reimers (1985), a value of $E(B-V) = 0.05$ is adopted for the reddening toward NGC 2451 based on several earlier studies (see references therein). Hence, we speculated that our spectrum might actually be suffering from interstellar reddening. We used the above value of interstellar reddening to correct our observed spectrum, following the prescription of Seaton (1979), but the effect is negligible as we see in top panel of Figure 3.23. However, after searching for additional data regarding NGC 2451 on the NASA/IPC Extragalactic Database[6] (NED), we came across a much more recent value for the reddening towards the cluster of $E(B-V) = 0.677$ as determined from the maps of infrared dust emission of Schlegel et al. (1998). This is significantly larger than the previously determined values. When we apply this new value of reddening to our data we see, in the bottom of Figure 3.23, that the slopes are now in excellent agreement. We therefore conclude that the hot solution for 0737−384 is indeed the correct one and the discrepancy between the slopes of the observed spectrum and the spectroscopic solution are due to interstellar reddening. The spectroscopic fit to the corrected spectrum yields $T_{\rm eff} = 30{,}320$ K and $\log g = 7.84$.

0927−173 (LP 787-49)

As in the previous case, our first instinct was to verify if there might be a problem with our observations of 0927−173. As it turns out, 0927−173 was observed at an airmass of $z = 1.54$, which puts it at much greater risk of suffering from atmospheric extinction. However, other objects observed on the same night and at higher airmass ($z \geq 1.80$) do not manifest the same problem and the slopes of their optical spectra are in perfect agreement with those of their spectroscopic solutions. Once again, we are confident that there is nothing wrong with the data itself. Furthermore, previous determinations of $T_{\rm eff}$ for this object suggest that it is a rather cool DA star. Indeed, Kilkenny et al. (1997) find $T_{\rm eff} = 7000$ K while Zuckerman

[6] http://nedwww.ipac.caltech.edu/

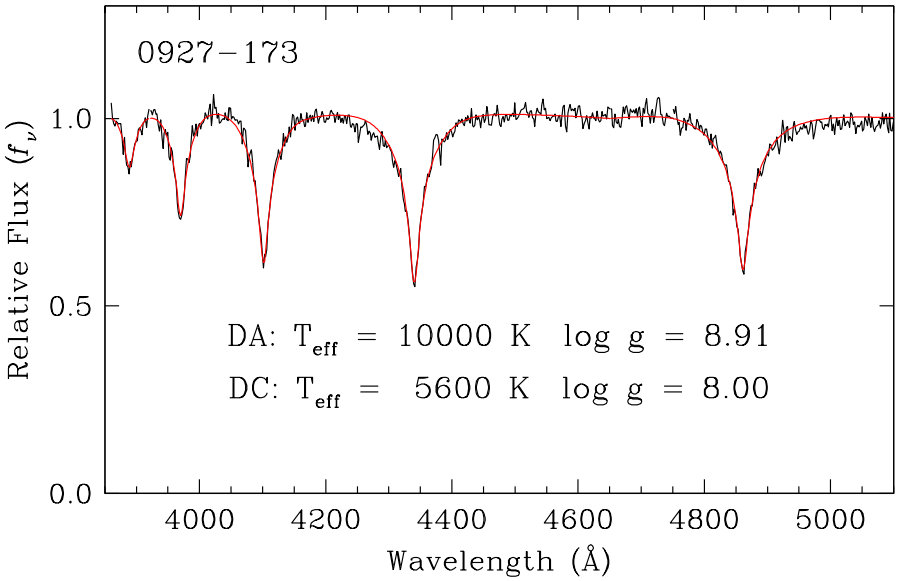

FIGURE 3.24 – Model fit (red) to the optical spectrum (black) for the DA+DC binary 0927−173. The atmospheric parameters corresponding to the spectroscopic solution are given in the figure. Both the observed and theoretical spectra are normalized to a continuum set to unity.

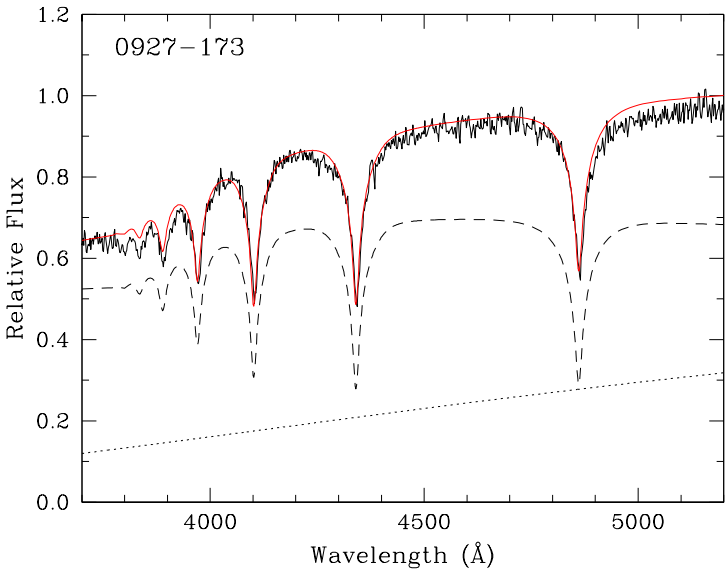

FIGURE 3.25 – Relative energy distributions for our best composite DA+DC fit displayed in Figure 3.24. The dashed line represents the contribution of the DA component while the dotted line represents the contribution of the DC component, both properly weighted by their respective radius. The red line corresponds to the total monochromatic flux of the composite system surperimposed on our spectrum of 0927−173 (black line), which has been scaled to the flux of the composite model at 4600 Å.

et al. (2003) find $T_{\rm eff}$ = 8000 K, in both cases the temperature is determined solely from a measurement of $(B-V)$. Combining the photometry from Kilkenny et al. (1997) with the available measurements of $JHK_{\rm s}$ from 2MASS, we performed a photometric fit using the same procedure described in Section 3.5.7. The results of this fit are displayed in the bottom panel of Figure 3.20. Assuming $\log g = 8.0$, our fit to the available photometry yields $T_{\rm eff}$ = 7530 K, in excellent agreement with the previous determinations, and we conclude that the cold solution must be the correct one. But how do we reconcile this temperature with the poor fit to the Balmer lines with the cold solution? The most likely explanation is that 0927−173 is a DA+DC binary system where the continuum flux of the DC component dilutes the observed Balmer lines leading to the results seen in Figure 3.19. In order to fit the composite spectrum, we employ exactly the same method as we did with the DA+DB systems analyzed in Section 3.5.3. Once again, $T_{\rm eff}$ and $\log g$ for the DA component and $T_{\rm eff}$ for the DC component are the free parameters as we fix $\log g = 8.0$ for the DC star. The results of our fit are shown in Figure 3.24 where we see that the fit to the composite spectrum is nearly perfect. We obtain $T_{\rm eff}$ = 10,000 K and a rather high surface gravity of $\log g = 8.91$ for the DA component, paired to a significantly cooler DC component with $T_{\rm eff}$ = 5600 K. More importantly, in Figure 3.25 we compare the model flux for the combined DA+DC system to our observed spectrum and we see that the slopes are in excellent agreement. Consequently, we conclude that the observed slope of 0927−173 can be explained by the additional presence of an unresolved companion, a cool DC white dwarf.

3.6 GLOBAL PROPERTIES & DISCUSSION

3.6.1 Adopted atmospheric parameters

The atmospheric parameters we have adopted for all the stars in our sample are summarized in Table 3.5. This includes all the normal DA white dwarfs in our sample as well as all the stars we have analyzed in detail in the preceding sections including the DAB and DAZ stars, and the DA+DB and DA+dM binaries. We also include the nine weakly magnetic white dwarfs from Section 3.5.6 and the three peculiar objects from Section 3.5.7. In all, a total of

1246 white dwarfs and their atmospheric parameters are listed in Table 3.5. The entries in Table 3.5 are ordered by their WD numbers, and we list the values of $T_{\rm eff}$ and $\log g$ as well as masses derived from the evolutionary models of Wood (1995) with thick hydrogen layers. Although the Montreal group has computed evolutionary models of their own (Fontaine et al. 2001), these are better suited for the cooler end of the white dwarf cooling sequence. At higher temperatures, the Wood and Fontaine et al. models are quite comparable and, in fact, the Wood models have the benefit of using post-AGB evolutionary sequences as a starting point (M. A. Wood, private communication). Furthermore, low-mass white dwarfs, below 0.46 $M_{\odot}$ and $T_{\rm eff} < 50{,}000$ K, are likely helium core white dwarfs, and we rely instead on the evolutionary models from Althaus et al. (2001) for those stars. For masses higher than 1.3 $M_{\odot}$, we use the zero temperature calculations of Hamada & Salpeter (1961). The values in parentheses represent the uncertainties of each parameter, calculated by combining the internal error, which is the dominant source of uncertainty, obtained from the covariance matrix of the fitting algorithm with the external error, obtained from multiple observations of the same object, estimated for DA stars at 1.2% in $T_{\rm eff}$ and 0.038 dex in $\log g$ (see LBH05 for details). The effect on the uncertainties caused by different values of S/N are included in the external error but are minimized by the fact that the majority of our data have rather high S/N (see Figure 12 of Gianninas et al. 2005). In addition, we list absolute visual magnitudes determined using the photometric calibrations from Holberg & Bergeron (2006). We also provide an updated spectroscopic classification for each star, with temperature indices[7] based on our determinations of $T_{\rm eff}$.

By coupling the absolute magnitudes we have determined with the apparent magnitudes available for each star in the literature, we computed *spectroscopic distances* that we also list in Table 3.5. However, these determinations come with the caveat that many of these apparent magnitudes are photographic or, when V was not available, we have substituted a B magnitude, or a g magnitude from the SDSS, or even a Stromgren y magnitude. Consequently, our distance estimates should be viewed with caution. Since there is a growing interest in identifying white dwarfs in the local neighborhood, in particular those within 20 pc (Holberg et al.

[7]See MS99 for a description of how the temperature index is calculated.

2008), we note that there is no strong evidence for new white dwarfs in our sample within that distance, with the exception perhaps of 0213+396 (16 pc). The distance to 1503−070 of 7 pc is obviously underestimated since we fitted this star with non-magnetic models (see Figure 3.18); the measured trigonometric parallax actually suggests a distance of $\sim$ 25 pc. We also have several objects with distances within 20 pc that are too cool ($T_{\rm eff} < 6500$ K) to derive meaningful atmospheric parameters with the spectroscopic technique, in particular $\log g$. One must also remember that the spectroscopic distances of cool DA stars located in the temperature range where the high log g-problem is encountered are clearly underestimated since their luminosity is also underestimated (smaller radii); this includes 0213+396, mentioned above, at $T_{\rm eff} = 9370$ K.

Finally, special notes have been added in Table 3.5 to designate objects that are known ZZ Ceti pulsators as well as stars that are photometrically constant. We note that all the stars analyzed in Gianninas et al. (2010) are also listed in Table 3.5. This includes both the DAO and DA+BP stars, with a note for all stars that exhibit the Balmer-line problem. For the DA white dwarfs that have been determined to belong to DA+DB, DA+DC, and DA+dM systems, we list only the parameters of the DA component. Finally, we include a note for the weakly magnetic stars that the listed parameters were determined with non-magnetic models.

Erratum: 0102−185

One of the reported DA+BP stars from Gianninas et al. (2010), 0102−185, is actually a much cooler DA white dwarf with $T_{\rm eff} = 23{,}410$ K and $\log g = 7.78$, in contrast to the parameters previously reported. An error during data reduction associated the wrong spectrum to this star. The spectrum that was analyzed as 0102−185 is actually a spectrum of 2211−495 from the same observing run. This reduces the number of DA+BP stars from 18 to 17.

TABLE 3.5 – Atmospheric Parameters of DA white dwarfs from MS99

WD	Name	ST	$T_{\rm eff}$(K)	$\log g$	$M/\,{\rm M}_\odot$	M_V	D (pc)	Notes
0000+171	PG 0000+172	DA2.4	21,130 (325)	8.00 (0.05)	0.63 (0.03)	10.68	108	
0000−186	GD 575	DA3.3	15,350 (265)	7.97 (0.05)	0.60 (0.03)	11.19	105	
0001+433	RE J0003+433	DA1.1	46,850 (1244)	9.05 (0.10)	1.23 (0.04)	11.24	118	
0004+061	PHL 670	DA2.1	24,400 (386)	8.51 (0.05)	0.94 (0.03)	11.23	100	
0004+330	GD 2	DA1.0	49,980 (898)	7.77 (0.06)	0.59 (0.02)	8.79	103	
0005−163	G158-132	DA3.4	14,920 (252)	7.93 (0.05)	0.57 (0.03)	11.18	104	1
0008+424	LP 192-41	DA7.0	7200 (107)	8.12 (0.07)	0.66 (0.05)	13.64	21	
0009+501	G217-37	DA7.6	6620 (103)	8.40 (0.09)	0.85 (0.06)	14.42	10	1
0009−058	G158-39	DA4.8	10,560 (156)	8.22 (0.06)	0.74 (0.04)	12.34	54	
0010+280	PG 0010+281	DA1.9	27,220 (407)	7.87 (0.05)	0.57 (0.02)	9.99	152	
0011+000	Wolf 1	DA5.2	9710 (140)	8.24 (0.05)	0.75 (0.04)	12.67	34	1
0012−173	PHL 752	DA.9	55,810 (1321)	7.88 (0.08)	0.65 (0.04)	8.85	379	
0013−241	Ton S 147	DA2.6	19,340 (301)	8.04 (0.05)	0.65 (0.03)	10.89	78	
0014+097	PG 0014+098	DA3.5	14,410 (273)	7.80 (0.05)	0.50 (0.03)	11.06	91	2
0016−220	Ton S 142	DA3.7	13,610 (346)	7.88 (0.05)	0.54 (0.03)	11.29	64	
0016−258	MCT 0016-2553	DA4.4	11,370 (166)	8.20 (0.05)	0.72 (0.03)	12.09	63	3
0017+061	PHL 790	DA1.7	29,120 (463)	7.82 (0.06)	0.55 (0.03)	9.75	100	
0018−339	BPM 46232	DA2.2	22,420 (339)	7.87 (0.04)	0.56 (0.02)	10.38	73	
0019+150	PHL 802	DA1.6	31,710 (484)	8.14 (0.06)	0.73 (0.03)	10.07	292	
0023+388	G171-B10A	DA4.6	10,980 (164)	8.21 (0.05)	0.73 (0.03)	12.21	56	
0023−109	G158-78	DA4.8	10,430 (153)	8.01 (0.06)	0.61 (0.03)	12.06	68	
0024−121	MCT 0024-1211	DA3.1	16,390 (275)	8.06 (0.05)	0.65 (0.03)	11.21	102	
0024−556	LTT 235	DA5.0	10,070 (145)	8.92 (0.05)	1.16 (0.02)	13.80	19	
0027−636	RE J0029-632	DA.8	63,640 (1531)	7.72 (0.08)	0.61 (0.03)	8.41	238	
0028−474	JL 192	DA2.8	17,780 (268)	7.78 (0.04)	0.50 (0.02)	10.66	86	
0030+444	G172-4	DA4.8	10,480 (152)	8.27 (0.05)	0.77 (0.03)	12.45	60	1
0030−181	KUV 00300-1810	DA3.5	14,270 (387)	7.94 (0.06)	0.58 (0.03)	11.27	104	
0031+150	G32-33	DA7.2	6980 (117)	8.07 (0.13)	0.64 (0.08)	13.70	43	
0032−175	G226-135	DA5.1	9910 (144)	8.26 (0.05)	0.76 (0.04)	12.62	29	1
0032−177	GD 623	DA2.9	17,580 (293)	7.93 (0.05)	0.58 (0.03)	10.89	92	
0033+016	LTT 10199	DA4.6	11,080 (161)	8.91 (0.05)	1.16 (0.02)	13.46	27	1
0033+771	LP 12-438	DA5.6	8940 (131)	8.61 (0.06)	0.99 (0.04)	13.63	30	
0033−176	KUV 00334-1738	DA2.2	23,290 (481)	8.04 (0.07)	0.65 (0.04)	10.56	256	
0033−178	KUV 00337-1749	DA2.0	24,620 (596)	7.28 (0.08)	0.39 (0.02)	9.14	516	
0034−211	LTT 329	DA3.5	14,600 (294)	7.53 (0.06)	0.41 (0.02)	10.60	61	2
0036+312	G132-12	DA4.0	12,610 (222)	8.01 (0.06)	0.61 (0.03)	11.61	83	3
0037+312	GD 8	DA1.0	51,350 (994)	7.77 (0.07)	0.59 (0.03)	8.75	152	
0037−006	PB 6089	DA3.2	15,690 (260)	7.98 (0.05)	0.60 (0.03)	11.17	51	1
0044−219	KUV 00442-2156	DA4.1	12,320 (218)	7.93 (0.06)	0.57 (0.04)	11.53	140	
0047−524	BPM 16274	DA2.7	19,020 (314)	7.97 (0.05)	0.60 (0.03)	10.81	48	
0048+202	PG 0048+202	DA2.4	21,050 (327)	8.02 (0.05)	0.64 (0.03)	10.72	106	
0050+357	RE J0053+360	DA1.8	27,810 (408)	7.99 (0.05)	0.64 (0.03)	10.12	69	
0050−332	SB 360	DA1.4	35,080 (506)	7.98 (0.05)	0.65 (0.02)	9.62	56	
0052+190	PG 0052+190	DA1.7	30,220 (449)	7.76 (0.05)	0.53 (0.02)	9.57	244	
0052+226	G69-31	DA5.2	9700 (143)	8.80 (0.06)	1.10 (0.03)	13.69	31	

TABLE 3.5 – Continued

WD	Name	ST	$T_{\rm eff}$(K)	log g	$M/\,{\rm M}_{\odot}$	M_V	D (pc)	Notes
0052−147	PHL 897	DA1.9	26,690 (398)	8.31 (0.05)	0.82 (0.03)	10.72	76	
0052−250	GD 661	DA3.7	13,760 (413)	8.00 (0.06)	0.61 (0.03)	11.43	105	
0053−117	LTT 524	DA7.1	7150 (108)	8.15 (0.08)	0.69 (0.05)	13.73	20	
0058−044	PHL 940	DA2.9	17,370 (292)	8.10 (0.05)	0.67 (0.03)	11.16	70	
0058−185	KUV 00582-1834	DA2.7	18,730 (342)	8.04 (0.06)	0.64 (0.03)	10.95	183	
0059+257	PG 0059+258	DA2.2	22,850 (443)	8.03 (0.06)	0.65 (0.03)	10.57	165	
0100−036	PHL 3287	DA5.7	8880 (202)	7.95 (0.24)	0.57 (0.14)	12.57	64	
0101+048	LTT 10380	DA5.9	8580 (124)	8.37 (0.05)	0.83 (0.04)	13.36	13	1
0101+059	PB 6250	DA3.4	14,890 (417)	8.45 (0.05)	0.89 (0.03)	11.99	67	
0102+095	PHL 972	DA2.0	25,810 (391)	7.96 (0.05)	0.61 (0.03)	10.23	70	
0102−142	PHL 980	DA2.4	20,950 (332)	7.99 (0.05)	0.62 (0.03)	10.67	161	
0102−185	PHL 975	DA2.2	23,430 (380)	7.78 (0.05)	0.52 (0.02)	10.16	223	
0103+558	GD 273	DA3.5	14,250 (382)	8.10 (0.05)	0.67 (0.03)	11.51	63	
0103−278	LTT 615	DA3.6	13,880 (356)	7.95 (0.05)	0.58 (0.03)	11.34	66	1
0104+015	LP 586-65	DA5.4	9320 (146)	8.33 (0.09)	0.81 (0.06)	12.97	73	
0104−464	LTT 632	DA4.4	11,550 (169)	8.29 (0.05)	0.79 (0.03)	12.20	41	3
0106+372	GD 11	DA1.7	30,020 (441)	7.84 (0.05)	0.57 (0.02)	9.71	125	
0106−358	GD 683	DA1.6	30,930 (456)	7.78 (0.05)	0.54 (0.02)	9.55	110	
0107+172	PG 0107+172	DA1.5	32,610 (491)	7.98 (0.06)	0.65 (0.03)	9.76	219	
0107+267	LTT 10425	DA3.5	14,490 (259)	7.99 (0.05)	0.61 (0.03)	11.33	53	
0107−192	GD 685	DA3.3	15,440 (263)	7.95 (0.05)	0.59 (0.03)	11.16	107	
0108+143	G33-45	DA5.4	9320 (136)	8.77 (0.06)	1.08 (0.03)	13.78	33	
0110−139	MCT 0110-1355	DA1.9	26,300 (408)	8.00 (0.05)	0.64 (0.03)	10.25	122	
0112−195	MCT 0112-1931	DA1.4	37,250 (751)	7.71 (0.08)	0.53 (0.03)	9.08	265	
0113−245	KUV 01138-2431	DA.9	58,880 (1587)	7.56 (0.09)	0.54 (0.03)	8.19	786	
0114−034	GD 821	DA2.5	20,390 (411)	7.92 (0.06)	0.58 (0.03)	10.63	130	
0115+521	GD 275	DA4.6	10,890 (164)	8.19 (0.06)	0.72 (0.04)	12.20	49	1
0115−257	KUV 01157-2546	DA3.2	15,690 (271)	8.06 (0.05)	0.65 (0.03)	11.29	133	
0116−231	Ton S 205	DA1.6	31,990 (492)	7.63 (0.06)	0.49 (0.02)	9.24	190	2
0118−166	GD 953	DA3.6	14,150 (370)	8.08 (0.05)	0.66 (0.03)	11.50	76	
0120+475	GD 276	DA4.6	10,980 (169)	8.17 (0.06)	0.71 (0.04)	12.15	74	
0124−257	Ton S 216	DA2.0	24,600 (406)	7.74 (0.05)	0.50 (0.02)	10.00	136	
0125+093	PB 6456	DA1.5	32,790 (513)	7.92 (0.07)	0.61 (0.03)	9.64	212	
0126+101	Wolf 72	DA5.8	8750 (125)	7.88 (0.06)	0.53 (0.03)	12.54	23	
0126+422	GD 13	DA2.2	23,270 (373)	7.85 (0.05)	0.55 (0.02)	10.28	86	
0126−532	BPM 16501	DA2.9	17,480 (358)	7.90 (0.06)	0.56 (0.03)	10.86	53	
0127+270	GD 14	DA1.9	25,930 (407)	7.86 (0.05)	0.57 (0.03)	10.08	150	
0127+581	Sh 2-188	DAO.6	87,140 (4901)	7.41 (0.18)	0.58 (0.04)	7.20	1116	1
0127−050	G271-81	DA3.0	16,790 (250)	7.99 (0.04)	0.61 (0.03)	11.07	70	
0129−205	PHL 1017	DA2.4	20,670 (333)	8.01 (0.05)	0.63 (0.03)	10.73	61	
0130−273	KUV 01308-2721	DA2.2	23,320 (388)	7.94 (0.05)	0.60 (0.03)	10.41	201	
0130−687	MCT 0130-6846	DA1.4	36,160 (546)	7.22 (0.05)	0.40 (0.01)	8.22	212	
0131−163	PHL 1043	DA1.0	50,110 (988)	7.87 (0.07)	0.63 (0.03)	8.95	101	
0132+254	PG 0132+254	DA2.4	20,650 (360)	7.45 (0.05)	0.41 (0.02)	9.81	179	
0133−116	Ross 548	DA4.0	12,480 (190)	8.05 (0.05)	0.64 (0.03)	11.68	31	3

TABLE 3.5 – Continued

WD	Name	ST	$T_{\rm eff}$(K)	$\log g$	$M/\,{\rm M}_\odot$	M_V	D (pc)	Notes
0134+181	PG 0134+181	DAO.8	59,540 (1809)	7.45 (0.10)	0.51 (0.03)	7.83	727	
0134+833	GD 419	DA2.6	19,240 (300)	8.06 (0.05)	0.66 (0.03)	10.93	27	
0135−052	LTT 888	DA6.9	7250 (103)	7.83 (0.05)	0.49 (0.03)	13.21	8	1
0136+152	PG 0136+152	DA6.2	8080 (116)	8.33 (0.05)	0.81 (0.03)	13.53	19	
0136+251	PG 0136+251	DA1.2	41,430 (785)	9.03 (0.07)	1.22 (0.03)	11.33	86	
0136+768	GD 420	DA3.0	16,910 (274)	7.79 (0.05)	0.51 (0.02)	10.77	66	1
0137−229	GD 1383	DA2.5	20,270 (369)	8.06 (0.06)	0.66 (0.03)	10.84	142	
0138−236	PHL 1100	DA1.4	35,920 (693)	7.77 (0.09)	0.56 (0.04)	9.24	236	
0140−392	SB 702	DA2.1	24,430 (376)	7.93 (0.05)	0.60 (0.03)	10.30	65	
0141−675	LTT 934	DA8.1	6250 (99)	7.81 (0.10)	0.48 (0.06)	13.81	10	
0142+312	G72-31	DA5.3	9480 (137)	8.38 (0.06)	0.84 (0.04)	12.99	23	
0143+216	Wolf 82	DA5.4	9340 (134)	8.57 (0.05)	0.96 (0.03)	13.38	22	1
0145+234	Mrk 362	DA3.9	13,060 (217)	8.13 (0.05)	0.69 (0.03)	11.71	36	1
0145−174	LP 768-500	DA6.9	7270 (127)	7.91 (0.15)	0.54 (0.08)	13.31	72	
0145−221	PHL 1159	DA4.1	12,150 (180)	8.21 (0.05)	0.74 (0.03)	11.96	47	3
0145−257	Ton S 231	DA1.9	26,700 (418)	7.95 (0.05)	0.61 (0.03)	10.15	74	
0147+674	GD 421	DA1.6	31,250 (452)	7.83 (0.05)	0.57 (0.02)	9.61	89	
0148+467	GD 279	DA3.6	14,000 (277)	8.04 (0.04)	0.63 (0.03)	11.45	16	1
0148+641	G244-36	DA5.6	9020 (129)	8.41 (0.05)	0.86 (0.03)	13.23	14	
0149−114	LP 708-538	DA5.5	9180 (137)	8.09 (0.07)	0.66 (0.05)	12.66	61	
0149−124	PHL 1204	DA4.0	12,640 (221)	8.34 (0.05)	0.82 (0.04)	12.08	106	
0151+017	G71-41	DA3.9	12,860 (212)	7.98 (0.05)	0.59 (0.03)	11.52	50	1
0151−094	PHL 1225	DA1.9	27,110 (480)	7.71 (0.06)	0.50 (0.03)	9.75	389	
0154−240	PHL 1248	DA.7	74,560 (2206)	7.85 (0.09)	0.68 (0.04)	8.46	381	
0155+069	Feige 17	DA2.2	22,840 (355)	7.84 (0.05)	0.55 (0.02)	10.30	102	
0155−070	LP 649-6	DA4.6	10,870 (172)	8.17 (0.07)	0.71 (0.04)	12.17	64	
0156+015	PB 6544	DA2.0	25,080 (376)	8.08 (0.05)	0.68 (0.03)	10.47	202	
0159+754	GD 422	DA3.7	13,740 (341)	7.96 (0.05)	0.59 (0.03)	11.37	84	
0159−111	KUV 01595-1109	DA4.4	11,360 (183)	8.29 (0.06)	0.78 (0.04)	12.24	86	
0203−138	GD 1104	DA1.0	49,850 (1105)	8.03 (0.08)	0.71 (0.04)	9.23	197	
0204−233	LP 829-17	DA3.7	13,680 (387)	7.91 (0.05)	0.56 (0.03)	11.31	72	
0205+133	PG 0205+134	DA.8	59,300 (1429)	7.42 (0.08)	0.50 (0.02)	7.90	235	2
0205+250	LTT 10723	DA2.4	21,190 (317)	7.91 (0.04)	0.57 (0.02)	10.53	35	
0205+551	GD 282	DA2.9	17,330 (281)	8.13 (0.05)	0.69 (0.03)	11.22	86	
0205−304	GD 1442	DA2.8	17,810 (276)	7.95 (0.05)	0.59 (0.03)	10.90	90	
0208+396	G74-7	DAZ6.9	7260 (110)	8.03 (0.09)	0.61 (0.05)	13.48	16	1
0208−153	MCT 0208-1520	DA2.2	22,620 (407)	7.92 (0.06)	0.59 (0.03)	10.44	106	2
0208−263	MCT 0208-2621	DA1.5	34,540 (518)	7.86 (0.06)	0.59 (0.03)	9.45	218	
0209+085	Feige 20	DAB1.4	36,550 (539)	8.00 (0.04)	0.67 (0.02)	9.59	73	
0212−231	Ton S 243	DA1.9	27,140 (451)	7.95 (0.06)	0.61 (0.03)	10.12	214	
0213+396	GD 25	DA5.4	9370 (135)	8.63 (0.05)	1.00 (0.03)	13.49	16	1
0214+568	H PER 1166	DA2.3	22,080 (344)	7.98 (0.05)	0.62 (0.03)	10.57	42	
0216+143	PG 0216+144	DA1.8	27,910 (411)	7.89 (0.05)	0.58 (0.02)	9.95	84	
0218+293	KUV 02185+2923	DA2.8	17,790 (304)	8.26 (0.05)	0.77 (0.03)	11.37	169	
0220+222	G94-B5B	DA3.1	16,240 (269)	8.05 (0.05)	0.65 (0.03)	11.21	88	

TABLE 3.5 – Continued

WD	Name	ST	$T_{\rm eff}$(K)	$\log g$	$M/\,{\rm M}_{\odot}$	M_V	D (pc)	Notes
0221+399	BD+39 0539	DA8.1	6250 (142)	8.31 (0.23)	0.79 (0.15)	14.52	38	
0222+422.2	LP 197-5	DA8.0	6320 (280)	8.17 (0.56)	0.69 (0.34)	14.25	41	
0224+317	KUV 02245+3145	DA3.3	15,280 (331)	7.90 (0.06)	0.56 (0.03)	11.10	144	
0226−329	MCT 0226-3255	DA2.1	24,240 (441)	7.89 (0.06)	0.58 (0.03)	10.26	52	
0227+050	Feige 22	DA2.5	19,920 (305)	7.93 (0.05)	0.58 (0.03)	10.67	25	
0229+270	LP 354-382	DA2.0	25,200 (388)	7.94 (0.05)	0.60 (0.03)	10.25	89	
0229+354	KUV 02295+3529	DA3.8	13,350 (360)	7.90 (0.07)	0.56 (0.04)	11.35	129	
0229−481	LB 1628	DA.8	66,260 (1650)	7.40 (0.08)	0.52 (0.02)	7.73	229	
0230+343	GD 30	DA3.3	15,270 (249)	7.98 (0.05)	0.60 (0.03)	11.21	91	
0231+050	PG 0231+051	DAO.6	89,470 (5011)	7.54 (0.18)	0.62 (0.05)	7.42	545	
0231+570	GD 283	DA3.6	13,860 (311)	8.02 (0.05)	0.62 (0.03)	11.45	41	
0231−054	PHL 1358	DA2.9	17,470 (274)	8.58 (0.05)	0.98 (0.03)	11.95	29	1
0232+035	Feige 24	DA.8	66,950 (1426)	7.40 (0.07)	0.52 (0.02)	7.71	81	2
0232+525	G174-5	DA2.8	17,880 (278)	8.37 (0.05)	0.85 (0.03)	11.55	28	
0235+064	PG 0235+064	DA3.5	14,340 (364)	8.11 (0.05)	0.68 (0.03)	11.51	52	
0235−125	PHL 1400	DA1.6	32,420 (473)	8.67 (0.05)	1.05 (0.03)	10.95	58	
0236+498	RE J0239+500	DA1.5	34,150 (510)	8.67 (0.05)	1.05 (0.03)	10.87	88	
0236+745	G221-2	DA5.5	9170 (140)	8.27 (0.08)	0.77 (0.05)	12.94	40	
0237+241	PG 0237+242	DA.7	70,480 (1811)	7.27 (0.08)	0.50 (0.02)	7.38	735	
0238+333	KUV 02386+3322	DA3.6	14,000 (299)	8.32 (0.05)	0.81 (0.03)	11.88	64	1
0239+109	LTT 10886	DA5.0	10,060 (142)	8.73 (0.04)	1.06 (0.02)	13.41	36	6
0242−174	BPS CS 22189-19	DA2.3	21,790 (391)	8.00 (0.05)	0.63 (0.03)	10.63	87	
0243+155	PG 0243+155	DA2.9	17,530 (281)	8.12 (0.05)	0.69 (0.03)	11.19	113	1
0243−026	LHS 1442	DA7.4	6800 (105)	8.09 (0.10)	0.64 (0.06)	13.83	22	
0246+326	KUV 02464+3239	DA4.2	11,940 (180)	8.21 (0.05)	0.73 (0.03)	11.98	58	3
0248+601	GD 425	DA3.0	17,050 (261)	8.03 (0.05)	0.64 (0.03)	11.09	96	
0250−007	BD-01 0407	DA6.0	8400 (126)	8.43 (0.07)	0.87 (0.05)	13.53	37	
0250−026	KUV 02503-0238	DA3.3	15,460 (254)	8.00 (0.05)	0.61 (0.03)	11.22	50	
0252−350	MCT 0252-3501	DA2.9	17,510 (278)	7.44 (0.05)	0.40 (0.02)	10.10	138	
0255−705	LTT 1419	DA4.7	10,770 (159)	8.23 (0.05)	0.75 (0.03)	12.30	23	1
0257+080	G76-48	DA7.8	6430 (103)	7.40 (0.14)	0.33 (0.05)	13.08	37	
0259+378	GD 38	DA1.6	32,040 (473)	7.84 (0.05)	0.57 (0.03)	9.56	174	
0302+027	Feige 31	DA1.4	35,790 (540)	7.80 (0.05)	0.57 (0.02)	9.29	127	
0302+621	GD 426	DA4.5	11,210 (166)	8.27 (0.05)	0.77 (0.03)	12.25	35	1
0303−007	KUV 03036-0043	DA3.0	17,050 (327)	7.77 (0.06)	0.49 (0.03)	10.72	125	2
0307+149	PG 0307+149	DA2.3	22,340 (361)	8.04 (0.05)	0.65 (0.03)	10.63	66	
0308+096	PG 0308+096	DA1.9	26,720 (456)	7.97 (0.06)	0.62 (0.03)	10.18	107	2
0308+188	PG 0308+188	DA2.7	18,730 (278)	7.92 (0.04)	0.58 (0.02)	10.77	42	
0309−275	MCT 0309-2730	DA.9	56,610 (2075)	7.53 (0.13)	0.53 (0.04)	8.19	402	2
0310−073	KUV 03106-0719	DA2.7	18,390 (334)	8.00 (0.06)	0.62 (0.03)	10.92	143	
0310−688	CPD-69 177	DA3.0	16,860 (244)	8.09 (0.04)	0.67 (0.03)	11.21	11	
0311+480	KPD 0311+4801	DA.5	97,080 (4750)	6.96 (0.12)	0.53 (0.03)	6.23	415	
0311+480	KPD 0311+4801	DA.5	97,080 (4750)	6.96 (0.12)	0.53 (0.03)	6.23	415	
0312+019	KUV 03123+0155	DA1.2	42,370 (899)	7.96 (0.08)	0.66 (0.04)	9.31	434	
0312+220	GD 43	DA2.7	18,600 (301)	7.89 (0.05)	0.56 (0.03)	10.74	105	

TABLE 3.5 – Continued

WD	Name	ST	$T_{\rm eff}$(K)	$\log g$	$M/\,{\rm M}_\odot$	M_V	D (pc)	Notes
0314+648	GD 427	DA2.9	17,610 (321)	7.89 (0.06)	0.56 (0.03)	10.83	139	
0316+345	BPM 85584	DA3.3	15,350 (249)	7.68 (0.05)	0.46 (0.02)	10.76	48	
0317+196	PG 0317+196	DA2.8	17,990 (276)	7.99 (0.05)	0.61 (0.03)	10.94	85	
0318−021	KUV 03184-0211	DA3.8	13,290 (231)	8.04 (0.05)	0.63 (0.03)	11.55	78	
0320−000	KUV 03205-0005	DA3.7	13,740 (537)	7.85 (0.07)	0.53 (0.04)	11.22	141	
0320−539	LB 1663	DA1.5	34,240 (499)	7.74 (0.05)	0.54 (0.02)	9.27	139	
0321+692.1	LP 31-422	DA1.3	37,490 (657)	7.95 (0.07)	0.64 (0.03)	9.46	256	
0321−026	KUV 03217-0240	DA1.8	27,370 (524)	8.45 (0.07)	0.91 (0.04)	10.91	225	5
0322+452	HDW 3	DAO.6	91,210 (4576)	7.32 (0.17)	0.57 (0.04)	6.95	1123	
0326−273	LTT 1648	DA5.4	9320 (134)	7.93 (0.06)	0.56 (0.03)	12.36	21	1
0328+008	KUV 03290+0053	DA1.4	35,190 (575)	7.99 (0.07)	0.66 (0.03)	9.64	271	
0329−011	KUV 03295-0108	DA2.8	17,870 (313)	7.85 (0.05)	0.54 (0.03)	10.75	193	
0330−009	KUV 03301-0100	DA1.5	34,010 (510)	7.96 (0.06)	0.64 (0.03)	9.64	176	
0330−017	KUV 03302-0143	DA1.6	31,100 (465)	7.87 (0.05)	0.59 (0.03)	9.68	334	
0332+320	G37-44	DA4.8	10,500 (153)	8.20 (0.05)	0.72 (0.03)	12.33	43	1
0333−350	MCT 0333-3500	DA1.5	34,480 (512)	7.85 (0.05)	0.59 (0.03)	9.44	163	
0335+027	KUV 03351+0245	DA3.0	16,750 (306)	8.07 (0.06)	0.66 (0.03)	11.18	175	
0336+040	KUV 03363+0400	DA5.7	8870 (129)	8.18 (0.06)	0.71 (0.04)	12.93	39	
0338−017	KUV 03383-0146	DA2.4	21,230 (382)	8.22 (0.05)	0.76 (0.03)	11.01	202	
0339+002	KUV 03399+0015	DA3.6	14,140 (199)	8.08 (0.04)	0.66 (0.03)	11.50	128	7
0339+523	Rubin 70	DA3.8	13,150 (292)	7.52 (0.05)	0.41 (0.02)	10.78	99	1
0339−035	LP 653-26	DA3.9	13,000 (212)	8.06 (0.05)	0.65 (0.03)	11.63	52	1
0341+021	KUV 03416+0206	DA2.2	22,770 (349)	7.47 (0.05)	0.42 (0.01)	9.67	168	
0341−459	BPM 31594	DA4.3	11,820 (174)	8.13 (0.05)	0.68 (0.03)	11.89	42	3
0342+374	HaWe 5	DA1.3	38,490 (1322)	8.18 (0.15)	0.77 (0.09)	9.81	346	
0343−007	KUV 03439-0048	DA.8	65,480 (1423)	7.73 (0.07)	0.61 (0.03)	8.39	201	
0344+073	KUV 03442+0719	DA4.5	11,180 (173)	7.92 (0.06)	0.56 (0.03)	11.73	75	3
0346−011	GD 50	DA1.2	42,700 (785)	9.20 (0.07)	1.30 (0.03)	11.65	29	
0347−137	GD 51	DA3.5	14,250 (281)	7.76 (0.05)	0.48 (0.03)	11.03	47	2
0348+339	GD 52	DA3.4	14,820 (350)	8.31 (0.05)	0.80 (0.03)	11.77	49	1
0349+247	LB 1497	DA1.5	32,650 (478)	8.67 (0.05)	1.05 (0.03)	10.94	130	
0349+495	LP 155-332	DA6.8	7430 (115)	8.26 (0.09)	0.76 (0.06)	13.74	39	
0352+018	KUV 03521+0150	DA2.2	22,840 (362)	7.95 (0.05)	0.60 (0.03)	10.46	89	
0352+049	KUV 03520+0500	DA1.4	36,920 (609)	8.74 (0.06)	1.09 (0.03)	10.89	115	
0352+052	GD 54	DA4.8	10,400 (152)	8.17 (0.06)	0.71 (0.04)	12.32	52	
0352+076	G80-34	DA3.1	16,380 (308)	7.87 (0.06)	0.55 (0.03)	10.94	146	
0352+096	HZ 4	DA3.4	14,670 (377)	8.30 (0.05)	0.80 (0.03)	11.76	36	1
0354+463	Rubin 80	DA6.1	8240 (126)	7.96 (0.10)	0.57 (0.06)	12.89	34	
0354+556	Rubin 79	DA6.0	8430 (123)	8.26 (0.06)	0.76 (0.04)	13.25	50	
0356+081	KUV 03561+0807	DA1.1	45,140 (875)	7.91 (0.07)	0.64 (0.03)	9.15	323	
0357−233	Ton S 392	DA.7	74,710 (2556)	7.86 (0.12)	0.68 (0.04)	8.47	320	
0401+250	LB 1240	DA3.9	12,790 (208)	8.06 (0.05)	0.64 (0.03)	11.64	27	1
0402+543	Rubin 89	DA2.9	17,120 (261)	8.04 (0.05)	0.64 (0.03)	11.10	72	
0406+169	LB 227	DA3.2	15,810 (288)	8.38 (0.05)	0.85 (0.03)	11.76	52	1
0406+592	2RE J0410+592	DA1.6	30,640 (443)	7.94 (0.05)	0.62 (0.02)	9.83	82	

TABLE 3.5 – Continued

WD	Name	ST	$T_{\rm eff}$(K)	$\log g$	$M/\,{\rm M}_\odot$	M_V	D (pc)	Notes
0407+179	HZ 10	DA3.5	14,210 (251)	7.92 (0.05)	0.56 (0.03)	11.25	38	1
0408−041	GD 56	DA3.3	15,270 (268)	8.09 (0.05)	0.67 (0.03)	11.38	67	
0410+117	HZ 2	DA2.3	21,600 (335)	7.98 (0.05)	0.61 (0.03)	10.60	45	
0413−077	40 Eri B	DA2.9	17,100 (256)	7.95 (0.04)	0.59 (0.03)	10.97	5	
0415+271	HL Tau 76	DA4.3	11,780 (180)	7.99 (0.05)	0.60 (0.03)	11.69	50	3
0416+334	GD 60	DA2.8	17,700 (272)	7.90 (0.05)	0.56 (0.03)	10.84	79	
0416+402	KPD 0416+4015	DA1.4	34,990 (522)	8.01 (0.05)	0.67 (0.03)	9.67	185	
0416+701	GD 429	DA4.1	12,230 (189)	7.60 (0.06)	0.43 (0.02)	11.06	55	1
0417+361	G38-29	DA4.4	11,480 (174)	8.00 (0.05)	0.60 (0.03)	11.77	59	3
0418+153	LB 212	DA3.6	14,060 (366)	8.10 (0.05)	0.67 (0.03)	11.54	104	1
0419−487	LTT 1951	DA7.8	6440 (113)	7.11 (0.19)	0.25 (0.05)	12.64	22	2
0420+520	KPD 0420+5203	DA2.1	23,950 (353)	8.10 (0.04)	0.69 (0.03)	10.59	77	
0421+162	LP 415-46	DA2.5	20,010 (315)	8.13 (0.05)	0.70 (0.03)	10.97	47	
0421+740	RE J0427+741	DA.9	53,880 (1103)	7.92 (0.07)	0.66 (0.03)	8.95	148	
0423+123	KUV 04234+1222	DA2.3	22,230 (500)	7.96 (0.07)	0.61 (0.04)	10.52	189	
0423+140	LB 216	DA2.6	19,550 (418)	8.88 (0.07)	1.15 (0.03)	12.33	75	
0425+168	LP 415-415	DA2.0	25,130 (381)	8.12 (0.05)	0.71 (0.03)	10.54	50	
0426+106	KUV 04262+1038	DA4.8	10,460 (155)	8.74 (0.06)	1.07 (0.03)	13.30	40	
0429+176	LTT 1951	DA2.9	17,620 (347)	8.02 (0.06)	0.63 (0.04)	11.02	39	2
0430+136	KUV 04304+1339	DA1.5	34,210 (614)	8.07 (0.09)	0.69 (0.05)	9.80	209	2
0431+126	HZ 7	DA2.3	21,890 (346)	8.11 (0.05)	0.69 (0.03)	10.78	49	
0433+406	Lanning 531	DA5.0	10,160 (151)	8.22 (0.06)	0.73 (0.04)	12.47	65	
0437+093	LP 475-247	DA8.1	6230 (122)	7.99 (0.20)	0.58 (0.12)	14.07	38	
0437+122	LP 475-249	DA3.8	13,260 (352)	8.08 (0.08)	0.66 (0.05)	11.61	165	
0437+152	KUV 04370+1514	DA2.6	19,300 (317)	7.48 (0.05)	0.42 (0.02)	10.00	147	
0438+108	HZ 14	DA1.8	27,540 (403)	8.15 (0.05)	0.73 (0.03)	10.39	49	
0439+466	LS V +46 21	DAO.6	86,980 (2389)	7.23 (0.08)	0.54 (0.02)	6.83	163	3
0440+510	G175-46	DA5.8	8700 (126)	8.26 (0.06)	0.76 (0.04)	13.12	37	1
0440−038	RE J0443-034	DA.8	60,080 (1965)	9.38 (0.11)	1.32 (0.06)	11.78	106	
0446−789	BPM 3523	DA2.1	24,440 (382)	7.88 (0.05)	0.57 (0.02)	10.23	44	
0452+103	LP 476-267	DA6.5	7700 (115)	8.10 (0.08)	0.66 (0.05)	13.36	50	
0453+418	GD 64	DA3.5	14,320 (256)	7.81 (0.05)	0.51 (0.03)	11.09	38	1
0453−295	MCT 0453-2933	DA2.4	20,640 (291)	7.61 (0.04)	0.45 (0.02)	10.11	101	7
0455+553	G191-16	DA4.3	11,760 (178)	8.13 (0.05)	0.68 (0.03)	11.90	65	3
0455−282	RE J0457-280	DA.8	63,540 (1199)	7.58 (0.06)	0.56 (0.02)	8.14	145	
0457−004	G84-26	DA4.4	11,410 (168)	8.98 (0.05)	1.19 (0.02)	13.52	23	
0458+407		DA3.4	14,920 (272)	8.08 (0.05)	0.66 (0.03)	11.39	105	
0458−303	MCT 0458-3020	DAO.6	91,010 (3156)	7.09 (0.10)	0.53 (0.02)	6.46	928	
0500−156	A66 7	DAO.6	82,710 (3820)	7.47 (0.13)	0.59 (0.04)	7.43	430	
0501+527	G191-B2B	DA.8	60,920 (993)	7.55 (0.05)	0.54 (0.01)	8.13	54	
0505+012	HS 0505+0112	DAOZ.8	60,340 (2283)	7.67 (0.12)	0.58 (0.04)	8.25	214	
0507+045.1	HS 0507+0435B	DA4.1	12,290 (186)	8.24 (0.05)	0.75 (0.03)	11.97	48	3
0507+045.2	HS 0507+0435A	DA2.3	21,550 (318)	8.08 (0.04)	0.67 (0.03)	10.76	49	
0509−007	RE J0512-004	DA1.6	32,450 (466)	7.40 (0.05)	0.42 (0.01)	8.79	121	
0511+079	G84-41	DA7.6	6660 (133)	8.25 (0.20)	0.75 (0.13)	14.16	22	

TABLE 3.5 – Continued

WD	Name	ST	$T_{\rm eff}$(K)	$\log g$	$M/\,{\rm M}_\odot$	M_V	D (pc)	Notes
0513+756	GD 433	DA3.6	14,130 (411)	7.88 (0.06)	0.55 (0.03)	11.22	101	1
0516+365	Lanning 32	DA1.6	31,850 (467)	7.90 (0.05)	0.60 (0.03)	9.67	130	
0517+307	GD 66	DA4.1	12,430 (197)	8.13 (0.05)	0.68 (0.03)	11.79	57	3
0518+005	GD 67	DA3.6	13,920 (369)	7.99 (0.05)	0.61 (0.03)	11.40	112	1
0518+333	G86-B1B	DA5.5	9080 (130)	8.27 (0.05)	0.77 (0.03)	12.97	44	
0518−105	RE J0521-102	DA1.5	33,200 (542)	8.74 (0.07)	1.08 (0.04)	11.04	93	
0525+526	LP 119-48	DA2.2	22,510 (343)	9.14 (0.05)	1.25 (0.01)	12.62	42	
0531−022	RE J0534-021	DA1.7	30,330 (433)	8.64 (0.04)	1.03 (0.02)	11.02	108	
0532+414	GD 69	DA6.5	7750 (112)	8.03 (0.06)	0.61 (0.04)	13.22	20	
0532−560	HE 0532-5605	DA4.3	11,830 (183)	8.54 (0.05)	0.95 (0.03)	12.56	31	3
0533+322	G98-18	DA3.0	16,970 (276)	7.59 (0.05)	0.43 (0.02)	10.42	159	1
0533+555	HDW 4	DA1.0	49,350 (1060)	8.00 (0.08)	0.69 (0.04)	9.19	304	
0543+436	G96-53	DAZ6.1	8260 (130)	7.46 (0.13)	0.36 (0.05)	12.11	99	
0543+579	GD 290	DA5.1	9960 (146)	8.26 (0.06)	0.77 (0.04)	12.62	40	
0546+265	GD 70	DA4.0	12,650 (273)	7.89 (0.08)	0.55 (0.04)	11.44	142	
0548+000	GD 257	DA1.1	46,860 (742)	7.78 (0.05)	0.59 (0.02)	8.88	152	
0548−241	RE J0550-240	DA.9	54,380 (1225)	8.02 (0.08)	0.71 (0.04)	9.13	260	
0549+158	LTT 11733	DA1.5	33,590 (483)	7.93 (0.05)	0.62 (0.02)	9.62	49	
0556+106	WeDe 1	DA.3	145,200 (8051)	8.81 (0.20)	1.09 (0.04)	9.80	316	
0556+172	KPD 0556+1712	DA2.6	19,280 (308)	8.34 (0.05)	0.83 (0.03)	11.37	77	
0557+237	G104-10	DA6.0	8360 (121)	8.18 (0.06)	0.70 (0.04)	13.15	56	
0558+165	KPD 0558+1631	DA2.9	17,210 (272)	8.42 (0.05)	0.88 (0.03)	11.68	63	
0559+158	G105-4	DA7.0	7230 (118)	8.41 (0.11)	0.85 (0.07)	14.08	35	
0606+282	GD 72	DA2.7	18,550 (293)	8.01 (0.05)	0.62 (0.03)	10.91	55	
0612+177	LTT 11818	DA1.9	26,150 (391)	7.99 (0.05)	0.63 (0.03)	10.25	43	
0615+556	PuWe 1	DAO.5	93,150 (3105)	7.57 (0.12)	0.64 (0.03)	7.42	452	
0615+655	HS 0615+6535	DA.6	77,780 (2811)	7.93 (0.11)	0.72 (0.04)	8.58	266	
0618+067	G105-30	DA8.5	5940 (209)	7.86 (0.55)	0.51 (0.29)	14.11	28	
0618+134	RE J0620+132	DA1.0	52,790 (1223)	7.89 (0.08)	0.65 (0.04)	8.92	189	
0621−376	RE J0623-374	DA.8	66,060 (1139)	7.12 (0.05)	0.41 (0.01)	7.30	91	
0625+415	GD 74	DA2.9	17,610 (278)	8.07 (0.05)	0.66 (0.03)	11.09	60	
0628−020	LP 600-42	DA7.3	6910 (136)	7.90 (0.20)	0.53 (0.11)	13.50	24	2
0630+200	RE J0633+200	DA.8	61,170 (2120)	8.97 (0.12)	1.21 (0.05)	10.84	215	
0630−050	RE J0632-050	DA1.1	45,560 (1094)	8.35 (0.09)	0.88 (0.05)	9.89	135	
0631+107	KPD 0631+1043	DA1.8	27,630 (403)	7.95 (0.04)	0.61 (0.02)	10.07	56	
0632+409	G107-9	DA6.3	7980 (122)	8.82 (0.08)	1.11 (0.04)	14.44	29	
0637+477	GD 77	DA3.4	14,650 (590)	8.30 (0.06)	0.80 (0.04)	11.77	40	1
0639+447	SA 26-82	DA2.0	25,580 (413)	7.83 (0.05)	0.55 (0.03)	10.06	213	
0641+438	LP 205-27	DA3.1	16,400 (266)	8.00 (0.05)	0.62 (0.03)	11.12	76	
0642−166	Sirius B	DA1.9	25,970 (378)	8.57 (0.04)	0.98 (0.03)	11.22	3	
0642−285	CD-28 3361	DA5.4	9370 (134)	8.15 (0.05)	0.69 (0.03)	12.66	32	
0644+025	G108-26	DA7.0	7190 (105)	8.55 (0.06)	0.95 (0.04)	14.34	19	
0644+375	LFT 487	DA2.3	22,290 (341)	8.10 (0.05)	0.69 (0.03)	10.73	19	
0646−253	RE J0648-252	DA1.8	28,380 (411)	7.99 (0.04)	0.64 (0.03)	10.08	52	
0648+641	LP 58-53	DA8.4	6000 (205)	8.26 (0.43)	0.76 (0.27)	14.63	25	

TABLE 3.5 – Continued

WD	Name	ST	$T_{\rm eff}$(K)	$\log g$	$M/\,{\rm M}_{\odot}$	M_V	D (pc)	Notes
0651−020	GD 80	DA1.5	34,220 (497)	8.28 (0.05)	0.82 (0.03)	10.16	86	
0654+324	KUV 06548+3225	DA2.2	22,690 (389)	8.11 (0.05)	0.69 (0.03)	10.71	300	
0658+624	GD 446	DA2.9	17,140 (262)	7.98 (0.05)	0.60 (0.03)	11.00	81	
0659−063	LP 661-3	DA7.6	6620 (105)	8.36 (0.10)	0.82 (0.07)	14.35	16	
0701−587	BPM 18394	DA3.5	14,560 (338)	8.56 (0.05)	0.96 (0.03)	12.21	28	
0706+294	KUV 07069+2929	DA3.4	14,690 (267)	7.97 (0.05)	0.60 (0.03)	11.27	68	
0709+194	LP 422-6	DA3.6	13,920 (435)	8.00 (0.06)	0.61 (0.03)	11.41	143	
0710+216	GD 83	DA4.7	10,630 (155)	8.15 (0.05)	0.69 (0.03)	12.21	41	1
0710+741	GD 448	DA2.6	19,690 (307)	7.52 (0.05)	0.43 (0.02)	10.03	97	
0715+125	G89-10	DA7.0	7200 (115)	8.12 (0.11)	0.66 (0.07)	13.64	34	
0717+368	KUV 07170+3653	DA2.0	25,260 (492)	8.00 (0.07)	0.63 (0.04)	10.34	196	
0718−316	RE J0720-318	DA.9	57,790 (1321)	7.80 (0.08)	0.62 (0.03)	8.66	308	
0721−276	RE J0723-274	DA1.4	36,750 (586)	7.98 (0.06)	0.65 (0.03)	9.54	59	
0725+276	RX J0728+275	DA1.0	49,200 (1445)	7.69 (0.11)	0.56 (0.04)	8.66	465	
0726+392	LP 207-7	DA3.8	13,240 (241)	7.97 (0.05)	0.59 (0.03)	11.46	74	
0730+487	GD 86	DA3.4	15,010 (331)	8.57 (0.05)	0.97 (0.03)	12.18	36	
0732−427	LTT 2884	DA3.2	15,570 (233)	8.12 (0.04)	0.68 (0.03)	11.38	36	
0737−384	NGC 2451-6	DA1.7	30,320 (460)	7.84 (0.06)	0.57 (0.03)	9.69	258	8
0740−570	BPM 18615	DA2.3	21,670 (318)	8.17 (0.04)	0.73 (0.03)	10.89	68	
0741+248	LP 366-3	DA3.9	12,990 (275)	8.16 (0.06)	0.70 (0.04)	11.76	89	1
0743+442	GD 89	DA3.3	15,220 (345)	8.47 (0.05)	0.91 (0.03)	11.98	39	1
0752+365	G90-28	DA6.4	7860 (116)	8.14 (0.07)	0.68 (0.05)	13.33	36	
0752−146	LTT 2980	DA2.6	19,440 (291)	7.92 (0.04)	0.58 (0.02)	10.71	37	
0752−676	BPM 4729	DA9.0	5600 (91)	7.78 (0.07)	0.46 (0.04)	14.30	9	
0754+402	KUV 07540+4015	DA2.6	19,720 (484)	7.98 (0.08)	0.61 (0.04)	10.77	154	
0800−533	BPM 18764	DA2.3	21,970 (331)	7.82 (0.04)	0.53 (0.02)	10.34	122	
0801+421	KUV 08016+4206	DA3.5	14,370 (562)	8.24 (0.06)	0.76 (0.04)	11.71	117	
0802+413	KUV 08026+4118	DA.9	53,220 (992)	7.68 (0.06)	0.56 (0.02)	8.55	155	
0803+400	KUV 08039+4003	DA3.3	15,210 (299)	8.04 (0.06)	0.63 (0.03)	11.30	166	
0805+654	PG 0805+655	DA1.1	44,090 (1077)	7.95 (0.10)	0.66 (0.05)	9.25	289	2
0808+423	KUV 08084+4221	DA3.2	15,590 (421)	8.98 (0.05)	1.19 (0.02)	12.91	59	
0808+595	PG 0808+595	DA1.8	28,100 (439)	7.40 (0.05)	0.42 (0.01)	9.09	242	
0810+234	GD 295	DA3.1	16,360 (264)	8.03 (0.05)	0.63 (0.03)	11.16	94	
0810+334	CBS 68	DA2.6	19,270 (329)	8.08 (0.05)	0.67 (0.03)	10.96	161	
0810+392	KUV 08100+3915	DA2.1	23,790 (468)	7.90 (0.06)	0.58 (0.03)	10.31	203	
0810−728	RE J0809-725	DA1.6	31,670 (455)	7.87 (0.05)	0.58 (0.02)	9.64	127	
0811+644	GD 457	DA3.7	13,700 (334)	7.91 (0.05)	0.56 (0.03)	11.31	46	
0812+478	PG 0812+478	DA.8	62,000 (1195)	7.63 (0.06)	0.57 (0.02)	8.26	246	
0813+217	G40-15	DA8.3	6050 (173)	7.40 (0.39)	0.33 (0.14)	13.36	54	
0814+569	PG 0814+569	DA1.3	38,390 (575)	7.93 (0.05)	0.63 (0.02)	9.39	282	
0815+376	KUV 08157+3739	DA2.2	22,420 (370)	8.02 (0.05)	0.64 (0.03)	10.60	120	
0815+397	KUV 08157+3946	DA1.3	37,910 (723)	7.91 (0.07)	0.62 (0.04)	9.38	402	
0816+297	PG 0816+297	DA2.9	17,200 (276)	7.93 (0.05)	0.58 (0.03)	10.93	100	
0816+387	G111-71	DA6.5	7700 (114)	8.07 (0.07)	0.64 (0.04)	13.31	45	1
0817+386	KUV 08172+3838	DA1.9	26,070 (399)	8.03 (0.05)	0.66 (0.03)	10.32	130	

TABLE 3.5 – Continued

WD	Name	ST	$T_{\rm eff}$(K)	$\log g$	$M/\,{\rm M}_\odot$	M_V	D (pc)	Notes
0819+363	PG 0819+364	DA2.6	19,580 (312)	8.11 (0.05)	0.69 (0.03)	10.97	119	
0820−585	L186-119	DA5.5	9180 (132)	8.09 (0.06)	0.65 (0.04)	12.65	61	
0821+632	PG 0821+633	DA2.9	17,480 (292)	7.90 (0.05)	0.56 (0.03)	10.86	100	
0823+316	Ton 320	DAO.7	72,510 (2128)	7.76 (0.09)	0.64 (0.03)	8.16	340	
0824+288	PG 0824+289	DA1.1	47,600 (823)	7.83 (0.06)	0.61 (0.03)	8.94	124	2
0826+418	KUV 08268+4150	DA4.8	10,390 (159)	8.19 (0.07)	0.72 (0.04)	12.36	77	
0826+455	LTT 12215	DA4.8	10,550 (152)	7.94 (0.05)	0.57 (0.03)	11.92	43	
0827+328	LTT 18061	DA6.8	7410 (108)	8.43 (0.06)	0.87 (0.04)	14.02	22	
0827+410	KUV 08273+4101	DA3.2	15,930 (274)	7.90 (0.05)	0.56 (0.03)	11.03	95	
0830+371	G115-9	DA5.5	9250 (134)	8.33 (0.06)	0.81 (0.04)	13.00	40	1
0830−535	RE J0831-534	DA1.6	31,030 (443)	7.82 (0.04)	0.56 (0.02)	9.61	93	
0831+412	KUV 08317+4117	DA1.6	32,070 (516)	8.46 (0.07)	0.93 (0.04)	10.59	201	
0834+500	PG 0834+501	DAO.8	64,070 (2120)	7.39 (0.10)	0.51 (0.03)	7.61	336	
0835+366	CBS 77	DA3.0	16,670 (298)	8.05 (0.05)	0.64 (0.03)	11.15	148	
0836+237	PG 0836+237	DA.9	55,490 (1177)	7.75 (0.07)	0.60 (0.03)	8.62	401	
0836+404	KUV 08368+4026	DA4.1	12,280 (192)	8.17 (0.05)	0.71 (0.03)	11.88	53	3
0837+378	KUV 08371+3754	DA3.4	15,020 (463)	8.29 (0.06)	0.79 (0.04)	11.70	144	
0837+395	KUV 08378+3934	DA2.3	21,640 (489)	7.94 (0.07)	0.59 (0.04)	10.54	158	
0838+035	RE J0841+032	DA1.3	37,870 (673)	7.85 (0.07)	0.60 (0.03)	9.29	109	
0838+376	KUV 08387+3737	DA2.5	19,780 (337)	7.94 (0.05)	0.59 (0.03)	10.71	182	
0839+231	PG 0839+232	DA2.0	25,830 (382)	7.87 (0.04)	0.57 (0.02)	10.09	73	
0839+345	KUV 08397+3435	DA2.8	18,230 (292)	8.15 (0.05)	0.71 (0.03)	11.16	102	
0839+379	KUV 08391+3800	DA2.5	19,920 (372)	8.10 (0.06)	0.68 (0.03)	10.92	104	
0839−327	CD-32 5613	DA5.5	9230 (131)	7.96 (0.05)	0.57 (0.03)	12.44	8	1
0841+336	KUV 08411+3340	DA2.0	25,290 (475)	8.10 (0.06)	0.69 (0.04)	10.49	174	
0841+411	KUV 08417+4112	DA2.9	17,170 (354)	8.02 (0.06)	0.63 (0.04)	11.06	185	
0841+603	PG 0841+603	DA1.5	33,580 (511)	7.95 (0.06)	0.63 (0.03)	9.65	199	
0842+382	GD 94	DA6.2	8070 (117)	8.06 (0.06)	0.63 (0.04)	13.12	38	
0843+516	PG 0843+517	DA2.0	24,670 (405)	7.93 (0.05)	0.60 (0.03)	10.28	149	
0846+249	Ton 353	DAO.7	70,180 (2874)	7.48 (0.12)	0.55 (0.03)	7.67	643	2
0846+346	Ton 953	DA6.6	7620 (110)	8.13 (0.06)	0.68 (0.04)	13.44	28	
0846+557	PG 0846+558	DA1.8	28,330 (417)	7.92 (0.05)	0.60 (0.02)	9.97	195	
0847+354	CBS 86	DA3.7	13,780 (471)	8.00 (0.06)	0.61 (0.04)	11.43	130	
0847+386	KUV 08473+3838	DA2.7	18,410 (305)	8.39 (0.05)	0.86 (0.03)	11.53	124	
0848−730	BPM 5102	DA2.8	18,180 (267)	7.87 (0.04)	0.55 (0.02)	10.74	81	
0850+419	KUV 08504+4155	DA2.7	18,920 (329)	7.98 (0.05)	0.61 (0.03)	10.84	163	
0850−617	BPM 5109	DA2.3	21,840 (322)	7.99 (0.04)	0.62 (0.02)	10.60	67	
0852+630	LP 60-359	DA6.2	8160 (124)	7.96 (0.09)	0.57 (0.05)	12.93	36	2
0852+658	PG 0852+659	DA2.5	20,050 (318)	8.15 (0.05)	0.71 (0.03)	10.99	93	
0854+404	GD 98	DA2.2	23,070 (353)	7.96 (0.05)	0.61 (0.03)	10.46	77	
0855+329	Ton 366	DA3.1	16,260 (287)	7.94 (0.05)	0.58 (0.03)	11.05	195	
0858+363	GD 99	DA4.1	12,380 (190)	8.24 (0.05)	0.75 (0.03)	11.96	33	3
0859+337	CBS 90	DA2.0	25,360 (440)	8.02 (0.06)	0.65 (0.03)	10.36	134	
0859−039	RE J0902-040	DA2.1	24,550 (374)	7.89 (0.05)	0.58 (0.02)	10.24	39	
0900+354	CBS 91	DA1.4	36,970 (649)	7.83 (0.07)	0.58 (0.03)	9.29	348	

TABLE 3.5 – Continued

WD	Name	ST	$T_{\rm eff}$(K)	$\log g$	$M/\,{\rm M}_{\odot}$	M_V	D (pc)	Notes
0900+378	CBS 92	DA1.2	43,250 (870)	7.94 (0.08)	0.65 (0.04)	9.26	354	
0901+140	PG 0901+140	DA5.4	9270 (134)	8.36 (0.06)	0.82 (0.04)	13.04	40	
0901+597	PG 0901+598	DA.9	53,170 (1689)	7.69 (0.11)	0.57 (0.04)	8.57	367	
0902+418	KUV 09029+4153	DA1.1	45,220 (1067)	8.15 (0.09)	0.76 (0.05)	9.56	338	
0903+290	Ton 383	DA3.5	14,610 (356)	8.13 (0.05)	0.69 (0.03)	11.52	119	
0904+391	PG 0904+391	DA1.9	26,190 (400)	8.07 (0.05)	0.68 (0.03)	10.37	142	
0904+511	PG 0904+512	DA1.5	32,760 (490)	8.32 (0.06)	0.84 (0.03)	10.30	166	
0905+605	Mrk 393	DA5.7	8860 (130)	8.37 (0.06)	0.83 (0.04)	13.24	42	
0906+296	LP 313-16	DA2.4	21,060 (340)	7.93 (0.05)	0.58 (0.03)	10.57	108	
0908+171	PG 0908+171	DA2.8	17,980 (290)	8.03 (0.05)	0.64 (0.03)	11.01	105	
0909+271	Ton 393	DA1.0	49,820 (1739)	8.09 (0.13)	0.74 (0.07)	9.34	149	
0911−076	EC 09119-0738	DA2.7	18,510 (294)	8.01 (0.05)	0.62 (0.03)	10.92	112	
0913+204	PG 0913+205	DA2.1	24,280 (460)	8.25 (0.06)	0.78 (0.04)	10.81	163	
0913+442	G116-16	DA5.8	8690 (124)	8.21 (0.05)	0.73 (0.03)	13.05	29	1
0914−195	RE J0916-194	DA.8	61,920 (2764)	9.32 (0.15)	1.30 (0.08)	11.62	150	
0915+201	LB 3016	DA.7	72,710 (2388)	7.49 (0.10)	0.56 (0.03)	7.79	588	
0915+526	PG 0915+526	DA3.1	16,370 (257)	8.09 (0.05)	0.67 (0.03)	11.25	70	
0916+064	PG 0916+065	DA1.1	44,960 (761)	7.79 (0.06)	0.58 (0.02)	8.94	258	
0920+216	LB 3025	DA2.7	18,910 (296)	7.94 (0.05)	0.59 (0.03)	10.78	139	1
0920+306	CBS 6	DA2.7	18,940 (303)	6.76 (0.05)	0.24 (0.01)	8.83	271	
0920+363	Ton 1054	DA2.0	24,940 (436)	7.70 (0.06)	0.49 (0.02)	9.91	169	
0920+375	PG 0920+375	DA2.6	19,250 (312)	8.47 (0.05)	0.91 (0.03)	11.59	108	
0921+354	G117-B15A	DA4.0	12,600 (193)	8.14 (0.05)	0.69 (0.03)	11.79	55	3
0921−120	EC 09214-1205	DA2.6	19,340 (374)	7.09 (0.06)	0.30 (0.01)	9.35	289	
0922+162	PG 0922+162	DA2.0	24,670 (385)	8.35 (0.05)	0.85 (0.03)	10.95	112	
0922+183	PG 0922+183	DA2.0	25,660 (443)	8.26 (0.06)	0.79 (0.04)	10.72	144	
0924+289	CBS 9	DA2.2	23,040 (407)	7.91 (0.05)	0.58 (0.03)	10.39	210	
0926−039	G161-36	DA3.6	13,860 (344)	8.03 (0.05)	0.63 (0.03)	11.46	46	1
0926−127	EC 09260-1244	DA2.8	18,290 (298)	7.89 (0.05)	0.56 (0.03)	10.77	146	
0927+394	KUV 09272+3930	DA2.0	25,000 (492)	8.35 (0.07)	0.85 (0.04)	10.92	227	
0927−173	LP 787-49	DA5.0	0000 (141)	8.91 (0.04)	1.16 (0.02)	13.80	28	6
0928+085	PG 0928+085	DA1.7	30,160 (442)	8.58 (0.05)	1.00 (0.03)	10.93	159	
0928+399	KUV 09288+3959	DA1.9	26,360 (515)	8.07 (0.07)	0.68 (0.04)	10.36	272	
0928−713	BPM 5639	DA5.9	8470 (121)	8.28 (0.05)	0.78 (0.03)	13.27	27	1
0929+290	Ton 16	DA3.6	13,880 (376)	8.01 (0.05)	0.61 (0.03)	11.43	130	
0930+294	G117-25	DA6.0	8400 (122)	8.65 (0.06)	1.01 (0.04)	13.94	25	
0933+025	PG 0933+026	DA2.4	20,780 (383)	7.84 (0.06)	0.54 (0.03)	10.47	130	2
0933+729	PG 0933+729	DA2.8	18,120 (277)	8.09 (0.05)	0.67 (0.03)	11.08	84	
0934+337	Ton 1080	DA2.0	25,290 (395)	7.27 (0.05)	0.39 (0.01)	9.07	286	
0934−587	BPM 19652	DA2.2	22,410 (328)	7.85 (0.04)	0.55 (0.02)	10.34	106	
0935−371.2	LTT 3537	DA6.4	7920 (113)	8.04 (0.05)	0.62 (0.03)	13.16	25	
0937+505	PG 0937+506	DA1.4	36,370 (536)	7.95 (0.05)	0.64 (0.02)	9.52	198	
0937−103	EC 09377-1020	DA3.5	14,400 (375)	8.86 (0.06)	1.14 (0.03)	12.80	43	
0938+286	Ton 20	DA3.3	15,150 (250)	7.95 (0.05)	0.58 (0.03)	11.19	74	
0938+299	Ton 443	DA2.4	20,870 (329)	8.14 (0.05)	0.71 (0.03)	10.92	108	

TABLE 3.5 – Continued

WD	Name	ST	$T_{\rm eff}$(K)	$\log g$	$M/\,{\rm M}_\odot$	M_V	D (pc)	Notes
0938+550	PG 0938+550	DA2.6	19,150 (315)	8.23 (0.05)	0.76 (0.03)	11.20	53	
0939+262	Ton 21	DA.7	70,580 (1452)	7.94 (0.07)	0.71 (0.03)	8.70	155	
0939−153	EC 09395-1518	DA3.7	13,760 (340)	7.98 (0.05)	0.60 (0.03)	11.41	80	
0941+225	LP 370-41	DA3.9	13,080 (249)	8.11 (0.06)	0.68 (0.04)	11.68	123	
0941+432	SA 29-906	DA1.9	26,660 (419)	7.95 (0.05)	0.61 (0.03)	10.16	175	
0941−068	G161-68	DA8.2	6170 (140)	8.09 (0.24)	0.64 (0.15)	14.24	27	
0942+236.1	LB 11089	DA7.0	7240 (111)	7.90 (0.09)	0.54 (0.05)	13.32	63	
0942+236.2	LB 11092	DA7.2	6960 (121)	8.21 (0.14)	0.72 (0.09)	13.91	52	
0943+330	G117-B11B	DA7.2	7000 (123)	8.61 (0.13)	0.99 (0.08)	14.56	34	
0943+441	SA 29-130	DA3.8	13,310 (276)	7.69 (0.05)	0.45 (0.02)	11.04	28	1
0944+262	LP 370-55	DA4.5	11,080 (189)	8.10 (0.07)	0.67 (0.04)	12.02	52	
0944+424	SA 29-965	DA2.1	24,370 (378)	8.06 (0.05)	0.67 (0.03)	10.50	218	
0946+501	HS 0946+5009	DA1.6	31,620 (475)	8.23 (0.06)	0.79 (0.03)	10.22	285	
0947+325	Ton 458	DA2.2	23,240 (359)	8.34 (0.05)	0.83 (0.03)	11.03	74	
0947+857	RE J0957+852	DA1.0	50,890 (920)	8.23 (0.06)	0.82 (0.03)	9.57	171	
0948+534	PG 0948+534	DA.4	139,500 (7734)	7.56 (0.14)	0.75 (0.20)	7.04	405	
0949+256	Ton 462	DA2.1	23,490 (377)	8.01 (0.05)	0.64 (0.03)	10.50	142	
0949+451	HS 0949+4508	DA3.3	15,160 (283)	7.74 (0.06)	0.47 (0.03)	10.89	95	2
0950+023	PG 0950+024	DA1.2	41,180 (709)	7.83 (0.06)	0.59 (0.03)	9.13	246	
0950+077	PG 0950+078	DA3.3	15,450 (266)	8.08 (0.05)	0.66 (0.03)	11.33	125	1
0950+139	PG 0950+139	DAO.5	93,230 (425)	7.37 (0.79)	0.59 (0.21)	7.00	647	
0950+185	PG 0950+186	DA1.7	29,460 (483)	7.54 (0.06)	0.46 (0.02)	9.25	166	2
0950−572	BPM 19738	DA3.9	12,790 (237)	7.81 (0.06)	0.50 (0.03)	11.30	53	1
0951−155	EC 09512-1534	DA2.7	18,590 (293)	8.01 (0.05)	0.63 (0.03)	10.92	108	
0953+340	KUV 09538+3405	DA2.9	17,570 (318)	7.99 (0.06)	0.61 (0.03)	10.98	143	
0954+134	PG 0954+135	DA3.1	16,370 (306)	7.94 (0.06)	0.58 (0.03)	11.03	119	
0954+697	PG 0954+697	DA2.2	22,410 (376)	7.95 (0.05)	0.60 (0.03)	10.50	123	
0954−710	BPM 6082	DA3.4	14,730 (226)	7.80 (0.04)	0.51 (0.02)	11.03	31	
0955+247	LTT 12661	DA5.8	8640 (125)	8.35 (0.06)	0.82 (0.04)	13.29	23	1
0955−008	LB 3090	DA2.1	24,170 (434)	8.02 (0.06)	0.64 (0.03)	10.46	179	
0956+020	PG 0956+021	DA3.0	16,630 (264)	7.93 (0.05)	0.58 (0.03)	11.00	81	
0956+045	PG 0956+046	DA2.7	18,950 (317)	7.89 (0.05)	0.56 (0.03)	10.71	104	1
0957−666	BPM 6114	DA1.8	27,640 (406)	7.25 (0.05)	0.39 (0.01)	8.83	143	
0958+353	KUV 09583+3520	DA1.2	41,870 (898)	7.85 (0.09)	0.60 (0.04)	9.15	355	
0959+297	CBS 18	DA.8	65,330 (2155)	7.90 (0.12)	0.68 (0.05)	8.71	181	
1000−001	LB 564	DA2.4	20,650 (339)	8.00 (0.05)	0.62 (0.03)	10.72	118	
1001+203	Ton 1150	DA2.4	21,010 (439)	7.88 (0.06)	0.56 (0.03)	10.50	93	2
1001+333	KUV 10010+3318	DA5.1	9830 (144)	8.29 (0.06)	0.78 (0.04)	12.70	52	
1001+362	KUV 10013+3614	DA5.3	9550 (143)	7.42 (0.09)	0.36 (0.03)	11.46	117	
1002+430	GD 111	DA2.4	20,980 (398)	8.03 (0.06)	0.64 (0.03)	10.73	122	
1003+445	RE J1006+443	DA.9	55,460 (1439)	7.77 (0.09)	0.60 (0.04)	8.66	465	
1003−023	PG 1003-023	DA2.4	21,010 (333)	8.01 (0.05)	0.63 (0.03)	10.70	88	
1005+642	GD 462	DA2.4	20,700 (322)	7.95 (0.05)	0.60 (0.03)	10.64	42	
1006+353	KUV 10063+3522	DA2.4	20,740 (468)	7.90 (0.07)	0.57 (0.04)	10.56	285	
1008+372	KUV 10090+3712	DA3.1	16,280 (286)	7.99 (0.05)	0.61 (0.03)	11.12	150	

TABLE 3.5 – Continued

WD	Name	ST	$T_{\rm eff}$(K)	$\log g$	$M/\,{\rm M}_{\odot}$	M_V	D (pc)	Notes
1008+382	KUV 10081+3817	DA3.7	13,740 (354)	7.98 (0.05)	0.60 (0.03)	11.40	120	
1010+043	PG 1010+043	DA1.7	28,810 (472)	8.05 (0.06)	0.67 (0.03)	10.13	175	
1010+064	PG 1010+065	DA1.1	45,280 (864)	7.93 (0.07)	0.65 (0.03)	9.18	301	
1011+335	KUV 10115+3332	DA2.5	20,560 (417)	8.11 (0.06)	0.69 (0.04)	10.90	200	
1012+083.1	LTT 12749	DA7.5	6720 (128)	8.02 (0.18)	0.60 (0.11)	13.78	30	
1013+256	Ton 494	DA2.2	22,840 (354)	8.05 (0.05)	0.66 (0.03)	10.61	118	
1013−010	G53-38	DA6.1	8280 (120)	8.04 (0.06)	0.62 (0.04)	12.99	29	
1013−050	RE J1016-053	DAO.9	57,250 (1528)	8.03 (0.08)	0.72 (0.04)	8.93	110	
1013−111	EC 10136-1111	DA3.0	17,020 (260)	8.04 (0.05)	0.64 (0.03)	11.11	135	
1015+161	PG 1015+161	DA2.5	20,420 (324)	8.11 (0.05)	0.69 (0.03)	10.91	88	
1015−173	EC 10150-1722	DA1.6	32,370 (574)	7.58 (0.09)	0.47 (0.03)	9.12	343	
1015−216	EC 10150-2138	DA1.6	31,960 (467)	7.96 (0.05)	0.63 (0.03)	9.77	151	
1016−308	Subasavage	DA3.1	16,340 (244)	8.19 (0.04)	0.73 (0.03)	11.40	45	
1017+125	PG 1017+125	DA2.2	22,620 (355)	7.95 (0.05)	0.60 (0.03)	10.48	113	
1017−138	EC 10174-1352	DA1.6	31,880 (481)	8.03 (0.06)	0.67 (0.03)	9.89	86	
1017−163	EC 10172-1618	DA1.9	27,050 (433)	8.03 (0.05)	0.66 (0.03)	10.24	154	
1018+410	PG 1018+411	DA2.1	24,440 (405)	8.11 (0.05)	0.69 (0.03)	10.57	100	
1018−103	EC 10188-1019	DA2.8	17,720 (348)	8.52 (0.06)	0.94 (0.04)	11.82	81	5
1019+129	PG 1019+129	DA2.6	19,030 (310)	8.02 (0.05)	0.64 (0.03)	10.89	87	
1019+462	GD 117	DA7.6	6600 (130)	8.54 (0.17)	0.94 (0.11)	14.65	26	
1019+637	LP 62-147	DA7.2	6970 (109)	8.29 (0.10)	0.78 (0.06)	14.03	14	
1020+315	SA 54-79	DA2.8	18,240 (309)	8.00 (0.05)	0.62 (0.03)	10.93	171	
1020−207	EC 10203-2044	DA2.5	20,550 (374)	7.99 (0.06)	0.62 (0.03)	10.71	75	
1022+050	LP 550-52	DA3.5	14,610 (241)	7.63 (0.05)	0.44 (0.02)	10.76	48	1
1022−301	RE J1024-302	DA1.4	35,880 (658)	9.11 (0.08)	1.26 (0.04)	11.69	66	
1023+009	PG 1023+009	DA1.4	36,470 (574)	7.88 (0.06)	0.60 (0.03)	9.39	252	
1026+002	PG 1026+002	DA2.9	17,210 (261)	7.96 (0.05)	0.59 (0.03)	10.97	38	2
1026+023	LP 550-292	DA3.8	13,140 (199)	8.06 (0.05)	0.64 (0.03)	11.60	33	1
1026+453	PG 1026+454	DA1.4	36,410 (543)	7.96 (0.05)	0.64 (0.03)	9.52	210	
1028+328	Ton 523	DA3.3	15,260 (288)	8.16 (0.05)	0.71 (0.03)	11.48	80	
1029+537	RE J1032+532	DA1.1	46,580 (879)	7.82 (0.07)	0.60 (0.03)	8.95	118	
1031+063	PG 1031+063	DA2.3	21,620 (371)	7.91 (0.05)	0.58 (0.03)	10.49	142	
1031−114	LTT 3870	DA1.9	26,310 (376)	7.92 (0.04)	0.59 (0.02)	10.13	37	
1031−147	EC 10315-1446	DA1.7	30,150 (453)	7.99 (0.05)	0.65 (0.03)	9.94	166	
1033+464	GD 123	DA1.7	30,260 (445)	7.90 (0.05)	0.60 (0.03)	9.78	82	
1034+492	GD 304	DA2.4	21,420 (353)	8.22 (0.05)	0.76 (0.03)	10.98	77	
1036+085	PG 1036+086	DA2.2	23,200 (365)	7.51 (0.05)	0.43 (0.02)	9.71	204	
1037+512	PG 1037+512	DA2.5	19,780 (346)	7.99 (0.05)	0.62 (0.03)	10.78	124	2
1038+633	PG 1038+634	DA2.0	25,400 (380)	8.42 (0.05)	0.89 (0.03)	11.00	68	
1038−277	EC 10381-2742	DA4.1	12,400 (191)	7.88 (0.05)	0.54 (0.03)	11.45	123	
1039+412	PB 520	DA4.2	12,040 (188)	8.19 (0.05)	0.72 (0.03)	11.95	66	3
1039+747	PG 1039+748	DA1.7	29,670 (465)	7.88 (0.06)	0.58 (0.03)	9.81	160	
1040+451	PG 1040+452	DA1.1	46,090 (1046)	7.99 (0.09)	0.68 (0.04)	9.26	343	
1040+492	RE J1043+490	DA1.0	48,070 (1021)	7.67 (0.08)	0.55 (0.03)	8.66	309	
1041+580	PG 1041+580	DA1.6	30,990 (451)	7.82 (0.05)	0.56 (0.02)	9.61	100	

TABLE 3.5 – Continued

WD	Name	ST	$T_{\rm eff}$(K)	$\log g$	$M/\,{\rm M}_\odot$	M_V	D (pc)	Notes
1042−690	LTT 3943	DA2.2	22,570 (331)	7.84 (0.04)	0.54 (0.02)	10.31	36	
1046+281	Ton 547	DA3.8	13,160 (215)	8.06 (0.05)	0.64 (0.03)	11.59	58	1
1046+301	CBS 27	DA3.0	16,970 (309)	7.95 (0.06)	0.59 (0.03)	10.99	100	
1047+335	CBS 130	DA4.3	11,630 (189)	8.20 (0.06)	0.73 (0.04)	12.04	98	
1047+694	PG 1047+694	DA1.5	33,810 (510)	7.99 (0.06)	0.65 (0.03)	9.69	187	
1048−150	EC 10481-1503	DA.9	55,550 (1387)	7.77 (0.09)	0.60 (0.03)	8.66	387	
1049+103	PG 1049+103	DA2.5	20,000 (345)	7.88 (0.05)	0.56 (0.03)	10.59	103	2
1049−158	EC 10498-1552	DA2.5	19,900 (328)	8.39 (0.05)	0.86 (0.03)	11.39	39	
1051−147	EC 10514-1447	DA2.4	20,570 (367)	8.33 (0.05)	0.83 (0.03)	11.24	102	
1052+273	Ton 556	DA2.1	24,080 (370)	8.42 (0.05)	0.89 (0.03)	11.11	40	
1052+342	CBS 131	DA3.5	14,540 (277)	7.60 (0.06)	0.43 (0.02)	10.72	181	
1053−092	PG 1053-092	DA2.1	23,570 (396)	7.77 (0.05)	0.51 (0.02)	10.13	174	
1053−290	EC 10532-2903	DA4.7	10,700 (154)	8.18 (0.05)	0.71 (0.03)	12.24	43	
1053−550	LTT 4013	DA3.4	14,770 (229)	8.00 (0.04)	0.61 (0.03)	11.30	40	1
1054−226	LP 849-31	DAZ6.4	7910 (118)	8.05 (0.08)	0.62 (0.05)	13.17	37	
1056+516	LB 1919	DA.7	68,510 (2150)	7.94 (0.11)	0.70 (0.05)	8.73	407	
1056−384	RE J1058-384	DA1.7	28,870 (420)	7.97 (0.05)	0.63 (0.03)	10.00	65	
1057+719	PG 1057+719	DA1.2	42,050 (645)	7.85 (0.05)	0.60 (0.02)	9.13	136	
1058−129	PG 1058-129	DA2.0	25,200 (369)	8.75 (0.04)	1.08 (0.02)	11.61	67	
1100+604	G197-4	DA2.7	18,990 (290)	8.08 (0.05)	0.67 (0.03)	10.98	37	
1101+242	Ton 53	DA1.6	31,310 (482)	7.89 (0.06)	0.60 (0.03)	9.70	231	
1101+364	PG 1101+364	DA3.7	13,770 (241)	7.41 (0.05)	0.37 (0.02)	10.49	62	1
1102+748	GD 466	DA2.4	20,660 (337)	8.38 (0.05)	0.86 (0.03)	11.31	54	
1102−183	EC 11023-1821	DA6.1	8290 (124)	8.19 (0.07)	0.72 (0.05)	13.21	36	
1102−281	EC 11023-2810	DA2.7	18,640 (280)	8.64 (0.04)	1.02 (0.03)	11.95	79	
1103+384	PG 1103+385	DA1.9	26,750 (426)	8.58 (0.05)	0.99 (0.03)	11.17	161	
1104+044	LP 551-66	DA2.3	21,750 (424)	7.91 (0.06)	0.58 (0.03)	10.48	101	2
1105−048	LTT 4099	DA3.1	16,110 (250)	7.98 (0.05)	0.60 (0.03)	11.11	23	
1105−340A	SCR J1107-3420A	DA3.6	13,970 (272)	8.05 (0.04)	0.64 (0.03)	11.48	27	
1106+316	CSO 75	DA1.7	29,370 (458)	7.84 (0.06)	0.56 (0.03)	9.76	244	2
1108+325	Ton 60	DA.8	64,050 (2060)	7.64 (0.11)	0.58 (0.04)	8.24	357	
1108+475	GD 129	DA3.8	13,250 (247)	8.26 (0.05)	0.77 (0.03)	11.89	50	1
1108+563	GD 305	DA5.5	9150 (135)	8.03 (0.07)	0.62 (0.04)	12.58	73	
1109+244	Ton 61	DA1.3	38,390 (615)	8.18 (0.06)	0.77 (0.03)	9.81	156	
1113+413	PG 1113+413	DA1.9	26,350 (390)	7.89 (0.05)	0.58 (0.02)	10.08	120	
1114+067	LTT 13038	DA7.8	6490 (130)	8.10 (0.20)	0.65 (0.12)	14.04	35	
1114+223	PG 1114+224	DA1.9	26,620 (431)	7.44 (0.05)	0.43 (0.02)	9.29	254	
1115+166	PG 1115+166	DA2.1	23,750 (335)	8.16 (0.04)	0.72 (0.03)	10.71	76	7
1116+026	GD 133	DA4.0	12,600 (192)	8.12 (0.05)	0.68 (0.03)	11.76	36	3
1116−307	EC 11167-3044	DA4.1	12,190 (187)	8.17 (0.05)	0.71 (0.03)	11.89	82	
1119+385	PG 1119+386	DA3.0	17,060 (259)	8.06 (0.04)	0.65 (0.03)	11.13	83	1
1119−243	EC 11191-2423	DA2.0	25,240 (436)	8.01 (0.06)	0.64 (0.03)	10.36	169	
1120+439	PG 1120+439	DA1.8	27,800 (402)	8.39 (0.04)	0.87 (0.03)	10.76	102	
1121+216	Ross 627	DA6.8	7430 (107)	8.16 (0.06)	0.69 (0.04)	13.58	14	
1121−507	BPM 20912	DA2.9	17,100 (250)	7.97 (0.04)	0.60 (0.03)	11.01	59	

TABLE 3.5 – Continued

WD	Name	ST	$T_{\rm eff}$(K)	$\log g$	$M/\,{\rm M}_\odot$	M_V	D (pc)	Notes
1122+426	GD 308	DA4.8	10,470 (157)	8.17 (0.06)	0.71 (0.04)	12.30	66	
1122+546	LB 2012	DA3.3	15,050 (244)	7.96 (0.05)	0.59 (0.03)	11.21	70	1
1122−324	EC 11221-3229	DA2.2	23,410 (351)	7.81 (0.04)	0.53 (0.02)	10.21	135	
1123+189	PG 1123+189	DA.9	53,220 (926)	7.92 (0.06)	0.66 (0.03)	8.97	107	
1124+595		DA4.7	10,750 (156)	8.88 (0.05)	1.14 (0.02)	13.49	21	
1124−018	PG 1124-019	DA2.0	25,180 (398)	7.74 (0.05)	0.51 (0.02)	9.95	201	
1124−190	EC 11249-1904	DA4.0	12,560 (233)	8.53 (0.06)	0.94 (0.04)	12.40	65	
1124−293	ESO 439-80	DA5.3	9490 (135)	8.17 (0.05)	0.70 (0.03)	12.65	30	
1125+175	PG 1125+175	DA.9	54,430 (1896)	7.87 (0.13)	0.64 (0.06)	8.85	263	
1125−025	PG 1125-026	DA1.6	31,560 (463)	8.25 (0.05)	0.80 (0.03)	10.26	107	
1126+384	Feige 43	DA2.0	25,800 (395)	8.00 (0.05)	0.64 (0.03)	10.30	82	
1128+564	LB 2033	DA1.8	27,490 (428)	7.87 (0.05)	0.57 (0.03)	9.96	199	
1129+071	PG 1129+072	DA3.6	13,910 (296)	8.02 (0.05)	0.62 (0.03)	11.44	49	
1129+155	PG 1129+156	DA2.8	17,990 (279)	8.24 (0.05)	0.76 (0.03)	11.32	35	
1129−537	BPM 21021	DA2.1	24,270 (352)	7.79 (0.04)	0.53 (0.02)	10.11	131	
1130+189	LP 433-6	DA4.5	11,200 (186)	8.55 (0.06)	0.95 (0.04)	12.72	66	
1130−125	EC 11307-1232	DA3.4	14,780 (390)	8.38 (0.05)	0.85 (0.03)	11.89	53	
1131+315	LB 10262	DA2.2	22,510 (626)	8.19 (0.09)	0.74 (0.05)	10.86	169	
1131+320	PB 2947	DA3.6	14,190 (308)	8.08 (0.05)	0.66 (0.03)	11.50	80	
1131+333	CBS 142	DA5.5	9170 (140)	8.75 (0.07)	1.07 (0.04)	13.79	44	
1132+470	G122-31	DA1.8	28,160 (466)	8.96 (0.06)	1.19 (0.03)	11.81	83	
1132−298	LDS 4119	DA6.7	7540 (134)	7.17 (0.22)	0.27 (0.06)	12.05	116	2
1133+293	Feige 45	DA2.1	24,050 (383)	7.89 (0.05)	0.58 (0.03)	10.28	88	
1134+300	LB 10276	DA2.2	22,470 (342)	8.56 (0.05)	0.97 (0.03)	11.48	20	
1135+321	CBS 48	DA3.2	15,970 (267)	8.04 (0.05)	0.64 (0.03)	11.22	36	
1136+667	HS 1136+6646	DAO.6	83,090 (2271)	7.31 (0.08)	0.55 (0.02)	7.06	233	
1137+423	KUV 11370+4222	DA4.1	12,230 (190)	8.22 (0.05)	0.74 (0.03)	11.95	83	3
1139+258	RX J1141+255	DA1.1	43,930 (1373)	8.03 (0.13)	0.70 (0.07)	9.39	331	
1139+424	KUV 11390+4225	DA1.8	28,000 (434)	7.92 (0.05)	0.60 (0.03)	10.00	174	
1141+077	PG 1141+078	DA.8	64,800 (1363)	7.53 (0.07)	0.55 (0.02)	8.01	205	
1141+504	LB 2094	DA2.3	21,640 (382)	7.94 (0.05)	0.59 (0.03)	10.54	160	
1141−316	EC 11411-3137	DA2.9	17,590 (261)	8.13 (0.04)	0.70 (0.03)	11.20	119	
1142+369	CBS 144	DA3.4	14,870 (240)	7.75 (0.05)	0.48 (0.02)	10.93	103	
1143+321	G148-7	DA3.1	16,290 (246)	8.17 (0.04)	0.72 (0.03)	11.39	28	
1143−314	EC 11437-3124	DA1.3	38,810 (596)	8.04 (0.05)	0.69 (0.03)	9.56	246	
1144−246	EC 11448-2438	DA1.6	31,410 (460)	7.18 (0.05)	0.38 (0.01)	8.42	287	
1145+187	PG 1145+188	DA1.8	27,390 (405)	7.87 (0.05)	0.57 (0.02)	9.96	71	
1147+255	LP 375-51	DA4.9	10,310 (149)	8.22 (0.05)	0.74 (0.03)	12.42	45	1
1147+389	KUV 11472+3858	DA2.8	18,160 (319)	8.00 (0.05)	0.62 (0.03)	10.94	170	
1148+544	LP 129-587	DA5.1	9970 (148)	8.22 (0.06)	0.74 (0.04)	12.54	69	
1149+057	LP 553-57	DA4.4	11,360 (167)	8.21 (0.05)	0.73 (0.03)	12.11	36	3
1149+410	GD 312	DA3.4	14,730 (288)	7.97 (0.05)	0.59 (0.03)	11.26	89	
1150−153	EC 11507-1519	DA4.0	12,640 (204)	8.22 (0.05)	0.74 (0.03)	11.90	66	3
1152+371	CBS 152	DA1.8	27,420 (465)	9.14 (0.07)	1.26 (0.02)	12.25	89	
1152−287	EC 11522-2843	DA2.3	21,650 (321)	7.69 (0.04)	0.47 (0.02)	10.17	174	

TABLE 3.5 – Continued

WD	Name	ST	$T_{\rm eff}$(K)	$\log g$	$M/\,{\rm M}_\odot$	M_V	D (pc)	Notes
1155+333	CBS 154	DA4.0	12,670 (613)	7.39 (0.09)	0.36 (0.03)	10.63	188	
1155−243	EC 11550-2422	DA3.6	13,830 (542)	7.95 (0.06)	0.58 (0.04)	11.35	106	
1156+291	CBS 50	DA5.4	9370 (137)	8.39 (0.06)	0.84 (0.04)	13.05	39	
1157+359	CBS 155	DA6.9	7330 (119)	8.57 (0.10)	0.96 (0.07)	14.31	35	
1158+432	PG 1158+433	DA3.4	14,810 (247)	7.98 (0.05)	0.60 (0.03)	11.27	95	
1159+803	G255-2	DA4.3	11,760 (180)	8.24 (0.05)	0.75 (0.03)	12.07	65	3
1159−098	LP 734-6	DA5.3	9580 (138)	8.90 (0.05)	1.15 (0.03)	13.94	25	
1200+548	LB 2181	DA1.7	29,030 (444)	7.97 (0.05)	0.63 (0.03)	9.99	183	
1201−001	PG 1201-001	DA2.4	20,600 (317)	8.33 (0.05)	0.83 (0.03)	11.24	60	
1201−049	PG 1201-049	DAOZ.9	57,260 (1902)	7.62 (0.11)	0.55 (0.04)	8.19	426	
1202+308	Ton 75	DA1.7	29,670 (465)	7.82 (0.06)	0.55 (0.03)	9.71	114	
1202+608	Feige 55	DAO.9	57,640 (1356)	7.33 (0.08)	0.47 (0.02)	7.65	155	
1202−232	LP 852-7	DA5.7	8770 (126)	8.27 (0.05)	0.77 (0.03)	13.11	9	
1203−272	EC 12037-2712	DA1.4	35,330 (523)	7.86 (0.05)	0.59 (0.02)	9.42	300	
1204+450	PG 1204+451	DA2.1	23,610 (383)	7.80 (0.05)	0.53 (0.02)	10.18	91	
1204−136	EC 12043-1337	DA4.4	11,420 (169)	8.31 (0.05)	0.80 (0.03)	12.26	45	1
1204−322	EC 12042-3217	DA2.2	22,440 (340)	7.97 (0.05)	0.61 (0.03)	10.52	107	
1207−157	EC 12075-1543	DA2.9	17,490 (311)	7.96 (0.06)	0.60 (0.03)	10.95	118	
1208+576	G197-47	DA8.6	5890 (135)	7.65 (0.16)	0.42 (0.07)	13.84	25	
1210+140	PG 1210+141	DA1.6	32,380 (479)	7.14 (0.05)	0.37 (0.01)	8.27	190	
1210+464	PG 1210+464	DA2.4	21,360 (600)	7.91 (0.09)	0.58 (0.04)	10.52	113	2
1210+533	PG 1210+533	DAO1.1	46,320 (703)	7.88 (0.05)	0.63 (0.02)	8.98	107	2
1211+320	CBS 54	DA3.9	12,990 (236)	8.09 (0.06)	0.66 (0.03)	11.66	74	1
1211+392	G198-B6A	DA2.7	18,970 (300)	7.98 (0.05)	0.61 (0.03)	10.83	135	
1213+528	Case 1	DA3.3	15,450 (356)	8.07 (0.06)	0.66 (0.04)	11.33	25	2
1214+267	LB 2	DAO.7	67,850 (2097)	7.72 (0.10)	0.62 (0.03)	8.18	309	
1216+036	PG 1216+036	DA3.5	14,420 (345)	7.98 (0.06)	0.60 (0.03)	11.31	86	
1218+497	LB 2318	DA1.4	35,810 (567)	7.99 (0.06)	0.66 (0.03)	9.60	212	
1218−198	EC 12185-1950	DA1.4	35,880 (592)	7.92 (0.07)	0.62 (0.03)	9.49	236	
1220+191	LP 435-58	DA4.6	10,900 (181)	8.26 (0.07)	0.77 (0.05)	12.32	71	
1220+234	Ton 610	DA2.0	24,680 (513)	9.12 (0.07)	1.25 (0.03)	12.41	44	5
1220−292	EC 12204-2915	DA2.7	18,670 (278)	7.91 (0.04)	0.57 (0.02)	10.76	101	
1222+339	CBS 351	DA3.1	16,030 (279)	8.02 (0.05)	0.63 (0.03)	11.19	145	
1223+478	PG 1223+478	DA1.6	31,550 (468)	7.88 (0.05)	0.59 (0.03)	9.66	255	
1223−659	BPM 7543	DA6.6	7590 (108)	7.85 (0.05)	0.51 (0.03)	13.06	15	
1224+309	CBS 60	DA1.7	29,750 (484)	7.48 (0.06)	0.44 (0.02)	9.12	238	
1225−164	EC 12252-1628	DA3.1	16,350 (299)	7.91 (0.06)	0.57 (0.03)	11.00	110	
1227+307	LB 11231	DA3.6	13,880 (523)	8.04 (0.06)	0.63 (0.04)	11.47	128	
1229−012	PG 1229-013	DA2.5	20,480 (337)	7.56 (0.05)	0.44 (0.02)	10.03	56	1
1230+417	HZ 28	DA2.5	20,310 (311)	8.03 (0.05)	0.64 (0.03)	10.79	97	
1230−308	EC 12303-3052	DA2.0	25,180 (366)	8.23 (0.04)	0.77 (0.03)	10.71	105	
1231+465	Ton 82	DA2.1	23,720 (372)	7.92 (0.05)	0.59 (0.03)	10.35	141	
1231−141	EC 12310-1408	DA2.9	17,390 (307)	8.02 (0.05)	0.63 (0.03)	11.04	104	
1232+238	PG 1232+238	DA1.1	47,600 (1278)	7.73 (0.10)	0.57 (0.04)	8.77	531	
1232+479	GD 148	DA3.3	15,070 (246)	7.95 (0.05)	0.59 (0.03)	11.20	46	

TABLE 3.5 – Continued

WD	Name	ST	$T_{\rm eff}$(K)	$\log g$	$M/\,{\rm M}_{\odot}$	M_V	D (pc)	Notes
1233+337	PG 1233+338	DA2.6	19,680 (317)	8.00 (0.05)	0.62 (0.03)	10.81	99	
1233−164	EC 12336-1625	DA2.0	24,950 (417)	8.31 (0.05)	0.82 (0.03)	10.86	70	
1234+481	PG 1234+482	DA.9	56,630 (1005)	7.86 (0.06)	0.64 (0.03)	8.80	133	
1235+294	KUV 12353+2925	DA2.6	19,400 (358)	7.95 (0.06)	0.59 (0.03)	10.75	141	
1236−495	LFT 931	DA4.2	11,920 (194)	8.81 (0.05)	1.11 (0.03)	13.05	15	3
1237−028	LP 615-183	DA4.9	10,310 (148)	8.66 (0.05)	1.02 (0.03)	13.19	35	
1237−230	LHS 339	DA8.8	5760 (251)	7.83 (0.61)	0.49 (0.32)	14.22	31	
1239+277	KUV 12399+2744	DA3.3	15,410 (265)	7.97 (0.05)	0.59 (0.03)	11.18	80	
1240+754	LB 261	DA2.6	19,580 (332)	7.93 (0.05)	0.58 (0.03)	10.70	91	
1241+235	LB 16	DA1.8	27,420 (424)	7.97 (0.05)	0.62 (0.03)	10.11	103	1
1241+296	KUV 12420+2938	DA2.7	18,660 (357)	7.90 (0.06)	0.57 (0.03)	10.75	112	
1241−010	PG 1241-010	DA2.1	24,480 (374)	7.37 (0.05)	0.41 (0.01)	9.33	86	
1243+301	KUV 12436+3011	DA3.4	14,900 (376)	7.89 (0.07)	0.55 (0.04)	11.14	196	
1243−194	EC 12431-1929	DA4.6	10,900 (163)	8.68 (0.05)	1.03 (0.03)	13.04	45	
1244+149	G61-17	DA4.6	10,870 (161)	8.15 (0.05)	0.69 (0.03)	12.14	55	1
1244−125	EC 12448-1232	DA3.6	13,880 (395)	8.02 (0.05)	0.62 (0.03)	11.44	45	
1247+310	KUV 12474+3105	DA4.1	12,370 (244)	8.39 (0.06)	0.85 (0.04)	12.20	100	
1247+575	LB 244	DA2.3	21,970 (416)	8.19 (0.06)	0.74 (0.04)	10.90	126	
1247−176	EC 12477-1738	DA2.3	21,620 (497)	8.16 (0.07)	0.72 (0.04)	10.88	116	2
1248−610	BPM 7755	DA2.0	24,870 (416)	8.05 (0.05)	0.66 (0.03)	10.44	125	
1249+044	HS 1249+0426	DA4.1	12,420 (191)	8.25 (0.05)	0.76 (0.03)	11.98	80	3
1249+160	GD 150	DA1.9	26,390 (413)	7.34 (0.05)	0.41 (0.01)	9.12	125	
1249+182	GD 151	DA2.5	20,400 (313)	7.84 (0.05)	0.54 (0.02)	10.50	99	
1249+296	LP 321-160	DA4.1	12,150 (236)	8.31 (0.07)	0.80 (0.04)	12.11	87	
1253+105	HS 1253+1033	DA3.8	13,380 (320)	7.94 (0.06)	0.57 (0.03)	11.39	40	1
1253+378	HZ 34	DAO.6	87,670 (3529)	7.02 (0.12)	0.50 (0.03)	6.38	716	
1253+482	GD 320	DA3.4	14,650 (301)	7.73 (0.06)	0.47 (0.03)	10.94	127	1
1254+223	BPM 88611	DA1.2	40,320 (626)	7.93 (0.05)	0.64 (0.03)	9.33	63	
1254−133	EC 12540-1318	DA2.1	23,710 (415)	7.92 (0.05)	0.59 (0.03)	10.35	138	
1255+426	PG 1255+426	DA1.3	39,960 (1298)	7.96 (0.14)	0.65 (0.07)	9.39	364	
1257+032	PB 4421	DA2.8	18,030 (278)	7.86 (0.05)	0.54 (0.02)	10.75	96	
1257+047	GD 267	DA2.2	23,260 (362)	8.01 (0.05)	0.63 (0.03)	10.51	81	
1257+278	LTT 13742	DA5.7	8810 (127)	8.44 (0.06)	0.88 (0.04)	13.38	25	
1257−723	BPM 7961	DA2.7	18,390 (276)	7.98 (0.04)	0.61 (0.03)	10.89	72	
1258+013	HE 1258+0123	DA4.3	11,740 (176)	8.11 (0.05)	0.67 (0.03)	11.88	73	3
1258+297	LP 322-329	DA3.2	15,540 (311)	8.03 (0.06)	0.63 (0.03)	11.26	256	
1258+593	LB 2520	DA3.3	15,160 (242)	8.00 (0.05)	0.61 (0.03)	11.26	65	
1300−098	PG 1300-099	DA3.1	16,060 (404)	8.33 (0.07)	0.82 (0.04)	11.66	85	1
1301+544	LB 248	DA1.5	34,050 (514)	8.19 (0.06)	0.77 (0.03)	10.01	137	
1304+227	LP 378-537	DA4.8	10,460 (179)	8.46 (0.09)	0.89 (0.06)	12.77	48	
1305+018	PG 1305+018	DA1.7	29,790 (449)	7.87 (0.05)	0.58 (0.03)	9.78	115	
1305−017	PG 1305-017	DAO1.1	44,400 (743)	7.76 (0.08)	0.57 (0.03)	8.80	448	
1307+354	GD 154	DA4.4	11,430 (171)	8.21 (0.05)	0.74 (0.03)	12.10	44	3
1307−141	EC 13077-1411	DA1.9	26,400 (457)	7.92 (0.06)	0.60 (0.03)	10.13	183	
1308+316	KUV 13088+3139	DA3.6	13,830 (421)	8.04 (0.06)	0.63 (0.03)	11.48	97	

TABLE 3.5 – Continued

WD	Name	ST	$T_{\rm eff}$(K)	$\log g$	$M/\,{\rm M}_\odot$	M_V	D (pc)	Notes
1308+329	CBS 342	DA2.7	18,370 (294)	7.99 (0.05)	0.61 (0.03)	10.91	104	
1308−301	EC 13085-3010	DA3.3	15,280 (233)	7.98 (0.04)	0.60 (0.03)	11.21	60	
1310+583	PG 1310+583	DA4.7	10,680 (156)	8.39 (0.05)	0.85 (0.03)	12.58	20	
1310−305	EC 13109-3035	DA2.4	21,320 (312)	7.91 (0.04)	0.58 (0.02)	10.53	62	
1314+293	HZ 43	DA.9	56,790 (1249)	7.89 (0.07)	0.65 (0.03)	8.84	64	2
1314−067	PG 1314-067	DA2.9	17,090 (289)	7.97 (0.05)	0.60 (0.03)	11.01	95	
1314−153	LP 737-47	DA3.2	15,670 (272)	7.91 (0.05)	0.56 (0.03)	11.07	57	
1317+453	G177-31	DA3.6	14,040 (243)	7.54 (0.05)	0.41 (0.02)	10.67	49	
1319+466	G177-31	DA3.5	14,500 (335)	8.30 (0.05)	0.79 (0.03)	11.78	36	
1319−288	EC 13198-2849	DA3.0	16,630 (308)	7.75 (0.06)	0.49 (0.03)	10.74	112	2
1320+645	PG 1320+645	DA1.8	28,200 (464)	7.52 (0.06)	0.45 (0.02)	9.30	260	
1321+607	LP 96-125	DA3.9	12,930 (277)	7.95 (0.07)	0.58 (0.04)	11.47	92	
1322+076	PG 1322+077	DA1.9	26,990 (474)	7.99 (0.06)	0.63 (0.03)	10.18	164	
1323−514	LFT 1004	DA2.5	19,930 (297)	7.85 (0.04)	0.54 (0.02)	10.56	64	
1324+077	PG 1324+077	DA1.9	27,150 (457)	8.45 (0.06)	0.91 (0.04)	10.91	124	
1325+167	PG 1325+168	DA2.7	18,800 (322)	8.25 (0.05)	0.77 (0.03)	11.27	91	
1325+279	PG 1325+279	DA2.2	22,690 (460)	7.97 (0.06)	0.61 (0.03)	10.50	119	
1325+581	G199-71	DA7.4	6850 (134)	7.95 (0.20)	0.56 (0.12)	13.60	42	
1326−236	EC 13266-2336	DA3.6	13,910 (459)	8.02 (0.06)	0.62 (0.03)	11.44	80	
1327−083	BD-07 3632	DA3.5	14,570 (235)	7.99 (0.04)	0.61 (0.03)	11.31	16	1
1328+343	PG 1328+344	DA2.9	17,160 (283)	7.97 (0.05)	0.60 (0.03)	11.00	78	
1328−152	EC 13288-1515	DA.9	57,980 (1385)	7.89 (0.08)	0.66 (0.03)	8.83	215	
1330+036	BPM 89123	DA2.8	18,330 (321)	7.91 (0.05)	0.57 (0.03)	10.79	103	
1330+473	PG 1330+473	DA2.2	23,320 (357)	7.95 (0.05)	0.60 (0.03)	10.41	94	
1332−229	EC 13324-2255	DA2.3	21,480 (414)	7.83 (0.06)	0.54 (0.03)	10.39	152	
1333+497	PG 1333+498	DA1.7	29,960 (448)	7.98 (0.05)	0.63 (0.03)	9.94	146	
1333+510	PG 1333+511	DA1.4	36,740 (672)	7.96 (0.07)	0.64 (0.04)	9.50	238	
1333+524	LB 2694	DA2.9	17,310 (297)	7.99 (0.05)	0.61 (0.03)	11.01	117	
1334+366	G165-18	DA7.4	6850 (127)	7.64 (0.19)	0.42 (0.08)	13.16	44	
1334−160	LDS 455B	DA2.6	19,580 (307)	8.41 (0.05)	0.87 (0.03)	11.45	60	
1334−678	LFT 1025	DA5.7	8840 (128)	8.16 (0.06)	0.70 (0.04)	12.91	34	
1335+369	PG 1335+369	DA2.4	21,260 (344)	7.80 (0.05)	0.52 (0.02)	10.37	69	
1335+700	PG 1335+701	DA1.6	30,820 (446)	8.34 (0.05)	0.85 (0.03)	10.45	102	
1337+705	LTT 18341	DA2.4	21,290 (325)	7.93 (0.05)	0.59 (0.03)	10.56	28	
1339+346	PG 1339+346	DA3.0	16,960 (264)	7.93 (0.05)	0.58 (0.03)	10.96	96	
1339+360	CBS 377	DA3.4	14,700 (282)	8.03 (0.05)	0.63 (0.03)	11.36	85	
1339+606	RE J1340+602	DA1.1	44,770 (1043)	7.75 (0.09)	0.57 (0.04)	8.89	407	
1340−307	ESO 445-249	DA7.8	6420 (101)	7.50 (0.12)	0.37 (0.05)	13.22	54	
1342+443	PG 1342+444	DA.7	74,830 (2418)	7.90 (0.11)	0.70 (0.04)	8.56	414	
1342−237	EC 13429-2342	DA4.5	11,300 (171)	8.17 (0.05)	0.71 (0.03)	12.07	61	
1343−135	EC 13436-1335	DA5.2	9700 (141)	8.00 (0.06)	0.60 (0.04)	12.31	51	
1344+106	G63-54	DA7.1	7140 (108)	8.14 (0.08)	0.68 (0.05)	13.71	19	
1344+509	PG 1344+509	DA2.4	21,430 (343)	8.12 (0.05)	0.69 (0.03)	10.83	106	
1344+572	G223-24	DA3.6	13,960 (294)	8.05 (0.05)	0.64 (0.03)	11.48	24	
1347+281	G150-43	DA6.9	7350 (124)	8.50 (0.12)	0.92 (0.08)	14.18	27	

TABLE 3.5 – Continued

WD	Name	ST	$T_{\rm eff}$(K)	$\log g$	$M/\,{\rm M}_{\odot}$	M_V	D (pc)	Notes
1348+442	PB 772	DA2.5	20,380 (344)	8.04 (0.05)	0.65 (0.03)	10.80	126	
1348−273	LTT 5382	DA5.0	10,010 (142)	8.21 (0.05)	0.73 (0.03)	12.51	31	
1349+144	PB 4117	DA2.9	17,330 (290)	7.78 (0.05)	0.50 (0.03)	10.70	85	
1349+552	LP 133-144	DA4.1	12,350 (192)	7.99 (0.05)	0.60 (0.03)	11.61	60	3
1350+656	G238-53	DA4.1	12,330 (194)	7.99 (0.05)	0.60 (0.03)	11.61	62	3
1350−090	LP 907-37	DA5.3	9580 (136)	8.44 (0.05)	0.88 (0.03)	13.06	20	5
1353+409	PB 999	DA2.1	24,280 (377)	7.59 (0.05)	0.46 (0.02)	9.75	144	
1354+340	BD+34 2473	DA3.5	14,490 (289)	8.06 (0.05)	0.65 (0.03)	11.42	89	
1356−233	EC 13563-2318	DA5.2	9700 (144)	8.20 (0.07)	0.72 (0.04)	12.61	30	
1400+454	CBS 253	DA2.4	20,860 (375)	7.95 (0.05)	0.60 (0.03)	10.62	189	
1401+005	PG 1401+006	DA.8	63,530 (3328)	7.88 (0.17)	0.67 (0.07)	8.70	463	
1401+523	GD 330	DA6.6	7620 (121)	8.49 (0.10)	0.91 (0.06)	14.01	30	
1401−147	EC 14012-1446	DA4.1	12,300 (190)	8.23 (0.05)	0.75 (0.03)	11.96	55	3
1403−077	PG 1403-077	DA1.0	52,070 (1104)	7.74 (0.07)	0.58 (0.03)	8.69	267	
1407+425	PB 1549	DA5.0	10,090 (145)	8.28 (0.05)	0.78 (0.03)	12.60	31	
1407−475	BPM 38165	DA2.2	23,090 (344)	7.75 (0.04)	0.50 (0.02)	10.13	68	
1408+323	LTT 14141	DA2.6	19,090 (289)	8.00 (0.05)	0.62 (0.03)	10.85	45	
1410+168	LP 439-387	DA2.3	22,260 (414)	7.98 (0.06)	0.62 (0.03)	10.55	107	
1410+317	PB 3534	DA2.5	20,480 (316)	8.07 (0.05)	0.67 (0.03)	10.84	144	
1410+425	PB 1665	DA3.1	16,020 (285)	8.01 (0.05)	0.62 (0.03)	11.18	96	
1411+135	US 3969	DA2.7	18,810 (345)	8.26 (0.06)	0.78 (0.04)	11.28	96	
1411+157	LP 439-356	DA3.1	16,170 (277)	7.62 (0.05)	0.44 (0.02)	10.57	134	
1412+160	US 3971	DA3.6	13,960 (487)	7.99 (0.06)	0.61 (0.03)	11.39	105	
1412+542	CBS 260	DA2.0	24,680 (415)	8.01 (0.05)	0.64 (0.03)	10.41	131	
1412−109	PG 1412-109	DA1.9	26,610 (395)	7.98 (0.05)	0.63 (0.03)	10.19	139	
1413+015	PG 1413+015	DAO1.1	47,770 (1040)	7.72 (0.08)	0.56 (0.03)	8.64	472	
1413+231	LTT 14182	DA2.1	24,200 (431)	7.75 (0.06)	0.51 (0.03)	10.05	224	
1413+241	KUV 14138+2408	DA2.9	17,210 (287)	8.17 (0.05)	0.72 (0.03)	11.29	139	
1413+432	CBS 173	DA3.5	14,440 (471)	8.21 (0.06)	0.74 (0.04)	11.66	74	
1415+132	Feige 93	DA1.5	34,570 (502)	7.42 (0.05)	0.43 (0.01)	8.70	208	
1416+633	LP 66-586	DA3.0	16,810 (507)	7.74 (0.10)	0.48 (0.04)	10.70	120	
1418−005	PG 1418-005	DA3.4	14,980 (301)	7.95 (0.06)	0.58 (0.03)	11.21	113	1
1418−088	G124-26	DA6.1	8210 (119)	8.31 (0.06)	0.79 (0.04)	13.43	24	
1420+228	KUV 14205+2251	DA2.8	18,170 (333)	7.94 (0.06)	0.59 (0.03)	10.86	154	
1420−244	EC 14205-2429	DA2.3	22,220 (408)	8.20 (0.06)	0.74 (0.03)	10.89	118	
1421+318	Ton 197	DA1.8	27,970 (417)	7.98 (0.05)	0.63 (0.03)	10.09	112	
1422+028	PG 1422+028	DA2.3	22,230 (397)	7.94 (0.05)	0.59 (0.03)	10.49	180	
1422+095	LTT 14236	DA4.1	12,440 (191)	8.14 (0.05)	0.69 (0.03)	11.80	32	3
1422+336	LP 271-15	DA3.5	14,370 (427)	8.25 (0.05)	0.77 (0.03)	11.73	119	
1422+433	CBS 183	DA2.2	22,850 (373)	7.83 (0.05)	0.54 (0.02)	10.28	139	
1424+503	CBS 268	DA1.6	31,250 (520)	8.23 (0.07)	0.78 (0.04)	10.24	56	2
1425−811	LTT 5712	DA4.1	12,330 (182)	8.17 (0.04)	0.71 (0.03)	11.86	24	3
1426−276	EC 14265-2737	DA2.7	18,440 (291)	7.72 (0.05)	0.48 (0.02)	10.52	120	
1427+410	CBS 187	DA1.4	35,880 (577)	7.90 (0.06)	0.61 (0.03)	9.45	324	
1428+102	PG 1428+102	DA2.1	24,060 (427)	7.97 (0.06)	0.62 (0.03)	10.39	157	

TABLE 3.5 – Continued

WD	Name	ST	$T_{\rm eff}$(K)	$\log g$	$M/\,{\rm M}_{\odot}$	M_V	D (pc)	Notes
1428+373	KUV 14287+3724	DA3.4	14,740 (232)	7.52 (0.05)	0.41 (0.02)	10.55	97	
1428+408	CBS 189	DA2.9	17,570 (320)	7.89 (0.06)	0.56 (0.03)	10.84	108	
1429+373	GD 336	DA1.4	35,000 (518)	8.14 (0.05)	0.74 (0.03)	9.88	123	
1429−037	HE 1429-0343	DA4.3	11,610 (178)	8.10 (0.05)	0.66 (0.03)	11.89	61	3
1429−216	EC 14293-2141	DA1.9	26,630 (493)	7.95 (0.07)	0.61 (0.03)	10.15	202	
1431+153	PG 1431+154	DA3.6	14,060 (499)	8.07 (0.06)	0.65 (0.04)	11.50	81	1
1431+257	KUV 14310+2542	DA2.1	23,690 (419)	7.27 (0.06)	0.39 (0.01)	9.20	363	
1433+538	GD 337	DA2.2	23,260 (379)	7.82 (0.05)	0.54 (0.02)	10.23	149	
1434+289	Ton 210	DA1.5	33,410 (504)	8.02 (0.06)	0.67 (0.03)	9.77	157	
1434−223	EC 14343-2218	DA1.8	28,460 (536)	7.58 (0.07)	0.47 (0.03)	9.39	247	
1435+370	CBS 194	DA3.2	15,580 (329)	7.99 (0.06)	0.61 (0.04)	11.20	91	2
1436+526	PG 1436+526	DA2.1	24,410 (450)	8.00 (0.06)	0.64 (0.03)	10.41	160	
1436−083	EC 14369-0823	DA3.4	14,860 (313)	8.09 (0.05)	0.67 (0.03)	11.43	92	
1436−216	EC 14363-2137	DA2.1	23,690 (577)	7.91 (0.08)	0.58 (0.04)	10.33	133	2
1436−781	L40-109	DA8.5	5960 (180)	7.18 (0.38)	0.26 (0.11)	13.12	40	
1439+304	PG 1439+305	DA2.2	23,010 (427)	7.96 (0.06)	0.61 (0.03)	10.47	188	
1441+323	CBS 391	DA3.9	12,890 (247)	8.05 (0.06)	0.64 (0.04)	11.62	75	1
1442+474	CBS 283	DA5.0	9990 (152)	8.13 (0.07)	0.68 (0.05)	12.39	53	
1443+295	HS 1443+2934	DA3.8	13,110 (216)	8.00 (0.05)	0.61 (0.03)	11.52	39	1
1443+336	PG 1443+337	DA1.8	28,120 (491)	7.78 (0.07)	0.53 (0.03)	9.77	211	2
1444+350	CBS 202	DA4.8	10,560 (156)	8.19 (0.06)	0.72 (0.04)	12.29	55	
1444+636	RE J1446+632	DA1.2	41,770 (813)	7.83 (0.07)	0.59 (0.03)	9.10	288	
1446+286	Ton 214	DA2.1	23,860 (364)	8.43 (0.05)	0.89 (0.03)	11.13	48	
1446+449	CBS 203	DA2.6	19,300 (465)	7.48 (0.08)	0.41 (0.03)	9.99	252	
1448+077	LFT 1146	DA3.4	14,870 (241)	7.88 (0.05)	0.55 (0.03)	11.12	74	1
1448+411	CBS 204	DA3.4	14,710 (334)	7.96 (0.06)	0.59 (0.03)	11.25	56	
1449+168	PG 1449+168	DA2.2	22,640 (348)	7.90 (0.05)	0.57 (0.02)	10.40	102	
1449+513	CBS 289	DA2.9	17,160 (308)	8.56 (0.05)	0.97 (0.03)	11.94	65	
1450+425	CBS 206	DA5.2	9610 (141)	8.21 (0.06)	0.73 (0.04)	12.66	47	
1451+006.1	GD 173	DA1.9	25,990 (395)	7.90 (0.05)	0.58 (0.02)	10.12	103	
1452+553	CBS 295	DA1.8	28,340 (436)	8.34 (0.05)	0.84 (0.03)	10.64	74	
1452−042	PG 1452-043	DA2.0	25,070 (509)	8.10 (0.07)	0.69 (0.04)	10.51	139	
1452−310	LEHPM 2-4029	DA5.4	9310 (133)	8.14 (0.05)	0.68 (0.03)	12.67	43	
1454+172	PG 1454+173	DA1.6	31,380 (484)	8.19 (0.06)	0.76 (0.04)	10.17	162	
1454−630.2	L151-81B	DA4.8	10,460 (151)	8.43 (0.05)	0.88 (0.03)	12.72	72	
1455+298	G166-58	DA6.8	7390 (106)	7.99 (0.06)	0.58 (0.03)	13.35	28	
1457−086	PG 1457-086	DA2.3	22,240 (364)	7.99 (0.05)	0.62 (0.03)	10.57	110	
1458+171	PG 1458+172	DA2.2	22,600 (490)	7.45 (0.07)	0.42 (0.02)	9.65	214	
1459+219	PG 1459+219	DA2.7	18,940 (292)	8.05 (0.05)	0.65 (0.03)	10.94	103	
1459+305	PG 1459+306	DA1.9	26,230 (402)	7.95 (0.05)	0.61 (0.03)	10.19	57	
1459+333	CBS 220	DA3.5	14,300 (406)	7.90 (0.07)	0.55 (0.04)	11.22	91	
1459+347	PG 1459+347	DA2.3	22,390 (363)	8.53 (0.05)	0.95 (0.03)	11.43	72	
1500−170	EC 15004-1700	DA1.5	32,580 (472)	7.98 (0.05)	0.65 (0.03)	9.76	126	
1501+032	PG 1501+032	DA3.5	14,370 (387)	7.99 (0.06)	0.61 (0.03)	11.34	67	
1502+349	CBS 223	DA2.3	22,300 (391)	7.97 (0.05)	0.61 (0.03)	10.53	124	

TABLE 3.5 – Continued

WD	Name	ST	$T_{\rm eff}$(K)	$\log g$	$M/\,{\rm M}_{\odot}$	M_V	D (pc)	Notes
1502+351	PG 1502+351	DA2.7	18,960 (290)	8.22 (0.05)	0.76 (0.03)	11.21	82	
1503+410	CBS 224	DA3.1	16,000 (339)	7.80 (0.06)	0.51 (0.03)	10.88	168	
1503−070	GD 175	DA7.3	6920 (190)	9.56 (0.24)	1.35 (0.12)	16.60	7	5
1503−093	EC 15036-0918	DA3.4	14,780 (254)	8.04 (0.05)	0.64 (0.03)	11.36	57	1
1504+461	CBS 300	DA2.5	20,200 (401)	7.95 (0.06)	0.60 (0.03)	10.69	116	
1504+546	CBS 301	DA2.2	23,120 (464)	7.88 (0.06)	0.56 (0.03)	10.33	136	2
1504−770	BPM 9323	DA2.9	17,540 (273)	7.93 (0.05)	0.58 (0.03)	10.90	71	
1505+297	CBS 395	DA3.6	13,830 (449)	7.97 (0.06)	0.59 (0.03)	11.37	133	
1507+021	PG 1507+021	DA2.5	20,270 (446)	7.90 (0.07)	0.57 (0.04)	10.61	150	
1507+220	PG 1507+220	DA2.5	20,540 (331)	7.91 (0.05)	0.58 (0.03)	10.60	78	
1507+465	CBS 303	DA1.7	29,600 (462)	7.68 (0.06)	0.49 (0.02)	9.50	317	
1507−105	GD 176	DA4.9	10,240 (148)	7.84 (0.05)	0.51 (0.03)	11.88	51	1
1508+548	PG 1508+549	DA2.9	17,630 (272)	7.98 (0.05)	0.61 (0.03)	10.97	85	
1508+637	GD 340	DA4.8	10,580 (151)	8.20 (0.05)	0.72 (0.03)	12.30	30	1
1509+322	GD 178	DA3.5	14,600 (278)	8.10 (0.05)	0.67 (0.03)	11.47	34	
1509+536	CBS 306	DA3.5	14,580 (320)	8.14 (0.05)	0.69 (0.03)	11.53	79	
1510+566	LP 135-154	DA5.4	9300 (133)	8.20 (0.05)	0.72 (0.03)	12.77	50	1
1511+009	LB 769	DA1.8	28,500 (421)	7.86 (0.05)	0.57 (0.02)	9.87	159	
1513+442	PG 1513+442	DA1.7	30,030 (439)	7.91 (0.05)	0.60 (0.02)	9.82	133	
1515+668	PG 1515+669	DA4.8	10,410 (157)	8.48 (0.06)	0.91 (0.04)	12.83	32	
1515−164	EC 15157-1626	DA3.5	14,560 (355)	8.09 (0.05)	0.67 (0.03)	11.46	82	
1517+373	CBS 239	DA2.0	25,430 (405)	7.91 (0.05)	0.59 (0.03)	10.19	145	
1518+541	CBS 313	DA3.0	16,660 (318)	7.96 (0.06)	0.59 (0.03)	11.03	99	
1518+558	CBS 314	DA3.5	14,350 (334)	7.98 (0.06)	0.60 (0.03)	11.32	86	
1518+636	LP 68-60	DA2.2	23,190 (410)	9.17 (0.06)	1.26 (0.02)	12.64	63	
1519+383	PG 1519+384	DA2.5	20,510 (362)	8.04 (0.05)	0.65 (0.03)	10.79	104	
1519+500	PG 1519+500	DA1.7	29,580 (521)	7.38 (0.07)	0.42 (0.02)	8.94	318	
1520+447	PG 1520+447	DA2.8	17,830 (329)	8.01 (0.06)	0.62 (0.03)	10.98	129	
1521+310	Ton 229	DA1.9	26,440 (400)	7.97 (0.05)	0.62 (0.03)	10.20	99	
1521+431	CBS 242	DA3.5	14,470 (301)	8.06 (0.05)	0.65 (0.03)	11.43	130	
1523+322	CBS 402	DA1.9	26,730 (430)	8.31 (0.05)	0.82 (0.03)	10.71	114	
1524−749	BPM 9518	DA2.0	25,190 (393)	7.69 (0.05)	0.48 (0.02)	9.87	163	
1525+257	LB 9733	DA2.2	23,410 (369)	8.30 (0.05)	0.81 (0.03)	10.96	87	
1526+013	PG 1526+013	DA1.0	50,000 (981)	7.89 (0.07)	0.64 (0.03)	8.99	346	
1527+090	PG 1527+091	DA2.3	22,250 (355)	8.04 (0.05)	0.65 (0.03)	10.65	53	
1527−171	EC 15277-1710	DA2.4	21,270 (395)	8.04 (0.06)	0.65 (0.03)	10.72	154	
1528+487	RE J1529+483	DA1.0	48,510 (879)	7.84 (0.06)	0.62 (0.03)	8.95	169	
1529+331	CBS 252	DA2.8	17,800 (672)	8.16 (0.12)	0.72 (0.07)	11.22	143	
1531+184	GD 186	DA3.7	13,720 (343)	8.05 (0.06)	0.64 (0.03)	11.51	87	1
1531+746	HS 1531+7436	DA3.8	13,370 (290)	8.50 (0.06)	0.92 (0.04)	12.25	62	3
1531−022	BPM 77964	DA2.6	19,540 (299)	8.46 (0.05)	0.91 (0.03)	11.55	31	
1532+033	PG 1532+034	DA.8	66,610 (2423)	7.67 (0.12)	0.59 (0.04)	8.25	358	
1534+503	GD 347	DA5.6	9010 (129)	8.14 (0.05)	0.69 (0.03)	12.81	38	
1535+293	Ton 797	DA2.0	25,200 (383)	7.97 (0.05)	0.62 (0.03)	10.30	143	
1537+651	GD 348	DA5.1	9820 (144)	8.23 (0.06)	0.74 (0.04)	12.61	25	1

TABLE 3.5 – Continued

WD	Name	ST	$T_{\rm eff}$(K)	$\log g$	$M/\,{\rm M}_\odot$	M_V	D (pc)	Notes
1537−152	LB 874	DA2.9	17,110 (270)	8.11 (0.05)	0.68 (0.03)	11.21	87	
1539+530	PG 1539+530	DA1.9	26,790 (404)	7.89 (0.05)	0.58 (0.02)	10.05	150	
1539−035	GD 189	DA5.0	10,160 (150)	8.37 (0.06)	0.84 (0.04)	12.73	31	1
1541+650	PG 1541+651	DA4.2	11,880 (182)	8.20 (0.05)	0.72 (0.03)	11.98	55	3
1541−381	LDS 539	DA2.7	18,970 (438)	7.71 (0.07)	0.47 (0.03)	10.44	68	2
1543−366	RE J1546-364	DA1.1	47,620 (808)	8.89 (0.06)	1.16 (0.03)	10.89	96	
1544+380	HS 1544+3800	DA3.6	13,820 (401)	8.05 (0.06)	0.64 (0.03)	11.50	38	1
1544−377	CD-37 6571B	DA4.8	10,610 (151)	8.20 (0.04)	0.72 (0.03)	12.29	13	1
1547+015	PG 1547+016	DA.6	80,660 (3670)	7.63 (0.15)	0.62 (0.05)	7.94	401	
1547+057	PG 1547+057	DA1.9	25,860 (387)	8.45 (0.05)	0.91 (0.03)	11.01	96	
1548+149	PG 1548+149	DA2.4	21,430 (336)	7.90 (0.05)	0.57 (0.03)	10.50	83	
1548+405	PG 1548+406	DA.9	55,440 (1181)	7.76 (0.07)	0.60 (0.03)	8.63	283	
1550+183	LTT 14705	DA3.4	14,910 (305)	8.36 (0.04)	0.84 (0.03)	11.84	41	1
1553+353	PG 1553+354	DA1.9	26,370 (396)	7.90 (0.05)	0.59 (0.02)	10.10	85	
1554+215	PG 1554+215	DA1.8	27,320 (414)	7.90 (0.05)	0.59 (0.03)	10.02	110	
1554+262	PG 1554+262	DA2.3	22,380 (371)	7.60 (0.05)	0.45 (0.02)	9.95	242	
1554+322	CBS 413	DA1.6	31,130 (472)	8.46 (0.06)	0.93 (0.04)	10.65	118	
1555−089	G152-B4B	DA3.4	14,620 (267)	7.96 (0.05)	0.59 (0.03)	11.27	51	1
1556+165	HS 1556+1634	DA4.1	12,300 (210)	7.56 (0.07)	0.41 (0.03)	10.98	92	1
1558+616	HS 1558+6140	DA2.6	19,420 (390)	7.98 (0.06)	0.61 (0.03)	10.79	145	
1559+128	PG 1559+129	DA1.7	30,040 (444)	8.04 (0.05)	0.67 (0.03)	10.02	235	
1559+369	Ross 808	DA4.4	11,440 (168)	8.10 (0.05)	0.67 (0.03)	11.93	31	3
1600+308	Ton 252	DA.9	59,150 (1780)	7.47 (0.10)	0.52 (0.03)	8.02	296	
1601+581	PG 1601+581	DA3.3	15,340 (248)	7.97 (0.05)	0.60 (0.03)	11.19	42	
1603+432	PG 1603+432	DA1.3	37,550 (565)	8.02 (0.05)	0.68 (0.03)	9.57	114	
1605+177	KUV 16055+1745	DA3.5	14,590 (277)	7.82 (0.05)	0.51 (0.03)	11.07	134	
1605+683	PG 1605+684	DA2.3	22,310 (430)	7.99 (0.06)	0.62 (0.03)	10.56	123	
1606+181	KUV 16069+1810	DA2.2	22,980 (384)	8.07 (0.05)	0.67 (0.03)	10.63	197	
1606+422	Case 2	DA3.8	13,110 (212)	7.87 (0.05)	0.53 (0.03)	11.33	32	1
1607+205	KUV 16075+2031	DA4.4	11,460 (186)	7.91 (0.06)	0.56 (0.03)	11.65	141	
1608+118	PG 1608+119	DA2.4	21,380 (355)	7.96 (0.05)	0.60 (0.03)	10.59	88	
1608+419	PG 1608+419	DA2.9	17,360 (338)	8.07 (0.06)	0.66 (0.04)	11.12	108	
1609+044	PG 1609+045	DA1.7	29,830 (433)	7.92 (0.05)	0.60 (0.02)	9.86	118	
1609+135	G138-8	DA5.4	9370 (134)	8.73 (0.05)	1.06 (0.03)	13.67	19	1
1609+631	PG 1609+631	DA1.6	31,150 (454)	8.68 (0.05)	1.05 (0.03)	11.05	134	
1610+166	BPM 91358	DA3.3	15,080 (251)	7.97 (0.05)	0.59 (0.03)	11.22	78	1
1610+383	KUV 16106+3820	DA3.3	15,140 (285)	7.96 (0.05)	0.59 (0.03)	11.20	110	
1611−084	RE J1614-083	DA1.2	41,440 (624)	7.85 (0.05)	0.60 (0.02)	9.16	93	
1612+554	HS 1612+5528	DA4.2	12,010 (205)	8.30 (0.06)	0.79 (0.04)	12.11	75	1
1614+136	PG 1614+137	DA2.2	23,190 (353)	7.38 (0.05)	0.41 (0.01)	9.45	144	
1614+160	PG 1614+160	DA2.8	18,020 (286)	8.03 (0.05)	0.64 (0.03)	11.00	104	
1614−128	LTT 6494	DA3.0	16,570 (257)	7.97 (0.05)	0.60 (0.03)	11.06	104	
1615−154	LTT 6497	DA1.7	30,200 (440)	8.02 (0.05)	0.66 (0.03)	9.98	31	
1616−591	BPM 24047	DA3.8	13,280 (231)	7.83 (0.05)	0.52 (0.02)	11.26	58	
1619+123	PG 1619+123	DA2.9	17,150 (259)	7.87 (0.04)	0.55 (0.02)	10.86	55	

TABLE 3.5 – Continued

WD	Name	ST	$T_{\rm eff}$(K)	$\log g$	$M/\,{\rm M}_\odot$	M_V	D (pc)	Notes
1619+414	KUV 16195+4125	DA3.5	14,540 (348)	7.88 (0.06)	0.55 (0.03)	11.16	134	2
1619+525	PG 1619+525	DA2.7	18,880 (282)	7.98 (0.04)	0.61 (0.03)	10.84	98	
1620+260	Ton 816	DA1.7	29,110 (427)	7.86 (0.05)	0.57 (0.02)	9.82	139	
1620+513	PG 1620+513	DA2.3	21,880 (398)	7.94 (0.06)	0.59 (0.03)	10.52	123	
1620+647	PG 1620+648	DA1.6	31,000 (447)	7.87 (0.05)	0.59 (0.02)	9.69	173	
1620−391	CD-38 10980	DA1.9	25,980 (369)	7.96 (0.04)	0.61 (0.02)	10.22	14	
1622+323	PG 1622+324	DA.8	66,480 (3712)	7.13 (0.19)	0.41 (0.05)	7.31	653	2
1623−540	BPM 24150	DA4.3	11,600 (168)	8.09 (0.04)	0.66 (0.03)	11.88	59	
1624+477	G202-49	DA5.5	9170 (147)	8.07 (0.11)	0.64 (0.07)	12.62	59	
1625+093	G138-31	DA6.9	7270 (146)	8.81 (0.17)	1.10 (0.09)	14.79	19	
1625+125	HS 1625+1231	DA4.2	11,990 (187)	8.12 (0.05)	0.68 (0.03)	11.85	71	3
1626+409	KUV 16268+4055	DA2.2	22,430 (446)	8.06 (0.06)	0.67 (0.04)	10.67	161	
1628+390	KUV 16288+3904	DA2.5	19,780 (350)	7.97 (0.05)	0.61 (0.03)	10.75	162	
1631+396	KUV 16319+3937	DA2.8	18,230 (290)	7.73 (0.05)	0.48 (0.02)	10.55	51	
1631+781	RE J1629+062	DA1.2	43,450 (774)	7.76 (0.06)	0.57 (0.03)	8.94	66	2
1632+177	PG 1632+177	DA4.9	10,220 (145)	8.04 (0.04)	0.62 (0.03)	12.17	15	
1633+433	G180-63	DAZ7.6	6650 (112)	8.07 (0.14)	0.63 (0.09)	13.89	15	
1633+676	PG 1633+677	DA2.1	24,450 (402)	8.07 (0.05)	0.67 (0.03)	10.51	140	
1635+137	G138-47	DA7.5	6740 (110)	7.70 (0.13)	0.44 (0.06)	13.31	53	
1635+608	PG 1635+608	DA1.9	26,560 (459)	7.95 (0.06)	0.61 (0.03)	10.15	136	
1636+057	G138-49	DA5.9	8560 (127)	8.85 (0.06)	1.13 (0.03)	14.25	20	
1636+160	GD 202	DA3.8	13,360 (277)	7.97 (0.06)	0.59 (0.03)	11.44	68	1
1636+351	KUV 16366+3506	DA1.4	37,250 (566)	8.07 (0.05)	0.70 (0.03)	9.68	111	
1637+335	LTT 14945	DA4.9	10,360 (149)	8.27 (0.05)	0.77 (0.03)	12.49	27	1
1639+153	G138-56	DA6.7	7550 (112)	8.52 (0.07)	0.93 (0.04)	14.10	21	
1640+113	PG 1640+114	DA2.5	20,410 (321)	8.06 (0.05)	0.66 (0.03)	10.82	110	
1640+457	LB 953	DA2.5	19,800 (333)	7.90 (0.05)	0.57 (0.03)	10.64	136	
1640+690	PG 1640+690	DA2.7	18,770 (298)	8.05 (0.05)	0.65 (0.03)	10.95	120	
1641+387	BPM 91679	DA3.1	16,320 (316)	8.10 (0.06)	0.67 (0.04)	11.27	43	
1641+715	HS 1641+7132	DA3.1	16,270 (283)	7.98 (0.05)	0.60 (0.03)	11.10	132	1
1642+385	PG 1642+386	DA1.1	47,420 (912)	7.72 (0.07)	0.56 (0.03)	8.75	368	
1642+413	PG 1642+414	DA1.7	29,520 (461)	8.26 (0.06)	0.80 (0.03)	10.42	144	
1643+143	PG 1643+144	DA1.8	28,040 (468)	7.77 (0.06)	0.53 (0.03)	9.76	133	2
1646+062	PG 1646+062	DA1.7	29,580 (466)	7.87 (0.06)	0.58 (0.03)	9.80	176	2
1647+375	KUV 16476+3733	DA2.2	22,640 (357)	7.93 (0.05)	0.59 (0.03)	10.44	82	
1647+591	G226-29	DA4.0	12,740 (201)	8.38 (0.05)	0.84 (0.03)	12.13	11	3
1648+371	KUV 16484+3706	DA1.1	44,510 (970)	7.61 (0.08)	0.52 (0.03)	8.64	284	
1648+407	RE J1650+403	DA1.3	39,240 (743)	8.05 (0.07)	0.70 (0.04)	9.57	179	
1654+637	GD 515	DA3.2	15,780 (313)	7.76 (0.06)	0.49 (0.03)	10.85	89	1
1655+210	GD 203	DA1.3	38,280 (666)	7.83 (0.06)	0.59 (0.03)	9.24	297	
1655+215	G169-34	DA5.4	9370 (134)	8.27 (0.05)	0.77 (0.03)	12.86	17	1
1657+343	PG 1657+344	DA.9	53,760 (1329)	7.62 (0.09)	0.55 (0.03)	8.42	398	
1658+440	PG 1658+441	DA1.6	31,010 (503)	9.72 (0.07)	1.38 (0.06)	13.34	18	5
1659+303	PG 1659+303	DA3.6	14,150 (352)	8.07 (0.05)	0.65 (0.03)	11.48	50	
1659+662	GD 518	DA4.2	12,030 (214)	9.08 (0.06)	1.23 (0.02)	13.59	38	

TABLE 3.5 – Continued

WD	Name	ST	$T_{\rm eff}$(K)	log g	$M/\,{\rm M}_{\odot}$	M_V	D (pc)	Notes
1659−531	BPM 24601	DA3.2	15,570 (231)	8.07 (0.04)	0.65 (0.03)	11.31	27	
1704+481.1	Sanduleak A	DA3.6	14,170 (294)	8.08 (0.05)	0.66 (0.03)	11.49	40	
1704+481.2	Sanduleak B	DA5.4	9370 (135)	7.93 (0.06)	0.56 (0.03)	12.34	26	
1706+332	G181-B5B	DA3.7	13,560 (393)	7.94 (0.06)	0.57 (0.03)	11.37	81	1
1707+475	PG 1707+476	DA1.8	27,440 (420)	7.82 (0.05)	0.55 (0.02)	9.89	113	
1709−575	LTT 6859	DA2.7	18,370 (266)	7.82 (0.04)	0.53 (0.02)	10.67	77	
1710+683	LP 70-172	DA7.6	6630 (232)	7.90 (0.51)	0.53 (0.28)	13.67	58	
1711+668	RE J1711+664	DA.9	54,630 (1756)	8.54 (0.12)	1.00 (0.06)	10.05	257	
1713+332	BPM 92172	DA2.2	22,870 (350)	7.49 (0.05)	0.42 (0.01)	9.70	88	
1713+695	LTT 18455	DA3.2	15,950 (241)	7.99 (0.04)	0.61 (0.03)	11.15	27	
1714−547	BPM 24754	DA4.5	11,140 (167)	8.09 (0.05)	0.66 (0.03)	11.98	52	3
1716+020	LFT 1339	DA3.7	13,630 (342)	7.89 (0.05)	0.55 (0.03)	11.30	39	1
1717−345	SC 171751.1-343	DA2.0	25,140 (915)	7.79 (0.13)	0.53 (0.06)	10.03	186	2
1720+360	PG 1720+361	DA3.5	14,270 (304)	7.95 (0.05)	0.58 (0.03)	11.30	64	
1721+294	RX J1723+293	DA1.3	40,180 (703)	7.57 (0.06)	0.49 (0.02)	8.73	327	
1724−359	RE J1727-355	DA1.5	34,040 (492)	9.02 (0.05)	1.22 (0.02)	11.58	60	
1725+586	LB 335	DA.9	58,220 (1257)	8.40 (0.07)	0.92 (0.04)	9.72	157	
1730−350	SC 173010.6-350	DA2.6	19,310 (288)	7.88 (0.04)	0.56 (0.02)	10.66	116	
1735+610	GD 525	DA3.1	16,470 (278)	8.00 (0.05)	0.62 (0.03)	11.11	95	
1736+052	G140-2	DA5.6	9040 (132)	8.43 (0.06)	0.88 (0.04)	13.27	33	
1737+419	GD 363	DA2.3	21,640 (327)	7.87 (0.04)	0.56 (0.02)	10.44	103	
1738+669	RE J1738+665	DA.6	79,320 (2183)	8.04 (0.08)	0.77 (0.04)	8.76	147	
1739+804	LB 1048	DA1.9	26,490 (484)	7.75 (0.06)	0.51 (0.03)	9.85	139	
1740−706	RE J1746-703	DA1.0	52,260 (1045)	8.75 (0.07)	1.10 (0.03)	10.52	157	
1742−722	LEHPM 2-1166	DA2.8	17,930 (265)	7.85 (0.04)	0.54 (0.02)	10.74	91	
1743−132	G154-B5B	DA3.9	12,970 (210)	8.01 (0.05)	0.61 (0.03)	11.55	35	1
1745+607	HS 1745+6043	DA1.4	35,820 (552)	8.52 (0.06)	0.97 (0.03)	10.50	126	
1749+717	HS 1749+7145	DA.7	74,560 (2335)	7.37 (0.10)	0.54 (0.03)	7.52	433	
1755+194	GD 370	DA2.0	25,470 (398)	7.95 (0.05)	0.61 (0.03)	10.24	136	
1756+827	LP 9-231	DA6.8	7380 (109)	7.97 (0.07)	0.57 (0.04)	13.33	17	
1800+685	KUV 18004+6836	DA1.1	45,230 (789)	7.88 (0.06)	0.63 (0.03)	9.10	152	
1802+213	GD 372	DA3.0	16,960 (278)	7.90 (0.05)	0.56 (0.03)	10.91	95	
1809+284	BPM 92960	DA2.7	18,610 (298)	7.99 (0.05)	0.61 (0.03)	10.88	70	
1811+327.1	G206-17	DA6.6	7590 (124)	7.89 (0.14)	0.53 (0.07)	13.11	45	
1811+327.2	G206-18	DA7.9	6420 (219)	7.64 (0.56)	0.42 (0.25)	13.43	58	
1819+580	RE J1820+580	DA1.0	49,240 (848)	7.87 (0.06)	0.63 (0.03)	8.98	98	
1820+709	GD 530	DA4.4	11,410 (179)	8.58 (0.05)	0.97 (0.03)	12.73	72	1
1821−131	G155-15	DA7.8	6490 (113)	8.73 (0.12)	1.06 (0.07)	15.08	13	
1822+008	Sh 2-68	DAOZ.6	84,460 (7824)	7.24 (0.18)	0.54 (0.05)	6.93	859	1
1824+040	Ross 137	DA3.5	14,350 (224)	7.63 (0.05)	0.44 (0.02)	10.80	42	1
1824+600	HS 1824+6000	DA4.3	11,800 (178)	7.77 (0.05)	0.48 (0.03)	11.39	73	3
1826−045	LTT 7347	DA5.4	9270 (133)	8.23 (0.05)	0.74 (0.03)	12.83	22	1
1827+778	HS 1827+7753	DA.7	72,950 (2565)	7.46 (0.12)	0.55 (0.03)	7.73	393	
1827−106	G155-19	DA3.6	13,890 (271)	7.76 (0.05)	0.48 (0.02)	11.07	43	1
1828+668	KUV 18284+6650	DA4.6	10,980 (169)	8.27 (0.06)	0.77 (0.04)	12.31	50	

TABLE 3.5 – Continued

WD	Name	ST	$T_{\rm eff}$(K)	$\log g$	$M/\,{\rm M}_{\odot}$	M_V	D (pc)	Notes
1833+644	KUV 18332+6429	DA1.1	47,160 (1535)	7.87 (0.13)	0.62 (0.06)	9.02	376	2
1834−781	BPM 11593	DA2.6	19,060 (283)	7.79 (0.04)	0.51 (0.02)	10.56	95	
1840+042	GD 215	DA5.6	9050 (130)	8.43 (0.05)	0.88 (0.03)	13.26	21	
1840−111	LTT 7421	DA4.9	10,260 (148)	8.30 (0.05)	0.79 (0.03)	12.57	21	1
1844−223	RE J1847-221	DA1.5	32,610 (468)	8.31 (0.05)	0.84 (0.03)	10.30	48	
1845+019	BPM 93487	DA1.7	30,190 (436)	7.88 (0.05)	0.59 (0.02)	9.77	43	
1845+683	KUV 18453+6819	DA1.4	37,310 (579)	8.30 (0.05)	0.83 (0.03)	10.05	123	
1855+338	LTT 15569	DA4.1	12,390 (189)	8.42 (0.05)	0.87 (0.03)	12.24	30	3
1857+119	G141-54	DA5.0	10,020 (145)	8.20 (0.06)	0.72 (0.04)	12.49	40	1
1858+393	G205-52	DA5.3	9530 (137)	8.26 (0.05)	0.76 (0.03)	12.78	37	
1911+135	G142-B2A	DA3.6	13,820 (328)	7.97 (0.05)	0.59 (0.03)	11.38	33	1
1914+094	KPD 1914+0929	DA1.5	33,560 (490)	7.94 (0.05)	0.62 (0.03)	9.63	145	
1914−598		DA2.4	20,830 (305)	7.84 (0.04)	0.54 (0.02)	10.46	61	
1918+110	GD 218	DA2.5	20,340 (359)	8.02 (0.05)	0.64 (0.03)	10.77	124	
1918+725	GD 533	DA2.2	22,780 (360)	7.95 (0.05)	0.60 (0.03)	10.47	85	
1919+145	BPM 94172	DA3.3	15,280 (247)	8.21 (0.04)	0.74 (0.03)	11.55	19	
1932−136	LDS 683B	DA2.9	17,520 (265)	7.87 (0.05)	0.55 (0.02)	10.81	106	
1935+276	G185-32	DA4.0	12,630 (194)	8.12 (0.05)	0.68 (0.03)	11.76	18	3
1936+327	BPM 94484	DA2.3	22,230 (344)	7.94 (0.05)	0.59 (0.03)	10.49	42	
1942+499	RE J1943+500	DA1.4	34,910 (523)	8.12 (0.05)	0.73 (0.03)	9.86	89	
1943+163	LTT 15765	DA2.5	20,320 (310)	7.94 (0.05)	0.59 (0.03)	10.65	47	
1948−389	BPS CS 22964-60	DA1.3	38,490 (587)	7.73 (0.05)	0.54 (0.02)	9.05	130	
1950+250	LTT 15808	DA4.2	12,110 (185)	8.12 (0.05)	0.68 (0.03)	11.83	46	3
1950−432	MCT 1950-4314	DA1.2	43,390 (684)	7.64 (0.05)	0.52 (0.02)	8.74	168	
1952−206	LTT 7873	DA3.5	14,370 (263)	7.98 (0.05)	0.60 (0.03)	11.32	54	1
1953−011	LFT 1503	DA6.4	7910 (115)	8.39 (0.06)	0.84 (0.04)	13.70	10	1
1953−715	BPM 12843	DA2.5	20,020 (324)	7.98 (0.05)	0.61 (0.03)	10.74	76	
1957+225	NGC 6853	DAO.6	86,680 (5379)	7.36 (0.18)	0.57 (0.05)	7.13	259	
1958+675	GD 539	DA2.1	24,570 (403)	7.76 (0.05)	0.51 (0.02)	10.04	170	
1958−501	BPS CS 30302-17	DAO.9	56,870 (1473)	7.97 (0.09)	0.69 (0.04)	8.85	184	
1959+059	GD 226	DA4.6	10,980 (166)	8.20 (0.06)	0.72 (0.04)	12.19	70	3
2003+437	GD 387	DA2.9	17,350 (272)	7.87 (0.05)	0.55 (0.03)	10.83	130	1
2004−605	RE J2009-605	DA1.2	43,360 (678)	8.19 (0.05)	0.78 (0.03)	9.68	61	
2007−219	LTT 7983	DA5.0	10,030 (146)	8.23 (0.06)	0.74 (0.04)	12.53	24	
2007−303	LTT 7987	DA3.1	16,150 (233)	7.98 (0.04)	0.60 (0.02)	11.12	16	
2008+510	G230-30	DA3.6	14,080 (467)	7.95 (0.06)	0.58 (0.04)	11.32	95	
2009+622	GD 543	DA1.9	26,520 (415)	7.76 (0.05)	0.52 (0.02)	9.88	133	
2010+613	GD 544	DA3.7	13,750 (361)	7.96 (0.05)	0.59 (0.03)	11.37	67	
2011+398	RE J2013+400	DAO1.0	49,650 (984)	7.94 (0.07)	0.66 (0.04)	8.97	134	1
2014−575	BPM 26691	DA1.8	28,320 (434)	7.96 (0.05)	0.62 (0.03)	10.03	54	
2018−233	BPS CS 22955-37	DA3.2	15,700 (276)	8.06 (0.05)	0.65 (0.03)	11.28	42	
2020−425	RE J2023-422	DA1.6	31,220 (477)	8.03 (0.06)	0.67 (0.03)	9.93	97	
2021−128	BPS CS 22950-12	DA2.3	21,730 (373)	7.99 (0.05)	0.62 (0.03)	10.61	52	
2022+198	RE J2024+200	DA1.0	52,970 (1094)	8.02 (0.07)	0.71 (0.04)	9.16	194	
2025+488	GD 390	DA4.6	10,900 (161)	8.13 (0.05)	0.68 (0.03)	12.11	56	1

TABLE 3.5 – Continued

WD	Name	ST	$T_{\rm eff}$(K)	$\log g$	$M/\,{\rm M}_\odot$	M_V	D (pc)	Notes
2025+554	GD 546	DA1.6	31,390 (460)	7.83 (0.05)	0.57 (0.02)	9.60	161	
2028+390	GD 391	DA2.0	24,830 (383)	8.06 (0.05)	0.67 (0.03)	10.47	38	
2029+183	GD 230	DA3.7	13,560 (310)	7.91 (0.05)	0.56 (0.03)	11.33	99	1
2031−277	RX J2034-275	DA.9	54,230 (962)	7.95 (0.06)	0.68 (0.03)	9.00	199	
2032+188	BPM 95701	DA2.6	19,090 (321)	7.57 (0.05)	0.44 (0.02)	10.17	115	
2032+248	HD 340611	DA2.4	20,700 (322)	8.02 (0.05)	0.64 (0.03)	10.75	14	
2035−174	LP815-45	DA2.9	17,530 (283)	7.92 (0.05)	0.57 (0.03)	10.89	84	
2035−336	MCT 2035-3337	DA2.6	19,460 (292)	7.92 (0.04)	0.58 (0.02)	10.70	55	
2039−202	LTT 8189	DA2.5	20,160 (300)	7.98 (0.04)	0.61 (0.03)	10.73	21	
2039−682	LTT 8190	DA3.0	16,970 (289)	8.59 (0.05)	0.98 (0.03)	12.01	18	
2040−392	MCT 2040-3914	DA4.5	11,300 (163)	8.26 (0.04)	0.76 (0.03)	12.20	26	3
2043−635	BPM 13537	DA1.8	27,740 (426)	8.23 (0.05)	0.78 (0.03)	10.51	101	
2044−043	LP 696-5	DA4.8	10,480 (156)	8.25 (0.06)	0.76 (0.04)	12.41	84	
2046+396	KPD 2046+3940	DA.8	66,600 (1532)	7.57 (0.07)	0.56 (0.02)	8.05	189	
2046−220	BPS CS 22880-12	DA2.1	24,080 (407)	8.01 (0.05)	0.64 (0.03)	10.45	101	
2047+372	LTT 16093	DA3.4	14,710 (285)	8.31 (0.04)	0.81 (0.03)	11.78	17	1
2048+809	LP 25-436	DA6.0	8440 (125)	8.34 (0.07)	0.81 (0.05)	13.37	40	
2051+095	LP 516-13	DA3.2	15,670 (250)	7.95 (0.05)	0.59 (0.03)	11.13	103	
2051−208	BPS CS 22880-13	DA2.3	21,460 (343)	9.10 (0.05)	1.24 (0.02)	12.63	31	
2056+033	PG 2056+033	DA1.0	51,900 (1467)	7.85 (0.10)	0.63 (0.04)	8.87	300	
2058+083	HS 2058+0823	DA1.3	37,420 (732)	7.95 (0.08)	0.64 (0.04)	9.47	134	
2058+181	GD 232	DA2.8	17,760 (276)	7.98 (0.05)	0.61 (0.03)	10.95	64	
2058+499	KPD 2058+4958	DA2.4	21,140 (339)	7.87 (0.05)	0.56 (0.02)	10.48	184	
2058+506	GD 393	DA5.1	9850 (141)	8.30 (0.05)	0.79 (0.03)	12.72	31	
2059+190	G144-51	DA7.2	6980 (111)	8.44 (0.10)	0.87 (0.07)	14.27	27	1
2059+247	G187-16	DA7.8	6460 (187)	8.71 (0.31)	1.04 (0.18)	15.06	20	
2105−820	LTT 8381	DA4.8	10,600 (153)	8.24 (0.05)	0.75 (0.03)	12.36	18	
2111+261	LTT 16224	DA5.8	8650 (125)	8.33 (0.06)	0.81 (0.04)	13.26	19	
2111+498	GD 394	DA1.3	39,660 (636)	7.88 (0.05)	0.61 (0.03)	9.26	58	
2114−376	MCT 2114-3737	DA2.1	24,050 (369)	7.73 (0.05)	0.50 (0.02)	10.04	132	
2115+010	PG 2115+011	DA1.9	26,210 (459)	7.95 (0.06)	0.61 (0.03)	10.19	121	
2115+118	HS 2115+1148	DAOZ.8	62,240 (2318)	7.76 (0.12)	0.62 (0.04)	8.36	424	1
2115−560	LTT 8452	DA5.1	9880 (141)	8.27 (0.05)	0.77 (0.03)	12.66	21	1
2116+675	GD 547	DA3.6	14,060 (340)	8.07 (0.05)	0.65 (0.03)	11.50	83	
2116+736	KUV 21168+7338	DA.9	54,580 (1213)	7.70 (0.08)	0.58 (0.03)	8.56	195	
2117+539	G231-40	DA3.4	14,680 (239)	7.91 (0.05)	0.56 (0.03)	11.19	17	1
2119+581	GD 548	DA6.2	8190 (120)	8.14 (0.07)	0.68 (0.04)	13.18	36	
2120+054	PG 2120+055	DA1.4	36,220 (549)	7.86 (0.05)	0.60 (0.02)	9.37	252	
2124+550	Ross 198	DA3.6	14,040 (253)	8.41 (0.05)	0.87 (0.03)	12.03	35	1
2124−224	BPS CS 29506-51	DA1.0	48,800 (838)	7.81 (0.06)	0.60 (0.02)	8.89	160	
2126+734	LTT 18524	DA3.1	16,110 (236)	7.97 (0.04)	0.60 (0.03)	11.11	22	1
2132+367	BPM 96804	DA6.8	7420 (121)	8.16 (0.11)	0.69 (0.07)	13.59	29	
2133−366	MCT 2133-3637	DA1.9	26,940 (490)	7.75 (0.06)	0.52 (0.03)	9.82	153	
2134+218	GD 234	DA2.6	19,180 (314)	8.14 (0.05)	0.70 (0.03)	11.05	48	
2136+229	G126-18	DA4.9	10,320 (149)	8.18 (0.05)	0.71 (0.03)	12.35	38	1

TABLE 3.5 – Continued

WD	Name	ST	$T_{\rm eff}$(K)	$\log g$	$M/\,{\rm M}_{\odot}$	M_V	D (pc)	Notes
2136+828	LFT 1649	DA2.8	17,700 (263)	7.97 (0.04)	0.60 (0.03)	10.95	26	
2138+214	LP 398-18	DA4.8	10,510 (178)	8.27 (0.09)	0.77 (0.06)	12.44	124	
2139+115	GD 235	DA3.1	16,300 (257)	7.97 (0.05)	0.60 (0.03)	11.09	88	
2139+132.1	G126-25	DA6.6	7660 (130)	8.22 (0.13)	0.73 (0.08)	13.56	40	
2143+353	GD 396	DA1.9	26,100 (411)	7.88 (0.05)	0.58 (0.03)	10.09	121	
2146−433	MCT 2146-4320	DA.6	78,090 (3178)	7.30 (0.10)	0.53 (0.03)	7.31	501	
2148+539	G232-38	DA4.2	11,900 (187)	8.09 (0.05)	0.66 (0.03)	11.82	96	3
2148−291	MCT 2148-2910	DA4.3	11,810 (181)	8.14 (0.05)	0.69 (0.03)	11.91	68	3
2149+021	G93-48	DA2.8	18,170 (266)	8.01 (0.04)	0.62 (0.03)	10.95	23	
2149+372	GD 397	DA3.7	13,640 (308)	7.98 (0.05)	0.60 (0.03)	11.41	59	1
2150+021	PG 2150+021	DA1.2	42,150 (673)	7.83 (0.05)	0.59 (0.02)	9.10	289	
2150+338	GD 398	DA2.7	18,660 (286)	7.94 (0.05)	0.59 (0.03)	10.81	73	
2151−015	LTT 8747	DA5.5	9190 (133)	8.28 (0.06)	0.77 (0.04)	12.94	20	
2151−307	RE J2154-302	DA1.7	30,360 (444)	8.16 (0.05)	0.74 (0.03)	10.19	84	
2152−045	BPS CS 22965-20	DA2.4	20,630 (334)	7.55 (0.05)	0.43 (0.02)	10.00	100	
2154+408	KPD 2154+4048	DA1.7	29,100 (508)	7.71 (0.07)	0.50 (0.03)	9.58	134	2
2154−061	PB 7026	DA1.4	36,930 (556)	7.83 (0.05)	0.58 (0.02)	9.28	139	
2157+161	GD 272	DA2.5	19,810 (378)	8.05 (0.06)	0.65 (0.03)	10.87	117	
2159−754	LFT 1679	DA5.7	8860 (130)	8.79 (0.06)	1.09 (0.03)	13.99	16	
2200−136	BPS CS 22892-17	DA2.0	25,820 (407)	7.71 (0.05)	0.49 (0.02)	9.86	126	
2203−485	BPM 44347	DA2.2	23,420 (369)	7.88 (0.05)	0.57 (0.03)	10.31	112	
2204+070	PG 2204+070	DA2.0	25,630 (400)	8.00 (0.05)	0.64 (0.03)	10.31	131	
2205+250	RE J2207+252	DA1.9	27,210 (399)	8.39 (0.05)	0.87 (0.03)	10.81	54	
2205−139	BPS CS 22892-38	DA1.9	25,950 (384)	8.33 (0.05)	0.83 (0.03)	10.81	72	
2207+142	LTT 16482	DA6.6	7580 (113)	8.22 (0.07)	0.73 (0.05)	13.59	25	
2207−303	RE J2210-300	DA1.7	29,010 (426)	7.91 (0.05)	0.59 (0.02)	9.90	96	
2211−495	RE J2214-491	DA.7	71,530 (1532)	7.46 (0.06)	0.55 (0.02)	7.74	64	
2212−279	BPS CS 30337-19	DA1.0	48,400 (1032)	7.63 (0.08)	0.53 (0.03)	8.57	335	
2213+317	LP 343-34	DA6.8	7440 (119)	8.30 (0.10)	0.79 (0.07)	13.79	44	
2214−376	MCT 2214-3740	DA1.5	32,780 (487)	8.00 (0.05)	0.66 (0.03)	9.78	153	
2216+484	GD 402	DA8.3	6080 (186)	8.74 (0.31)	1.06 (0.17)	15.39	14	
2218+706	DeHt 5	DA.7	76,750 (1952)	7.38 (0.07)	0.54 (0.02)	7.48	383	
2220+133	PG 2220+134	DA2.1	23,780 (364)	8.46 (0.05)	0.91 (0.03)	11.19	76	
2226+061	GD 236	DA3.1	16,240 (251)	7.76 (0.05)	0.49 (0.02)	10.80	60	1
2226−210	NGC 7293	DAO.5	94,640 (3349)	7.62 (0.12)	0.65 (0.03)	7.49	152	
2231−295	Ton S 56	DA3.1	16,360 (256)	8.07 (0.05)	0.65 (0.03)	11.22	80	
2232−575	LTT 9082	DA2.9	17,390 (264)	7.93 (0.05)	0.58 (0.03)	10.92	64	
2235+082	PG 2235+082	DA1.4	36,140 (570)	7.98 (0.06)	0.66 (0.03)	9.58	148	
2237+819	HS 2237+8154	DA2.8	18,180 (387)	8.50 (0.06)	0.93 (0.04)	11.74	74	2
2239+081	PG 2239+082	DA2.1	24,310 (463)	7.80 (0.06)	0.53 (0.03)	10.11	197	
2240+125.1	HS 2240+1234A	DA3.1	16,170 (269)	8.08 (0.05)	0.67 (0.03)	11.27	97	
2240+125.2	HS 2240+1234B	DA3.6	14,130 (482)	8.10 (0.06)	0.67 (0.03)	11.52	99	
2240−017	G28-13	DA5.4	9250 (133)	8.26 (0.06)	0.76 (0.04)	12.89	45	
2240−045	Feige 106	DA1.1	45,780 (770)	7.81 (0.06)	0.59 (0.02)	8.96	181	
2244+031	PG 2244+031	DA.8	60,740 (1166)	7.79 (0.06)	0.62 (0.03)	8.58	367	

TABLE 3.5 – Continued

WD	Name	ST	$T_{\rm eff}$(K)	$\log g$	$M/\,{\rm M}_\odot$	M_V	D (pc)	Notes
2246+066	HS 2246+0640	DA.4	125,790 (4516)	6.86 (0.12)	0.64 (0.04)	5.51	1812	
2246+223	LTT 18580	DA4.7	10,720 (155)	8.89 (0.05)	1.14 (0.02)	13.51	15	1
2247+583	Lanning 23	DA.9	56,780 (956)	8.02 (0.05)	0.72 (0.03)	9.08	108	
2248+293	G128-7	DA8.1	6230 (150)	8.85 (0.22)	1.12 (0.11)	15.49	10	
2248−504	BPM 28016	DA3.0	16,540 (252)	7.95 (0.05)	0.59 (0.03)	11.02	61	
2251−634	MCT 2251-6326	DA2.5	20,340 (301)	7.95 (0.04)	0.60 (0.02)	10.67	53	
2253+054	LTT 16738	DA8.1	6240 (154)	8.61 (0.24)	0.98 (0.15)	15.03	17	
2253−081	BD-08 5980B	DA7.4	6770 (126)	7.87 (0.18)	0.52 (0.10)	13.55	39	
2254+126	GD 244	DA4.2	12,060 (185)	8.15 (0.05)	0.70 (0.03)	11.88	75	3
2256+249	GD 245	DA2.2	22,840 (355)	7.84 (0.05)	0.54 (0.02)	10.29	46	
2257+138	KUV 22570+1349	DA1.8	28,340 (413)	8.39 (0.05)	0.87 (0.03)	10.72	164	
2257+162	KUV 22573+1613	DA2.0	25,450 (396)	7.54 (0.05)	0.45 (0.02)	9.56	207	
2258+406	G216-B14B	DA5.0	10,050 (147)	8.42 (0.06)	0.87 (0.04)	12.85	34	1
2259−267	MCT 2259-2646	DA2.5	20,050 (314)	8.03 (0.05)	0.64 (0.03)	10.82	75	
2302+457	GD 404	DA2.1	24,010 (378)	7.94 (0.05)	0.60 (0.03)	10.35	124	
2303+017	PHL 400	DA1.2	42,210 (995)	7.71 (0.10)	0.55 (0.04)	8.89	278	
2303+242	PG 2303+243	DA4.3	11,820 (189)	8.16 (0.05)	0.70 (0.03)	11.94	52	3
2306+124	KUV 23061+1229	DA2.4	21,010 (335)	8.09 (0.05)	0.68 (0.03)	10.82	63	
2306+130	KUV 23060+1303	DA3.7	13,800 (284)	8.03 (0.05)	0.62 (0.03)	11.46	53	1
2306−274	MCT 2306-2726	DA3.0	16,960 (348)	7.33 (0.06)	0.37 (0.02)	9.98	151	
2307+636	G241-46	DA2.7	18,800 (297)	7.87 (0.05)	0.55 (0.03)	10.69	55	
2308+050	PB 5280	DA1.4	36,500 (578)	7.58 (0.06)	0.48 (0.02)	8.89	267	
2308+167	KUV 23083+1642	DA2.6	19,240 (342)	8.03 (0.05)	0.64 (0.03)	10.89	183	
2309+105	BPM 97895	DA.9	56,160 (975)	7.98 (0.06)	0.70 (0.03)	9.03	66	
2311+552	GD 556	DA3.0	16,970 (286)	7.86 (0.05)	0.54 (0.03)	10.86	116	1
2311−260	Ton S 94	DA1.0	51,340 (1198)	7.98 (0.08)	0.69 (0.04)	9.11	244	
2312+119	KUV 23128+1157	DA2.7	18,860 (309)	7.78 (0.05)	0.51 (0.02)	10.56	285	
2313+682	GD 557	DA5.6	9060 (132)	8.48 (0.06)	0.90 (0.04)	13.33	38	
2313−330	BPS CS 22888-45	DA1.3	39,260 (713)	7.10 (0.07)	0.38 (0.01)	7.86	376	
2314+064	PB 5312	DA2.7	18,470 (290)	8.05 (0.05)	0.65 (0.03)	10.99	97	1
2314+141	KUV 23149+1408	DA2.7	18,600 (309)	7.85 (0.05)	0.54 (0.03)	10.68	176	
2314+471	GD 405	DA3.5	14,580 (331)	8.42 (0.05)	0.88 (0.03)	11.98	77	
2317+268	Mrk 320	DA1.6	31,890 (486)	7.71 (0.06)	0.52 (0.02)	9.37	243	
2318+090	PB 5342	DA1.7	29,510 (473)	8.08 (0.06)	0.69 (0.04)	10.14	236	
2318+126	LP 522-34	DA3.6	14,020 (379)	8.03 (0.05)	0.63 (0.03)	11.44	97	
2319+691.1	GD 559	DA2.5	20,420 (331)	7.96 (0.05)	0.60 (0.03)	10.68	61	
2321−549	RE J2324-544	DA1.1	45,920 (795)	7.82 (0.06)	0.60 (0.03)	8.98	175	
2322+093	KUV 23220+0921	DA3.4	14,750 (318)	7.94 (0.06)	0.58 (0.03)	11.22	125	
2322+098	KUV 23223+0953	DA2.4	20,960 (352)	7.90 (0.05)	0.57 (0.03)	10.54	215	
2322+206	PG 2322+207	DA3.7	13,560 (266)	7.96 (0.05)	0.58 (0.03)	11.40	96	1
2322−181	LP 822-81	DA2.2	22,900 (363)	8.03 (0.05)	0.65 (0.03)	10.57	87	
2323+256	G128-62	DA8.5	5960 (199)	7.62 (0.35)	0.41 (0.16)	13.74	46	
2324+060	PB 5379	DA3.0	16,660 (253)	8.02 (0.04)	0.63 (0.03)	11.11	71	
2325+263.1	LP 402-29	DA7.3	6860 (134)	8.56 (0.17)	0.96 (0.11)	14.55	29	
2326+049	G29-38	DA4.1	12,200 (187)	8.22 (0.05)	0.74 (0.03)	11.95	17	3

TABLE 3.5 – Continued

WD	Name	ST	$T_{\rm eff}$(K)	$\log g$	$M/\,{\rm M}_{\odot}$	M_V	D (pc)	Notes
2326−224	PHL 535	DA2.6	19,590 (330)	8.01 (0.05)	0.63 (0.03)	10.82	102	
2328+107	KUV 23282+1046	DA2.2	22,860 (370)	7.86 (0.05)	0.56 (0.03)	10.33	110	
2329+267	LTT 16922	DA4.2	11,940 (252)	9.03 (0.07)	1.21 (0.03)	13.50	22	1
2329+407	Case 3	DA3.0	16,640 (257)	8.02 (0.05)	0.63 (0.03)	11.12	35	
2331+290	GD 251	DA1.8	28,410 (456)	7.53 (0.06)	0.45 (0.02)	9.31	203	
2331−475	LB 1526	DA.9	58,290 (1019)	7.63 (0.06)	0.56 (0.02)	8.35	112	
2333−049	G157-82	DA4.6	10,940 (165)	8.17 (0.06)	0.71 (0.04)	12.16	50	1
2333−165	BPM 82758	DA3.7	13,790 (294)	7.96 (0.05)	0.59 (0.03)	11.37	31	
2336+063	PB 5486	DA2.9	17,500 (278)	8.13 (0.05)	0.70 (0.03)	11.20	76	
2336−079	GD 1212	DA4.5	11,270 (165)	8.18 (0.05)	0.71 (0.03)	12.08	17	3
2336−187	G273-97	DA6.4	7920 (116)	7.91 (0.07)	0.54 (0.04)	12.97	34	
2336−199	MCT 2336-1955	DA2.4	20,810 (363)	7.97 (0.05)	0.61 (0.03)	10.66	134	
2337−760	LTT 9648	DA3.5	14,420 (277)	7.61 (0.06)	0.43 (0.02)	10.75	61	1
2341+322	LTT 16991	DA3.8	13,130 (198)	8.02 (0.04)	0.62 (0.03)	11.54	18	1
2341−164	G273-B15B	DA3.6	13,830 (359)	8.00 (0.05)	0.61 (0.03)	11.42	81	
2342+806	GD 561	DAO.7	74,160 (3038)	7.16 (0.11)	0.48 (0.03)	6.94	328	
2345+304	PG 2345+305	DA1.7	29,850 (495)	7.78 (0.07)	0.54 (0.03)	9.64	223	
2347+128	G30-20	DA4.4	11,470 (171)	8.14 (0.05)	0.69 (0.03)	11.98	61	3
2347+292	G130-15	DA8.5	5900 (232)	7.80 (0.59)	0.48 (0.30)	14.07	21	
2347−192	GD 1248	DA1.8	27,370 (458)	7.99 (0.06)	0.64 (0.03)	10.16	111	
2348−244	LTT 58183	DA4.2	11,880 (176)	8.17 (0.05)	0.71 (0.03)	11.94	48	3
2349+286	PG 2349+286	DA1.3	38,380 (603)	7.98 (0.05)	0.66 (0.03)	9.48	227	
2349−031	LHS 4033	DA4.7	10,770 (163)	9.58 (0.06)	1.36 (0.03)	15.08	24	
2349−283	Ton S 126	DA2.8	18,300 (399)	8.04 (0.07)	0.65 (0.04)	10.99	81	
2350−083	G273-B1B	DA2.6	19,270 (313)	7.90 (0.05)	0.57 (0.03)	10.69	125	
2350−248	PHL 580	DA1.7	29,710 (435)	8.45 (0.05)	0.91 (0.03)	10.73	79	
2351−335	LDS 826A	DA5.7	8810 (128)	8.25 (0.06)	0.76 (0.04)	13.07	13	1
2353+026	PB 5617	DA.8	62,600 (1561)	7.66 (0.08)	0.58 (0.03)	8.31	319	
2354−151	PHL 599	DA1.4	35,770 (550)	7.32 (0.06)	0.41 (0.01)	8.45	207	
2357+296	PG 2357+297	DA.9	53,190 (1107)	7.60 (0.07)	0.54 (0.02)	8.40	219	
2359−434	L362-81	DA5.8	8650 (123)	8.56 (0.05)	0.96 (0.03)	13.66	8	5

Notes. – (1) Photometrically constant; (2) DA+dM binary; (3) ZZ Ceti; (4) Balmer-line problem (5) based on non-magnetic models; (6) DA+DC binary; (7) DA+DB binary; (8) Suffers from interstellar reddening.

3.6.2 Comparison with SPY

In establishing the reliability of the results of large surveys such as the one presented here, we believe it is both interesting and important to compare our results with other studies that include many of the same objects. As mentioned earlier, recent analyses of large numbers of white dwarfs were presented both by LBH05 and Limoges & Bergeron (2010), and although virtually all of the white dwarfs in those studies are included here, we are also using the exact same observations and analysis techniques making any meaningful comparison a rather futile endeavor. Instead, what we require is an independent analysis, which is exactly what the SPY sample analyzed by Koester et al. (2009) represents. The DA white dwarfs in the SPY sample had initially been analyzed in Voss (2006), however Koester et al. (2009) have re-analyzed the same stars with a new generation of models presented in Koester (2010). We must stress that these models did not yet include the improved Stark profiles of TB09. Consequently, as previously discussed, we will be using the results obtained with the Lemke (1997) broadening profiles in order to compare with the SPY sample. More importantly, the white dwarfs from SPY have been observed and analyzed with models and techniques completely independent from our own and thus represent a truly distinct data set.

The sample presented in Koester et al. (2009) consists of a total of 615 DA white dwarfs of which 362 are in common with our sample. The reason there is not a greater overlap is two-fold. First, many of the stars selected for the SPY project were taken from the Hamburg-ESO (Christlieb et al. 2001) and Hamburg-Schmidt (Homeier et al. 1998) surveys and these stars were not yet listed in MS99. Second, as we mentioned earlier, many of the white dwarfs for which we were unable to obtain spectra were situated in the southern hemisphere, and this also contributed to the smaller overlap. In order to be sure we are comparing all stars on an equal footing, we choose to compare only single DA white dwarfs; any known double-degenerate systems or magnetic white dwarfs are excluded. Furthermore, we also omit stars with $T_{\rm eff} > 50{,}000$ K and $T_{\rm eff} < 8000$ K for the same reasons outlined in Koester et al. (2009). Namely, the models used by Koester et al. (2009) do not include effects due to departures from local thermodynamic equilibrium at higher temperatures, and the spectra become less sensitive to changes in $\log g$ at lower temperatures. These last two criteria reduce the number

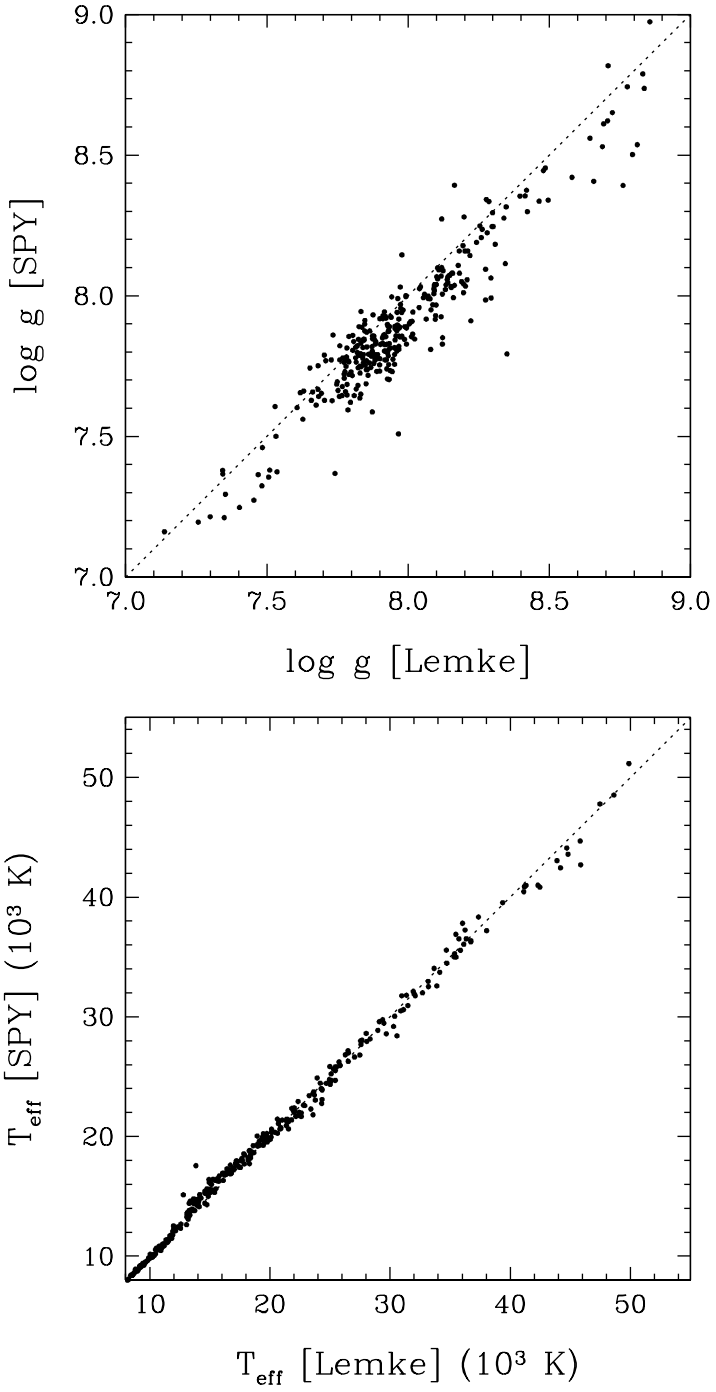

FIGURE 3.26 – Comparison of $\log g$ (top) and $T_{\rm eff}$ (bottom) values between this work using the Lemke (1997) Stark profiles and the results of Koester et al. (2009) for 330 DA white dwarfs common to both samples. The dotted lines represent the 1:1 correlation.

of viable white dwarfs to 330.

The results of our comparison are presented in Figure 3.26. We see that with the exception of a couple of outliers near $T_{\rm eff} \sim 14{,}000$ K, the agreement between our $T_{\rm eff}$ values and those from SPY is excellent. The two outliers (0318−021 and 0937−103) are stars where both the cold and hot seeds lead to the same spectroscopic solution (see LBH05 for a discussion about the hot and cold solutions). Clearly, this is not the case in the SPY analysis of the same objects as they derive larger values for $T_{\rm eff}$ in both cases. In contrast, the $\log g$ determinations show a clear trend where our measurements tend toward higher values than those from SPY. Koester et al. (2009) had noted this problem (see their Figure 3) and discussed several possibilities in an attempt to understand this discrepancy. In particular, they point out that differences between the "Bergeron" and "Koester" models could be the cause. Indeed, LBH05 showed a comparison between their results and those of several other studies. Three of those analyses used Koester models and all three seemed to exhibit the same trend we see here. Another possibility is that the apparent shift in $\log g$ could be caused by differences in the fitting procedures. Finally, Koester et al. (2009) speculate that the very nature of the SPY data could be the origin of the problem. The SPY spectra were obtained with the UV-Visual Echelle Spectrograph (UVES) at the Very Large Telescope (VLT), and the stitching together of the various orders might have introduced artifacts in the spectra. For the complete discussion, we refer the reader to Koester et al. (2009).

In an effort to better understand this shift in $\log g$ values, we decided to independently fit the SPY spectra , which were very kindly provided to us by D. Koester, using our models and fitting procedures. In Figure 3.27 we show the comparison between these new values derived from the SPY spectra and those from our spectra, all analyzed with the Lemke (1997) Stark profiles. First, we note that the agreement between the $T_{\rm eff}$ determinations (bottom panel) remains very good. Second, and more importantly, we do not observe any systematic shift in the $\log g$ values (top panel)! There is more scatter in the $\log g$ plot but the overall agreement is markedly better than was seen in Figure 3.26. Since we obtain a satisfactory agreement between the atmospheric parameters measured from both sets of spectra, we must conclude that there is no problem, a priori, with the SPY spectra themselves. Differences between our

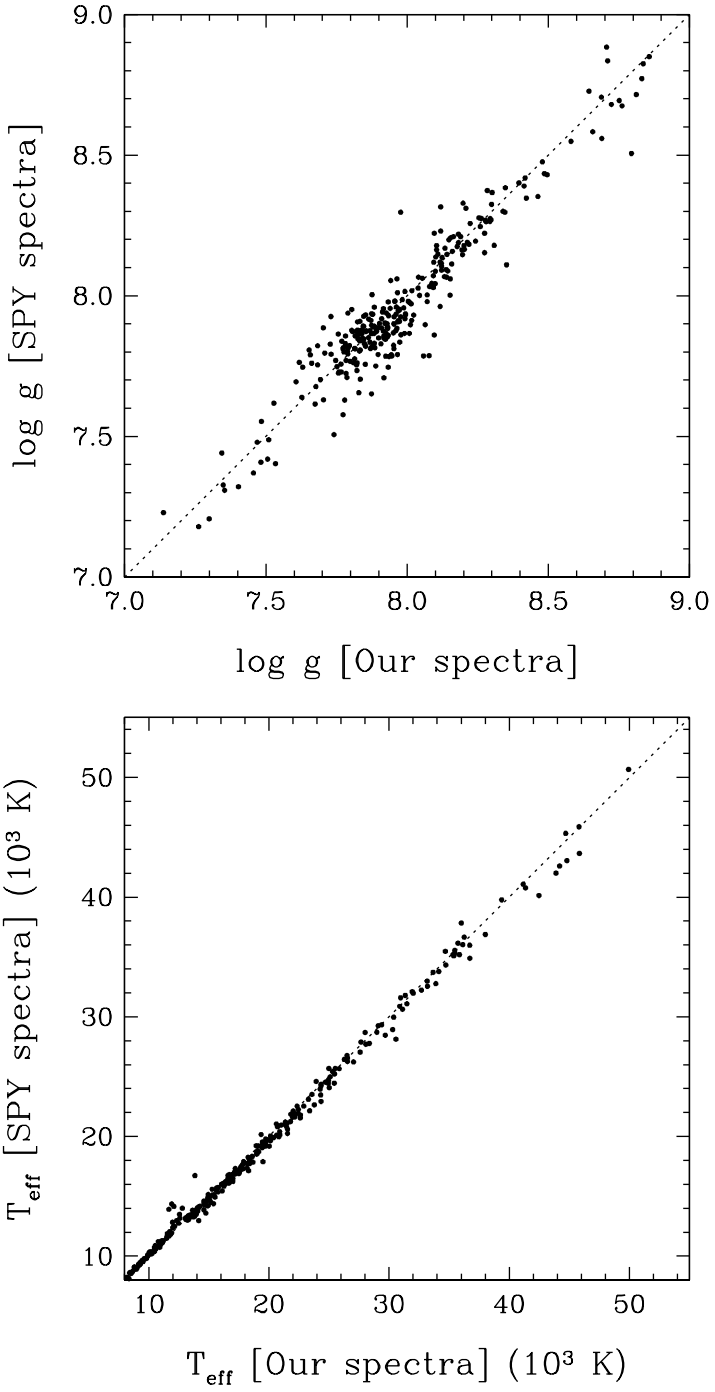

FIGURE 3.27 – Comparison of $\log g$ (top) and $T_{\rm eff}$ (bottom) values between this work using the Lemke (1997) Stark profiles and the results of our fits to the SPY spectra using the same models. The dotted lines represent the 1:1 correlation.

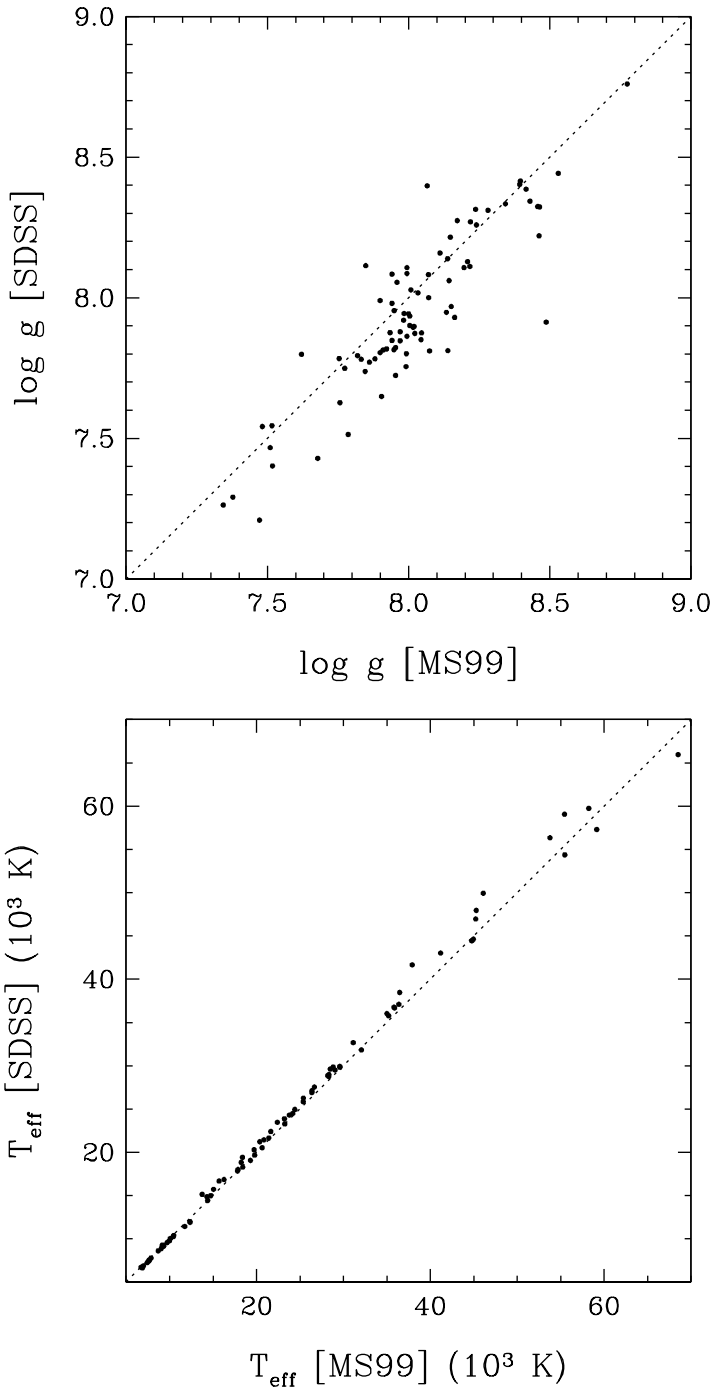

FIGURE 3.28 – Comparison of $\log g$ (top) and $T_{\rm eff}$ (bottom) values derived from our observations and from fits to SDSS spectra of 83 DA white dwarfs common to both samples. The dotted lines represent the 1:1 correlation.

results and those of Koester et al. (2009) must necessarily arise from differences in the models or the fitting techniques used. Nonetheless, the fact that the $T_{\rm eff}$ determinations agree so well in both of the previous comparisons is encouraging. Furthermore, when using an independent data set and relying on our own theoretical framework, we succeed in getting both $T_{\rm eff}$ and $\log g$ values that match rather well.

3.6.3 Comparison with SDSS

Another independent source of spectra is the SDSS. Despite the thousands of new white dwarfs discovered in the SDSS, very few are in common with our sample. As we showed in Figure 3.1, the much fainter sample of white dwarfs observed by the SDSS is the reason the two samples are so mutually exclusive. Nonetheless, we have retained 83 DA white dwarfs in common with both samples[8]. We obtained the SDSS spectra for these stars from the SDSS SkyServer[9] and proceeded to fit them with the new models that include the TB09 Stark broadening profiles. The comparison between our $T_{\rm eff}$ and $\log g$ determinations and those obtained from the SDSS spectra is presented in Figure 3.28. As in the case of the comparison with SPY, we note a very good agreement between both sets of $T_{\rm eff}$ values (bottom panel). However, we also note a second similarity with our SPY comparison as the $\log g$ values also seem to be systematically shifted towards lower values from those determined from the SDSS spectra. This concurs with the results of Tremblay et al. (2011) who explained that any differences must be due to the different spectra employed as they are being analyzed within the same theoretical framework and the same fitting method. Tremblay et al. (2011) conclude that issues with the reduction of the SDSS data still remain and are the reason for the observed shift.

3.6.4 Comparison with parallax measurements

Yet another way of testing the reliability of our results is to compare our derived values of absolute magnitudes with those obtained from parallax measurements. The added incentive here is that the absolute magnitudes obtained from parallaxes are completely model inde-

[8]We omit DA+dM binaries, DAO stars, and magnetic white dwarfs from this comparison.
[9]http://cas.sdss.org/dr7/en/

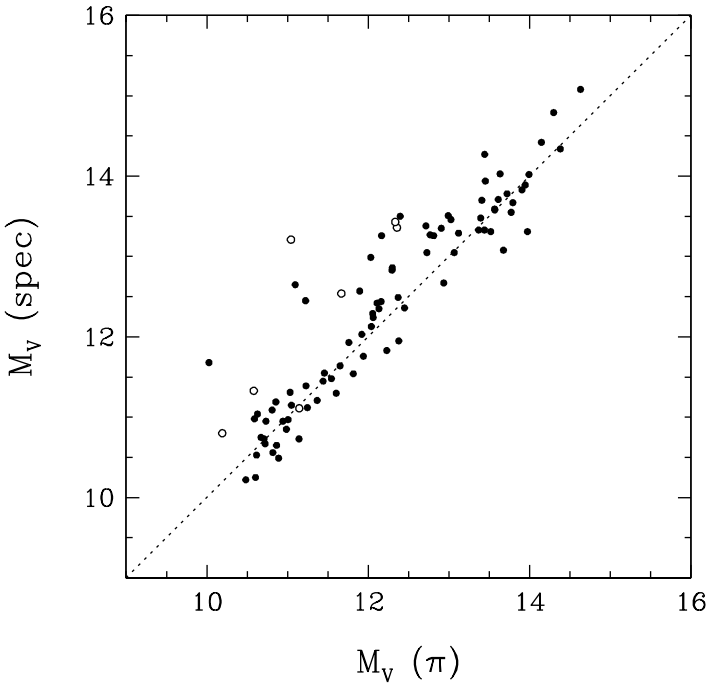

FIGURE 3.29 – Comparison of absolute magnitudes derived from parallax measurements with the absolute magnitudes derived from our spectroscopic determinations of $T_{\rm eff}$ and $\log g$ for 92 DA white dwarfs. The open circles represent known or suspected double-degenerate binary systems. The dotted lines represent the 1:1 correlation.

pendent. We have 92 DA white dwarfs in our sample with available parallax measurements from either the Yale Parallax Catalogue (van Altena et al. 1995), or *Hipparcos* (Perryman & ESA 1997). We present in Figure 3.29 the comparison between the M_V values from parallax measurements and those obtained through our spectroscopic analysis. We can see that the overall agreement is quite good and this reinforces our confidence that our results are accurate.

There are a number of obvious outliers in this figure that can be easily explained as unresolved double degenerates (open circles), the most important of which is L870-2 (0135−052), discovered by Saffer et al. (1988). But this is not always the case. For instance, we find M_V(spec) = 11.68 for Ross 548 (0133−016, ZZ Ceti itself), for a corresponding distance of 31 pc, while the distance obtained from the trigonometric parallax measurement from the Yale Parallax Catalogue is more than twice as large at 67 pc. We cannot find an easy explanation for this discrepancy unless Ross 548 is also an unresolved degenerate binary. As well, the absolute magnitudes of cool DA stars found in the temperature range where the high-log g

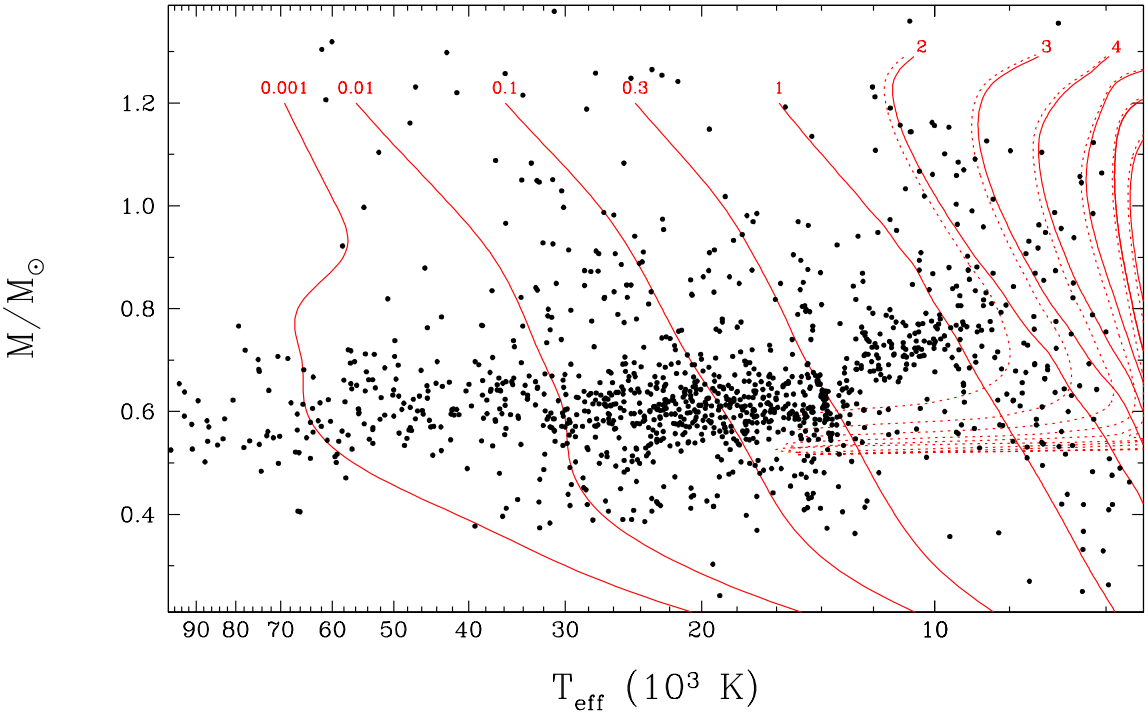

FIGURE 3.30 – Mass distribution as a function of $T_{\rm eff}$ for all the stars listed in Table 3.5. The solid red lines represent isochrones that take into account only the white dwarf cooling time whereas the dotted red lines include also the main sequence lifetime. Each isochrone is labeled by its age in Gyr. Isochrones for $\tau < 1$ Gyr are taken from Wood (1995) whereas those for $\tau \geq 1$ Gyr are taken from Fontaine et al. (2001).

problem is found are likely to be overestimated; this accounts for the clump of objects away from the 1:1 correlation in the range $12.5 < M_V < 13.5$.

We must finally mention that the observed agreement is very good within the parallax uncertainties for *both* model grids. As TB09 pointed out, despite the fact that the new models yield higher values of $T_{\rm eff}$ and $\log g$ (i.e., smaller radii), the two effects nearly cancel each other out and the predicted luminosities (or M_V) remain largely unchanged.

3.6.5 Mass distribution

We display in Figure 3.30, the mass distribution as a function of $T_{\rm eff}$ for all the stars listed in Table 3.5. As previously noted, the bulk of the distribution is centered around 0.6 $M_{\odot}$ for $T_{\rm eff} > 13{,}000$ K. Below this temperature, the well known "high-$\log g$ problem" manifests itself. Several solutions to this problem have been explored over the years. First, Bergeron et al.

(1990b) showed how helium, spectroscopically invisible below 13,000 K, might explain this problem. If analyzed with pure hydrogen models, DA white dwarfs containing helium would appear to have higher $\log g$ values because the presence of helium increases the pressure in the atmosphere, which is analogous to increasing the surface gravity. Recently, Tremblay et al. (2010) attempted to detect the presence of the He I λ5877 line in six DA white dwarfs using high resolution spectroscopy. They found no evidence of the helium line and concluded that helium was not the solution. The reason helium was thought to be the key ingredient in explaining the high-$\log g$ problem is because it was expected that convective mixing would bring it to the surface. In addition, properly calibrating the mixing length theory used to describe convection was deemed crucial. Bergeron et al. (1995) addressed this issue but even with the mixing length properly calibrated, the high-$\log g$ problem remained. The advent of the TB09 profiles was also thought to represent a possible element of the solution. However, as we have seen, the new profiles succeed in "straightening out" the mass distribution, but do not seem to contribute in fixing the masses at lower $T_{\rm eff}$. One of the few remaining avenues of research is the computation of full 3D hydrodynamic models of convection as a replacement to the mixing length theory that has always been used, but ultimately constitutes an approximation.

At the hotter end of the white dwarf sequence, we note in Figure 3.30 that the distribution remains essentially continuous around 0.6 $M_{\odot}$ unlike the previous determination shown in Figure 3 of Gianninas et al. (2009)[10] where there is a noticeable "dip" toward lower masses at higher $T_{\rm eff}$. Our new result is a consequence of the new determinations of $T_{\rm eff}$ and $\log g$ for the DAO stars from Gianninas et al. (2010). As it was demonstrated, the use of the CNO models to solve the Balmer-line problem also resulted in higher masses for the DAO stars, consistent with the remainder of the hydrogen-rich white dwarf population.

We show in Figure 3.31 the histogram that represents the mass distribution of our sample regardless of effective temperature. Besides the full distribution, we also plot the mass distributions for stars above and below $T_{\rm eff} = 13{,}000$ K (in blue and red, respectively). The reason for this split is that we want to analyze the mass distribution for stars that are not affected

[10]Please refer to Annexe D

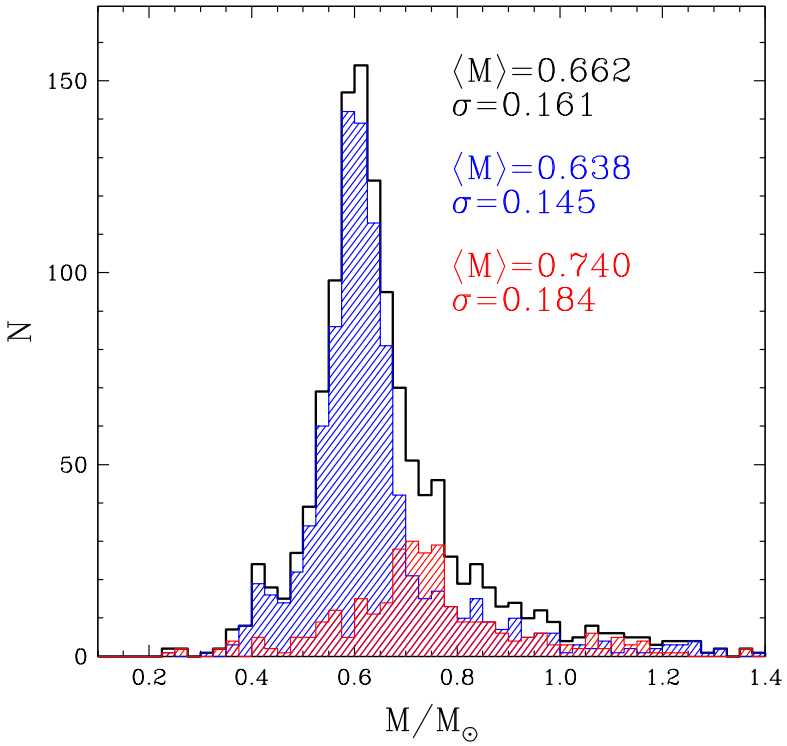

FIGURE 3.31 – Mass distribution for all the stars listed in Table 3.5 (solid line histogram). Also shown are the mass distributions for stars with $T_{\rm eff} > 13{,}000$ K (blue histogram) and for stars with $T_{\rm eff} < 13{,}000$ K (red histogram). The mean mass and dispersion for each distribution are indicated in the figure in units of solar masses.

by the high-log g problem. The overall shape of the distribution is in good agreement with the latest determination of the SDSS DA mass distribution presented by Tremblay et al. (2011), the only other large scale analysis of DA white dwarfs employing the new TB09 Stark profiles. In both cases, the mass distribution is strongly peaked near 0.6 $M_{\odot}$. The other notable features are the high-mass tail and the low-mass component that peaks near 0.45 $M_{\odot}$. The mean mass of the entire sample is $\langle M \rangle = 0.662$ $M_{\odot}$. However, if we consider only stars with $T_{\rm eff} \geq 13{,}000$ K, we get a lower mean mass of $\langle M \rangle = 0.638$ $M_{\odot}$. This is higher than the value of 0.613 $M_{\odot}$ obtained by Tremblay et al. (2011) for the SDSS DR4 sample. However, as stated in Tremblay et al., the mean mass is sensitive to outliers and as we will discuss below, the MS99 sample contains a number of high-mass white dwarfs that are systematically missed by many surveys. This fact is also evidenced in Figure 18 of Tremblay et al. (2011) where we note a dearth of stars for $M > 1.0$ $M_{\odot}$ and $T_{\rm eff} \geq 20{,}000$ K.

We note in Figure 3.30 a number of rather high mass white dwarfs. In particular, if we restrict ourselves to stars with $T_{\rm eff} > 13{,}000$ K, thus avoiding the troublesome lower temperature regime where the high-$\log g$ problem reigns, we find there are 20 white dwarfs with a mass M $\geq 1.1\ M_{\odot}$. Of these, 11 were detected by *ROSAT* (Fleming et al. 1996). This trend is not at all surprising. By definition, white dwarfs with a higher mass have a smaller radius, which, in turn, means they are intrinsically fainter at a given $T_{\rm eff}$. As such, magnitude-limited UV-excess surveys (PG, KUV), and many of the other surveys looking for bright blue objects (MCT, EC) would have skipped these stars because they are fainter. On the other hand, X-ray surveys like the one conducted with *ROSAT*, catalog *all* sources, regardless of the brightness of the object. Consequently, since ours is not a magnitude-limited sample, these white dwarfs make their way into our sample by virtue of being included in MS99.

At the other end of the mass spectrum, the presence of stars below the dotted lines in Figure 3.30 is significant. Those isochrones include the main sequence lifetime of the white dwarf's progenitor. This represents a cutoff of sorts in that the possible progenitor stars would not have had sufficient time to become white dwarfs within the lifetime of the Galaxy, nor to have cooled down to those temperatures. However, it is clear that there exists a non-negligible low-mass component in the mass distribution. The presence of these stars can be explained if we consider binary star evolution under different guises. First, several of these stars are known to be unresolved double-degenerate binary systems that have been discovered through searches for radial velocity variations (Maxted & Marsh 1999; Maxted et al. 2000). In such cases, the measured atmospheric parameters are misleading if we assume only a single star is present. A second possibility involves the merger of two white dwarfs. Indeed, the recent results presented by Kilic et al. (2011, and references therein) seem to suggest that there are several very low mass ($\sim 0.2\ M_{\odot}$) white dwarfs that are in close binary systems. If these white dwarfs merge, they could potentially form a white dwarf with a mass near $0.4\ M_{\odot}$. Finally, there is the possibility of a helium core white dwarf (Althaus et al. 2001). Helium-core white dwarfs are formed when stars lose a significant amount of their envelope's mass to a companion before the progenitor reaches the tip of the red giant branch. Regardless which of these scenarios is the most likely to account for the population of low-mass white dwarfs,

one thing is clear. These low-mass white dwarfs represent a separate evolutionary channel distinct from the usual post-AGB models that explain the evolution of the vast majority of white dwarfs.

3.6.6 Revisiting the PG luminosity function

Besides revising the atmospheric parameters of all the normal DA stars from the complete sample with the use of the TB09 profiles, there is also a number of white dwarfs whose atmospheric parameters are further refined from the LBH05 analysis as they are members of certain distinct classes of objects. In particular, there are 16 DA+dM binaries, 10 DAO stars[11], 5 DA+BP stars, 7 magnetic white dwarfs and finally the DA component from the 1115+166 DA+DB binary system. For the magnetic white dwarfs not included in Table 3.5, we adopt the parameters listed in Table 3.3. With these up to date atmospheric parameters in hand, we proceed to recompute the PG luminosity function in exactly the same manner described in LBH05. We compare our new determination of the PG luminosity function with that of LBH05 in Figure 3.32. We see some variations in the individual magnitude bins with respect to the LBH05 result, but this is to be expected considering the revised atmospheric parameters we have employed in computing the luminosity function. We can also compare the space densities, in other words, the total number of DA white dwarfs per pc^{-3}. This is determined by integrating the area under the luminosity function. LBH05 had determined a value[12] of 3.07×10^{-4} pc^{-3} for $M_V < 12.75$. Our new determination of the PG luminosity function yields a slightly lower value of 2.92×10^{-4} pc^{-3} for the same magnitude range. This represents only a 5.1% difference with the value from LBH05. At first glance, one might think that the somewhat higher temperatures produced by the new TB09 Stark profiles means that stars are intrinsically brighter than we once thought, meaning they can potentially be further away thus reducing the local density of white dwarfs. However, our earlier comparison between the absolute magnitudes obtained from spectroscopy and those determined from

[11]PG 1305−017 is included in this sample but, as outlined in Gianninas et al. (2010), the parameters obtained by Bergeron et al. (1994) using their stratified models are adopted, as such, the parameters for this star remain unchanged.

[12]LBH05 actually give a value of 5.0×10^{-4} pc^{-3} but this number is inaccurate for reasons unknown to one of the co-authors of both studies (P.B.) who obtained the correct number provided here.

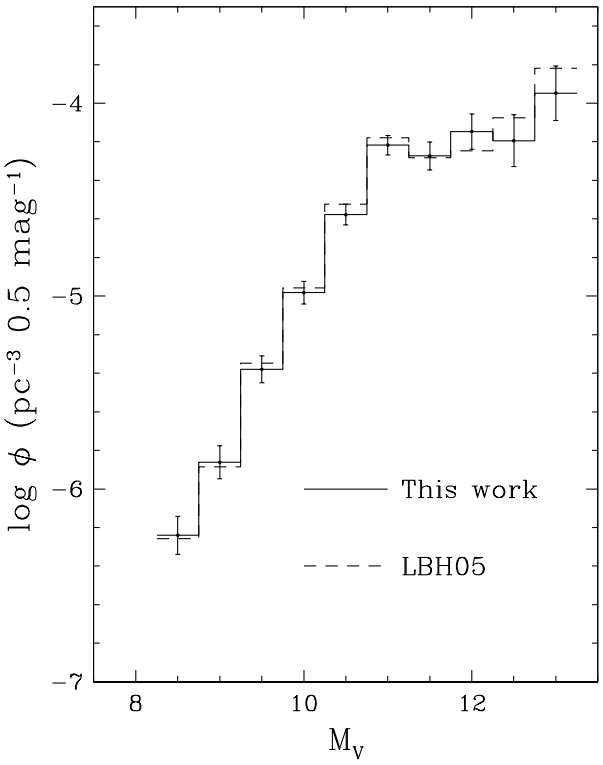

FIGURE 3.32 – Luminosity function of all DA stars in the complete PG sample using the atmospheric parameters derived in this work (solid line) presented in half-magnitude bins, assuming a scale height for the Galaxy of $z_0 = 250$ pc. The dashed line represents the results of LBH05 shown here for comparison.

parallax measurements showed that the intrinsic brightness of these white dwarfs has not changed in an appreciable way since the stellar radii are also smaller (higher masses). Under these circumstances, the luminosity function should remain almost unaffected. However, closer inspection of the individual values of $T_{\rm eff}$, $\log g$, and M_V reveals that small differences do cause stars to jump from one magnitude bin to the next, which can ultimately affect the determination of the space density of white dwarfs.

3.6.7 ZZ Ceti instability strip

In Table 3.5 we list a number of stars that have been observed in high-speed photometry in order to ascertain if they are photometrically variable. In total, we identify 136 white dwarfs that are photometrically constant and 53 stars that are known ZZ Ceti pulsators. Using this photometric sample of 189 white dwarfs, we wish to re-visit the empirical determination of

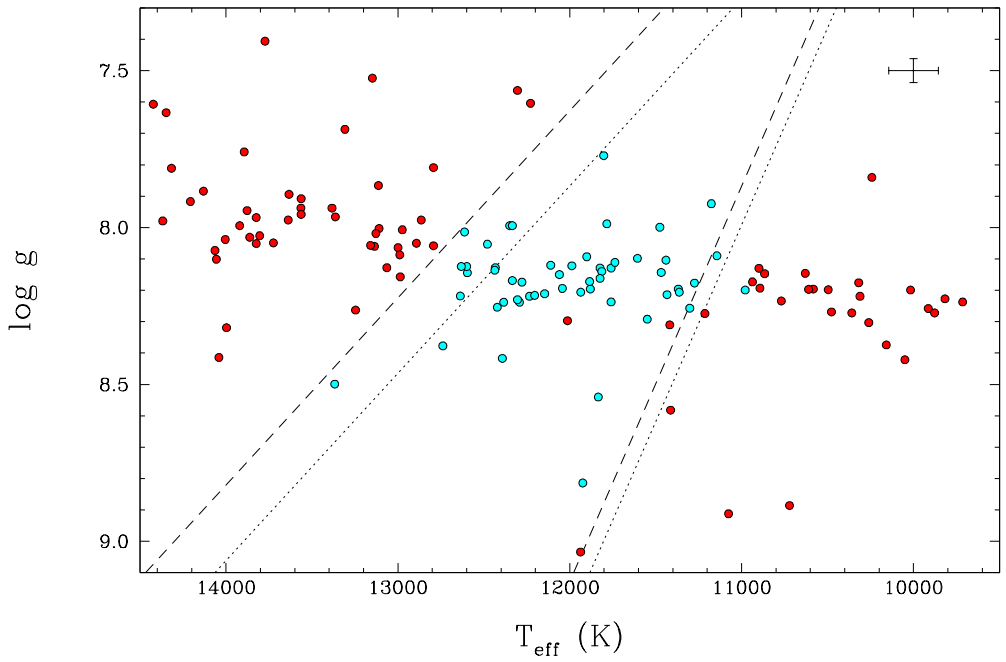

FIGURE 3.33 – $T_{\rm eff}$ - $\log g$ distribution for DA white dwarfs with high-speed photometric measurements. The cyan circles represent the 53 ZZ Ceti stars in our sample and the red circles are the 136 photometrically constant DA stars from Table 3.5. The dotted lines represent the empirical boundaries of the instability strip as established in Gianninas et al. (2006) whereas the dashed lines correspond to our new determinations. The error bars represent the average uncertainties of the spectroscopic method in the region of the ZZ Ceti instability strip.

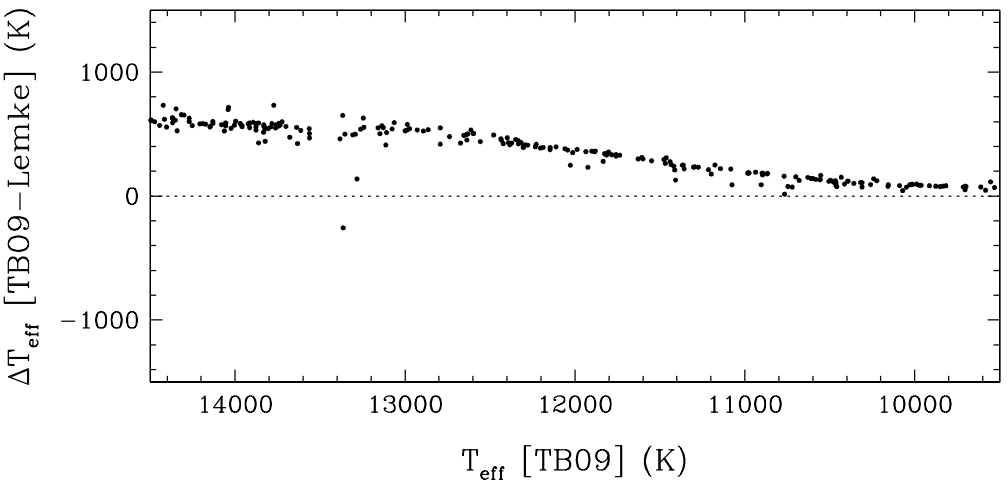

FIGURE 3.34 – Differences in $T_{\rm eff}$ determinations between the improved Stark profiles of TB09 and the VCS profiles of Lemke (1997) as a function of $T_{\rm eff}$ for stars near the ZZ Ceti instability strip. The dotted line represents the 1:1 correlation.

the boundaries of the ZZ Ceti instability strip. In particular, we wish to see how the use of the TB09 Stark broadening profiles has affected the location of the instability strip as compared to our last result in Gianninas et al. (2007). We plot in Figure 3.33 the location of these 166 white dwarfs in the $T_{\rm eff}$-$\log g$ plane. For the purposes of comparison, we plot as dotted lines the empirical boundaries of the instability strip as determined in Gianninas et al. (2007). Our new determination of these boundaries is shown as dashed lines. First, we notice that the entire strip has shifted by a few hundred kelvins towards higher $T_{\rm eff}$. Second, we see that the strip has also widened by several hundred kelvins. These changes are a direct result of the use of the new TB09 broadening profiles. We plot in Figure 3.34 differences in $T_{\rm eff}$ obtained by using the old Lemke (1997) profiles versus the calculations of TB09, focusing on the range of $T_{\rm eff}$ where the ZZ Ceti instability strip lies. We see that the new values of $T_{\rm eff}$ are systematically higher than the old values, this explains why the whole instability strip is shifted toward higher effective temperatures. However, we also notice that $\Delta T_{\rm eff}$ increases as a function of $T_{\rm eff}$ from $\sim$ 200 K near $T_{\rm eff}$ = 11,000 K, to $\sim$ 600 K at $T_{\rm eff}$ = 13,000 K. This is the reason the instability strip is now wider than previously established.

One aspect of the instability strip that remains unchanged is its purity. With the exception of the two "offending" stars discussed below (one pulsator and one non-variable), only pulsating white dwarfs are to be found within the instability strip and only photometrically constant white dwarfs without, within the uncertainties. We stress that the significance of a pure instability strip is two-fold. First, if the strip is pure, one can predict the variability of white dwarfs whose atmospheric parameters places them within the confines of the instability strip. Second, if the strip is pure, then it represents an evolutionary phase through which all hydrogen-rich white dwarfs must pass. As a result, asteroseismological analyses of these stars can yield important information about their internal structure, in particular the thickness of the hydrogen layer. This in turn can be applied to the the entire population of hydrogen-rich white dwarf stars.

We also note that the blue edge seems to be quite clearly defined whereas there is a certain level of ambiguity associated with the location of the red edge. As far as the blue edge is concerned, the sharp transition between non-variable to variable stars is probably a

consequence of very specific conditions being required for the driving mechanism to ignite pulsations at the surface of the white dwarf. On the other hand, the dying off of pulsations at the red edge is not so well understood and it is speculated that the interaction between convection and the pulsations is what ultimately signals the demise of variability. It is conceivable that this process is not as clear cut and thus the exact temperature at which a star will cease pulsating is more ambiguous, producing a red edge whose precise location is more difficult to nail down.

As mentioned above, there are two notable exceptions to the "pure" instability strip. The first of the two offending white dwarfs is 1959+059. This is a ZZ Ceti star that lies outside the instability strip near $\sim$ 11,000 K. This star was first reported as being variable by Voss et al. (2007). Our spectrum for this object was one of the many provided to us by C. Moran (1999, private communication) and we have not obtained a new spectrum subsequent to its discovery as a ZZ Ceti star. It is likely that our spectrum was not averaged over several pulsation cycles as is necessary in order to obtain a proper measure of the atmospheric parameters for ZZ Ceti stars. Indeed, Voss et al. (2007) report a period of 1350 s and an amplitude of 5.69 mma, consistent with cooler ZZ Ceti stars that have longer periods and larger amplitudes as compared to their hotter counterparts. These large amplitudes signify that $T_{\rm eff}$ can easily swing back and forth by several hundred kelvins resulting in the star moving in and out of the instability strip (Fontaine & Brassard 2008). A new spectrum, averaged over several pulsation cycles, would need to be secured to get a more reliable measurement of $T_{\rm eff}$ and $\log g$ for this star. As such, its current location outside the instability strip is not inconsistent with the notion of a pure instability strip.

The second offending star is HS 1612+5528, the non-variable white dwarf lying in the heart of the instability strip. This star was reported as "not observed to vary" by Voss et al. (2006). Gianninas et al. (2009) independently observed HS 1612+5528 and also detected no variations down to a limit of 0.2%. However, there are ZZ Ceti stars with amplitudes as low as 0.05%. It is possible that in both cases the star was observed during a period of destructive interference. Alternatively, HS 1612+5528 could represent the first ZZ Ceti star whose pulsations are hidden from us due to geometric considerations. In other words, since we cannot resolve the surface

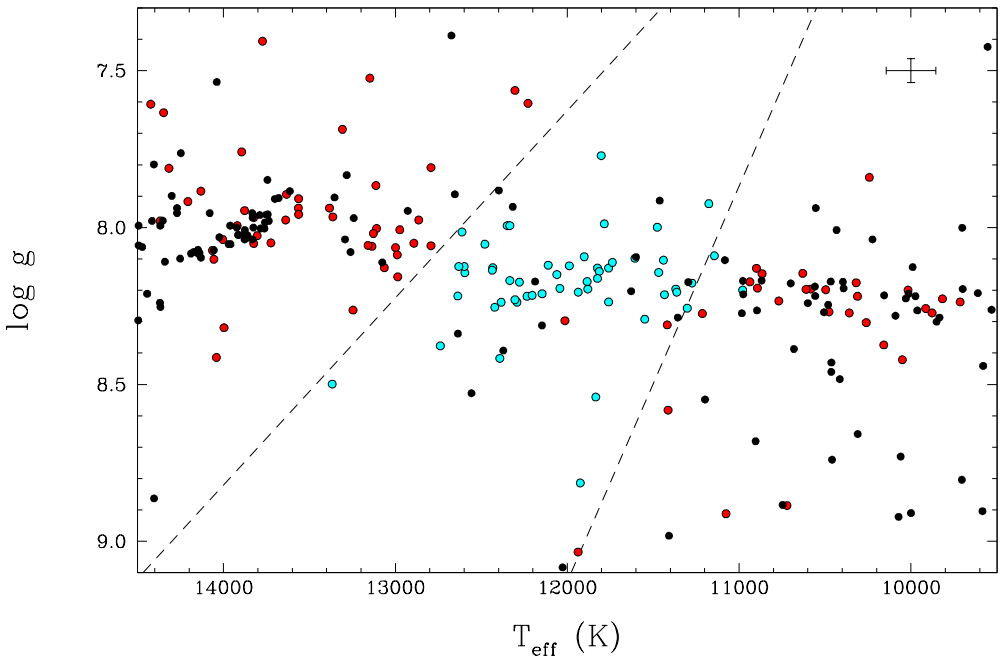

FIGURE 3.35 – Same as Figure 3.33 but for our entire sample of white dwarfs. The black circles represent the stars for which we do not have any high-speed photometric data. The dashed lines correspond to our new determination of the empirical boundaries of the ZZ Ceti instability strip.

of the star, the excited pulsation mode, or modes, might produce no detectable variations if the combined effect of the alternating hot and cold areas is nil. This would likely require a chance alignment where, for example, the rotation axis of the star is perpendicular to our line of sight. Whatever the case may be, we are planning to secure new high-speed photometry for this star during the next trimester to settle, once and for all, the issue of its photometric status.

Finally, in Figure 3.35 we add all the remaining stars from our survey whose photometric status is unknown. We can identify a total of 13 ZZ Ceti candidates that lie within the empirical boundaries of the instability strip. However, as Gianninas et al. (2006) demonstrated, it is important and worthwhile to observe all white dwarfs that are near either edge of the instability strip as well. It could be argued that adding a few more ZZ Ceti stars to the mix is not especially important since hundreds have now been identified through the SDSS and follow-up work. However, the SDSS variables are, for the most part, a few magnitudes

fainter than the white dwarfs shown here. Besides the discovery lightcurves, it is hard to conceive of meaningful asteroseismological studies of the ZZ Ceti stars from SDSS. In contrast, these brighter candidates could be studied on small to medium-sized telescopes equipped with proper instrumentation.

The most intriguing of all the candidates is certainly 1659+662 (GD 518). With $\log g = 9.08$, it would easily become the most massive ZZ Ceti star ever discovered, surpassing even 1236−495 (BPM 37093, LTT 4816) the current heavyweight of the group. High-speed photometric measurements of this object are being planned as well.

3.7 CONCLUSION

We have presented the results of our spectroscopic survey of hydrogen-rich white dwarfs from MS99. First, we discovered that many stars listed in the catalog are still erroneously classified as white dwarfs. In particular, we list a total of 67 stars that are misclassified, 26 of which need to be reclassified as the result of our observations. We then examined the spectroscopic content of our survey. The majority of stars in our sample are simple DA white dwarfs but a number of them show more than just the characteristic Balmer lines of hydrogen. Indeed, our sample includes both DAB and DAZ white dwarfs as well as DA+dM binaries and magnetic white dwarfs. In addition, there are several white dwarfs that are cool enough that no Balmer-lines are present, at least not within the spectral range covered by our observations. With the exclusion of the magnetic stars and the cool, featureless white dwarfs, we have analyzed the spectra of all the white dwarfs in our sample. In order to do so, and with the goal of obtaining the most accurate atmospheric parameters possible, we have endeavored to use the most modern, up-to-date, and appropriate model atmospheres in our analyses of these white dwarfs.

First, for the analysis of all the hydrogen-rich white dwarfs we have used models that include the new Stark broadening profiles from TB09. The analysis of the hot DAO and DA+BP stars was presented in Gianninas et al. (2010) and featured models to which CNO, at solar abundances, was added in order to overcome the Balmer-line problem. The results of that analysis were incorporated here. Furthermore, we used updated helium atmosphere

models to analyze several DA+DB double-degenerate binary systems and we developed a technique that uses M dwarf templates to correct for the contamination in the composite spectra of DA+dM binary systems. We also analyzed several DAZ stars by including calcium in the calculation of the synthetic spectrum only. Two of these are newly identified DAZ stars and they should be checked for any infrared excess. This would betray the presence of a circumstellar disk that would be the logical source of the metal pollutants.

In switching from the older Stark broadening profiles of Lemke (1997) to those of TB09, we also explored how our atmospheric parameters have changed as a result. We observed that the values of $T_{\rm eff}$ are shifted slightly toward higher temperatures while the values of $\log g$ show a more obvious and significant trend to towards higher values. With that said, we also saw how the new profiles improved the overall shape of the mass distribution as a function of $T_{\rm eff}$. The distribution now remains largely constant around 0.60 $M_{\odot}$ until $\sim$ 13,000 K where the well known high $\log g$ problem takes over. It is hoped that new 3D hydrodynamic models of convection might finally solve this problem by replacing the more approximate mixing length theory used to this day.

We also wanted to test the reliability of our results by comparing them with those of an independent study. The Koester et al. (2009) analysis of DA white dwarfs from the SPY sample was ideal for this purpose since several hundred white dwarfs were in common with both samples but were observed and analyzed in a completely independent fashion. We showed that our $T_{\rm eff}$ determinations are in excellent agreement with those of Koester et al. (2009) despite a trend towards higher $\log g$ values in the Koester et al. analysis.

Our mass distribution yields a mean mass of 0.638 $M_{\odot}$ when considering only white dwarfs with $T_{\rm eff} \geq$ 13,000 K. The mean mass is somewhat higher than other determinations, but it is understood to be caused by high-mass white dwarfs that are missed in many surveys but included here. We also note the presence of a low-mass component, consistent with the results of most other large scale studies of DA white dwarfs. The low-mass stars are necessarily the product of binary evolution either through mergers or a common envelope phase where a significant fraction of their mass may have been lost.

We also recomputed the PG luminosity function and found a space density which is only

slightly lower than that determined by LBH05. It would be easy to point the finger at the new TB09 Stark broadening profiles since they yield higher temperatures, but they also yield higher $\log g$ measurements that translate to smaller radii. These facts coupled together produce two very similar values of M_V. However, even small differences can cause stars to switch magnitude bins, which explains our marginally lower value.

Finally, we re-examined the ZZ Ceti instability strip and found that the TB09 Stark broadening profiles produce a wider instability strip that is also systematically shifted toward higher $T_{\rm eff}$. Furthermore, we have identified over a dozen new ZZ Ceti candidates among which might be the most massive ZZ Ceti star ever discovered. High-speed photometric observations are planned for all candidates in the very near future.

We thank the director and staff of Steward Observatory and of the Carnegie Observatories for the use of their facilities. We are also grateful to D. Koester for providing us with all of the SPY spectra, and M.-M. Limoges for obtaining several of the optical spectra analyzed in this paper. This work was supported in part by the NSERC Canada and by the Fund FQRNT (Québec). M. T. R. acknowledges support from FONDAP (15010003) and Proyecto BASAL PB06 (CATA). P. B. is a Cottrell Scholar of Research Corporation for Science Advancement.

3.8 REFERENCES

Achilleos, N., & Wickramasinghe, D. T. 1989, ApJ, 346, 444

Althaus, L. G., Serenelli, A. M., & Benvenuto, O. G. 2001, MNRAS, 323, 471

Angel, J. R. P., Borra, E. F., & Landstreet, J. D. 1981, ApJS, 45, 457

Asplund, M., Grevesse, N., & Sauval, A. J. 2005, Cosmic Abundances as Records of Stellar Evolution and Nucleosynthesis, 336, 25

Aznar Cuadrado, R., Jordan, S., Napiwotzki, R., Schmid, H. M., Solanki, S. K., & Mathys, G. 2004, A&A, 423, 1081

Beauchamp, A. 1995, Ph.D. Thesis, Univ. de Montréal

Beauchamp, A., Wesemael, F., & Bergeron, P. 1997, ApJS, 108, 559

Beauchamp, A., Wesemael, F., Bergeron, P., Fontaine, G., Saffer, R. A., Liebert, J., & Brassard, P. 1999, ApJ, 516, 887

Beauchamp, A., Wesemael, F., Bergeron, P., Liebert, J., & Saffer, R. A. 1996, in ASP Conf. Ser. 96, Hydrogen-Deficient Stars, ed. S. Jeffery & U. Heber (San Francisco, CA: ASP), 295

Becklin, E. E., Farihi, J., Jura, M., Song, I., Weinberger, A. J., & Zuckerman, B. 2005, ApJ, 632, L119

Bergeron, P., et al. 2010, American Institute of Physics Conference Series, 1273, 7

Bergeron, P., Leggett, S. K., & Ruiz, M. T. 2001, ApJS, 133, 413

Bergeron, P., & Liebert, J. 2002, ApJ, 566, 1091

Bergeron, P., Greenstein, J. L., & Liebert, J. 1990a, ApJ, 361, 190

Bergeron, P., Ruiz, M.-T., & Leggett, S. K. 1993, ApJ, 407, 733

Bergeron, P., Saffer, R. A., & Liebert, J. 1992, ApJ, 394, 228

Bergeron, P., Wesemael, F., Beauchamp, A., Wood, M. A., Lamontagne, R., Fontaine, G., & Liebert, J. 1994, ApJ, 432, 305

Bergeron, P., Wesemael, F., Fontaine, G., & Liebert, J. 1990b, ApJ, 351, L21

Bergeron, P., Wesemael, F., Lamontagne, R., Fontaine, G., Saffer, R. A., & Allard, N. F. 1995, ApJ, 449, 258

Billères, M., Wesemael, F., Bergeron, P., & Beauchamp, A. 1997, ApJ, 488, 368

Bochanski, J. J., West, A. A., Hawley, S. L., & Covey, K. R. 2007, AJ, 133, 531

Bohlin, R. C., & Gilliland, R. L. 2004, AJ, 127, 3508

Bowyer, S., Lieu, R., Lampton, M., Lewis, J., Wu, X., Drake, J. J., & Malina, R. F. 1994, ApJS, 93, 569

Catalán, S., Isern, J., García-Berro, E., Ribas, I., Allende Prieto, C., & Bonanos, A. Z. 2008, A&A, 477, 213

Christlieb, N., Wisotzki, L., Reimers, D., Homeier, D., Koester, D., & Heber, U. 2001, A&A, 366, 898

Cutri, R. M., et al. 2003, The IRSA 2MASS All-Sky Point Source Catalog, NASA/IPAC Infrared Science Archive

Dufour, P., et al. 2010, ApJ, 718, 647

Dufour, P., Fontaine, G., Liebert, J., Schmidt, G. D., & Behara, N. 2008, ApJ, 683, 978

Eisenstein, D. J., et al. 2006, ApJS, 167, 40

Farihi, J., Becklin, E. E., & Zuckerman, B. 2005, ApJS, 161, 394

Farihi, J., Hoard, D. W., & Wachter, S. 2006, ApJ, 646, 480

Ferrario, L., Wickramasinghe, D. T., Liebert, J., Schmidt, G. D., & Bieging, J. H. 1997, MNRAS, 289, 105

Finley, D. S., Koester, D., & Basri, G. 1997, ApJ, 488, 375

Fleming, T. A., Snowden, S. L., Pfeffermann, E., Briel, U., & Greiner, J. 1996, A&A, 316, 147

Fontaine, G., & Brassard, P. 2008, PASP, 120, 1043

Fontaine, G., Brassard, P., & Bergeron, P. 2001, PASP, 113, 409

Gänsicke, B. T., Euchner, F., & Jordan, S. 2002, A&A, 394, 957

Gänsicke, B. T., Koester, D., Girven, J., Marsh, T. R., & Steeghs, D. 2010, Science, 327, 188

Gänsicke, B. T., Koester, D., Marsh, T. R., Rebassa-Mansergas, A., & Southworth, J. 2008, MNRAS, 391, L103

Gianninas, A., Bergeron, P., Dupuis, J., & Ruiz, M. T. 2010, ApJ, 720, 581

Gianninas, A., Bergeron, P., & Fontaine, G. 2007, in ASP Conf. Ser. 372, 15th European Workshop on White Dwarfs, ed. R. Napiwotzki & M. R. Burleigh, (San Francisco, CA:ASP), 577

Gianninas, A., Bergeron, P., & Fontaine, G. 2006, AJ, 132, 831

Gianninas, A., Bergeron, P., & Fontaine, G. 2005, ApJ, 631, 1100

Gianninas, A., Bergeron, P., & Ruiz, M. T. 2009, J. Phys. Conf. Ser., 172, 012021

Gianninas, A., Dufour, P. & Bergeron, P. 2004, ApJ, 617, L57

Giclas, H. L., Burnham, R., & Thomas, N. G. 1965, Lowell Observatory Bulletin, 6, 155

Glenn, J., Liebert, J., & Schmidt, G. D. 1994, PASP, 106, 722

Green, R. F., Schmidt, M., & Liebert, J. 1986, ApJS, 61, 305

Greenstein, J. L. 1986, ApJ, 304, 334

Hamada, T., & Salpeter, E. E. 1961, ApJ, 134, 683

Heber, U., Napiwotzki, R., Lemke, M., & Edelmann, H. 1997, A&A, 324, L53

Heller, R., Homeier, D., Dreizler, S., & Østensen, R. 2009, A&A, 496, 191

Holberg, J. B., & Bergeron, P. 2006, AJ, 132, 1221

Holberg, J. B., Sion, E. M., Oswalt, T., McCook, G. P., Foran, S., & Subasavage, J. P. 2008, AJ, 135, 1225

Homeier, D., Koester, D., Hagen, H.-J., Jordan, S., Heber, U., Engels, D., Reimers, D., & Dreizler, S. 1998, A&A, 338, 563

Hubeny, I., & Lanz, T. 1995, ApJ, 439, 875

Hügelmeyer, S. D., Dreizler, S., Homeier, D., Krzesiǹski, J., Werner, K., Nitta, A., & Kleinman, S. J. 2006, A&A, 454, 617

John, T. L. 1994, MNRAS, 269, 871

Jordan, S., Heber, U., Engels, D., & Koester, D. 1993, A&A, 273, L27

Kawka, A., Vennes, S., & Thorstensen, J. R. 2004, AJ, 127, 1702

Kepler, S. O., Kleinman, S. J., Nitta, A., Koester, D., Castanheira, B. G., Giovannini, O., Costa, A. F. M., & Althaus, L. 2007, MNRAS, 375, 1315

Kilic, M., Brown, W. R., Allende Prieto, C., Agüeros, M. A., Heinke, C., & Kenyon, S. J. 2011, ApJ, 727, 3

Kilic, M., von Hippel, T., Leggett, S. K., & Winget, D. E. 2006, ApJ, 646, 474

Kilic, M., von Hippel, T., Leggett, S. K., & Winget, D. E. 2005, ApJ, 632, L115

Kilkenny, D., Heber, U., & Drilling, J. S. 1988, South African Astronomical Observatory Circular, 12, 1

Kilkenny, D., O'Donoghue, D., Koen, C., Stobie, R. S., & Chen, A. 1997, MNRAS, 287, 867

Koester, D. 2010, Mem. Soc. Astron. Italiana, 81, 921

Koester, D., et al. 2001, A&A, 378, 556

Koester, D., & Reimers, D. 1985, A&A, 153, 260

Koester, D., Voss, B., Napiwotzki, R., Christlieb, N., Homeier, D., Lisker, T., Reimers, D., & Heber, U. 2009, A&A, 505, 441

Kondo, M., Noguchi, T., & Maehara, H. 1984, Ann. Tokyo Astron. Obs., 20, 130

Lacombe, P., Wesemael, F., Fontaine, G., & Liebert, J. 1983, ApJ, 272, 660

Lemke, M. 1997, A&AS, 122, 285

Liebert, J., Bergeron, P., & Holberg, J. B. 2005, ApJS, 156, 47 (LBH05)

Liebert, J., Bergeron, P., & Saffer, R.A. 1991, in 7th European Workshop on White Dwarfs, NATO ASI Series, ed. G. Vauclair & E. M. Sion (Dordrecht: Kluwer Academic Publishers), 409

Liebert, J., Bergeron, P., Schmidt, G. D., & Saffer, R. A. 1993, ApJ, 418, 426

Limoges, M.-M., & Bergeron, P. 2010, ApJ, 714, 1037

Lisker, T., Heber, U., Napiwotzki, R., Christlieb, N., Han, Z., Homeier, D., & Reimers, D. 2005, A&A, 430, 223

Marsh, M. C., et al. 1997a, MNRAS, 286, 369

Marsh, M. C., et al. 1997b, MNRAS, 287, 705

Martin, B., & Wickramasinghe, D. T. 1984, MNRAS, 206, 407

Maxted, P. F. L., & Marsh, T. R. 1999, MNRAS, 307, 122

Maxted, P. F. L., Marsh, T. R., & Moran, C. K. J. 2000, MNRAS, 319, 305

McCook, G. P., & Sion, E. M. 1999, ApJS, 121, 1 (MS99)

Monet, D. G., et al. 2003, AJ, 125, 984

Noguchi, T., Maehara, H., & Kondo, M. 1980, Ann. Tokyo Astron. Obs., 18, 55

Pereira, C., Bergeron, P., & Wesemael, F. 2005, ApJ, 623, 1076

Perryman, M. A. C., & ESA 1997, ESA Special Publication, 1200

Pounds, K. A., et al. 1993, MNRAS, 260, 77

Press, W. H., Flannery, B. P., Teukolsky, S. A., & Vetterling, W. T. 1986, Numerical Recipes (Cambridge: Cambridge Univ. Press)

Putney, A. 1997, ApJS, 112, 527

Putney, A., & Jordan, S. 1995, ApJ, 449, 863

Rebassa-Mansergas, A., Gänsicke, B. T., Schreiber, M. R., Koester, D., & Rodríguez-Gil, P. 2010, MNRAS, 402, 620

Saffer, R. A., Liebert, J., & Olszewski, E. M. 1988, ApJ, 334, 947

Saffer, R. A., Liebert, J., Wagner, R. M., Sion, E. M., & Starrfield, S. G. 1989, AJ, 98, 668

Schlegel, D. J., Finkbeiner, D. P., & Davis, M. 1998, ApJ, 500, 525

Schmidt, G. D., & Smith, P. S. 1994, ApJ, 423, L63

Schmidt, G. D., West, S. C., Liebert, J., Green, R. F., & Stockman, H. S. 1986, ApJ, 309, 218

Seaton, M. J. 1979, MNRAS, 187, 73P

Silvestri, N. M., et al. 2006, AJ, 131, 1674

Silvestri, N. M., Oswalt, T. D., Wood, M. A., Smith, J. A., Reid, I. N., & Sion, E. M. 2001, AJ, 121, 503

Smith, R. J., Croom, S. M., Boyle, B. J., Shanks, T., Miller, L., & Loaring, N. S. 2005, MNRAS, 359, 57

Strand, K. A., Dahn, C. C., & Liebert, J. W. 1976, BAAS, 8, 506

Stroeer, A., Heber, U., Lisker, T., Napiwotzki, R., Dreizler, S., Christlieb, N., & Reimers, D. 2007, A&A, 462, 269

Subasavage, J. P., Henry, T. J., Bergeron, P., Dufour, P., Hambly, N. C., & Beaulieu, T. D. 2007, AJ, 134, 252

Tremblay, P.-E., & Bergeron, P. 2009, ApJ, 696, 1755 (TB09)

Tremblay, P.-E., Bergeron, P., & Gianninas, A. 2011, ApJ, 730, 128

Tremblay, P.-E., Bergeron, P., Kalirai, J. S., & Gianninas, A. 2010, ApJ, 712, 1345

van Altena, W. F., Lee, J. T., & Hoffleit, E. D. 1994, The General Catalogue of Trigonometric Parallaxes (New Haven: Yale Univ. Obs.)

Vanlandingham, K. M., et al. 2005, AJ, 130, 734

Vennes, S., Christian, D. J., & Thorstensen, J. R. 1998, ApJ, 502, 763

Vennes, S., Ferrario, L., & Wickramasinghe, D. T. 1999, MNRAS, 302, L49

Vennes, S., Smith, R. J., Boyle, B. J., Croom, S. M., Kawka, A., Shanks, T., Miller, L., & Loaring, N. 2002, MNRAS, 335, 673

Vennes, S., Thejll, P. A., Galvan, R. G., & Dupuis, J. 1997, ApJ, 480, 714

Vennes, S., Thejll, P. A., Wickramasinghe, D. T., & Bessell, M. S. 1996, ApJ, 467, 782

Voss, B. 2006, Ph.D. Thesis, Univ. Kiel

Voss, B., Koester, D., Østensen, R., Kepler, S. O., Napiwotzki, R., Homeier, D., & Reimers, D. 2006, A&A, 450, 1061

Voss, B., Koester, D., Østensen, R., Napiwotzki, R., Homeier, D., & Reimers, D. 2007, in ASP Conf. Ser. 372, 15th European Workshop on White Dwarfs, ed. R. Napiwotzki & M. R. Burleigh, (San Francisco, CA:ASP) 583

Werner, K. 1996, ApJ, 457, L39

Wesemael, F., et al. 1994, ApJ, 429, 369

Wickramasinghe, D. T., & Ferrario, L. 2000, PASP, 112, 873

Wolff, B., Jordan, S., Koester, D., & Reimers, D. 2000, A&A, 361, 629

Wood, M. A. 1995, in Proceedings of the 9th European Workshop on White Dwarfs, eds. D. Koester & K. Werner (Berlin: Springer), 41

Zuckerman, B., Koester, D., Melis, C., Hansen, B. M., & Jura, M. 2007, ApJ, 671, 872

Zuckerman, B., Koester, D., Reid, I. N., Hünsch, M. 2003, ApJ, 596, 477

Chapitre 4

Conclusion

4.1 Résumé

Dans cette thèse, nous avons présenté les résultats de notre relevé spectroscopique d'étoiles naines blanches brillantes et riches en hydrogène tirées, en majorité, du catalogue de McCook & Sion (1999). Ceci représente à ce jour, le plus grand échantillon de naines blanches brillantes ($V < 17.5$) analysées de manière homogène. Sur un échantillon de 1495 étoiles, nous avons obtenu des spectres pour 1339 de ces étoiles.

Dans un premier temps, nous avons présenté une analyse détaillée et complète des étoiles naines blanches chaudes de type DA et DAO. Pour ce faire, nous avons calculé des nouvelles grilles de modèles d'atmosphère afin de résoudre le problème des raies de Balmer (Werner 1996). L'utilisation de ces nouveaux modèles entraîne un bien meilleur accord entre les données observationnelles et nos spectres synthétiques. De plus, nos valeurs révisées des paramètres atmosphériques des naines blanches de type DAO indiquent qu'elles sont plus chaudes et plus massives que les déterminations précédentes nous laissaient croire (Bergeron et al. 1994). Conséquemment, nous avons pu conclure que les naines blanches de type DAO proviennent de l'évolution d'étoiles de la branche asymptotique des géantes (AGB) comme la vaste majorité des naines blanches. En ce qui concerne le problème des raies de Balmer, un examen des spectres ultraviolets du satellite *FUSE* nous a permis de montrer que la présence de métaux dans l'atmosphère est bel et bien à l'origine de ce phénomène. Finalement, nous avons proposé

un scénario cohérent où un faible vent stellaire, soutenu par la présence des métaux, explique à la fois la présence de l'hélium dans les étoiles DAO mais rend aussi compte du problème des raies de Balmer de façon générale.

Deuxièmement, nous avons présenté les résultats complets de notre relevé de McCook & Sion (1999). Le premier objectif de notre relevé était de confirmer la classification spectrale de chaque objet. À cet égard, nous avons pu exclure 67 étoiles dont 26 qui ont été reclassifiées grâce aux données obtenues spécifiquement pour ce projet. Un examen minutieux des spectres nous a permis d'identifier plusieurs sous-types de naines blanches, outre les naines blanches DA simples dans notre échantillon. Plus précisément, nous retrouvons des naines blanches de type DAB, DAZ, des systèmes binaires DA+dM ainsi que des étoiles DA magnétiques. Pour analyser l'ensemble de ces objets, nous avons utilisé la toute dernière génération de modèles d'atmosphère qui inclut les récents calculs de profils d'élargissement Stark de Tremblay & Bergeron (2009). L'utilisation de ces modèles améliorés est nécessaire puisque notre méthode pour évaluer les paramètres atmosphériques repose sur notre capacité à reproduire en détail les profils observés des raies de Balmer. En fin de compte, nous fournissons des mesures de la température effective, $T_{\rm eff}$, et de la gravité de surface, $\log g$, pour 1246 naines blanches. À partir de ces valeurs, nous calculons des masses, des magnitudes absolues et également des distances pour chaque objet. Avec ces données, nous comparons nos résultats avec ceux d'autres échantillons importants de naines blanches dont nous avons des étoiles en commun, tel que les échantillons SPY et SDSS. On note une bonne correspondance pour les valeurs de $T_{\rm eff}$ mais dans les deux cas, nous obtenons des masses plus élevées. Dans le cas de SPY, ces différences sont attribuables aux différents modèles et aux différentes méthodes d'analyse tandis que des problèmes dans la calibration des données seraient à l'origine de la disparité avec les étoiles du SDSS.

Nous avons par la suite étudié les propriétes globales de notre échantillon. La distribution de masse en fonction de $T_{\rm eff}$ montre toujours le problème des masses élevées à basses températures mais la nouvelle analyse des étoiles DAO et les nouveaux profils d'élargissement Stark ont pour effet de redresser la distribution de masse à haute température et également autour de 13,000 K. En considérant uniquement les naines blanches avec $T_{\rm eff} > 13{,}000$ K, nous

déterminons une masse moyenne de 0.638 $M_{\odot}$, une valeur plus élevée que celle déterminée à partir de données du SDSS (Tremblay et al. 2011). Cette différence est reliée au fait que notre relevé contient des naines blanches plus massives qui sont systématiquement exclues dans bien des relevés, incluant le SDSS. Nous avons également recalculé la fonction de luminosité de l'échantillon PG (Liebert et al. 2005). Nous remarquons surtout des différences dans les intervalles de plus faibles magnitudes ce qui entraînent une légère baisse de la valeur de la densité locale de naines blanches. Finalement, nous redéterminons l'emplacement des frontières chaudes et froides de la bande d'instabilité des naines blanches variables de types ZZ Ceti. L'utilisation des nouveaux profils Stark produit un décalage de la bande d'instabilité vers des températures plus chaudes, cette dernière étant également plus large qu'auparavant. De plus, nous identifions plusieurs nouveaux candidats dont le statut photométrique devra être vérifié. Dans cette liste, nous incluons une étoile qui pourrait être l'étoile de type ZZ Ceti la plus massive jamais détectée.

4.2 Importance des résultats

Comme nous l'avons indiqué dans la section précédente, nous avons analysé le plus grand échantillon de naines blanches brillantes et ce, de manière homogène. Ceci représente une ressource importante pour la communauté des naines blanches puisque nous avons démontré que nos méthodes sont robustes et nos résultats sont fiables. Notre analyse ne présentent pas les problèmes qui affligent les données et/ou les résultats d'autres relevés comme SPY et SDSS. Notre analyse deviendra donc une référence importante et un point d'ancrage auquel d'autres chercheurs compareront leurs résultats.

Nous tenons à souligner que le passage aux nouveaux profils Stark de TB09 est important en terme de notre capacité de reproduire de manière précise les profils observés des raies de Balmer. Cependant notre but n'est pas d'étudier les effets d'inclure ces nouveaux calculs dans les modèles ou de commenter sur l'importance de ces nouveaux profils pour l'étude des naines blanches en général. Cela à déjà été fait dans par TB09.

Ensuite, de nombreux projets cherchent à définir et étudier des échantillons locaux de naines blanches, c'est-à-dire, à l'intérieur d'un rayon de 20-25 parsecs du soleil, comme Giam-

michele et al. (2010) par exemple. Dans ces cas, il devient intéressant d'avoir des mesures précises des paramètres atmosphériques pour toutes les naines les plus brillantes connues.

D'autre part, les naines blanches servent souvent comme étoiles de calibration pour les observatoires spatiales. Ainsi, l'accès à une banque de naines blanches avec des mesures précises de $T_{\rm eff}$ et $\log g$ peut aussi servir pour générer des listes d'étoiles de références potentielles pour le *James Webb Space Telescope* (*JWST*), par exemple.

Les résultats de cet thèse pourront également servir de point de départ pour de nouvelles études. Par exemple, du temps d'observation a déjà été obtenu pour observer plusieurs des étoiles dont les paramètres atmosphériques les placent dans la bande d'instabilité des naines blanches variables de type ZZ Ceti. De plus, les nouvelles déterminations des limites empiriques de la bande d'instabilité sont très importantes pour les modèles asterosismologiques. Notamment, l'emplacement exact de la frontière chaude de la bande d'instabilité est très sensible à l'efficacité convective dans les modèles. On peut donc exploiter ce fait pour contraindre la valeur de celle-ci.

D'autre part, nous avons identifié deux nouvelles étoiles de type DAZ qui seraient d'excellents candidats pour la présence d'un disque circumstellaire. Des observations dans le domaine infrarouge seraient nécessaires pour déceler la présence de tels disques. Même pour les naines blanches qui ne sont pas de type DAZ, nos déterminations de $T_{\rm eff}$ peuvent servir à la comparaison avec des données infrarouges et ainsi voir si un excès est détecté. Ceci pourrait mener à des nouvelles identifications de disques ou de compagnons froids.

4.3 Perspectives d'avenir

Dans un futur proche, il y a encore plusieurs relevés qui vont nous permettre d'approfondir davantage nos connaissances sur les étoiles naines blanches.

Le relevé *Lépine-Shara Proper Motion* (LSPM, Lépine & Shara 2005) exploite les données du *Digitized Sky Survey* en effectuant une nouvelle analyse des plaques POSS-I et POSS-II acquises à deux époques différentes, à des intervalles allant de 25 à 40 ans. Le logiciel SUPERBLINK est utilisé pour déterminer de manière précise le mouvement propre de toutes les étoiles dans chaque champ. Le catalogue final compte plus de 1.3 million d'objets. Limoges

et al. (2010) présente des résultats préliminaires d'un projet visant la découverte de nouvelles naines blanches à partir du relevé LSPM, en jumelant les données de mouvement propre avec toute photométrie disponible (UV lointain, visible, infrarouge). Ces candidats sont ensuite observés en spectroscopie pour confirmer leur statut. À ce jour, 147 nouvelles naines blanches ont été découvertes.

D'autre part, le *Sloan Extension for Galactic Understanding and Exploration* (SEGUE, Yanny et al. 2009) représente une extension du SDSS visant spécifiquement le contenu stellaire de notre Galaxie. Des spectres pour 240,000 étoiles avec des magnitudes $20 > g > 14$ ont été obtenus. Entre autres, des spectres pour plus de 4000 candidats ont été identifiés comme naines blanches chaudes potentielles.

Finalement, la sonde GAIA, un projet du *European Space Agency* (ESA), sera lancée dans les prochaines années. Le but de cette mission sera de créer la carte tri-dimensionnelle la plus vaste et la plus précise de notre Galaxie en fournissant des mesures de positions, de photométries et de vitesses radiales pour près de 1 milliard d'étoiles dans notre Galaxie et le Groupe Local. GAIA comptera trois instruments pour effectuer à la fois des mesures d'astrométrie (parallaxe), de photométrie et de spectroscopie (vitesses radiales). Jordan (2007) rapporte que l'échantillon de naines blanches de GAIA devrait être complet jusqu'à 100 pc. De plus, des simulations montrent que GAIA devrait détecter près de 400,000 naines blanches au total. Malheureusement, les spectres obtenus par GAIA ne seront pas dans une plage de longueur d'onde (8470 – 8740Å) particulièrement propice à l'identification ou l'étude de naines blanches. Cependant, les mesures de parallaxe de GAIA mèneront à des mesures précises de la masse ce qui permettra de vérifier la relation masse-rayon des naines blanches.

Ces grands projets révolutionneront sûrement le domaine des naines blanches dans les années à venir. Cependant, l'achèvement d'un vieux projet, arrêté depuis plus de 15 ans, pourrait également apporter une contribution. Nous parlons ici du relevé MCT (voir Section 1.4). Des centaines de candidats demeurent sans observations spectroscopiques. Ces observations seraient d'autant plus faciles à obtenir avec la panoplie d'observatoires d'envergure maintenant disponible dans l'hémisphère sud et surtout au Chili, mais également parce que les candidats qui sont tous relativement brillants ($B < 16.5$). Déjà, plusieurs objets intéressants

avaient été identifiés dans le relevé MCT et il est certain que d'autres s'y trouvent. Dans ces cas, des études subséquentes (spectroscopie à haute dispersion, mesures de vitesses radiales, astérosismologie) seraient, encore une fois, facilitées par la brillance de ces objets. Nous croyons que la conclusion du relevé MCT représente une tâche qui mériterait d'être entreprise.

Bibliographie

Adams, W. S. 1914, PASP, 26, 198

—. 1915, PASP, 27, 236

Adams, W. S. & Pease, F. G. 1914, PASP, 26, 258

Bergeron, P., Wesemael, F., Beauchamp, A., Wood, M. A., Lamontagne, R., Fontaine, G., & Liebert, J. 1994, ApJ, 432, 305

Cannon, A. J. & Pickering, E. C. 1912, Annals of Harvard College Observatory, 56, 115

Christlieb, N., Wisotzki, L., Reimers, D., Homeier, D., Koester, D., & Heber, U. 2001, A&A, 366, 898

Darling, G. W. 1994, PhD thesis, Dartmouth College

Demers, S., Béland, S., Kibblewhite, E. J., Irwin, M. J., & Nithakorn, D. S. 1986, AJ, 92, 878

Eggen, O. J. & Greenstein, J. L. 1965, ApJ, 141, 83

Eisenstein, D. J., et al. 2006, ApJS, 167, 40

Fleming, T. A., Liebert, J., & Green, R. F. 1986, ApJ, 308, 176

Giammichele, N., Bergeron, P., & Dufour, P. 2010, American Institute of Physics Conference Series, 1273, 101

Giclas, H. L. 1958, Lowell Observatory Bulletin, 4, 1

Giclas, H. L., Burnham, R., & Thomas, N. G. 1965, Lowell Observatory Bulletin, 6, 155

—. 1971, Lowell proper motion survey Northern Hemisphere. The G numbered stars. 8991 stars fainter than magnitude 8 with motions greater than 0".26/year, ed. Giclas, H. L., Burnham, R., & Thomas, N. G.

Green, R. F., Schmidt, M., & Liebert, J. 1986, ApJS, 61, 305

Greenstein, J. L. 1960, in Stellar Atmospheres, ed. J. L. Greenstein, 676

Hagen, H., Groote, D., Engels, D., & Reimers, D. 1995, A&AS, 111, 195

Homeier, D., Koester, D., Hagen, H., Jordan, S., Heber, U., Engels, D., Reimers, D., & Dreizler, S. 1998, A&A, 338, 563

Jordan, S. 2007, in Astronomical Society of the Pacific Conference Series, Vol. 372, 15th European Workshop on White Dwarfs, ed. R. Napiwotzki & M. R. Burleigh, 139–144

Kilkenny, D., O'Donoghue, D., Hambly, N., & MacGillivray, H. 2010, Ap&SS, 329, 49

Kilkenny, D., O'Donoghue, D., Koen, C., Stobie, R. S., & Chen, A. 1997, MNRAS, 287, 867

Kleinman, S. J. 2010, in American Institute of Physics Conference Series, Vol. 1273, American Institute of Physics Conference Series, ed. K. Werner & T. Rauch, 156–159

Kondo, M., Noguchi, T., & Maehara, H. 1984, Annals of the Tokyo Astronomical Observatory, 20, 130

Kuiper, G. P. 1941, PASP, 53, 248

Lamontagne, R., Demers, S., Wesemael, F., Fontaine, G., & Irwin, M. J. 2000, AJ, 119, 241

Lépine, S. & Shara, M. M. 2005, AJ, 129, 1483

Liebert, J., Bergeron, P., & Holberg, J. B. 2005, ApJS, 156, 47

Limoges, M. & Bergeron, P. 2010, ApJ, 714, 1037

Limoges, M., Bergeron, P., & Lépine, S. 2010, in American Institute of Physics Conference Series, Vol. 1273, American Institute of Physics Conference Series, ed. K. Werner & T. Rauch, 193–196

Luyten, W. J. 1922a, PASP, 34, 54

—. 1922b, PASP, 34, 356

—. 1923, Lick Observatory Bulletin, 11, 1

—. 1950, AJ, 55, 86

—. 1952, ApJ, 116, 283

—. 1957, A catalogue of 9867 stars in the Southern Hemisphere with proper motions exceeding 0.”2 annually., ed. Luyten, W. J.

—. 1963, Bruce proper motion survey; the general catalogue

—. 1979, LHS catalogue. A catalogue of stars with proper motions exceeding 0.”5 annually, ed. Luyten, W. J.

McCook, G. P. & Sion, E. M. 1977, A Catalogue of spectroscopically identified white dwarfs, ed. McCook, G. P. & Sion, E. M.

—. 1983, A catalogue of spectroscopically identified white dwarfs., ed. McCook, G. P. & Sion, E. M.

—. 1987, ApJS, 65, 603

—. 1999, ApJS, 121, 1

Noguchi, T., Maehara, H., & Kondo, M. 1980, Annals of the Tokyo Astronomical Observatory, 18, 55

Schatzman, E. L. 1958, White dwarfs

Sion, E. M., Greenstein, J. L., Landstreet, J. D., Liebert, J., Shipman, H. L., & Wegner, G. A. 1983, ApJ, 269, 253

Stobie, R. S., Morgan, D. H., Bhatia, R. K., Kilkenny, D., & O’Donoghue, D. 1987, in IAU Colloq. 95: Second Conference on Faint Blue Stars, ed. A. G. D. Philip, D. S. Hayes, & J. W. Liebert, 493–496

Tremblay, P. & Bergeron, P. 2009, ApJ, 696, 1755

Tremblay, P., Bergeron, P., & Gianninas, A. 2011, ApJ, 730, 128

van Maanen, A. 1917, PASP, 29, 258

Werner, K. 1996, ApJ, 457, L39

Wisotzki, L. 1994, in IAU Symposium, Vol. 161, Astronomy from Wide-Field Imaging, ed. H. T. MacGillivray, 723–727

Yanny, B., et al. 2009, AJ, 137, 4377

Annexe A

Solutions spectroscopiques pour les étoiles DAO et DA+BP

Nous présentons ici l'ensemble de nos solutions spectroscopiques pour les étoiles DAO et DA+BP présentées au Chapitre 2 puisque ces solutions n'y figuraient pas toutes étant donnés les contraintes d'espace pour la publication dans l'*Astrophysical Journal* (ApJ).

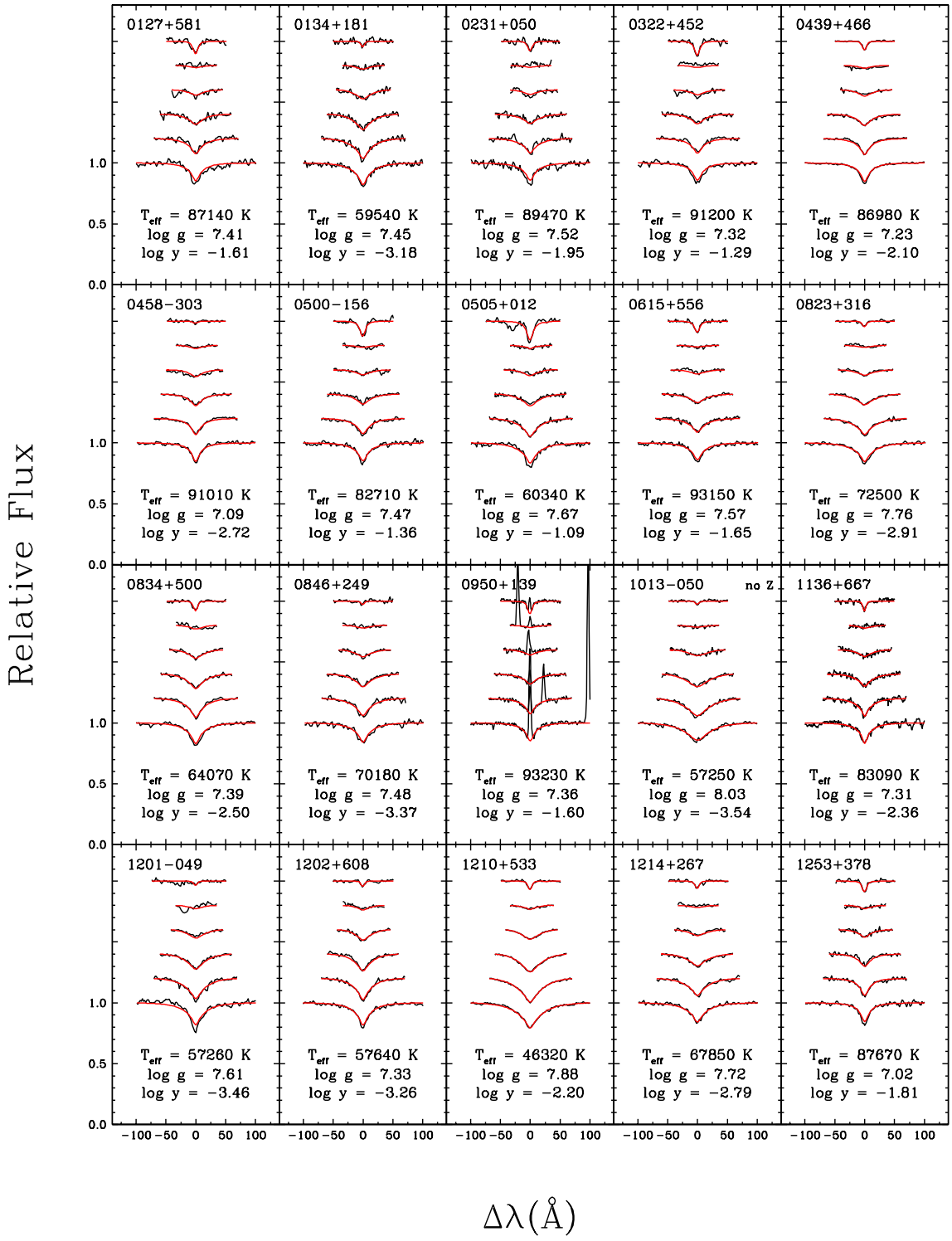

FIGURE A.1 – Solutions spectroscopiques pour les étoiles DAO présentées au Chapitre 2 sauf la DAO stratifiée, PG 1305-017. L'indicatif *no Z* dans le coin supérieur droit d'une case signifie que les modèles sans métaux ont été utilisés.

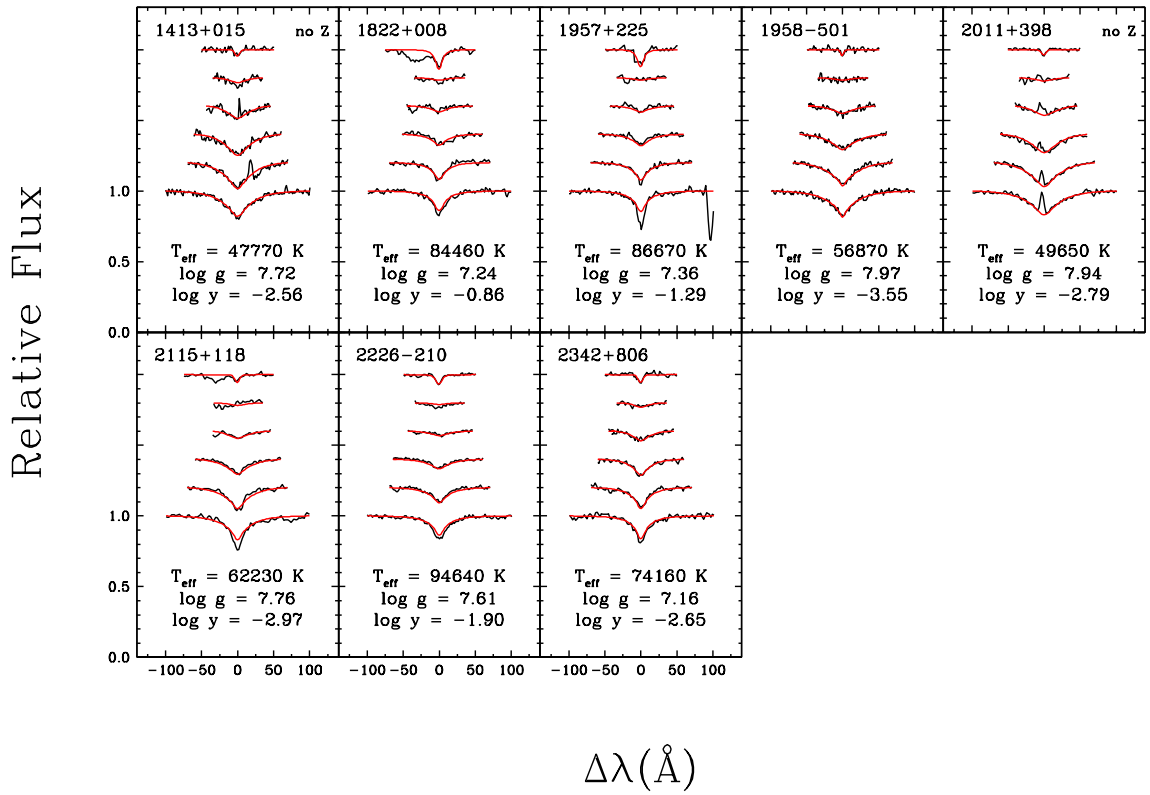

FIGURE A.1 – Suite

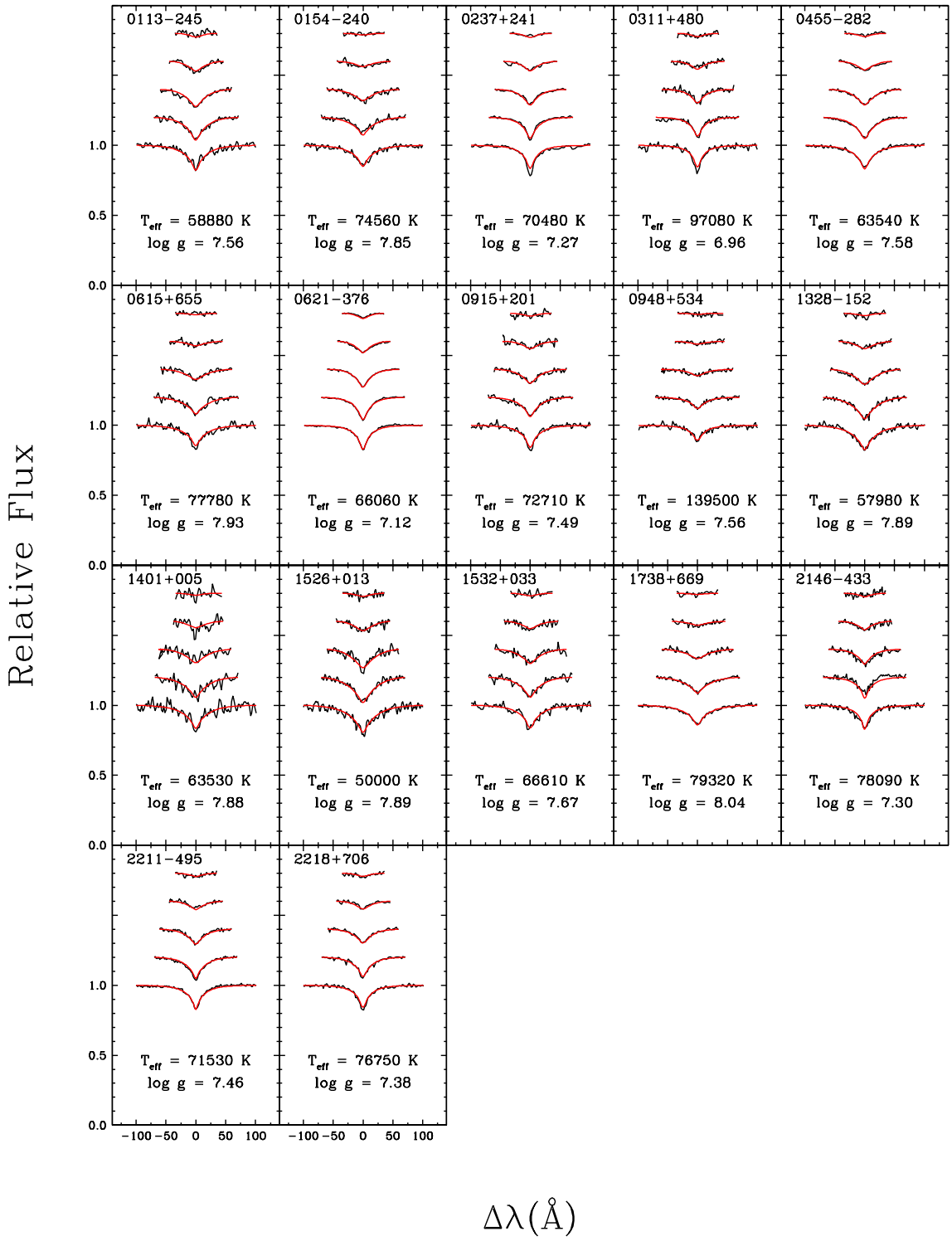

FIGURE A.2 – Solutions spectroscopiques pour les 17 étoiles DA+BP présentées au Chapitre 2.

Annexe B

Solutions spectroscopiques pour les étoiles DA

Nous présentons ici l'ensemble de nos solutions spectroscopiques pour les étoiles DA présentées au Chapitre 3 puisque ces solutions n'y figuraient pas toutes étant donnés les contraintes d'espace pour la publication dans l'*Astrophysical Journal* (ApJ).

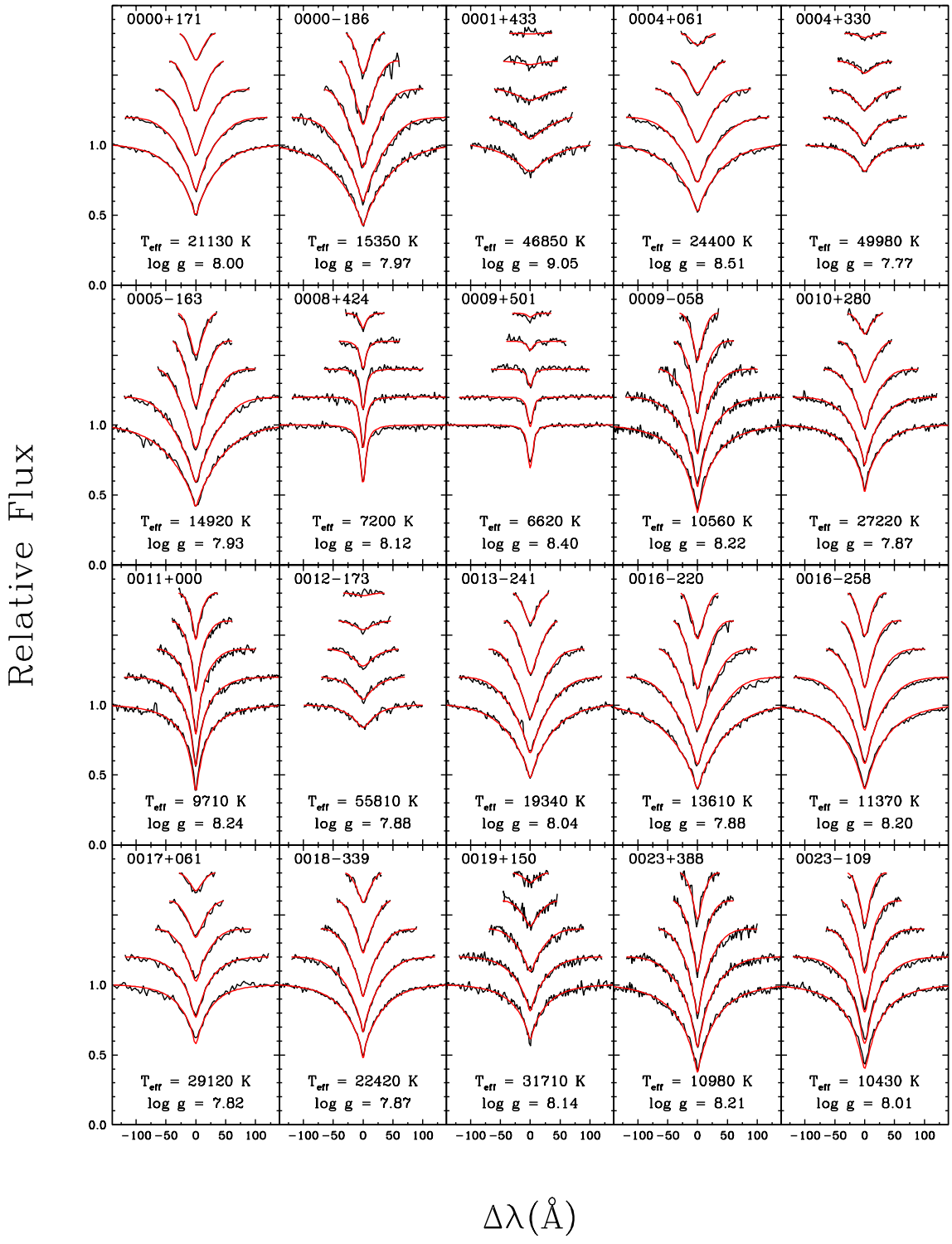

FIGURE B.1 – Solutions spectroscopiques pour les étoiles DA présentées au Chapitre 3.

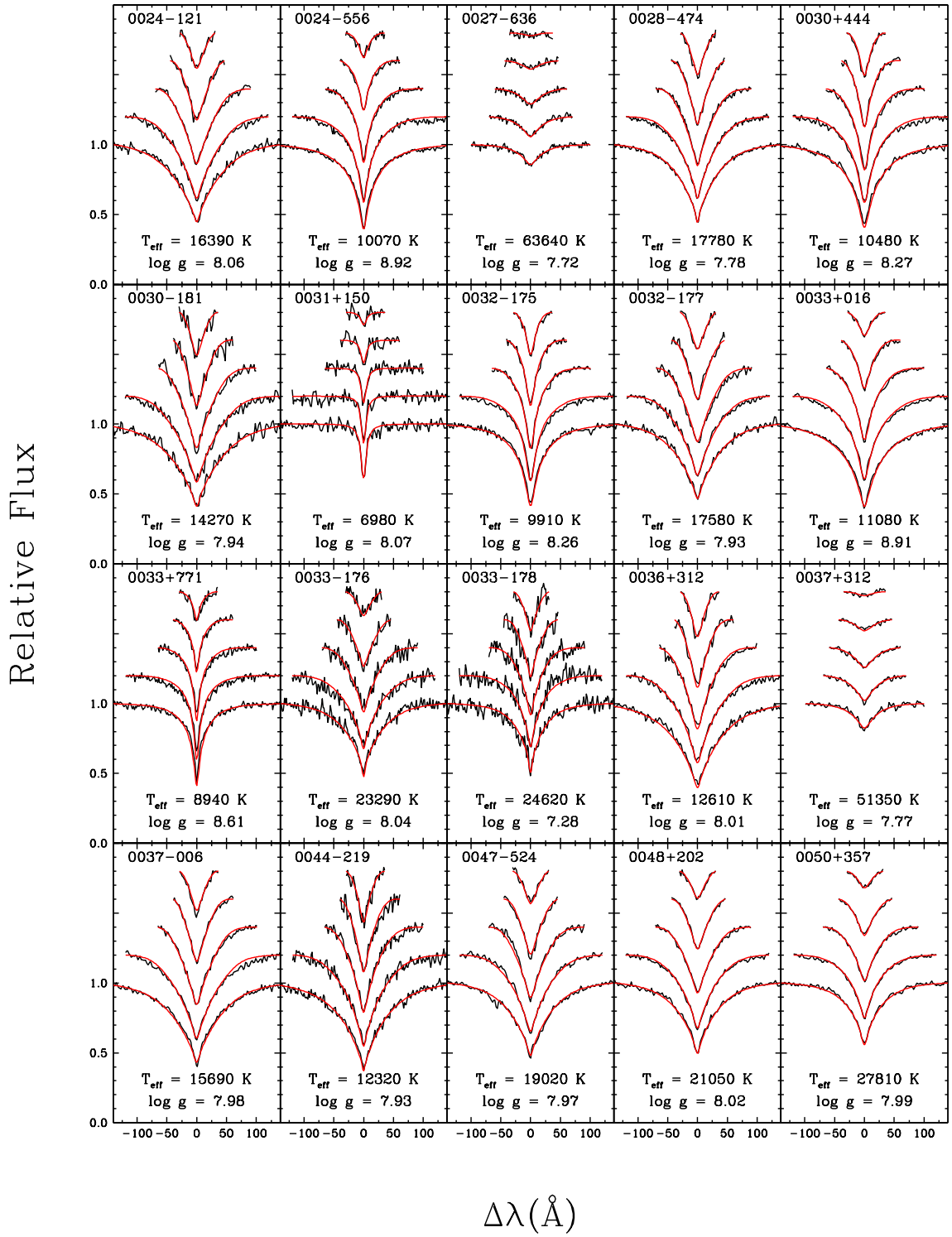

FIGURE B.1 – Suite

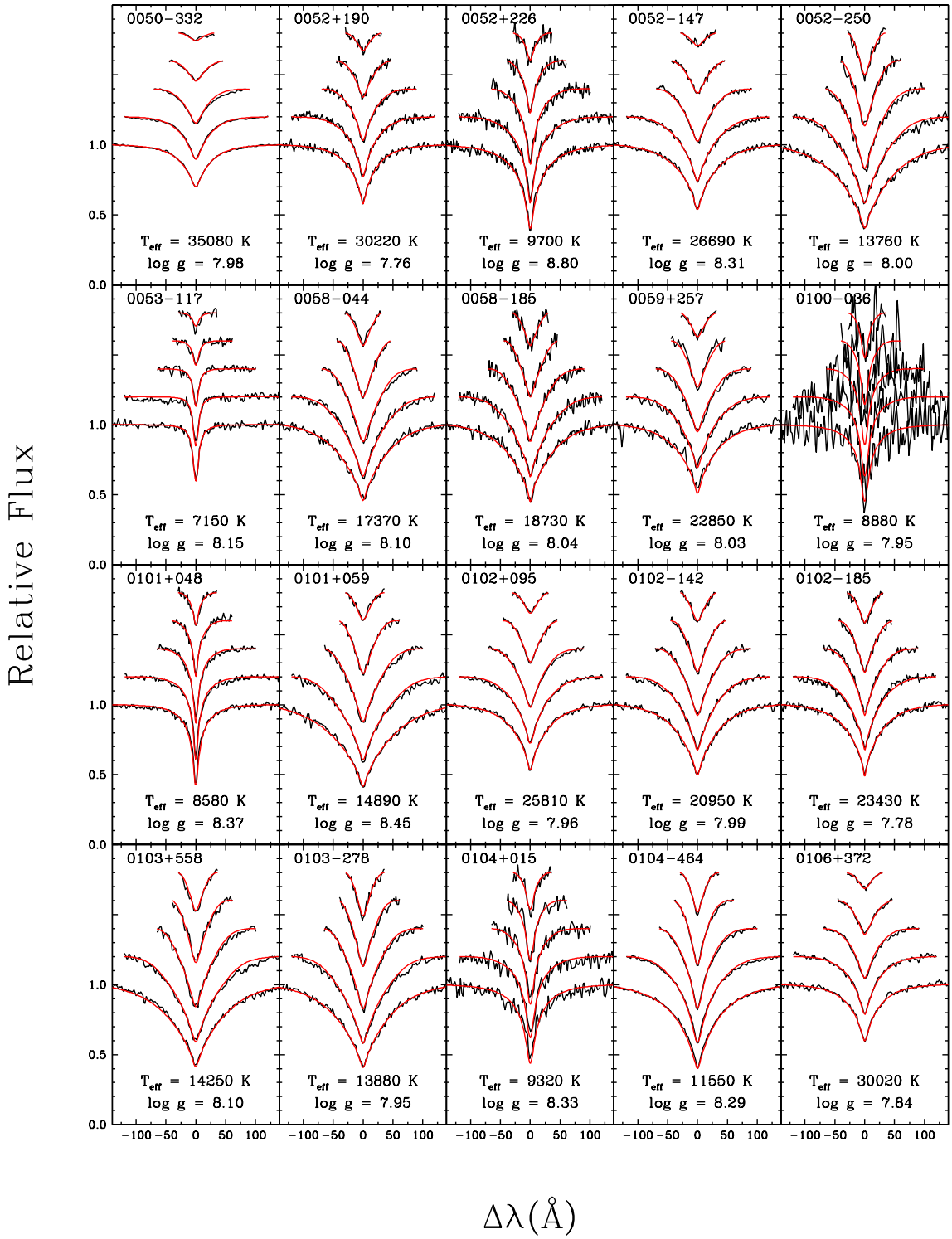

FIGURE B.1 – Suite

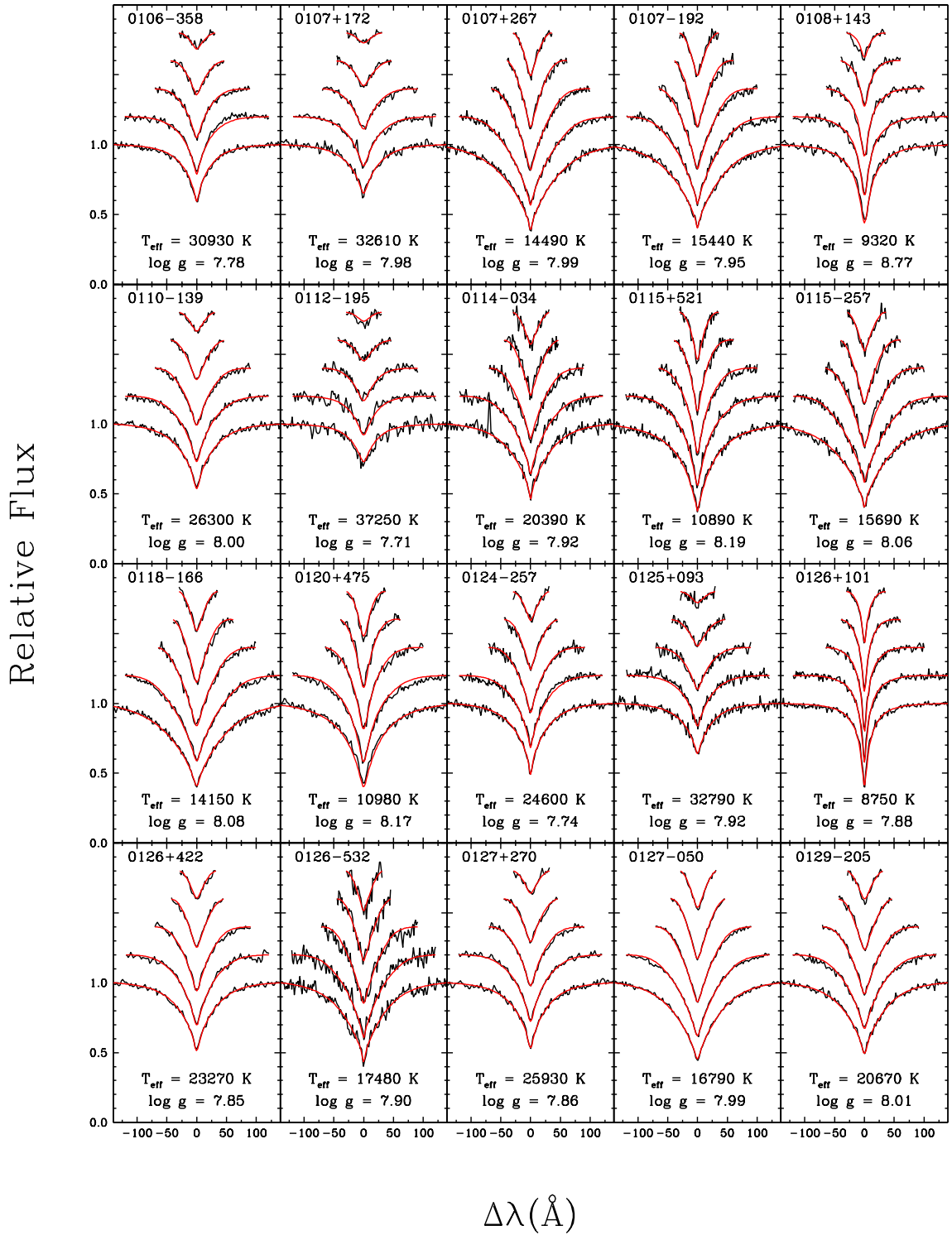

FIGURE B.1 – Suite

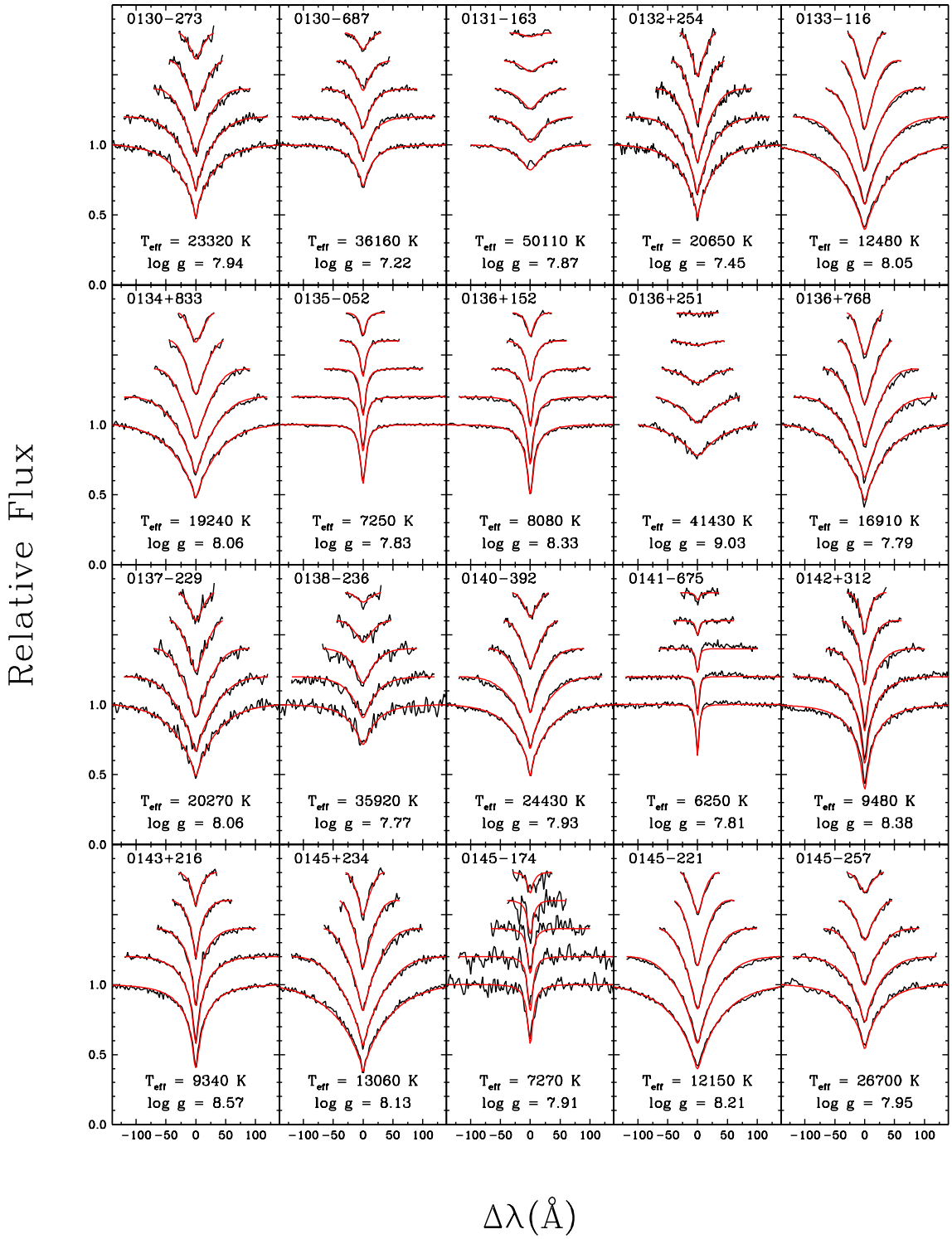

FIGURE B.1 – Suite

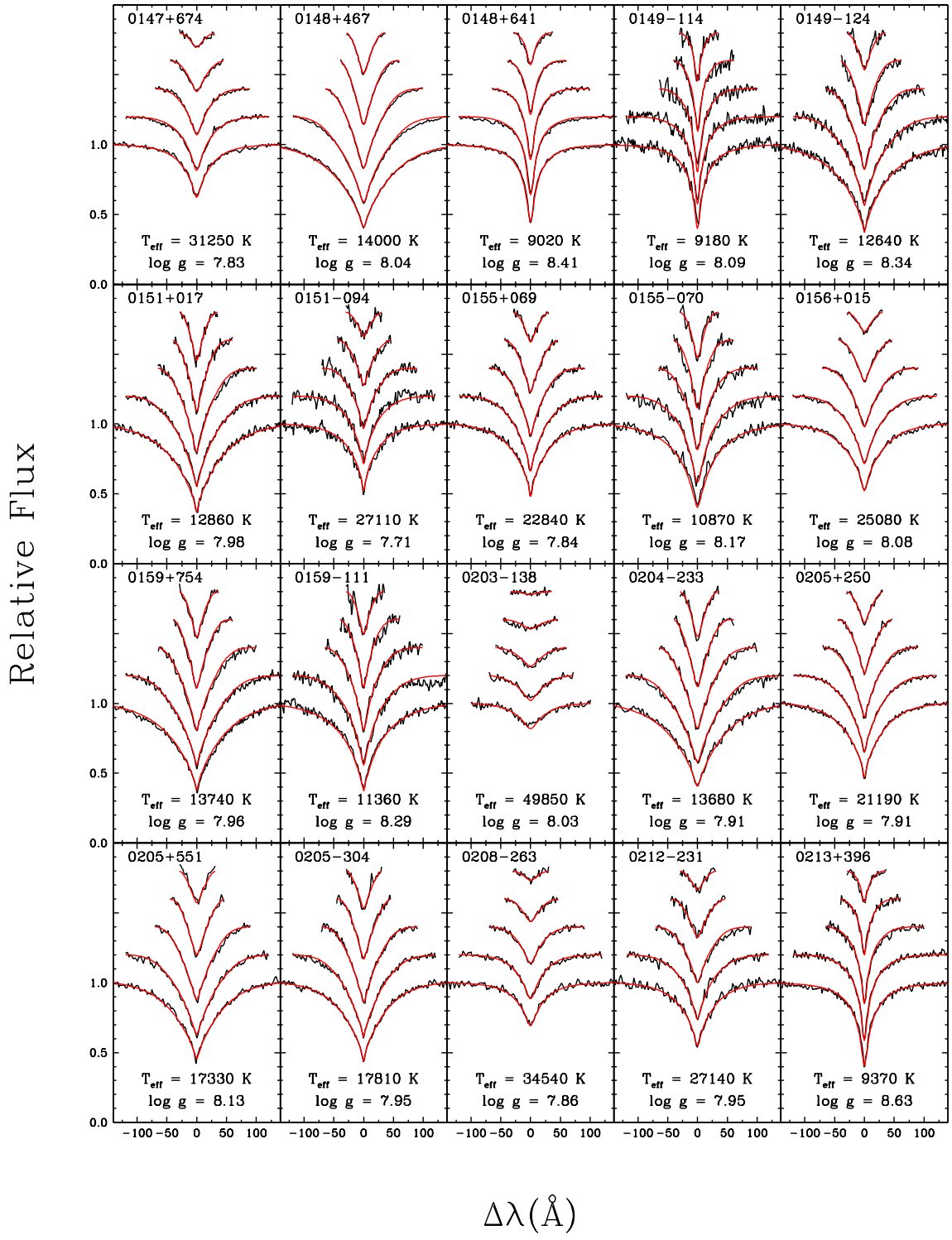

FIGURE B.1 – Suite

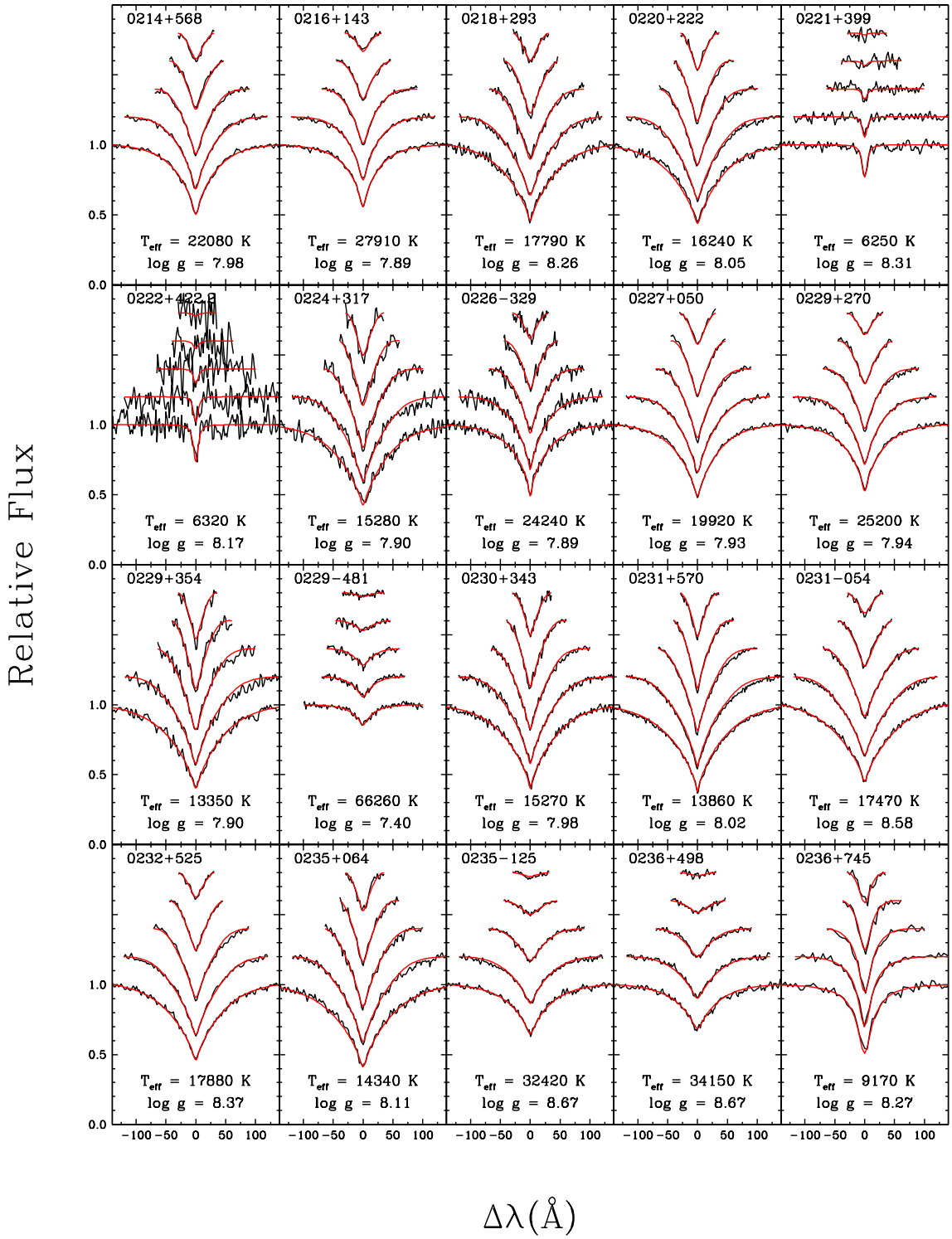

FIGURE B.1 – Suite

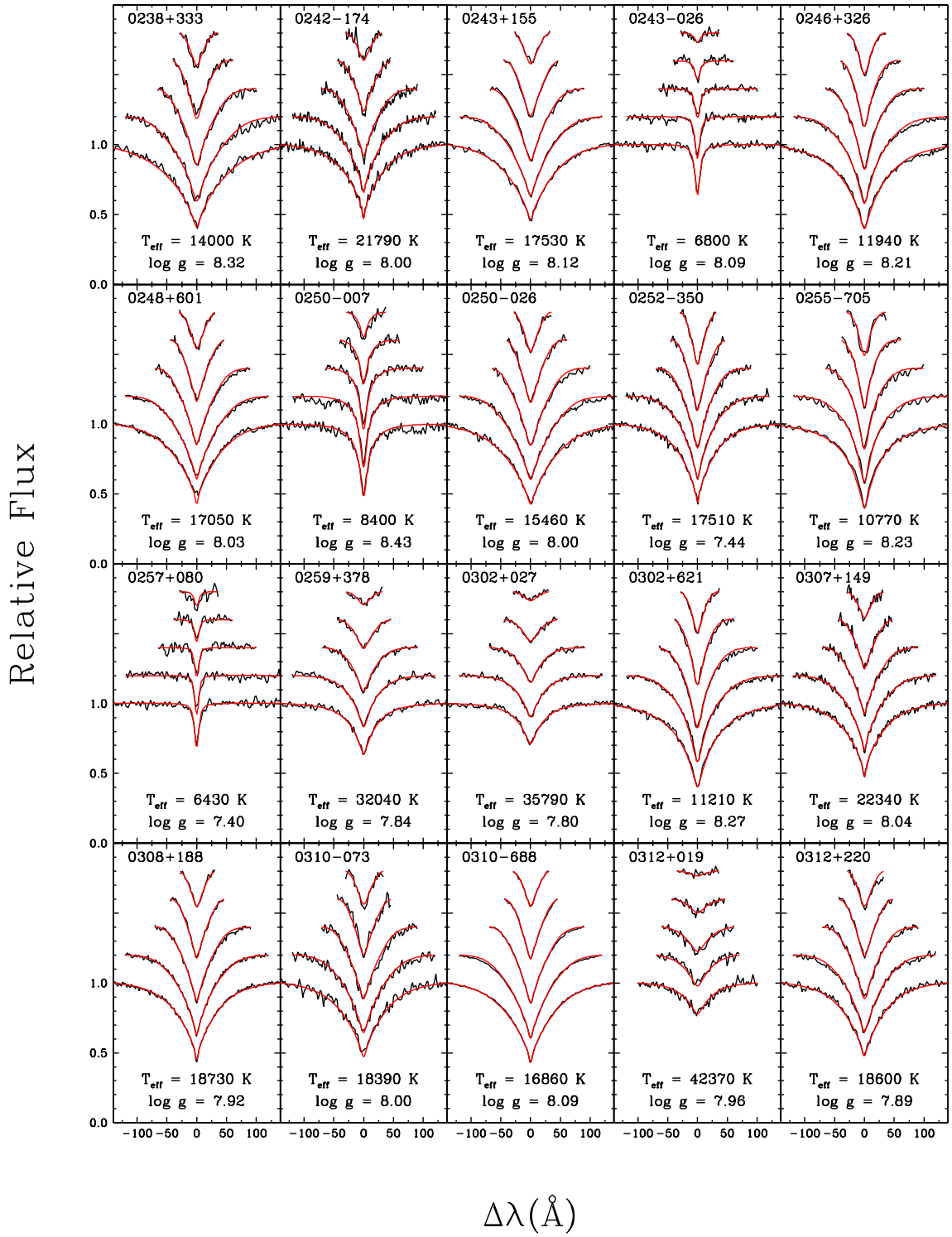

FIGURE B.1 – Suite

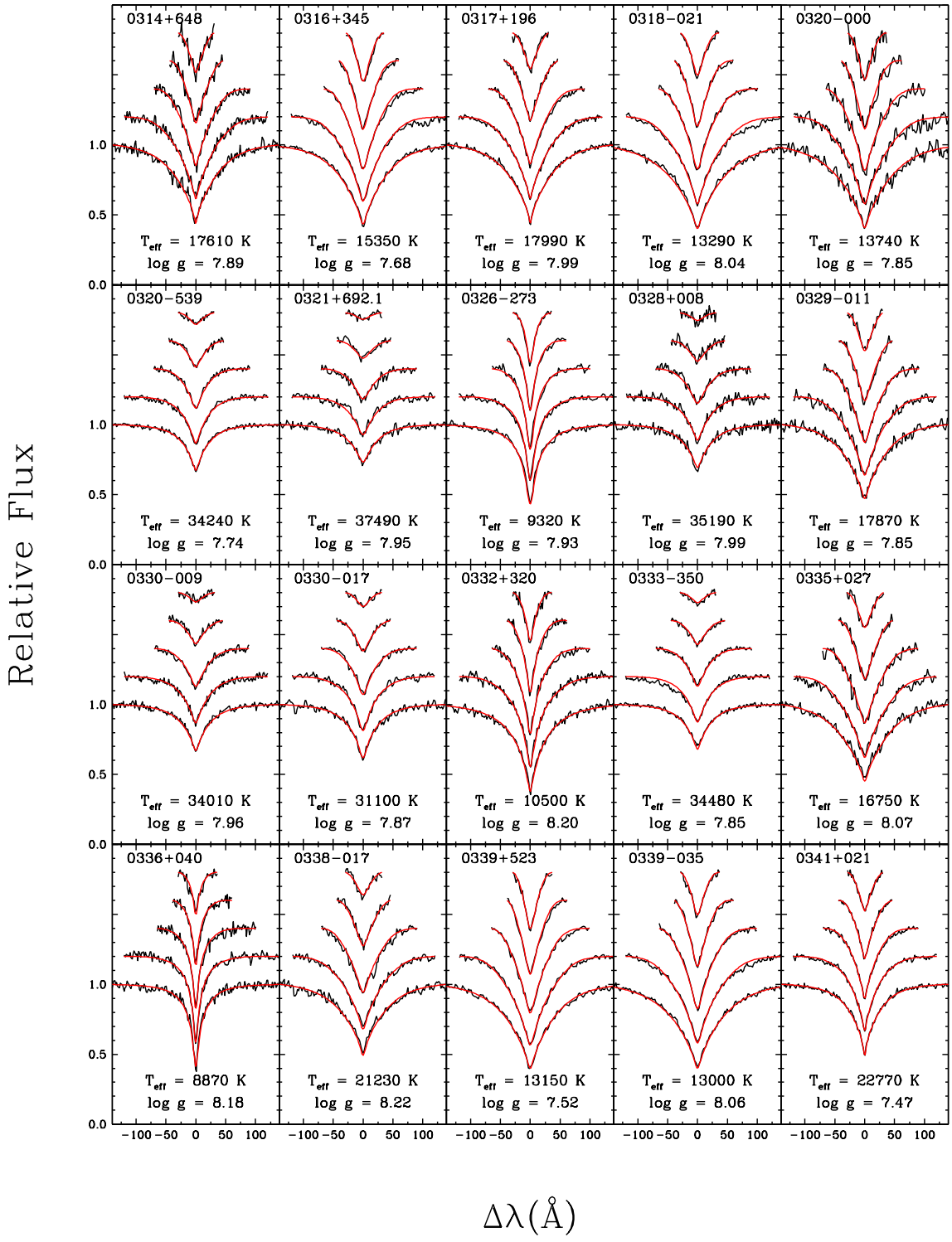

FIGURE B.1 – Suite

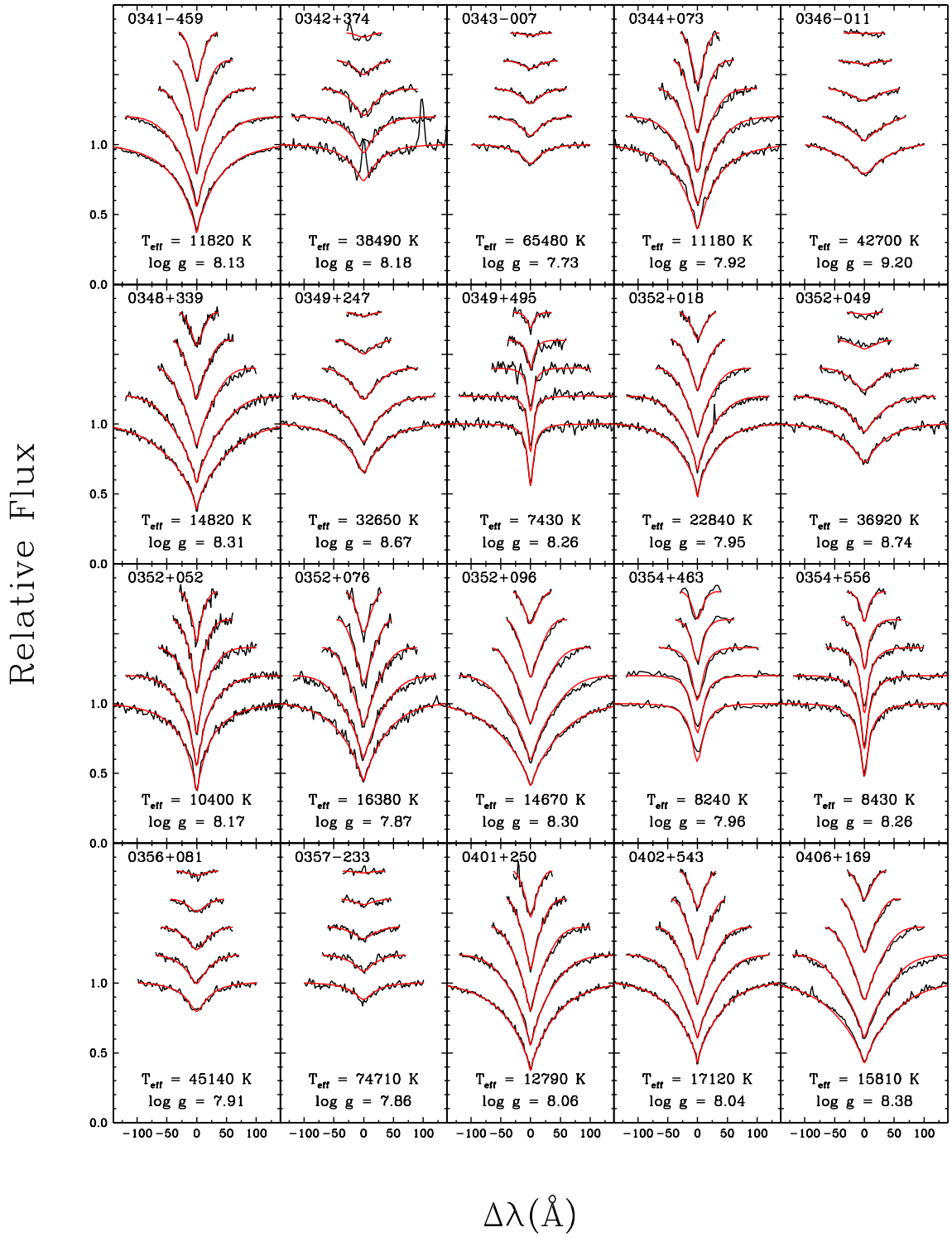

FIGURE B.1 – Suite

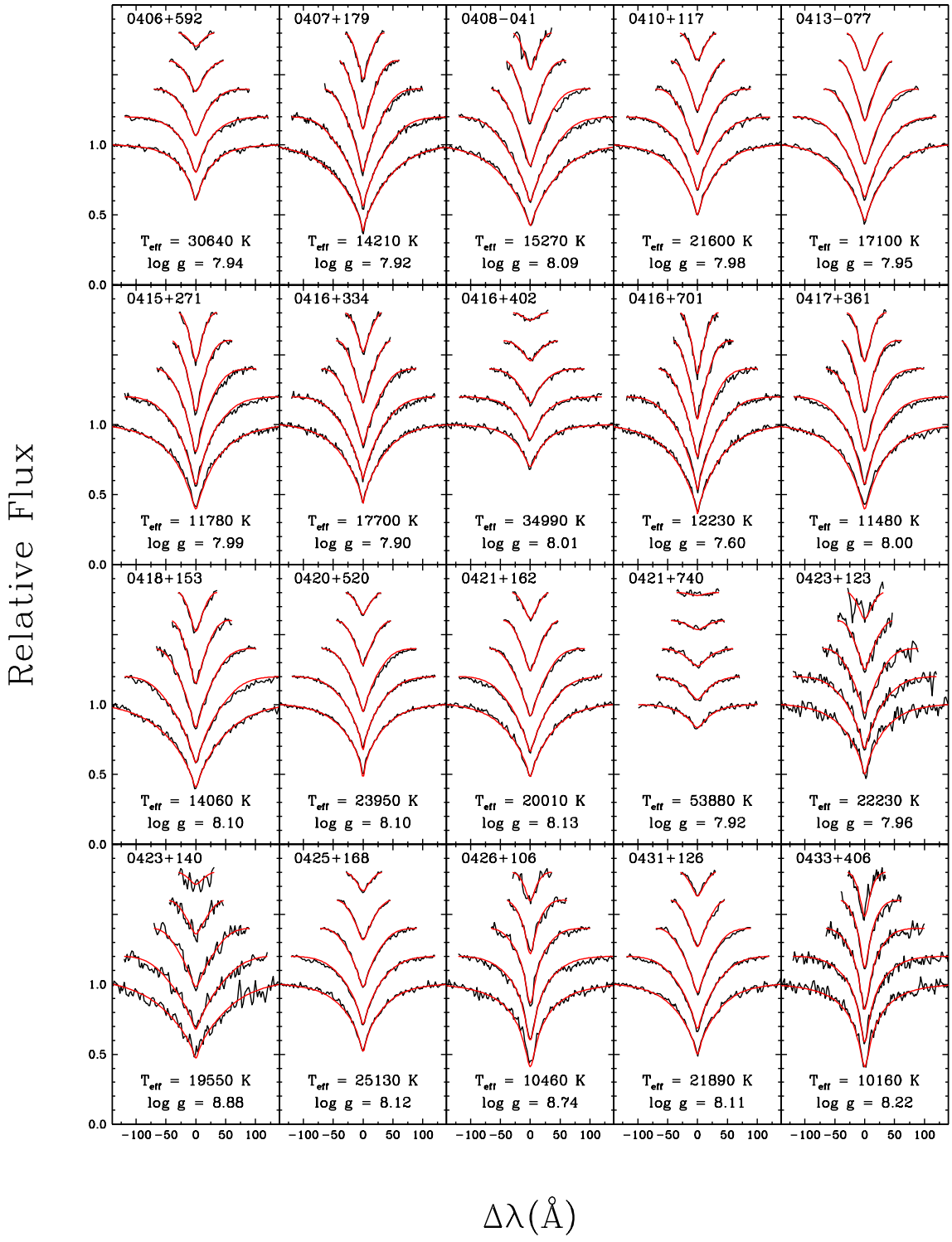

FIGURE B.1 – Suite

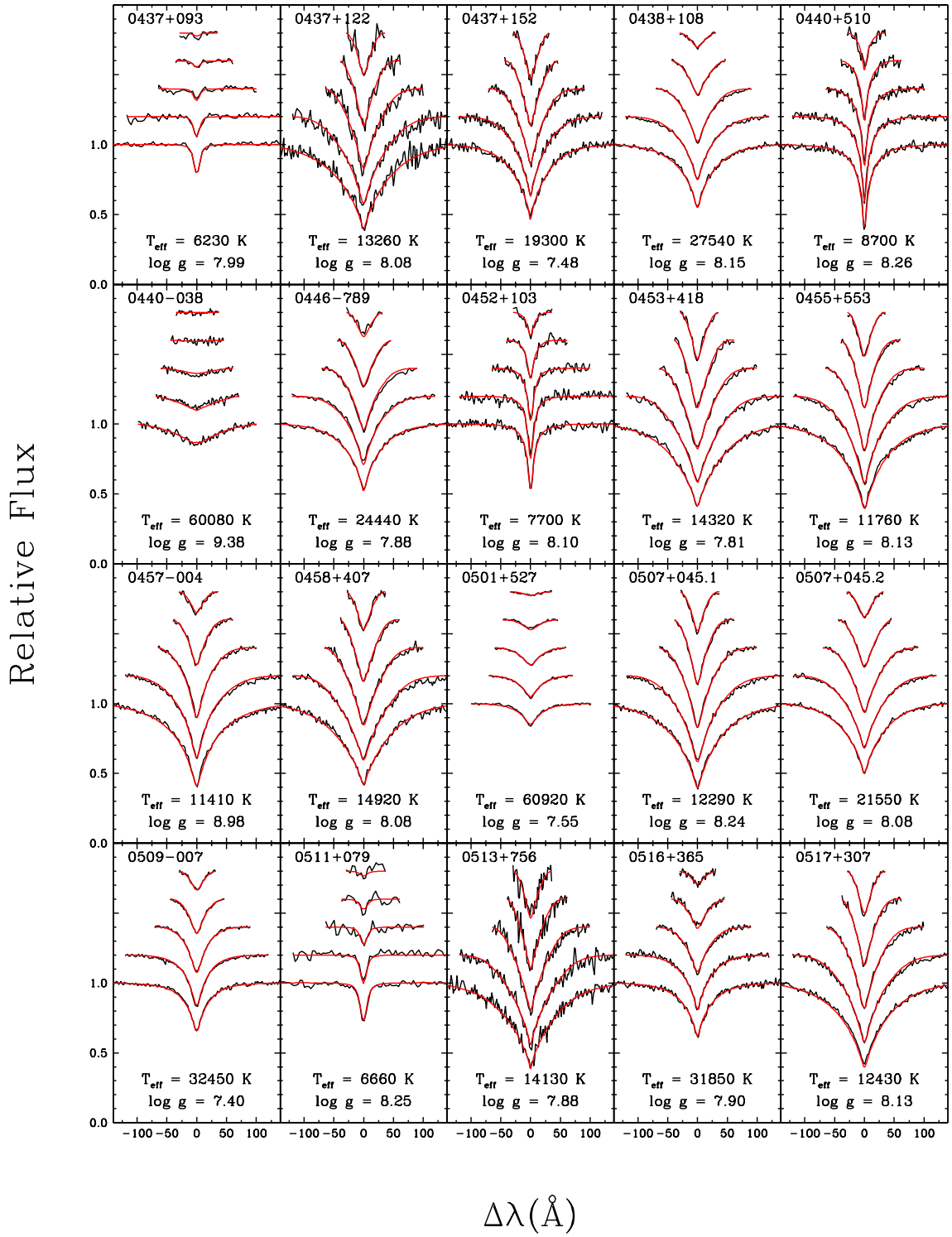

FIGURE B.1 – Suite

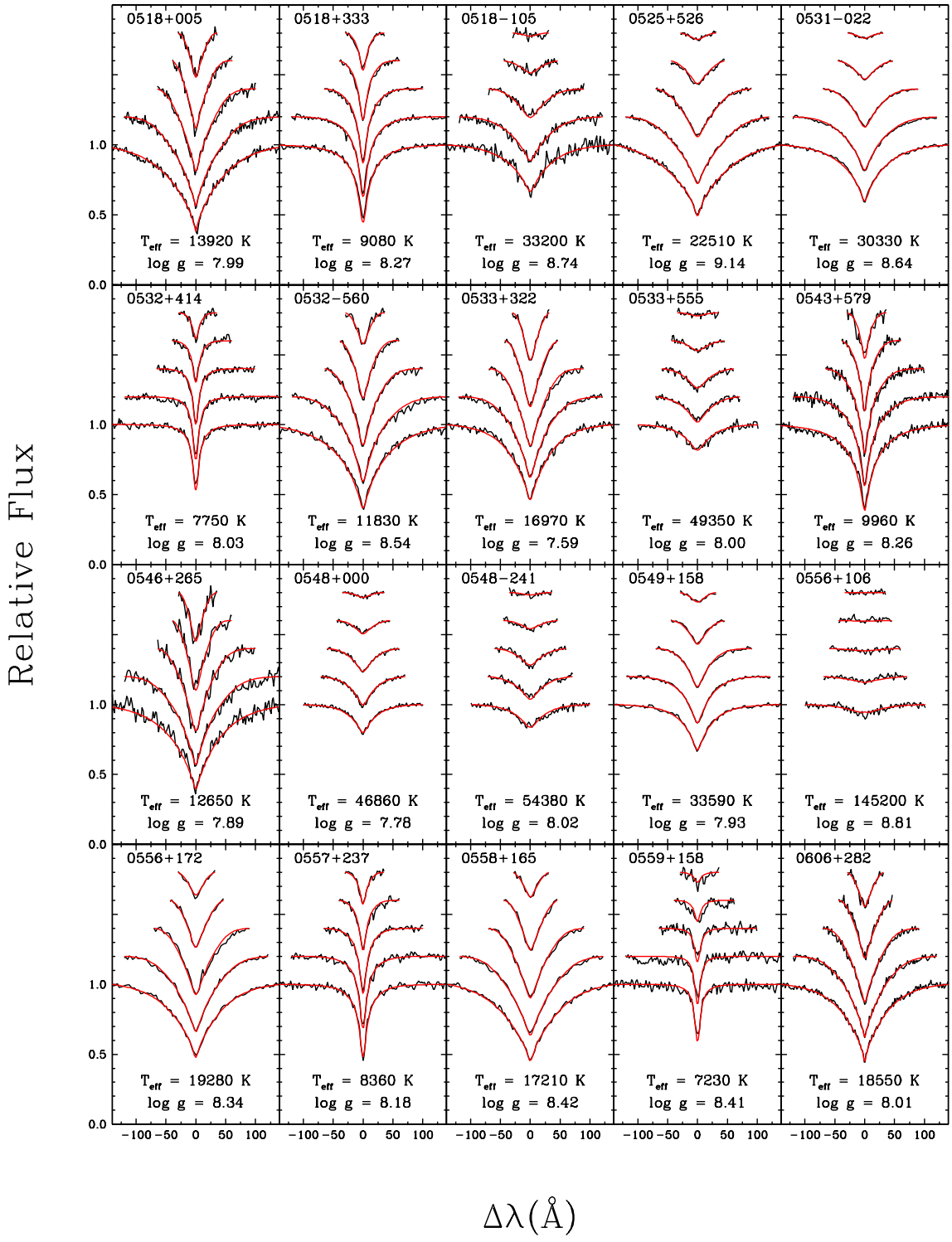

FIGURE B.1 – Suite

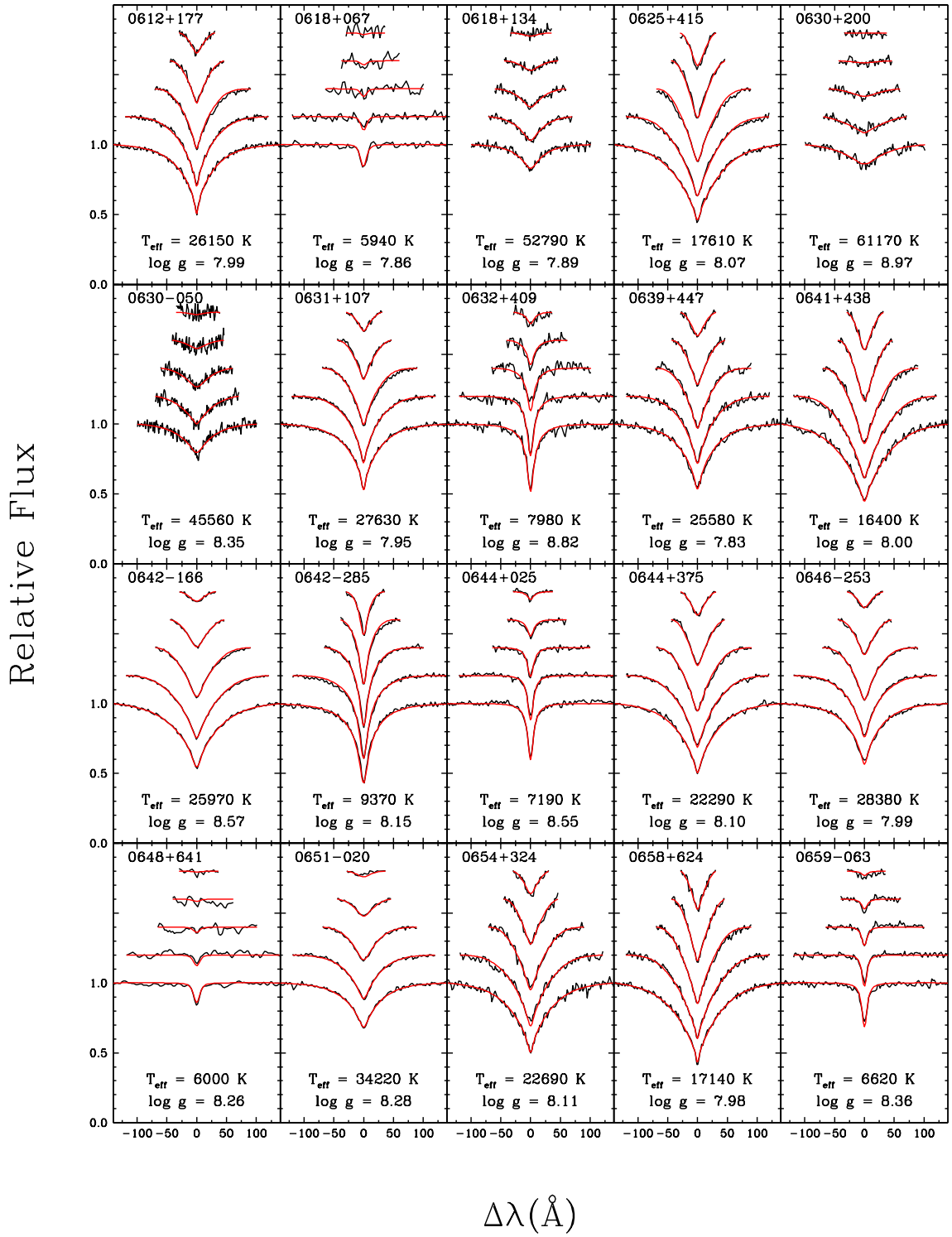

FIGURE B.1 – Suite

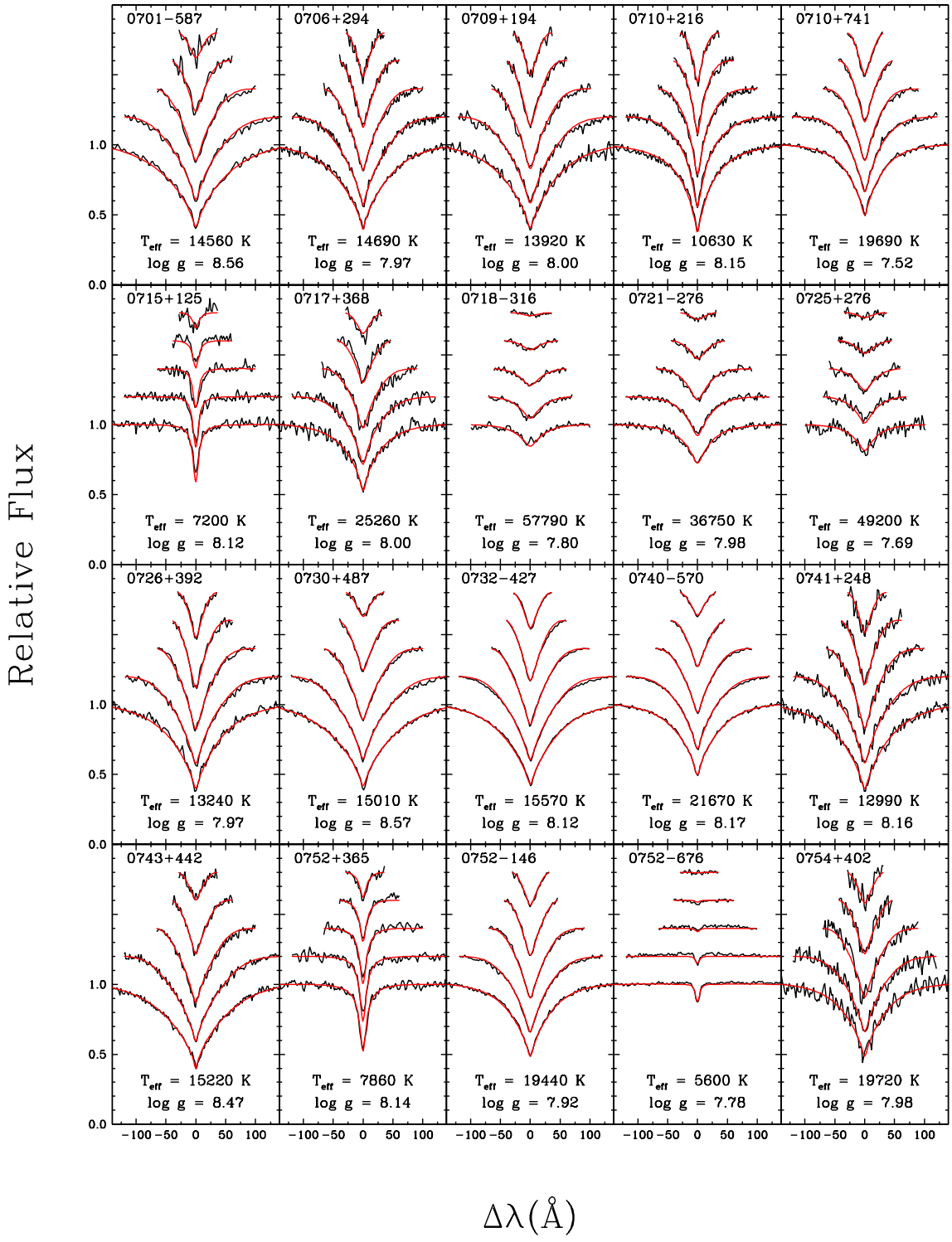

FIGURE B.1 – Suite

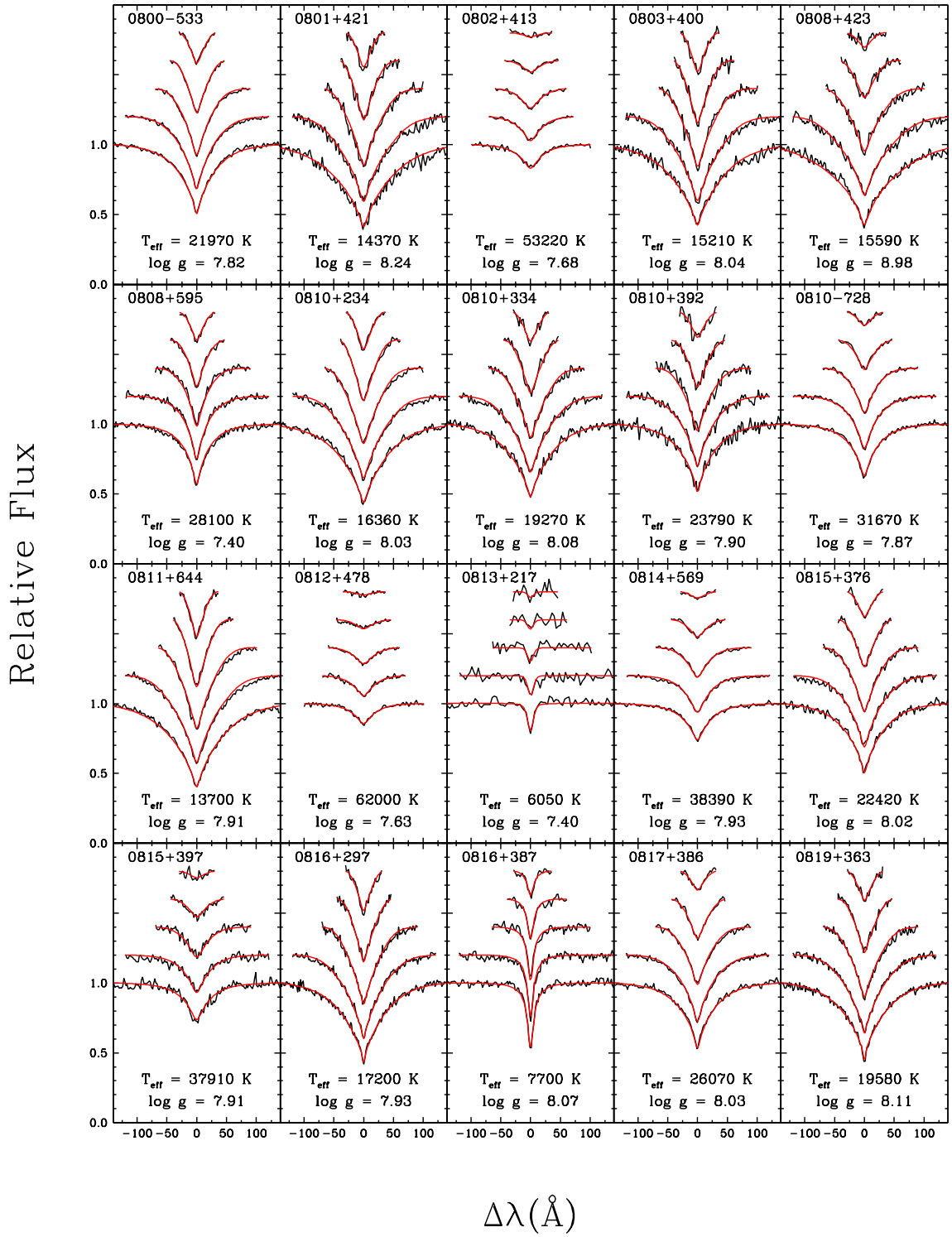

FIGURE B.1 – Suite

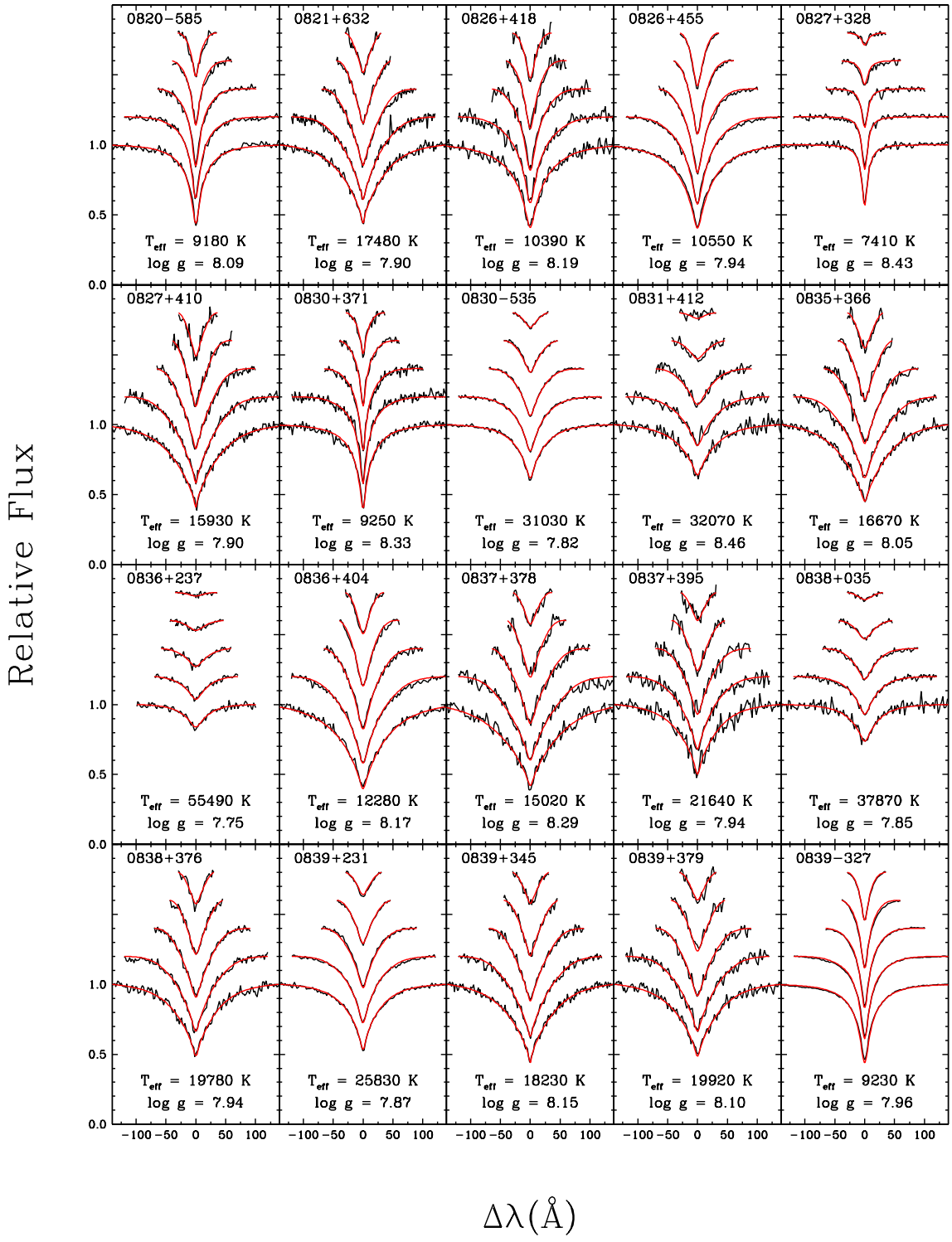

FIGURE B.1 – Suite

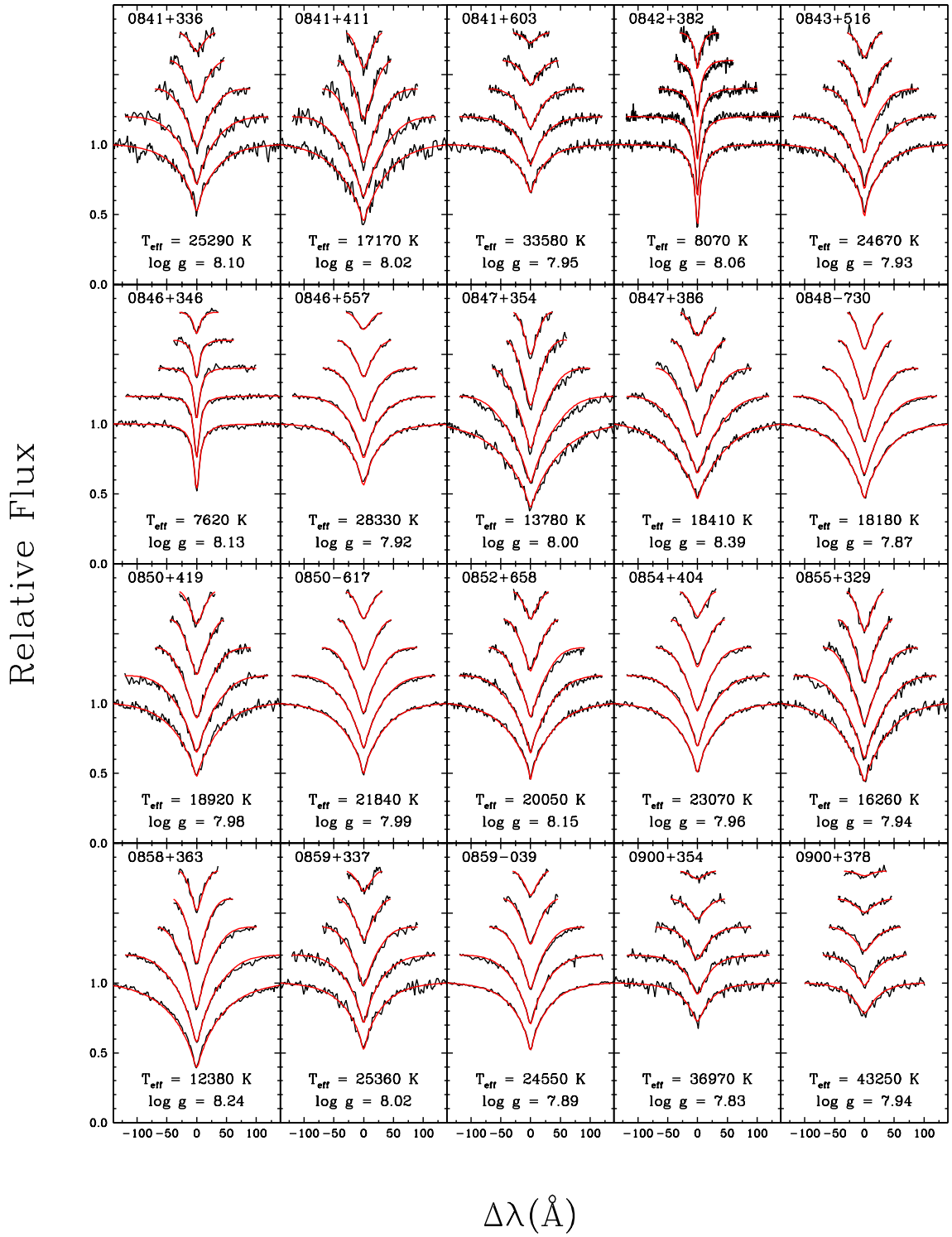

FIGURE B.1 – Suite

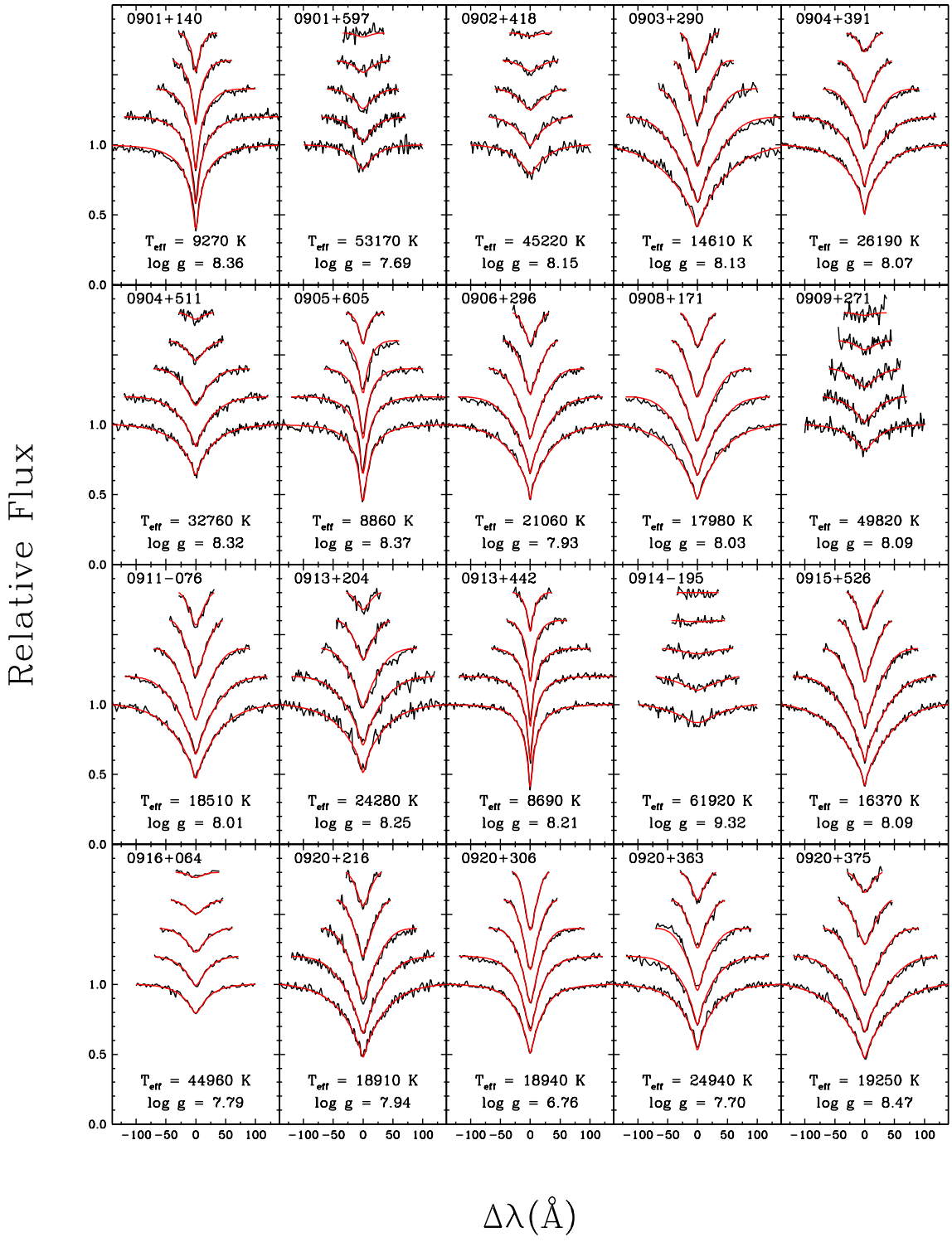

FIGURE B.1 – Suite

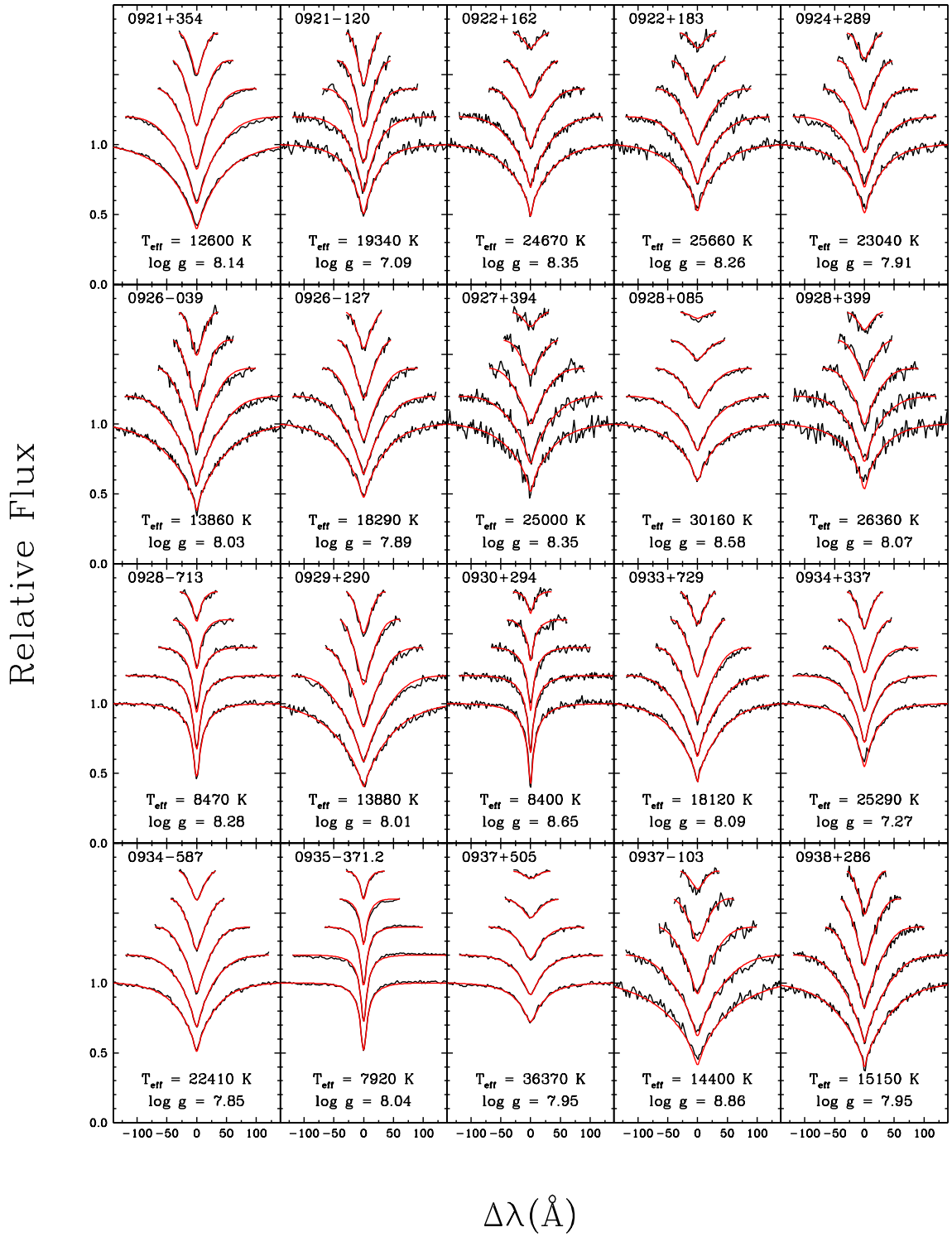

FIGURE B.1 – Suite

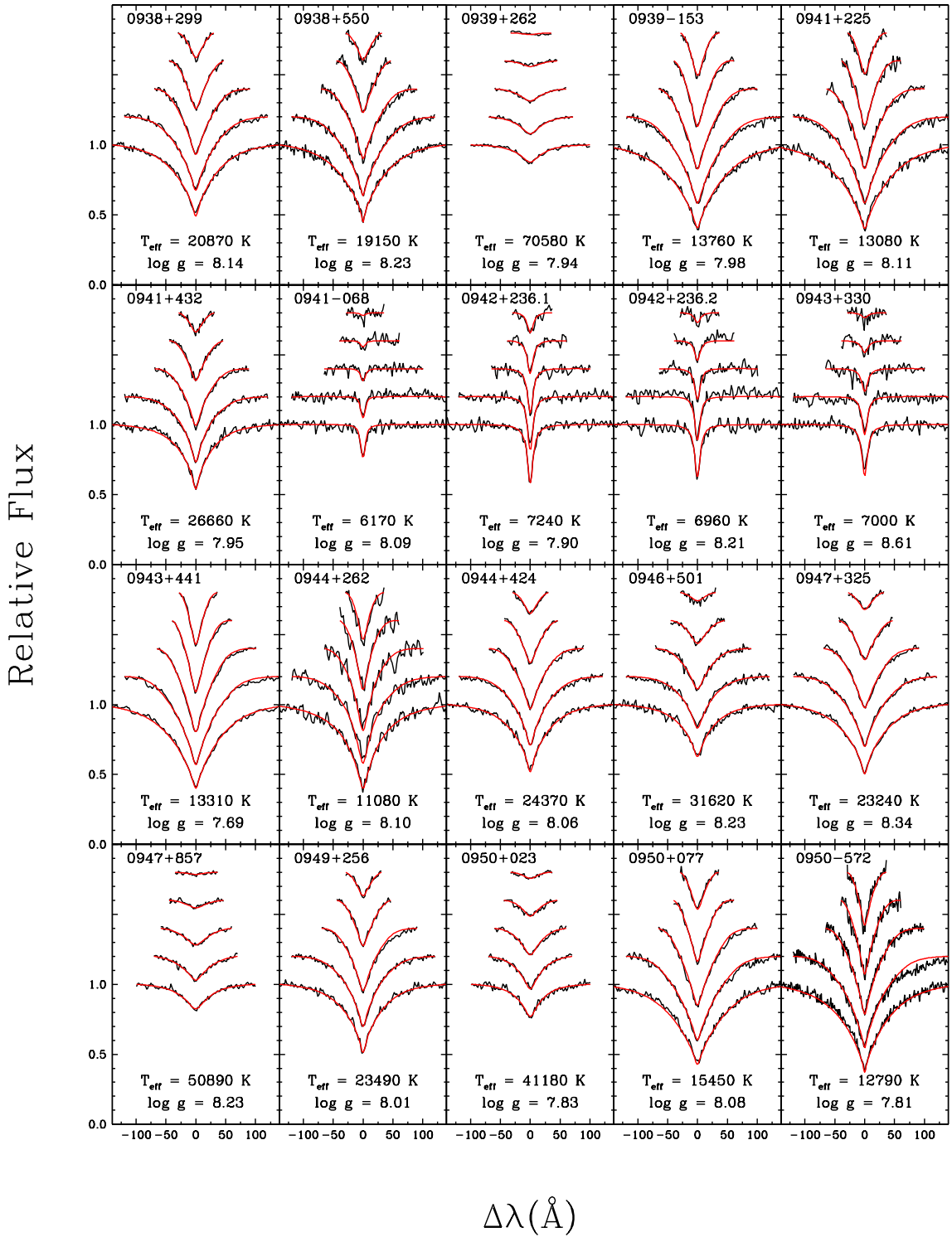

FIGURE B.1 – Suite

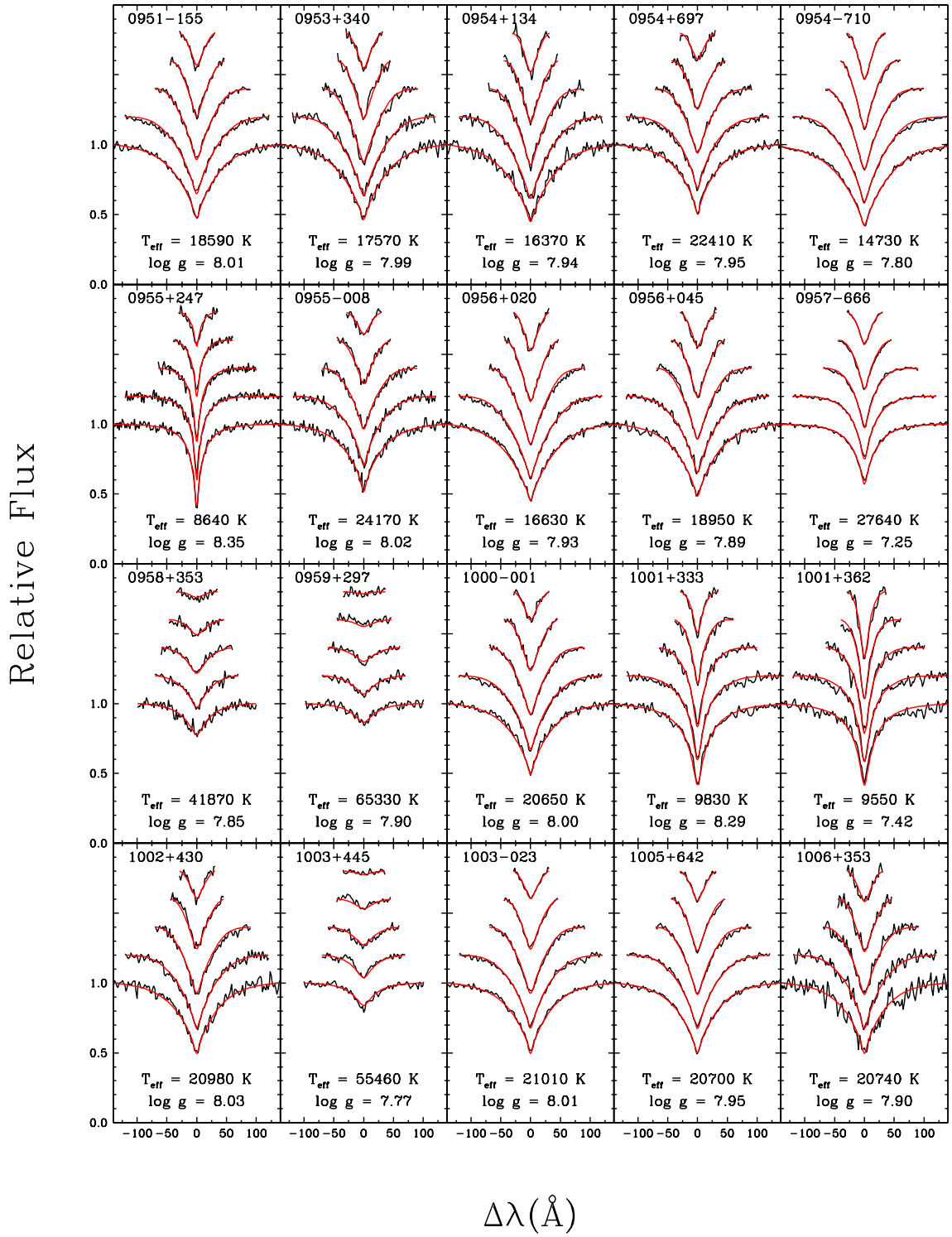

FIGURE B.1 – Suite

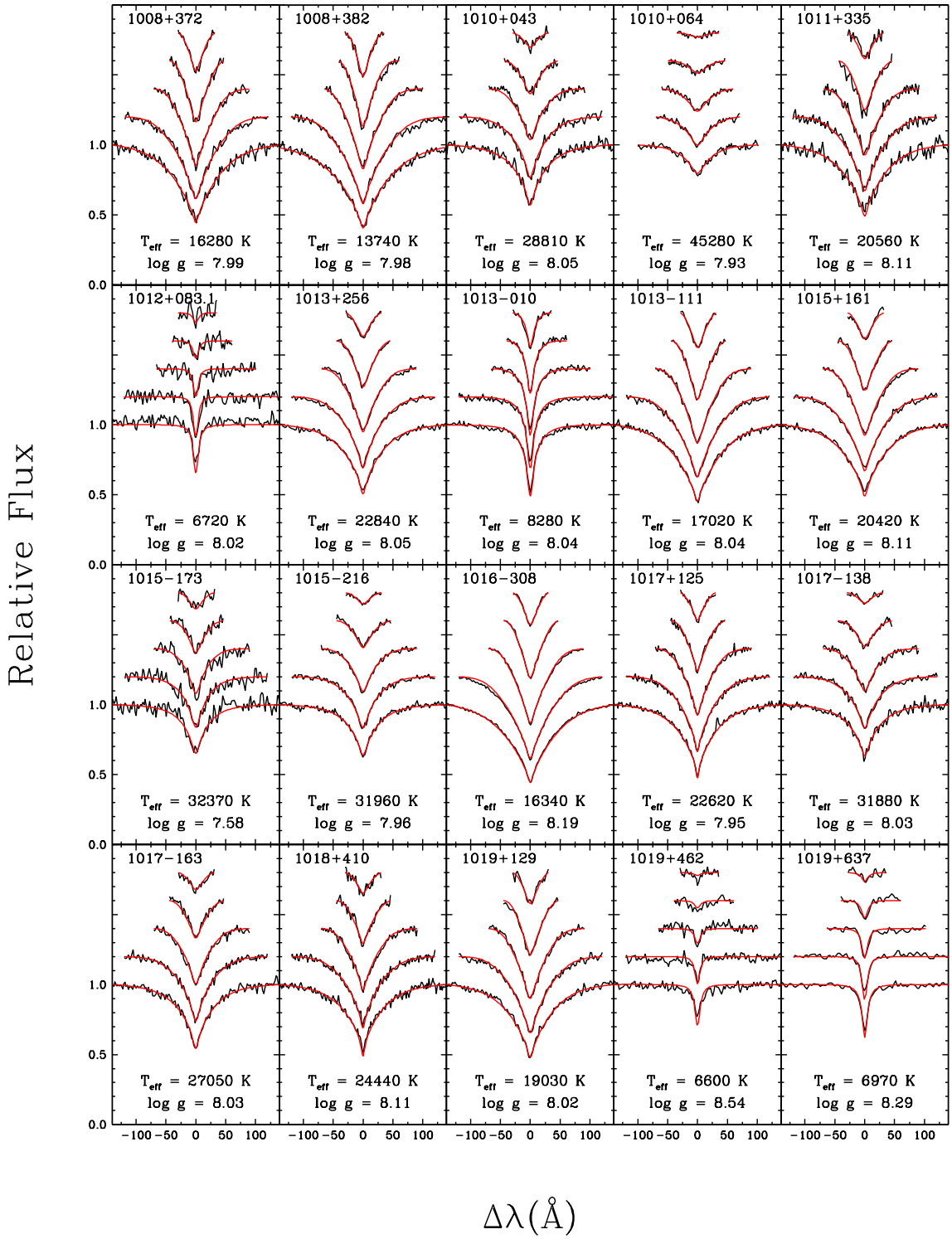

FIGURE B.1 – Suite

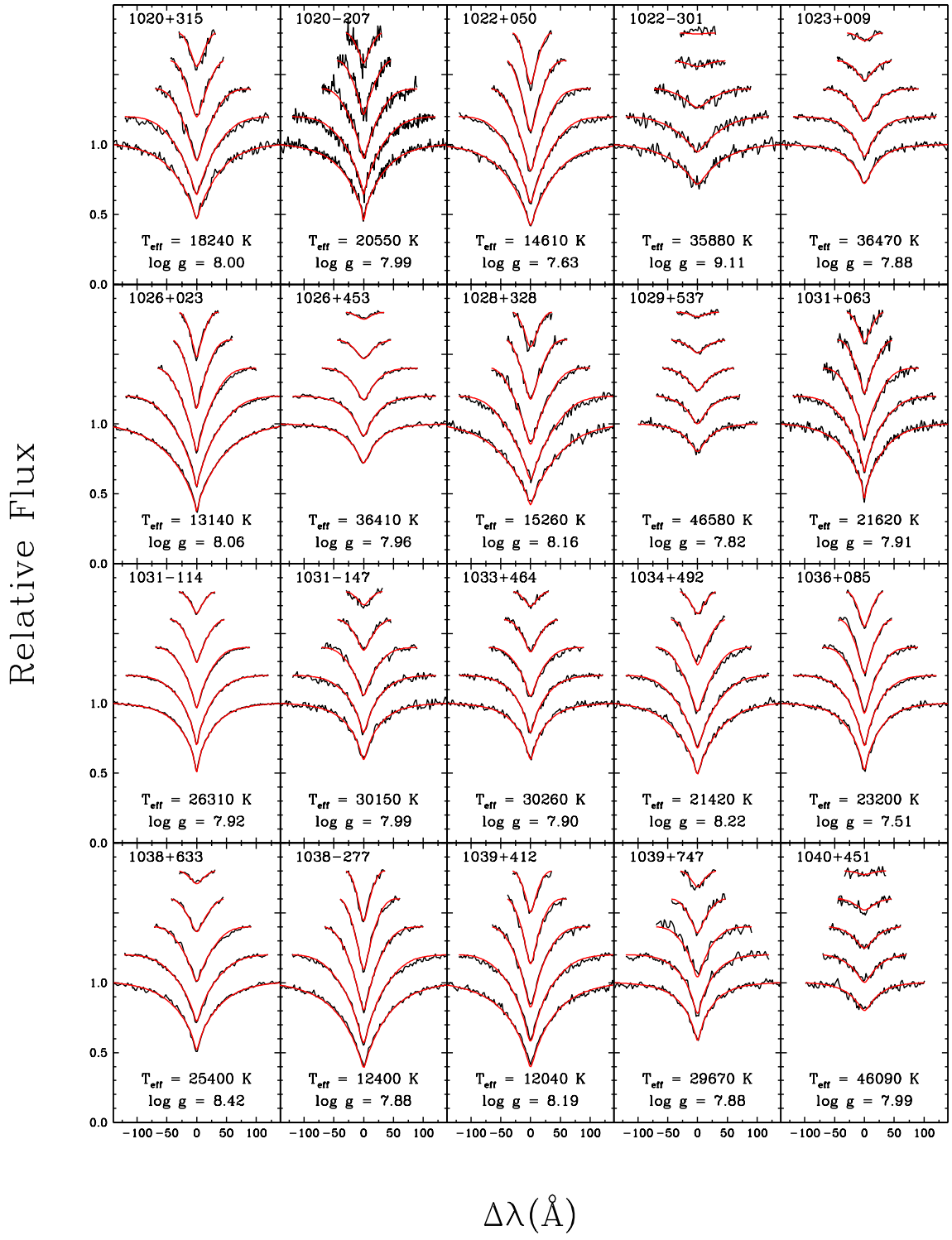

FIGURE B.1 – Suite

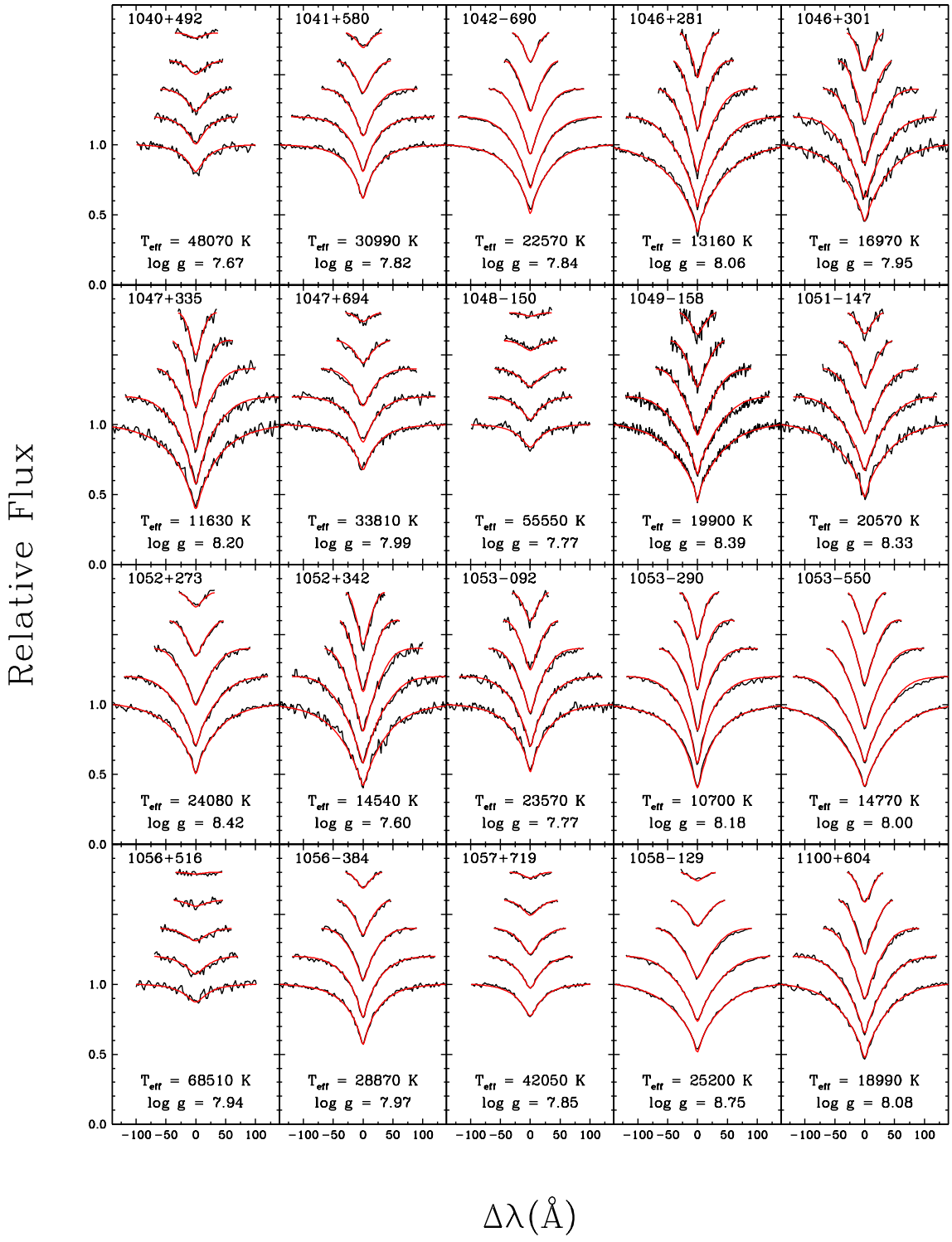

FIGURE B.1 – Suite

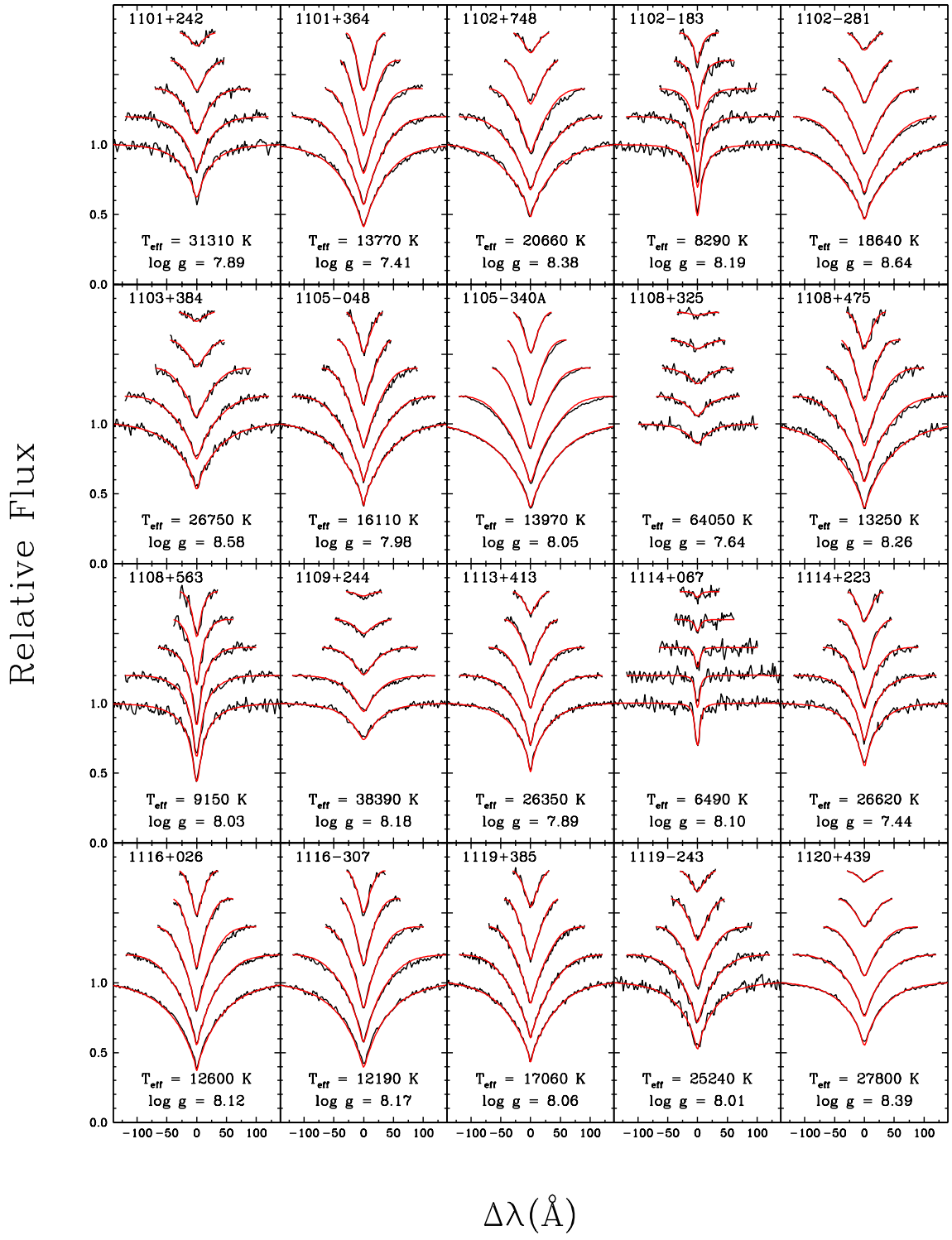

FIGURE B.1 – Suite

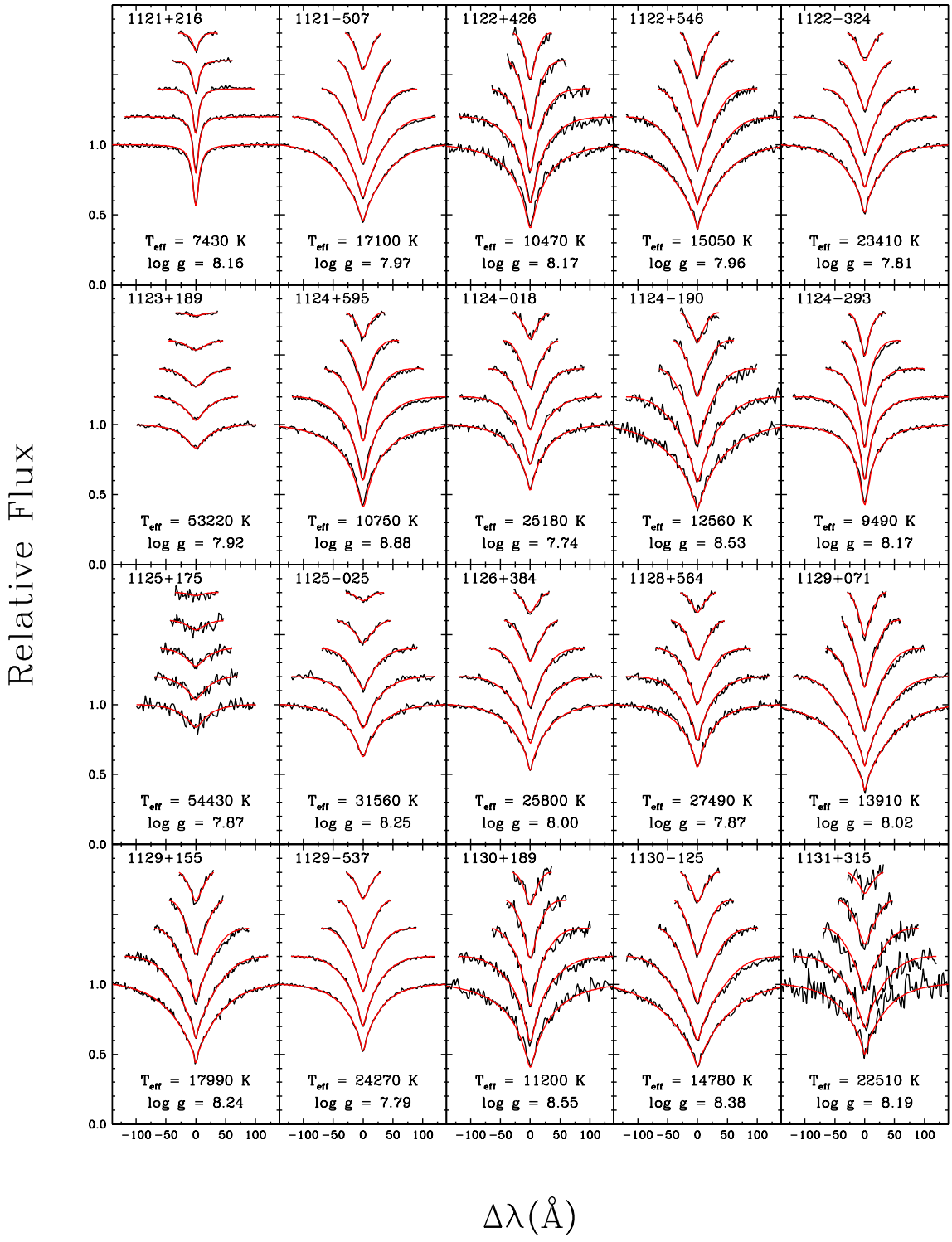

FIGURE B.1 – Suite

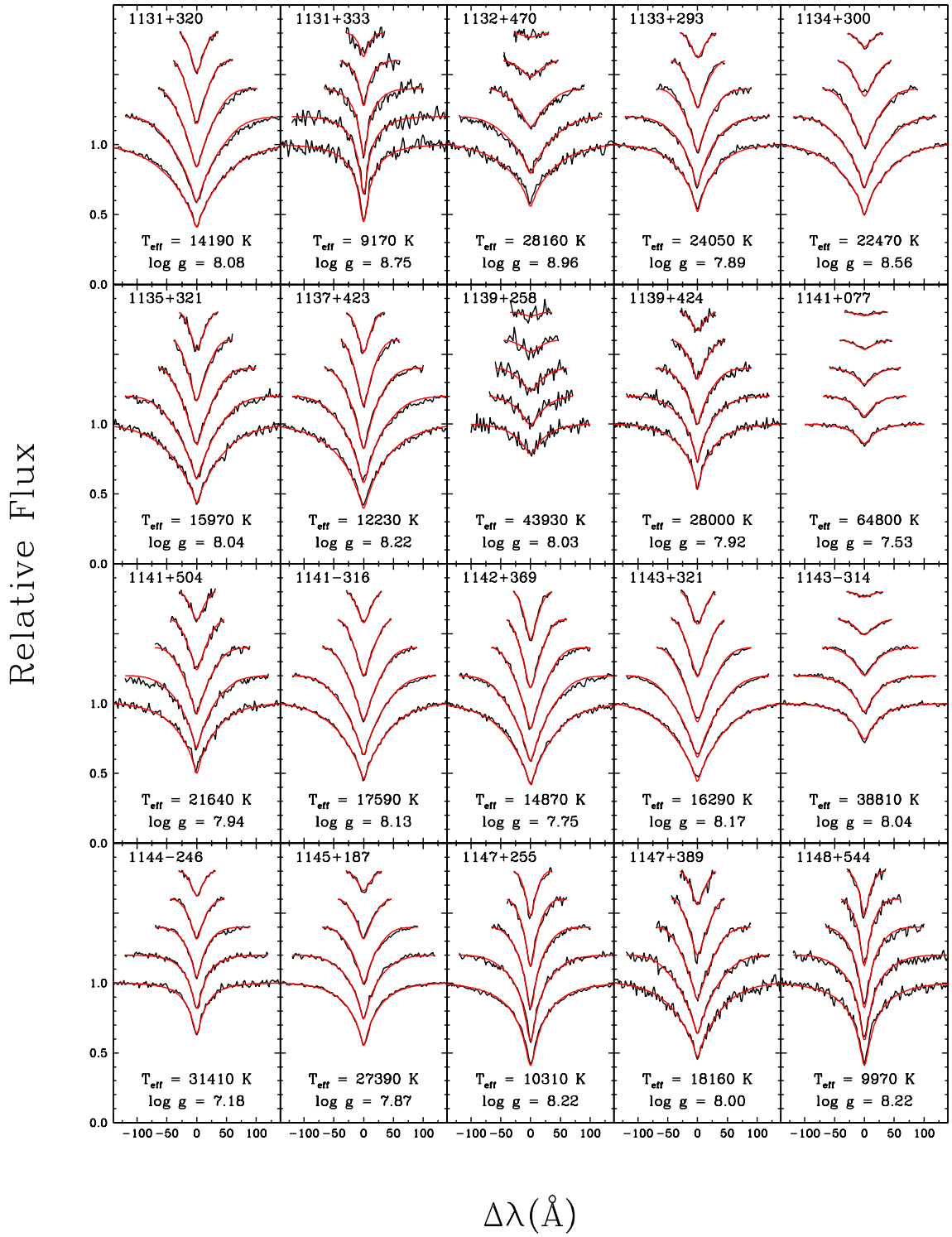

FIGURE B.1 – Suite

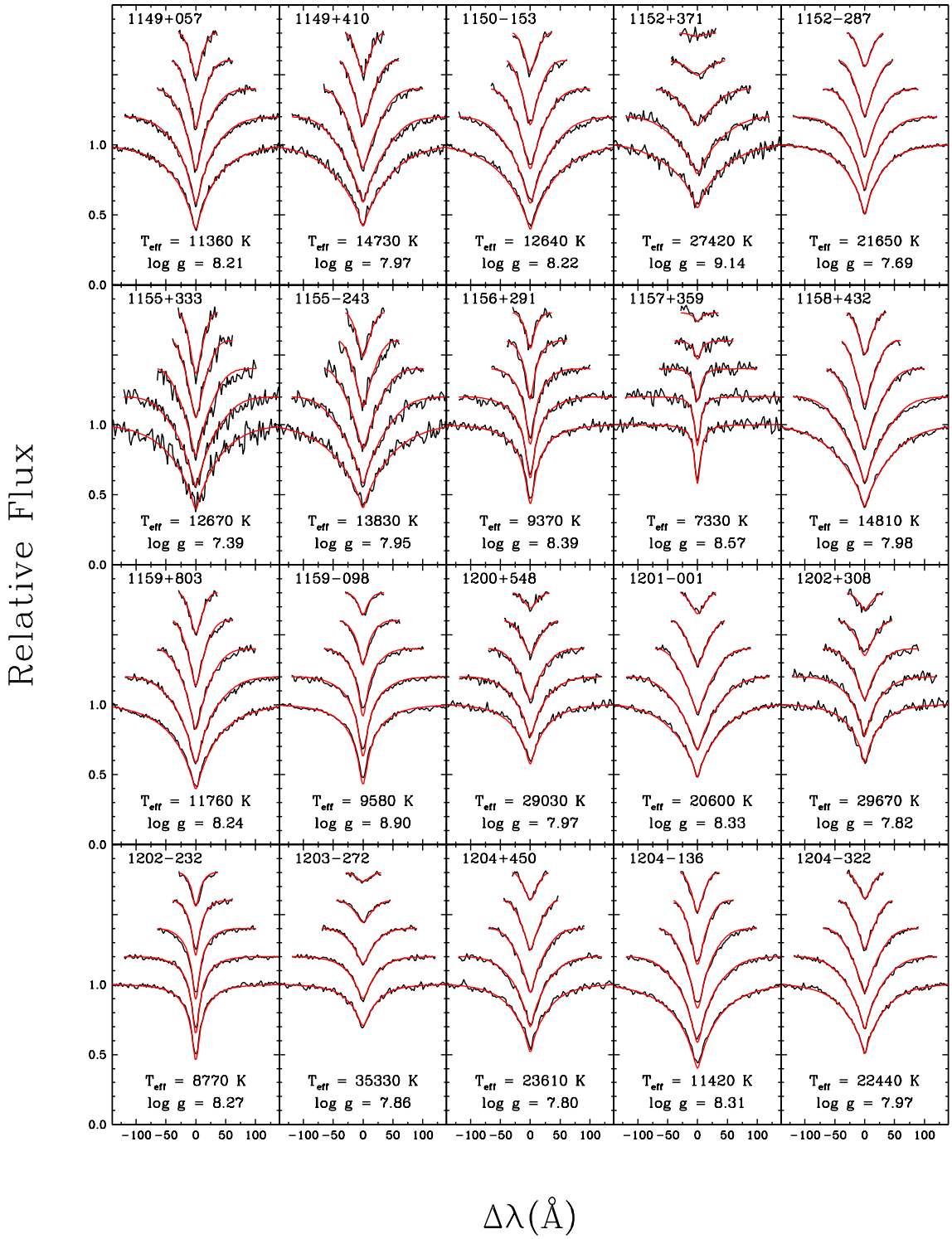

FIGURE B.1 – Suite

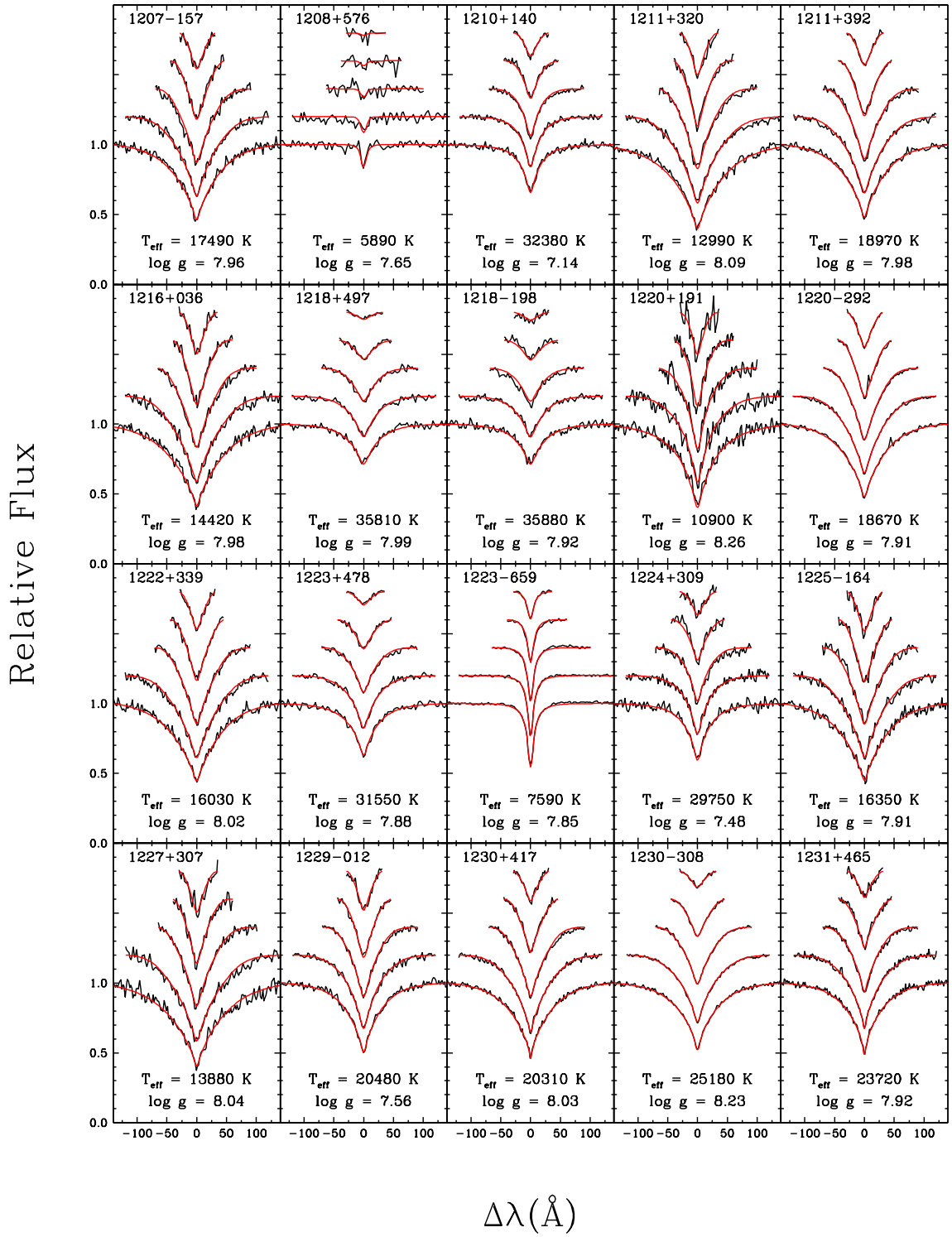

FIGURE B.1 – Suite

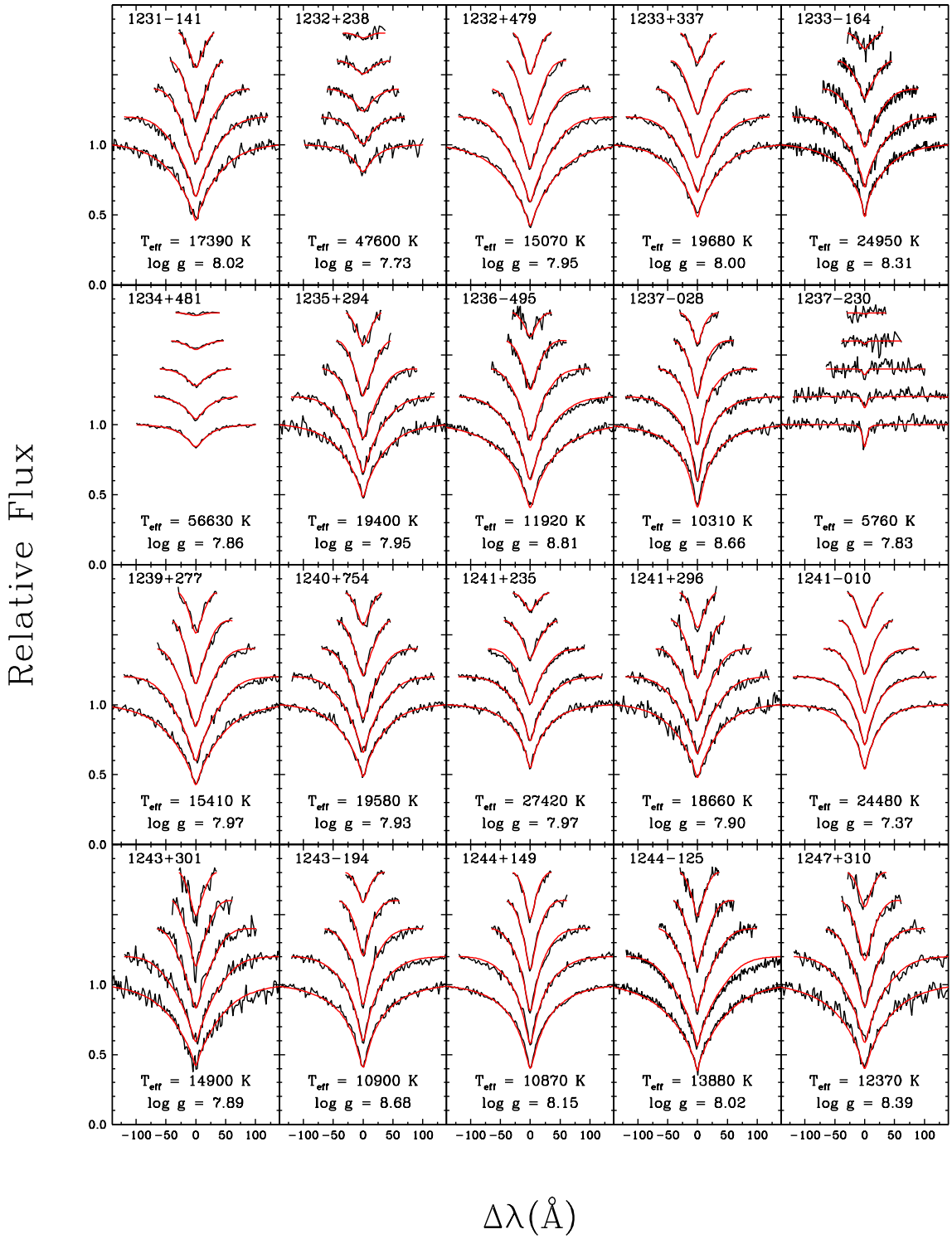

FIGURE B.1 – Suite

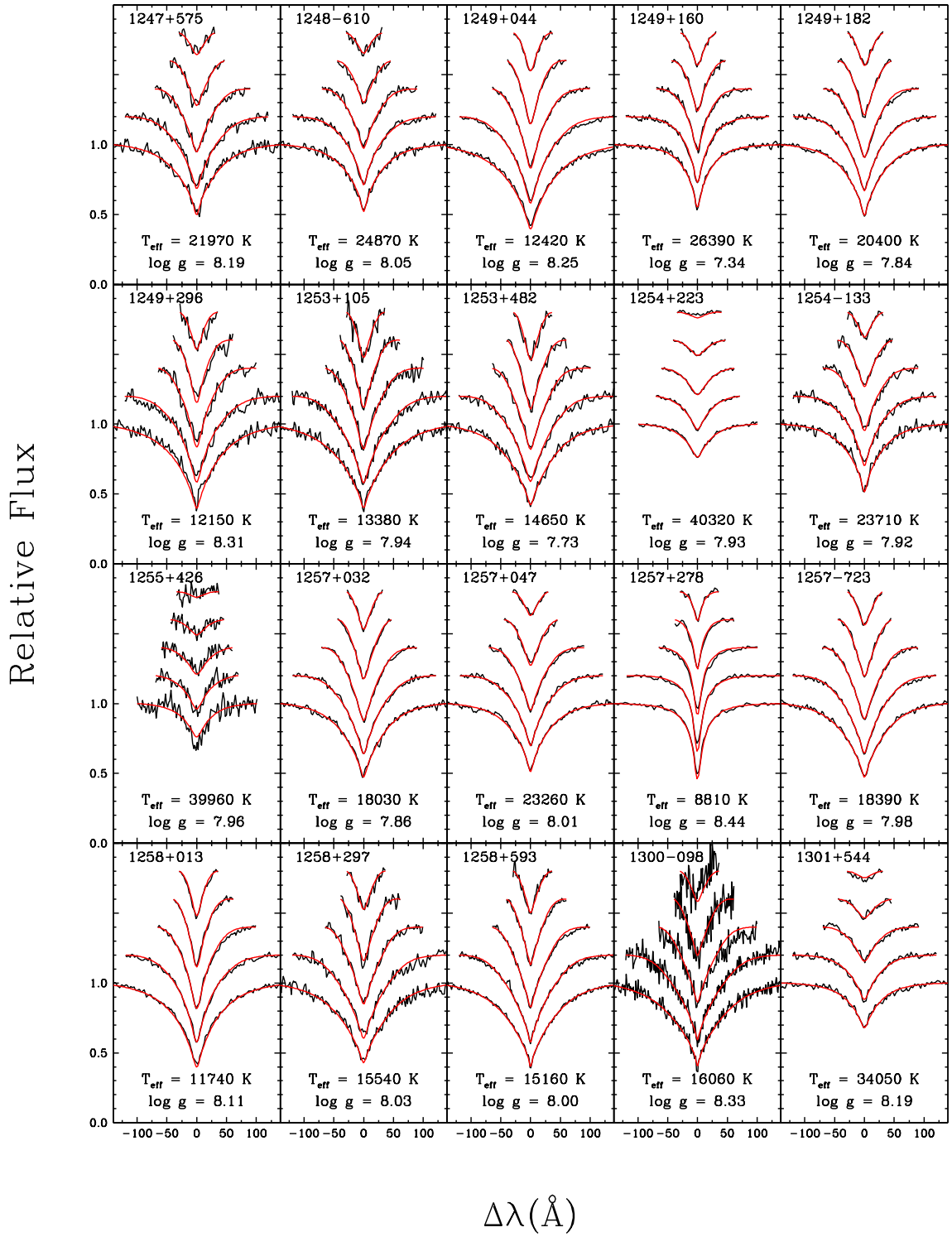

FIGURE B.1 – Suite

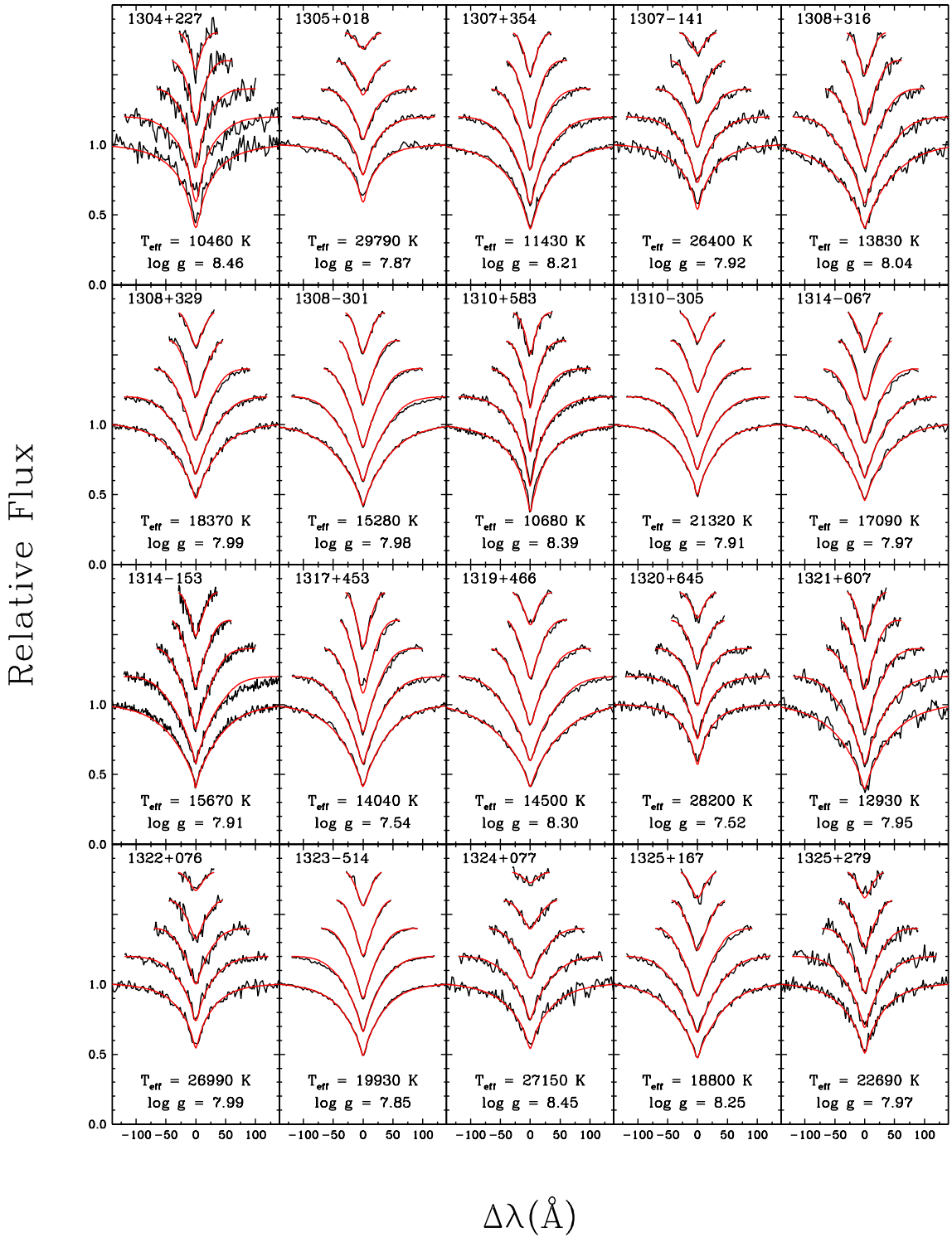

FIGURE B.1 – Suite

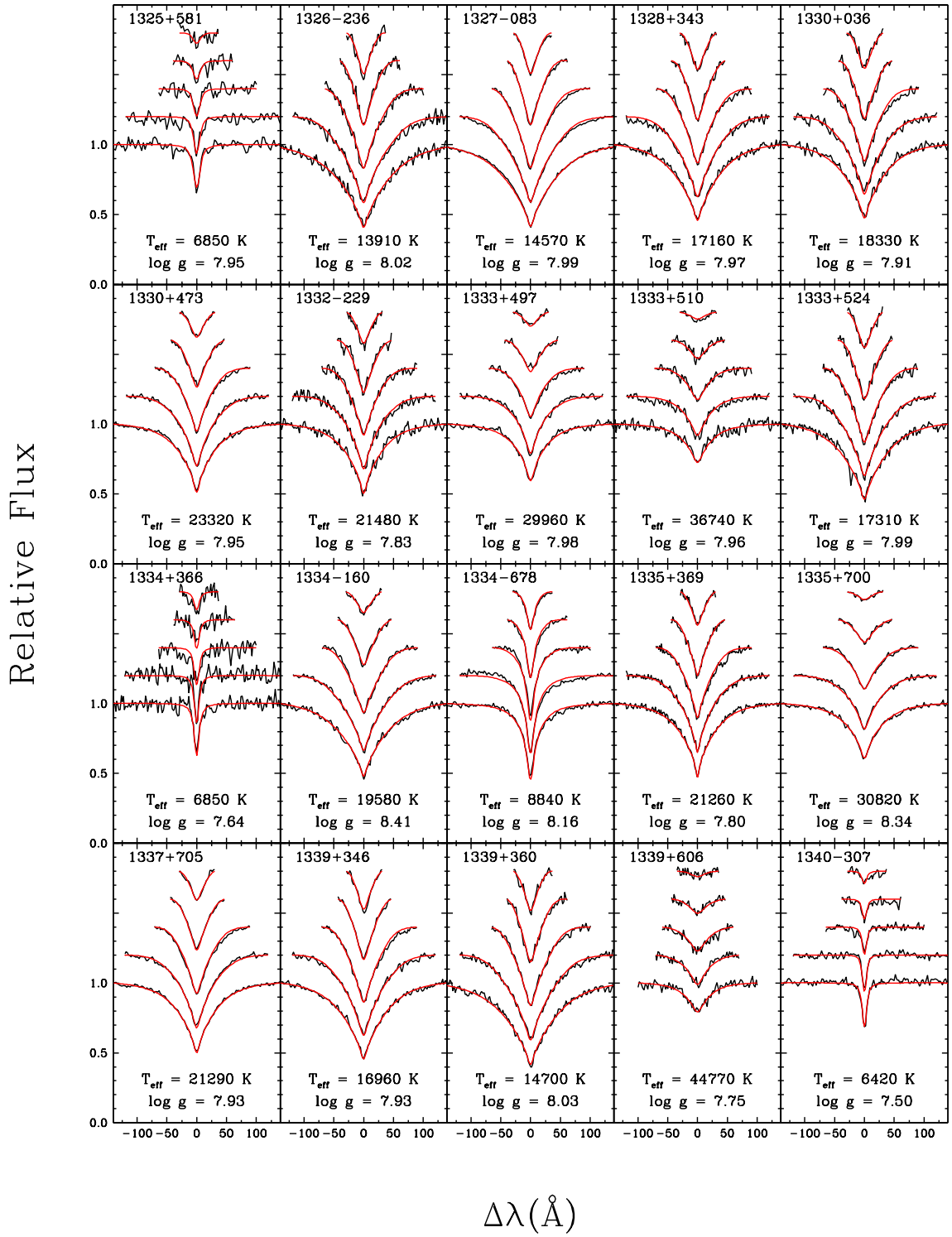

FIGURE B.1 – Suite

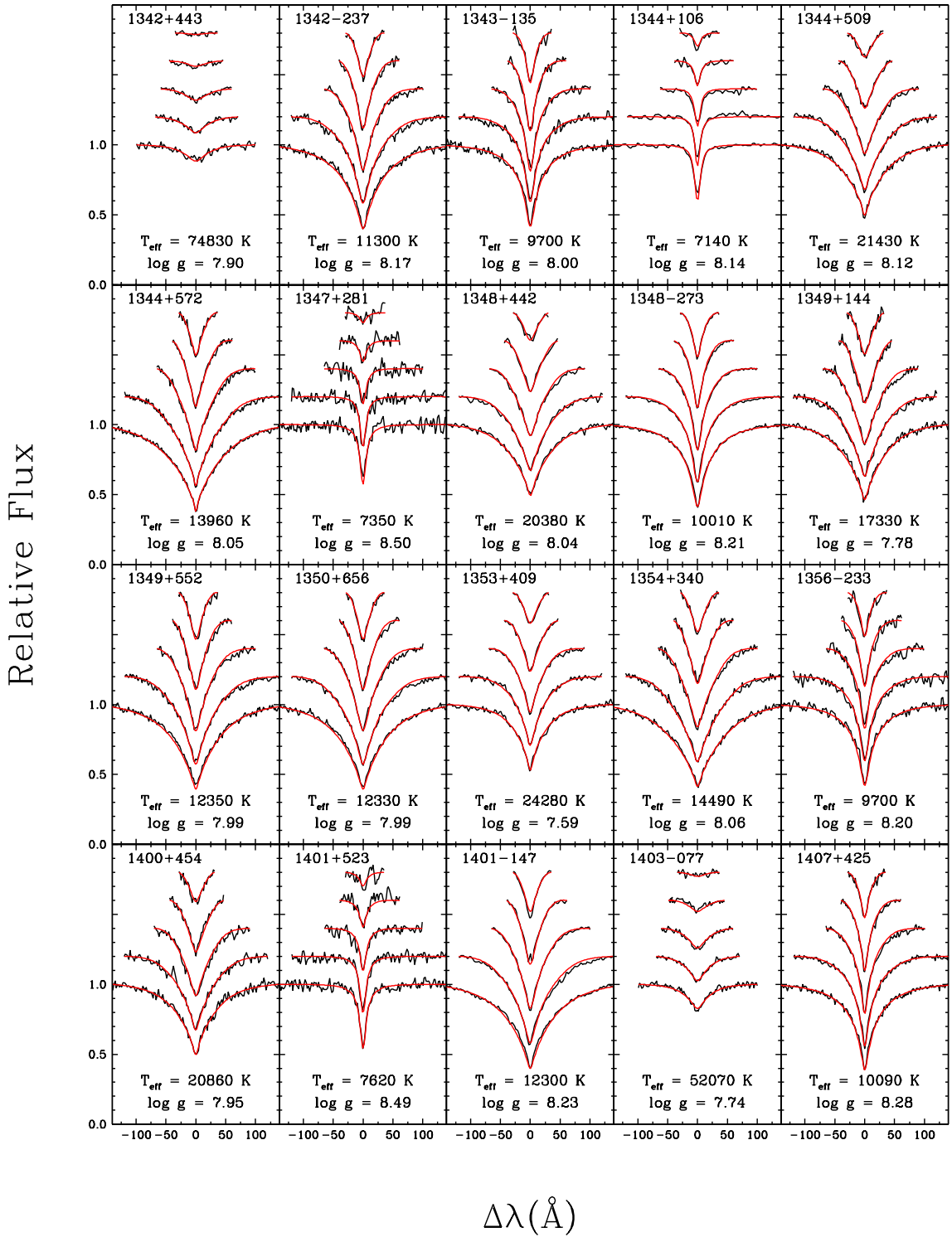

FIGURE B.1 – Suite

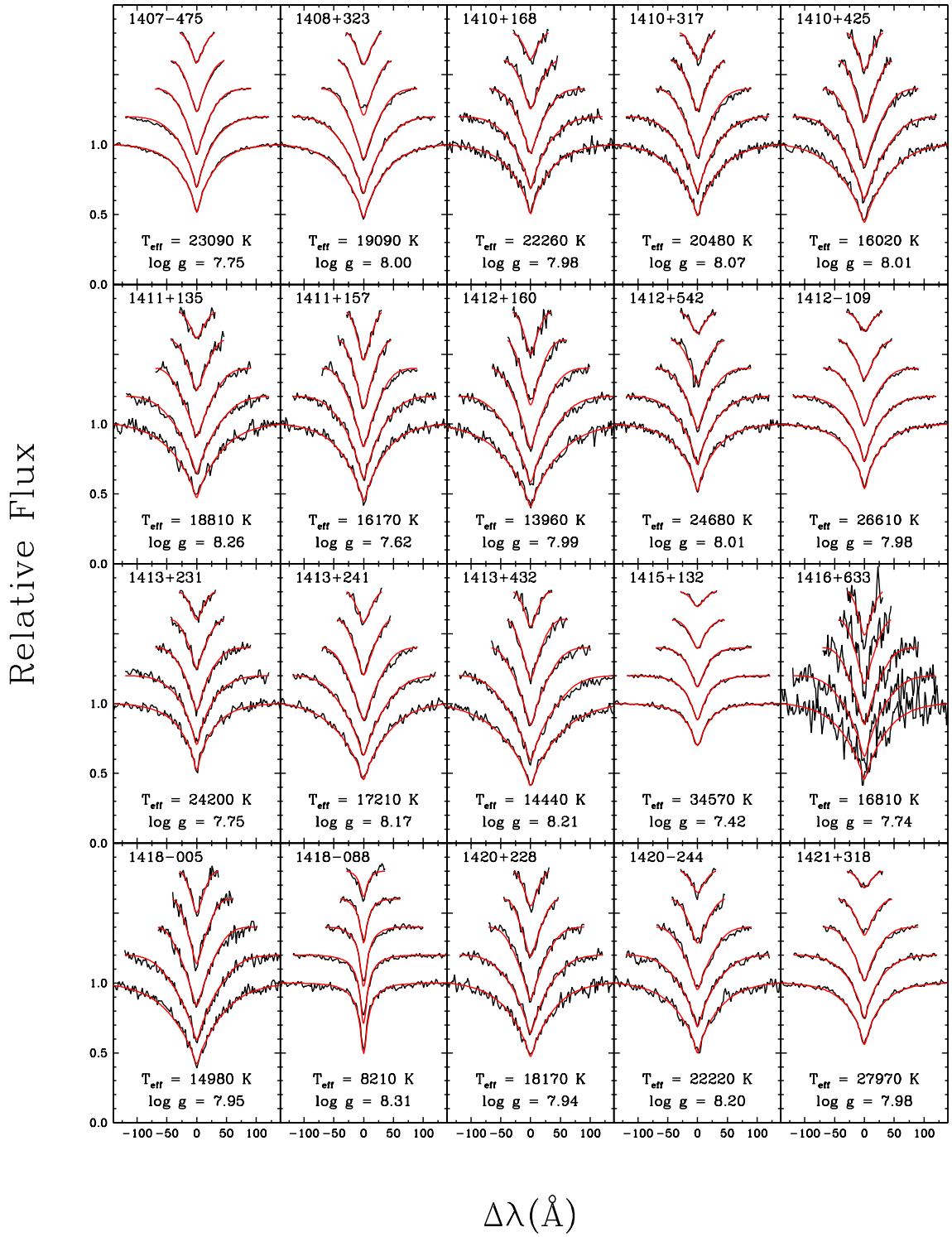

FIGURE B.1 – Suite

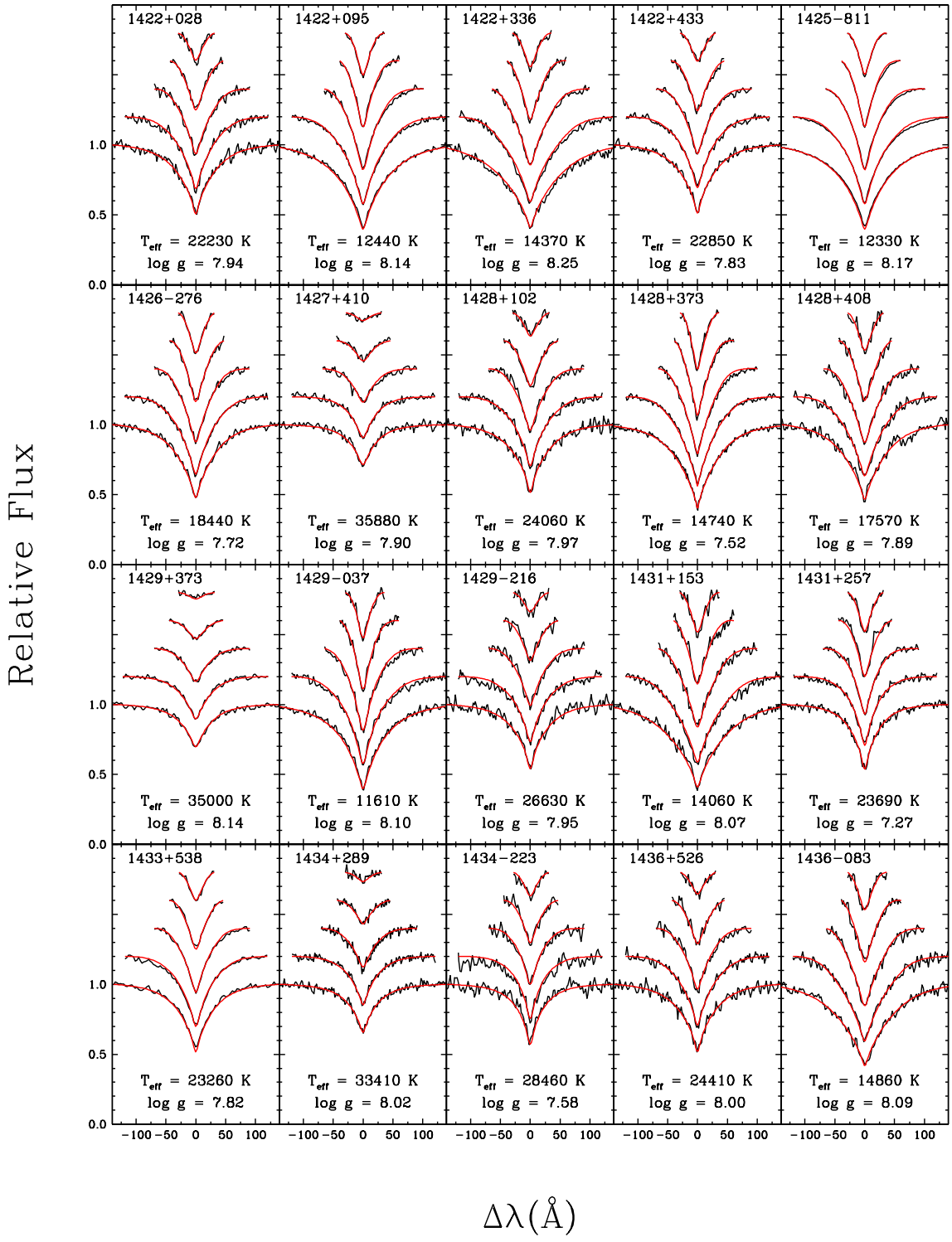

FIGURE B.1 – Suite

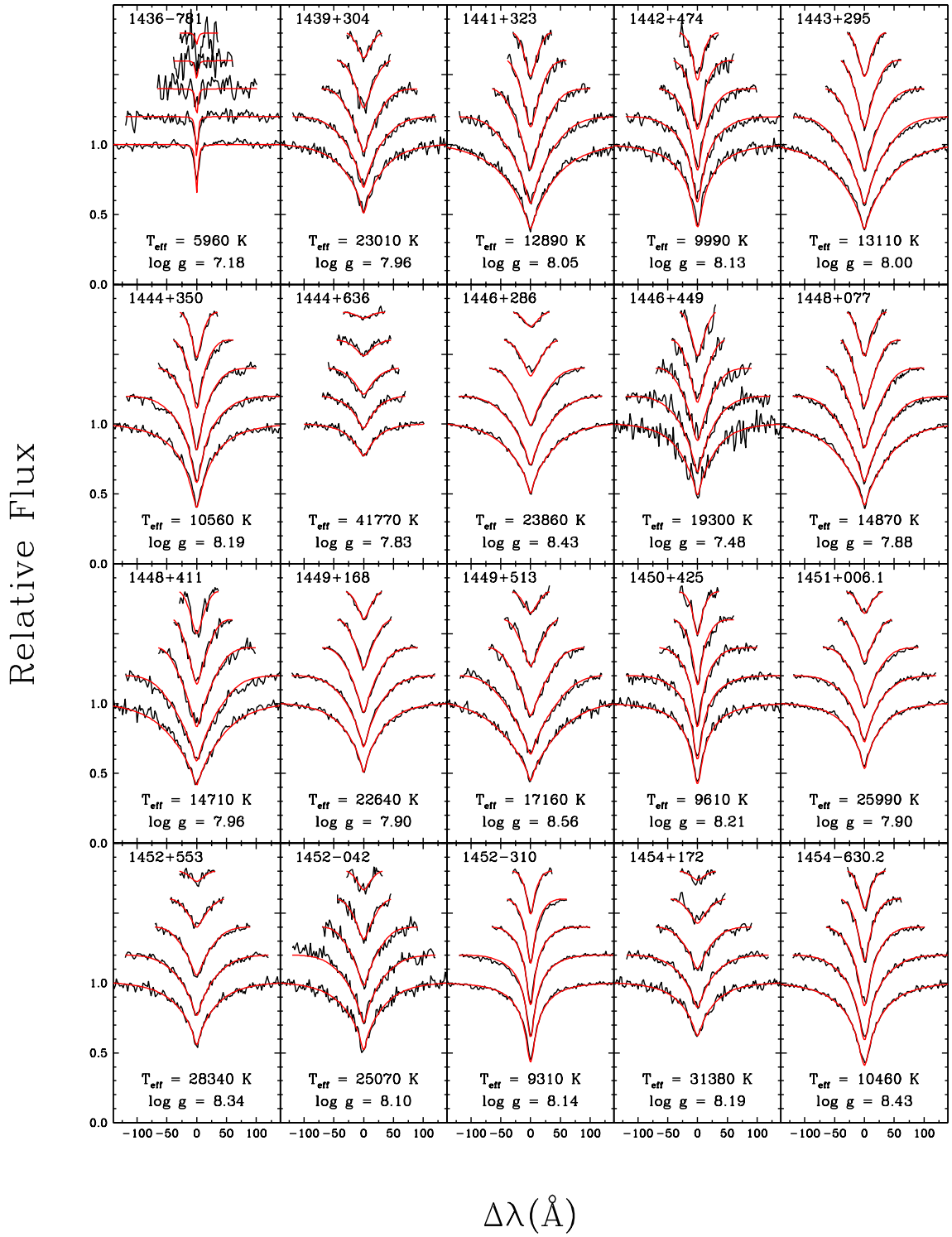

FIGURE B.1 – Suite

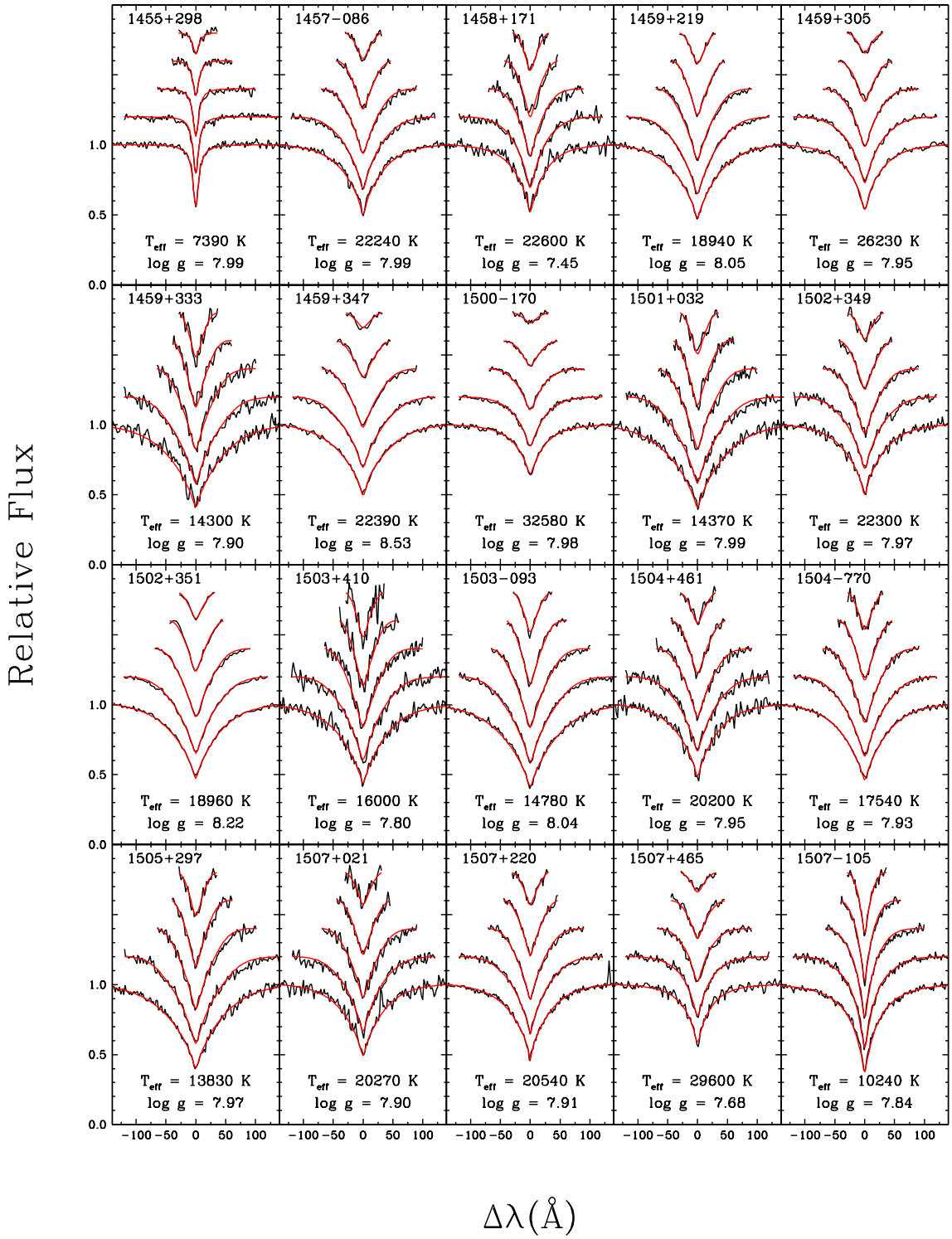

FIGURE B.1 – Suite

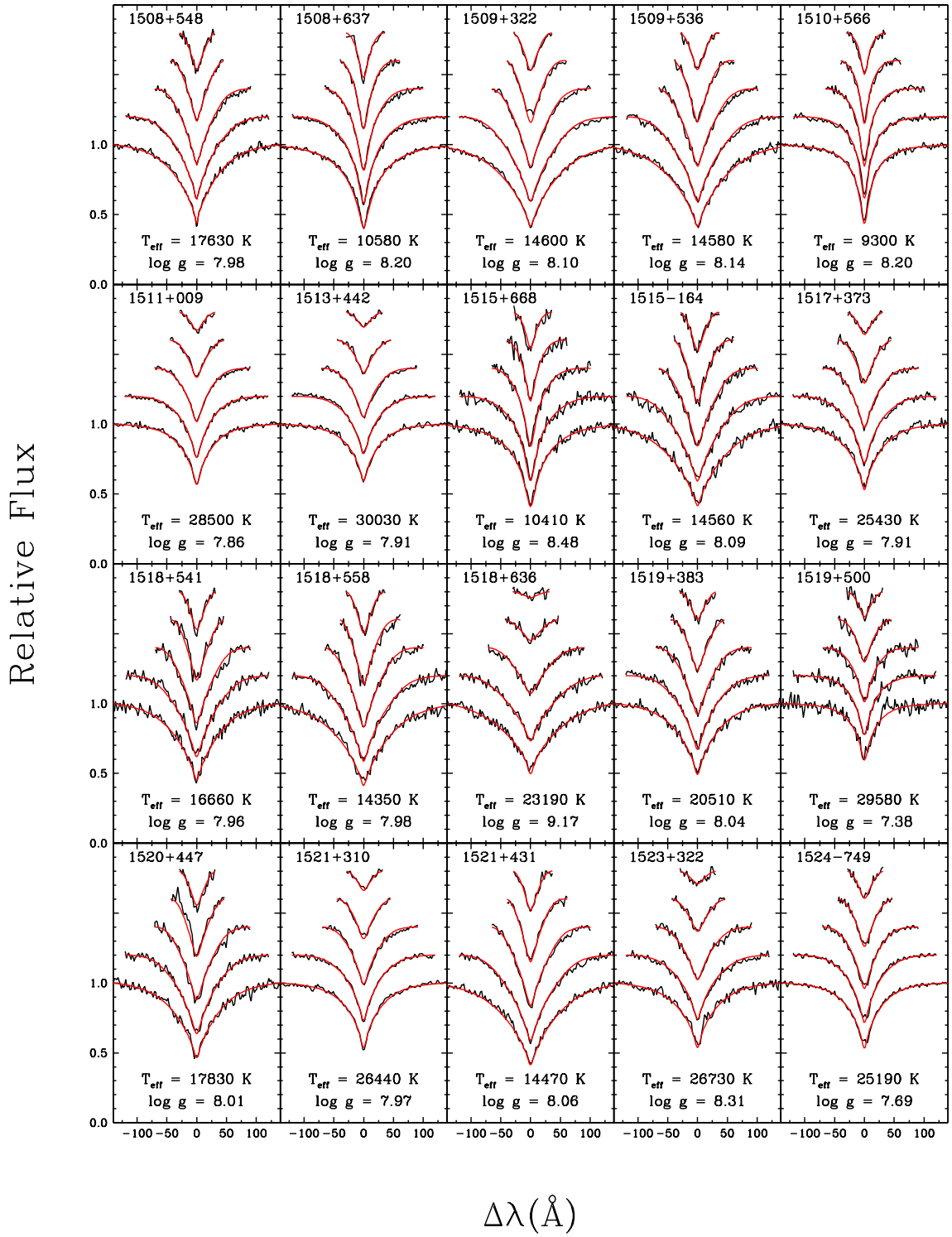

FIGURE B.1 – Suite

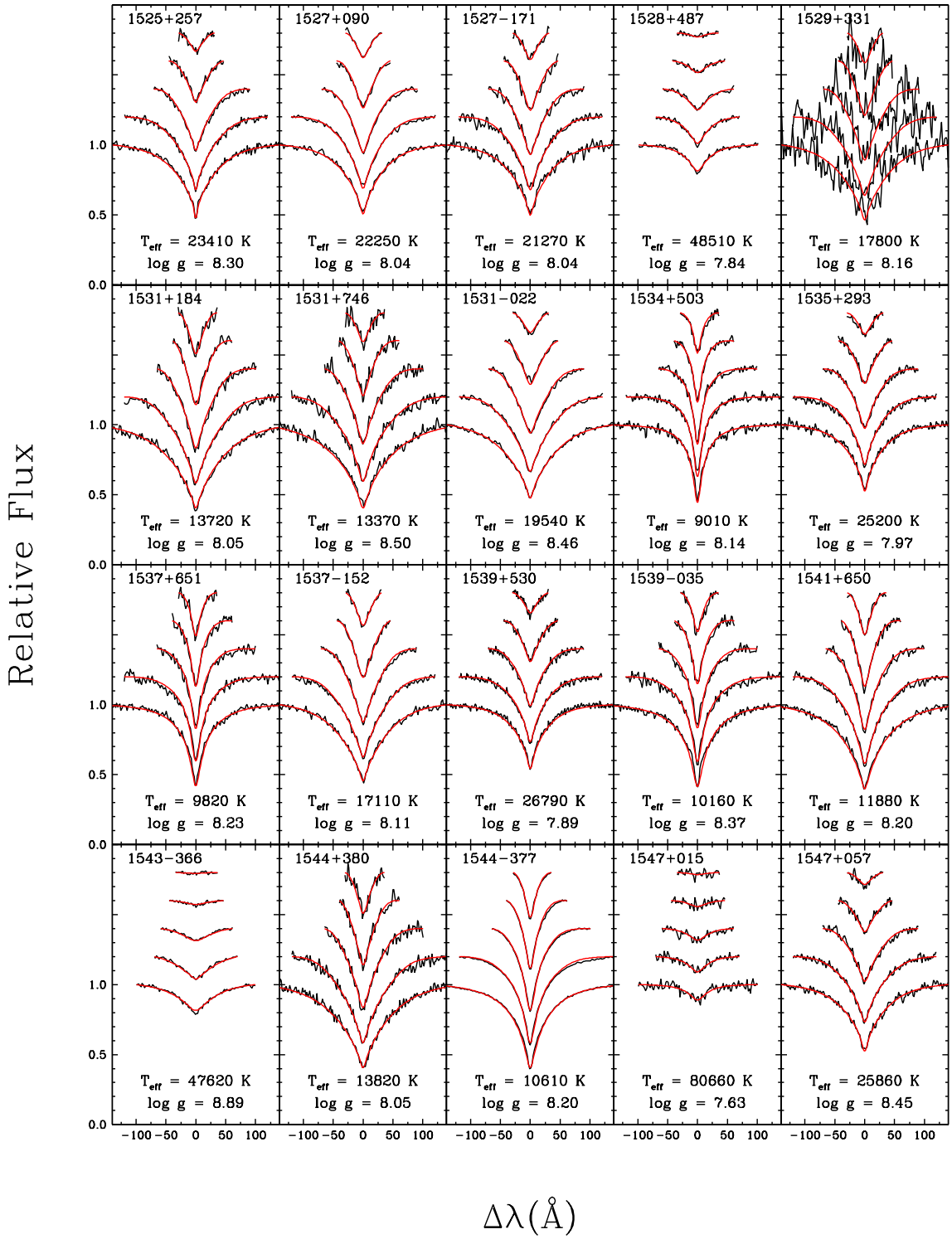

FIGURE B.1 – Suite

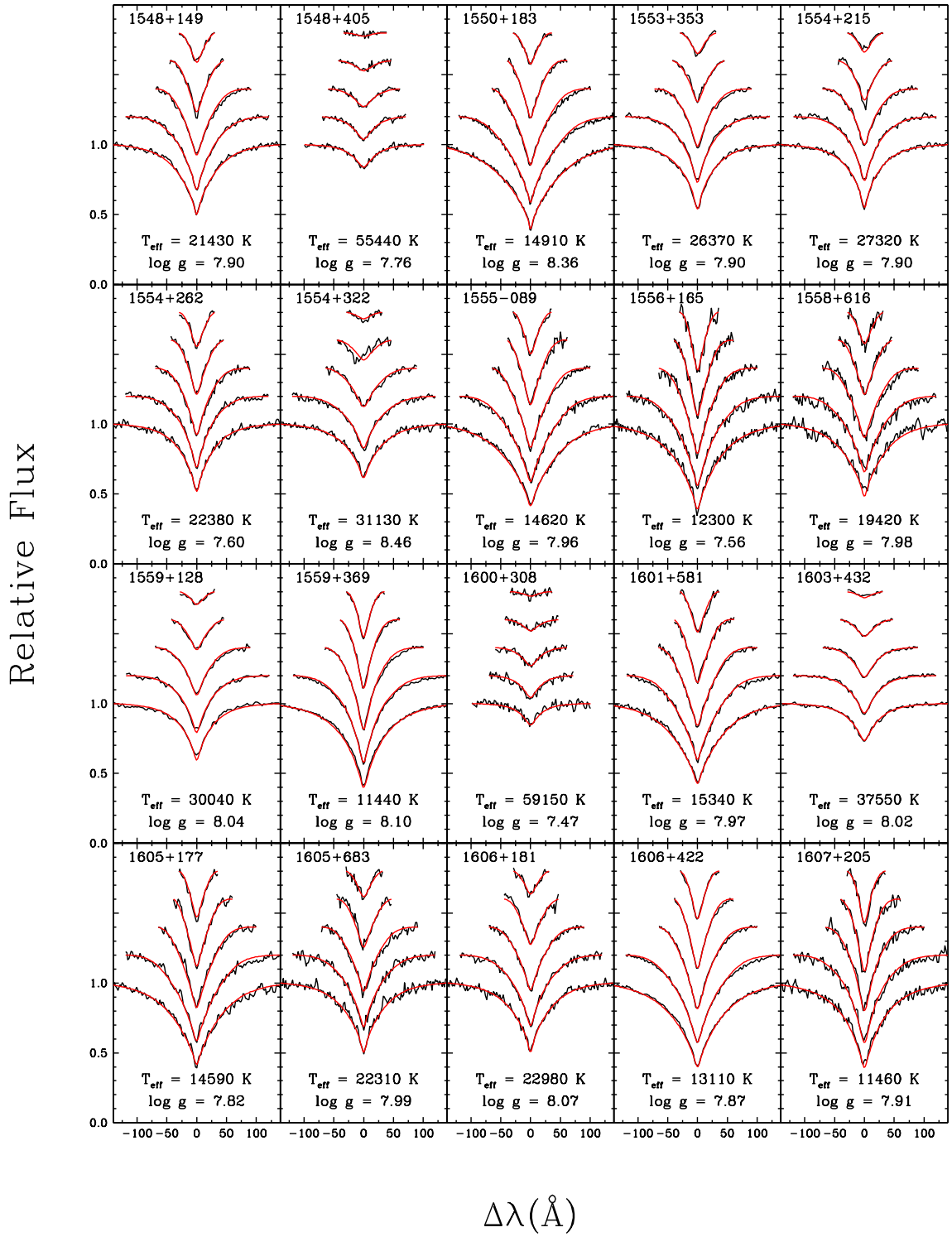

FIGURE B.1 – Suite

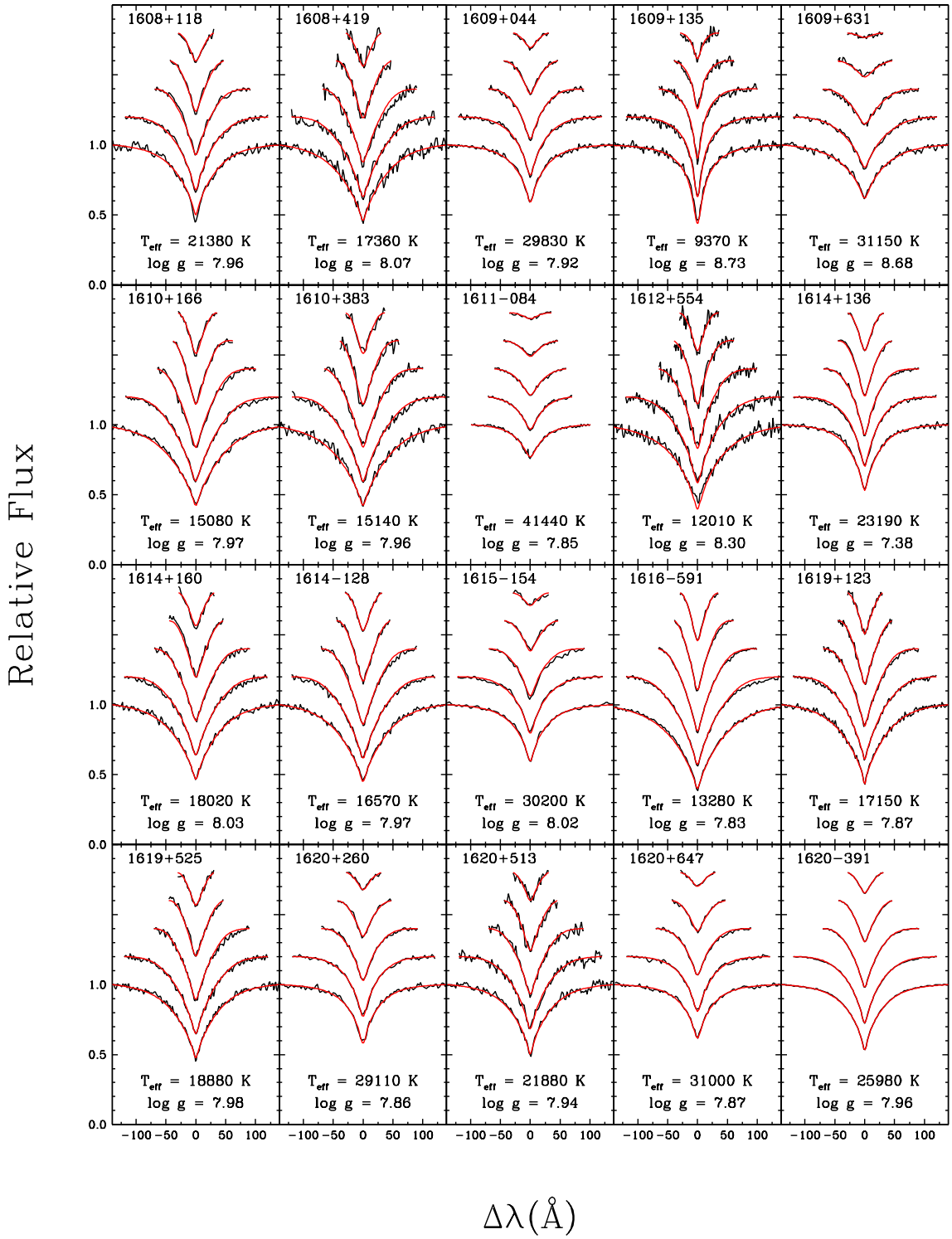

FIGURE B.1 – Suite

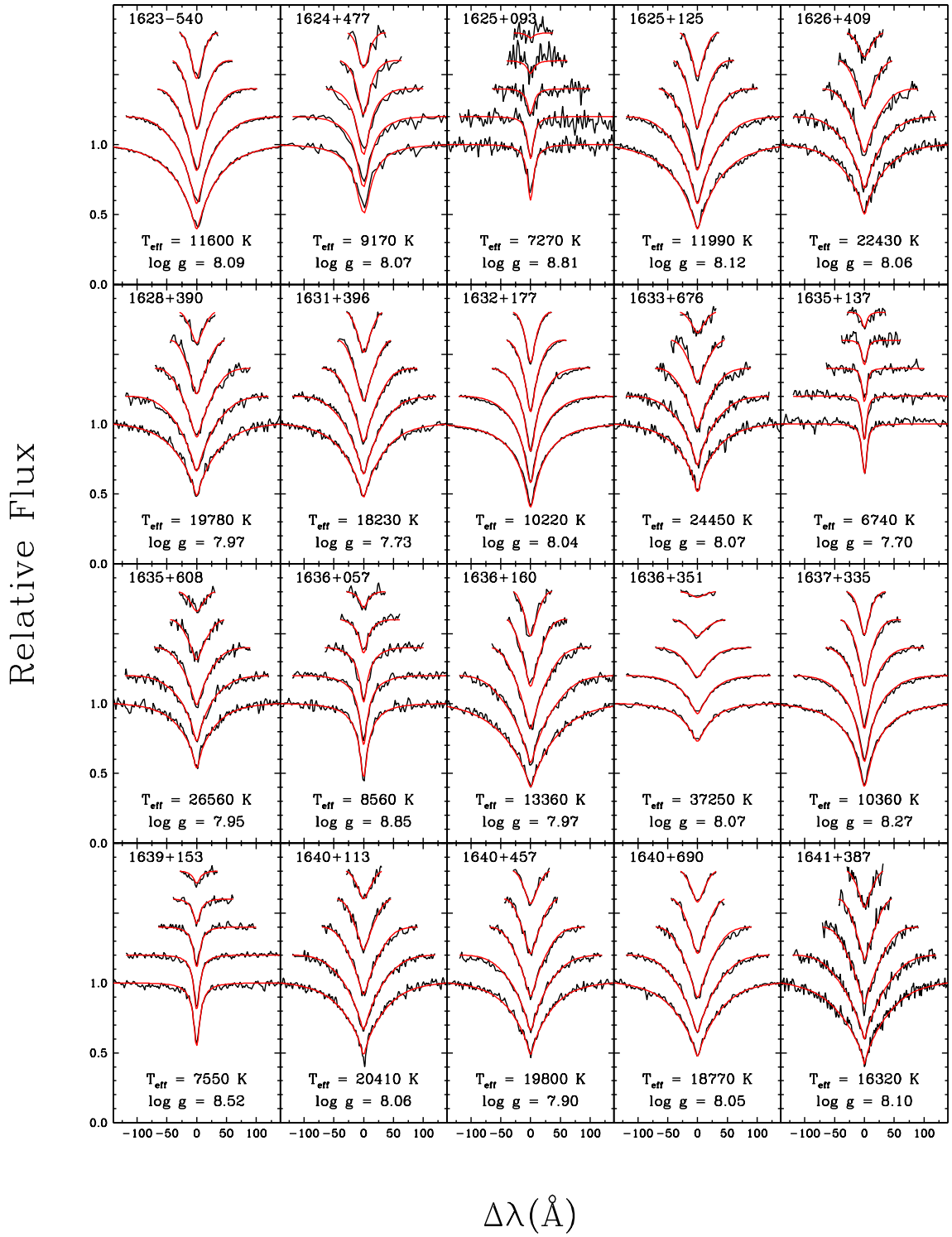

FIGURE B.1 – Suite

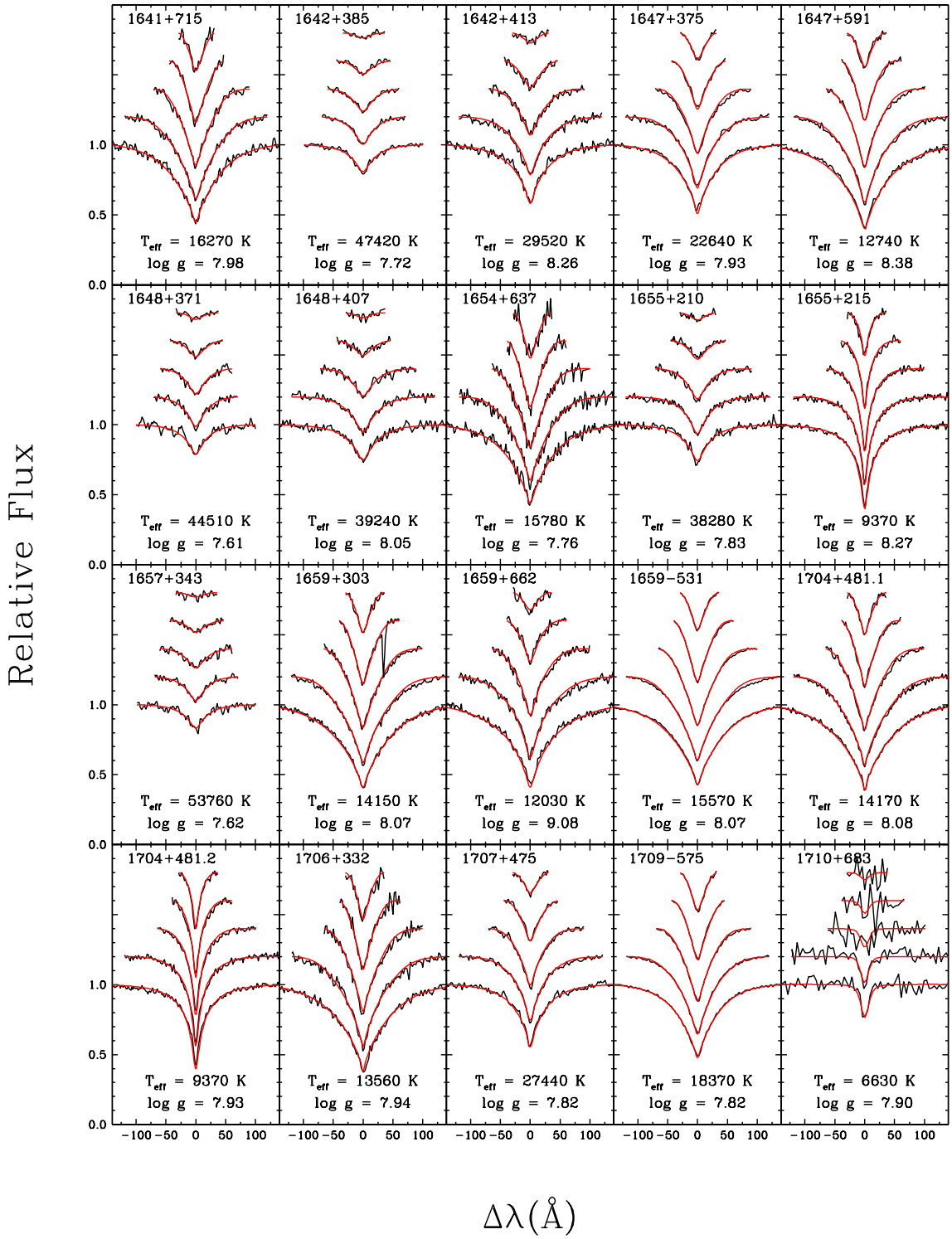

FIGURE B.1 – Suite

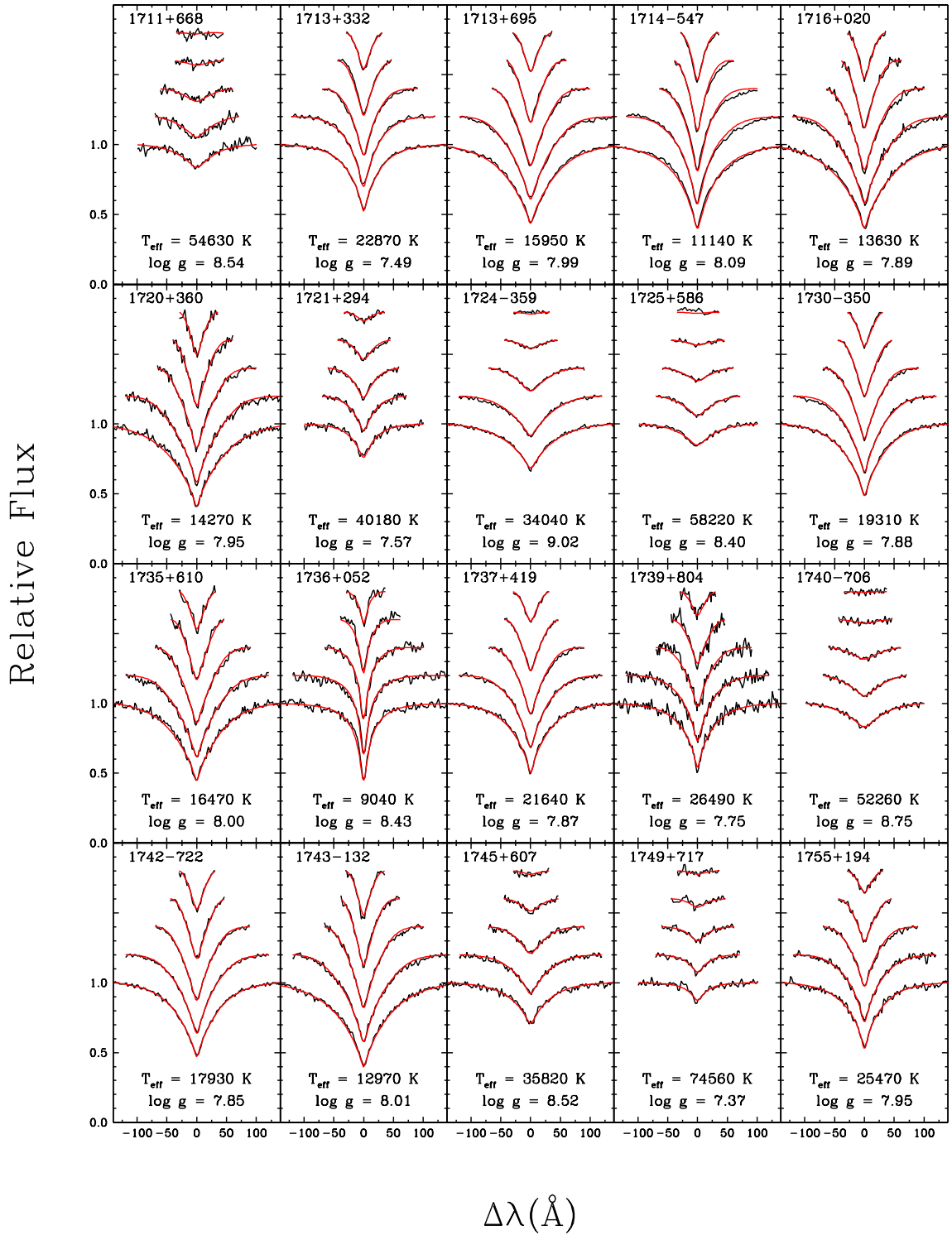

FIGURE B.1 – Suite

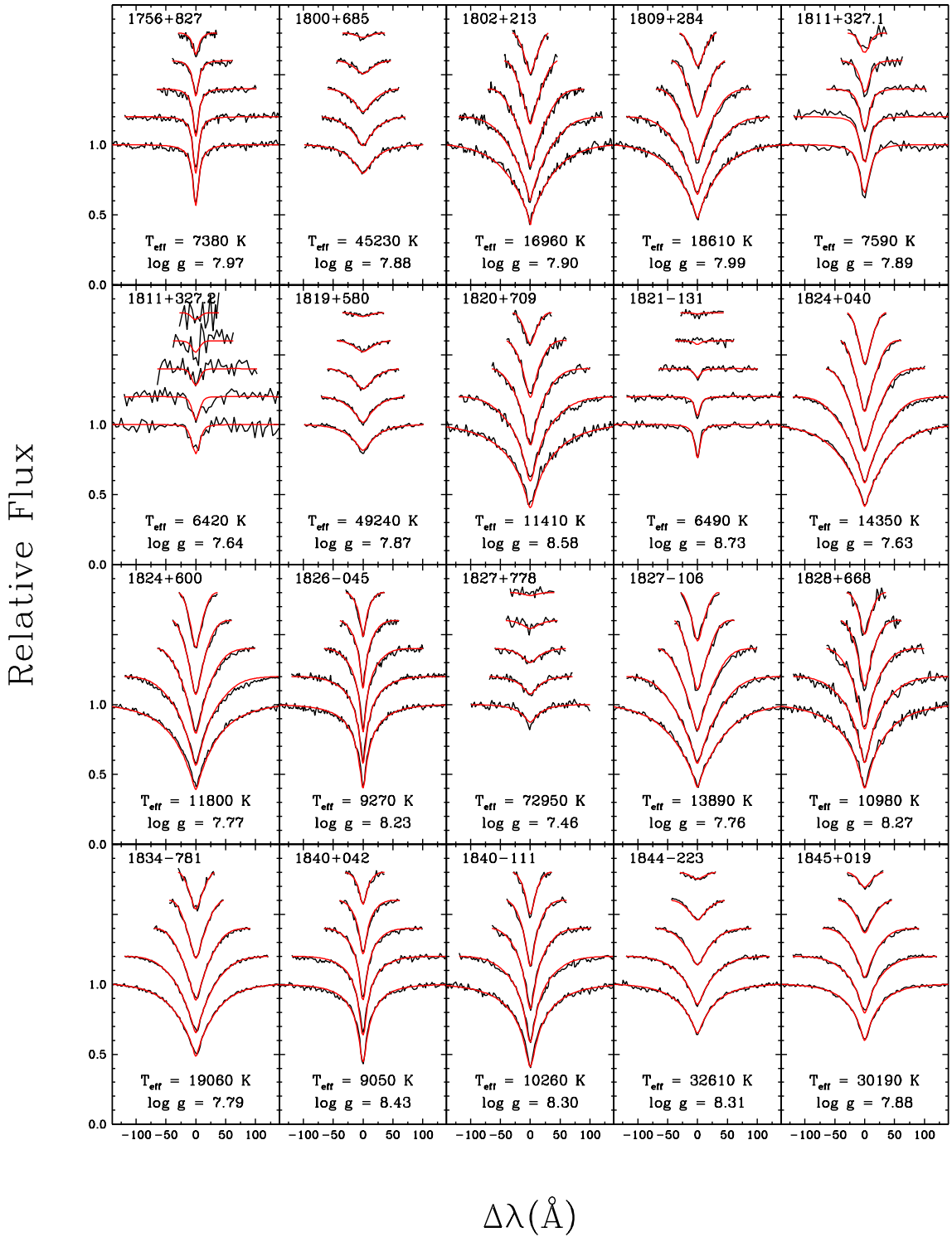

FIGURE B.1 – Suite

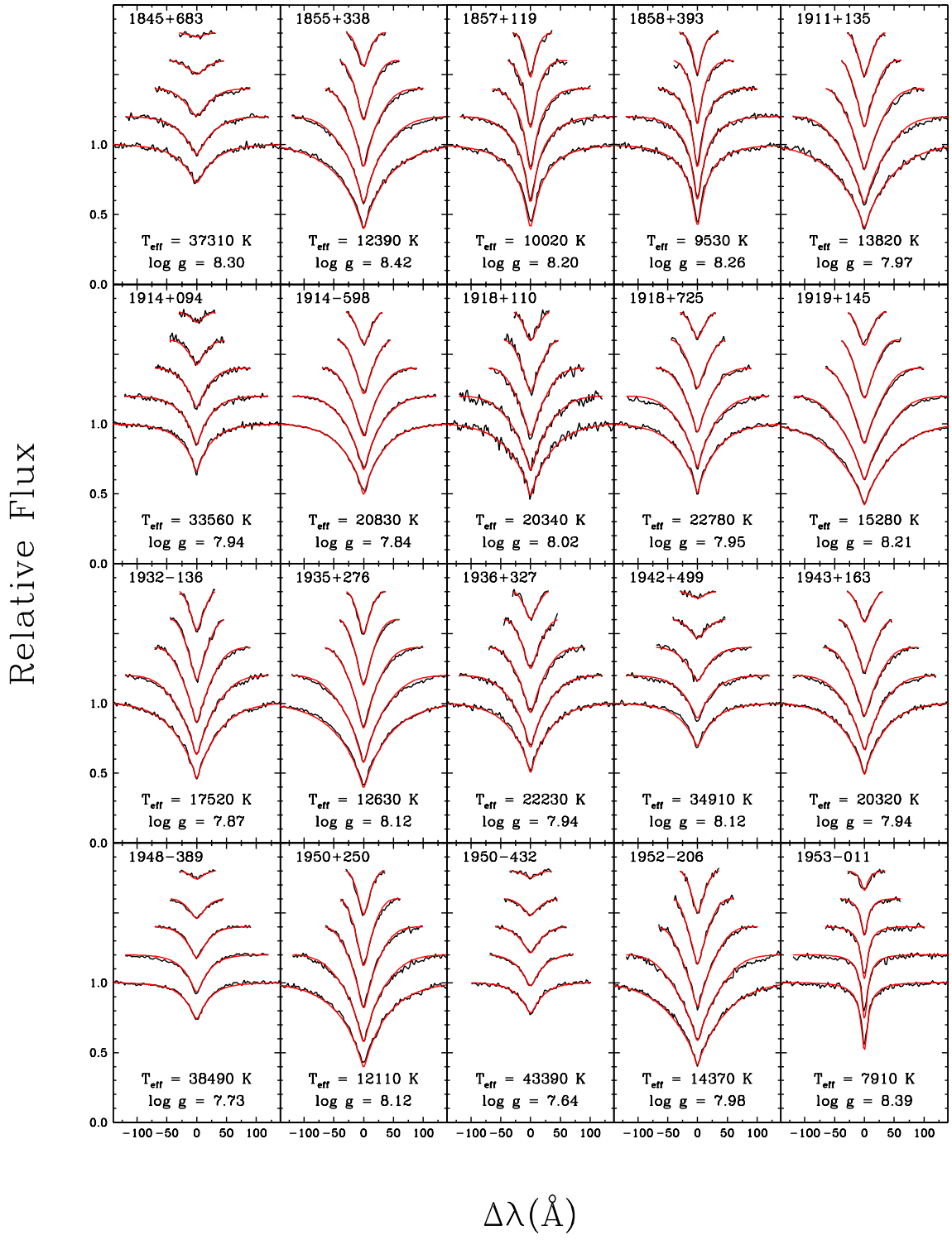

FIGURE B.1 – Suite

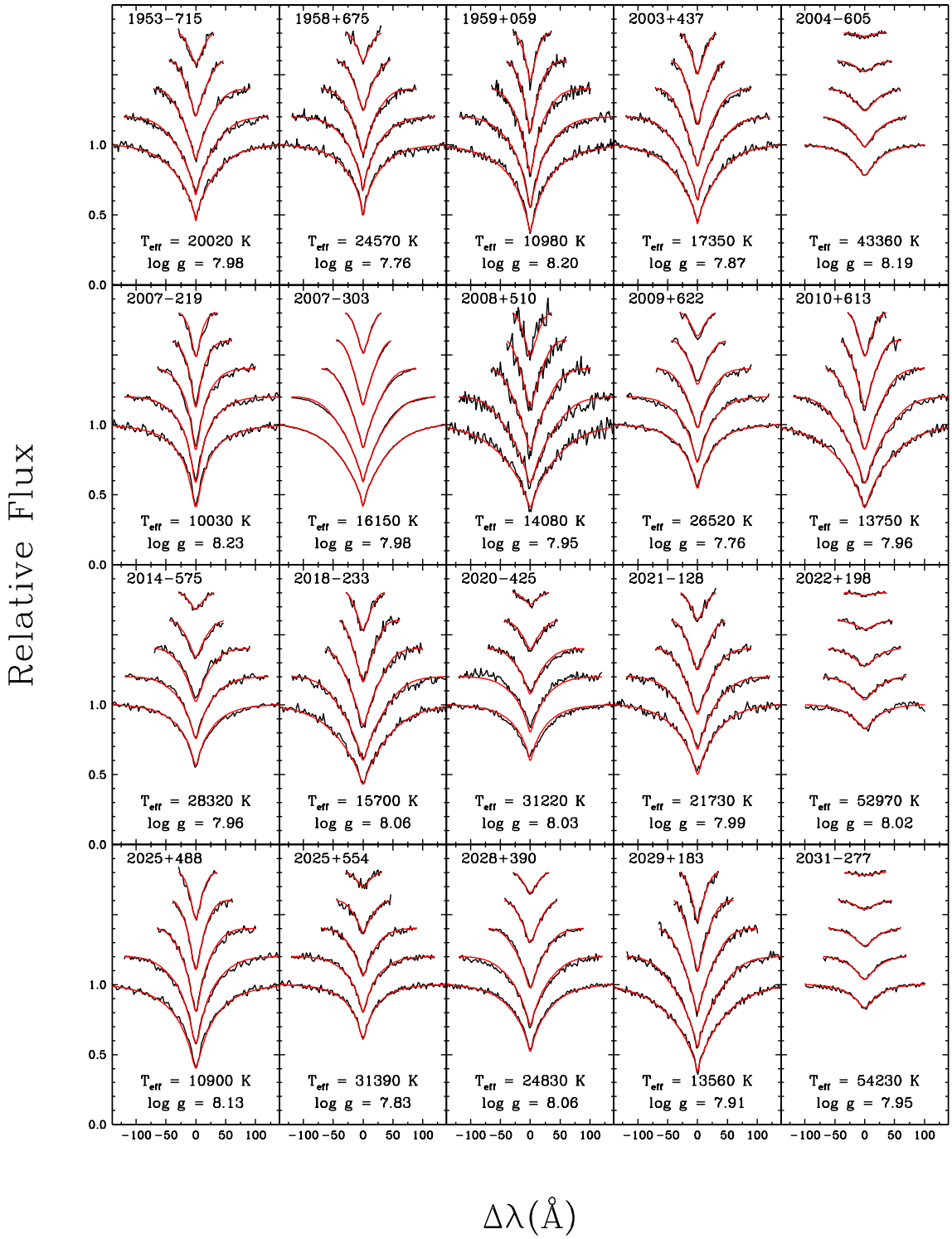

FIGURE B.1 – Suite

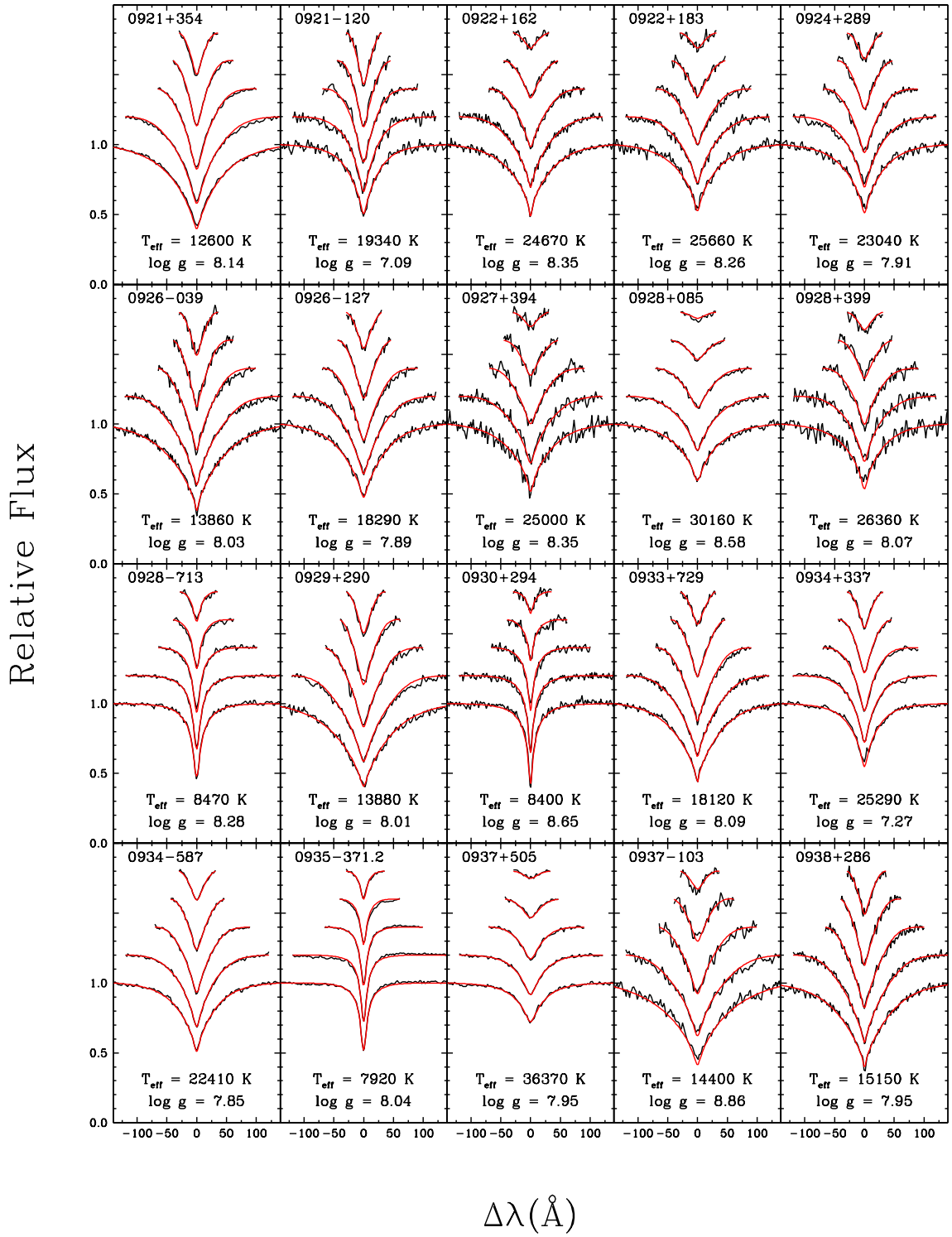

FIGURE B.1 – Suite

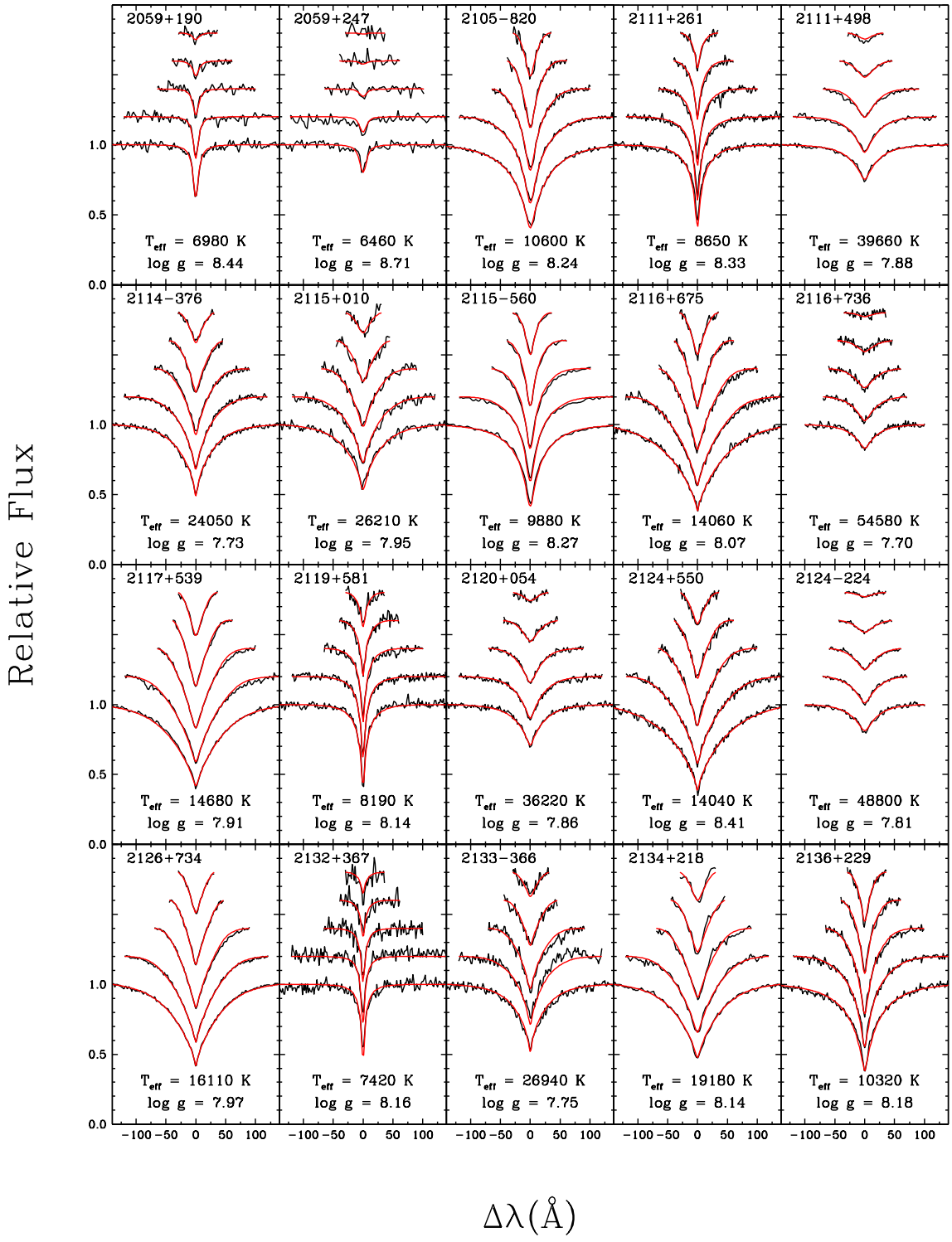

FIGURE B.1 – Suite

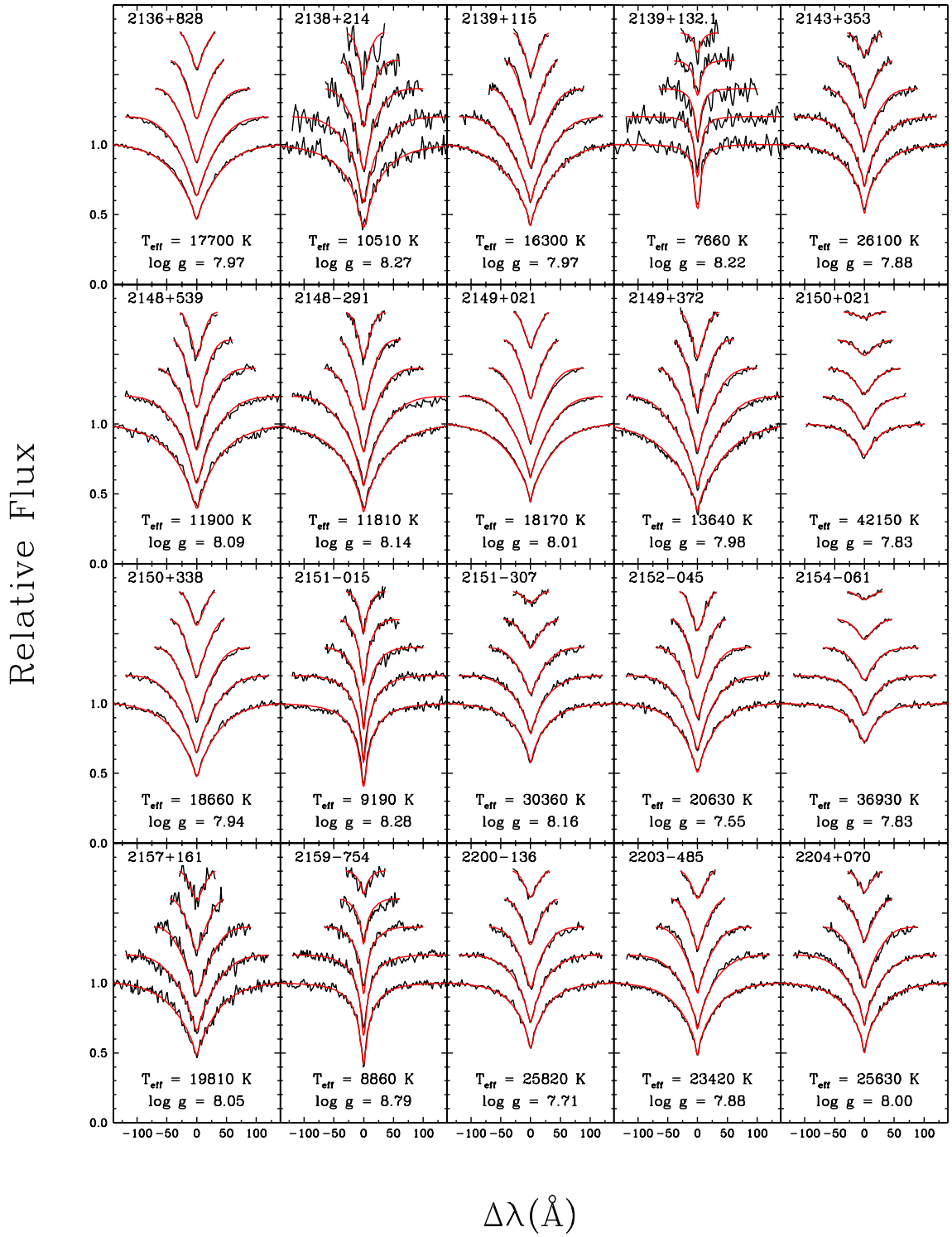

FIGURE B.1 – Suite

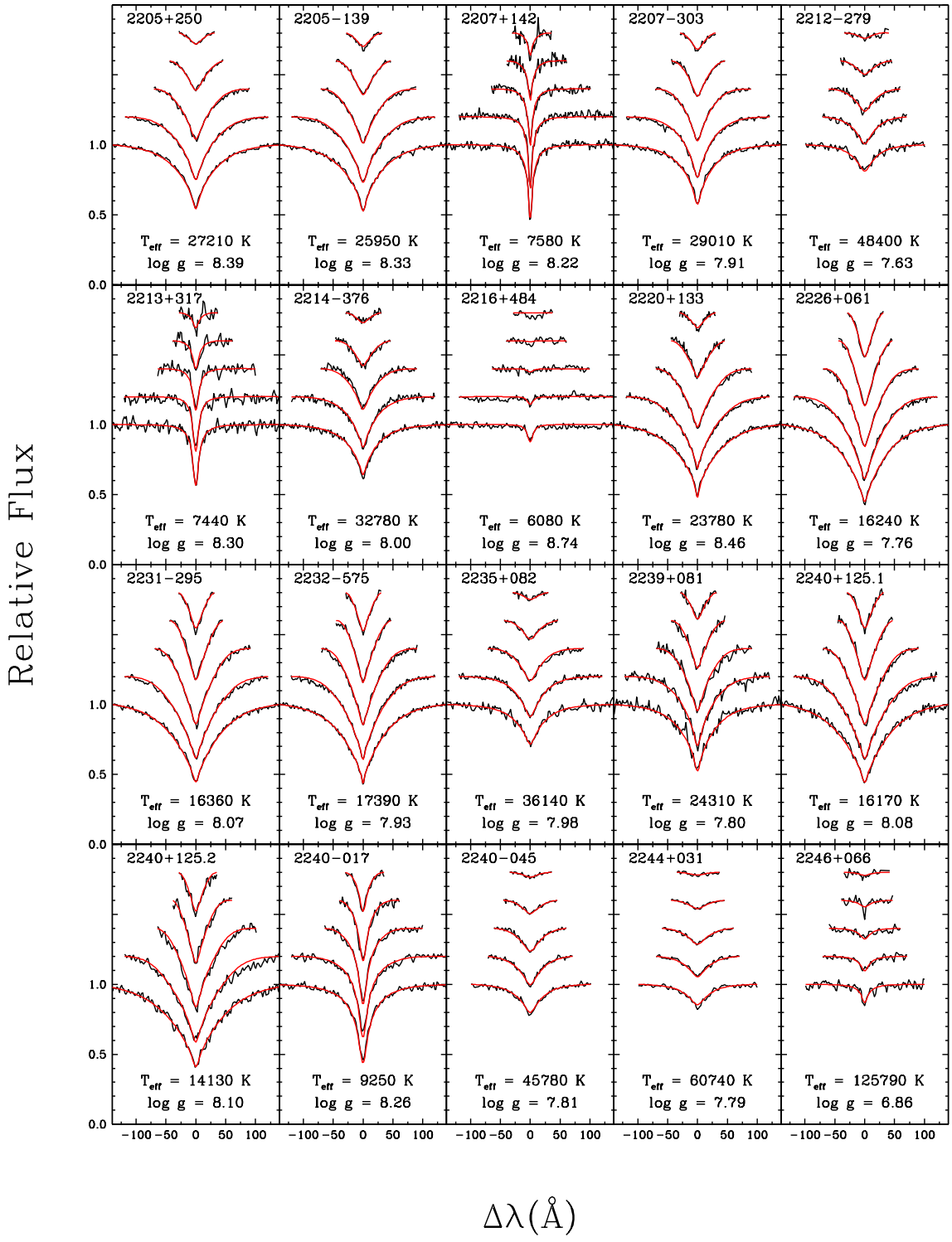

FIGURE B.1 – Suite

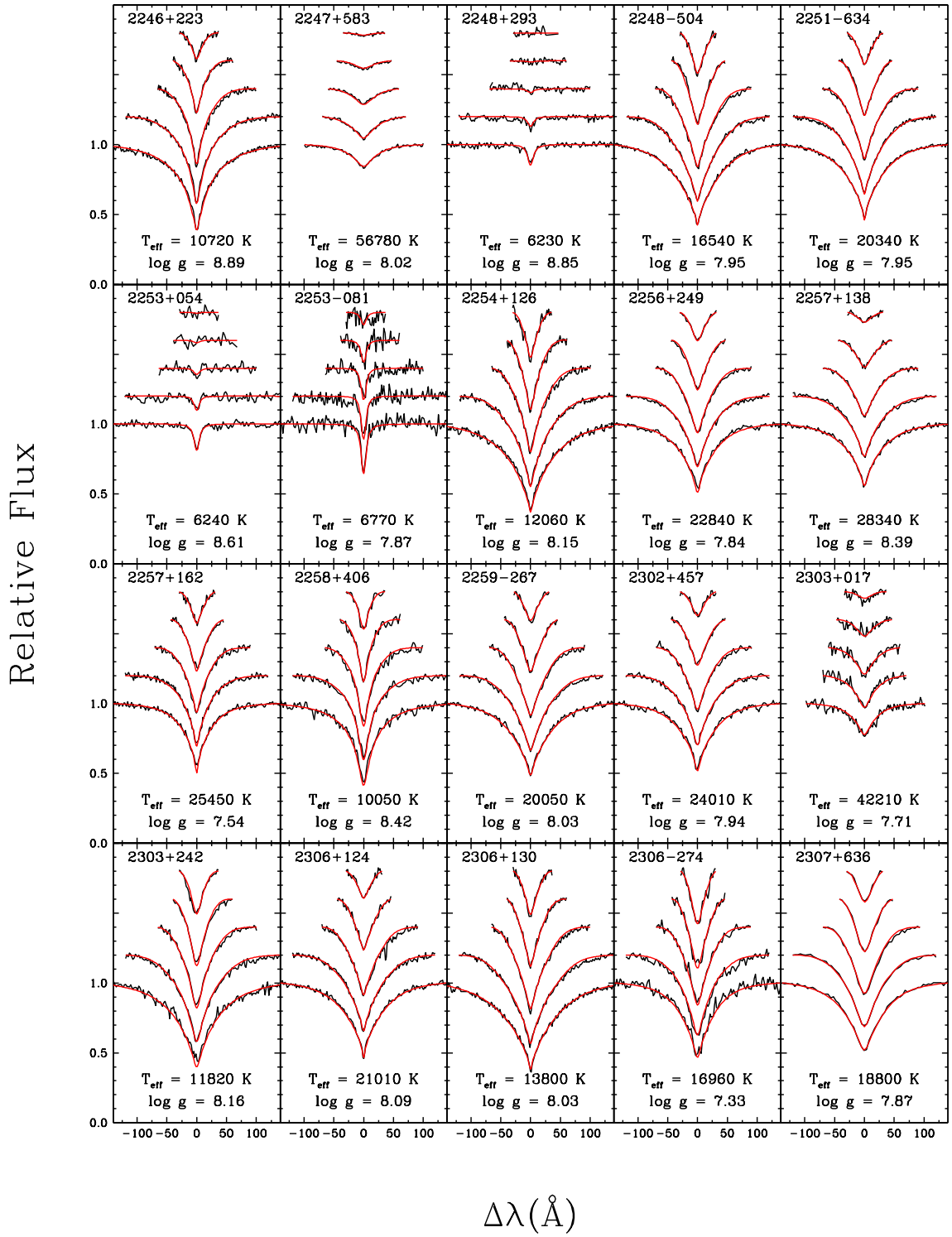

FIGURE B.1 – Suite

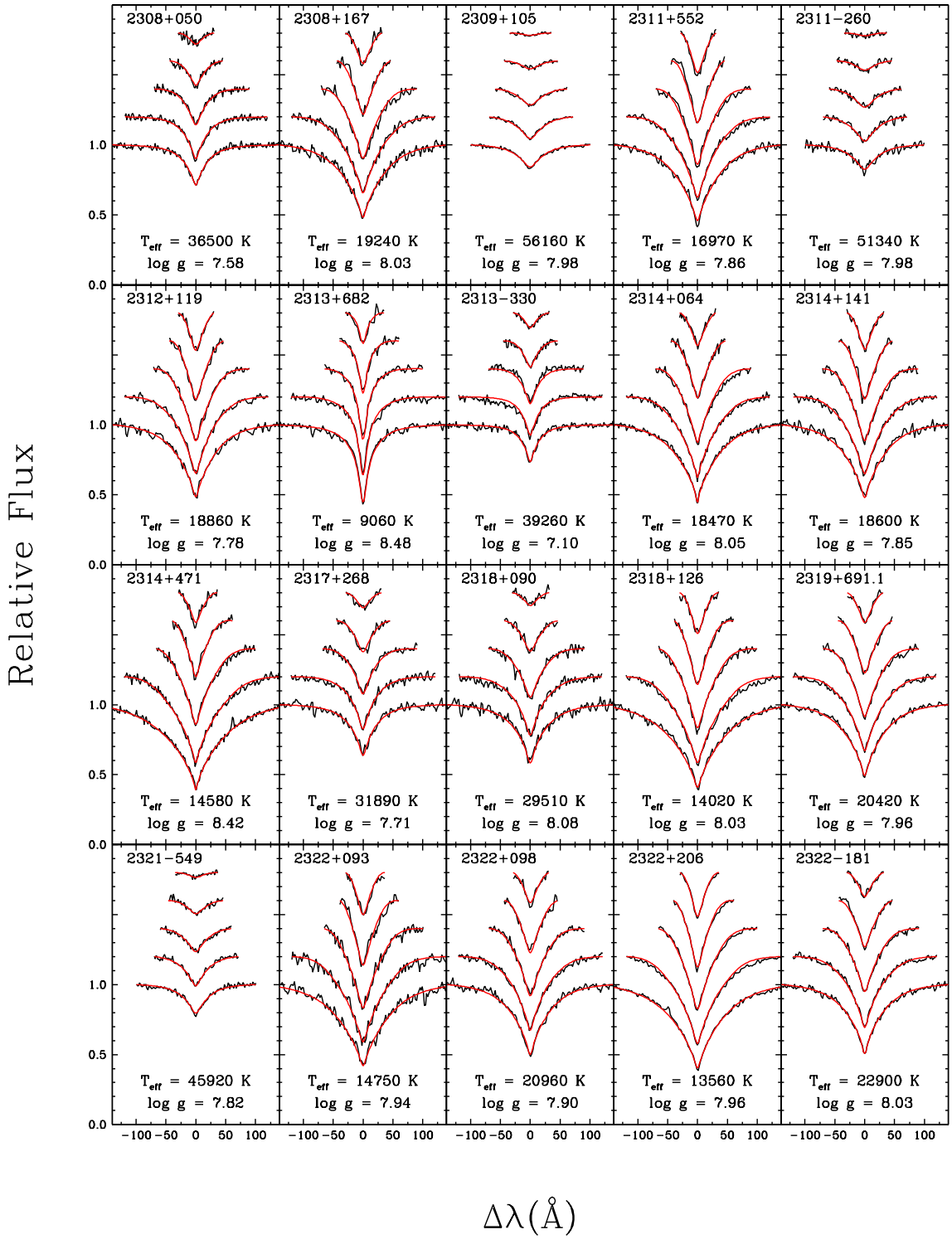

FIGURE B.1 – Suite

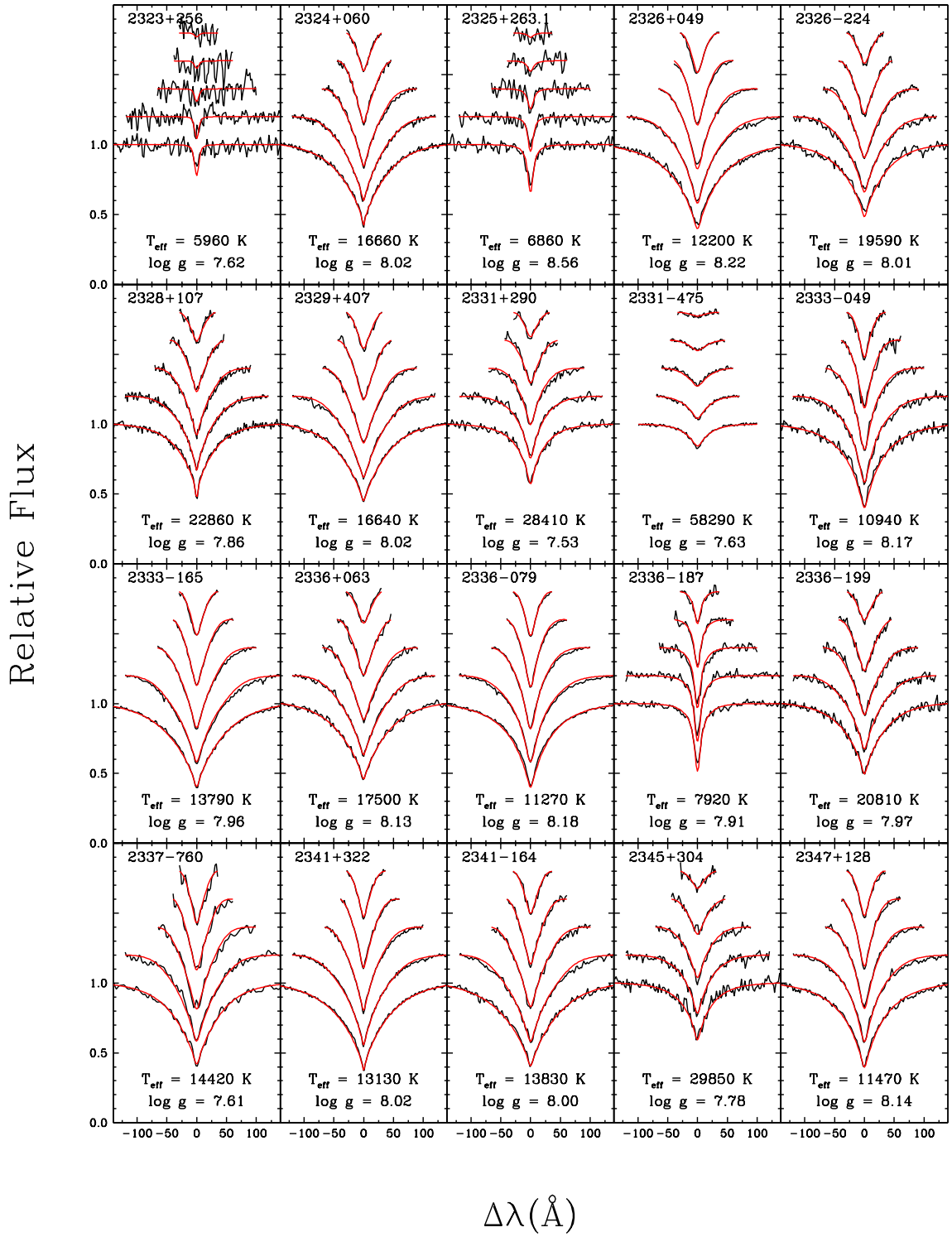

FIGURE B.1 – Suite

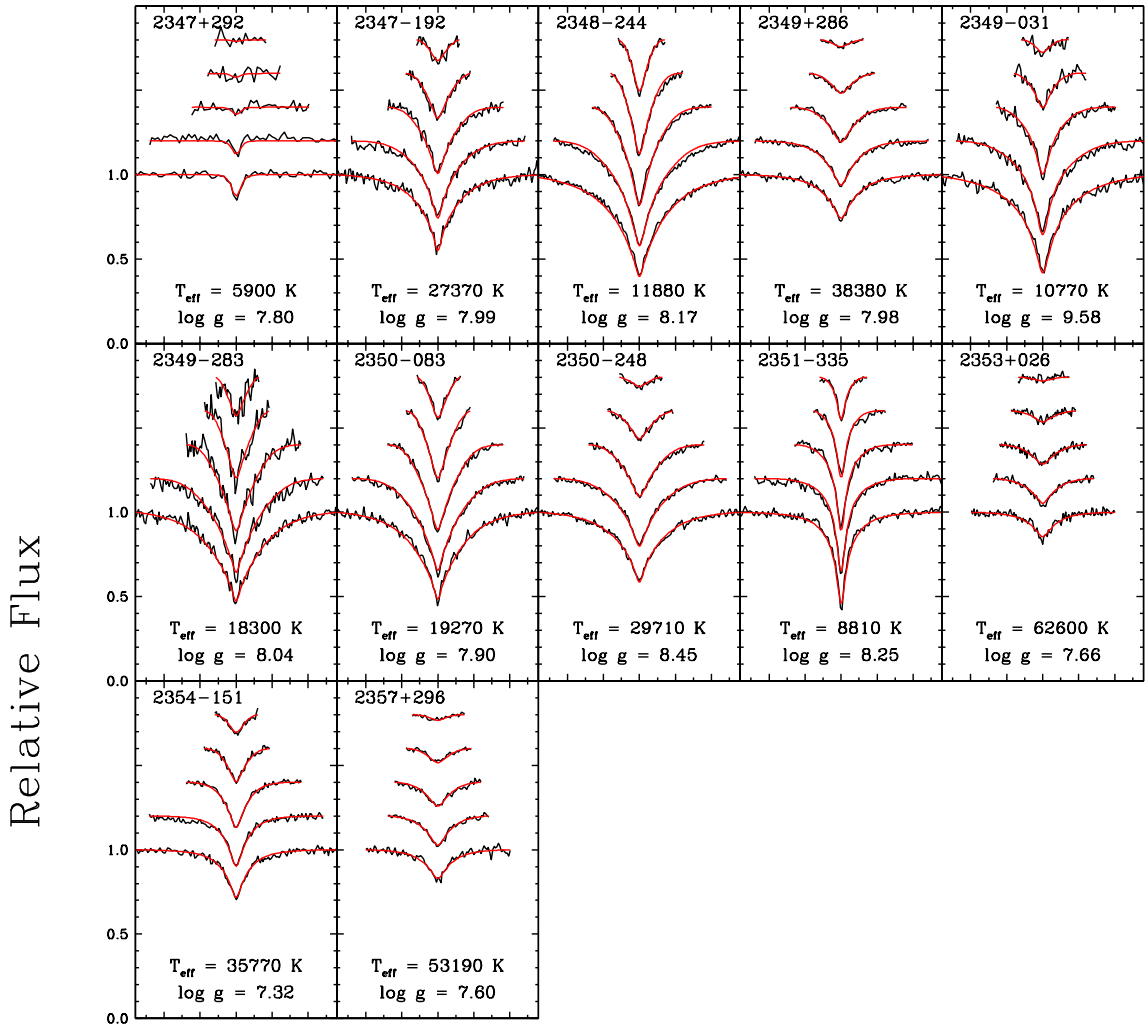

FIGURE B.1 – Suite

Annexe C

Solutions spectroscopiques pour les systèmes binaires DA+dM

Nous présentons ici l'ensemble de nos solutions spectroscopiques pour les systèmes bianires DA+dM présentées au Chapitre 3 puisque ces solutions n'y figuraient pas toutes étant donnés les contraintes d'espace pour la publication dans l'*Astrophysical Journal* (ApJ). Les noms suivis de la lettre "F" indiquent les cas où nous avons forcé les valeurs de $T_{\rm eff}$ et $\log g$ aux valeurs obtenues en analysant les spectres bleus de ces mêmes étoiles.

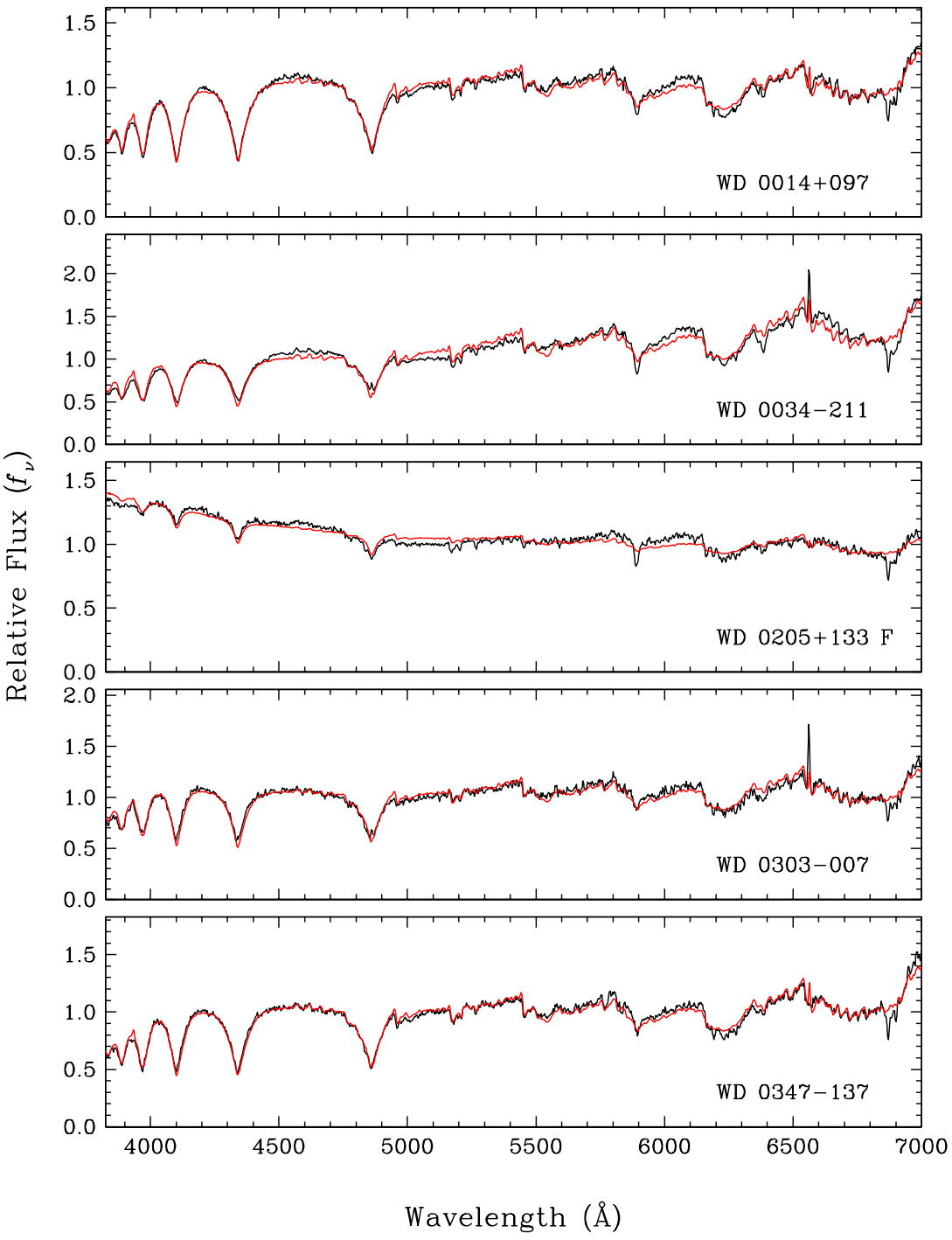

FIGURE C.1 – Solutions spectroscopiques pour les systèmes binaires DA+dM présentées au Chapitre 3.

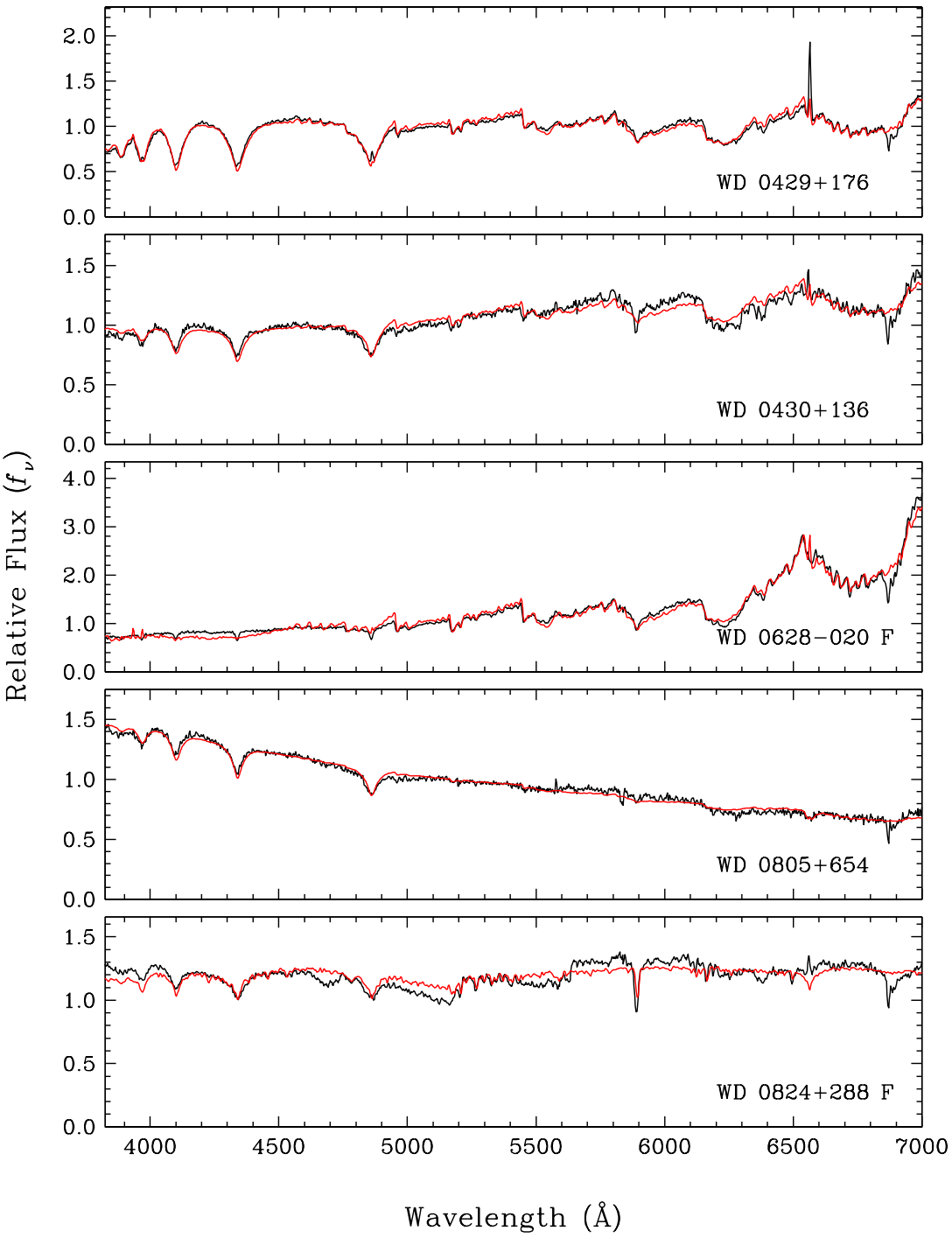

FIGURE C.1 – Suite

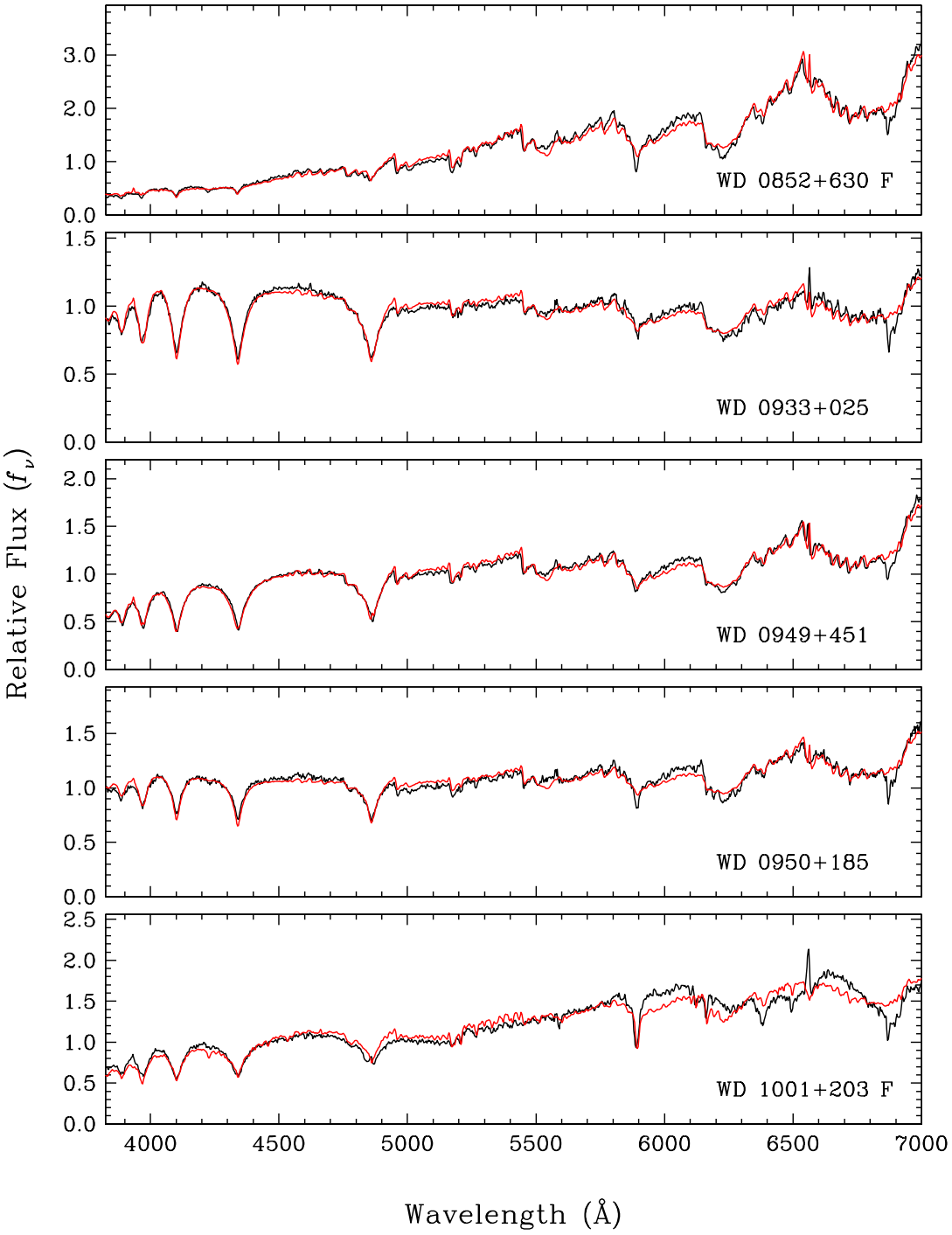

FIGURE C.1 – Suite

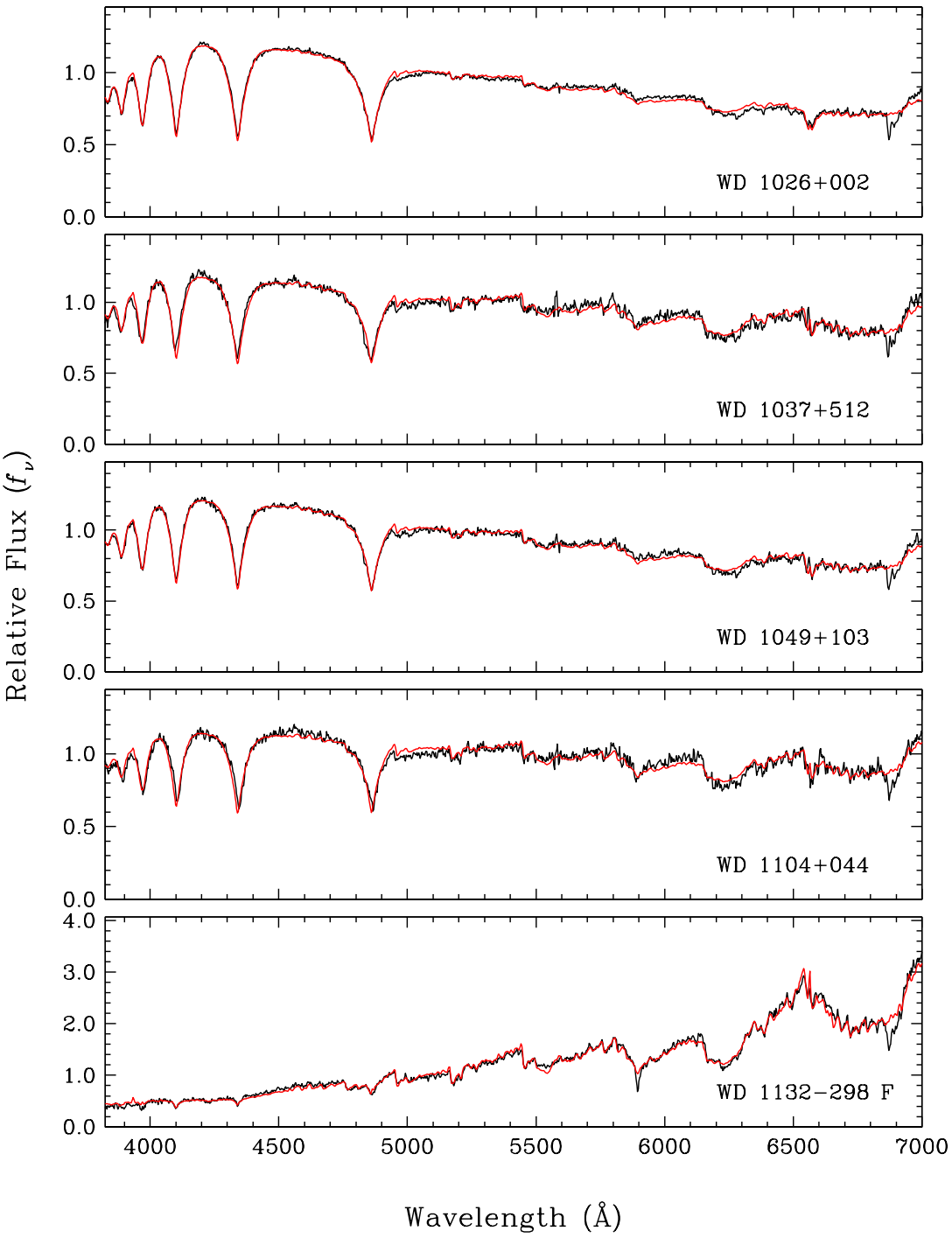

FIGURE C.1 – Suite

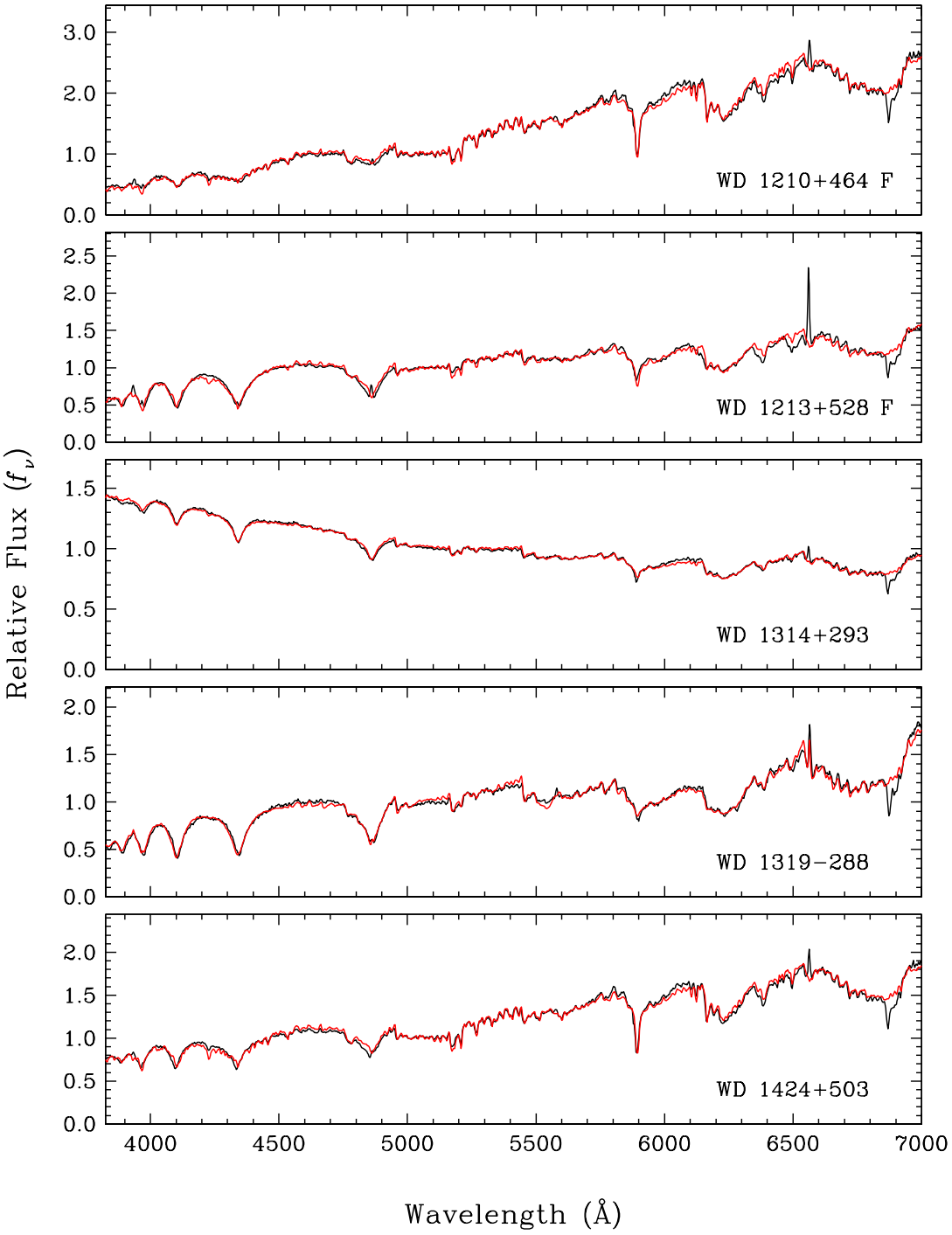

FIGURE C.1 – Suite

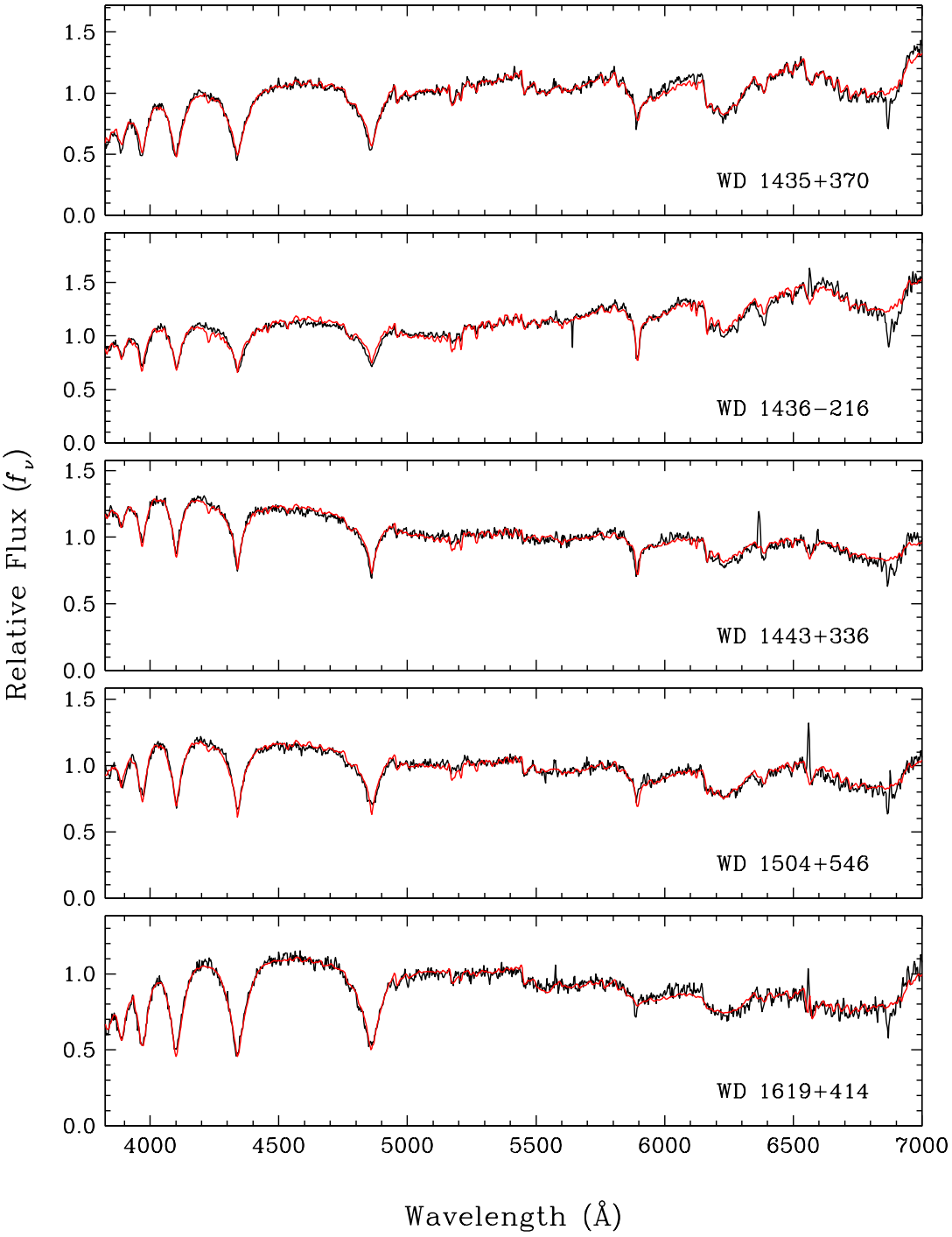

FIGURE C.1 – Suite

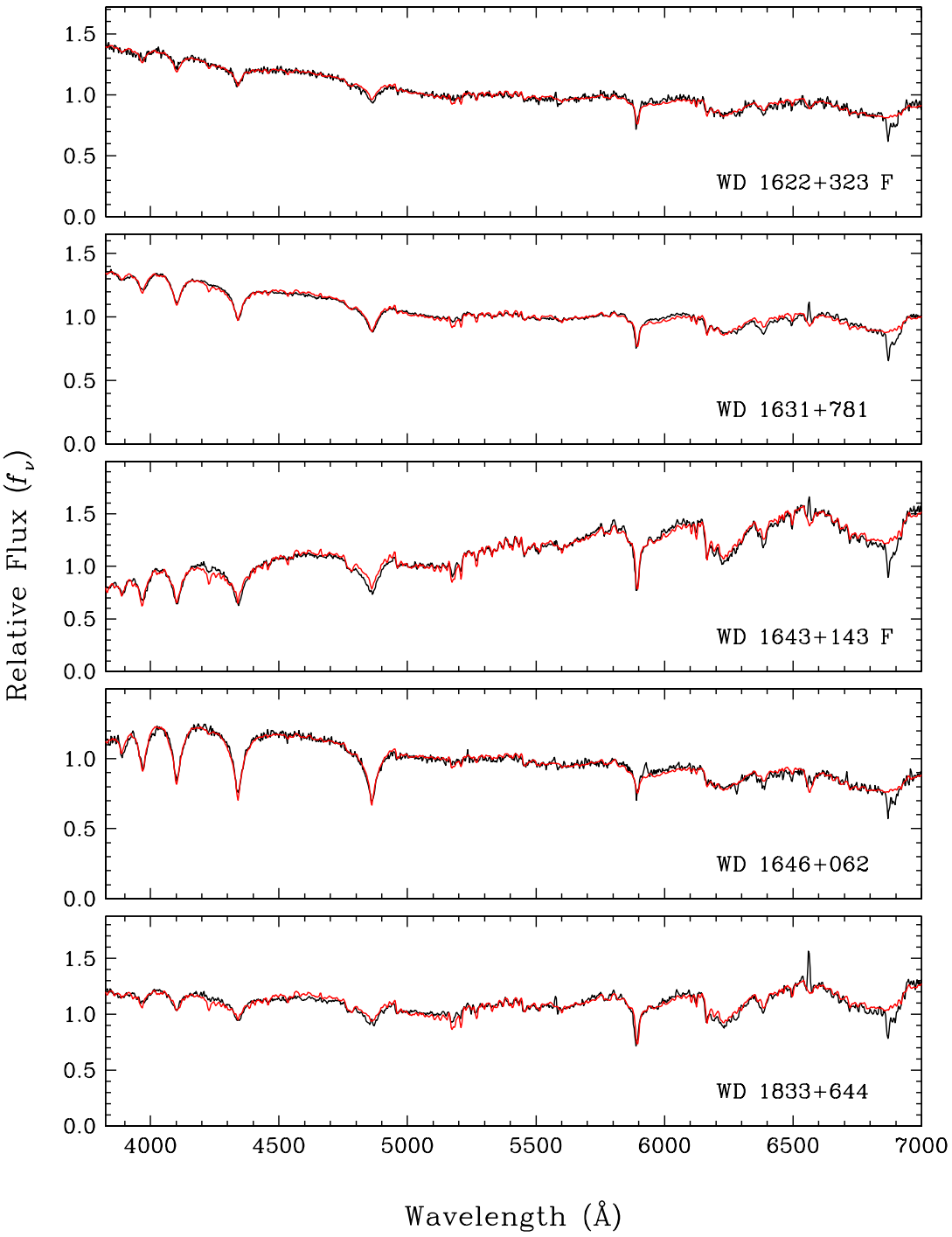

FIGURE C.1 – Suite

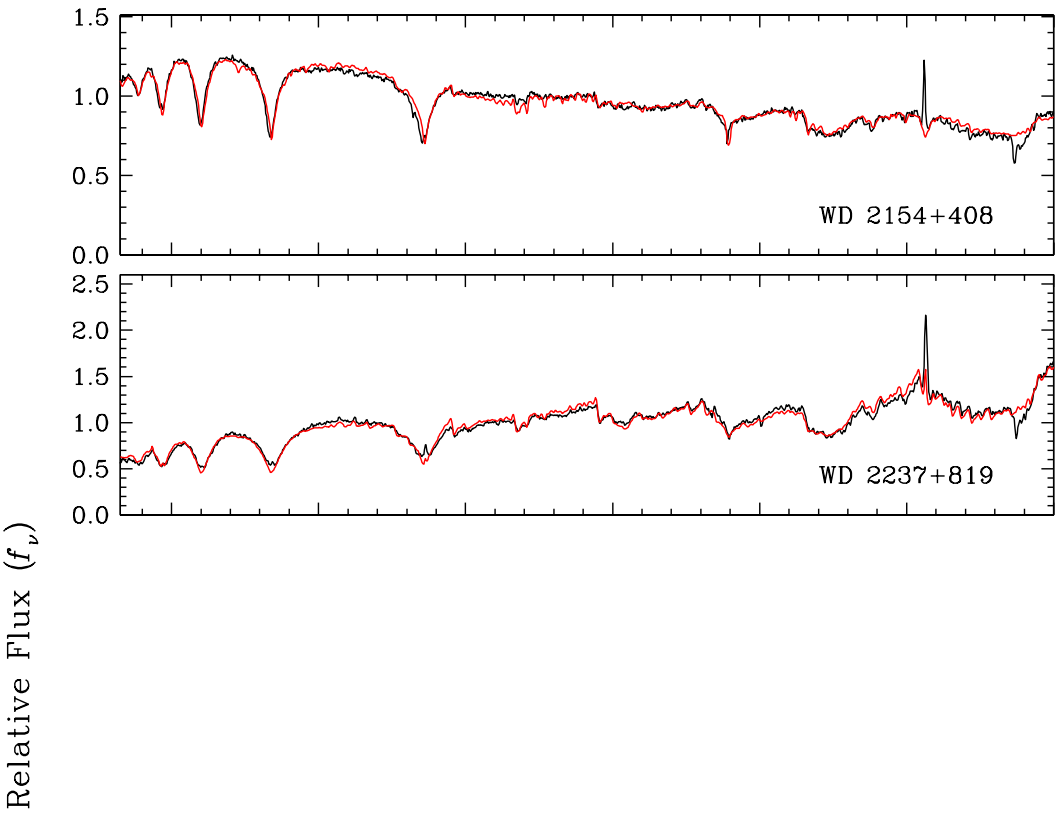

FIGURE C.1 – Suite

Annexe D

Spectroscopic analysis of DA white dwarfs from the McCook & Sion catalog

Nous présentons ici un article publié dans le compte rendu du 16th European Workshop on White Dwarfs, tenu à Barcelone, en Espagne, du 30 juin au 4 juillet 2008. Cette publication présente des résultats partiels et/ou préliminaires de ce projet de thèse et nous l'incluons en annexe pour des fins de comparaisons avec les résultats finaux.

Journal of Physics: Conference Series **172** (2009) 012021 doi:10.1088/1742-6596/172/1/012021

Spectroscopic analysis of DA white dwarfs from the McCook & Sion catalog[1]

A Gianninas[1], P Bergeron[1] and M T Ruiz[2]

[1] Département de Physique, Université de Montréal, C.P. 6128, Succ. Centre-Ville, Montréal, Québec H3C 3J7, Canada

[2] Departamento de Astronomía, Universidad de Chile, Casilla 36-D, Santiago, Chile

Abstract. For some years now, we have been gathering optical spectra of DA white dwarfs in an effort to study and define the empirical ZZ Ceti instability strip. However, we have recently expanded this survey to include all the DA white dwarfs in the McCook & Sion catalog down to a limiting visual magnitude of V=17.5. We present here a spectroscopic analysis of over 1000 DA white dwarfs from this ongoing survey. We have several specific areas of interest most notably the hot DAO white dwarfs, the ZZ Ceti instability strip, and the DA+dM binary systems. Furthermore, we present a comparison of the ensemble properties of our sample with those of other large surveys of DA white dwarfs, paying particular attention to the distribution of mass as a function of effective temperature.

1. Introduction

Although the Sloan Digital Sky Survey (SDSS) has unearthed thousands of new white dwarfs, it is our belief that there is a significantly brighter sample of white dwarfs whose scientific potential has never truly been exploited. With this in mind, we have undertaken a systematic survey of DA white dwarfs based, in large part, on the last published version of the catalog of spectroscopically identified white dwarfs of McCook & Sion (1999). We will first describe our survey and how it compares to other large surveys of DA white dwarfs and examine some of the ensemble properties of our current sample. We will then take a closer look at a few choice subsamples of objects. In particular, we will look at the DAO white dwarfs, the ZZ Ceti instability strip, and the DA+dM binaries. Finally, we will look at one specific object, CBS 229, which we believe to be a binary system with a magnetic component.

2. Survey Overview

Over the last few years, we have been obtaining optical spectra for DA white dwarfs near the ZZ Ceti instability in an effort to constrain its empirical boundaries. More recently, we expanded this observational survey to include all the DA white dwarfs from the McCook & Sion catalog down to a limiting visual magnitude of V=17.5. Many of these stars have never been analyzed with modern CCD spectroscopy and the only information available is a spectral classification, which

[1] Based on observations made with ESO Telescopes at the La Silla or Paranal Observatories under program ID 078.D-0824(A) and with the Las Campanas 2.5 m Irénée du Pont telescope.

is often erroneous. The bulk of this project has been conducted using Steward Observatory's 2.3 m telescope at Kitt Peak. However, we were also able to obtain time on the ESO 3.6 m telescope at La Silla (Chile) as well as Carnegie Observatories' 2.5 m du Pont telescope at Las Campanas (Chile), allowing us to extend our survey into the southern hemisphere.

How does our work compare to other large surveys of DA white dwarfs? The SPY project (Koester et al. 2001), which obtained high resolution spectra for several hundred white dwarfs, had a limiting magnitude of $V = 16.5$ and was conducted in the southern hemisphere at the VLT. There is actually quite a large overlap with our own sample of stars. Indeed, close to 80% of the stars surveyed in SPY are included in this work. In contrast, we have only a very small overlap with the SDSS (see Figure 1) owing to the fact that the majority of their objects are quite faint due to the nature of the SDSS itself. The faintness of the objects in the SDSS also limits the quality of their spectra since a single exposure time is set for all the objects observed on a given plate. Therefore, the dimmer an object, the lower the signal-to-noise ratio (S/N) of the spectrum. This makes for an extremely inhomogeneous sample of data as far as S/N is concerned. In contrast, we observe one star at a time and adjust our exposure times to obtain spectra with a minimum S/N of approximately 50 (see Fig. 2). Thus our sample, although not as large as the SDSS, comprises data of much higher quality overall. This is key as we have shown in Gianninas, Bergeron & Fontaine (2005) the importance of high S/N for measuring the atmospheric parameters of DA white dwarfs.

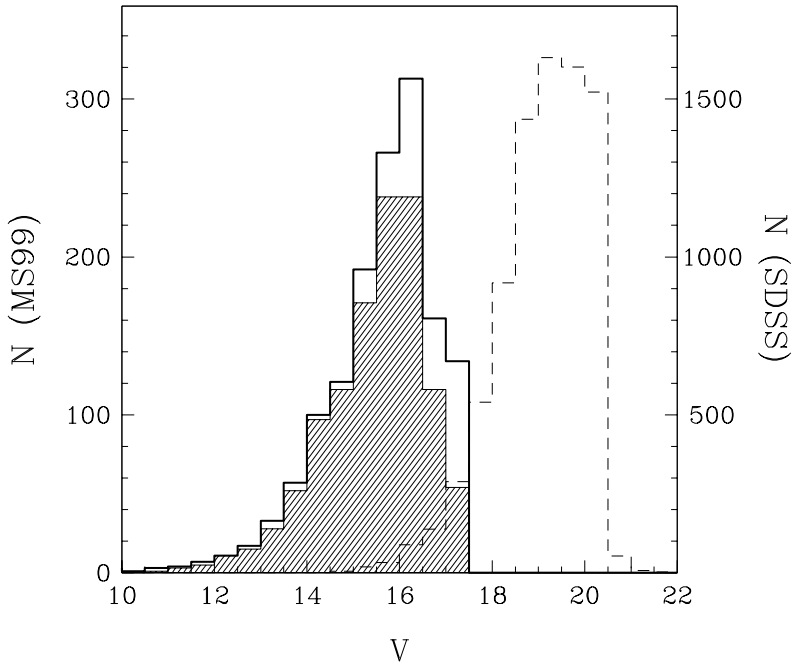

Figure 1. Distribution of visual magnitudes, V, for our sample selected from McCook & Sion (1999; *bold histogram*) and for the white dwarfs we have observed to date (*hatched histogram*). In comparison, the distribution for the SDSS sample as of Data Release 4 (Eisenstein et al. 2006) is also shown (*dashed histogram*). Note that the scale is different for the McCook & Sion sample (*left*) and the SDSS sample (*right*).

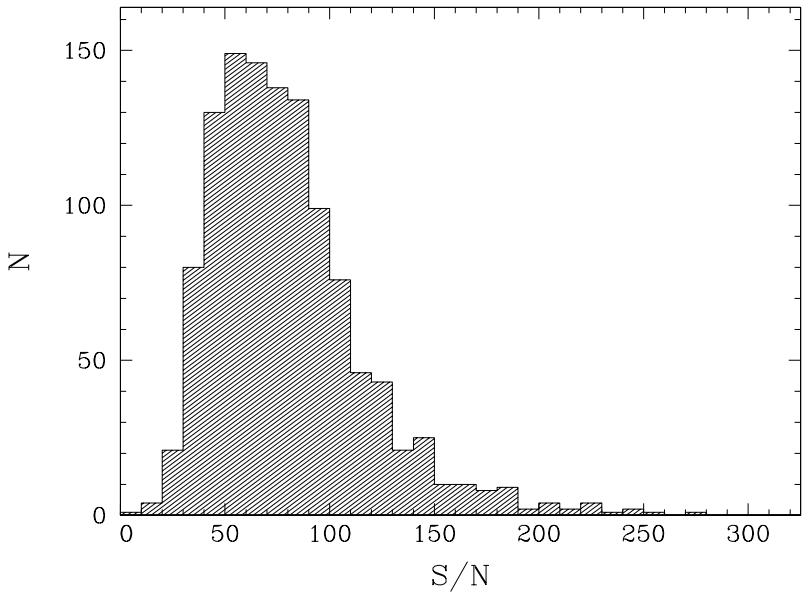

Figure 2. Distribution of S/N for the sample of DA white dwarfs for which we have obtained optical spectra. The majority of the spectra have a S/N of 50 or greater.

3. Mass distribution

We show in Figure 3 the mass distribution of our sample as a function of effective temperature. The atmospheric parameters, $T_{\rm eff}$ and $\log g$, are determined using the spectroscopic technique described in Bergeron, Saffer & Liebert (1992; see also Liebert, Bergeron & Holberg 2005) and the masses are derived from evolutionary models with carbon/oxygen cores and thick hydrogen layers (see references in Liebert et al. 2005). Our mass distribution shows the usual increase in mass at lower temperatures as seen in the PG sample (Liebert et al. 2005), for example. This phenomenon is still not understood although many possible solutions have been proposed over the years (Bergeron, Gianninas & Boudreault 2007). We also notice a certain number of white dwarfs with masses less than $\sim$0.45 $M_{\odot}$. This population of low mass white dwarfs is necessarily the product of binary evolution as a progenitor with the appropriate mass could not yet have evolved to the white dwarf stage. As such, these objects are important as they represent a separate evolutionary channel for white dwarf stars.

4. DAO white dwarfs

DAO stars are hydrogen atmosphere white dwarfs whose optical spectra also contain lines of ionized helium, usually He II λ4686. The mechanism which maintains the helium in the atmosphere is still unclear, although a weak stellar wind has already been proposed. Figure 4 shows the location of the DAO stars from our sample in the $T_{\rm eff}$-$\log g$ plane along with the regular DA white dwarfs that populate that same region of the diagram. First, we notice that the sequence of DAO stars seems to be best reproduced by the 0.5 $M_{\odot}$ cooling track in contrast with the DA stars that follow the 0.6 $M_{\odot}$ cooling track, which is consistent with the accepted mean mass for white dwarfs. This can be explained if we assume that these DAO stars are the product of post-EHB evolution whereby the progenitor was not massive enough to climb back up the asymptotic giant branch (AGB) and evolved to the white dwarf stage directly from the extreme horizontal branch (EHB). We note, however, that this scenario does not apply to all DAO white dwarfs. As shown in Napiwotzki (1999), there is a sequence of DAO stars that are

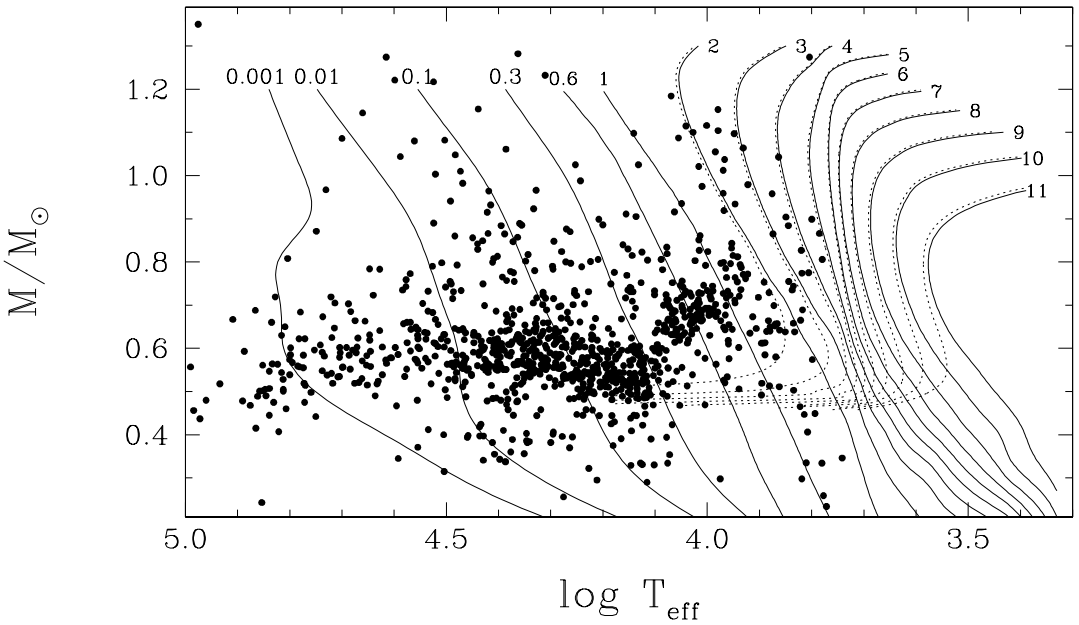

Figure 3. Mass distribution as a function of effective temperature for our entire sample. The solid lines represent isochrones which take into account only the white dwarf cooling time whereas the dotted lines include also the main sequence lifetime. Each isochrone is labeled by its age in Gyr.

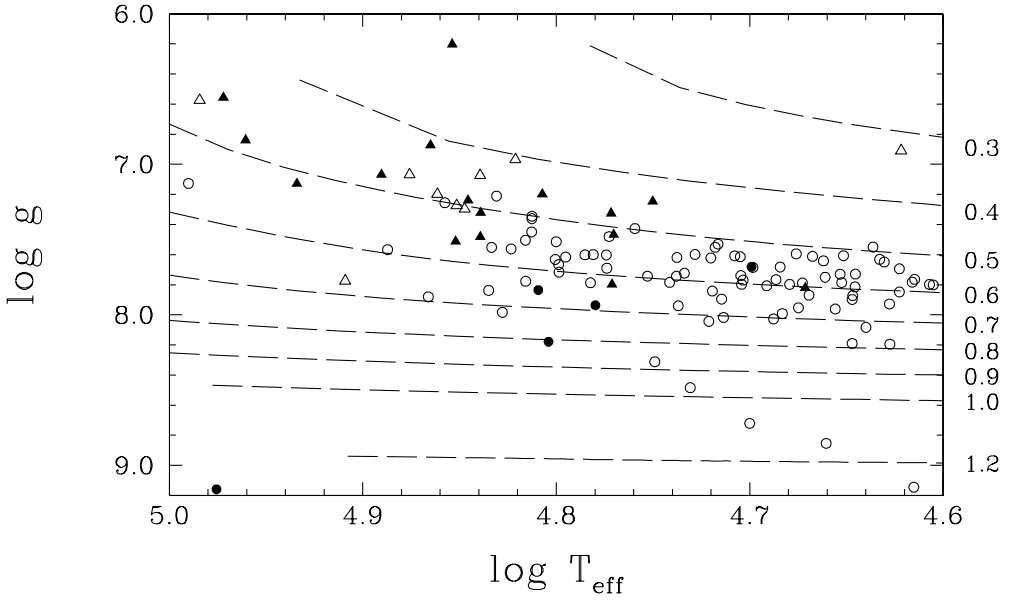

Figure 4. Section of the $\log g$ vs $\log T_{\rm eff}$ diagram showing the hot end of the DA white dwarf cooling sequence. Circles represent DA white dwarfs and triangles correspond to the DAO stars. The filled symbols indicate those stars that exhibit the Balmer line problem. The dashed lines are white dwarf cooling tracks with thick hydrogen layers and masses (in $M_{\odot}$) indicated to the right of the figure.

consistent with normal post-AGB evolution like the majority of white dwarfs.

We also notice in Figure 4 that most of the DAO stars exhibit the Balmer line problem as first reported by Napiwotzki (1992). The problem manifests itself as an inability to obtain consistent values of $T_{\rm eff}$ and $\log g$ from the spectroscopic fitting technique for the individual Balmer lines. Werner (1999) eventually showed that the problem could be solved by including C, N, and O in the models with proper Stark broadening of the metallic lines. We hope to include this solution within the next generation of our models in order to properly analyze these DAO white dwarfs as well as the other DA stars which exhibit the same phenomenon.

5. The ZZ Ceti instability strip

Figure 5 shows our most up to date vision of the ZZ instability strip. In particular, we have re-observed several of the variables in the strip and with the exception of one pulsator, we have spectra with S/N $\gtrsim$ 70 for all our ZZ Ceti stars. However, one also notices the presence of a photometrically constant star in the middle of the instability strip, HS 1612+5528. This object had been reported as NOV (not observed to vary) by Voss et al. (2006). We obtained our own spectrum of this star and confirmed its position within the instability strip. Consequently, we decided to conduct our own observations to determine whether this star was variable or not. We observed HS 1612+5528 at the Observatoire du mont Mégantic using the Montréal three-channel photometer LAPOUNE for several hours on the night of 2006 July 20 and we detected no variations down to a limit of 0.2%. However, there are known ZZ Ceti stars that pulsate with amplitudes as low as 0.05% so we hope to obtain new high-speed photometry to determine once and for all the status of this object. For the moment, it is the only photometrically constant star contaminating the strip, but it is entirely possible that we, and Voss et al., observed HS 1612+5528 during a period of destructive interference. Alternatively, HS 1612+5528 could also represent a ZZ Ceti star whose pulsations are not detectable due to our line of sight with respect to the pulsation modes of the star.

Finally, we see that our survey as once again uncovered several new objects which lie near or within the empirical boundaries of the strip and we are exploring the possibility of obtaining high-speed photometric measurements for these stars as well.

6. DA+dM binary systems

Although the majority of stars in our survey are isolated DA white dwarfs, there are several objects whose optical spectra contain the tell-tale signs pointing to the presence of a main sequence companion, usually an M dwarf. The spectrum of the M dwarf will contaminate one or several of the Balmer lines from the white dwarf spectrum which renders our normal technique of fitting the observed Balmer line profiles very difficult. To try and get around this problem, we either exclude certain spectral lines or certain portions of the spectral lines from our fitting procedure. However, this means that our determinations of the atmospheric parameters for these stars are quite uncertain. In an effort to determine more accurately the atmospheric parameters of these white dwarfs, we have begun gathering spectra which cover the entire Balmer series from Hα to H8 thus providing sufficient wavelength coverage to determine the spectral type of the M dwarf.

Our analysis will involve a 5-parameter fit to the entire spectrum: the effective temperature and surface gravity of the white dwarf primary, the spectral type of the M dwarf secondary and the relative intensities of the two energy distributions. We will essentially be co-adding our usual synthetic spectra of DA white dwarfs with the M dwarf spectral templates from Bochanski et al. (2007). We will then use the results of the fit to subtract an appropriate template, with the proper flux level, from our initial spectrum. We see in Figure 6 a sample of some of the spectra we have obtained so far. The kink we see in the red wing of Hβ is due to a TiO band. Some spectra also show a MgH band in the blue wing of Hβ as well as Ca I between Hγ and Hδ. We

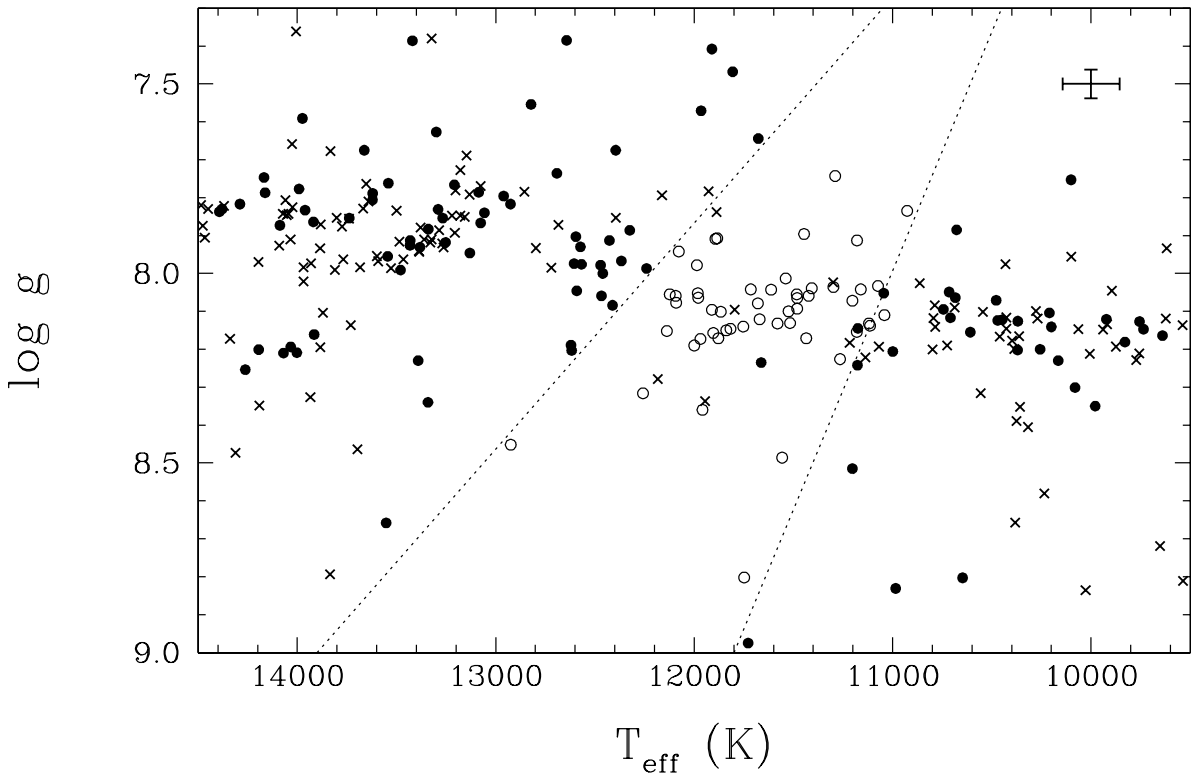

Figure 5. Section of the $\log g$ vs $T_{\rm eff}$ diagram showing the ZZ Ceti instability strip. Open circles correspond to ZZ Ceti stars while filled circles represent stars that are photometrically constant. The $\times$ symbols are stars from our survey which have never been observed for variability. The dashed lines correspond to the empirical boundaries of the instability strip and the typical error bars in this region of the $T_{\rm eff}$-$\log g$ plane are shown in the upper right corner.

also notice the prominent Na D line at 5895 Å. Furthermore, hydrogen-line emission from the M dwarf can contaminate the center of the Balmer lines of the white dwarf.

7. CBS 229

Large surveys often uncover unique and interesting objects. In the course of our survey of the DA+dM binaries described in the previous section, we came across CBS 229, an object which turned out to be rather interesting. We had initially thought that the feature in the red wing of Hβ observed in our blue spectrum (not shown here) was the usual TiO absorption band produced by the presence of an M dwarf. But our full optical spectrum, shown at the top of Figure 7, does not show any signs of an M dwarf companion. We became aware after the fact that CBS 229 had also been observed as part of SDSS, and classified as magnetic with an estimated polar magnetic field of $B_p \sim 20$ MG (Vanlandingham et al. 2005). Indeed, the SDSS spectrum (also displayed in Fig. 7) with a better spectral resolution shows what are clearly magnetic components near Hα. But the observed profile at Hβ, or even at Hα, is really at odds with the predictions of magnetic models. For instance, the models for KPD 0253+5052 shown in Figure 6 of Wickramasinghe & Ferrario (2000), with a comparable magnetic field, predict a much weaker Hα central Zeeman component with respect to the shifted components than observed in CBS 229. Furthermore, the predicted Hβ profile and the higher Balmer lines are totally smeared out, in sharp contrast with the strong and sharp Balmer lines observed in CBS 229.

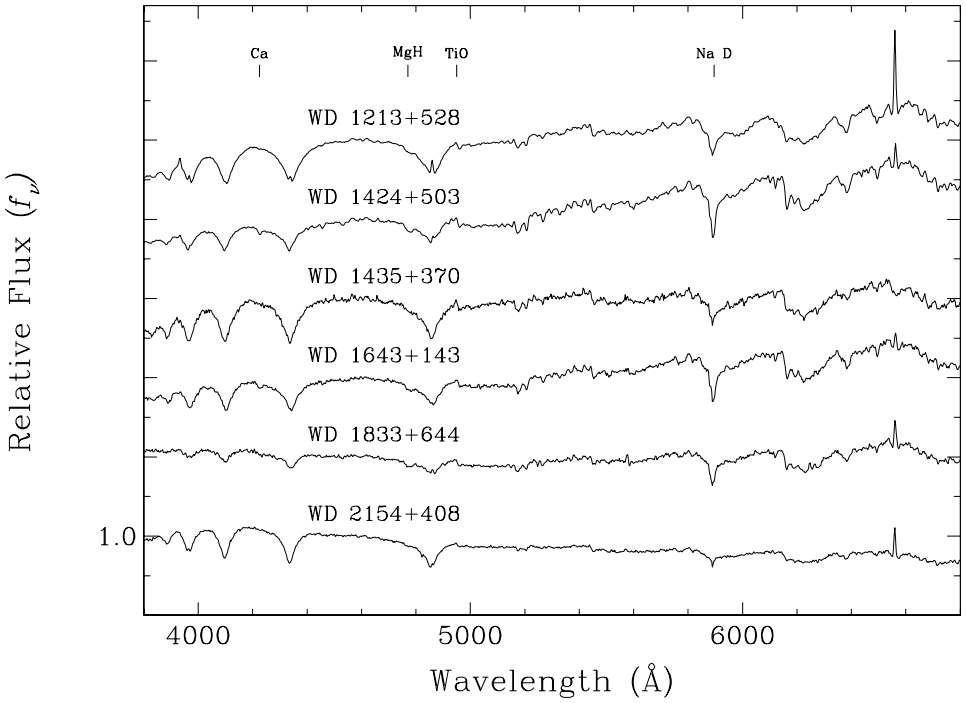

Figure 6. Optical spectra of DA+dM binary systems. Tick marks indicate metallic features in the spectrum of the M dwarf companion's spectrum.

Instead, we suggest that CBS 229 is an unresolved double degenerate binary composed of a magnetic DA star and a normal DA star. We show in Figure 7 a very preliminary attempt to deconvolve the spectrum into its two separate components. We subtracted from the SDSS data a synthetic spectrum with $T_{\rm eff} = 15,000$ K and $\log g = 8.5$. We assumed that the non-magnetic DA contributes 40% of the flux at 5500 Å; this sets the relative intensities of the spectra. The residual spectrum clearly shows magnetic features at Hα and Hβ that bear a strong resemblance with the 17 MG model shown in Figure 6 of Wickramasinghe & Ferrario (2000). To our knowledge, there are not many double degenerate systems with only one magnetic component that have been discovered and analyzed, with the exception of the LB 11146 system reported by Liebert et al. (1993), for which the companion to the non-magnetic DA white dwarf turned out to be a highly magnetic helium-atmosphere white dwarf. We plan a more detailed analysis of CBS 229 that can hopefully shed some more light on the evolution of such unique systems.

8. Future Outlook

We have several upcoming observing runs at Kitt Peak during which we hope to complete our survey of the McCook & Sion catalog in the northern hemisphere. In parallel, we will continue to obtain spectra for the remaining DA+dM binary systems that we have identified in our sample. We are also securing telescope time in Chile to complete our survey in the southern hemisphere. We hope that within a year's time our survey will essentially be complete.

Our analysis of these stars is ongoing on several fronts. We are working on adding the necessary physics in our models to analyze the DAO stars exhibiting the Balmer line problem. Our analysis of the DA+dM binaries, and in particular, our ability to extract the white dwarf spectrum will soon yield results as will our analysis of CBS 229.

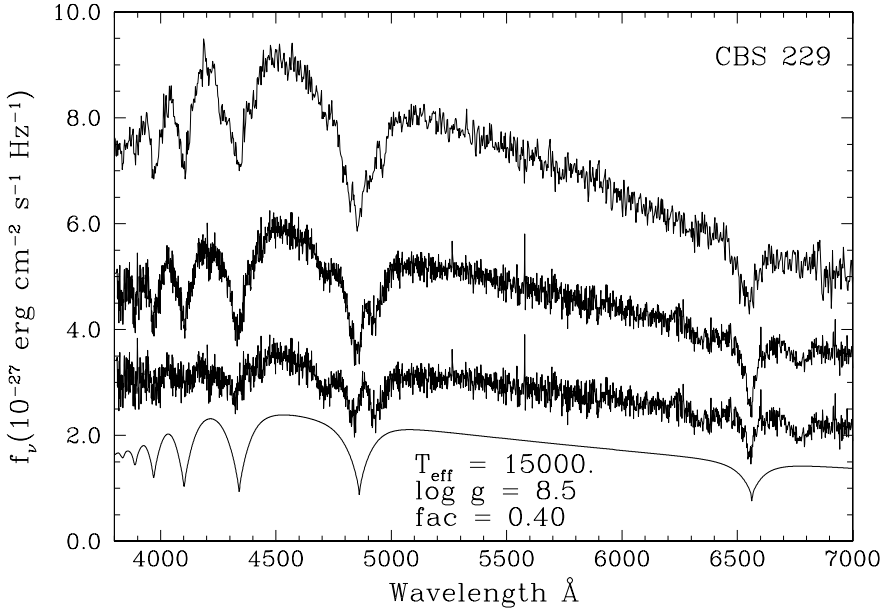

Figure 7. Our own spectrum (first from the top) and the SDSS spectrum (second from the top) of CBS 229. At the bottom, a synthetic spectrum of a DA white dwarf corresponding to the atmospheric parameters indicated in the figure. The quantity $fac = 0.40$ implies that the synthetic spectrum contributes 40% of the flux of the sytem at 5500 Å. The spectrum just above is the residual left over from subtracting the synthetic DA model from the SDSS spectrum.

Acknowledgments

We would like to thank the director and staff of Steward Observatory for the use of their facilities. We would also like to thank G. Fontaine for his assistance in conducting the high-speed photometry and analysis of HS 1612+5528. This work was supported in part by the NSERC Canada and by the Fund FQRNT (Québec). A. G. acknowledges the contribution of the Canadian Graduate Scholarships. P. B. is a Cottrell Scholar of Research Corporation for Science Advancement. M. T. R. received support from FONDAP 15010003 and PFB-06 (CONICYT).

References

Bergeron P Gianninas A and Boudreault S 2007 *ASP Conf. Series* vol 372, eds R Napiwotzki and M R Burleigh (San Francisco: ASP) p 29
Bergeron P Saffer R and Liebert J 1992 *ApJ* **394** 247
Bochanski J J, West A A, Hawley S L and Covey K R 2007 *AJ* **133** 531
Eisenstein et al. 2006 *ApJS* **167** 40
Gianninas A Bergeron P and Fontaine G 2005 *ApJ* **631** 1100
Koester D et al. 2001 *A&A* **378** 556
Liebert J Bergeron P and Holberg J B 2005 *ApJS* **156** 47
Liebert J Bergeron P Schmidt G D and Saffer R A 1993 *ApJ* **418** 426
McCook G P and Sion E M 1999 *ApJS* **121** 1
Napiwotzki R 1992 *Lecture Notes in Physics* vol 401, ed U Heber and C S Jeffery (Berlin: Springer) p 310
Napiwotzki R 1999 *A&A* **350** 101
Vanlandingham K M et al. 2005 *ApJ* **130** 734
Voss B Koester D Ostensen R Kepler S O Napiwotzki R Homeier D and Reimers D 2006 *A&A* **450** 1061
Werner K 1999 *ApJ* **457** L39
Wickramasinghe D T and Ferrario L 2000 *PASP* **112** 873